

UNCLASSIFIED

AD 273 334

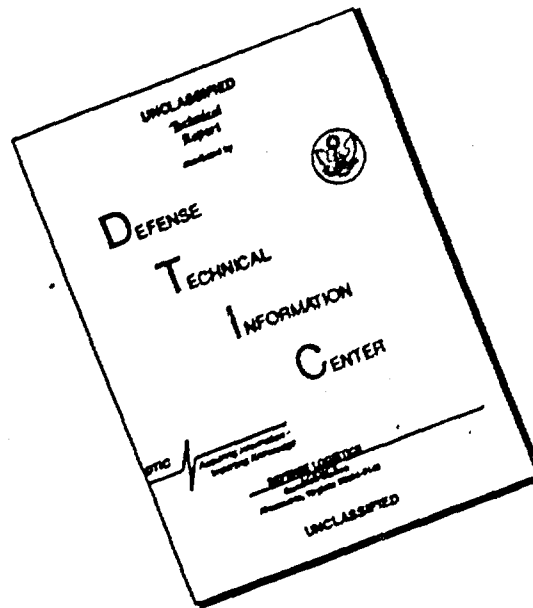
*Reproduced
by the*

**ARMED SERVICES TECHNICAL INFORMATION AGENCY
ARLINGTON HALL STATION
ARLINGTON 12, VIRGINIA**



UNCLASSIFIED

DISCLAIMER NOTICE



THIS DOCUMENT IS BEST QUALITY AVAILABLE. THE COPY FURNISHED TO DTIC CONTAINED A SIGNIFICANT NUMBER OF PAGES WHICH DO NOT REPRODUCE LEGIBLY.

NOTICE: When government or other drawings, specifications or other data are used for any purpose other than in connection with a definitely related government procurement operation, the U. S. Government thereby incurs no responsibility, nor any obligation whatsoever; and the fact that the Government may have formulated, furnished, or in any way supplied the said drawings, specifications, or other data is not to be regarded by implication or otherwise as in any manner licensing the holder or any other person or corporation, or conveying any rights or permission to manufacture, use or sell any patented invention that may in any way be related thereto.

273334 WADD TECHNICAL REPORT 61-42
16 260

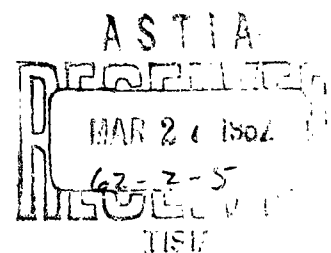
646 100

STRUCTURAL VIBRATIONS IN SPACE VEHICLES

K. ELDRED
WM. ROBERTS
R. WHITE

NORTHROP CORPORATION
NORAIR DIVISION
AND
WESTERN ELECTRO ACOUSTIC LABORATORY

DECEMBER 1961



AERONAUTICAL SYSTEMS DIVISION

CATALOGED BY ASTIA
AS AD NO. —

273 334

NOTICES

When Government drawings, specifications, or other data are used for any purpose other than in connection with a definitely related Government procurement operation, the United States Government thereby incurs no responsibility nor any obligation whatsoever; and the fact that the Government may have formulated, furnished, or in any way supplied the said drawings, specifications, or other data, is not to be regarded by implication or otherwise as in any manner licensing the holder or any other person or corporation, or conveying any rights or permission to manufacture, use, or sell any patented invention that may in any way be related thereto.

Qualified requesters may obtain copies of this report from the Armed Services Technical Information Agency, (ASTIA), Arlington Hall Station, Arlington 12, Virginia.

This report has been released to the Office of Technical Services, U. S. Department of Commerce, Washington 25, D. C., for sale to the general public.

Copies of ASD Technical Reports and Technical Notes should not be returned to the Aeronautical Systems Division unless return is required by security considerations, contractual obligations, or notice on a specific document.

STRUCTURAL VIBRATIONS IN SPACE VEHICLES

K. ELDRED, WM. ROBERTS AND R. WHITE

**NORTHROP CORPORATION
NORAIR DIVISION
HAWTHORNE, CALIFORNIA
AND
WESTERN ELECTRO ACOUSTIC LABORATORY
LOS ANGELES, CALIFORNIA**

DECEMBER 1961

**FLIGHT DYNAMICS LABORATORY
CONTRACT No. AF 33(616)-6486
PROJECT No. 1370
TASK No. 14004**

**AERONAUTICAL SYSTEMS DIVISION
AIR FORCE SYSTEMS COMMAND
UNITED STATES AIR FORCE
WRIGHT-PATTERSON AIR FORCE BASE, OHIO**

FOREWORD

This report was prepared by the Norair Division of Northrop Corporation, Hawthorne, California, in conjunction with Western Electro-Acoustic Laboratory, acting as an associate contractor under Contract AF33(616)-6486. This contract was initiated under Project No. 1370 "Dynamic Problems in Flight Vehicles," Task No. 14004, "Methods of Vibration Prediction, Control and Measurement," for "A Study of Structural Vibration Sources and Methods of Response Prediction and Reduction of These Responses". The work was administered under the direction of the Dynamics Branch, Flight Dynamics Laboratory, Deputy for Technology, Aeronautical Systems Division, with Lt. N. Wrobel acting as project engineer. This report covers work completed in January 1961

The authors express their appreciation for the contributions of Mr. Robert Wilkus, Dr. O. R. Rogers and other ASD personnel, and of a number of Aerospace companies for reports and data. In addition to the principal authors, contributing personnel from Northrop including Dan Van Ert, Arthur Cross, Bruce Vernier, and Roy Mustain; and Jose Ortega, Milton Cottis and Myron Mann from Western Electro-Acoustic Laboratory.

ABSTRACT

in view of the present satellite and space travel developments, a study of vehicle structural vibration was deemed necessary. Continuous exposure to vibration environments may cause serious structural and equipment failures resulting in impairment of function or complete mission failure. The scope of the study is a preliminary investigation of the forcing functions and their characteristics, the methods of estimating a combined response, and the proof tests required to qualify structure and equipment. The study owes its timeliness and importance to its fundamental concern with structural integrity. The general fatigue problem has become more important while simultaneously the acoustic fatigue problem crosses the threshold at which ordinary structure no longer withstands the repeated acoustical forces. Since developed power will continue to rise with time, fatigue due to acoustic excitation is certain to become an increasingly important design problem.

This report is presented in three parts, Sources, Responses, and Simplified Composite Response for Testing.

Part One discusses the various sources of vibratory energy which can result in vehicle vibration including rocket noise, aerodynamic pressure fluctuations (boundary layer, base pressure, wakes, cavities, projections, oscillating shock, separate flow and panel flutter), wind shear and gust, meteorites and direct mechanical coupling.

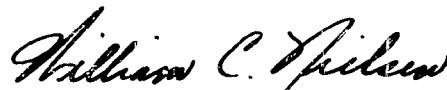
Part Two discusses the prediction of vibratory response through both empirical and analytical approaches, and includes a thorough discussion of the single degree of freedom system, resonance-on-resonance, panels, shells, mobility, generalized force, joint acceptance, correlations and other statistical tools, and in addition, comparisons of empirical data from a variety of aircraft and missiles.

Part Three contains a discussion of fatigue and malfunction, the properties of an ideal test, implications of and methods for obtaining a simplified composite response and an examination of various test equivalences.

PUBLICATION REVIEW

This report has been reviewed and is approved.

FOR THE COMMANDER:



WILLIAM C. NIELSEN

Colonel, USAF

Chief, Flight Dynamics Laboratory

TABLE OF CONTENTS

	<u>Page</u>
FOREWORD	
ABSTRACT	iii
LIST OF ILLUSTRATIONS	ix
LIST OF TABLES	xxii
LIST OF SYMEOLS	xxiii
 PART I	
SOURCES OF VIBRATIONS	
SECTION I INTRODUCTION	1
SECTION II ROCKET NOISE EXCITATION	4
Characteristics and Origin of Jet and Rocket Noise	4
Estimation of Noise Environment During Launch	16
Effect of Motion	20
Ground Effects	25
References	30
SECTION III AERODYNAMIC EXCITATION	32
Turbulent Boundary Layer Flow	32
Impingement of Jet Turbulence on the Vehicle	40
Separated Flows and Oscillating Shocks	42
Flow Over Cavities	50
Flow Past Projections	54
Base Pressure Fluctuations	58
Panel Flutter	64
References	66
SECTION IV ATMOSPHERIC WIND AND TURBULENCE ENVIRONMENTS	69
Introduction	69
General Discussion, Aerodynamic Forces	69
Types of Disturbances	70
Methods of Analysis	72
Application	73
Wind Profiles and Wind Shear	74
Continuous Atmospheric Turbulence	80
References	90

TABLE OF CONTENTS (Cont'd)

	<u>Page</u>
SECTION V	THE METEORITE ENVIRONMENT 93 Areas of Interest 93 The Asteroidal Materials 93 Cometary Material 94 Daily Influx and Interplanetary Debris 94 Velocities 95 Estimated Data on Other Parameters 95 Field Data 100 Inferences on Puncture and Vibration 101 References 103
SECTION VI	DIRECT VIBRATION EXCITATION 104 Rocket Engine Combustion Instability 104 Liquid Rocket Engines 104 Solid Rocket Engines 110 Thrust Variations 111 Liquid Rocket Engine Vibration and Thrust Variations 112 Advanced Propulsion Systems and Power Units for Space 130 Auxiliary Equipment Vibration Excitation 133 References 140
SECTION VII	NOISE EXPOSURE FOR HYPOTHETICAL VEHICLE AND MISSION 141
BIBLIOGRAPHY	151
PART II	RESPONSE TO VIBRATIONS 157
SECTION I	INTRODUCTION 159
SECTION II	PROPERTIES OF THE SINGLE DEGREE OF FREEDOM SYSTEM 161 Free Vibration and Transient Excitation 162 Forced Sinusoidal Vibration 167 Motion Excitation 171 Transmissibility 173 Random Excitation 175 Dynamic Analogies 181 Mathematical Derivation and Summary of Responses of Single Degree of Freedom System 183

TABLE OF CONTENTS (Cont'd)

SECTION II (Cont'd)

Equivalence of Lumped Parameter and Continuously Distributed Single-Degree-of-Freedom System	183
Derivation and Summary of Responses of the Lumped Parameter SDF System	187
References	197

SECTION III

SUMMARY OF VIBRATION DATA FROM JET AIRCRAFT AND MISSILES	198
Introduction	198
Origin of Vibration Data	199
Vibration in Jet Aircraft	206
Vibration in Missiles	209
Comparison of Aircraft and Missile Vibration Trends	212
Empirical Prediction of Vehicle Vibration	218
Direct Correlation of Noise Adjacent Structure Vibration in Aircraft	243
Correlation of Ballistic Missile Launch Noise and Response	230
References	239

SECTION IV

GENERAL CONCEPTUAL APPROACH TO STRUCTURAL VIBRATIONS	241
Introduction	241
Excitation Sources	243
Structural Forcing Function	245
Statistical Properties of the Random Force, $F(t)$	246
Interpretation of the Statistical Averages, $F(t)$	259
Space-Time Correlations	271
Generalized Force	275
Mobility of the Structure	281
Response of the Structure	286
Vibration of a Panel Due to Far Field Acoustic Excitation	287
Resonance-On-Resonance	293
Introduction	293
Discussion	294
Rules for Addition for Random Processes	298
Method of Estimating Vibration Response to Many Sources	299
References	300

TABLE OF CONTENTS (Cont'd)

SECTION V	PANEL VIBRATIONS	301
	General Description of Panels	301
	Natural Response Characteristics of Panels	303
	Mode Shapes and Natural Frequencies of Panels	303
	Panel Damping	335
	Attenuation of Vibration with Distance in Typical Structure	342
	Structural Damping	344
	References	346
SECTION VI	FATIGUE	352
	Introduction	352
	Combined Stresses	359
	Variable Amplitude Loading	363
	The Stress Concentration Factor	364
	Cumulative Damage	366
	Application to Engineering Problems	366
	References	368
CONCLUSIONS		370
PART III	SIMPLIFIED COMPOSITE RESPONSE	373
SECTION I	INTRODUCTION	375
SECTION II	CONSIDERATIONS IN THE DESIGN OF THE TEST	377
SECTION III	SIMPLIFIED COMPOSITE RESPONSE	379
SECTION IV	NONLINEARITIES ASSOCIATED WITH ACCELERATED TESTING	382
SECTION V	SINUSOIDAL-RANDOM EQUIVALENCE FOR CUMULATIVE FAILURES	385
	Acceleration in Time	387
	Equivalence of two Particular Response Patterns	387
	Work as Basis of Equivalence	388
	Why Do Random Vibration Testing	389
	Studies Presently Completed	390

TABLE OF CONTENTS (Cont'd)

SECTION VI	EQUIPMENT MALFUNCTION AND DAMAGE	393
	Equipment Failure	394
SECTION VII	ANALYTICAL EQUIVALANCES FOR LABORATORY TESTING	415
	Sine Random Equivalences	417
	Sinusoidal Sweep-Random Equivalences	424
	Narrow Band Random-Sweep Equivalences	427
SECTION VIII	CONCLUSIONS	435
	REFERENCES	437
APPENDIX A		441
APPENDIX B		449

LIST OF ILLUSTRATIONS

<u>Figure</u>	<u>Page</u>
1 Typical Contours of Equal Over-all SPL in db re .0002 dyne/cm ² for a Turbojet at Military Power (Reference 1, and WADC Unpublished Data) and a Rocket (Reference 2), with Distance Expressed in Terms of Nozzle Exit Diameter (d_e) .	5
2 Sketch of Jet Flow for a Sonic Turbojet at Military Power and a Supersonic Rocket	6
3 Total Acoustic Power for Rockets as a Function of Rocket Stream Power. Data from WADC and NASA (References 2, 9, 10). .	9
4 Normalized Acoustic Power Per Cycle for Jet Flows as a Function of a Non-Dimensional Frequency Parameter (from Reference 11).	11
5 Total Acoustic Power for Jet Flows Compared to a Revised Lighthill Parameter Based on Characteristic Velocity and Diameter	13
6 Coefficient for the Revised Lighthill Parameter of Figure 5 as a Function of Throat Temperature	14
7 Far Field Directivity of Jet Noise for Three Types of Flow Giving the rms Acoustic Pressure at a Constant Radius as a Function of the Maximum Pressure and Angle (from References 8, 9, 12)	15
8a Estimated Mean Square Pressure Per Cycle as a Function of a Dimensionless Frequency Parameter at Various Axial Distances Forward of the Rocket Nozzle for a Stationary Rocket at Sea Level with an Undisturbed Flow	17
8b Estimated Mean Square Pressure Per Cycle as a Function of a Dimensionless Frequency Parameter at Various Axial Distances Forward of the Rocket Nozzle for a Stationary Rocket at Sea Level with an Undisturbed Flow	18
8c Estimated Mean Square Pressure Per Cycle as a Function of a Dimensionless Frequency Parameter at Various Axial Distances Forward of the Rocket Nozzle for a Stationary Rocket at Sea Level with an Undisturbed Flow	19
9 Relationship Between the Geometric Angle Between Moving Source and Receiver and the Angle of Source Radiation for Various Vehicle Mach Numbers	22

<u>Figure</u>		<u>Page</u>
10	Reduction of Noise Level as a Function of the Angle of Source Radiation for Various Vehicle Mach Numbers	23
11	Variation of Exponent n as a Function of Angle of Source Radiation for Jets with Maximum Total Temperature of Approximately 1460°R	24
13	Illustration of the Turbulent Flow Resulting from Impingement on the Ground During Surface Launch, with a Far Field Contour of Equal Sound Pressure Superimposed. The Ratio R/R_0 is the Ratio of the Radius of the Contour at any Angle to the Reference Radius at the Angle of Maximum Radiation	26
13	Examples of the Increase of Vehicle Noise Exposure During Launch at Two Positions on the Vehicle (Reference 15)	27
14	Data from 1/6 Scale Unlined Model Silo Tests (Reference 16) Corrected to Full-Scale Frequencies	28
15	Exit Corridor	33
16a	Sketch of the Development of a Turbulent Boundary Layer Along a Flat Plate	34
16b	Illustration of the Definition of the Boundary Layer Thickness (δ)	34
17	Over-all Sound Pressure Level and Mean Square Fluctuating Pressure (p^2) in the Turbulent Boundary Layer as a Function of Freestream Dynamic Pressure (References 3, 8, 9, 10, 11, 13) .	37
18	Fractional Mean Square Pressure Per Cycle $[P^2(f)]$ in the Turbulent Boundary Layer Normalized by $\frac{a_0 \delta \omega}{U_\infty^2 \nu_\infty}$ as a function of the Dimensionless Frequency Parameter $\frac{f \delta a_0 \nu_\infty}{U_\infty^2 \nu_0}$ (Data from References 8, 10, 11, 13) .	39
19	Engine Air Inlet Duct Microphone Data	43
20	Curves Relating Pressure Pulsations with Normal-Force Changes on the NACA 65A009 Airfoil (from Reference 18)	45
21	Separation Pressure Coefficients (from Reference 19)	46
22	Sketch of Shock Oscillation as a Result of Interaction with a Laminar Boundary Layer	47

<u>Figure</u>		<u>Page</u>
23	Intensity of the Neutrally Stable Oscillating Shock Wave as a Function of Upstream Mach Number	48
24	Illustration of Flow Past Cavity, Showing Vortex Formation in Cavity and Effect of Vortex Velocity on Propagation of an Acoustic Wave	51
25	Strouhal Number of Dominant Cavity Resonance as a Function of Mach Number from Data of References 2 and 3	53
26	Illustration of Vortex Formation in the Wake of a Cylinder at a Reynolds Number Below 150, and Illustration of the Acoustical Radiation Pattern at the Fluctuating Lift and Drag Frequencies	55
27	Comparison of the Strouhal Number Associated with the Shedding of Vortex Pairs from Cylinders as a Function of Reynolds Number, Including Data from Many Investigations (taken from Etkin et al, Reference 31)	57
28	Aft Fuselage Microphone Data	59
29	Sketch Illustrating Wake Formation of a Blunt Based Body of Revolution	60
30	Variation of Over-all Level of Base Pressure Fluctuations with Freestream Velocity	62
31	Mean Square Pressure Per Cycle Relative to the Dynamic Pressure, Normalized by $\frac{U_\infty^2}{d}$ for Both Microphones	63
32	Illustration of Turbulent Wakes from Two Types of Blunt Bodies at Supersonic Speeds	65
33	Sample Wind Profiles Taken at Silver Hill, Maryland, During 1953-1954 (Reference 12)	75
34	Wind Speed Vs. Altitude	78
35	One Per Cent Synthetic Wind Profile Obtained During Geophysical Year (Reference 23)	79
36	Gust Strength	80
37	Eddy Model of Turbulence	80

<u>Figure</u>		<u>Page</u>
38	Velocity Profile in Continuous Turbulence	81
39	Summary of Airplane Measurements of the Power Spectrum of Atmospheric Turbulence (Reference 25)	82
40	Wind Shear and Gust Velocity	83
41	Distribution of Root-Mean-Square Gust Velocity with Weather Condition (Reference 25)	84
42	Distribution of Root-Mean-Square Gust Velocity with Altitude for Routine Operations (Reference 25)	86
43	Analytical Turbulent Spectrum for Various Turbulent Scales . .	87
44	Power Spectral Density of Atmospheric Turbulence for a Vertical Rising Hypothetical Space Vehicle in Thunderstorm and Clear Air Turbulence	89
45	Distribution of Velocities for 285 Sporadic and 75 Shower Meteors	96
46	Mean Heights of Beginning, Maximum Light, and End for Sporadic Meteors of Various Velocities	97
47	Normal Acoustical Modes for a Cylindrical Combustion Chamber .	106
48	Calculated Range of Frequencies for the Fundamental Modes of a Closed-Closed Cylindrical Chamber as a Function of Chamber Dimensions	109
49	Sketch of Rocketdyne B2C Rocket Engine Vibration Instrumentation	117
50	Thrust Variation During Mainstage Burning - S-3D Rocketdyne Engine 150,000 lbs. Static Thrust	118
51	Low Frequency Vibration of Attach Points - S-3D Rocketdyne Engine Frequency Analysis	120
52	Variation in Cutoff Vibration During Separate Firings at the Three Attach Points (S-3D Engine)	122
53	Vibration at the Attach Points in the Thrust Direction. Only the Amplitudes of the Most Dominant Frequencies are Shown (S-3D Engine)	123

<u>Figure</u>		<u>Page</u>
54	Vibration at the Attach Points Perpendicular to the Thrust Direction - S-3D	124
55	Vibration at the Attach Points Perpendicular to the Thrust Direction - S-3D Engine	125
56	Vibration at the Lox Injector in the Thrust Direction (S-3D Engine)	126
57	Vibration on the Head of the Combustion Chamber in the Thrust Direction (S-3D Engine)	127
58	Snark Launch Vibration Measurement During 1st 0.2 Secs. Taken by a Trailing Wire	128
59	Reduction in Noise Due to the Use of a Reignition Inhibitor . .	129
60	Variation of Amplitude with Time During Launch at F.S. 204 . . .	129
61	Vibration Ranges on XJ85-5 Engines Used in the T-38	135
62	Range of Turbopump Vibrations	139
63	Sketch of Hypothetical Three-Stage Vehicle	142
64	Exit Profile for Hypothetical Vehicle Showing Velocity and Altitude as a Function of Time	143
65	Re-Entry Profile for Hypothetical Vehicle Showing Velocity and Altitude as a Function of Time	144
66	Estimated Variation in Over-all Sound Pressure Level for Two Positions on Hypothetical Three-Stage Vehicle as a Function of Mission Time (from Figures 64 and 65)	145
67	Estimated Variation in Over-all Sound Pressure Level and the Level in Three Octave Bands as a Function of Time (from Figure 66) at Position A on the First Stage of the Hypothetical Vehicle	147
68	Estimated Variation in Over-all Sound Pressure Level and Level in Three Octave Bands as a Function of Time (from Figure 66) at Position B on the First Stage of the Hypothetical Vehicle . . .	148
69	Estimated Mean Square Pressure Per Cycle at Several Times During Mission for Position A.	149
70	Estimated Mean Square Pressure Per Cycle at Several Times During Mission for Position B	150

<u>Figure</u>		<u>Page</u>
71	Force Excitation of a Single Degree of Freedom System	163
72	Vibration Response for Various Damping.	164
73	Response to Step and Impulse Forcing Functions	166
74	Resonant Amplification Factor	169
75	Phase Angle vs. Frequency Ratio	170
76	Resonant Amplification Factor for a Vibrating Base	172
77	Transmissibility	174
78	Probability Density for Rayleigh and Normal Distribution . . .	176
79	Normal and Rayleigh Probability Distribution Functions	178
80	Mechanical-Electrical Analogies for the Single Degree of Freedom System	182
81	Example of Missile Vibration Data Without and With Correction for Bracket Resonance from Blake (Reference 1)	201
82	Comparison of Analysis of a Spectrum with Filters Having Different Frequency Bandwidths and Reduction to a Per-Cycle Basis	203
83	Comparison of the Analysis of a Spectrum with Filters Having Differing Frequency Bandwidths, and Presentation of the Data as the Mean Square Amplitude for the Total Bandwidth	205
84	Acceleration in Jet Fighter Aircraft (After Crede & Lunney, Reference 6)	207
85	Acceleration in Jet Bomber Aircraft (After Crede & Lunney, Reference 6)	208
86	Graphic Level Recording of Variation of Over-all Noise Level Inside Forward Compartment of a Small Missile During its Flight	210
87	Missile Launch Accelerations Obtained on Structure in Forward Half of Vehicle	211
88	Missile Flight Accelerations on Structure in Forward Half of Vehicle and Obtained Near Maximum Dynamic Pressure, Flight Phase	213

<u>Figure</u>		<u>Page</u>
89	Missile Flight Accelerations on Structure Adjacent to Rocket Engine	214
90	Range of Accelerations for Four Types of Self-Excited Missile Equipment	215
91	Summary of Median Curves for Aircraft and Missile Accelerations	216
92	Internal and External Acoustic Environment of the Snark Missile	219
93	Correlation Between the Vibration Level and the External Acoustic Excitation of the Snark Missile - OAL Levels	221
94	Correlation Between the Vibration Level and the External Acoustic Excitation of the Snark Missile - 20-75 cps Octave Band	222
95	Correlation Between the Vibration Level and the External Acoustic Excitation of the Snark Missile - 75-150 cps Octave Band	223
96	Correlation Between the Vibration Level and the External Excitation of the Snark Missile - 150-300 cps Octave Band	224
97	Correlation Between the Vibration Level and the External Acoustic Excitation of the Snark Missile - 300-600 cps Octave Band	225
98	Correlation Between the Vibration Level and the External Acoustic Excitation of the Snark Missile - 600-1200 cps Octave Band	226
99	Sound Pressure Level vs. rms Acceleration for Two Frequency Bands	228
100	Summary of Aircraft Empirical Correlation of External Noise with Acceleration of Adjacent Structure	229
101	Variation of the Parameter β with k_r for the Data of Figure , where $\beta = \frac{4\left(\frac{a}{g}\right)^2 W^2}{w_n Q F^2(f)}$	233
102	Variations of the Parameter β with Frequency for the Data of Figure where $\beta = \frac{4\left(\frac{a}{g}\right)^2 W^2}{w_n Q F^2(f)}$	234

<u>Figure</u>		<u>Page</u>
103	Histogram of vs the Regression Line in Figure 101	235
103a	Approximate Trend for Surface Launch Acceleration as a Function of Gross Launch Weight Based on Present Vehicles and Engines	238
104	General Vibration Flow Diagram from the Source of Excitation to Final Response	242
105	An Ensemble of Measured Time Histories of Force	247
106	Histogram for Approximating the First Probability Density Function	249
107	Method for Determining the First Joint Probability Density Function	250
108	Time Record of a Nonstationary Random Force Function	254
109	Amplitude Sampling of $F(t)$ at Even Intervals of Time	255
110	Block Diagrams of Electronic Analog Circuits for Computing Statistical Averages	257
111	Periodic Time Function with Three Sinusoidal Components	260
112	Typical Filter Characteristic	261
113	Amplitudes of Filtered Frequency Components of $F(t)$	262
114	Modulated Wave Obtained When Two Discrete Frequency Components Lie Within the Bandwidth of the Filter	262
115	Bar Graph of the Amplitudes of Filtered Discrete Frequency Components	262
116	Time Function, $F(t)$, and a Bar Graph of the Discrete Frequency Components of $F(t)$	263
117	Finite Isolated Pulses and Their Fourier Transforms	264
118	Bar Graph of the Mean Square Amplitudes of Discrete Frequency Components of $F(t)$	267
119	Time-Correlation Coefficient for a Pure Sinusoidal Function . . .	269
120	Correlation Length and Correlation Area on Vehicle Surface Associated with Surface Pressure Fluctuations	272

<u>Figure</u>		<u>Page</u>
121	Propagations of Acoustical Pressure Waves Over Surface of a Missile	272
122	Typical Time-Correlation Coefficient Obtained in Practice . . .	273
123	Variation of Correlation Coefficient with Frequency	274
124	Rigid Panel with Propagating Acoustical Pressures Over the Surface	278
125	Joint Acceptance of a Rigid Panel to Far Field Acoustic Pressure Fluctuations	279
126	Joint Acceptance of Flexible Panel to Far Field Acoustical Pressure Fluctuations	280
127	Dynamic Response Factor for Transient Response of Linear Structures to Shock Excitation	282
128	Flexible Panel Excited by Propagating Acoustic Pressure Waves. .	288
129	Two-Degree-of-Freedom System	293
130a	Response of Primary Structure and Secondary Items as a	
130b	Function of the Mass Ratio	295
131a	Response of Primary Structure and Secondary Items as a	
131b	Function of the Mass Ratio	296
132	Power Spectral Density of the Input and Response	297
133	Probability Density Function	298
134	Power Spectral Density	298
135	Free Flexural Velocity, C_0 ; Pressurized Cylinder not Loaded by a Liquid	312
136	Free Flexural Velocity, C_0 ; Pressurized Cylinder not Loaded by a Liquid	313
137	Free Flexural Velocity, C_0 ; Pressurized Cylinder not Loaded by a Liquid	314
138	Axial and Circumferential Mode Shapes of a Uniform, Thin, Circular Cylinder	315
139	Comparison of Frequencies Predicted by Exact and Approximate Shell Theories	316

<u>Figure</u>		<u>Page</u>
140	Conditions at the Lowest Frequency	317
141	Typical Frequency Response Curve of a Thin Pressurized Cylindrical Shell	317
142	Natural Frequencies of Square Flat Plate with Various Edge Conditions	319
143	Large Static Deflections of Flat Rectangular Panels for a Uniform Surface Pressure, P. Reference 64, page 350	325
144	Stress Factor for Large Static Deflection of Flat Rectangular Panel with Uniform Surface Pressure P; Stress for Longest Edge of Panel	327
145a	Static Stress vs. Static Pressure for 11" x 13" Flat Rectangular Aluminum Panels of Thicknesses .032, .040, .064, and .081 Inches	328
145b	Static Stress vs. Static Pressure for Curved Panels with 11" x 13" Rectangular Base with Various Radii of Curvature	328
146	Peak Stress Amplitude vs. Frequency for .040 Inch Thick Flat Panel with Acoustical Siren Normal Pressure Loading	329
147	Peak Stress Amplitude vs. Frequency for a Curved Panel with Acoustical Siren Normal Pressure Loading	330
148	Maximum Stress vs. Panel Thickness	331
149	Amplification Factor vs. Sound Pressure Level	332
150	Fundamental Axi-Symmetric Vibration Frequencies of Shallow Spherical Shells, Reference 35	333
151	Added Surface Mass of a Liquid in a Cylinder (Reference 61)	334
152	Hysteresis Loop for Two Stress Levels	335
153	Damping Energy vs. Panel Deflection	336
154	Slip Damping	337
155	Energy Loss per Cycle for Various Loadings of a Riveted and Integral Beam	338
156	Beam with Visco-Elastic Layer	339
157	Elastic and Viscous Energy Dissipation	339

<u>Figure</u>		<u>Page</u>
158	Schematic for Showing Fluid Damping	340
159	Ratio of Total Damping to Visco-Elastic Material Damping for a Visco-Elastic Overlay on a Plate	341
160	Vibration Attenuation in Snark Fuselage	343
161	Compilation of Structural Damping Data - Equivalent Viscous Damping of Primary Structural Modes of Completed Vehicles . . .	345
162	Mean Time to Failure for Complete System for 2-year Mission Into Space	352
163	Conventional Presentation of S-N Data	353
164	Hysteresis Loop	354
165	Bending Moment Required to Produce Constant Strain	354
166	Fatigue Data from Controlled Strain Tests (Reference 3)	355
167	Hypothetical Variation of Plastic Strain	356
168	Asymptotic Endurance Limit	356
169	Hypothetical Variation of Plastic Strain	356
170	Cutoff Endurance Limit	357
171	Affine Crack Growth Curves	357
172	S-N Family to Display Preload Effect	358
173	Interaction Between Alternating and Steady Stress	358
174	Octahedral Shear Failure Criterion	359
175	Effect of Mean Axial Stress on Axial Fatigue	360
176	Effect of Static Normal Stress on Torsional Fatigue	360
177	Definitions of f_0 and f_1	361
178	A Suggested Presentation of the Damage, the Load History, and the Strength	363

<u>Figure</u>		<u>Page</u>
179	S-N Comparison	363
180	Influence of Stress Interaction	364
181	Notch Sensitivity	365
182	Effect of Preload	379
183	Load History Related to Mean Stresses	380
184	Over-all Mean Stress	380
185	Alternating Stress	380
186	Influence of Stress Interaction	386
187	Typical S-N Curve	386
188	Miner's Fraction	386
189	Typical S-N Curves	387
190	Cumulative Damage	388
191	Response Spectrum	388
192	Log Stress	388
193	Hysteresis Loop	388
194	Cost Comparison	390
195a 195b 195c 195d	Idealized Models of Equipment Packages for Which Spacing is Important	411
196	Response of the Single Degree of Freedom System Shown in Figure 195c for the Case of Low Damping	412
197	Actual Environmental Surface	413
198	Actual Fragility Surface	413
199	Actual Environmental Blanket	413
200	Actual Fragility Blanket	414

<u>Figure</u>		<u>Page</u>
201	Comparison of Actual Environmental Blanket with Actual Fragility Blanket	414
202	Non-Dimensional Transmissibility Function for the Single- Degree-of-Freedom System	433
203	Probability Distributions for Peak Response of the Single- Degree-of-Freedom System to Wide-Band Random Excitation and to Narrow-Band Random Sweep Excitation	434
204	Probability Density of the Phase Angle.	450
205	Probability Density of a Steady Sinusoidal Disturbance.	452
206	Relations between the Coordinates	455
207	Probability Density of Envelope R of $Z(t) = S(t) + N(t)$	457

LIST OF TABLES

<u>Table</u>		<u>Page</u>
I	Major Sources of Vibratory Energy in Missiles and Space Vehicles	2
II	Data Concerning Meteoroids and Their Penetrating Probabilities	98
III	Characteristic Values of μ_n for the Cylindrical Chamber (Reference 4)	107
IV	Summary of Maximum Acceleration Results PFRT Vibration Study for the B2C Rocket Engine . .	113
V	Summary of Maximum Acceleration Results PFRT Vibration Test for the B2C Rocket Engine . . .	114
VI	Summary of Maximum Acceleration Results PFRT Vibration Test for the B2C Rocket Engine . . .	115
VII	Summary of Maximum Acceleration Results PFRT Vibration Test for the B2C Rocket Engine . . .	116
VIII	Summary of Propulsion Engines for Space Vehicles	131
IX	Summary of Response Functions for the Lumped Parameter Single Degree of Freedom System	195
X	Values for α	320
XI	Values for β	321
XII	Gaussian Probability Distribution Function . .	409
XIII	Probability of Collision of Two Masses Separated by Distance	409
XIV	Probability of Occurrence of Damage at Any Frequency	410
XV	Summary of Sinusoidal Frequency Sweep Relations	432

LIST OF SYMBOLS

- a = radius of thin cylindrical shell
- a = acceleration
- A = area; area of panel
- a = speed of sound
- a_{∞} = ambient speed of sound in the surrounding atmosphere
- a_* = the critical speed of sound in the jet; the speed of sound in the throat
- A_c = cross-sectional area of rocket flow
- a_0 = speed of sound at S.L.
- a_n = parameters
- b = length of panel
- b_n = parameters
- $c_{0,1,2}$ = free flexural wave velocity
- c = viscous damping constant
- C_c, C_{cr} = critical value of damping
- c_n = unfiltered amplitude \sim component amplitudes
- C_n = normal coefficient
- C = velocity of wave propagation
- C_D = coefficient of drag
- C_F = coefficient of friction
- C_L = coefficient of lift
- C_p = coefficient of pressure
- CF = correlation coefficient
- d = diameter; depth
- d_c = characteristic diameter of the jet

d_e = nozzle exit diameter
 D = deflection (panel)
 d_t = nozzle throat diameter
 D = damage
 $\sum D$ = cumulative damage
 E = voltage drop across resistor
 E = modulus of elasticity of material (Young's)
 F = force
 F_G = generalized force
 f = frequency
 f_0 = system natural frequency
 f_L = longitudinal acoustic resonance
 F = rocket thrust (lbs.)
 F_0 = steady force
 $F(t)$ = exciting force as a function of time
 g = gravitational force (ft/sec²)(in/sec²)
 h = thickness (shell)
 J_i = stress invariants
 k = spring constant
 K = constant of proportionality for lift, L
 K_t = stress concentration factor
 K_f = fatigue notch factor
 L, ℓ = length (cylinder, panel) cavity; scale of turbulence
 L, L = lift
 ℓ_c = characteristic jet dimension
 M = mass flow (ft/sec)

m = mass (secondary)
 M = mass (primary)
 m, n, q = integer wave numbers for various modes
 \bar{M} = molecular weight of the combustion gases
 M = mobility
 M = Mach number
 \bar{m} = mean value of a random process
 n = number of nodal diameters
 N = number of response peaks
 P_d = average damping power
 p = pressure
 P_0 = atmospheric pressure
 P_t = total pressure or chamber pressure of rocket
 P = power; total acoustic power
 P_{ave} = average power
 psd = power spectral density
 P_i = power input
 \bar{p}_m^{-2} = mean square pressure (moving)
 \bar{p}_s^{-2} = mean square pressure (stationary)
 q_{∞}, q = dynamic pressure (freestream) (psi or psf)
 q = damped natural frequency
 $Q = \frac{1}{2(\zeta/\zeta_{cr})}$ = one divided by twice the damping ratio
 r = radius
 Re = Reynold's number
 R = chamber radius
 $Re(c)$ = Reynold's number of cylinder

S, S = similarity parameter
 S = Strouhal number $S = \frac{fd}{V_\infty}$, area
 T = time duration
 \mathcal{T} = transmissability
 t = (temp) $^\circ$ F
 T = temperature ($^\circ$ R)
 T_c = chamber temperature
 $T_{G,F}; T(\Omega)^2$ = transfer function
 T = torque
 u_1 = perturbation velocity
 U = fluid velocity; mean local velocity; velocity forward speed
 U_∞ = freestream velocity
 U_c = mean convection velocity
 v_c = characteristic jet velocity
 V_e = nozzle exit velocity
 V_N = magnitude of atmospheric velocity disturbance normal to the flight path
 V_∞ = vehicle forward velocity
 W = weight
 $W(f)$ = acoustic power per cycle
 W = total amount of work done in energy dissipation
 W_t = total acoustic power
 x = displacement
 \dot{x} = velocity
 \ddot{x} = acceleration

(Alpha)

α = angle of attack
 α = angular acceleration

(Beta)

β = parameter

(Gamma)

γ = ratio of specific heats
for rocket stream

(Delta)

δ = boundary layer thickness

(Epsilon)

ϵ_p = plastic strain

(Zeta)

$\zeta = (c/c_{cr})$

(Eta)

η = constant of proportionality
between the rms velocity
and V_c

(Theta)

θ = incidence angle

(Iota)

ι =

• (Lambda)

λ = wavelength

WADD TR 61-62

(MU)

μ = mass ratio

(NU) ν = Poisson's ratio

ν = kinematic viscosity of
the fluid

ν_∞ = freestream kinematic
viscosity

ν_s = sea level standard
kinematic viscosity

(XI) = deflection of panel

ξ

(RHO)

ρ = density of air at altitude

ρ_∞ = density of atmosphere

ρ_c = characteristic jet density

ρ_o = ambient density of surrounding
atmosphere

(Sigma)

σ = stress

$\overline{\sigma}^2$ = intensity of turbulence; mean²
square gust velocity (ft/sec)²

σ_a = alternating stress

σ_m = mean static stress

(Tau)

τ = shear

τ_{octa} = octagonal shear

(Phi)

ϕ = phase angle

(Chi)

x = representative of a position of a point in a given coordinate system

(Psi)

ψ = the direction of a vector in a given coordinate system

(Omega)

ω = angular velocity

ω = frequency of oscillating force

ω_n = natural frequency of isolated system

ω_L = lower cutoff frequency

ω_o = natural frequency

σ = rms value or standard deviation in a random process

Ω = reduced frequency

$\phi(\Omega)$ = power spectral density

\sim = cycles per second

PART I - SOURCES OF VIBRATIONS

I. INTRODUCTION

It is well known that the noise from rocket motors during launch often results in high amplitude vehicle vibrations. Although rocket noise is generally responsible for the most severe vibration environment in missiles, other sources, such as the aerodynamic boundary layer, thrust oscillation, motor resonances, wind shear and gust, internal equipment, etc., affect the vibration environment in varying degrees, depending upon the mission profile and vehicle design.

The major vibration sources are summarized in Table I, together with a brief description of their characteristic forcing functions, the portion of flight where they may occur, and an estimate of their relative severity.

It may be fairly stated at the outset that many of these sources cannot be quantified with the degree of precision often desired by an engineer. This results both from the complex nature of some of the sources and the short historical transition which is occurring from subsonic manned aircraft to supersonic and hypersonic missiles and space vehicles. Fortunately, the relative importance of these sources can be readily determined and their parameters can be roughly estimated. Further, and perhaps more important, the fundamentals of the major sources are becoming better understood.

This knowledge of the fundamental factors governing source characteristics is felt to be of paramount importance to the designer, as it can provide the framework for analysis of the relative merits of various competing mission and vehicle concepts in terms of their potential vibration environments. It should be noted that this statement applies particularly to the launch configuration which often occasions the most severe vibration environments.

For these reasons the following chapters will stress the fundamental factors affecting each source. The descriptions will be amplified by available experimental data and, where possible, generalized to enable design estimates.

Manuscript released by authors on June 3, 1961, for publication as a WADD Technical Report.

TABLE I

MAJOR SOURCES OF VIBRATORY ENERGY
IN MISSILES AND SPACE VEHICLES

<u>Source</u>	<u>Type of Forcing Function</u>	<u>Important During</u>	<u>Relative Severity*</u>	<u>Relative Pressure</u>
Rocket noise (generated in exhaust stream)	Continuous spectra random amplitude	(a) Launch (b) Flight below Mach 1	1 2	
Aerodynamic Excitation				$(\frac{P^2}{q})^{1/2}$
(a) Boundary Layer Turbulence	Continuous spectra random amplitude	Atmospheric flight	1**	.005
(b) Cavity Resonances	Discrete frequencies dependent on flight speed	Atmospheric flight	1**	.03-.06
(c) Projection wakes	Discrete frequencies & continuous spectra	Atmospheric flight	1**	.01
(d) Impingement of propulsion exhaust	Continuous spectra random amplitude	Atmospheric or space flight	2**	
(e) Fluctuating wake drag	Continuous spectra random amplitude	Atmospheric flight	1**	.007-.015
(f) Oscillating shock waves	Primarily discrete frequencies	Primarily in Low supersonic range	1**	to .1
(g) Skin flutter	Discrete frequency	Atmospheric flight	1**	
(h) Buffet and other separa- ted flows	Narrow band random	Atmospheric	1**	to .1
Wind Shear & Gust Excitation	Continuous spectra predominantly low frequency	Atmospheric flight	2**	
Meteorite Impinge- ment	Intermittent or quasi-continuous spectra	Space flight	4	
Internal Vibration Excitation				
(a) Propulsion System	Primarily discrete frequencies plus starting transients & random thrust variations	Whenever operating	1**	

TABLE I (Continued)
MAJOR SOURCES OF VIBRATORY ENERGY
IN MISSILES AND SPACE VEHICLES

<u>Source</u>	<u>Type of Forcing Function</u>	<u>Important During</u>	<u>Relative Severity*</u>	<u>Relative Pressure</u>
(b) Internal equipment	Primarily discrete frequencies	Whenever operating	3	
(c) Fuel sloshing	Primarily low frequency	Whenever fuel tanks are par- tially filled & vehicle alters direction	2**	

*This estimate is very simplified and primarily qualitative.

**Occurrence and severity depend upon design and/or mission profile.

II. ROCKET NOISE EXCITATION

The noise generated by the exhaust stream of a rocket motor is generally responsible for the most severe vibration environment occurring in vehicles which are launched from earth or any other solar body which has an atmosphere. This noise from the rocket exhaust is characterized by a very broad spectral distribution throughout the entire audible and subaudible frequency range. As a result, it contains energy at most of the frequencies where vehicle structure, skin and equipment have resonances.

Fortunately, as will be seen in Part II, although the rocket noise extends into the subaudible frequency range where the fundamental vehicle vibration modes are usually found, these modes are not strongly excited because the vehicles dimensions are relatively small compared to the wave length of the very low frequency noise. Therefore, the change in pressure along any vehicle dimension is small and very little energy is absorbed. However, at the higher frequencies, on the order of 100 to 10,000 CPS, where skin and equipment resonances are encountered, most vehicles are no longer small in comparison to the acoustic wave lengths which are of the order of 1.0 to .1 feet. Consequently, much of the acoustic energy incident on the vehicle is absorbed, particularly at the resonant frequencies of the outer skin and its substructure. Thus, at these frequencies, the skin and substructure have a considerable vibration response and this vibration is mechanically transmitted throughout the vehicle to equipment and other internal structure.

The noise resulting from subsonic and sonic jets and turbojets has been extensively studied during the last decade, both in England and in this country. However, the noise from rockets has been investigated only since about 1955. Although this research has answered many fundamental questions regarding jet and rocket noise generation, there are still several questions which are unanswered. These areas where knowledge is lacking will be discussed as they arise in the following sections.

CHARACTERISTICS AND ORIGIN OF JET AND ROCKET NOISE

Figures 1(a) and (b) illustrate the near field contours of the over-all sound pressure level (SPL) measured for a typical turbojet (Reference 1) and for a typical rocket (Reference 2). Comparison of the two figures illustrates a significant difference between the noise generation of the sonic and supersonic flows in that the maximum noise levels occur much further downstream in the supersonic rocket flow than in the sonic turbojet flow. The reason for this difference becomes evident when the actual flows are compared.

Figure 2(a) illustrates a schematic of a subsonic or sonic jet flow and Figure 2(b) gives a similar sketch of a supersonic rocket flow. It can be seen that the sonic jet is characterized by a conical core in which the jet velocity is equal to the nozzle exit velocity (v_e). The shear between the high velocity jet stream and the quiescent atmosphere produces a turbulent boundary layer surrounding the core almost immediately downstream from the nozzle. This turbulent boundary layer grows in size

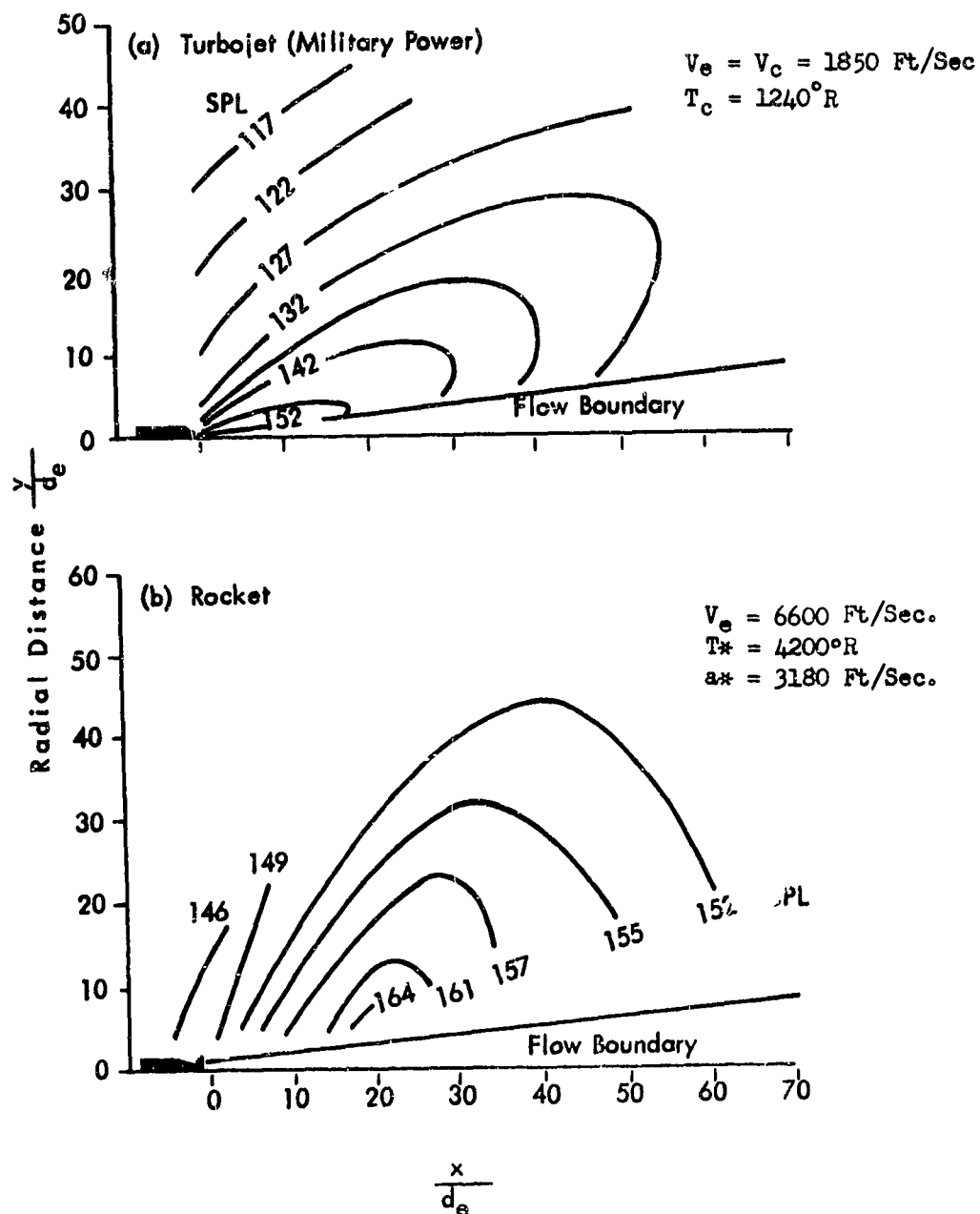
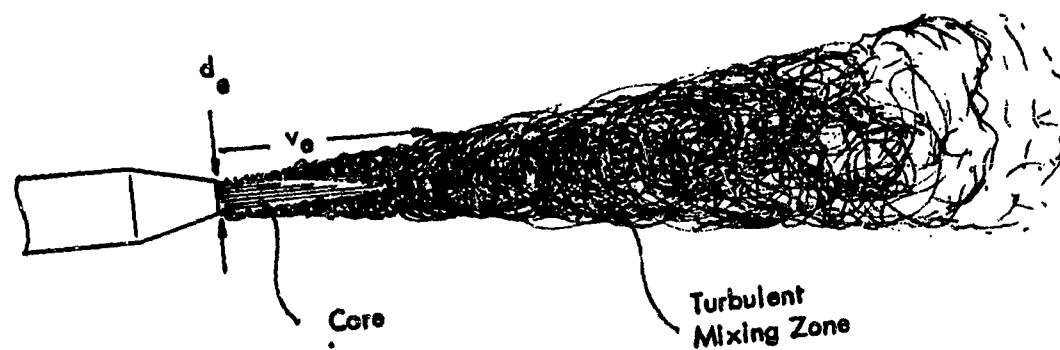


Figure 1. Typical Contours of Equal Overall SPL in db re .0002 dyne/cm² for a Turbojet at Military Power (Reference 1, and WADC Unpublished Data) and a Rocket (Reference 2), with Distance Expressed in Terms of Nozzle Exit Diameter (d_e).

(a) Subsonic or Sonic Jet Flow



(b) Supersonic Jet Flow

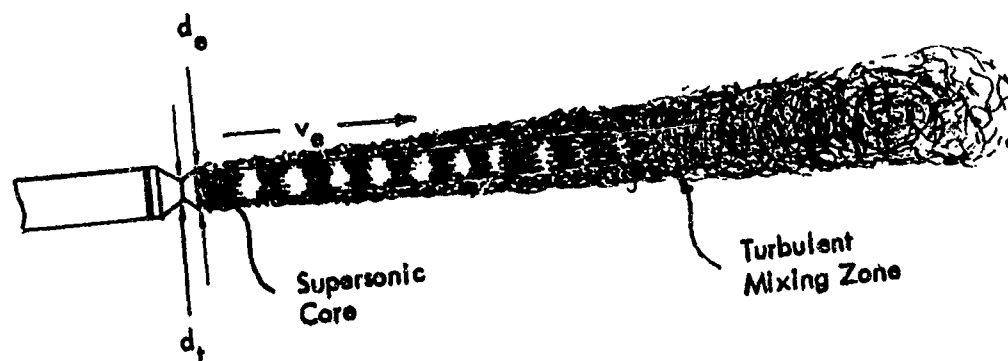


Figure 2. Sketch of Jet Flow for a Sonic Turbojet at Military Power and a Supersonic Rocket.

as more momentum is transferred from the jet core to the turbulent eddies and is used to accelerate the entrained air. As this process continues downstream, the turbulent jet expands at the one-half angle of about 7.5° and beyond the tip of the core, the centerline velocity decreases rapidly with increasing distance.

The supersonic rocket stream in Figure 2(b) has been found to be similar to the subsonic jet at all points downstream from the tip of its core (Reference 3). However, it is clear from the figure that the two are very dissimilar upstream of the core tip for, unlike the subsonic jet, the rocket's cylindrical supersonic core extends for a considerable distance from the nozzle before it begins to taper and only a thin turbulent boundary layer is formed along the cylindrical portion. It also should be noted that the flow inside the supersonic core is not uniform; rather, it is characterized by a complex shock wave structure which extracts mechanical energy from the flow, converting it into heat energy. Thus, after considerable distance downstream, the internal shocks slow the flow and the mixing becomes similar to that of the sonic jet.

A comparison of the jet structures just described, with the contours of equal noise level in Figure 1, clearly demonstrates that, in each case, the maximum noise is generated near the tip of the jet core. Laurence of NASA (Reference 4) has found the maximum amount of turbulent energy in this same location. Additional comparison by Howes et al (Reference 1) of the noise measurements along the boundary of a turbojet exhaust stream and the measurements of turbulence in a cold jet (Reference 4) demonstrates excellent correlation between the frequency spectra of noise and turbulence at similar positions. Here, it was conclusively proved that the high frequencies are generated near the beginning of the flow where the mixing zone is thin and the turbulent eddies are relatively small, whereas the low frequencies are generated further downstream where the turbulent eddies have a much larger characteristic size.

The factors which govern the conversion of the turbulent energy in the jet to noise in subsonic flows have been theoretically examined by Lighthill (References 5 & 6). From an analysis of the dimensional and physical relationships expressed in his general theoretical equations (Reference 5) he suggested that the total acoustical power should be proportional to the characteristic jet flow parameters, as expressed by the following:

$$W \sim \frac{\rho_c^2 l_c^2 v_c^5}{\rho_0 a_0^5}$$

where W is the total acoustical power,

ρ_c is a characteristic jet density

l_c is a characteristic jet dimension

v_c is a characteristic jet velocity

ρ_0 is the ambient density in the surrounding atmosphere

and a_0 is the ambient speed of sound in the surrounding atmosphere

Callagan of NACA (Reference 7) and others have correlated the results of an extensive series of cold model jets and turbojets with a modified form of this relationship. This modified Lighthill parameter,

$$W \sim \frac{\rho_0 A_e v_e^8}{a_0^5}$$

where A_e is the nozzle exit area and

v_e is the nozzle exit velocity

gives excellent correlation for all model and turbojet noise data with the exception of afterburning turbojets, where the measured acoustical power is always lower than the predicted power. However, the early use of this modified Lighthill parameter in the prediction of supersonic rocket noise led to values which were as much as 100 times greater than those actually measured.

As a result of the apparent inability to extend the theory to supersonic flows, several empirical relationships between the jet stream power and its radiated acoustical power were developed. A revised version of one of these relationships (Reference 8) illustrating data from rockets in the thrust range between 1000 and 133,000 pounds is given in Figure 3. It is felt that this empirical relationship can be used for preliminary prediction of the total acoustical power of conventionally fueled rockets at, or near, sea level. However, because of its empirical derivation, it cannot be trusted for prediction of noise from unconventional supersonic flows, or where the atmospheric conditions differ substantially from the standard sea level conditions.

However, it is possible to relate rocket noise to the Lighthill theory as was accomplished above by NASA for cold and hot subsonic and sonic jets. In the previous discussion of supersonic and subsonic jet flows, it was seen that they are essentially similar downstream of their cores. Further, in both cases the region of maximum noise generation was in the subsonic turbulent flow near the core tip. Therefore, it might be suspected that a sonic flow could be defined which would be similar to the rocket flow in all characteristics, except that it would not have the long cylindrical supersonic core surrounded by a very thin turbulent boundary layer. However, it would mix with the atmosphere in the same manner downstream of the core as does the rocket, producing similar turbulence and noise.

The reasoning has been followed in Reference 11, to determine the physical similarities of these two types of jet flows and their noise generation mechanisms.

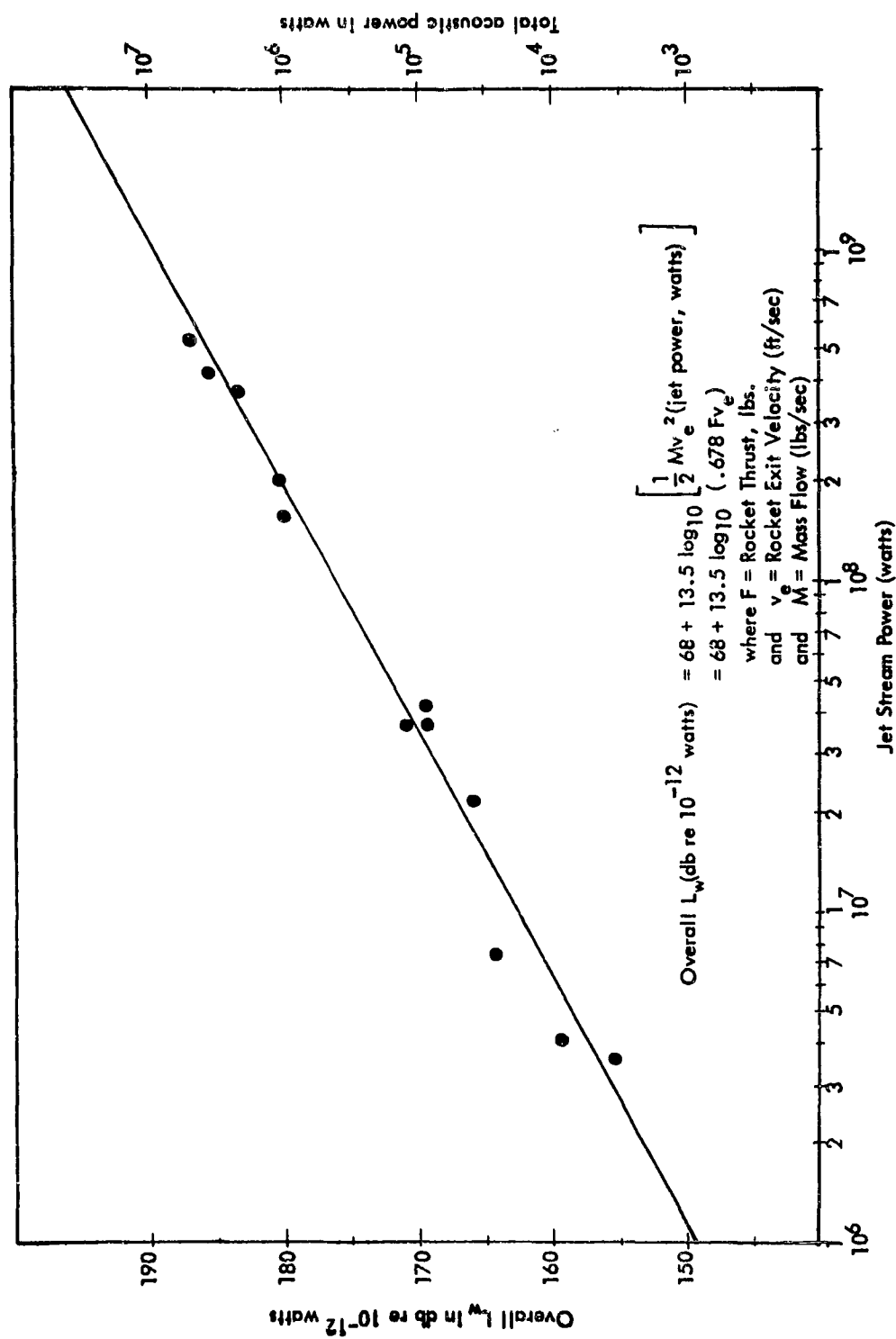


Figure 3. Total Acoustic Power for Rockets as a Function of Rocket Stream Power.
 Data from WADC and NASA (References 2, 9, 10).

The results indicate that the noise from the supersonic rocket is essentially similar to that of a sonic jet whose characteristic (v_c) is equal to the critical speed of sound (a_*) in the rocket flow, and whose characteristic diameter (d_c) is determined by continuity of mass flow in the rocket stream.

Figure 4 shows the normalized acoustical power spectrum for all types of jet flows as a function of the dimensionless frequency parameter,

$$\frac{f d_c a_*}{v_c a_0}$$

where d_c is the characteristic diameter of the jet

a_* is the critical speed of sound in the jet,
the speed of sound in the throat

a_0 is the speed of sound in the atmosphere

f is the frequency, and

v_c is the characteristic velocity of the flow,
velocity at the throat

It can be seen that this dimensionless frequency parameter is reduced to

$$\frac{f d_c}{a_0}$$

when the flow is sonic or supersonic, for, in this case $v_c = a_*$. The data in Figure 4 from subsonic cold and heated air jets, turbojets, afterburner and rockets exhibit good correlation over a wide frequency range. Note that this acoustical power spectrum is fairly constant over almost a decade of frequency, and contains considerable energy throughout several decades.

This correlation demonstrates that the frequency spectrum of the acoustical power of sonic and supersonic jets is dependent only on the characteristic diameter of the jet flow and the speed of sound in the surrounding medium. Hence, the frequency region of maximum acoustic energy will shift to lower frequencies as the characteristic flow diameter is increased, but will shift to higher frequencies when the speed of sound in the surrounding atmosphere is increased. The characteristic diameter for the rocket flow, which conforms to continuity of mass flow where the velocity is a_* , is given by

$$d_c = d_t \left[\left(\frac{2}{\gamma+1} \right)^{\frac{\gamma}{\gamma-1}} \left(\frac{P_t}{P_0} \right) \right]^{\frac{1}{2}}$$

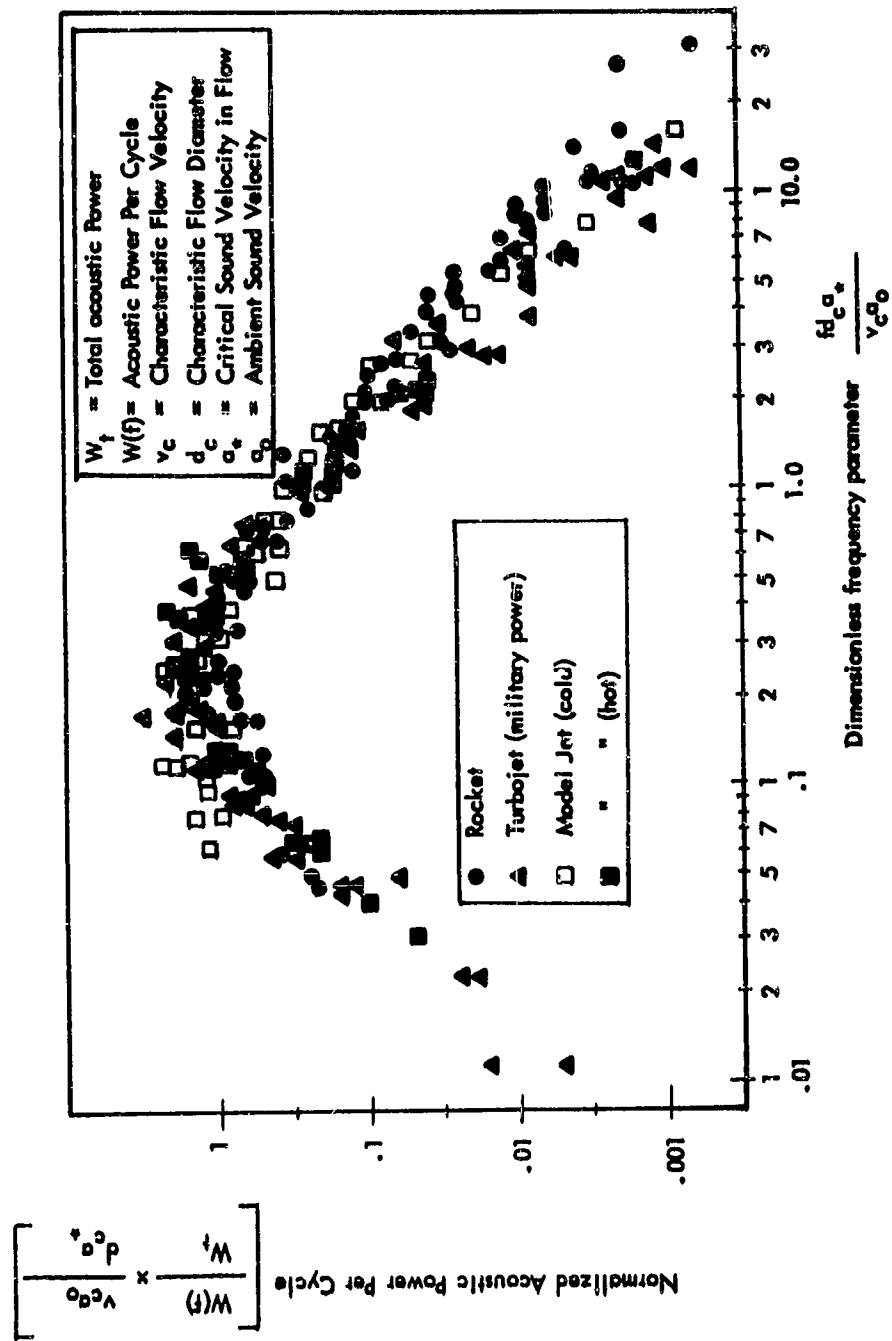


Figure 4. Normalized Acoustic Power per Cycle for Jet Flows as a Function of a Non-dimensional Frequency Parameter (From Reference 11).

where P_t is the total pressure of the rocket at the rocket throat

P_o is the atmospheric pressure

γ is the ratio of specific heats for the rocket stream, and

d_t is the nozzle throat diameter.

Hence, the frequency region of maximum acoustic energy is dependent upon the rocket pressure ratio as well as its nozzle geometry.

When the value of d_c , computed above, and v_c , which equals a for supersonic flows and v_c for subsonic flows, are substituted in the NACA modified Lighthill parameter the acoustic power appears more linearly related to the parameter, as shown in Figure 5. However, it is evident that the rocket and afterburner data depart from the curve at its highest end. This is primarily a temperature effect as discussed in Reference 11 and illustrated in Figure 6.

Thus, the total acoustic power can be calculated approximately from the relationship

$$W = 5 \times 10^{-5} \left[\frac{P_o A_c v_c^8}{a_o^5} \right] F(t),$$

where $F(t)$ can be evaluated from Figure 6.

The preceding has discussed the relationships between the rocket flow characteristics and its generation of acoustical power. However, the acoustical power incident on the missile and exciting vibration is generally only a small fraction of the total acoustical power. Figure 7 illustrates spacial distribution of the noise radiated by a cold jet, turbojet and rocket. It is apparent that the noise is quite directional with the greater proportion of the energy radiated to the rear of the nozzle. This illustrates the desirability of placing the engine nozzles at the aftermost position on the vehicle to minimize the vehicle's noise environment. The figure also shows that the angle of maximum noise radiation is very close to the jet boundary for the cold jet, but is further forward for the turbojet, and still further forward for the rocket. This change in directivity for these sources is considered to result from the refraction of the acoustical energy within the flow in accordance with the change in the local speed of sound encountered as the acoustical energy is propagated toward the jet boundary. Hence, in the figure this effect is most noticeable for the conventional rocket which has the highest characteristic sound velocity. It should also be noted that the directional characteristic of the noise in jet flows is a function of frequency. The angle of maximum radiation for the high frequencies is forward of

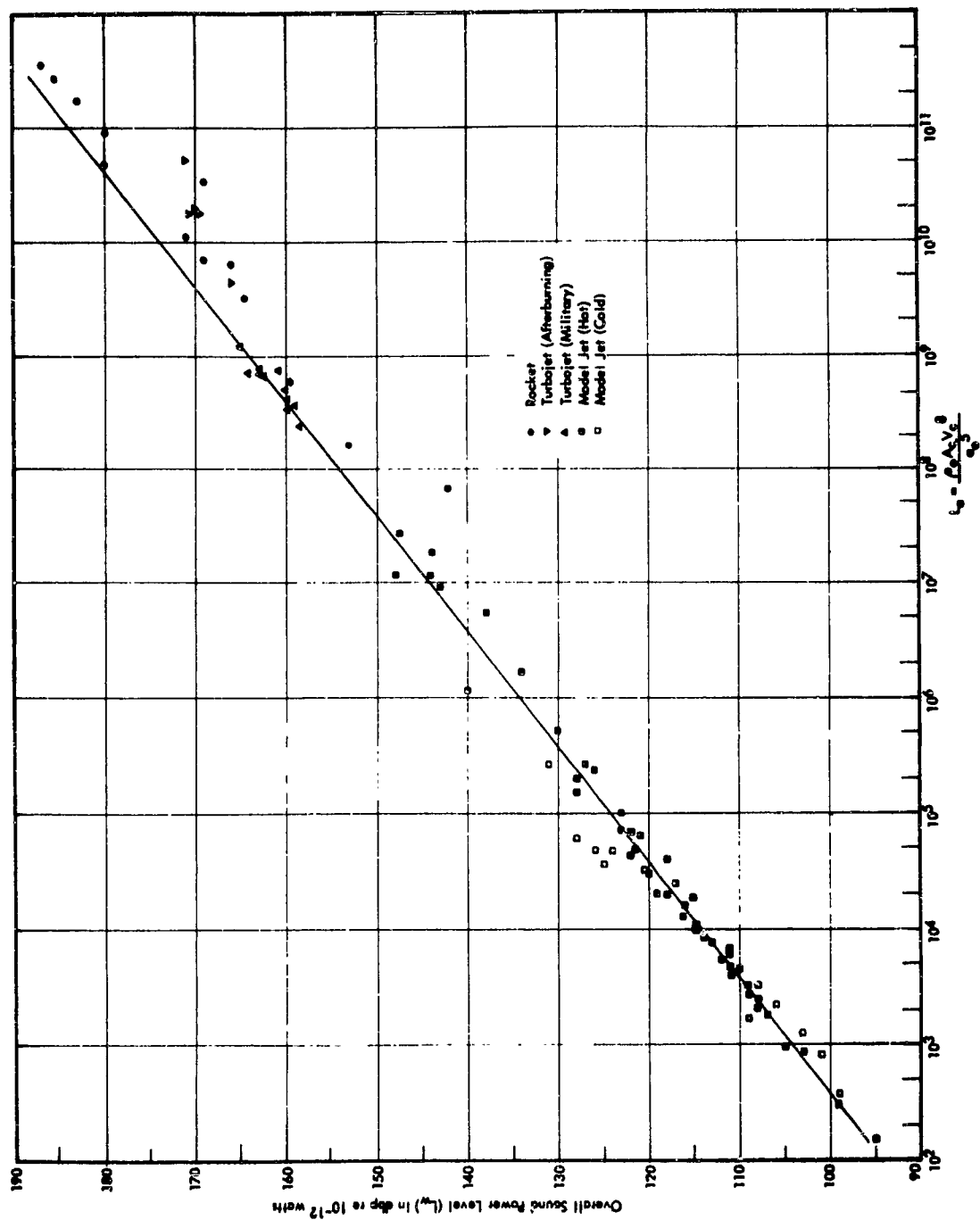


Figure 5. Total acoustic power for jet flows compared to a revised Lighthill parameter based on characteristic velocity and diameter.

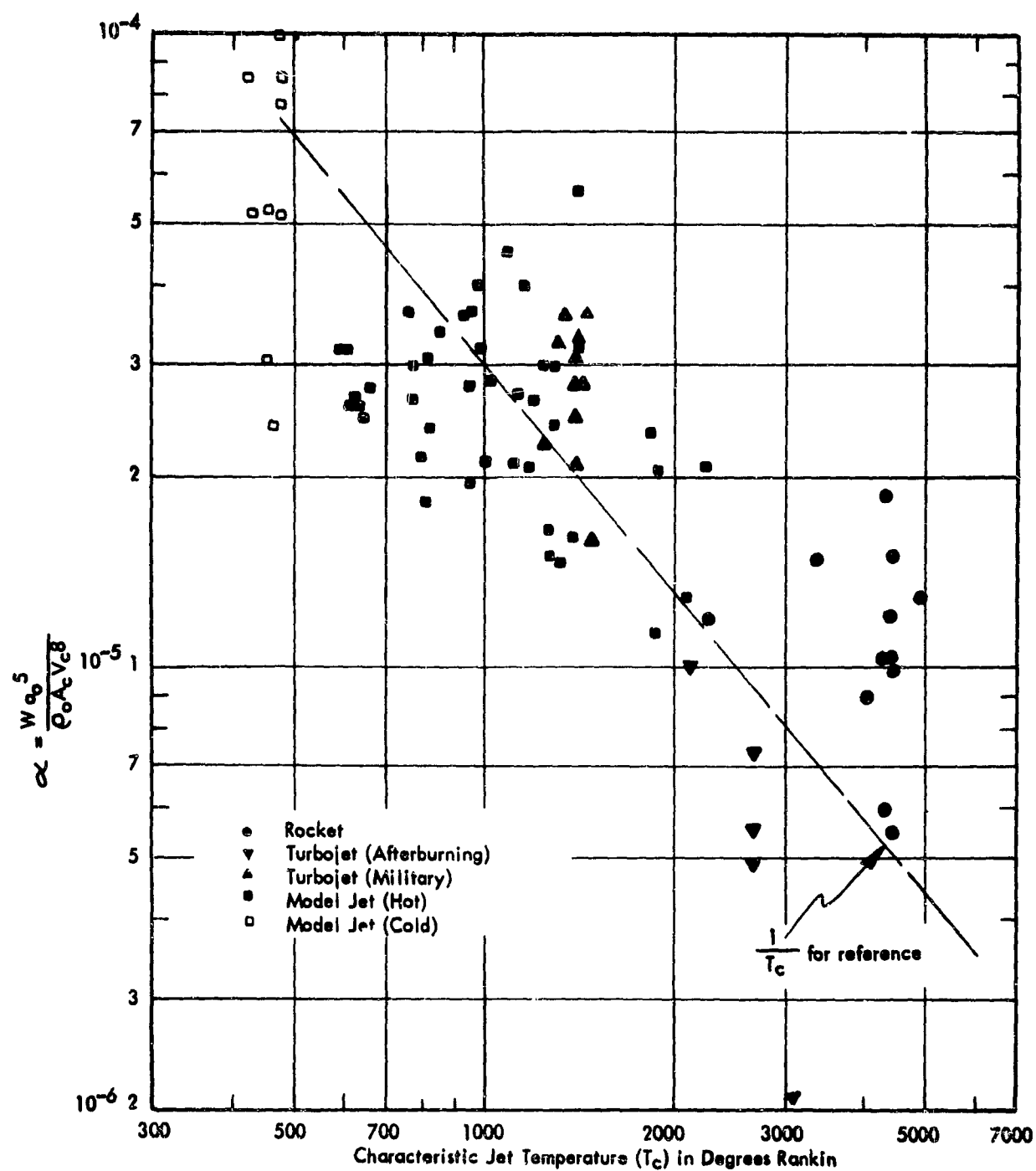


Figure 6. Coefficient for the revised Lighthill parameter of figure 5 as a function of throat temperature.

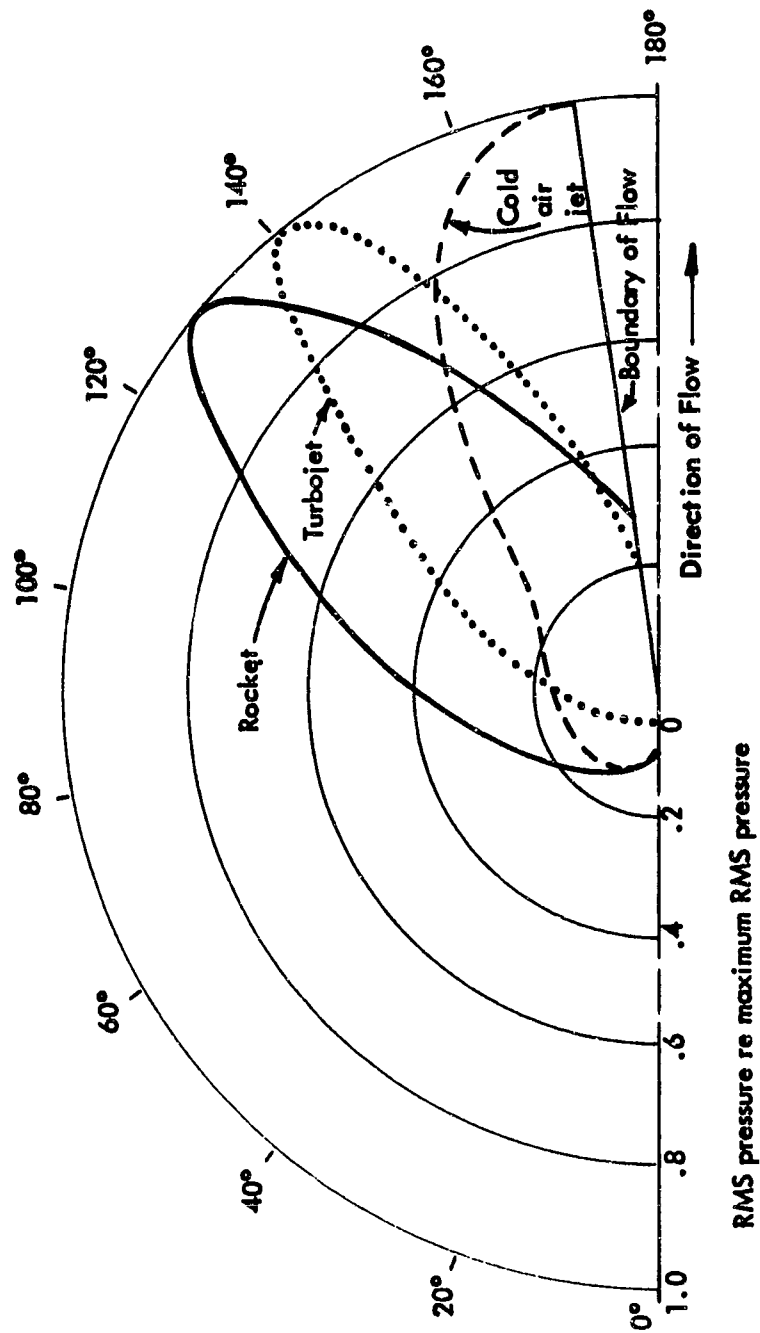


Figure 7. Far Field directivity of Jet Noise for Three Types of Flow Giving the RMS Acoustic Pressure at a Constant Radius as a Function of the Maximum Pressure and Angle (From Reference 8, 9, 12).

the angle of maximum radiation for the over-all; whereas the angle of maximum radiation for the low frequencies is aft of the angle of the over-all. This is consistent with the refraction effect, for the high frequency noise is generated upstream where the local speed of sound is high, whereas the low frequencies are generated further downstream where the jet has been partially cooled by the mixing process and the local speed of sound is much closer to the ambient speed of sound.

One of the implications of Figure 7 is the difficulty encountered in attempting to duplicate noise environment on a model scale with the use of cold supersonic flows, since their directional characteristics would be radically different from those of the full scale hot flow. On the other hand, the correlation of the spectra of Figure 4 and the total power of Figures 5 and 6 indicate that the noise can be exactly scaled using nozzle dimensions alone to define the scale factor as long as all other rocket flow parameters (pressure ratio, specific heats, temperature and density) are held constant.

ESTIMATION OF NOISE ENVIRONMENT DURING LAUNCH

In order to estimate the noise environment of a missile or space vehicle during launch in the atmosphere, it is necessary to supplement the previously developed generalized relationships with experimental data pertaining to the launch configuration. This results from the fact that the launch pad and deflector, etc., actually modify the rocket's flow during the first few critical seconds until the vehicle attains sufficient altitude to allow the flow to behave as indicated in Figure 2. These modifications of the flow affect its basic noise generation and its directional radiation characteristics. Consequently, the noise environment surrounding the vehicle during the first phase of launch depends upon the launch configuration.

For the purpose of preliminary estimation of environment and a general understanding of the launch effects it is convenient to consider first the noise environment of a vehicle which is launched from a point well above the ground. Figure 8 gives the estimated external noise environment at various forward positions along a typical vehicle which has its rocket motor mounted aft and which is at an altitude of at least 50 nozzle exit diameters. The estimated mean square pressure per cycle is given for three values of the rocket characteristic flow velocities as a function of the dimensionless frequency parameter $\frac{fd_c}{a_0}$ which was found earlier to be appli-

cable to the rocket power spectra. The estimated levels are given for several positions forward of the nozzle at various non-dimensional distances (x/d_t) where d_t is the nozzle throat diameter. The solid curves have been derived from Cole (Reference 14) and other data applying to single nozzle rockets. The dashed curves in the low frequency region of Figure 8a were taken from Dyer (Reference 13) and apply to one case of dual nozzled rocket propulsion plants. They illustrate the general effect of multiple nozzles on the generation of rocket noise where the high frequency spectra are generally controlled by the individual rocket flows, whereas the low frequencies are generated primarily in the combined flow. Thus, depending on the number of nozzles, their spacing, and the axial distance prior to the mixing of the individual streams, the high frequency portion of the noise spectrum is best

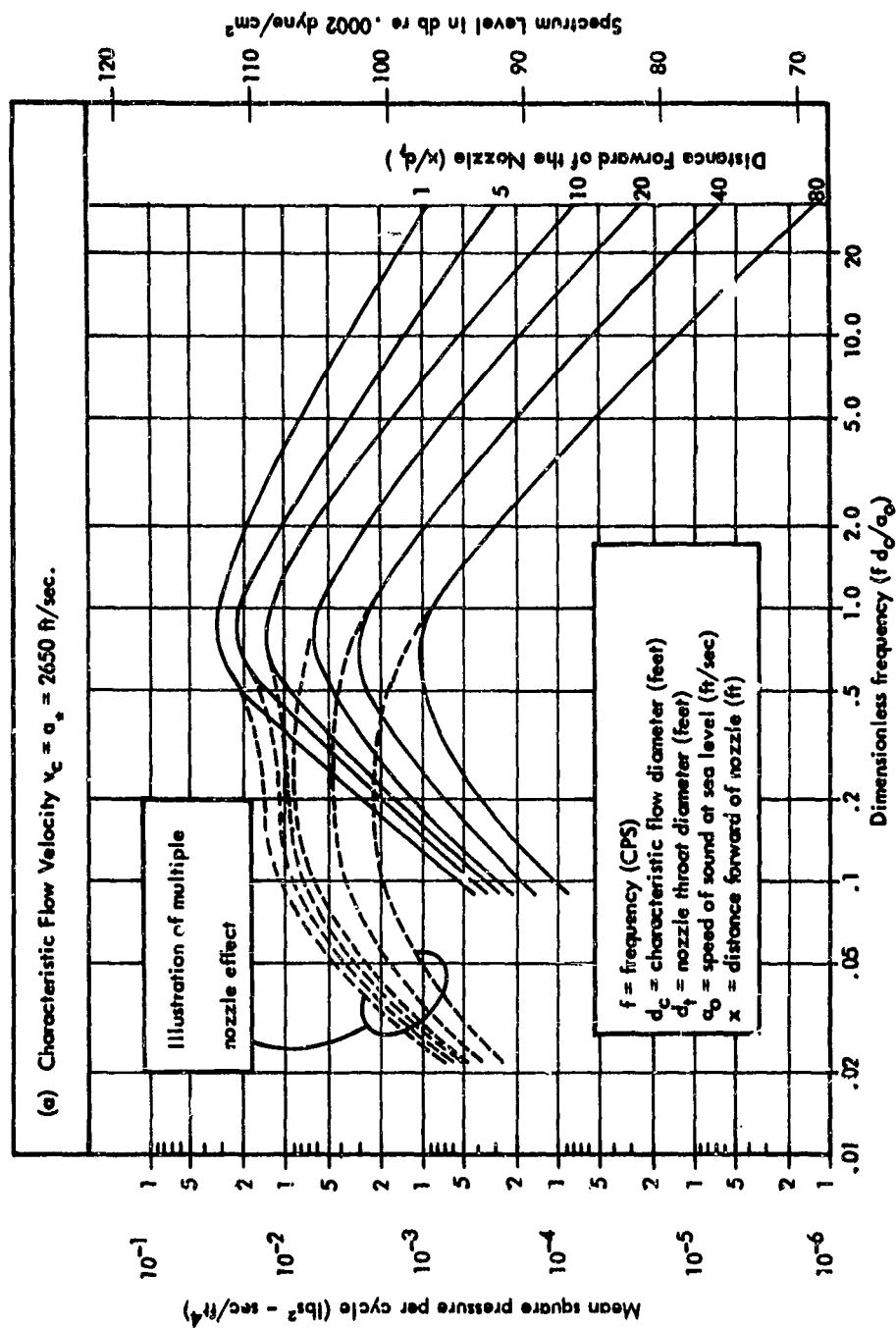


Figure 8a, Estimated Mean Square Pressure Per Cycle as a Function of a Dimensionless Frequency Parameter at Various Axial Distances Forward of the Rocket Nozzle for a Stationary Rocket at Sea Level with an Undisturbed Flow.

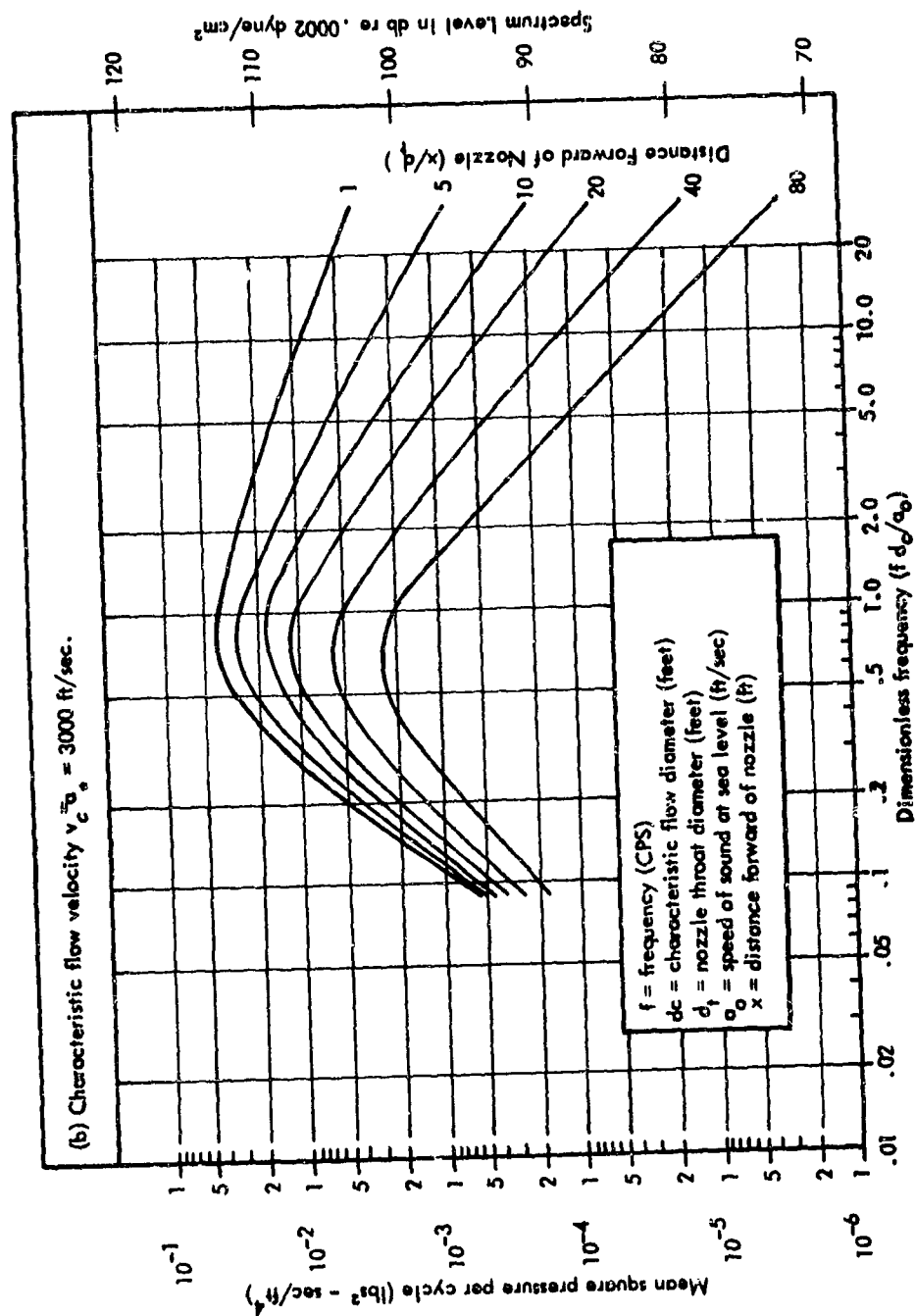


Figure 8b. Estimated Mean Square Pressure Per Cycle as a Function of a Dimensionless Frequency Parameter at Various Axial Distances Forward of the Rocket Nozzle for a Stationary Rocket at Sea Level with an Undisturbed Flow.

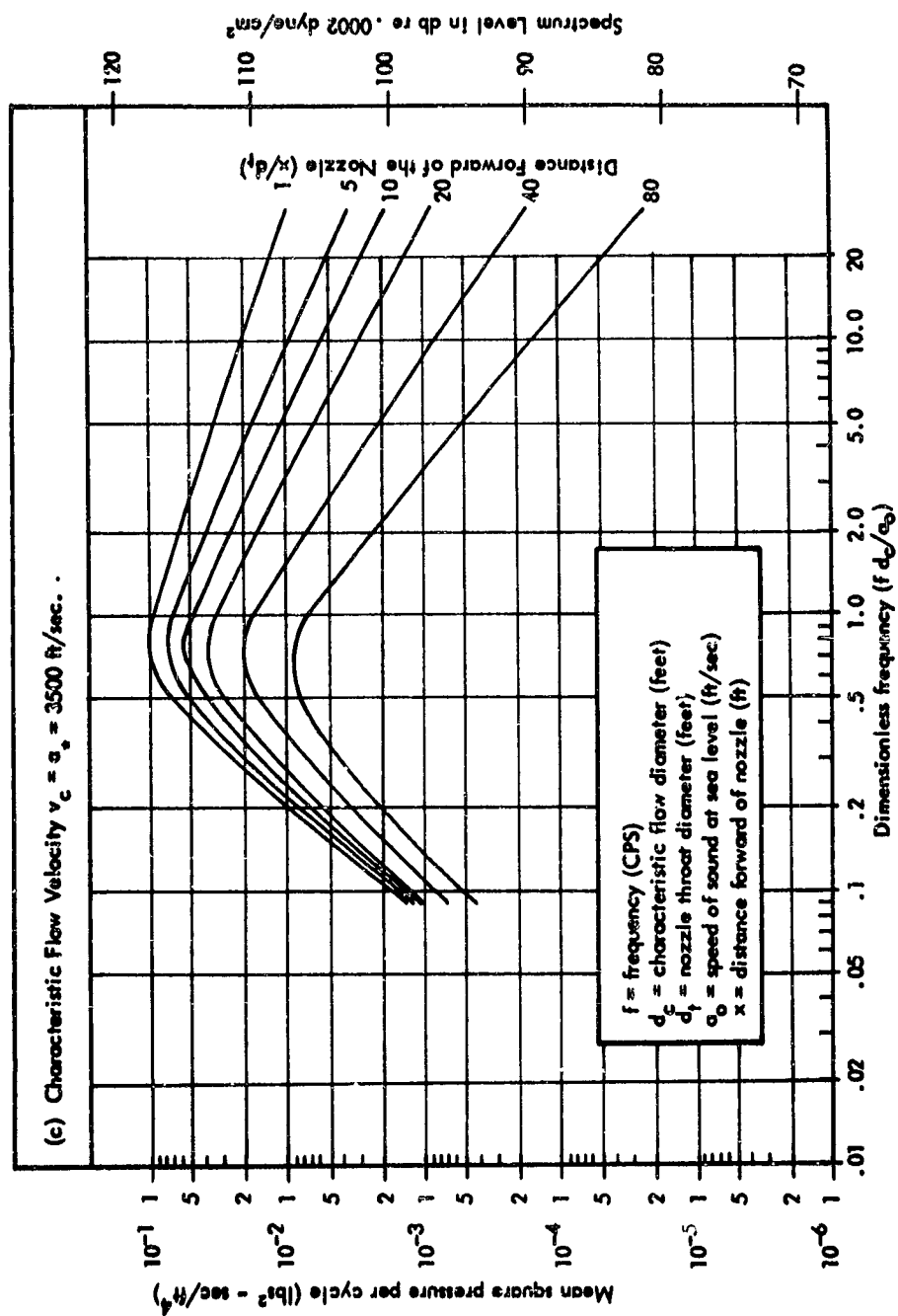


Figure 8c. Estimated Mean Square Pressure Per Cycle as a Function of a Dimensionless Frequency Parameter at Various Axial Distances Forward of the Rocket Nozzle for a Stationary Rocket at Sea Level with an undisturbed flow.

predicted from the individual flow characteristics of the combined flows. This results in the tendency toward two peaks in the spectrum. Note that, since the actual positioning of multiple nozzles will influence the magnitude in this low frequency region, these curves should be used with caution.

In addition, experience dictates that the wording "tentative" be applied to all of the curves shown in Figure 8. This results, both from the small body of reliable rocket noise data forward of the nozzle which are available, and from anticipation that variation of certain nozzle parameters will, in general, vary these estimates.

Although Figure 8 considers the magnitude of the change of noise level forward of the rocket nozzle resulting as a function of characteristic velocity ($v_c = a_*$), there is evidence that the distance between the apparent noise source and the nozzle is also affected by nozzle exit velocity. The data of Reference 3 show that the distance between the nozzle and the tip of the supersonic core is given approximately by

$$6.5 d_e [1 + (M_e - 1)^2] \quad (\text{from Reference 3 data,}) \text{ where}$$

d_e is the nozzle exit diameter and

M is the nozzle exit flow Mach number.

Therefore, it is expected that the distance from the nozzle to any apparent source will be a function of the square of the exit Mach number or exit velocity. This would suggest that this distance is also a function of the over or under expansion of the nozzle and pressure ratio. Unfortunately, the available data do not enable any clear generalizations of these factors.

Examination of the near field data of Reference 9 discloses that the reignition of the gases in the rocket flow was responsible for a large increase in the noise. This increase, on the order of 10 to 100 times the mean square pressure measured without reignition, was attributed primarily to unstable oscillations of, and turbulence associated with, the flame front. Consequently, the stabilization of the flame front by a flame holder such as the jetavator of Reference 9, materially reduced the near field levels.

Reignition and other unexpected phenomena may often accompany the development of successful rocket propulsion units. Because of the considerable import of these phenomena on any estimates of near field noise forward of the nozzle, it is desirable to obtain full scale noise data for the basic rocket which is intended to be used for the boost of a vehicle. These data should be obtained as early as practicable in the vehicular design stage to supplement the preliminary design estimates of noise environment.

EFFECT OF MOTION

The environment given by Figure 8 pertains to a stationary vehicle. However, as the vehicle begins to move and as its forward velocity increases, several factors

combine to reduce its rocket noise environment. Among these factors are the increased time required for the noise to travel forward from its source in the flow behind the missile and the reduction in total acoustic power, resulting from a reduction of the relative velocity between the jet flow and the atmosphere. Other factors, such as the decrease of pressure with altitude which increases the characteristic diameter of the flow and lowers its total power, will have minor effects on the frequency spectrum of the noise.

However, the first two factors are expected to predominate. Figures 9 and 10 summarize the steps for applying the correction resulting from the first of these motion factors to any vehicle. As shown in the sketch in Figure 9, when the vehicle is in motion, sound radiated at the source, S, does not reach the receiver, R, at its geometrical position relative to the source which is defined by the angle θ_0 . Instead, the sound radiated from θ_0 reaches the receiver when it has moved from R_0 to R_1 . These relationships for the moving source and receiver are given by Figure 9. In addition to the change in the angle of source radiation, the additional distance traveled by the sound in the undisturbed medium when both source and receiver are in motion results in a greater inverse square loss than in the stationary case. This additional inverse square loss is given as a function of source angle for various vehicle Mach numbers in Figure 10. Note that for a vehicle which has a conventional cylindrical missile configuration, the geometrical angle (θ_0) and the angle of source radiation (θ_1) are both essentially zero degrees. In this case, Figure 9 is unnecessary and Figure 10 or the simple formula:

$$\Delta M = 20 \log (1 - M_{\infty})$$

can be used directly. It is easily seen that no sound reaches the vehicle when the flight Mach number equals or exceeds unity.

The second major factor affecting the noise radiated when the vehicle is in motion results from the decrease of the relative velocity between the jet flow (V_c) and the atmosphere. Unpublished data from WADD Aero-Space Medical Division, and from Reference 14 for a 10,000 lb. thrust jet engine demonstrate that the variation in noise resulting from a variation in nozzle velocity and temperature for the stationary jet varies as a function of angular position. This variation is illustrated in Figure 11 which is compiled from the two references. The curve shown for rocket flow is estimated from knowledge of rocket directivity and at present has little experimental support. Thus, the total forward speed effect, combining both the change in relative jet velocity and the change in angle and distance previously discussed can be estimated from

$$\frac{p_m^2}{p_s^2} = \left[\frac{V_c - V_{\infty}}{V_c} \right]^n f(M_{\infty})$$

where p_m^2 is the mean square acoustic pressure at a point on the moving vehicle,

p_s^2 is the mean square acoustic pressure at the θ_1 angle source radiation when stationary, n is evaluated from Figure 11, and θ_1 and $f(M_{\infty})$ are evaluated from Figures 9 and 10

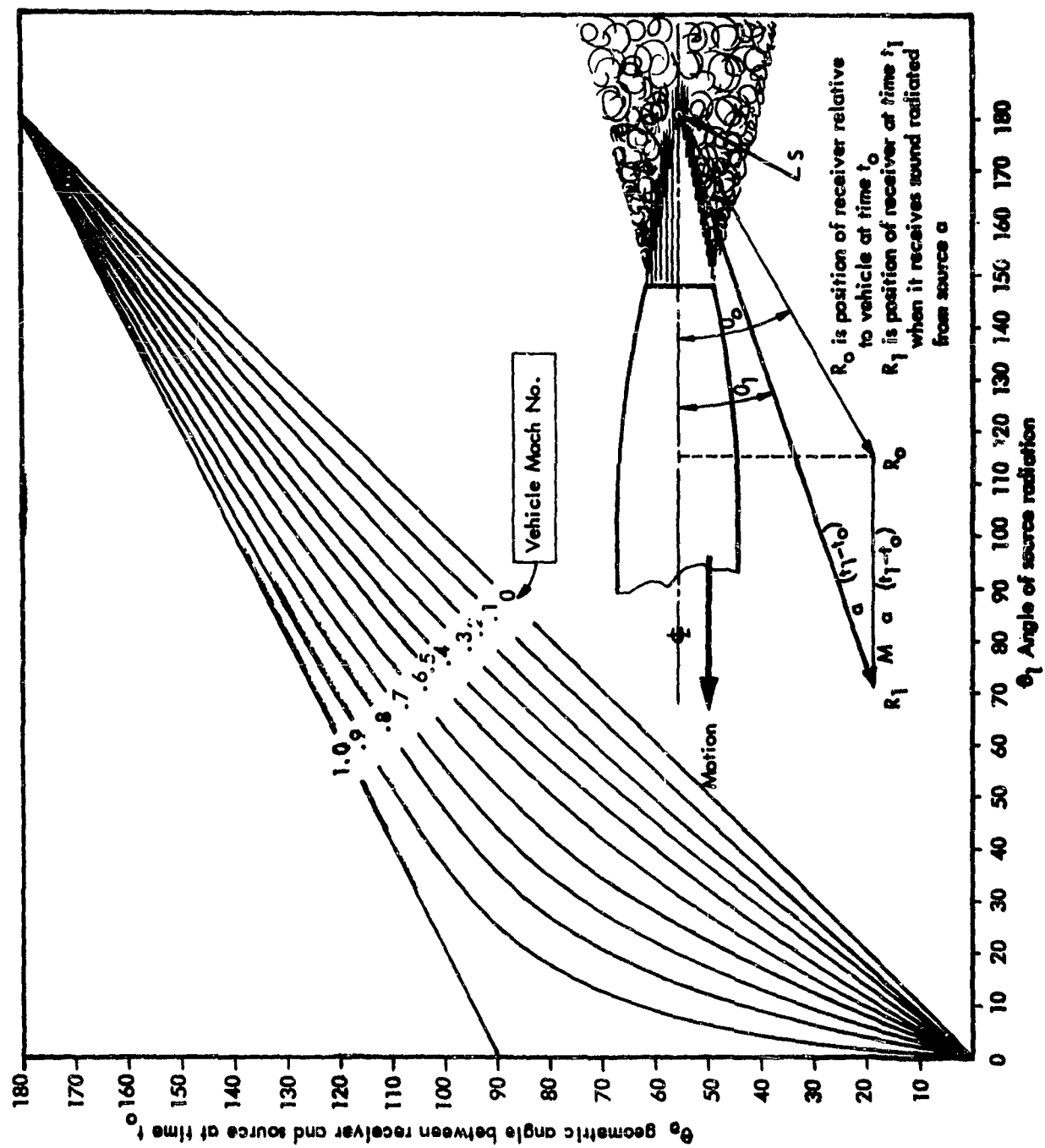


Figure 9. Relationship Between the Geometric Angle Between Moving Source and Receiver and the Angle of Source Radiation for Various Vehicle Mach Numbers.

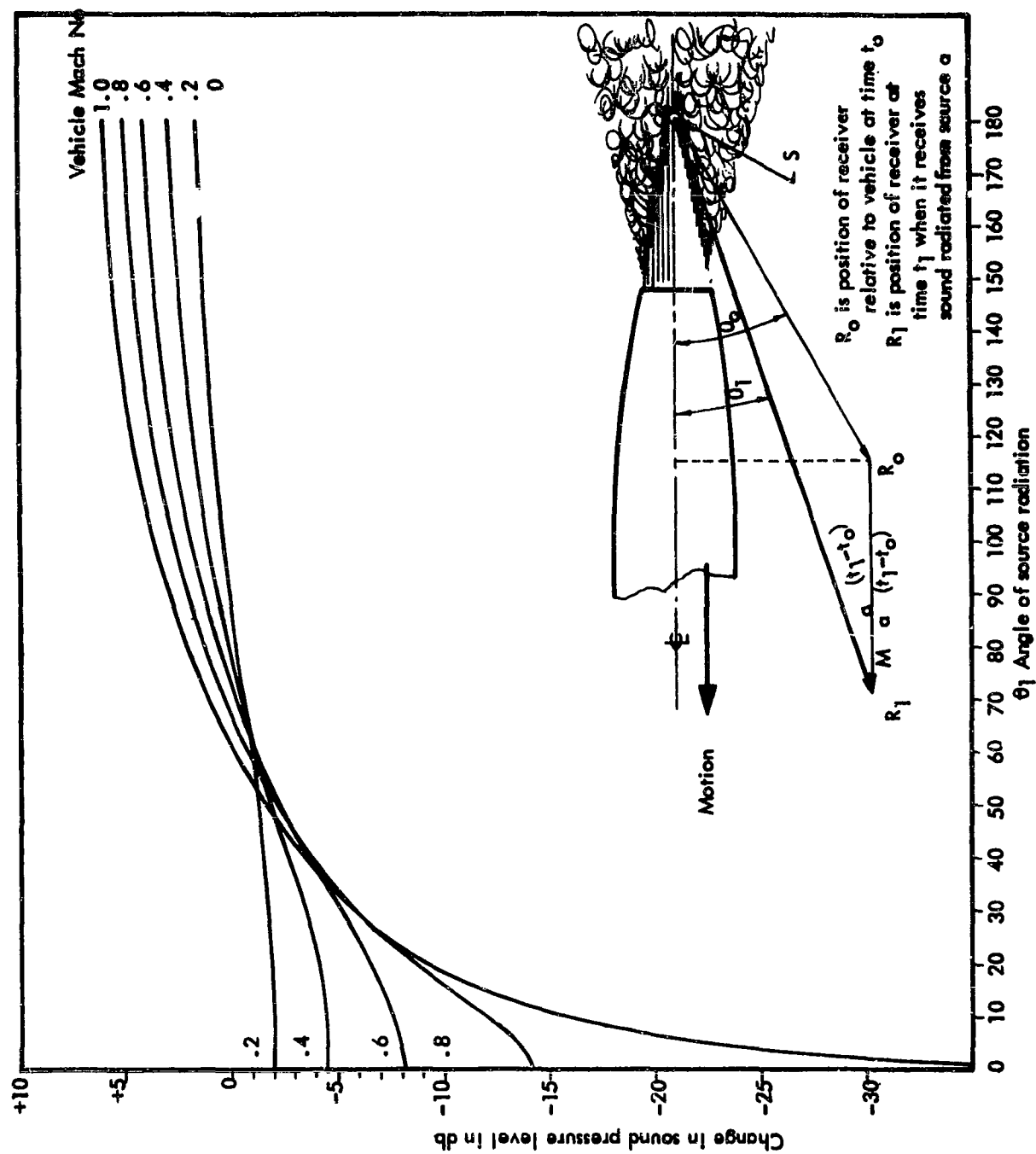


Figure 10. Reduction of Noise Level as a Function of the Angle of Source Radiation for Various Vehicle Mach Numbers.

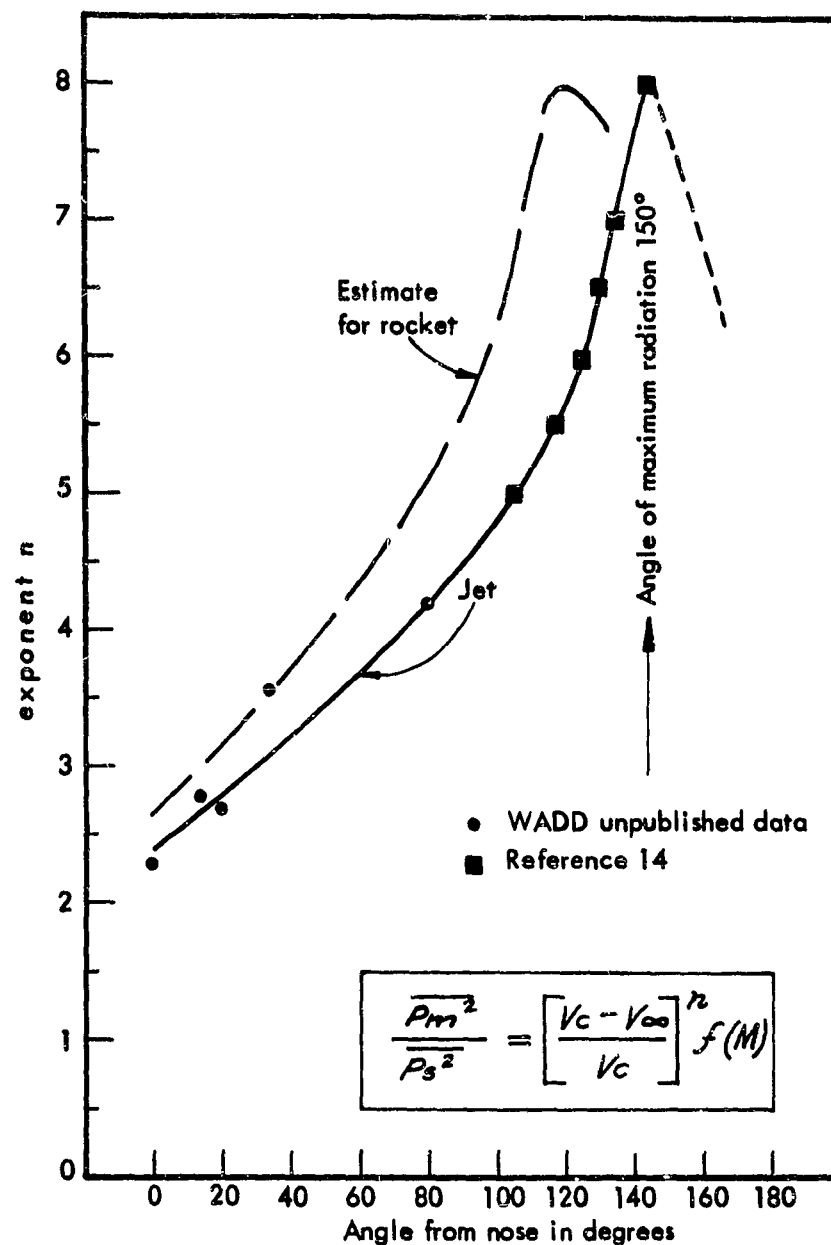


Figure 11. Variation of exponent n as a function of angle of source radiation for jets with maximum total temperature of approximately 1460°R

GROUND EFFECTS

The preceding estimation of the rocket noise environment of the vehicle which is above an altitude of at least 50 nozzle exit diameters, is simplicity itself, when compared to estimation of the environment of altitudes less than 50 nozzle exit diameters. These difficulties result from the impingement of the rocket flow on the ground or flow deflector. Figure 12 illustrates the rocket flow when the nozzle is a few diameters above a flat ground plane. As can be seen, the supersonic core impinges directly on the ground or on some type of deflector, losing much of its kinetic energy. After the impingement, the now turbulent flow spreads radially along the ground, slowing rapidly with increased distance.

It has been shown by Cole, et al, of WADC (Reference 15) that the rocket's total acoustical power is considerably less than that generated by a normal flow because of this impingement. However, it was also shown in these experiments that the sound pressures at any point along a vertical vehicle were increased. This apparent anomaly can be resolved by considering the directional characteristics of rocket noise previously mentioned in connection with Figure 7. In the normal flow, the angle of maximum radiation is approximately 120° from the nose of the vehicle, or 60° from the direction of flow. Assuming, for a first approximation, that the refraction effects in the ground flow are similar to those of the normal flow, the angle of maximum radiation would remain at 60° to the flow. But, since the flow is now at 90° from the vehicle's nose, the angle of maximum radiation would be only 30° from the missile. In addition, it can also be shown that the decreased area for acoustic energy radiation perpendicular to the rocket flow results in an additional increase in the sound pressure along the vehicle's axis. These effects combine to give the maximum angle of radiation at 0° along the vehicle's axis, as shown by the experimental curve in Figure 12. Thus, although the total acoustical power from the rocket is reduced by the launch configuration, the change in directivity increases the proportion of this power which is intercepted by the vertical standing vehicle and may actually increase the sound pressures on the vehicle.

A few examples of the increase in noise along the vehicle, taken from WADC experiments with many launch configurations, are given in Figure 13. It can be seen that the noise increase is of considerable magnitude. Further, the increase is greater when the flow is symmetrical about the base than when a deflector is used to concentrate the flow to one side of the vehicle. This result could also be anticipated from the above, for the diversion of the flow to the side will result in an angle of maximum radiation about 30° away from the vehicle's axis and the axial concentration of the noise from the symmetrical flow outward from the base will not exist. Hence, the increase in noise exposure for the vehicle is less.

Another launch configuration which is being given much consideration is the underground silo. Comparison of the silo configuration of Figure 14 with the surface launch of Figure 12 shows that the base of the silo affects the rocket stream in a manner similar to the flat ground reducing its momentum and energy. Therefore, it would be expected that the total acoustic power from the rocket would be least when the nozzle is at its minimum height close to the bottom of the silo, and would

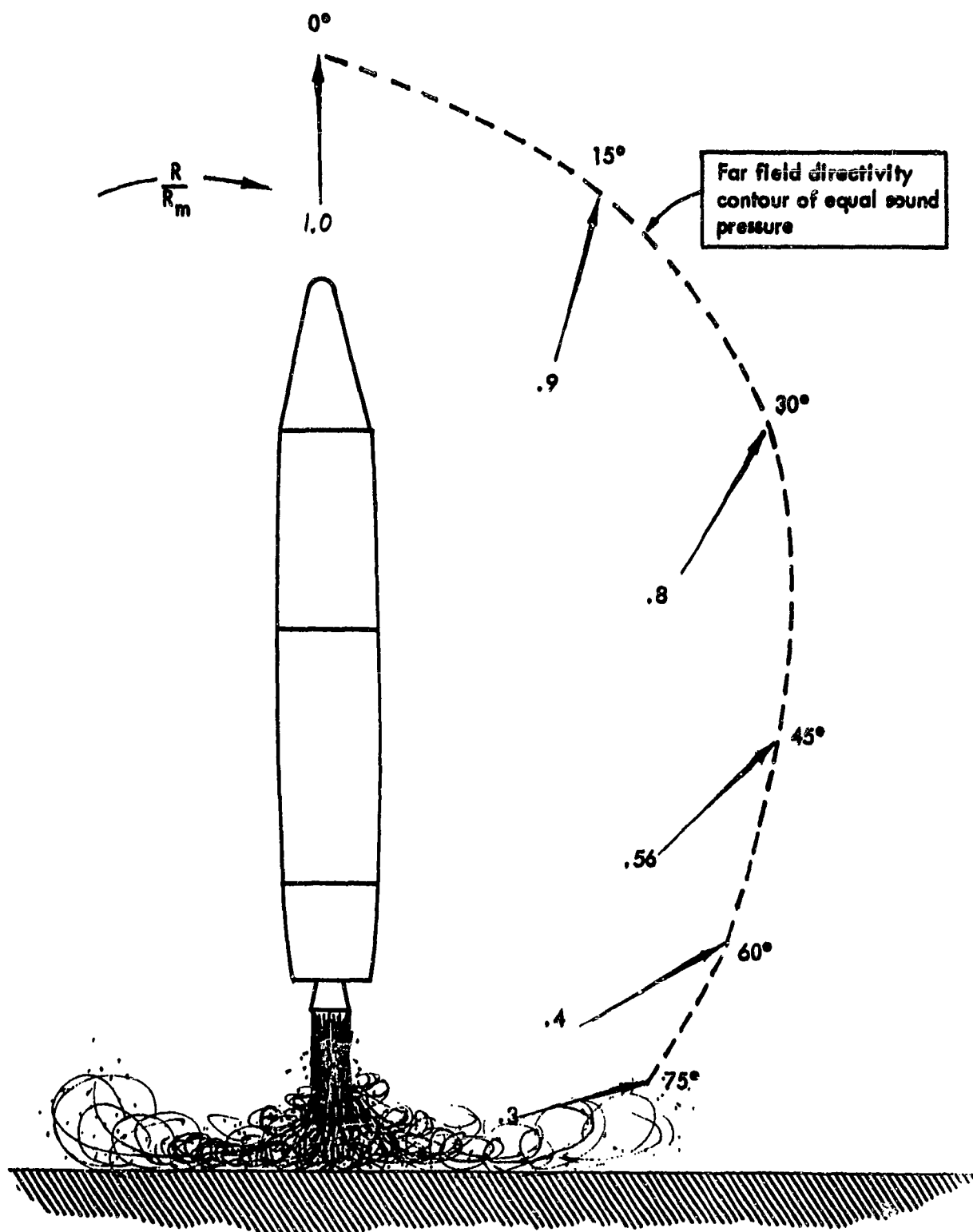


Figure 12. Illustration of the Turbulent Flow Resulting from Impingement on the Ground during Surface Launch, with a Far Field Contour of Equal Sound Pressure Superimposed. The Ratio R/R_m is the Ratio of the Radius of the Contour at any Angle to the Reference Radius at the Angle of Maximum Radiation.

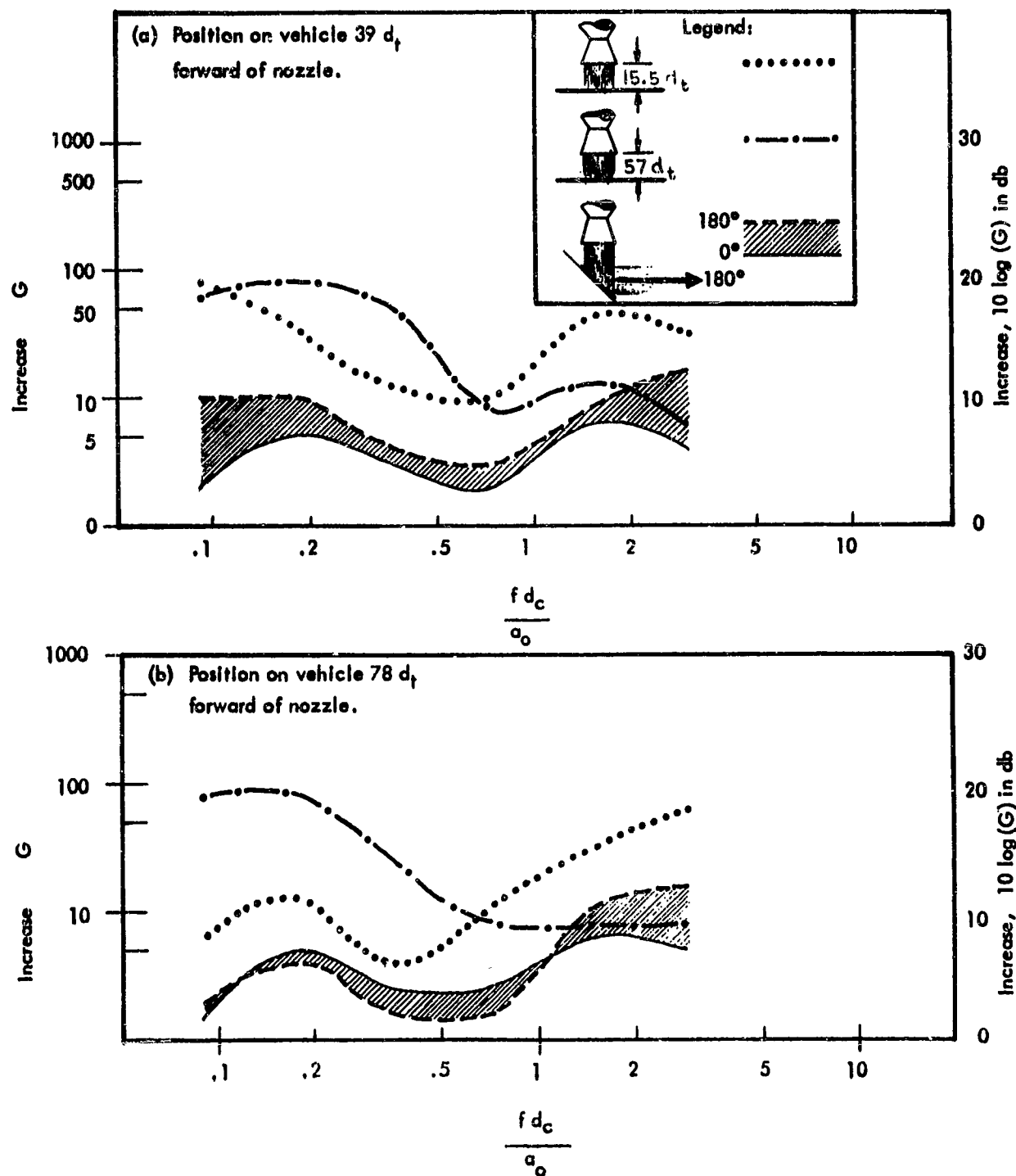


Figure 13. Examples of the Increase of Vehicle Noise Exposure During Launch at Two Positions on the Vehicle (From Reference 15).

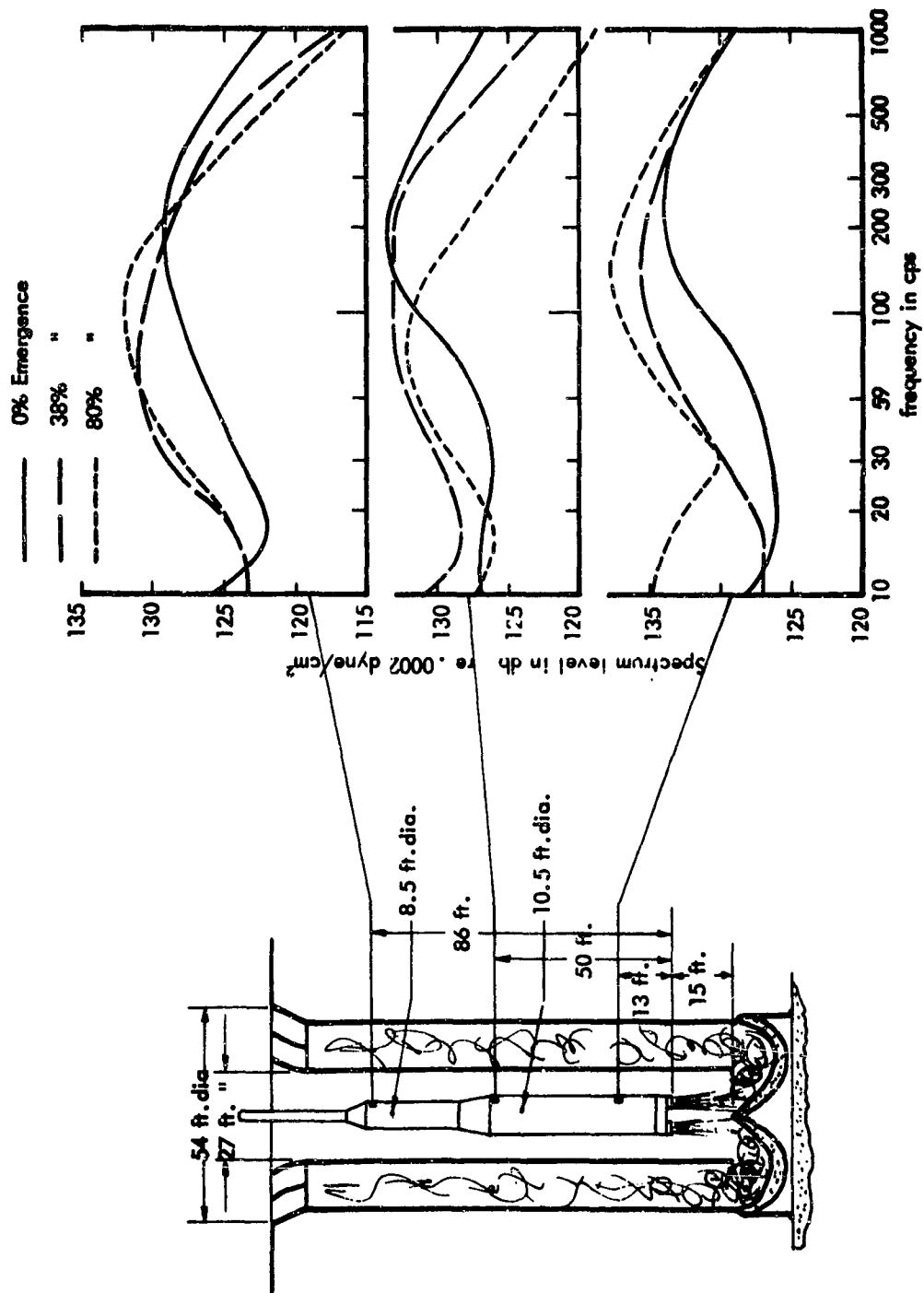


Figure 14. Data from 1/6 scale unlined model silo tests (reference 16) corrected to full scale frequencies.

increase as the distance between the nozzle and the base increases to about 50 nozzle exit diameters, until the base no longer absorbs a significant portion of the stream energy. Because the silo completely surrounds the vehicle, this acoustic power must either be absorbed in the silo walls or radiate toward the opening.

An example of the noise levels which may be expected on a missile in an unlined silo of the "W" configuration is given in Figure 14. These data were obtained for an experimental 1/6 scale silo in Reference 16 and have been scaled in frequency to full scale for presentation in Figure 14. As would be expected, the low frequency noise increases as the vehicle emerges from the silo, whereas the high frequency noise on the missile decreases as the microphone emerges from the silo. Comparison of this estimated silo environment with that for other launch configurations (Figures 8 and 13) indicates that a significant increase in noise results, particularly for forward positions on the vehicle. However, this noise could be substantially reduced by a variety of means, including incorporating absorbent walls, increasing silo diameter, separating the bottom of the silo from the portion occupied by the vehicle with a moving ring partition, etc.

In fact, the addition of a thick Fiberglas duct liner gives reductions of as much as 24 db at the forward position and 16 db at the aft position in the frequency range of 30 - 100 cps, as measured by the authors of Reference 16 on the scale model. However, the measurements also showed that the noise reduction given by the liner decreased markedly at frequencies above 100 cps to the order of 3 - 6 db at 1000 cps, as correctly predicted by Reference 17. Hence, the use of a liner, alone, without auxiliary baffles to scatter the beamed high frequency sound offers little reduction at frequencies where panel resonances and equipment malfunction may be most serious.

From the foregoing discussion, it is clear that the large variation in the noise environment during launch which can result from launch geometry, emphasizes that the design and concept of the launch configuration for any vehicle are controlling factors in its final launch noise environment. Hence, these factors are subject to study from the initiation of any vehicle design. Although it is felt that the development of optimum configurations for specific purposes can be guided by calculations based on the principles of rocket flow characteristics and noise generations, experimentation is necessary for precise definition because the complex flow defies accurate prediction. Fortunately, the correlation of rocket noise generation with flow parameters demonstrates that very small scale rockets, such as the JATO rockets of Reference 15, may be used for this purpose, as long as all flow parameters except nozzle diameters are maintained constant.

Furthermore, phenomena such as reignition in the flow with its oscillating flame front (Reference 9) may substantially increase the vehicle's noise environment above that which would otherwise result. Therefore, it is desirable to perform acoustical measurements on each basic type of rocket engine during its final development stage to provide the vehicle designer data which either substantiates his estimates or warns of unexpected increases in the estimated acoustic and vibration environments.

GENERAL REFERENCE: von Gierke, E. E., "Aircraft Noise Sources," Chapter 33 of "Handbook of Noise Control," edited by Cyril Harris, McGraw Hill Book Company, Inc., New York, 1957

REFERENCES

1. Howes, W. L. et al, "Near Noise Field of a Jet Engine Exhaust," NACA Report 1338
2. Mayes, W. H. Lanford, W. E., Hubbard, H. H., "Near Field and Far Field Noise Surveys of Solid Fuel Rocket Engines for a Range of Nozzle Exit Pressure," NASA TN D-21, August 1959.
3. Anderson, A. E. and Johns, F. R., Jet Propulsion 25, 13-15 (1955)
4. Laurence, J. C., "Intensity, Scale and Spectra of Turbulence in Mixing Region of Free Subsonic Jet," NACA Report 1292, 1956.
5. Lighthill, M. J., Proceedings of Royal Society of London, 1951.
6. Lighthill, M. J., Proceedings of Royal Society of London, A211; 545 (1952).
7. Callaghan, E. E. and Coles, W. D., "Far Noise Field of Air Jets and Jet Engines" NACA Report 1329 (1957).
8. Eldred, K. M. et al, "Prediction of Rocket and Turbojet Noise," Presented at 52nd Acoustical Society of American Meetings, 1956.
9. Cole, J. N. et al, "Noise Radiation from Fourteen Types of Rockets in the 1000 to 130,000 Pounds Thrust Range," WADC Technical Report No. 57-354, December 1957.
10. Lassiter, L. W., Heitkotter, R. H., "Some Measurements of Noise from Three Solid Fuel Rocket Engines," NACA TN 3316, December 1954.
11. Eldred, K. M., "Review of the Noise Generation of Rockets and Jets," JASA 32 (1502) 1960
12. Lee, Robert, "Free Field Measurements of Sound Radiated by Subsonic Air Jets," Navy Dept. The David W. Taylor Model Basin, Report 868, December 1953.
13. Dyer, Ira, Franken, P. A., "The Acoustic Environment of a Missile," Shock and Vibration Bulletin, Part 1, No. 25; December 1957.
14. Wolfe, M. O. W., "Near Field Jet Noise," Royal Aircraft Establishment, Technical Note No. Structures 228, September 1957.
15. Cole, J. N., England, R. T., Powell, R. G., "Effects of Various Exhaust Blast Deflection on the Acoustic Noise Characteristics of 1000-lb. Thrust Rockets."

REFERENCES (continued)

16. Loya, Gaede, Knowles, AFMD TR 60-39.
17. Gallaway, Bolt Beranek and Newman Report 713, 6 May 1960.

III AERODYNAMIC EXCITATION

There are several aerodynamic phenomena associated with high speed flight in the atmosphere which can excite vehicle vibration. These phenomena include:

- (a) Turbulent boundary layer flow
- (b) Separated flows and oscillating shocks
- (c) Impingement of jet turbulence
- (d) Flow over cavities
- (e) Flow past projections
- (f) Base pressure fluctuation
- (g) Panel flutter

With the exception of the pressure fluctuations associated with turbulent boundary layer flow, each of these phenomena may be controlled by the designer. This control is not necessarily an easy task, particularly when one considers the tremendous range of flow velocities from subsonic to hypersonic which are encompassed by the corridor of continuous flight shown in Figure 15. Furthermore, although model testing can be extremely valuable in investigating some of these factors for a particular vehicle, it is probably unreliable at present in the hypersonic regime for the investigation of dynamic phenomena encountered in quasi steady state flight.

Regardless of these and other difficulties, it is important that the aerodynamic design and flight profile of each new vehicle be investigated analytically and/or experimentally for each of the phenomena discussed in this section, to insure that potentially serious vibration problems are not accidentally designed into the vehicle.

TURBULENT BOUNDARY LAYER FLOW

The turbulent boundary layer which forms along the skin of any body moving at high speed in an atmosphere is a source of skin vibration. This source has been often referred to as "aerodynamic noise," "boundary layer noise," or "pseudo sound." As will be seen, the strength of this source is proportional to the freestream dynamic pressure (q_∞)* and hence it generally is of most importance during the high q portion of the flight.

The boundary layer external to the vehicle is a region of retarded flow which forms about any surface moving through a fluid medium. As illustrated for the smooth flat plate in Figure 16, the boundary layer slowly develops from the leading edge of the plate. If the freestream turbulence is negligible, the leading edge relatively blunt, and the plate smooth, the initial portion of the boundary layer has laminar streamline flow. However, as the distance from the leading edge increases, the laminar boundary layer becomes unstable and the flow changes from laminar to turbulent.

* The dynamic pressure is given by $q = \frac{1}{2} \rho_\infty U_\infty^2$ where ρ_∞ is the freestream density of the atmosphere and U_∞ is the freestream velocity.

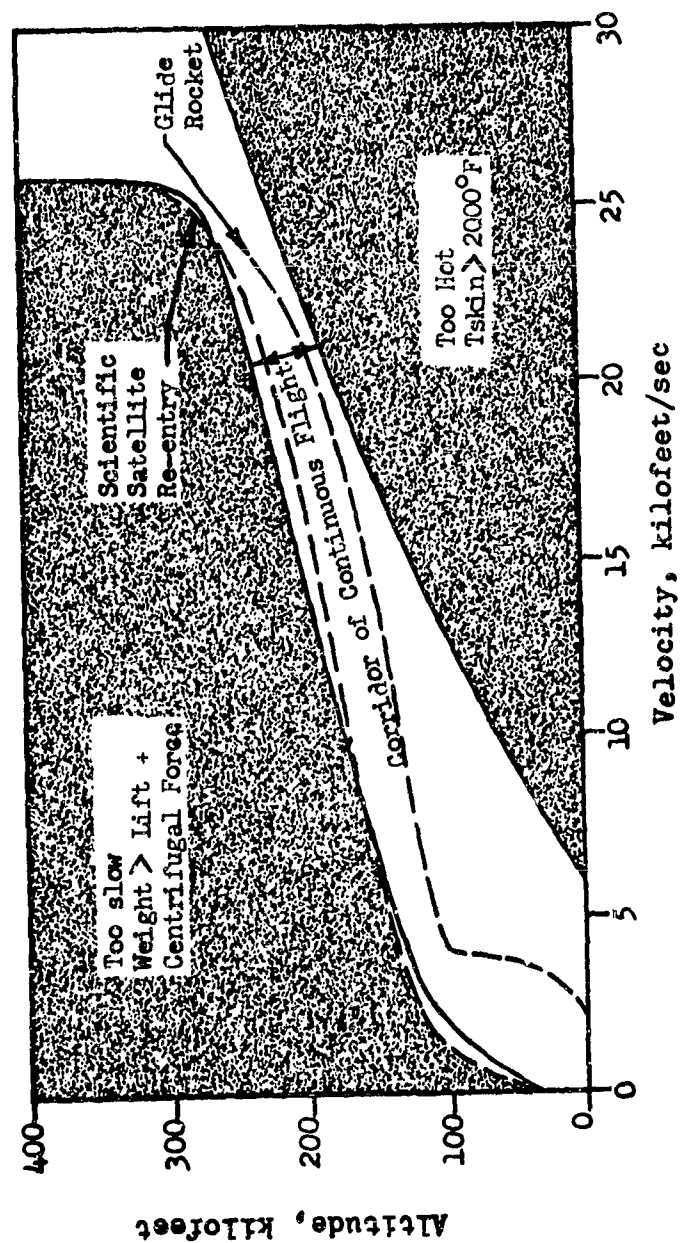


Figure 15. Exit Corridor.

Figure 16a. Sketch of the Development of a Turbulent Boundary Layer Along a Flat Plate.

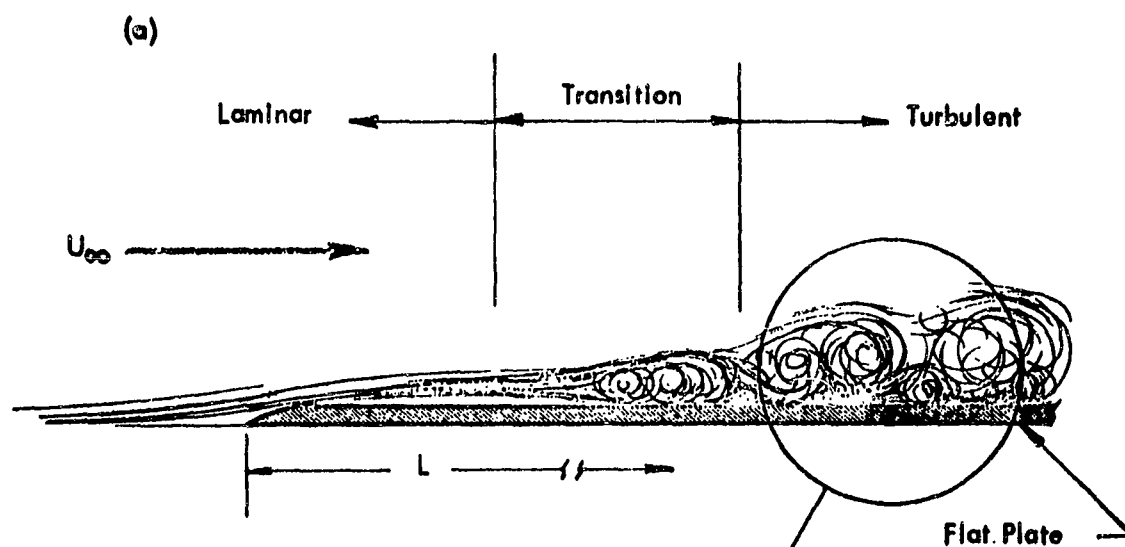


Figure 16b. Illustration of the Definition of the Boundary Layer Thickness (δ)

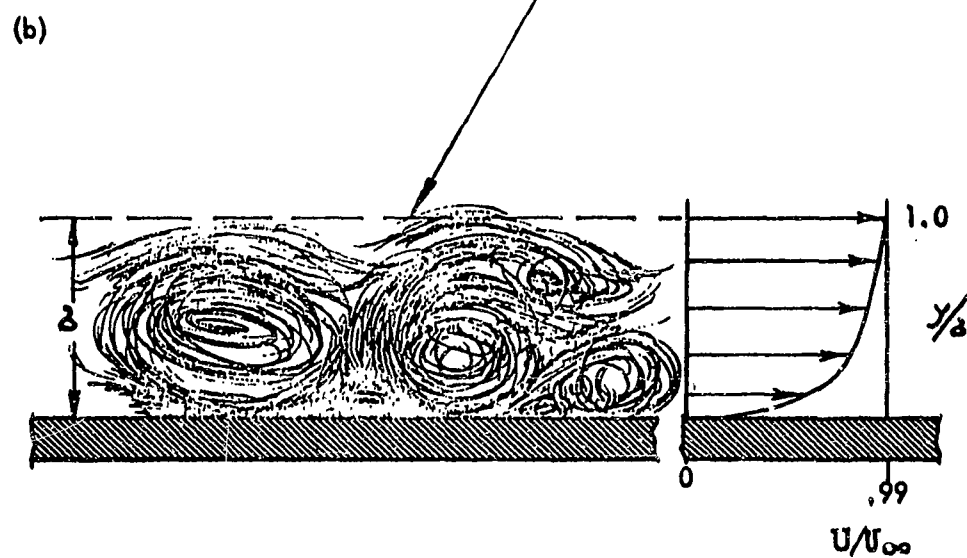


Figure 16

The distance between the leading edge and the transition region for a streamlined body is dependent on the turbulence in the atmosphere and upon Reynolds number. The Reynolds number (Re), which is a dimensionless ratio of the inertia forces in the flow to the viscous forces in the flow, is an important similarity parameter for all fluid flow phenomena, and is given by

$$Re = \frac{U L}{\nu}$$

when U is the fluid velocity

L is the length from the leading edge of the vehicle

ν is the kinematic viscosity of the fluid

Generally, if there is little atmospheric turbulence and the flow along the vehicle is smooth, the transition region in the boundary layer will begin at the distance from the leading edge where the Reynolds number becomes 3×10^5 . It should be noted that this distance is relatively small for high speed vehicles.

The physical thickness (δ) of the boundary layer can be defined, as shown in Figure 16, as the distance from the surface at which the mean velocity is 99% of the freestream velocity. For a flat plate this mean thickness is given approximately by (References 1 and 2):

$$\delta = .37 L Re^{-1/5}$$

Although this formula is strictly applicable only to a smooth flat plate, it can be used approximately with many types of aircraft surfaces, because the surface dimensions are much greater than the boundary layer thickness. However, in an actual vehicle, many additional factors including pressure gradients, angle of attack, flow separation, etc., combine in determining the boundary layer parameters.

The turbulent boundary layer can be considered as an assortment or randomly sized eddies or vortices which flow past the vehicle's skin at a mean convection velocity (U_c). Experimental data (References 3 and 4) indicate that U_c is approximately .8 times the velocity external to the boundary layer. As would be expected, the individual eddies lose their identity in a relatively short distance as they shed fluid and energy as a result of interaction with the skin or with other eddies. Thus, each large eddy which is formed taking energy from the shear in the boundary layer between the vehicle and the surrounding atmosphere, decomposes into successively smaller and smaller eddies. It was found in Reference 3 that a large eddy begins to change significantly after it has travelled a distance of only two boundary layer thicknesses and has lost all identity when it reaches a distance of 10δ . Therefore, it can be seen that the pressure fluctuations associated with these eddies are in phase, or correlated for only short distances over the vehicle's surface, and that these distances are generally much smaller than those associated with normal acoustic pressures of similar frequency.

Because the skin is almost in direct contact with the convected swirling vortices which characterize the turbulent boundary layer, the fluctuating pressures at the skin are actually the direct dynamic pressures of the velocity fluctuations normal to the skin. The overall mean square value of these fluctuating pressures has been found proportional to the freestream dynamic pressure by the theoretical investigators (References 5, 6, 7, 8) and by most of experimenters (References 3, 4, 8, 9, 10, 11, 12). This relationship is illustrated in Figure 17 where data from several types of experiments, including aircraft, wind tunnels and rotating cylinders, have been plotted. As can be seen, the majority of the data conforms to a linear relationship between the overall root mean square fluctuating pressure and q . It is interesting to note that the major departure which is shown, results from data taken at a forward position on the F102A. It is felt that this may be typical of areas toward the nose of an aircraft or space vehicle where the development of the turbulent boundary layer may be delayed by the negative pressure gradient formed longitudinally along the skin by the velocity increase. It is also interesting to note that the overall levels calculated from Sandborn's measurements of velocity fluctuations in the boundary layer of a low speed wind tunnel (Reference 13) also fit on the

curve. The mean value of $\sqrt{P^2}/q$ for these pressure data in Figure 17, not including the four Sandborn velocity points or the F102A position 3 data in the average, is 5.2×10^{-3} with a standard deviation of 1.3×10^{-3} .

The majority of these data are limited to the subsonic and transonic speed range. Preliminary data from Jordan and McCloud on a F104 and by North American on an F4J indicate that, for some cases at least, the pressure fluctuations are lower at supersonic speeds (above M 1.5) than at subsonic speeds when compared at the same dynamic pressures. Also, current work of Kistler and Laufer at CIT Jet Propulsion Laboratory indicates that the ratio of $\sqrt{p^2}$ decreases

to approximately 2×10^{-3} at Mach 4. Thus, utilization of the subsonic^q relationship for prediction of the overall value of boundary layer pressure fluctuations at Mach numbers exceeding approximately 1.5, may result in conservative estimates.

The spectrum of these pressure fluctuations has been found to correlate with the dimensionless frequency parameter:

$$\frac{f \delta a_0 \gamma_{\infty}}{U_{\infty}^2 \gamma_0}$$

where f is frequency (cps)

δ is boundary layer thickness (ft.)

a_0 is sea level standard speed of sound (ft/sec)

γ_0 is sea level standard kinematic viscosity (ft²/sec)

γ_{∞} is freestream kinematic viscosity (ft²/sec)

and U_{∞} is freestream velocity (ft/sec).

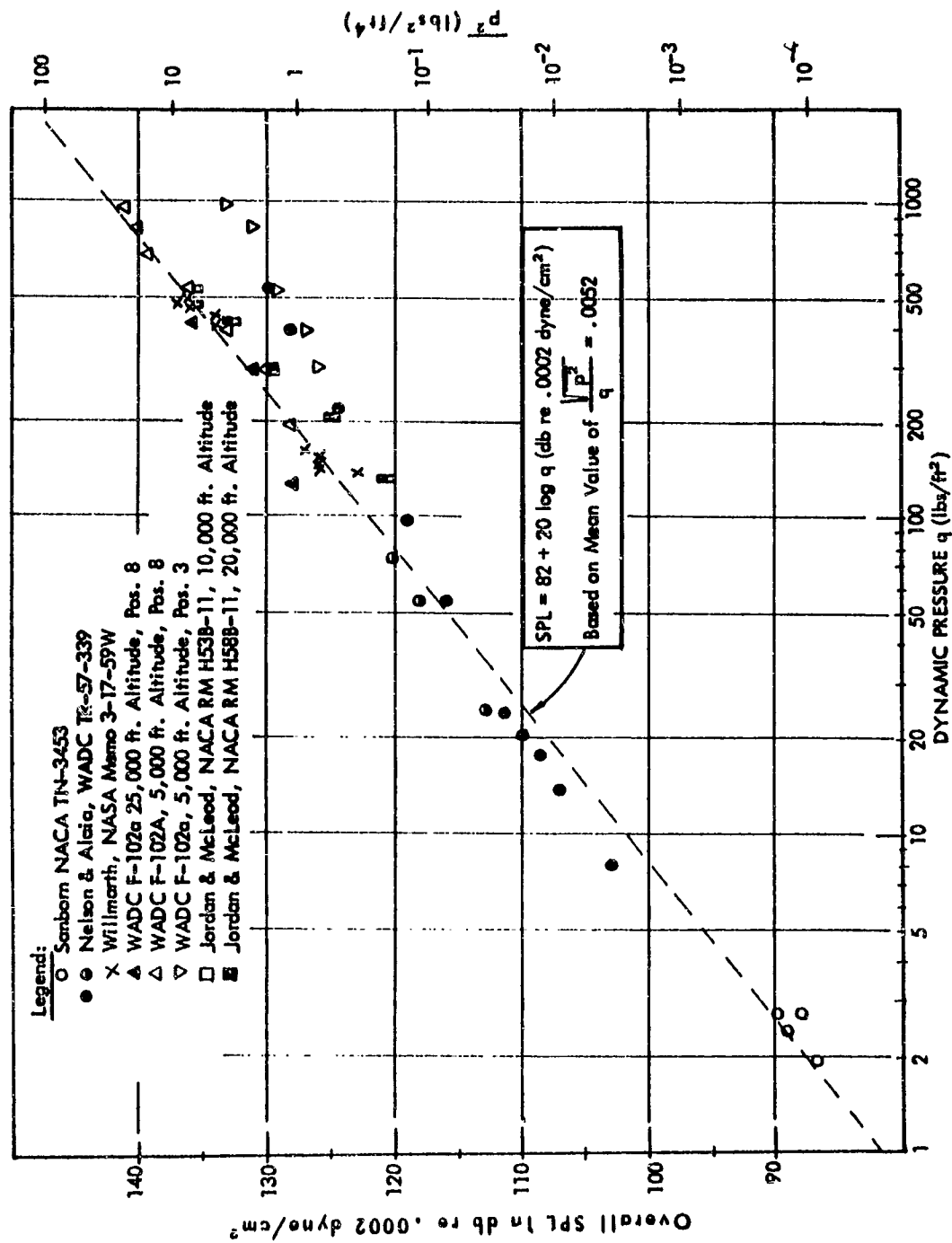


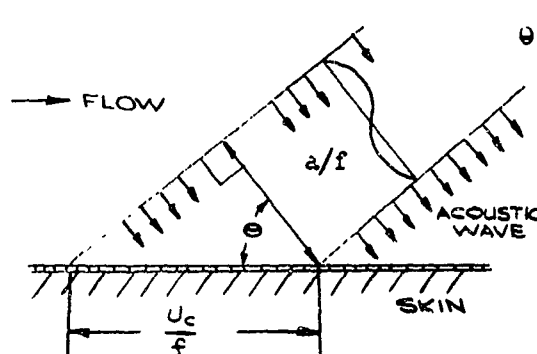
Figure 17. Overall Sound Pressure Level and Mean Square Fluctuating Pressure ($\overline{p^2}$) in the Turbulent Boundary Layer as a Function of Freestream Dynamic Pressure (data from Refs. 3, 8, 9, 10, 11 and 13).

Figure 18, from Reference 15, gives the mean square fluctuating pressure per cycle as a fraction of the overall mean square fluctuating pressure. As can be seen, the normalized data appear to form a general curve with a constantly increasing negative slope with increasing frequency. This effect is the result of the increased viscous damping associated with the high frequency small scale eddies which have correspondingly small Reynolds numbers.

The factors which ordinarily will have the greatest effect on the spectrum are the velocity and the boundary layer thickness. As the velocity increases, the energy at high frequencies tends to increase more rapidly than the total energy, which comes from the steep slope at the high frequency side of the Figure 18, whereas when the boundary layer thickness increases, the low frequency energy increases. It is noted that for many applications to high speed vehicles, the frequency range of interest will extend below that given in Figure 18. Although no data are available in this region, it is expected that the curve will become flat at lower values of the frequency parameter.

It should be noted that the frequency of these pressure fluctuations is equal to their convection velocity divided by the distance between successive pressure maxima. Hence, if the mean convection velocity is $.8 U_{\infty}$, then the wavelength (λ) associated with any frequency (f) is given by $\lambda = \frac{.8U}{f}$

Thus, at velocities where the convection velocity is less than the speed of sound, the wavelength of the boundary layer pressure fluctuation along the skin is less than the wavelength of an acoustical pressure at the same frequency. However, when the convection velocity is greater than the speed of sound, an acoustic wave of the same frequency can be made equivalent as long as the component of its propagation velocity along the surface equals the convection velocity of turbulence. If the angle of incidence (θ), required to give an equivalent wavelength, is measured from the skin, then



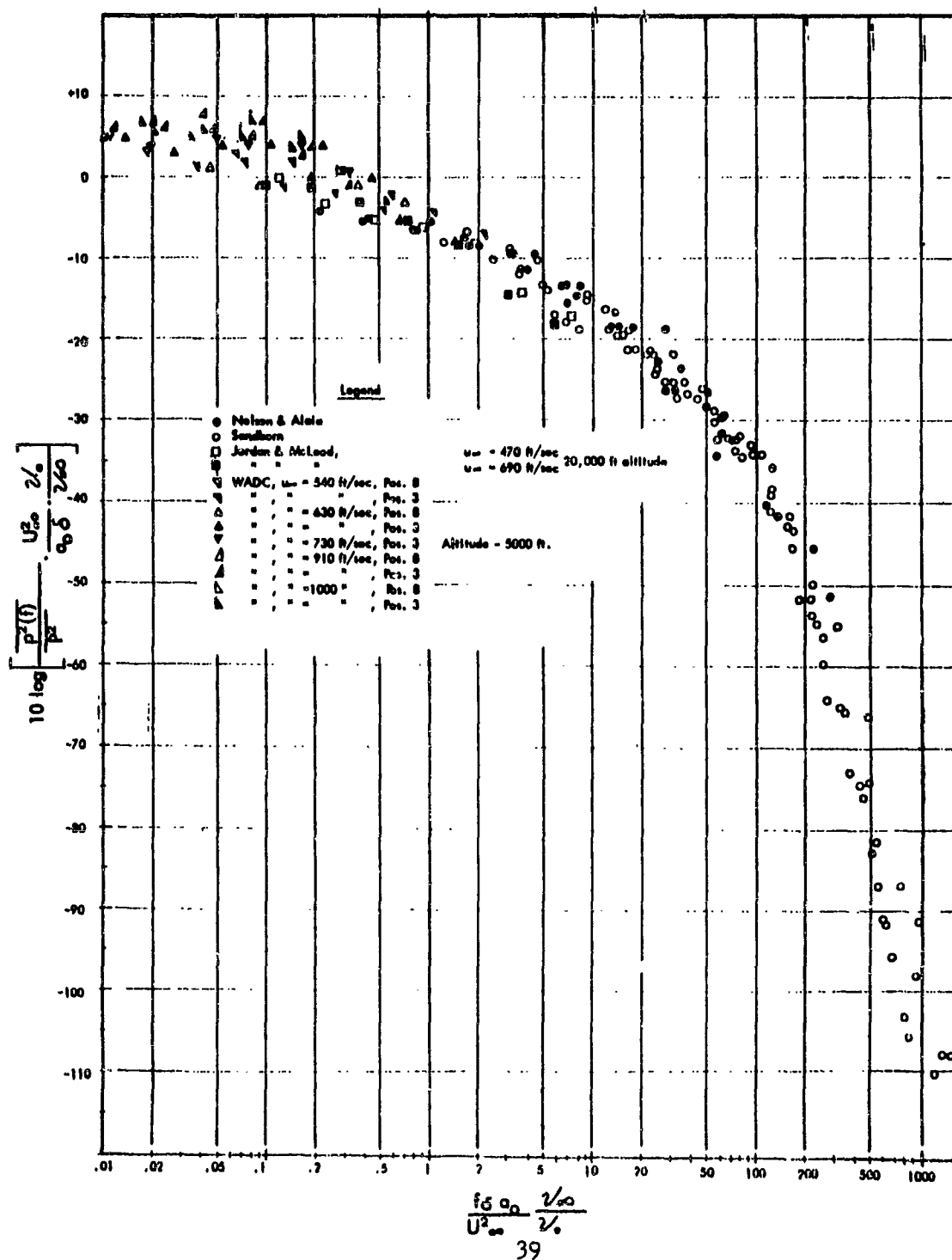
WAVE LENGTH ON SKIN

$$\theta = \cos^{-1} \frac{a}{U_c} = \cos^{-1} \frac{a}{.8U_{\infty}}$$

where a is the speed of sound
 U_c is convection velocity
and U_{∞} is the freestream velocity.

Generally, the boundary layer pressure fluctuations will be most important as vibration sources during the high q flight portions of exit and re-entry when the vehicle is supersonic. For all flight velocities above the transonic

Figure 18. Fractional Mean Square Pressure Per Cycle $\left[\frac{\overline{p^2(f)}}{\rho \frac{U_\infty^3}{2\delta} \frac{2\delta}{\rho}} \right]$ in the Turbulent Boundary Layer Normalized by $\frac{\rho \frac{U_\infty^3}{2\delta} \frac{2\delta}{\rho}}$ as a function of the dimensionless frequency parameter $\frac{f \delta \rho}{U_\infty^2}$ (Data from Refs. 8, 10, 11 and 13).



speed range, considerable differences may exist between the freestream velocity and the local velocity external to the boundary layer. Consequently, when the data of Figures 17 and 18 are applied in the prediction of external pressure fluctuations, the local quantities external to the boundary layer predicted for the vehicle should be substituted for the freestream values. In addition, it is quite possible that the flow will remain laminar for very considerable distances, particularly during high Mach number exit and re-entry, resulting in insignificant pressure fluctuations. This extension of laminar flow at high Mach numbers beyond the normal point of transition can result from the stabilizing effect of heat extraction from the boundary layer by the vehicle. These factors emphasize the necessity of obtaining realistic estimates of the boundary layer from the aerodynamicists prior to attempting estimates of the pressure fluctuations.

IMPINGEMENT OF JET TURBULENCE ON THE VEHICLE

The impingement of a jet exhaust stream on the surface of a vehicle will excite vibration in the same manner as does the turbulent boundary layer. Although this impingement of hot exhaust gas is normally avoided in design for many reasons, it may be unavoidable in some cases, particularly when vernier rockets are utilized for control purposes. Note that the probability of the impingement of supersonic flows increases with vehicle altitude because of the increased angle through which the supersonic flow expands as the atmospheric pressure decreases (see Reference 23).

Measurements of the turbulent fluctuations in a subsonic jet by Laurance (Reference 24) indicate that the velocity fluctuations (rms) range between 8 and 20% of the characteristic jet flow velocity with the high value close to the nozzle. The resulting fluctuating pressures should be proportional to the dynamic pressure (q_c) in the jet flow. Following the analysis of boundary layer fluctuations in Reference 15, the total mean square fluctuating pressure is given by

$$\overline{p^2} = 3/4 \rho_c^2 \eta^4 v_c^4 = 3 \eta^4 q_c^2$$

where ρ_c is the characteristic density in the jet (see Section II)

v_c is the characteristic velocity in the jet (see Section II)

and η is the Constant of proportionality between the

rms velocity fluctuations and v_c (approximately .08 to .2)

Estimation of this total root mean square pressure fluctuation for typical jet flows gives values ranging between 15 and 100 lbs/ft². For a sonic turbojet, the fluctuating pressure is maximum very near the nozzle and decreases rapidly with distance along the flow until the lower pressure is reached at a distance of approximately 40 nozzle exit diameters downstream. Unfortunately, similar measurements are not available for rocket flows; however, it would be expected that the equation given above would apply to the turbulent portion of the rocket flow, and although the proportionality constant, η , may vary, the values for the jet probably can be used for a first approximation. It would also be expected that the region of maximum pressure fluctuations in the rocket flow would be centered a few nozzle exit diameters forward of the tip of the supersonic core.

It should be noted that the magnitude of these pressure fluctuations will be much lower at altitude, since they are proportional to the jet density and hence to the atmospheric pressure. This variation with altitude was demonstrated by the data of Reference 25, in which the pressure fluctuations of the boundary of the jet from an F-94 aircraft were measured at various altitudes up to 30,000 ft.

The spectra of these pressure fluctuations vary with axial position in the same manner as the near field jet noise. Reference 26 gives actual velocity spectra as a function of axial position along a subsonic jet. Note that these spectra must be squared to obtain the pressure spectra. Reference 27 compares the axial location of the peaks of these subsonic spectra with acoustical data for a turbojet at military power. Reference 42 gives near field data for a rocket which enables an approximate estimate of the acoustic spectrum as a function of axial position. The data from these three references can be combined to estimate the approximate spectrum of the fluctuating pressures at any desired axial distance.

Admittedly, this estimation procedure is somewhat crude, necessarily resulting from the lack of data for the pressure fluctuations in the rocket flow. However, it is felt that this procedure will give realistic estimates of the fluctuating pressures resulting from flow impingement on the vehicle which are sufficient for preliminary design. Further, it is expected that the magnitude of these fluctuations, together with the associated high temperatures, will generally be sufficient to persuade the designer to avoid such flow impingement, although this may not always be possible at high altitudes where the jet flow expands through a fairly large angle.

SEPARATED FLOWS AND OSCILLATING SHOCKS

The preceding section discussed the wall pressure fluctuations associated with normal stable turbulent boundary layers which may be anticipated on the skin of a vehicle throughout most of its flight regime. There are, however, two other types of boundary flow irregularities which can result in considerable increases in the fluctuating wall pressures. These may be generally categorized as buffet, which is associated with flow separation, and oscillating shock waves which interact with the boundary layer and oscillate longitudinally. Flow separation usually occurs when the air in the boundary layer is forced to flow around sharp corners, or abrupt convex changes in geometry such as some cockpit canopies. More generally, flow separation occurs when the pressure gradient in the direction of the flow is positive and of a magnitude that causes a reversal of the flow near to the wall. This situation can usually be found on airfoils which are operating close to the stall region.

An example of the high level of turbulent pressure fluctuations downstream of a sharp-edged inlet duct is summarized in Figure 19. Here, measurements were made in the wall of the T-38's inlet duct at a station located approximately 2 ft. downstream of the sharp-edged inlet. The value of $\frac{\sqrt{p^2}}{q}$ obtained during

stationary ground runs is approximately 0.1, whereas in flight this ratio is approximately .008, which is of the order of magnitude expected for boundary layer pressure fluctuations previously discussed. Furthermore, the figure shows that the addition of a bellmouth to the intake for the ground runs reduced $\frac{\sqrt{p^2}}{q}$ from .1 to the flight value of .008. Thus, the data clearly show

that when the flow enters the duct smoothly, either on ground with the bellmouth or in flight where the streamlines are parallel to the duct, that the pressure fluctuations are similar to those found on the skins of other surfaces. However, when the flow is forced around a corner as in the ground operation, with the sharp-edged duct, separation occurs with an attendant tenfold increase in the fluctuating pressures. It might be noted that the acoustic environment during ground operation was sufficiently severe to cause fatigue failures in original riveted single skin panels. Consequently, these flat panels have been replaced with honeycomb construction.

In an analysis of the buffet problems associated with separated flows on lifting surfaces, Leipmann, Reference 16, has indicated from dimensional considerations that for certain conditions the buffet loads should vary with the square root of the dynamic pressure instead of the direct variation. This result is due to the importance of the aerodynamic damping in limiting the response. Similarly, dimensional analysis indicates that if wings of different stiffness were subjected to the same buffeting pressure, the deflections would vary inversely with the square root of the stiffness. Rainey, Reference 17,

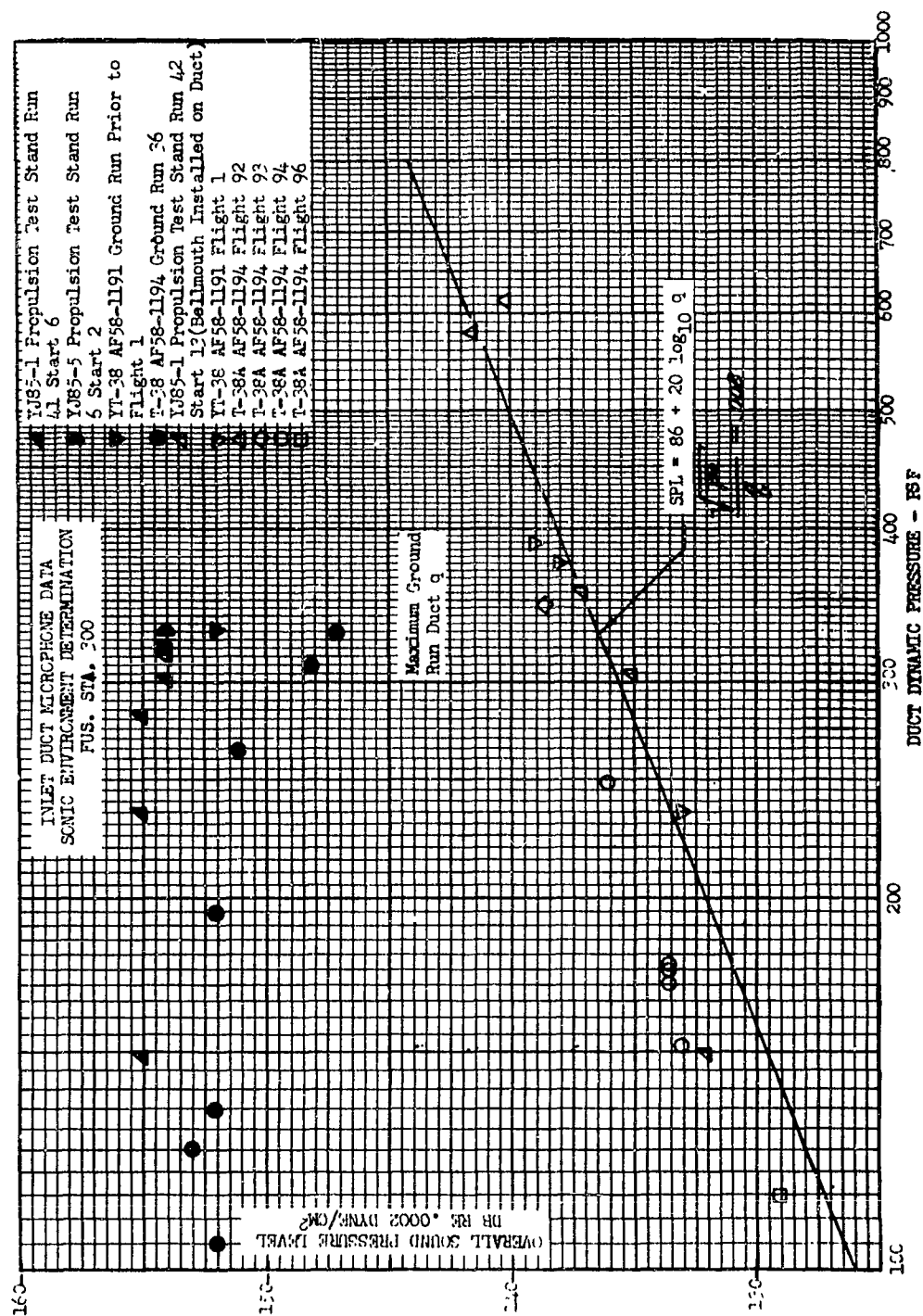


Figure 19. Engine Air Inlet Duct Microphone Data.

confirms this, as well as showing the buffeting forces are not independent external forces but are lessened by the amount of the resulting oscillations. Gross wing stiffness was under discussion in this case, but the conclusion would probably also apply to panels.

An example of the region wherein separated flow and resultant buffet would be expected by the aerodynamicist is given for a NACA 65A009 airfoil in Figure 20 from Reference 18. The figure shows the variation of the normal coefficient, c_n , with Mach number for several angles of attack. Superimposed are given values of the pressure oscillations $\frac{\Delta p}{q}$ where Δp is the peak double amplitude of the pressure fluctuations measured at the skin. Assuming approximately sinusoidal fluctuations, a coefficient of $\frac{\Delta p}{q}$ of .2 would correspond to $\sqrt{\frac{2}{\frac{p}{q}}}$ of the order of .07.

Note that this value compares closely with the value found for the T-38 duct.

Separation of a turbulent boundary layer often occurs behind a normal shock, which is formed when local supersonic flow is slowed to subsonic velocity. Figure 21, taken from Reference 19, gives the minimum ratio of the differential of static pressure (Δp) across the shock to dynamic pressure (q) required for separation of the turbulent flow behind the shock from the skin. At ratios to the left of the curve, separation is not expected.

Another phenomenon of increasing importance is the oscillating shock. This phenomenon was well illustrated by a recent movie of tests on the Mercury capsule presented by NASA which showed very strong shocks near the nose of the vehicle which resulted from several discontinuities in the forward body lines.

The mechanism for oscillation of a shock which interacts with a laminar boundary layer has been investigated by Trilling (References 20 and 21) and is illustrated in Figure 22. Since the shock resulting from the body discontinuity cannot extend to the wall because of finite boundary layer, the differential pressure behind the shock (p_f) is communicated through the boundary layer to the flow ahead of the shock. If the pressure gradient ($\Delta p = p_f - p_i$) across the shock is of sufficient magnitude, the laminar boundary layer will separate and a reverse flow will occur near the wall. Since any motion of the shock affects the pressure differential and, hence, the reverse flow and position of the separated boundary layer; and conversely, any change in the position or shape of the separated boundary layer affects the potential flow and thus, the shock, oscillations are possible whenever these interrelated factors produce an instability.

Figure 23, from Reference 20, gives the magnitude of the pressure coefficient (ΔC_p) across the shock required for oscillations as a function of Mach number. As can be seen in the figure, ΔC_p is approximately one at Mach 1.6 and this is equal to the pressure coefficient for a normal shock. However, at Mach numbers

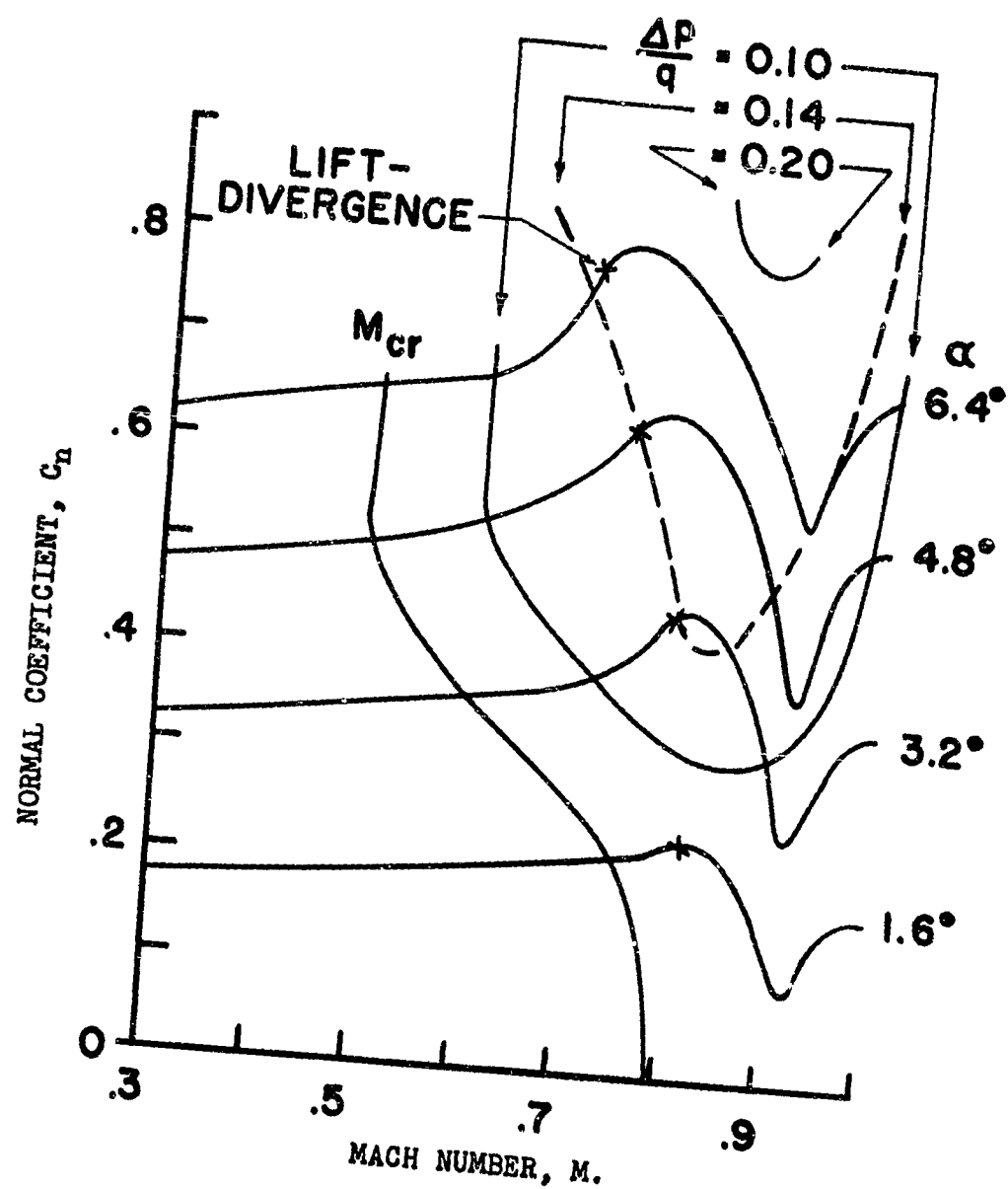


Figure 20. Curves Relating Pressure Pulsations with Normal-force Changes on the NACA 65A009 Airfoil. (from reference 18)

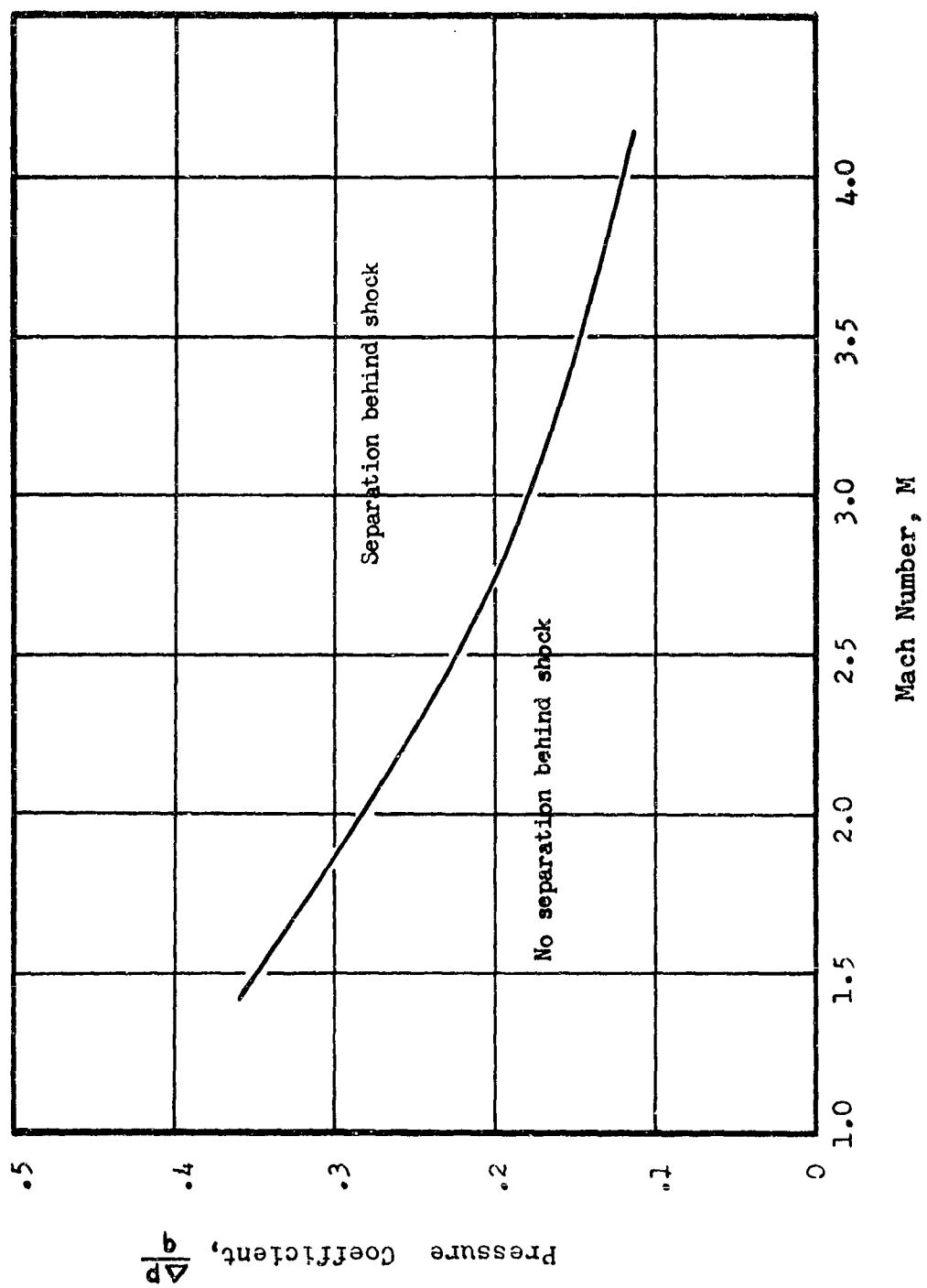


Figure 21. Separation Pressure Coefficients, from reference 19.

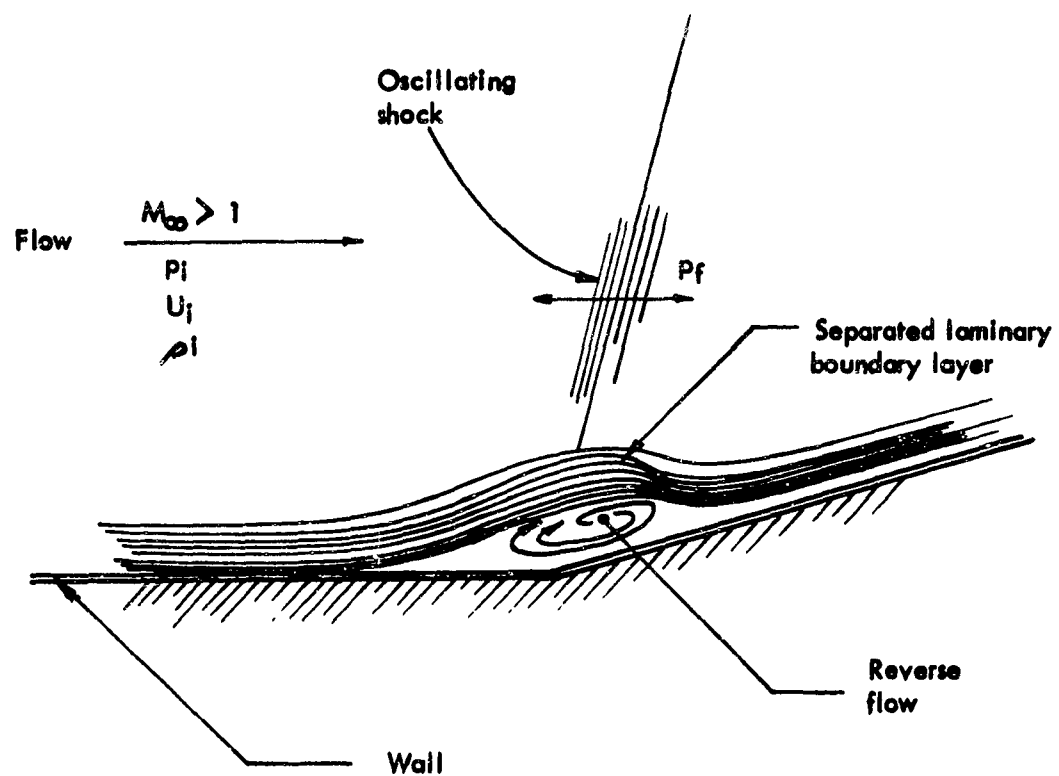


Figure 22. Sketch of shock oscillation as a result of interaction with a laminar boundary layer.

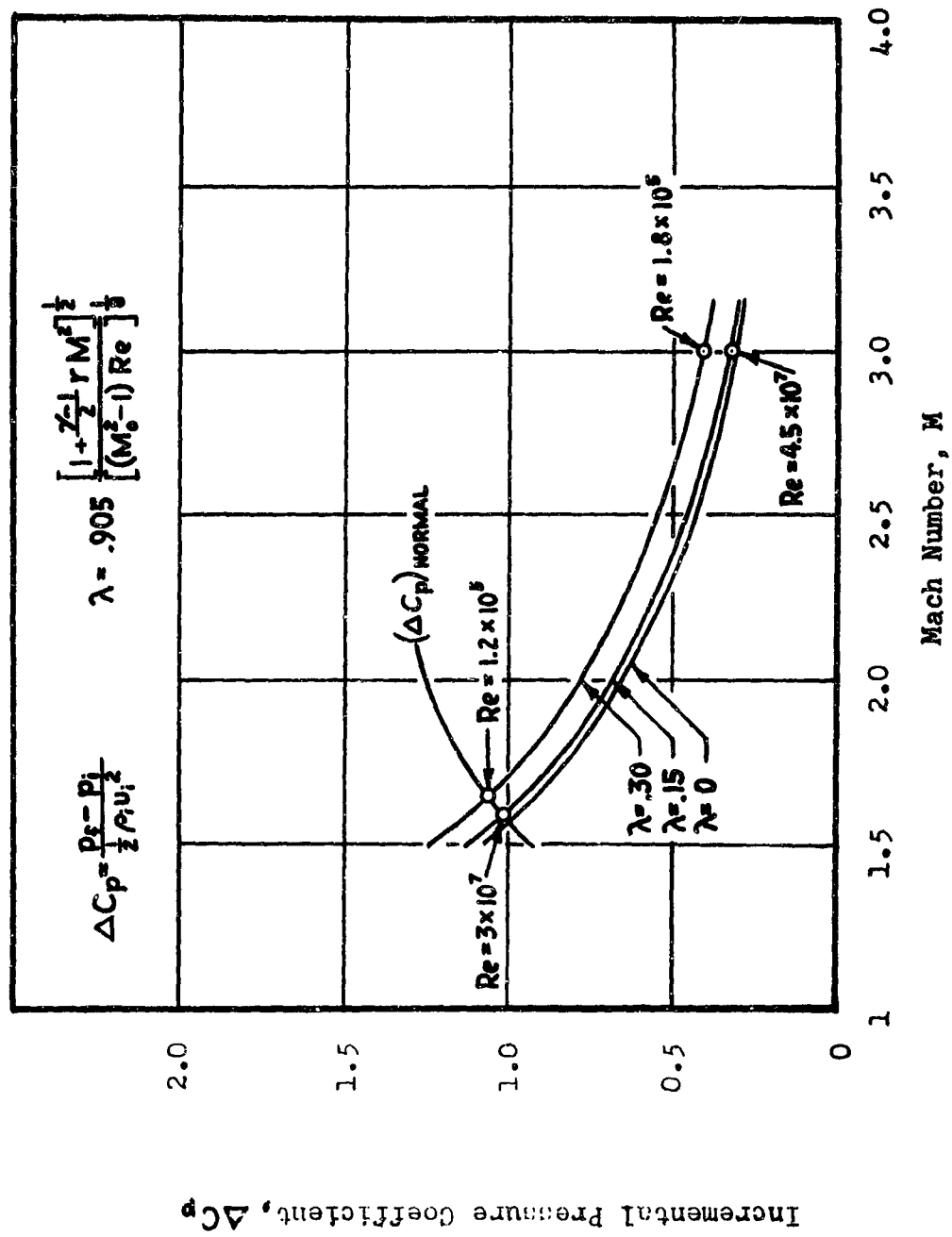


Figure 23. Intensity of the Neutrally Stable Oscillating Shock Wave as a Function of Upstream Mach Number.

above 1.6, ΔC_p decreases below that of a normal shock rather quickly. Hence, at the higher Mach numbers, oscillations occur with the relatively weak shocks associated with small changes in the direction of the wall toward the flow, as in Figure 22.

The frequency of the oscillation predicted by Reference 20 is given for high Reynolds numbers approximately by

$$f = \frac{K U_\infty}{4 \pi L S^n \Delta C_{psh}}$$

where K is the reduced frequency and

$$K_1 \sim 1.8, K_2 \sim 4.8$$

U_∞ is the freestream velocity

L is the length from the leading edge

S is the ratio of the freestream density divided by the wall density

n is the exponent of the viscosity - temperature relationship, and equals .76 in the range of interest

and ΔC_{psh} is the pressure coefficient across the shock alone.

A calculation for the frequency of an oscillating shock - laminar boundary layer for a shock located at a body discontinuity four ft. aft of the nose, for Mach 1.6 gave a frequency of 26 cps. Examination of factors in the formula affecting the frequency show it to be approximately proportional to $M^{2.5}$ and therefore, for the example just considered, the frequency at Mach 3.2 would be about 150 cps.

The interaction between a shock and a turbulent boundary layer on an airfoil operating in the transonic regime is described by Lambourn in Reference 22. As the Mach number increases, the flow over the top of the wing becomes supersonic through the region of maximum thickness and slows down through a shock toward the trailing edge. As the Mach number increases further, the shock moves further toward the trailing edge and becomes stronger, until in some cases it causes separation of the flow and the shock moves forward. Since this separation of flow results in a loss of lift, the angle of attack must be increased to maintain altitude, and this change causes the shock to move aft again increasing the lift once more. Note that this cycle could occur at speeds near a wing flutter region and accelerate failure.

It is doubtful whether oscillating shock wave phenomena on a complex configuration can be predicted analytically with satisfactory accuracy. Hence, it is

important to investigate these phenomena carefully by wind tunnel tests where considerable effort should be exerted toward simulating the full scale boundary layer flow.

FLOW OVER CAVITIES

Many severe vibration problems have resulted in aircraft when bomb bay and other similar compartments have been opened during flight. These vibrations, which may be very intense are caused by a combined acoustic and flow oscillation in the recessed bay or cavity. Although space vehicles will not have open weapon bays or wheel wells during the atmospheric portion of their flight, they may have recesses and cavities along their exterior, particularly where sections of the vehicle have been joined together. Often the frequency of the vibration resulting from aerodynamic excitation of these smaller cavities will be in the range where electronic tubes are most susceptible to microphonics. Consequently, it is desirable to eliminate these external cavities wherever possible, thus eliminating one source of vibration excitation.

The cavity resonance phenomenon is not completely understood. However, several experimental studies have been undertaken which enable an estimate of the resonance frequency and pressure amplitude. The following paragraphs will briefly review these data and discuss possible causes of the resonance phenomenon.

Figure 24 illustrates the flow past and within a cavity of length, L , and depth, d . As can be seen the boundary layer flow over the cavity transfers some of its momentum to the air in the cavity, creating one or more vortices within the cavity. Measurements made by Roshko (Reference 28) in a cavity mounted in a wind tunnel indicate that the maximum vortex velocity along the downstream cavity wall is approximately $.45 U_{\infty}$ decreasing to $.2 U_{\infty}$ along the bottom and the forward wall. His measurements also showed that pressure maxima were present at each corner, the largest found at the intersection of the boundary layer and the downstream cavity wall.

The effect of the vortex's circulation on a series of constant phase surfaces of an acoustic wave radiated from the lower downstream corner is increased with forward direction along the bottom and forward vertical wall by the vortex velocity and decreased vertically along the aft wall of the cavity by the vortex. Note that the magnitude of this effect on the propagation velocity and, hence, the shape of these constant phase contours is dependent upon the Mach number of the flow and the number of vortices in the cavity. The vortex circulation velocity also modifies the normal acoustical resonances within the cavity. For example, based on Roshko's data, the frequency (f) for the longitudinal one-half wave acoustical resonance in the lower portion of the cavity, away from the opening, is modified by the vortex flow in the cavity so that the resonance frequency is given approximately by:

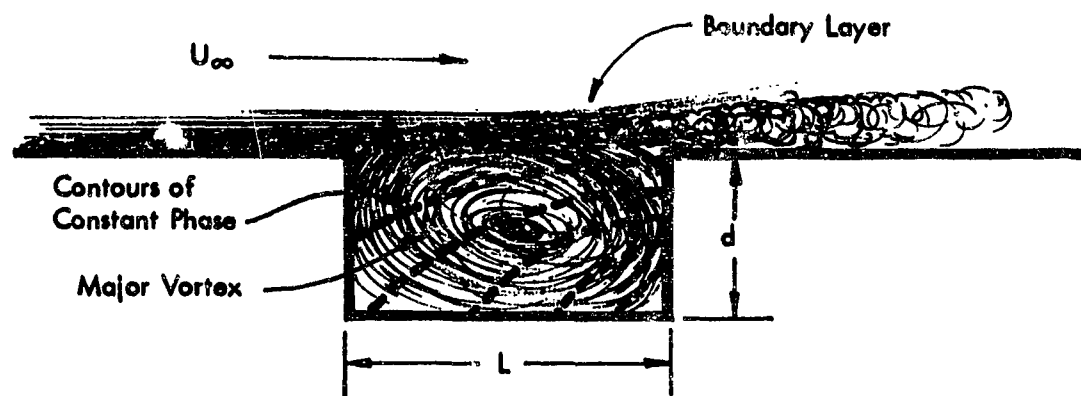


Figure 24. Illustration of Flow Past Cavity, Showing Vortex Formation in Cavity and Effect of Vortex Velocity on Propagation of an Acoustic Wave.

$$f_L = \frac{a(1 - M_\infty^2)}{2L}$$

where a is the local speed of sound,
 M_∞ is the freestream Mach number, and
 L is the length of the cavity

This formula indicates that the one-half wave longitudinal resonance is decreased from its zero flow value as the freestream Mach number is increased. A calculation of the one-quarter wave acoustical resonance between the base of the cavity and the opening of the cavity indicates that its frequency will also decrease with increasing Mach number. In addition, both of these resonances vary in frequency as a function of position in the cavity because of the variation in circulation velocity. Consequently, it would not be expected that either of these resonant phenomena would be self-sustaining except, perhaps, at very low Mach numbers.

The investigators of cavity resonance phenomena (References 28, 29, 30) have all suggested that the resonance results from interaction between an acoustic wave and the boundary layer - vortex flow, where an acoustic wave propagated from the aft bottom corner of the cavity affects the boundary layer flow over the cavity. This interaction with the boundary layer results in a modulation of the momentum transferred from the boundary layer to the vortex and, hence, a modulation of the vortex circulation velocity and the resultant stagnation pressures in corners of the cavity. Although the exact form of this interaction is unknown, experimental evidence suggests that the length of the cavity is on the order of one wavelength at the dominant resonant frequency. Figure 25 gives the cavity Strouhal number associated with the dominant resonant frequency as a function of freestream Mach number for the data of References 29 and 30. As can be seen, the fundamental cavity resonant frequency is inversely proportional to its length and directly proportional to approximately the two-thirds power of the freestream velocity. Examination of the full scale data from Reference 30 indicates an additional small altitude effect on the frequency.

Other cavity resonance frequencies, including one-half, one and one-half, and two times the dominant frequency, have been found together with the dominant frequency. The occurrence of these other frequencies in both experiments (References 29 and 30) was dependent upon either boundary layer turbulence or the dimensions of the cavity.

The maximum rms amplitude of the pressure fluctuation appears to be on the order of .03 to .06 of the freestream dynamic pressure (q) (References 28 and 30). Note that these values are on the order of 5 to 10 times greater than the ratio of the overall rms turbulent boundary layer pressure fluctuations to the freestream dynamic pressure, previously discussed in this section. Also, when the cavity resonant frequency coincides with the frequency of one of the cavity's acoustical modes, the pressure amplitude would be expected to be even greater.

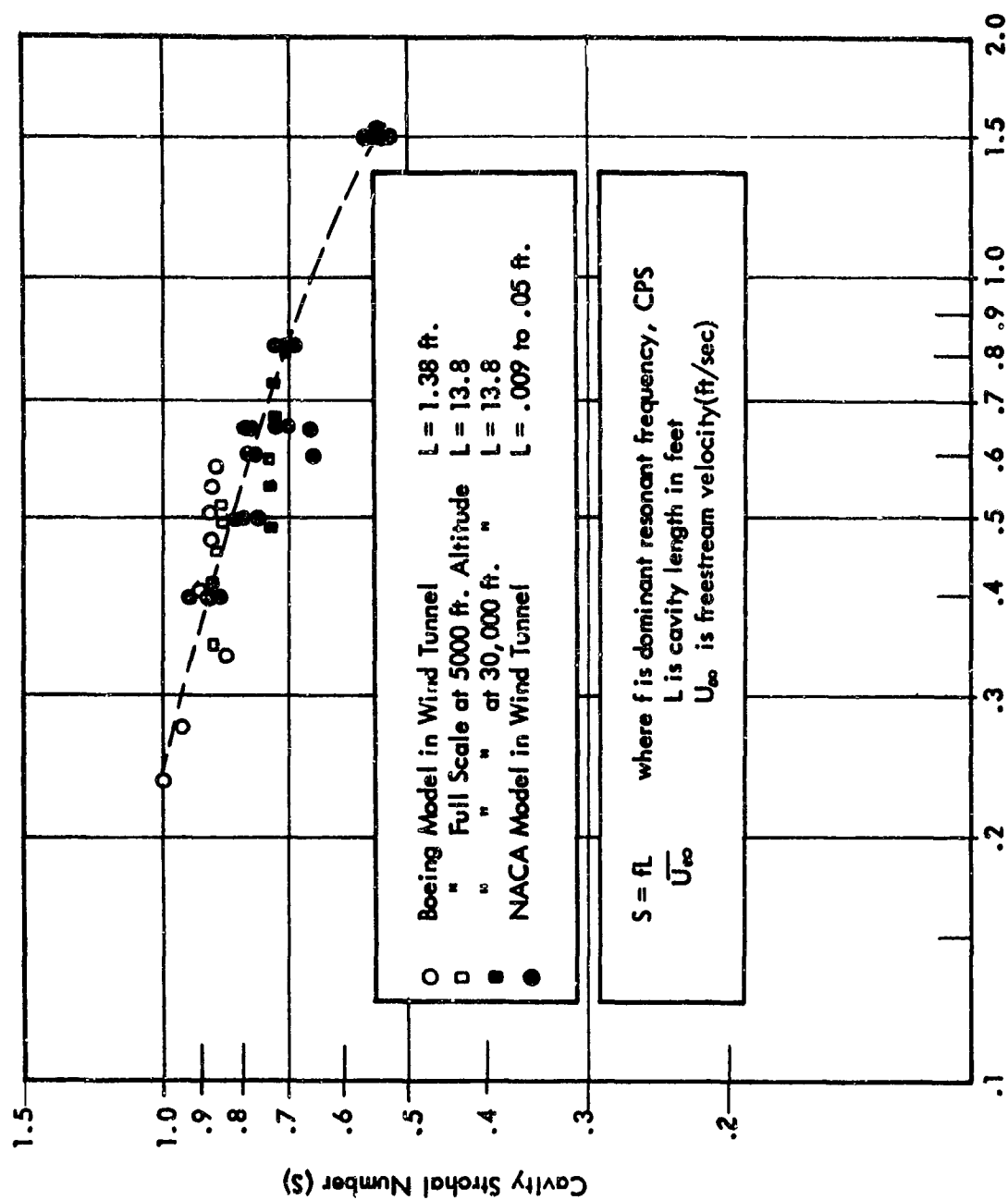


Figure 25. Strouhal Number of Dominant Cavity Resonance as a Function of Mach Number from Data of Refs. 2 and 3.

This suspicion is confirmed in analysis of the Reference 30 data where the ratio of rms pressure to freestream dynamic pressure increased to .1 when the cavity resonant frequency coincided with the modified longitudinal one-half wave acoustical resonance. Thus, cavity resonances can be expected to be most serious either during the high q portions of flight, or at any flight condition when the cavity resonant frequency is coincident with the modified acoustical modes of the cavity.

It should also be mentioned that openings which connect the flow past the missile with a large volume within the missile can be expected to behave as classical Helmholtz resonators, which are treated in the normal acoustical texts. The Helmholtz resonant frequencies will be much lower than those considered here for the cavity phenomena and will be approximately constant over a wide range of vehicle velocities.

FLOW PAST PROJECTIONS

Space vehicles and hypersonic gliders may have guidance fins, antennas, or other projections extending from the body of the vehicle into the surrounding atmosphere. When the vehicle moves, these projections generate turbulent wakes in the flow. Although these wakes radiate acoustical energy to the body of the vehicle, their major importance as a vibration source is their direct effect on the projection or impingement on the vehicle. Since, as will be shown, the fluctuating pressures associated with this type of wake are concentrated about two discrete frequencies, these pressure fluctuations are often responsible for the apparent superposition of discrete frequency energy on otherwise random pressure spectra. Therefore, a brief discussion of this phenomenon is of interest. It is also noted that these phenomena are of importance to the entire vehicle when it is stationary on the launch pad and exposed to wind.

Generally, little energy is contained in the wake of streamlined projections. However, when the flow on the projection separates from the surface, vortices are formed which contain considerable energy. Figure 26 illustrates the wake of a cylinder which is at a relatively low Reynolds number (R_e) (below approximately 150). Here, the flow is characterized by the alternate shedding of discrete paired vortices from the cylinder, forming the well known Karmen Vortex Street. However, as the Reynolds number increases, the vortices lose their individual identity, and the wake becomes generally turbulent.

The frequency (f) at which the vortex pairs are shed from a cylinder is proportional to the freestream velocity (U_∞) and inversely proportional to the cylinder diameter (d). The correlation between the Strouhal number (S), where $S = \frac{fd}{U_\infty}$ and the cylinder Reynolds number is given as a function

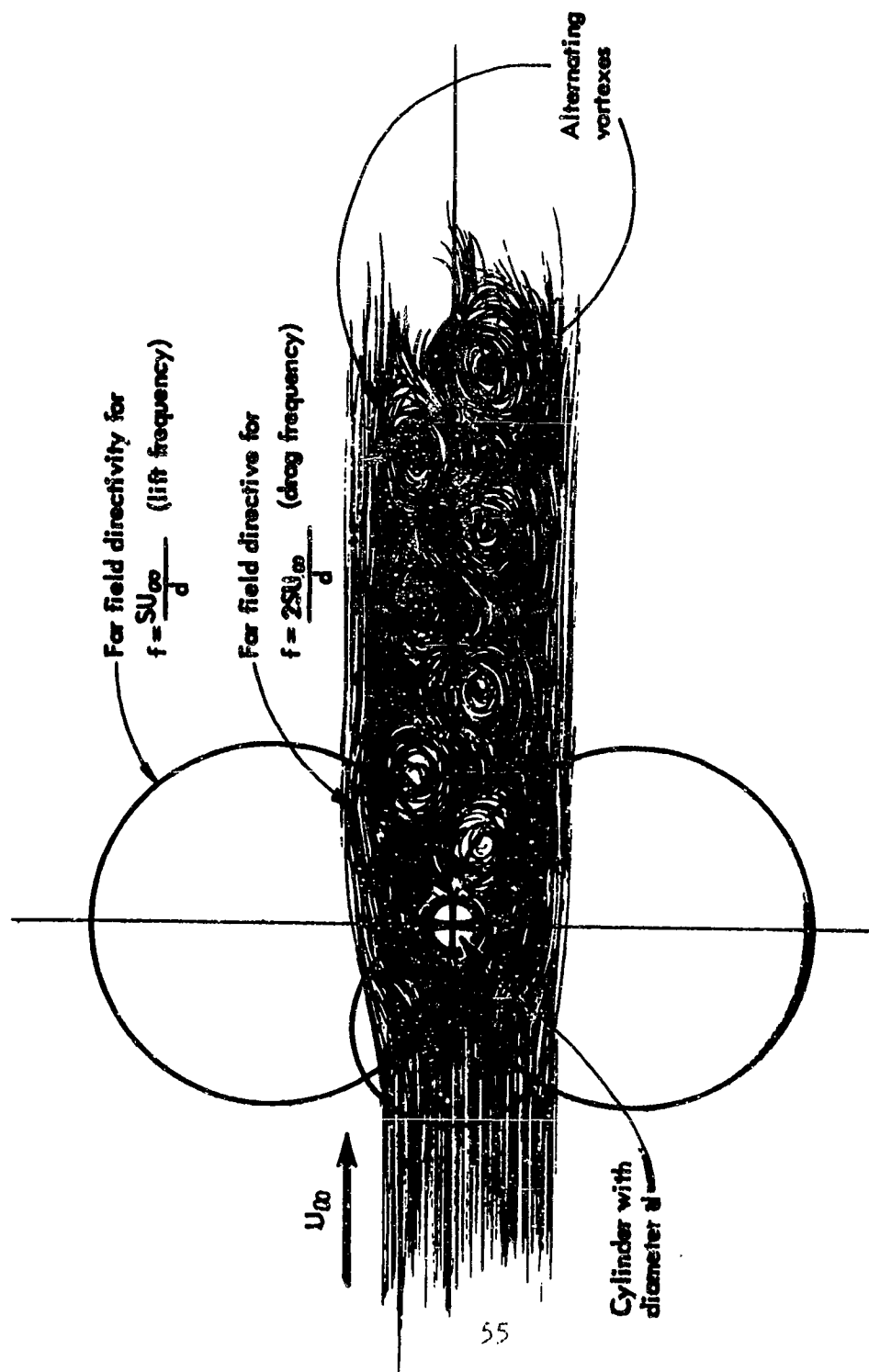


Figure 26. Illustration of Vortex Formation in the Wake of a Cylinder at a Reynolds Number Below 150, and Illustration of the Acoustical Radiation Pattern at the fluctuating Lift and Drag Frequencies.

of cylinder Reynolds number, $R_e(c)^*$ in Figure 27. This figure, taken from Reference 31, includes the results of many experimental investigations. As can be seen, the frequency for the shedding of a pair of vortices is approximately $\frac{2 U_\infty}{d}$ over a considerable range of Reynolds number above $R_e(c) = 150$.

It should be noted that this frequency is characteristic of the flow even at higher Reynolds numbers where the idealized flow of Figure 26 is made considerably more complex by turbulence (see Reference 32).

This shedding of vortices from alternate sides of the cylinder results in an alternating lifting force on the cylinder which is perpendicular to both the cylinder axis and the flow. In addition, as each individual vortex is shed, the cylinder's drag is suddenly varied, with the result that the cylinder is subjected to an alternating drag force in the direction of the flow. The frequency of this fluctuating drag is twice that of the fluctuating lift. It is noted that although the vortices become rather unidentifiable when the Reynolds number exceeds 300, the fluctuating pressures are still found to be concentrated at these two frequencies. However, as the velocity increases the bandwidth of the fluctuating pressure frequency spectrum widens and the pressures are expected to be in phase over progressively smaller distances along the projection. Generally, the fluctuating drag has a considerably lower force than the fluctuating lift (see, for example, References 33 and 34); however, any estimates of the magnitudes of either of these forces depend entirely upon the geometry of the projection.

These wakes have been generalized by Krzywoblocki, Reference 37. A permanent vortex sheet attaches to a wing or body producing lift, but as it deforms and rolls up rapidly behind a delta wing or behind a cylindrical body, its regular character is soon lost and the flow changes to isotropic turbulence with the transition dependent on the Reynolds number. The transition from a defined vortex sheet to turbulent flow occurs in a short distance at high Reynolds number and it is interesting to note the analogy between the boundary layer transition and the transition of the Von Karman vortices behind the cylinder. In each case at low Reynolds number very regular flow patterns persist even though laminar boundary layer flow is irrotational and the vortex sheet flow is rotational. This follows since the Reynolds number is the ratio of the fluid inertia forces to the viscous forces, and at low Reynolds number the viscous forces predominate and have the ability to damp completely the stray fluctuations which at high Reynolds number can grow to eventually cause chaotic flow.

*The Reynolds number for a cylinder $R_e(c)$ is given by:

$$R_e(c) = \frac{U_\infty d}{\gamma_\infty}$$

where U_∞ is the freestream velocity,

d is the cylinder diameter

and γ_∞ is the freestream kinematic viscosity

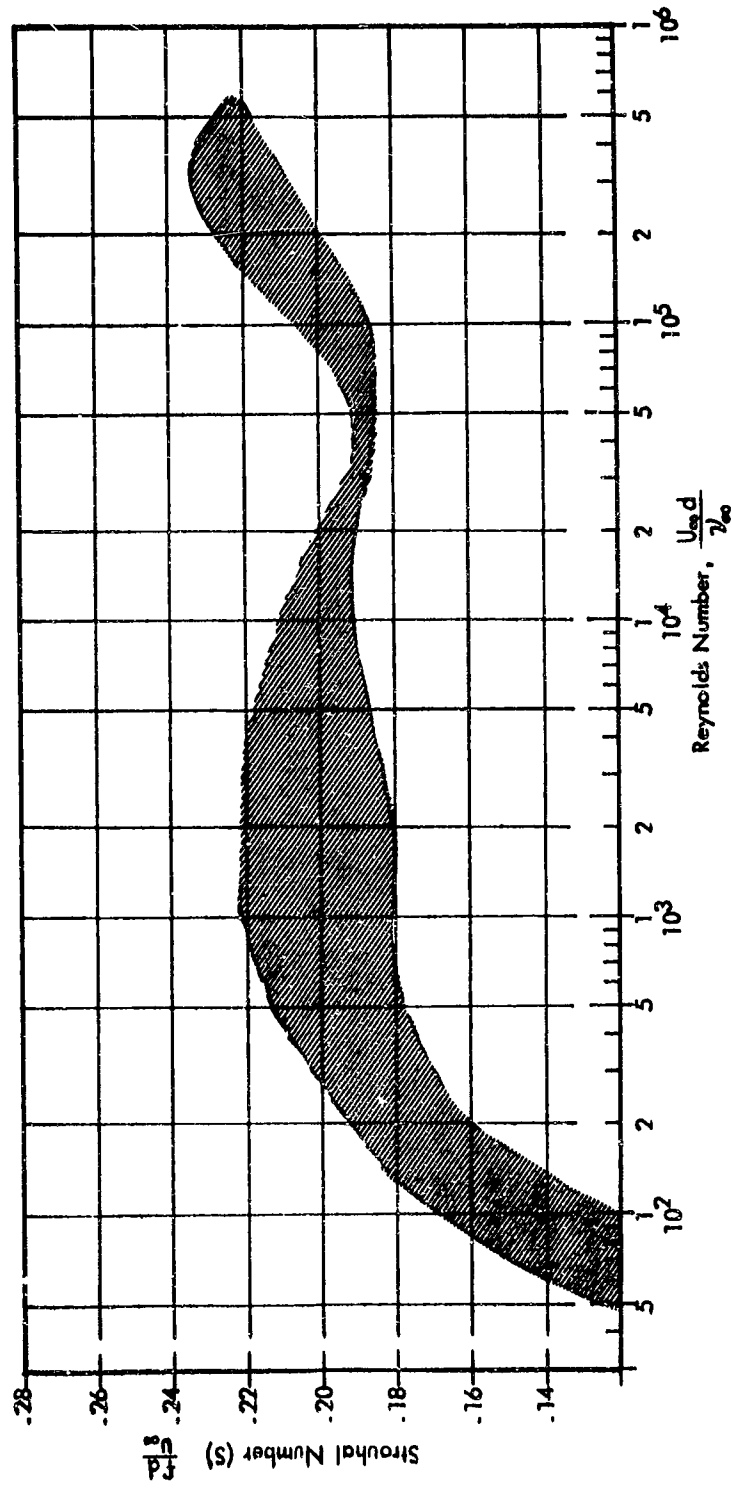


Figure 27. Comparison of the Strouhal Number Associated with the Shedding of Vortex Pairs from Cylinders as a Function of Reynolds Number, Including Data from Many Investigations (taken from Etkin, et al, Ref.31)

These fluctuations are also responsible for the radiation of acoustic energy. Figure 26 shows that the far field directivity of the acoustic pressures at the vortex shedding frequency is maximum at right angles to the flow, whereas the directivity of the acoustic pressures associated with the fluctuating drag has a maximum in line with the flow. It is noted that the maximum at right angles to the flow should shift forward with increasing subsonic Mach number (Reference 35). The magnitude of the acoustic power has been found, from theoretical considerations, to depend upon the sixth power of velocity, the square of the projection's area, and on the fluctuating lift or drag coefficient (References 31 and 36). An additional dependence on velocity would be expected because of the forward motion of the source in accordance with Reference 35. However, experimental data indicate that the acoustic power is proportional to a lower power of velocity than the sixth, varying between 4 and 5.5 which makes prediction difficult.

Another vibration source associated with projections from a vehicle is the direct impingement of the wake from the projection on the skin of the vehicle. An example of the fluctuating pressures on the skin at a position several feet downstream of the speed brake on the T-38 is given in Figure 28. As can be seen, the ratio of $\frac{\sqrt{p^2}}{q}$ increases by a factor of three from that experienced

with a normal turbulent boundary layer to approximately .02 when the brake is extended and the skin experiences the wake turbulence. It might be noted that the velocity ratio η utilized in the estimation of jet impingement on the skin is of the order of .01 for this example of wake impingement.

BASE PRESSURE FLUCTUATIONS

Recently, considerable vibration has been experienced at the fundamental longitudinal mode and at other internal resonance frequencies of a vehicle which had a blunt nose during the maximum dynamic pressure phase of flight (Reference 38). This vibration was believed to result from the turbulent fluctuations in the wake of the base or drag device, as shown in Figure 29. Correlation of the vibration response with flight parameters indicated a direct relationship between rms vibration response and $(q \sim U_\infty)$, where q_∞ is the freestream dynamic pressure and U_∞ , the freestream velocity. From this empirical relationship it is clear that the vibration from blunt base excitation becomes of increasing concern at very high speed flight in the atmosphere.

Although the author of Reference 38 felt that pressure fluctuations on the blunt base, as shown in Figure 28, were responsible for the excitation in the same manner as the previously discussed fluctuating drag on projections, no data were available to give the magnitude and spectra of these fluctuations. However, a subsonic experiment designed to measure these base pressure fluctuations has been completed (Reference 39). In this wind tunnel experiment data were taken at two microphone locations (center and 65% radius) in the base of a 5-in. diameter body of revolution at velocities up to 352 ft/sec.

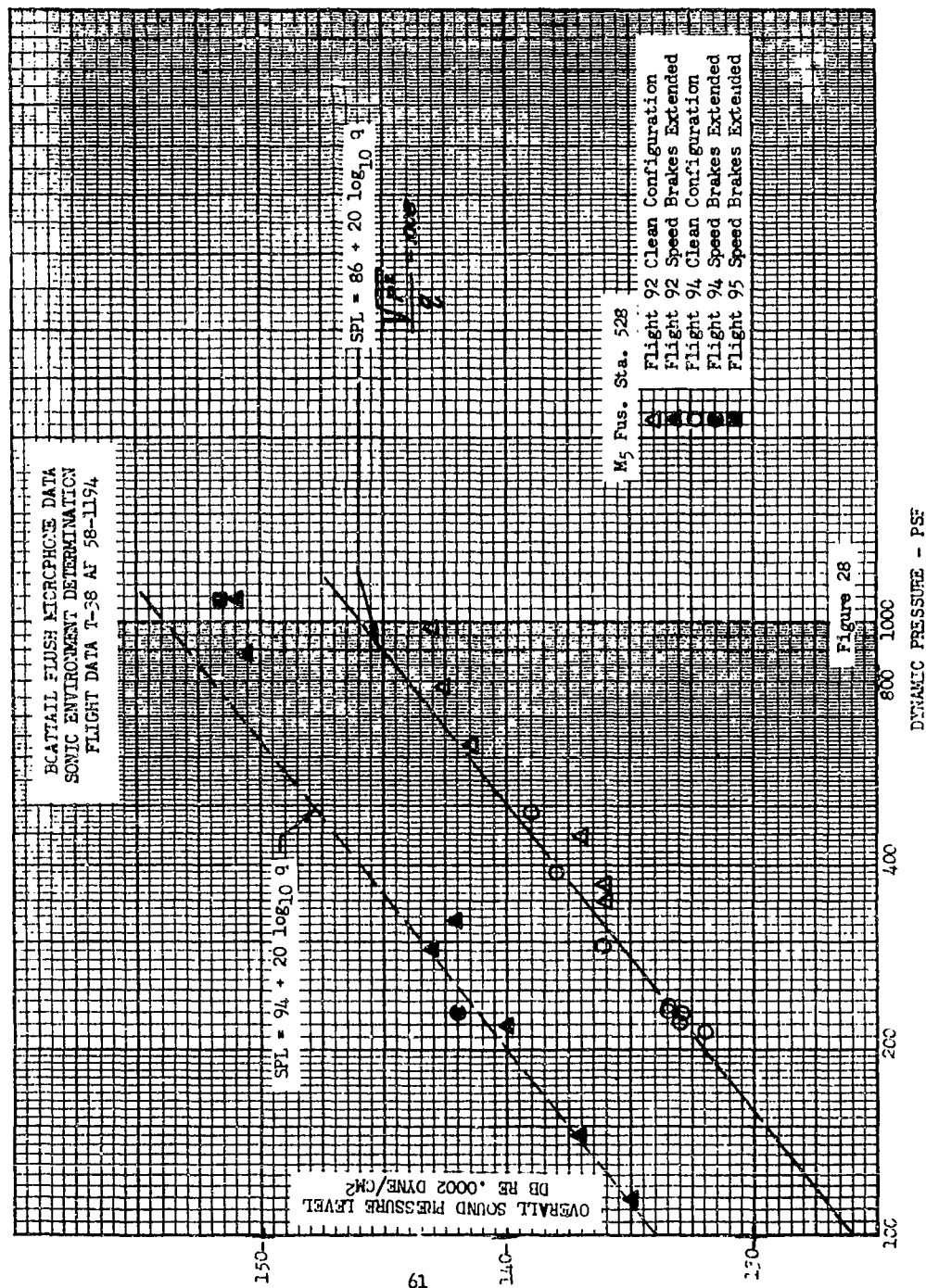


Figure 28. Aft Fuselage Microphone Data

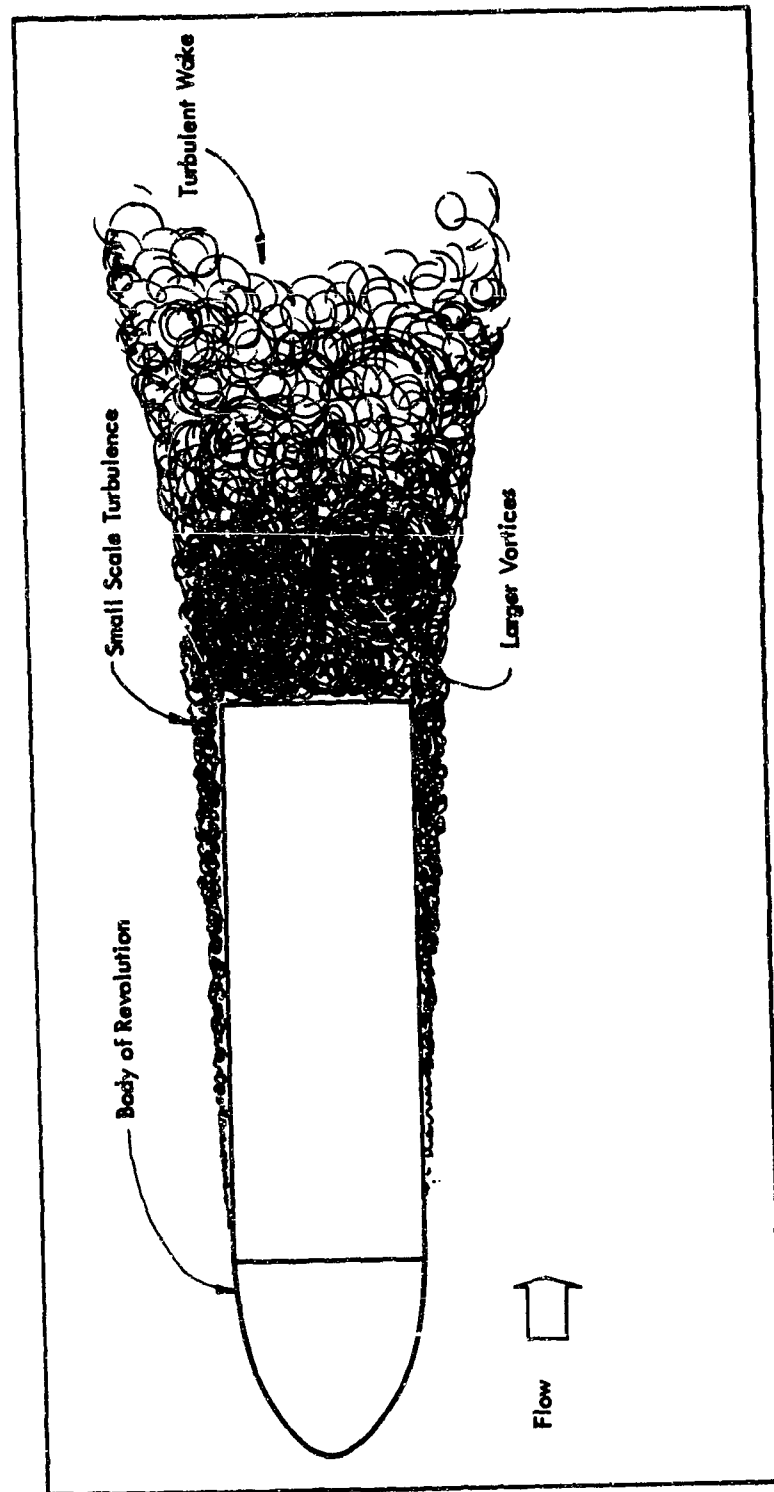


Figure 29. Sketch Illustrating Wake Formation of a Blunt Based Body of Revolution

Figure 30 gives the variation of the overall level of base pressure fluctuations as a function of freestream velocity. It is clear from the data that the overall fluctuation level at the center position is approximately 7 db below that measured at the outer microphone position (65% radius). Further, as the freestream velocity is increased, the fluctuation level at each position is asymptotic to a constant value of root mean square pressure divided by free-stream dynamic pressure. Figure 31 gives the mean square pressure per cycle, divided by the freestream dynamic pressure and normalized by $\frac{U_{\infty}^2}{d}$, as a

function of Strouhal number. The results illustrate that the spectra at the two positions are similar at frequencies above a Strouhal number of .5. However, for frequencies below a Strouhal number of .5, the energy per cycle is greater at the outer microphone than at the center microphone.

This suggests that only the outer portions of the base are affected by large scale vortices shed from the edge of the cylinder, as illustrated in Figure 29. This result is consistent with the variation in pressure measured by Gerrard (Reference 33) at the surface of a cylinder which has an axis normal to the flow. As it would be expected that the larger scale vortices are randomly shed from all portions of the base circumference, it is probable that the integrated loading on the base can be summed on an energy basis.

It should also be noted that the spectra given in Figure 31 explain the departure from a linear relationship between the overall fluctuating pressures and the freestream dynamic pressure. The lower cutoff frequency of the recording instrumentation was 18 cps, which corresponds to a Strouhal number of approximately .11 at 68 ft/sec. and .052 at 146 ft/sec. Hence, little of the maximum energy per cycle was included in the 68 ft/sec. measurement, and some energy was not included even at the 146 ft/sec. velocity. A rough calculation of the overall level of base pressure fluctuation at the 68 ft/sec. velocity, which includes the energy estimated below 18 cps from Figure 31 gives a constant of $\frac{\sqrt{p^2}}{q_{\infty}}$ equal to .013 for the outer microphone, which is consistent with the constant of .015 determined from the higher velocity data.

Although the data of Reference 38 does not allow prediction of the magnitude of the missile's vibration response, the variation of vibration amplitude with flight parameters can be directly compared to the variation which would be estimated from Figure 30. It was stated in Reference 38 that the response was almost entirely at the frequency of the fundamental longitudinal mode. The Strouhal number at this resonance frequency varies inversely with the freestream velocity, since both frequency and diameter are constant. Now, from Figure 31 it is seen that the relative mean square pressure per cycle varies inversely as the square of the Strouhal number for all Strouhal numbers above approximately .3, and is essentially independent of Strouhal numbers below the Strouhal number of .1. Therefore, at any fixed resonant frequency in an airframe or missile of diameter (d) which results in a Strouhal number greater than .3, the relative mean square pressure per cycle is directly proportional to the square of the freestream velocity times the square of its dynamic

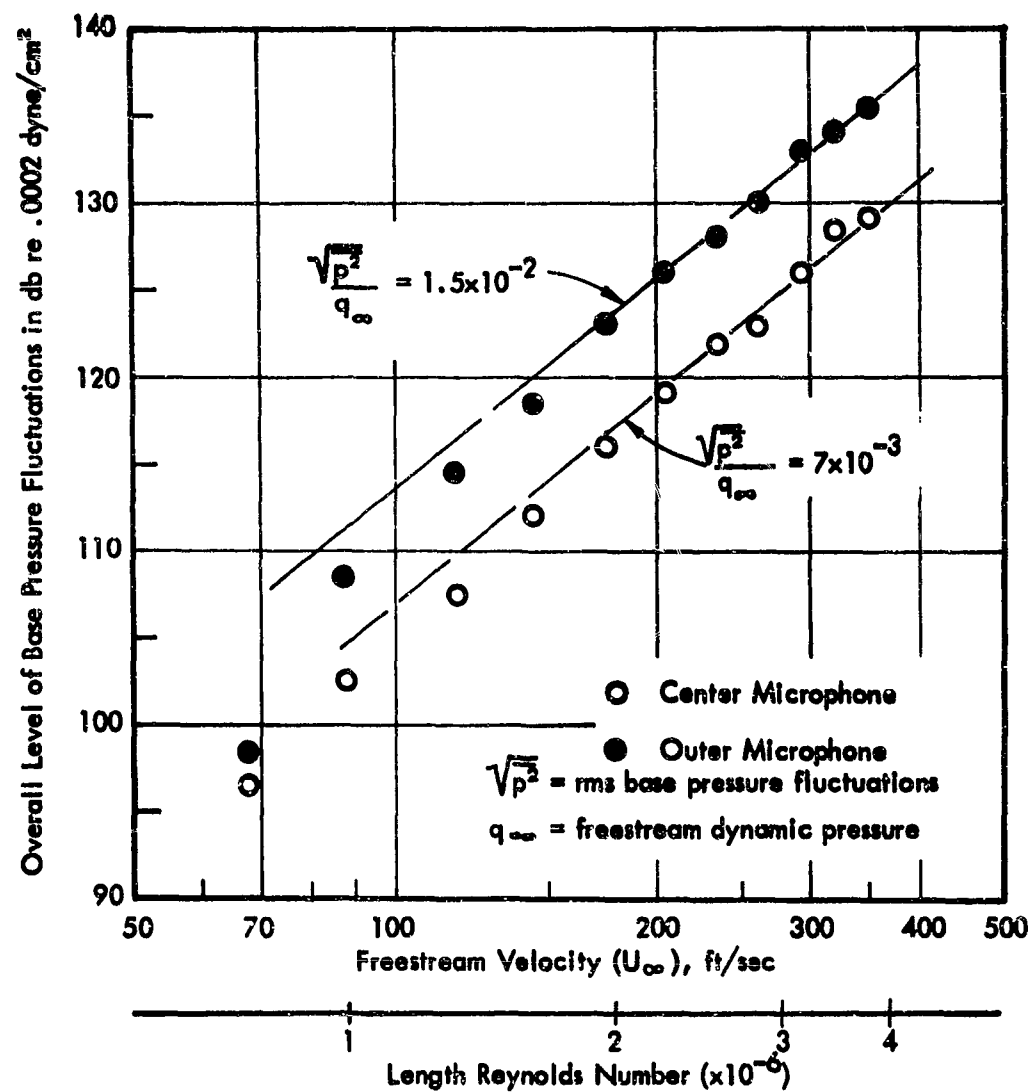


Figure 30. Variation of Overall Level of Base Pressure Fluctuations with Freestream Velocity

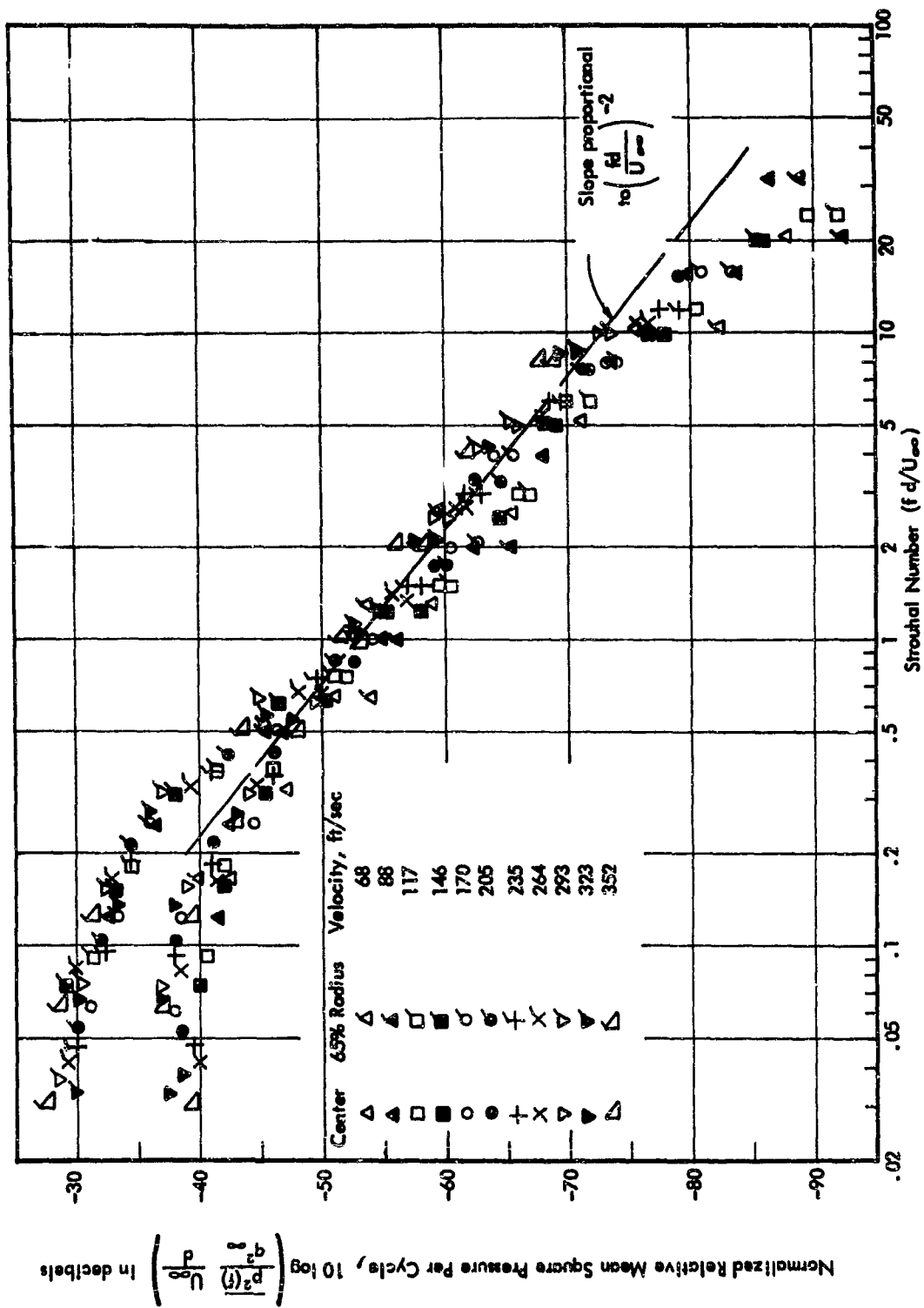


Figure 31. Mean Square Pressure Per Cycle Relative to the Dynamic Pressure, Normalized by $\frac{p}{U_\infty}$ for Both Microphones.

pressure; thus, the rms pressure per cycle is

$$\sqrt{p^2(f)} \sim q_{\infty} U_{\infty}^{1/2}, \text{ for } \frac{fd}{U_{\infty}} > .3$$

which is similar with the measured rms vibration response.

It is felt that the data obtained from the model qualitatively explain the variation of vibration response with flight parameters. However, it must be noted that much of the flight vibration data were obtained at supersonic velocities, whereas the model data are entirely subsonic. Consequently, since the supersonic wake flow differs from subsonic wake flow, as can be seen in the illustration of Figure 32, some question exists regarding the applicability of these data to the supersonic case. It would be expected that the larger vortices, which increased the low frequency levels at the outer microphone, would be absent in the supersonic flow, and that the pressure fluctuations over the base from the turbulent wake would have the general character observed at the center microphone in these tests.

PANEL FLUTTER

Panel flutter is a self-excited oscillation of an external structural skin panel exposed to supersonic flow. The mechanism producing the instability is the same as in classical flutter; i.e., the free vibration modes of the panel are coupled by the aerodynamic forces to yield certain definite combinations of the modes which are capable of extracting energy from the airstream. The motion is characterized by a high degree of structural non-linearity due to the non-linear spring rate of the panel. The panel is quite flexible at low loads and very stiff at high loads. The spring rate depends also on the non-linearities associated with the nearness to buckling, transverse static pressure difference, and the curvature of the panel. The effect of these non-linearities is usually to limit the amplitude of the instability so that the typical mode of failure is through fatigue of the panel rather than through exceeding the strength limit.

While panel flutter is a possible source of outer skin panel vibration, the cure must lie with prevention of the instability and not with treatment as a fatigue problem in which a portion of the life of the panel is expended in normal service. Panel flutter is a true instability and there does not exist a method capable of defining the upper limit to the motion. However, panel flutter can be prevented through the use of the empirical design data of References 40, 41, and 42. Reference 43 shows failure to include the boundary layer in previous theoretical work leads to skin requirements too high by as much as one order of magnitude.

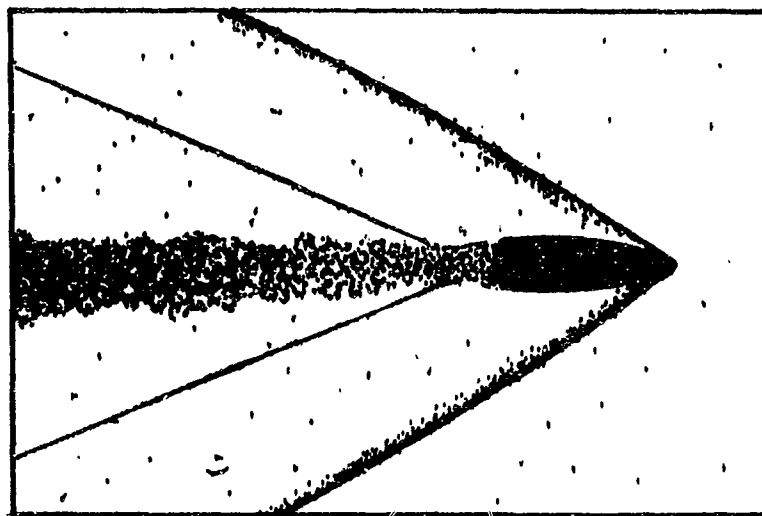
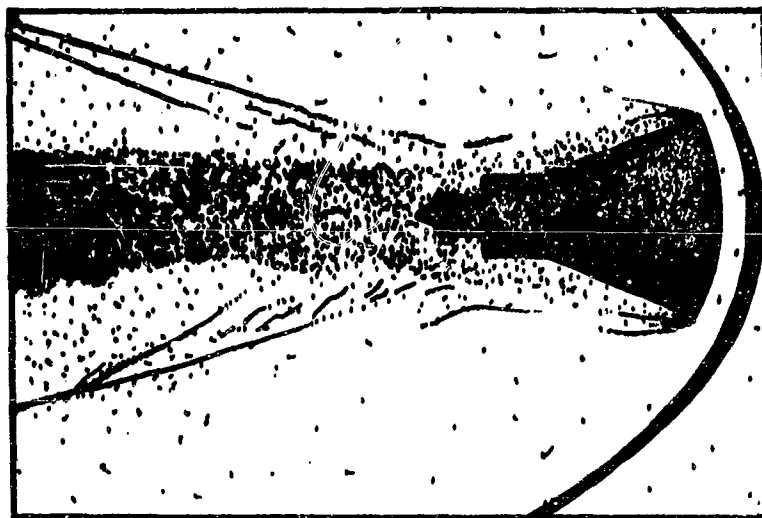


Figure 32. Illustration of Turbulent Wakes from Two Types of Blunt Bodies at Supersonic Speeds.

REFERENCES

1. Schlichting, Dr. Hermann, "Boundary Layer Theory," per Gamon Press, New York, 1955.
2. Howarth, L. (Ed), "Modern Developments in Fluid Dynamics," High Speed Flow, Vol. II, Clarendon Press Oxford, 1953.
3. Willmarth, W. W., "Space-Time Correlations and Spectra of Wall Pressure in a Turbulent Boundary Layer," NASA 3-17-59W, March 1959.
4. Harrison, Mark, "Pressure Fluctuations on the Wall Adjacent to a Turbulent Boundary Layer," ASTIA 1260, Dec. 1958.
5. Kraichnan, Robert H., "Pressure Fluctuations in Turbulent Flow over a Flat Plate," JASA, May 1956.
6. Kraichnan, Robert H., "Noise Transmission from Boundary Layer Pressure Fluctuation," JASA, Jan. 1957.
7. Ribner, H. S., "Boundary Layer-Induced Noise in the Interior of Aircraft," UTIA No. 37.
8. McLeod, Norman J. and Jordan, Gareth H., "Boundary Layer Noise at Subsonic and Supersonic Speeds," Published in NACA Symposium Proceedings, Langley, 1959.
9. McLeod, Norman J. and Jordan, Gareth H., "Preliminary Flight Survey of Fuselage and Boundary Layer Sound Pressure Levels," NACA RM H58H11, May 13, 1958.
10. Leech, "Boundary Layer Noise Measurements on the F102A Aircraft," to be published by Aero Medical Lab as WADC Tech. Note.
11. Nelson, W. L., and Alaia, C. M., "Aerodynamic Noise and Drag Measurements on a High-Speed Magnetically-Suspended Rotor," WADC TR 57-339, ASTIA No. AD 142153, January 1958.
12. Mull, Harold R. and Algranti, Joseph S., "Preliminary Flight Survey of Aerodynamic Noise on an Airplane Wing," NACA RM E55K07, March 2, 1956.
13. Sandborn, Virgil A. and Slogar, Raymond J., "Longitudinal Turbulent Spectrum Survey of Boundary Layers in Adverse Pressure Gradients," NACA TN 3453, May 1955.
14. Kistler, Alan L., "Fluctuation Measurements in Supersonic Turbulent Boundary Layers," ASTIA No. AD 211278, August 1958.
15. Eldred, Kenneth M., "Review of Experimental Data Regarding Boundary Layer Pressure Fluctuations and Noise," to be published.

16. Liepmann, "Parameters for Use in Buffeting Flight Test," SM-14631, Douglas Aircraft, January 1953.
17. Rainey, "Examination of Methods of Buffet Analysis Based on Experience with Wings of Varying Stiffness," NASA TN D-3, August 1959.
18. Humphreys, "Pressure Pulsations on Rigid Airframes at Transonic Speeds," NACA RM L51-112, 1951.
19. Mager, "Prediction of Shock-Induced Turbulent Boundary Layer Separation," Journal of the Aero/Space Sciences, March 1955.
20. Trilling, "Oscillating Shock - Boundary Layer Interaction," Journal of the Aero/Space Sciences, May 1958.
21. Hakkinen, R. J., Greber, I., Trilling, L., and Arbarbanel, S. S., "The interaction of an Oblique Shock Wave with a Laminar Boundary Layer," MIT, FDRG Report #57-1, May 1957. To be published as an NACA Technical Note.
22. Lambourne, "Some Instabilities Arising from Interactions Between Shock Waves and Boundary Layers," Agard Report 182, April 1958.
23. Love, E. S., Lee, Louise P., "Shape of Initial Portion of Boundary of Supersonic Axisymmetric Free Jets at Large Jet Pressure Ratios," NACA TN 4195, January 1958.
24. Laurence, J. C., "Intensity, Scale and Spectra of Turbulence in Mixing Region of Free Subsonic Jet," NACA Report 1292, 1956.
25. Fakan, J. C., and Mall, H. R., "Effect of Forward Velocity on Sound Pressure Level in the Near Noise Field of a Moving Jet," NASA TN D-61, October 1959.
26. Howes, W. L. et al, "Near Noise Field of a Jet Engine Exhaust," NACA Report 1338.
27. Hayes, W. H., Lanford, W. E., Hubbard, H. H., "Near Field and Far Field Noise Surveys of Solid Fuel Rocket Engines for a Range of Nozzle Exit Pressures," NASA TN D-21, August 1959.
28. Roshko, A., "Some Measurements of Flow in a Rectangular Cutout," NACA TN 3488, August 1955.
29. Krishnamurty, K., "Acoustic Radiation from Two-Dimensional Rectangular Cutouts in Aerodynamic Surfaces," NACA TN 3487, August 1955.
30. Yorton, D. A., "Investigation of B-47 Bomb Bay Buffet," Boeing Document D-12675, ASTIA 150-742, dated 16 May 1952.

31. Etkin, B., Korbacher, G. K., Keefe, R. T., "Acoustic Radiation from a Stationary Cylinder in a Fluid Stream," Journal of the Acoustical Society, January 1957.
32. Roshko, A., "On the Development of Turbulent Wakes from Vortex Sheets," NACA TN 2913, 1953.
33. Gerrard, J. H., "Measurements of the Fluctuating Pressure on the Surface of a Circular Cylinder," Part 1, "Cylinder of 1-in. Diameter," ASTIA AD 200922, January 1958.
34. McGregor, D. M., "An Experimental Investigation of the Oscillating Pressures on a Circular Cylinder in a Fluid Stream," UTIA TN No. 14, 1957.
35. Oestreicher, Hans L., "Field of a Spatially-Extended Moving Sound Source," Journal of the Acoustical Society of America, November 1957.
36. Gerrard, J. H., "Measurement of the Sound from Circular Cylinders in an Air Stream," Aeronautical Research Council F.M. 2271, June 1955.
37. Krzywoblocki, "Investigation of the Wing-Wake Frequency with Application of the Strouhal Number," Journal of the Aero/Space Sciences, Vol. 12, No. 1, 1945.
38. Blake, R., Kuoppamäki, K., and Paul, V. R., Lockheed Aircraft Corporation Confidential Communication to Norair Division of Northrop Corporation.
39. Eldred, K. M., "Base Pressure Fluctuations," Journal of the Acoustical Society of America, Vol. 33, No. 1 (59-63), January 1961.
40. Widmayer, "Experimental Investigation of the Flutter Behavior of Curved Panels at Supersonic Speeds," IAS Proceedings of the National Specialists Meeting on Dynamics and Aeroelasticity, November 1958.
41. Sylvester, Nelson and Cunningham, "Experimental and Theoretical Studies of Panel Flutter at Mach Numbers 1.2 to 3.0," NACA RM L55E18b, July 1955.
42. Sylvester, "Experimental Studies of Flutter of Buckled Rectangular Panels at Mach Numbers from 1.2 to 3.0 Including Effects of Pressure Differential and of Panel Width-Length Ratio," NACA RM L55130, December 1955.
43. Miles, "On Panel Flutter in the Presence of a Boundary Layer," Journal of Aero/Space Sciences, Vol. 26, No. 2, February 1959.

IV ATMOSPHERIC WIND AND TURBULENCE ENVIRONMENTS

INTRODUCTION

To the space vehicle in the launch and re-entry phase, the earth's atmosphere with its prevalent upper troposphere winds and its general turbulent structure represents a potential source of vehicle structural vibration. These vibrations are induced by a variety of oscillating aerodynamic lift forces acting on the vehicle which are caused by continuous changes in the magnitude and direction of atmospheric winds and gusts encountered along the flight path. The severity of the elastic structural response depends upon the magnitude of these lift forces, the low frequency response characteristics of the vehicle structure, and the frequency content of the atmospheric disturbances as experienced by the forward moving vehicle.

GENERAL DISCUSSION, AERODYNAMIC FORCES

Launch and re-entry through the atmosphere, for any given vehicle, create wide variations in the parameters which affect these forces and moments. Except for lift and drag forces developed at very high altitudes, the perturbing aerodynamic forces acting on the vehicle generally depend upon the vehicle external geometry, altitude, forward speed, Mach number, Reynolds number, and angle of attack. However, different types of aerodynamic forces usually have different functional dependences upon each of these parameters.

The generalized form of the equation for these unsteady aerodynamic forces is:

$$L = C_F \cdot q \cdot \ell^2 \quad \text{Lift}$$

where

$$C_F = C_F(\alpha, R_e, M, S) \quad \text{Lift Coefficient}$$

$$\alpha = v_N/U \quad \text{Angle of Attack}$$

$$R_e = \rho U \ell / \mu \quad \text{Reynolds Number}$$

$$S = V/bw \quad \text{Similarity Parameter}$$

$$q = 1/2 \rho U^2 \quad \text{Dynamic Pressure}$$

$$\ell = \quad \text{Characteristic Length}$$

It is necessary therefore to determine the functional dependence of C_F on α , R_e , M , and S for each type force being considered. This dependence varies considerably between forces developed on lifting surfaces and those developed on non-lifting surfaces, so that it is best to consider these two types of forces separately.

Relatively large cross wind viscous drag forces may develop when the total wind or gust component normal to the vehicle axis of symmetry is large, say on the order of Mach .30 or greater. Such forces might develop in the regions of the jet stream,

where the horizontal winds attain velocities of 200 or 300 ft/sec. The equation of force for these viscous drag forces requires slight modification of the generalized form given above, in that the dynamic pressure is that associated with the cross wind component. That is,

$$L = \frac{1}{2} \rho \cdot v_N^2 \cdot C_F \cdot \ell^2,$$

where ℓ is some characteristic length, which for a circular cylinder is a function of the radius of the cylinder and its length. Since the axial boundary layer flow is turbulent, the drag coefficient, C_F , is relatively insensitive to Reynolds number and Mach number. For a cross wind having a sharp edge profile, the peak magnitude of C_F may be as high as twice the corresponding steady state value. Detailed discussion of these viscous drag forces are found in References 6 through 9.

The aerodynamic forces acting on hypersonic space vehicles operating at very high altitudes, say 50 miles or greater, are not developed by a flow of "continuous" air around the vehicle, but actually result, in a sense, from the "individual" reactions of air molecules colliding with the surface of the vehicle. The regime of fluid flow classified as a continuum corresponds to negligibly small ratios of the mean free path of air molecules to the size of the vehicle. However, at these high altitudes where the air is semi-rarefied, the mean free path may be as large as one inch or more and for rarefied gases the mean free paths may exceed the size of the vehicle. References 10 and 11 are listed as possible sources of information concerning the theoretical aspects of this problem.

In the analysis of elastic structural response to atmospheric disturbances, other very important secondary lift and drag forces are developed as a result of the additional angles of attack of the vehicle caused by the elastic deformations and rigid body pitch and translation of the vehicle about its flight path. The responses ultimately obtained from a consideration of gust and wind shear forces are responses of the lowest gross vehicle modes and the lowest modes of its lifting surfaces.

TYPES OF DISTURBANCES

Essentially two distinct types of free air flow disturbances exist in the earth's atmosphere. These are 1) fairly steady horizontal winds, with highest flow velocities and largest changes in wind speed in and around a relatively thin core called the jet stream, and 2) gust components associated with continuous random atmospheric turbulence resulting from the general overturning of air masses caused by the non-uniform heating of the atmosphere. The normal velocity, v_N , of the air flow associated with the horizontal winds can change significantly in both magnitude and direction with altitude intervals of 1,000 to 10,000 feet, while for continuous turbulence similar changes may occur over distances as short as 10 to 500 feet.

Since the forward velocity of a vehicle causes these changes in wind and gust velocity to occur in relatively short periods of time, there is associated with each of these atmospheric disturbances a frequency range over which the resulting lift

forces fluctuate. The magnitude of this frequency is directly proportional to the forward speed of the vehicle and inversely proportional to the size of the region, or distance interval along the flight path, over which these velocity fluctuations take place. Thus, since continuous turbulence is a smaller scale phenomenon than wind fluctuations, the frequency content of continuous turbulence as felt by the space vehicle, is higher than that associated with the horizontal wind fluctuations. The relative structural vibration severity of these two phenomena, thus, depends in part upon the frequency response characteristics of the vehicle under consideration. More detailed discussions to be given below show possible frequency ranges for each type of disturbance. The turbulence problem is generally more severe because of larger forces and larger dynamic responses.

Structural response is determined by the rate of change of wind or gust velocity with respect to distance in the atmosphere. This is defined as wind shear. Because of the physical limitations of the measuring devices used, true wind shear at any one point cannot be determined. Measurements of this quantity can only be in the form of average wind shear. Average wind shear is the ratio of the difference in the speed of parallel components of wind or gust velocity at two points in the atmosphere to the distance of separation of the points.

Experimental data indicate that the wind shear ratio for horizontal winds, measured along the vertical, rarely exceed $.10 \text{ sec.}^{-1}$, corresponding to a $\Delta v_n = 100 \text{ ft./sec.}$ per 1,000 ft. of altitude difference. Generally this value is not more than $.07 \text{ sec.}^{-1}$. However, for continuous turbulence, the gust gradients can be as high as $.35 \text{ sec.}^{-1}$ over 100 ft. intervals and $.65 \text{ sec.}^{-1}$ over about 20 ft. intervals. These latter values indicate that the continuous turbulence will be generally more severe than the horizontal winds as a vibration source. Of course, the high frequencies associated with short distances as 20 ft. and with a high forward vehicle velocity may be high relative to the vehicle resonant frequencies so that the induced structural response of the gross vehicle modes at these frequencies will be very small. In addition, the frequencies corresponding to $.10 \text{ sec.}^{-1}$ wind shear for 1,000 ft. will usually be less than 1.0 cps, which is generally lower than the fundamental body modes for most missiles and rockets.

Vehicle perturbations from horizontal winds actually pose a much greater stability and control problem than a structural vibration problem for vertical rising vehicles being launched from the surface of the earth, References 12 and 13. According to Telefsen, Reference 12, the acceleration increments of a conventional ballistic-type missile associated with even the highest wind shears will be small, less than 1.5 g's. However, Reference 13 points out that vertical wind gradients may be sufficiently large as to represent critical design conditions for control components such as the throw of a gimbaled rocket motor required to overcome wind shear in the jet stream. Wind shear data are presented here, however, because of the possibility of future designs being considered which have fundamental body bending modes on the order of 1 cps for which these accelerations may be more significant. Such configurations might result from the design of large nuclear-powered rockets in which it is desirable to separate the crew from the reactor by as large a distance as possible.

Although, in a complete dynamic response analysis, the small scale effects of the turbulence phenomenon will be added to the larger scale wind effects, this division of atmospheric velocity disturbances into two categories also acts as a division in the method of dynamic response analysis of the space vehicle structure. Continuous turbulence, being an essentially random natural process, is most effectively characterized by velocity-spectral density functions and certain probability distributions, Reference 14. Thus, the vibration response analysis for this phenomenon will be centered around the following equation:

$$\Phi_{\text{Response}}(\Omega) = |T(\Omega)|^2 \cdot \Phi_{\text{Input}}(\Omega)$$

where Ω is a reduced frequency in radians/foot ($2\pi f/U$), $\Phi_{\text{Input}}(\Omega)$ is the velocity spectral density of the continuous atmospheric turbulence, $T(\Omega)$ is the structural transfer function, and $\Phi_{\text{Response}}(\Omega)$ is the response spectral density, given in terms of the units appropriate to the desired response quantity. However, according to Reference 14, it is anticipated that a spectrum need not be defined for the horizontal winds because of the relatively high stability of the jet stream winds in both speed and direction. Hence, a structural vibration analysis which accounts for this phenomenon need be performed only for a single typical, but severe, horizontal wind condition; that is, a discrete disturbance.

METHODS OF ANALYSIS

In the past, discrete gust analyses have often been used to test the structural integrity of airplanes and missiles to atmospheric turbulence, by considering those gusts encountered which may be exceeded by only a few per cent for all flight time in any weather condition. With the recent mathematical developments in the field of generalized harmonic analysis, much attention is being focused upon the application of power spectral density methods for describing structural response to continuous turbulence. There are several advantages to this approach. As mentioned above, it is the wind shear through a gust which determines the severity of structural response. This quantity is reflected in the shape of the gust profile. According to Reference 13, this shape is rarely known so that it has been necessary to assume approximate gust profiles such as ramps, one cycle for a 1-cosine function, sharp edge profiles, etc. With the spectral approach, this deficiency is eliminated. In addition, it is felt that the probability of experiencing a series of gusts of varying wave length is greater than that of encountering a discrete gust having a wave length and profile which is critical for the vehicle being analysed. However, recent parametric studies, Reference 15, in which both the discrete gust and the spectral approach have been used, indicate that the two methods give comparable results since they both depend upon the statistical measurement of gust velocity.

Atmospheric air flow disturbances exist from the surface of the earth to very high altitudes, on the order of 300,000 ft. Except for viscous drag forces and non-continuum aerodynamic forces, the simplified lift equations given above aid in

limiting this entire altitude range to those altitudes at which first order vehicle structural vibrations will be produced due to atmospheric disturbances. Ground cross winds may induce structural vibrations in a missile-type vehicle sitting in firing position on the launch pad. These winds cause alternating vortices to be shed from the main structure in a manner similar to that described in a previous section, "Flow Past Projections." However, this is a ground handling problem for which the magnitude of the response can often be limited by the choice of proper weather conditions for launching or by the use of sufficient constraints on the vehicle until the missile leaves the pad.

As the altitude and speed of the vehicle increase, sensitivity to disturbances increases, reaching a peak sensitivity usually at about 30,000 to 40,000 ft. Gust magnitudes in the field of continuous turbulence often remain nearly constant from above the friction layer to these altitudes. Thus, the response due to continuous turbulence increases with altitude since the forward speed increases rapidly to large magnitudes. It is coincidental, however, that the sensitivity usually reaches its peak at the altitude where wind shears are highest for the prevalent atmospheric horizontal winds. Above this region and up to altitudes of 70,000 to 80,000 ft. wind shears and gust magnitudes generally decrease, with a gradual decrease up to about 100,000 ft. Above this altitude range, the density of the air drops to such low magnitudes that even extreme atmospheric disturbances, Reference 17, fail to produce lift forces significant to first order structural vibrations. For re-entry the situation is expected to be quite similar as very high forward velocities are attained at very high altitudes, with a subsequent decrease in velocity as the vehicle descends further into the atmosphere, reaching relatively low velocities at the low altitudes.

APPLICATION

The problem of structural vibrations induced by atmospheric disturbances is not confined to the earth's atmosphere, but will exist for high-speed flight through the atmospheres of all planets to which future reconnaissance flights will be made. It is expected that the severity of these vibrations in the atmospheres of the foreign planets could be significantly different from that experienced in the earth's atmosphere. This results from the dissimilarities in the gaseous composition of the atmosphere held by each planet, and in the influence of direct solar radiation in heating the atmosphere. Presently, little is known about disturbances existing in foreign planetary atmospheres. The limited information available is based upon conjecture from the known proximity of the planets to the sun, order of magnitude estimates on the amount of gaseous composition of these atmospheres, and extrapolation of data concerning the earth's atmosphere. Once reliable data do become available, the method of handling the disturbance phenomena will be the same as that used for the earth's atmosphere.

A considerable amount of wind and gust data for various climatic conditions have been tabulated during the last few decades. Unfortunately, most of this meteorological information is in the form of averages which are of little value to design since the magnitude of the wind and gust velocities recorded will be exceeded about 50% of the time. A few measurements of extreme atmospheric disturbances have also

been made. As design criteria, these extremes would impose costly structural strength requirements. Based on the purpose and over-all cost of a given vehicle being designed, a certain tolerable risk is usually allowable. It is thus desirable to obtain wind and gust data for which a probability of exceeding a certain value of wind shear or gust gradient distance can be established.

WIND PROFILES AND WIND SHEAR

The usual method for presenting data on the structure of the prevalent horizontal atmospheric winds is by means of wind profiles which are accompanied by magnitudes of the vertical wind gradients, called wind shear, for the portions of the profile with the largest fluctuations in wind speed and/or direction. A wind profile is defined as a plot of the horizontal wind velocities in the atmosphere as a function of altitude for a given time and for a given location above the surface of the earth. Two graphs are normally required for this purpose: one for the speed and one for the direction as a function of altitude.

A considerable mass of wind data has been collected over the past ten years for many regions in the United States and abroad, and for various altitude ranges. Most of these data consist of small sized samplings in the lower altitude regions, in the regions of the jet stream where the highest velocities usually exist, and in high altitude regions up to 400,000 ft. Although for vibration purposes it is probably not necessary to define a spectrum for the wind structure, some sort of probability of occurrence of various sized vertical wind shears and various shaped wind profiles should be determined in order to establish a realistic criteria for the design of space vehicles which must pass through the atmosphere. Most of the data available are either not in the proper form or are too limited in accuracy or sample size to permit determination of such probability functions. Reference 18 contains detailed data on the variations in wind fields from surfaces up to 30,000 ft. References 19 and 20 contain samplings of large wind shears measured in the vicinity of the jet streams. Average wind conditions for higher altitudes as measured by balloon soundings, sound propagation studies, and the drift of smoke puffs from bursting smoke shells are discussed in Reference 21. Reference 17 discusses the wind and turbulence measurements made at 200,000 to 400,000 ft. by observing the motions of persisting meteor trails.

Some successful attempts have been made to accurately define the wind structure with altitude for specific locations in the United States and for various seasons of the year by making frequency measurements of profiles and accompanying wind shears over extended periods of time, References 12, 22, and 23. Large variations in wind structure exist for different geographical locations so that for vehicles being launched from different locations of the earth, the vibration specifications for winds could be significantly different depending upon the particular wind structure usually found above that location. Figure 33 shows two examples taken from Reference 12 of wind profiles measured at Silver Hill, Md. Of the more than 700 soundings taken during a one-year investigation at Silver Hill (1953, 1954), these are representative of the more extreme profiles obtained. However, many other shapes are possible. These profiles show two important features of winds which are well known to investigators in this field: the variation of wind speed

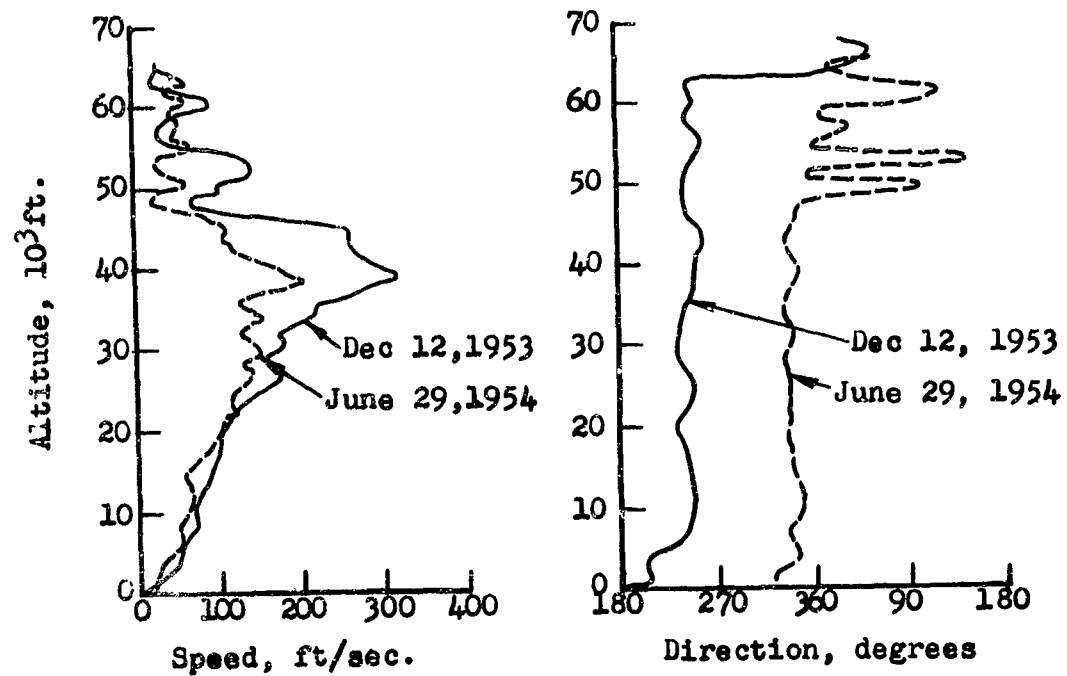


Figure 33. Sample Wind Profiles taken at Silver Hill, Maryland, During 1953 - 1954 (Reference 12)

and direction with seasonal changes, and the stability of the flow direction associated with the higher velocity winds. During the winter and spring months, the speed is usually much higher than for the other two seasons, especially in the region of the jet stream. The direction of flow during the windiest season is generally from west to east, while during the summer months the flow often makes a complete reversal in direction. Also, as seen from these profiles, the direction of flow as a function of altitude is quite constant for the stronger winds. Winds in the frictional layer of air near the surface of the earth which often reflect the make-up of the local terrain, and winds aloft which have relatively low speeds have flow directions which are not nearly as constant as the stronger winds. In any season, these particular winds may completely reverse direction. For the lower velocity winds, Seissenwine, in Reference 13, presents some arbitrary recommendations for direction changes with altitude of the lower velocity winds:

Surface to 2000 ft.	180°/1000 ft.	with 15 fps winds
3000 to 4000 ft.	10°/1000 ft.	with 50 fps winds
6000 to 8000 ft.	40°/1000 ft.	with 40 fps winds

The existence of the previously mentioned jet stream between the altitudes of 30,000 and 45,000 ft. is clearly evident in Figure 33. The jet stream is a thin core of high velocity air which more or less encircles the Northern Hemisphere in a narrow band at about the middle latitudes. Its horizontal axis is generally located somewhere in the altitude range indicated in Figure 33. Also, N. Sissenwine, in Reference 23, indicates that in the United States the thickness of the jet core is about 10,000 ft., independent of the location of the horizontal axis in this altitude range. These are generally the strongest winds aloft, except for extremely high altitude winds which are of little interest here. Measurements of the jet stream velocities indicate an average value of about 200 ft/sec. with maximum speeds over the United States of about 300 ft/sec. Although of questionable accuracy, much higher speeds on the order of 400 to 500 knots have been recorded over Japan and North Africa, Reference 12. Jet streams are not separate entities from the other winds aloft such as a tornado, but are strong winds which are characteristically a part of the over-all wind structure of the atmosphere. During the windiest seasons of the year, jet streams always exist somewhere in the United States, with oscillations of 5 to 10 degrees about their mean monthly positions, Reference 13. Some measurements of wind steadiness have been made for the jet stream, which show that fluctuations in speed and velocity of the strongest winds are quite small. According to Reference 13, during the winter season and for the latitudes covering the United States, wind steadiness is higher than 90%. Magnitudes as high as 95% to 98% have been recorded over the Western Pacific region. Wind steadiness is defined as the ratio of the wind speed to the mean wind speed, measured in percentage. As a specific example, Reference 13, wind constancy maps indicate that at 18,000 ft. over the United States, 90% of the wind directions will be within 45 degrees of the mean direction.

In addition to wind shear, defined above, the shear layer thickness is also important to wind-induced vehicle vibration response. A shear layer is merely the altitude interval associated with a given wind shear. It is mentioned in Reference 24 that because of the accuracy limitations of equipment used to measure wind shear, the

minimum unattainable shear layer thickness is 500 ft. for a wind shear of any significant magnitude. With this restriction, the wind shear at any given altitude must actually be an average wind shear obtained over a shear layer. Average wind shears are usually specified for 1,000, 3,000, and 5,000 ft. shear layers, with the accuracy of the wind shear decreasing with decreasing layer thickness. Since the averaging process effectively reduces the magnitudes of the actual existing wind shears, peak average wind shears for say 1,000 ft. layers will be larger in magnitude, by as much as 1.5, than wind shear in a 3,000 ft. layer. Thus, in many cases the wind shears for a given region will be given for more than one shear layer, sometimes all three layers. As an example of this, a maximum 3,000-ft. shear for 30,000 to 40,000 ft. altitude range indicates a .051 sec.⁻¹ wind shear association with 181 knot (306 fps) wind and a .077 sec.⁻¹ wind shear for a 1,000 ft. layer within the 3,000 ft. layer, Reference 22.

The highest wind shears are found in the region of the jet stream. Reference 22 indicates that the wind velocity drops off faster above the axis of the jet stream than below so that higher wind shears are generally obtained immediately above the jet stream core. High wind shears have been recorded in regions other than the jet stream. For example, high wind shears have been recorded in the regions of low altitude surface winds; however, the probability of occurrence is small and the vehicle sensitivity to wind is low in this region due to its low forward velocity. It may also happen that significant wind shears may develop in regions of lower wind speed where the flow direction of the winds changes radically, reaching complete reversal at times.

For certain types of wind structures, intense shears may not be confined to a single shear layer, since as shown in Figure 33 several "fingers" of adjacent high wind flow may exist simultaneously. No data are presently available which estimate the probability of encountering more than one high shear layer.

The following table contains the per cent winter risk of encountering, at 40,000 ft. altitude, a given wind speed and its associated wind shear based on 3,000 ft. shear layers. These data, obtained for Patrick Air Force Base, are taken from Reference 22.

Winter Risk (%)	Wind Speed (fps)	Average Shear for a Layer of 3000 ft. Thickness (fps/1000 ft.)
1	298	46
5	246	28
10	214	22
20	181	18

These wind conditions are presently considered to be as severe as those anticipated for the worst locations in the United States. Similar data are also available from soundings taken at Bedford, Mass., but differ only slightly from those presented in this table.

The wind profiles presented in Figure 33 represent the wind structure with altitude for individual soundings. Of greater interest to the designer are per cent wind profiles which show the wind speeds which are exceeded only a given percentage of the time. Four such profiles and their accompanying wind shears, for Patrick Air Force Base, are presented in Figure 34 for 1%, 5%, 10%, and 20% winter risk. Here the percentage risk is associated with the peak wind speed of each profile and the remainder of the profile in each case represents the typical wind structure accompanying such a jet stream speed. These wind structures obtained from Reference 22 were measured during January 1955.

Figure 35 also shows a 1% synthetic wind profile obtained from wind measurements taken during the recent Geophysical year. The maximum speed in the jet stream core is 300 fps and will be exceeded only 1% of the time. Wind speeds at the other altitudes are considered typical. It is recommended in Reference 23 that this profile be used for design of vehicles with sharp maximum wind response between 30,000 and 45,000 ft., and which may be launched during the windiest seasons of the year from areas in the U. S. with the highest winds. The horizontal axis of the jet stream is to be shifted to the most critical vehicle altitude between 30,000 and 45,000 ft. while maintaining the shapes of the 10,000 ft. layer in which it is centered. The direction of the flow is to be held constant with altitude with the wind blowing from the most critical azimuth. The 1% wind shears associated with the peak are:

±1000 ft. shear layer	.076 sec ⁻¹
±3000 ft. shear layer	.050 sec ⁻¹
±5000 ft. shear layer	.033 sec ⁻¹

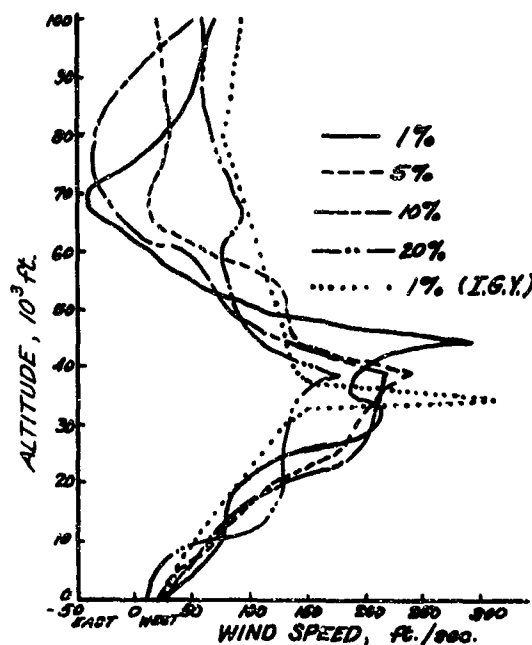


Figure 34. Wind Speed vs. Altitude

As future data become available, it is important to bear in mind that the wind shear to be used for design must be compatible, percentage-wise, with the maximum wind speed. Generally, if the probability of a maximum wind speed occurring is 1%, then it is likely that the associated wind shear will have a 1% probability of occurrence. However, it is possible to have high wind shears for high wind velocities. The probability of such an occurrence is small and it is presently felt, Reference 13, that these two effects will average out.

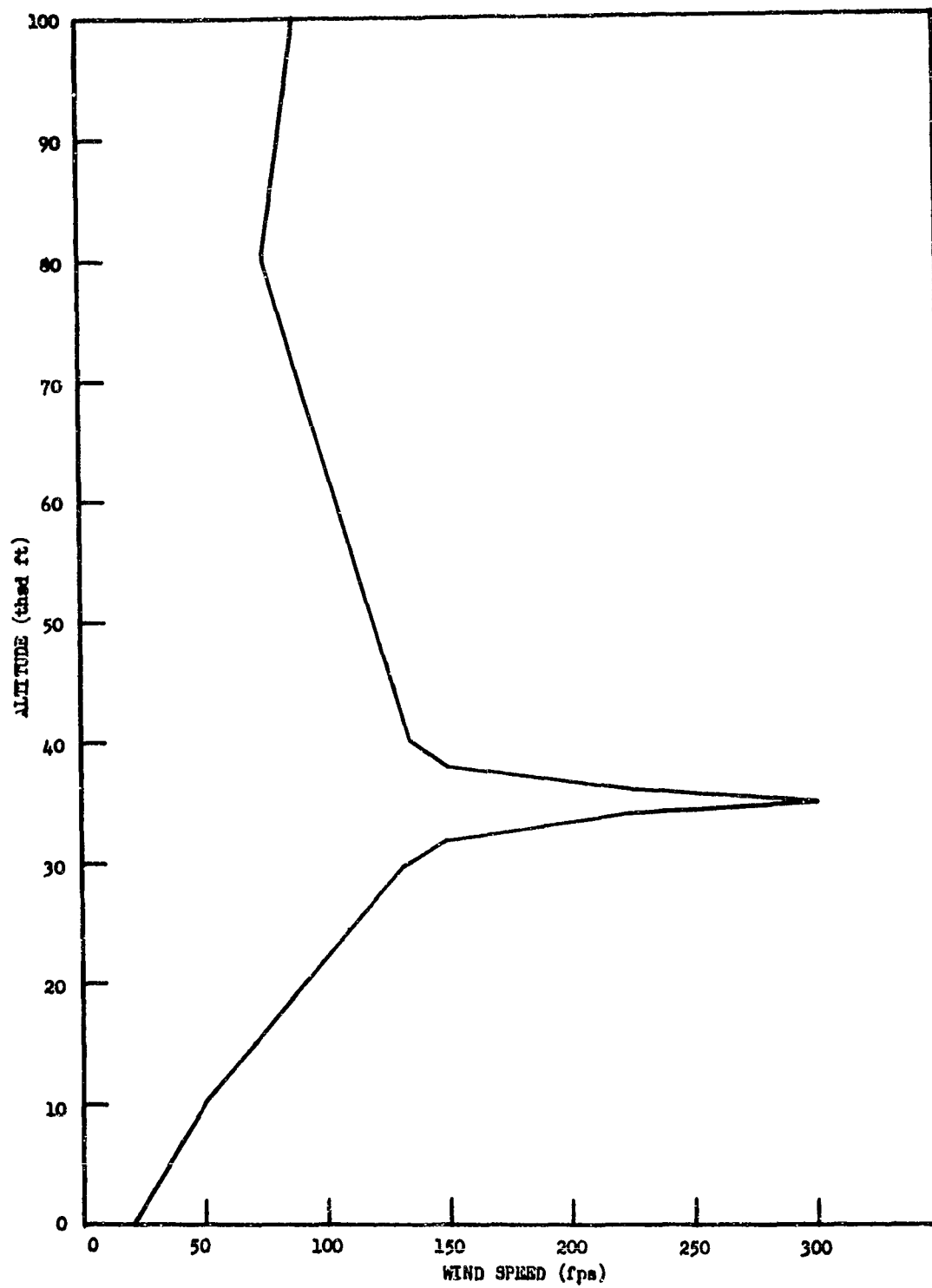


Figure 35. One Percent Synthetic Wind Profile Obtained During Geophysical Year (Reference 23).

Shown in Figure 36 is a plot of the lift parameter ($\rho \cdot U \cdot v_n$) versus time, for a hypothetical vehicle rising vertically through the atmosphere. The vehicle forward velocity time history is that presented in Figure 64, and the horizontal wind profile used is the 1% profile for Patrick Air Force Base, Figure 34. The axis of the jet stream is encountered at 48 seconds after launch as evidenced by the relatively sharp peak in the lift. Except for this peak, the oscillations shown do not represent vibration sources for the vehicle because of their very low associated frequencies. From this curve, it is seen that the frequency content of the peak is on the order of 1 cps and less. For vehicles attaining higher forward velocities in the vicinity of the jet stream, the frequency experienced at such a peak will increase; but since it is not likely that the forward speed of any such vehicle will be more than twice used here, frequency will certainly be no greater than 2 cps. Vehicles having a fundamental body mode in this low frequency range will experience bending oscillations. Very long vehicles may be relatively flexible in bending so that some consideration should be given to the horizontal winds as a potential source of vibration.

CONTINUOUS ATMOSPHERIC TURBULENCE

Atmospheric turbulence is a continuous random velocity disturbance described by power-spectral-density functions and certain probability distributions. Physically, turbulence can be thought of as being made of eddies or vortices of the type shown in Figure 37. Such eddies might be quite distinct in the atmosphere, acting much like independent vortices, with their lifetime depending upon their size and associated kinetic

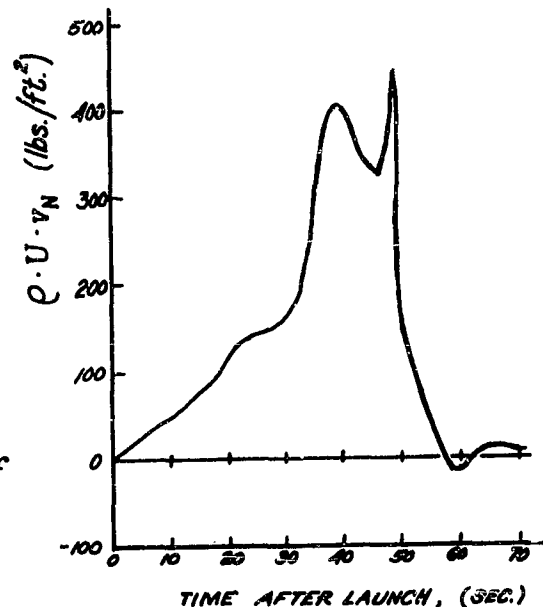


Figure 36. Gust Strength

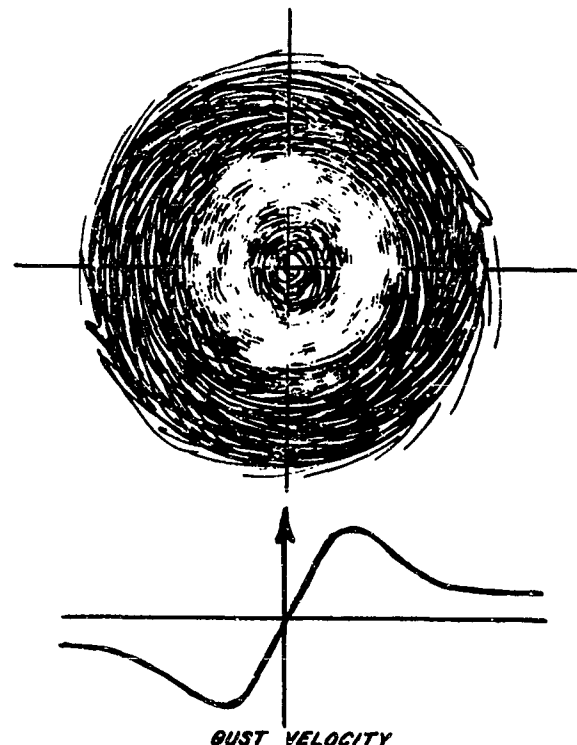


Figure 37. Eddy Model of Turbulence.

energy. The velocity profile through such an eddy will be roughly approximated by that shown in Figure 37. Conceptually, these eddies are generally superimposed upon each other, or fused together, so as to lose their individual identity, thus creating random air flows classified as continuous turbulence. The velocity profile at any instant of time through a region of continuous turbulence might appear as that shown in Figure 38. This shows the random nature of the gust velocity disturbances in a continuous turbulent field and the need for a statistical characterization by means of power spectral methods. Also, shown are high velocity discrete gust peaks which have been used in the past as a design criteria for airplanes in turbulent environments.

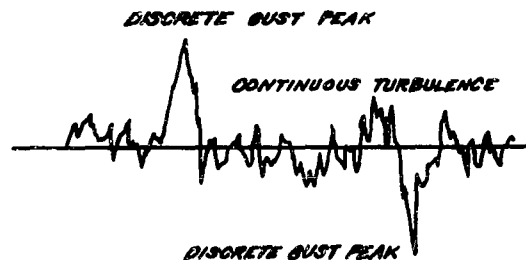


Figure 38. Velocity Profile in Continuous Turbulence

Turbulence may be caused by air friction, due to viscosity, between adjacent layers of air moving with different velocities. The high wind shears in the region of the jet stream thus act as sources of significant amounts of turbulence. Vortices and eddies formed in the shear layers are carried downstream by the horizontal winds which aid in distributing turbulence formed in one region into other regions of the atmosphere.

Other causes of turbulence are (1) convergence of large moving air masses, having different temperature, humidity, and stability, (2) surface winds deflected by local terrain, and (3) convective activity due to the general overturning and lifting of air masses by non-uniform heating of the atmosphere. Convection is a significant contributor to turbulence, in that the rising air masses produce large eddies which eventually break up into smaller eddies with a transfer of energy. The energy in the smaller eddies is then dissipated through the action of the viscosity of the air. The rising air mass that triggered this action finally disappears.

From an energy standpoint, the spectrum of turbulence can be divided into the following three general categories, Reference 16:

1. Low frequency (large eddy size) mechanical and convective turbulence
2. Isotropic middle frequency turbulence (average eddy size) in which energy is neither created nor dissipated
3. High frequency (small eddy size) turbulence in which energy is dissipated by viscosity.

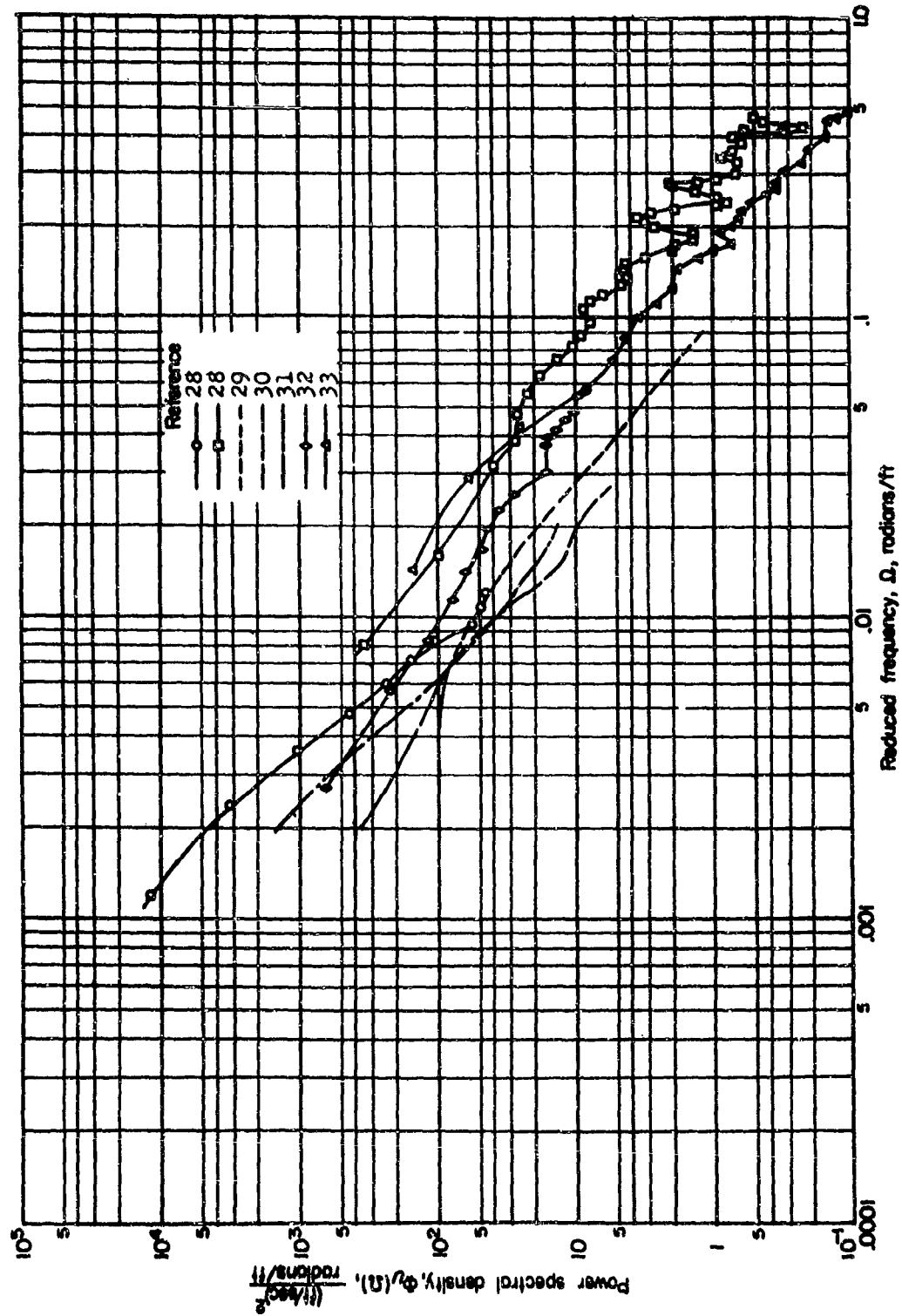


Figure 39. Summary of Airplane Measurements of the Power Spectrum of Atmospheric Turbulence (Reference 25).

Viscosity of the air is a helpful feature in the consideration of vehicle response to atmospheric turbulence in that it limits the magnitude of the gust gradients that build up over short distance intervals. Generally, the higher peak gust velocities are associated with air masses of large eddy size where gust gradient distances are correspondingly large. As the gust gradient distance decreases, as for the smaller sized eddies, the peak gust velocity also decreases. This effect is shown in Figure 39 by data presented in Reference 13 for discrete gusts having wind shears and corresponding gust gradient distances which are exceeded only one per cent of the time in thunderstorm-type turbulence. This, of course, does not mean that wind shear decreases with gust gradient distance, or eddy size, since wind shear is defined as the rate of change of gust velocity with distance into the gust. Figure 40 shows that wind shear actually increases, to some upper limit due to viscosity, for the discrete gust case with decreasing gust gradient distance.

Most of the continuous turbulence and discrete gust data presently available were obtained by NASA from analyses of the acceleration response of conventional transport and military aircraft to gustiness obtained over the past twenty years. Thus, the data are generally limited (1) by the standard storm avoidance procedures practiced by both military and transport aircraft, (2) to the portion of the turbulence spectrum which induces response in winged aircraft, (3) to the altitude range and to the airplanes in which flight is normally made, and (4) by the errors inherent in the data reduction procedures from the limited accuracy with which aircraft response characteristics are known.

As indicated in Reference 25, for standard transport operations, about 10% of all flight time is spent in clear air turbulence, 1% in cumulus cloudiness, and .05% in thunderstorms. Of all three of these turbulent conditions, thunderstorm turbulence is considered to be the most severe. Operational military missiles and rockets cannot generally avoid storm conditions. Similarly, time tables for space vehicle launchings may not permit weather delays. Therefore, special investigation by the military of thunderstorm turbulence have been made in order to supplement the lack of such data obtained in the above manner. A summary of these results is given in Figure 41. Reference 25 indicates that for these data, which were obtained by power-spectral-density methods, the relation between the actual gust velocity peaks

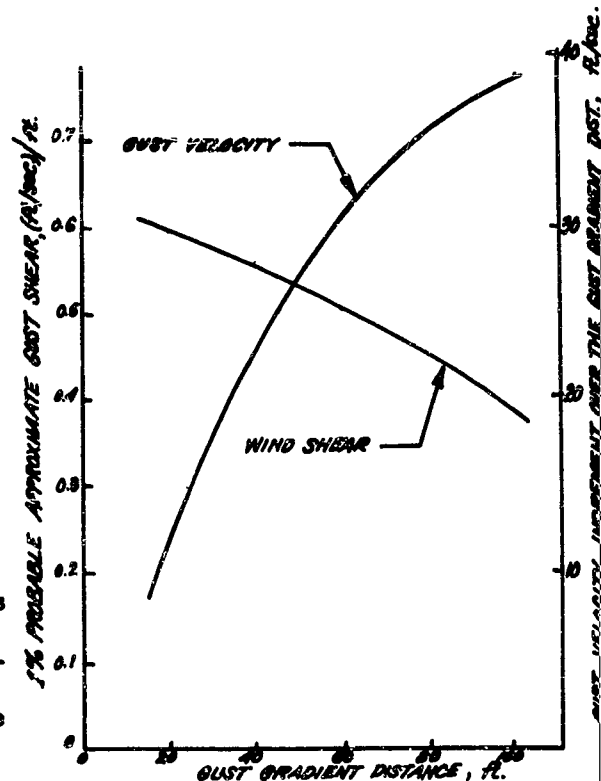


Figure 40. Wind Shear and Gust Velocity.

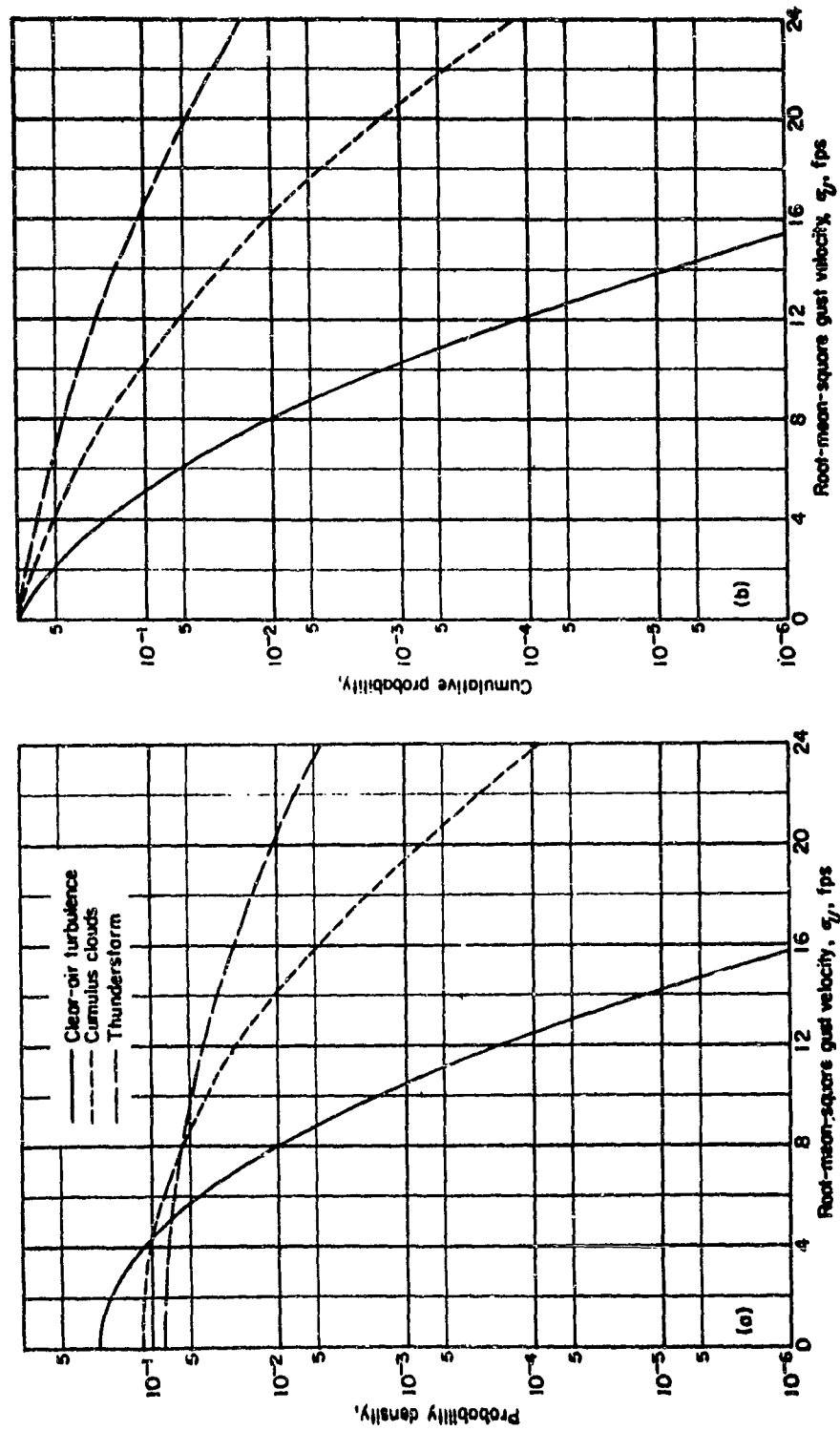


Figure 41 Distribution of Root-mean-square Gust Velocity with weather condition (Reference 25).

and these root-mean-square gust velocities is approximately 2 to 1.

Donely, in Reference 26, indicates that atmospheric turbulence data obtained from response measurements by conventional aircraft are applicable to response calculations for missiles and rockets. However, for high-speed space vehicles, whose forward velocity determines the effective turbulence frequencies experienced, considerable response might be induced by large scale turbulence to which airplanes, with their slower speeds, would be insensitive. Also, the unconventional geometries and aerodynamic properties may alter the range in the scale and frequency spectrum over which the sensitivities will exist. For this reason, it is not easy to anticipate the specific turbulence data requirements for each design consideration.

In considering the variation of gust velocity with altitude, Seissenwine, Reference 13, states that for convective cloudiness, this variation is small up to 35,000 ft., and that clear air turbulence exists near the jet stream between 30,000 and 40,000 ft. Figure 42 presents data from Reference 25, giving the cumulative probability distribution of the root-mean-square gust velocity for routine transport operations for the three altitude ranges, 0-10,000 ft., 10,000-30,000 ft., and 30,000-50,000 ft. It was assumed here that the turbulence varies only slightly within each altitude range. These data are based upon a limited number of gust measurements. However, it is felt that the data presented will give reasonably good first order approximations to the characteristics of atmospheric turbulence variations with altitude.

Estimates of the gust velocities encountered within various altitude ranges and for various weather conditions have been given. It has already been shown, however, that gust velocity varies with eddy size or gust gradient distance. That is, to the vehicle in flight through a turbulent region, the gust velocity varies with the effective frequency associated with these disturbances. Therefore, in applying the data discussed above to the problem of vehicle response to atmospheric turbulence, it is necessary to specify the variation with this frequency of the gust velocity about the root-mean-square gust velocity. From studies of turbulence artificially generated in wind tunnels by screens of various mesh sizes, the following very convenient analytical power-spectral-density function has been derived which adequately approximates this variation with frequency in the atmosphere:

$$\Phi(\Omega) = \bar{\sigma}_U^2 \left(\frac{L}{\pi} \right) \frac{1 + 3\Omega^2 L^2}{(\pi^2 + \Omega^2 L^2)^2}$$

This function, which is given in terms of the reduced frequency, Ω , contains two important parameters commonly used in describing continuous turbulence: the intensity of turbulence, $\bar{\sigma}_U^2$, and the scale of turbulence, L . The intensity of turbulence is the mean square gust velocity and the scale of turbulence is a measure of the average eddy size in a given field of continuous turbulence. Figure 43 shows plots of this function for various values of L , 2000, 1000, 600, 200 ft., and for the frequency range $.0001 \leq \Omega \leq 1.0$.

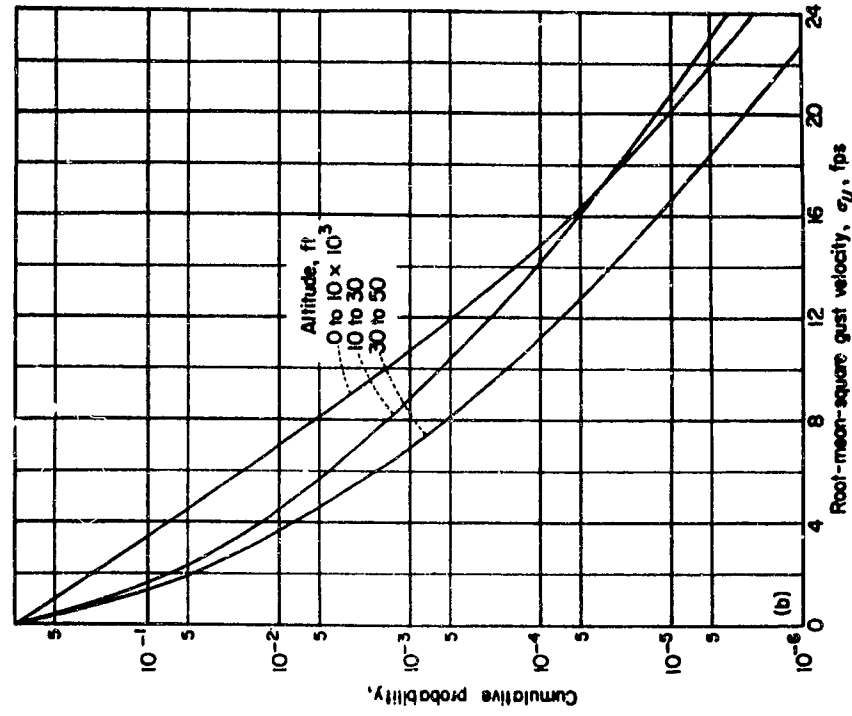
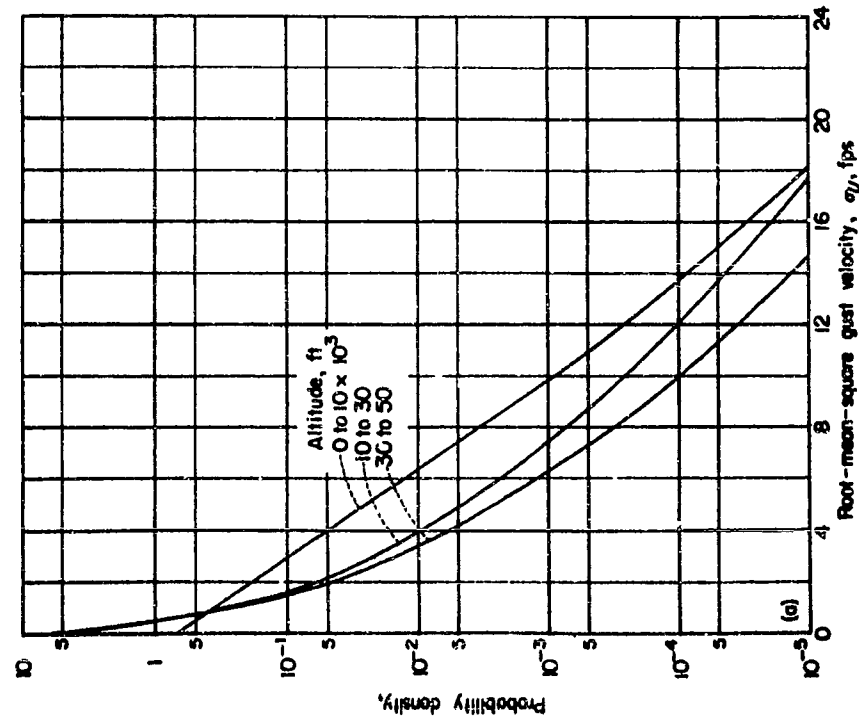


Figure 42. Distribution of Root-mean-square Gust Velocity with Altitude for Routine Operations (Reference 25).

In applying the analytical model of turbulence to space vehicle response calculations, it is necessary to divide the planned flight profile into segments, in such a manner that the statistical properties of the turbulence remain nearly constant within each segment. The scale of turbulence, L , is fairly insensitive to altitude variations and weather conditions, so that it is usually fixed at the previously mentioned constant value of 1000 ft. However, as was shown earlier, the intensity of turbulence does vary with altitude and varies significantly with weather conditions. Other problems are also of interest, such as (1) the variation of the statistical properties of turbulence with time and with geographical location, and (2) the distribution of the peak gust velocities about the mean. In order to answer these questions, a brief discussion will be given of four important properties of turbulence and their implications upon the response problem. These properties are homogeneity, isotropy, stationarity, and Gaussianness.

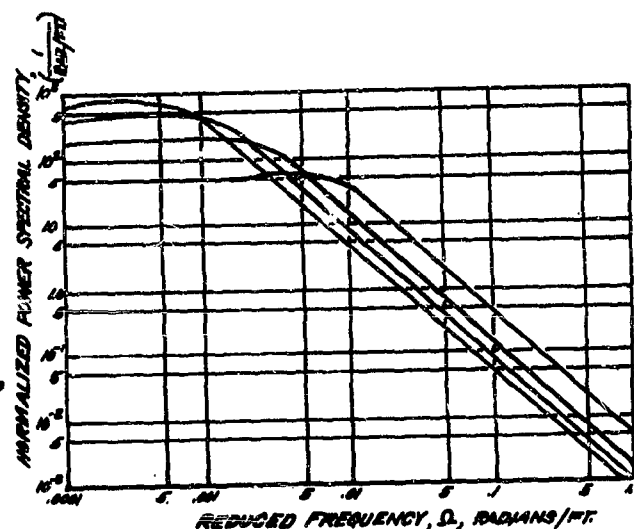


Figure 43. Analytical Turbulent Spectrum for Various Turbulent Scales

Turbulence is said to be homogeneous if the root-mean-square gust velocity in a given direction in the atmosphere is constant throughout a specific region. Altitude and weather conditions thus affect the homogeneity of the atmosphere. As a first approximation, each of the three altitude ranges of 0-10,000, 10,000-30,000, and 30,000-50,000 ft. shown in Figure 42 might be assumed to be approximately homogeneous for constant weather conditions in each. Weather conditions involve large scale patterns of air motion which change slowly, so that for the moderate to low altitudes, a 100-mile wide area might be homogeneous for a time lapse of about one hour, Reference 27.

Turbulence is said to be isotropic, if in addition to being homogeneous in a given direction the root-mean-square gust velocities in three orthogonal directions are equal. This is the simplest kind of turbulence, and can be generated in wind tunnels by mesh screens. Reference 27 contains plots of power spectral density functions for turbulence in the atmosphere for upwind and cross-wind measurements, and for vertical and lateral components. These show that the correlation in the statistical properties in various directions is considered to be quite good. There is a considerable amount of additional data which shows that the property of isotropy does exist in the atmosphere for limited time and space regimes. Reference 27 contains a detailed account of the measurements of this property.

Turbulence is said to be stationary if the root-mean-square gust velocity is not a

function of time. Reference 27 contains two measured turbulent spectra for a single airplane flight taken at two different times during the flight. A total of four minutes flying time is covered by the samplings with each corresponding to 15 miles of flight. A comparison of the two spectra indicates that some degree of stationarity does exist in the atmosphere at the higher frequency with some lack of stationarity at the lower frequencies. However, the forward speeds of missiles and space vehicles during exit and re-entry would seem to insure that stationarity would exist in any given region which was considered to be homogeneous.

Finally, one of the most important and most desirable statistical properties of any random process is that of a normal or Gaussian probability distribution. Normality states precisely the manner in which a variate fluctuates about its mean value. For random atmospheric turbulence, a Gaussian probability distribution function would indicate the probability of experiencing a certain gust velocity in terms of the difference between this gust velocity and the average root-mean-square gust velocity obtained for a specific region in which Gaussianness was assumed to be valid. Testing measured data for Gaussianness is a very difficult task. Suffice it to say that for small space and time regimes, as with the above properties, the property of Gaussianness is usually valid.

An illustrative example is presented in Figure 44 which shows the velocity spectral density functions of atmospheric turbulence at 10,000, 20,000, 30,000, 40,000, and 50,000 ft. altitude for a hypothetical vertical rising vehicle. The forward velocity profile of the vehicle is that shown in Figure 65. Thunderstorm conditions were assumed to exist from launch to 30,000 ft. along with clear air turbulence from 30,000 to 50,000 ft. The value of the root-mean-square gust velocity for the thunderstorm conditions is $\sigma_U = 26.0$ ft. per second. This value corresponds to a cumulative 1% value obtained by extrapolating the thunderstorm curve shown in Figure 41. Similarly, a cumulative 1% value of $\sigma_U = 8.0$ ft. per second was used for clear air turbulence. In order to present the results in more appropriate units than those used in the analytical model of turbulence discussed above, the following theoretical equation for the velocity spectral density was used:

$$\Phi(f) = \sigma_U^2 \cdot \frac{2L}{U} \cdot \frac{1 - 3\Omega^2 L^2}{(1 - \Omega^2 L^2)^2} \quad - \quad \frac{(\text{ft./sec})^2}{\text{cps}}$$

where

$$\Omega = \frac{2\pi f}{U}$$

$$L = 1000 \text{ ft.}$$

This equation is equivalent to the one shown on page 72.

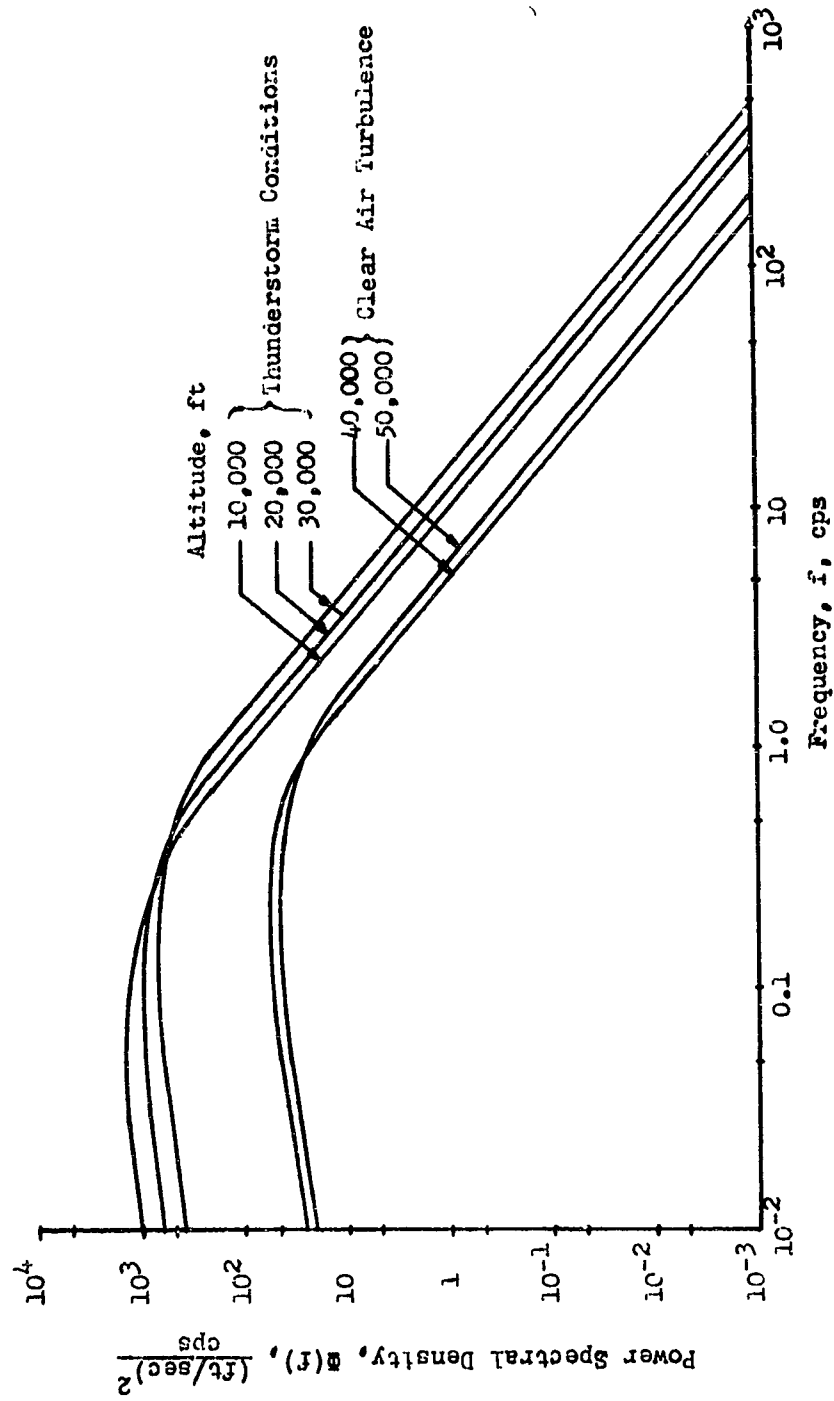


Figure 44. Power Spectral Density of Atmospheric Turbulence for a Vertical Rising Hypothetical Space Vehicle in Thunderstorm and Clear Air Turbulence.

REFERENCES

1. Bisplinghoff, R. L., Ashley, H., Halfman, R. L., "Aeroelasticity," Addison-Wesley Publishing Co., Inc., 1955.
2. Ashley, H., Zartarian, G., Neilson, D. G., "Investigation of Certain Unsteady Aerodynamic Effects in Longitudinal Dynamic Stability," USAF TR 5986, December 1951.
3. Allen, H. S., "Estimation of Forces and Moments Acting on Inclined Bodies of Revolution of High Fineness Ratio," NACA TN 3715.
4. Mello, J. F., "Investigation of Normal Force Distributions and Wake Vortex Characteristics of Bodies of Revolution at Supersonic Speeds," Journal of Aero/Space Sciences, Vol. 26, March 1959, Number 3.
5. Miles, J. W., "The Potential Theory of Unsteady Supersonic Flow," Cambridge Monographs on Mechanics and Applied Mathematics, Cambridge University Press, 1959.
6. Kelly, H. R., "The Estimation of Normal Force, Drag, and Pitching Moment Coefficients for Blunt-Nosed Bodies of Revolution at Large Angles of Attack," Journal of the Aeronautical Sciences, Vol. 21, August 1954.
7. Allen, H. J., Perkins, E. W., "A Study of Effects of Viscosity on Flow Over Slender Inclined Bodies of Revolution," NACA TR 1048, 1952.
8. Allen, H. J., "Pressure Distribution and Some Effect of Viscosity on Slender Inclined Bodies of Revolution," NACA TN 2044, 1950.
9. Schwabe, M., "Pressure Distribution in Non-uniform Two-Dimensional Flow," NACA TN 1039, 1943.
10. Maslen, S. H., "Second Approximation to Laminar Compressible Boundary Layer on Flat Plate in Slip Flow," NACA TN 2818, 1952.
11. Tsien, Houe-Shen, "Superaerodynamics, Mechanics of Rarefied Gases," Journal of the Aeronautical Sciences, Vol. 13, No. 12, December 1946.
12. Tolefson, H. B., "An Investigation of Vertical Wind-Shear Intensities from Balloon Soundings for Application to Airplane and Missile Response Problems," NACA TN 3732, 1956.
13. Sissenwine, N., "Wind Speed Profile, Wind Shear, and Gusts for Design of Guidance Systems for Vertical Rising Air Vehicles," Air Force Cambridge Research Center, Air Force Surveys in Geophysics, 10 March 1954.

14. Anderson, Oiva R., "Some Considerations of Structural Design Criteria for Guided Missiles," Allied Research Associates, Inc., January 1958, WADC TR 58-196.
15. Foss, K. A., McCabe, W. L., "Gust Loading of Rigid and Flexible Aircraft in Continuous Atmospheric Turbulence," Massachusetts Institute of Technology, WADC TR 57-704, ASTIA Document No. AD-142170, January 1958.
16. "Analysis of Turbulence Data Measured in Flight at Altitudes up to 1600 ft. Above Three Different Types of Terrain," Cornell Aeronautical Laboratory, Inc., February 1959, ASTIA Document No. AD-212231.
17. Greenhow, J. S., Neufeld, E. L., "Measurements of Turbulence in the Upper Atmosphere," Proceedings of the Physical Society, Vol. 74, Part 1, No. 475, 1 July 1959.
18. Widger, W. K., Jr., "A Survey of Available Information on the Wind Fields Between the Surface and the Lower Stratosphere," Air Force Surveys in Geophysics No. 25, Air Force Cambridge Research Center, December 1952.
19. Hurst, G. W., "The Profile of the Jet Stream Observed," Quarterly Journal of the Royal Meteorological Society, Vol. 78, No. 338, October 1952, pp. 613-615.
20. Alaka, M. A., Jordan, C. L., and Renard, R. J., "The Jet Stream," NAVAER 50-IR-249, Bureau of Aeronautics, 1 June 1953.
21. Jenkins, C. F., "A Survey of Available Information on Winds Above 30,000 ft.," Air Force Surveys in Geophysics, No. 24, Air Force Cambridge Research Center, December 1952.
22. Sissenwine, N., "Development of Missile Design Wind Profiles for Patrick AFB," Air Force Surveys in Geophysics, No. 69, Air Force Cambridge Research Center, March 1958.
23. Sissenwine, N., "Revised 1% Synthetic Wind Profile," Geophysics Research Directorate, AFRCR 30, June 1959.
24. Lees, S., "Study on Wind Shear Measurements," ASTIA No. 149929, U.S. Army Signal Corps. Engineering Laboratory, Fort Monmouth, New Jersey.
25. Press, H., Meadows, M. T., Hadlock, I., "A Re-evaluation of Data on Atmospheric Turbulence and Airplane Gust Loads for Application to Spectral Calculations," NACA Report 1272, 1956.
26. Donely, P., "Summary of Information Relating to Gust Loads on Airplane," NACA TN 1976, November 1949, also NACA Report No. 997, 1950.

27. Press, Harry, "Atmospheric Turbulence Environment with Special Reference to Continuous Turbulence," Advisory Group for Aeronautical Research and Development, Report No. 115, April-May 1957, ASTIA Document No. AD-157286.
28. Press, H., and Houbolt, H. C., "Some Applications of Generalized Harmonic Analysis to Gust Loads on Airplanes," Journal of Aeronautical Sciences, Vol. 22, No. 1, pp. 16-26, January 1955.
29. Connor, R. J., Hawk, J., and Levy, C., "Dynamic Analysis for the C-47 Airplane Gust Load Alleviation System," Report No. SM-14456, Douglas Aircraft Co., Inc., July 29, 1952.
30. Summers, R. A., "A Statistical Description of Large-Scale Atmospheric Turbulence," Sc.D. Thesis, MIT, 1954. Also Report T-55, Instrumentation Lab., MIT, May 17, 1954.
31. Clementson, G. C., "An Investigation of the Power Spectral Density of Atmospheric Turbulence," Ph.D. Thesis, MIT, 1950.
32. Notess, C. B., and Eakin, G. J., "Flight Test Investigation of Turbulence Spectra at Low Altitude Using a Direct Method for Measuring Gust Velocities," Report No. VC-839-F-1, Cornell Aeronautical Laboratories, Inc., July 1954.

V. THE METEORITE ENVIRONMENT

AREAS OF INTEREST

The space vehicle traveling within the solar system will be exposed to the potential hazards of extra-terrestrial material. An analysis of this hyper-environmental problem must encompass the following areas:

- a. The origin of these space debris.
- b. The distribution of these particles and masses throughout the solar system.
- c. The physical parameters such as size, composition, velocity, etc.
- d. The probability that these materials will impinge upon inter-planetary rockets and the concomitant probability of structural and/or puncture type damage.

It is reasonable to assume that the extra-terrestrial materials are distributed throughout the solar system in varying quantities and with variant physical parameters. Primarily, this space debris consists of cometary and asteroidal wastage. Whipple (Reference 1) states that photographic and visual meteors are clearly of cometary origin except for a small fraction not exceeding 10 percent that may be of asteroidal origin.

THE ASTEROIDAL MATERIALS

Asteroidal bodies are generally concentrated in the region between the orbits of Mars and Jupiter (Reference 3) and in the plane of the ecliptic. It is highly possible that these asteroidal bodies are fragments from planets that have disintegrated as a result of explosions or collisions. At various times some of these bodies come within a few million miles of the earth. Particles are continually being chipped from these asteroidal bodies by the forces of nature (collisions, explosions, gravitational forces, oscillations caused by unbalanced masses, etc.). The term meteorite (technically) refers to bits and pieces (from asteroids) which have survived the rigors of passage through the earth's atmosphere. These meteorites may vary from less than a grain to as much as 70 tons and are our only tangible space debris. They are composed of high-density materials that may be classed roughly as irons, stony-irons, and stones (Reference 4). Robey (Reference 5) states that 20 percent of the meteorites are of the iron-nickel composition.

It can be assumed that the asteroidal particles are distributed by a random process throughout the solar system with the center or mean of this distribution located in the asteroidal belt. Natural forces tend to remove these particles from the area of mean concentration. The randomly ejected particles that fall outside of the asteroidal belt may assume independent orbits in the

solar system. Statistically, the distribution of the asteroidal material may be described, approximately, by a modified normal or Gaussian curve with the peak in the region between Mars and Jupiter and with the tails of the curve influenced by the various larger bodies in the solar system.

COMETARY MATERIAL

Comets are low-density collections of orbital material in our solar system that contain rarefied gases, dust, and frozen ices. Comets disintegrate rapidly under exposure to strong solar heat during the perihelion phase (point nearest the sun) of their orbit. Cometary material has a low-density of 0.05 gm/cm^3 (Reference 6). Fragments and particles from the comets enter the earth's atmosphere to become meteors. The luminous phenomenon is called a meteor and the cometary particle or fragment that produces this phenomenon is a meteoroid. The smallest of these particles, in the form of dust, are called micrometeorites and are, generally, concentrated in the plane of the earth's orbit and along the orbit of comets. Some of the meteoroids can be expected to depart from the primary orbits of the comets and to travel in independent orbits. In any case, the solar distribution of these cometary particles will vary in intensity with the greatest concentration along the cometary orbits.

DAILY INFLUX AND INTERPLANETARY DEBRIS

The daily influx of space debris (from both asteroids and comets) provides some slight indication of the amount of material in the solar system. Unfortunately, estimates of this daily influx range over several orders of magnitude. Estimates of the daily influx of extra-terrestrial material entering the earth's atmosphere run from 10 tons per day to 1 million tons per day (References 2 and 3). In 1958, Soviet scientists reported an influx of 800,000 to 1 million tons per day based on satellite data. Whereas the earth's orbit lies between the orbits of Venus and Mars, it is reasonable to assume that near future interplanetary travel will be from earth to Venus and Mars. For this reason, investigations may be limited to the area bounded by the orbits of these two neighbors of earth. It may be concluded also that since the earth is in the middle of this interplanetary travel area, the amount of space debris surrounding the earth may be indicative of the material in space between Mars, earth, and Venus. Furthermore, the velocities and masses of meteorites that an interplanetary space vehicle might encounter are equivalent to those found near the earth. An exception of this generalization is that slightly higher velocities will be found near Venus and slightly lower velocities will be found near Mars. Proportionately, this would apply also to the magnitude of any vibrations induced on space vehicles by any meteoritic impingement.

VELOCITIES

Extra-terrestrial bodies enter the earth's atmosphere with velocities ranging from 11 km/sec to 72 km/sec (approximately 7 miles/sec to 45 miles/sec) (References 1, 2 and 3). Note that the velocity of space debris entering the earth's atmosphere cannot be less than 11 km/sec because of the earth's gravitational attraction. This lower velocity limit is equivalent to the condition wherein the meteorite and the earth are placed beside each other with zero relative velocity and the earth's gravitational pull causes the meteorite to attain a velocity of 11 km/sec. The highest velocity, 72 km/sec, is a summation of the earth's velocity about the sun, 30 km/sec, and the maximum attainable velocity, 42 km/sec, of a meteorite in the solar system when its distance from the sun is that of the earth. It is interesting to point out that meteorites with orbits closer to the sun will display higher velocities. This is substantiated by the fact that such bodies require higher velocities to maintain their orbits while counteracting the greater gravitational force near the sun.

Sample data on meteor velocities are presented in Figure 45. These grouped type data were taken from Reference 7 and represent the velocities for 285 sporadic and 75 shower meteors photographed by Baker Super-Schmidt cameras at Dona Ana and Soledad, New Mexico, from February, 1952, to July, 1954. The meteor photographs were selected on a random basis in order to eliminate any possible bias. This histogram shows that the meteor velocities are in good agreement with the 11 km/sec to 72 km/sec range. It can be seen that the velocity distribution is bimodal for both the sporadic and the shower meteors. The sporadic meteors display the highest peak in the 15 km/sec to 20 km/sec class, while the shower meteors display the highest peak in the 35 km/sec to 40 km/sec class. The mean velocities (calculated from the original ungrouped data) for the sporadic and the shower meteors are 33.6 km/sec and 42.8 km/sec, respectively. The mean velocity or grand average for the combined sporadic and shower meteor data is 35.5 km/sec.

Hawkins and Southworth (Reference 7) calculated the mean height for meteors of various velocities from observations of beginning light, maximum light, and end of light. These observed data, plotted in Figure 46, indicate that meteoric hazard is definitely nonexistent below an altitude of 80 km.

ESTIMATED DATA ON OTHER PARAMETERS

A valuable contribution on meteoric information has been presented in Reference 6 and is published herein as Table II. This table gives estimated data on mass, size, velocity, kinetic energy, influx, and penetration probabilities for meteoroids of visual magnitudes from zero to 31. The unit of visual magnitude is inversely proportional to mass. A mass of 25 grams is assigned to a meteor of visual magnitude zero according to the Harvard Photographic Meteor Program. The mass decreases by a factor of $10^{0.4}$ ($=2.512$) for each increment of visual magnitude. It should be mentioned that the fundamental characteristics of the meteoroids of Table II are extrapolations beyond the visual range, i.e., the particles discussed are below the range

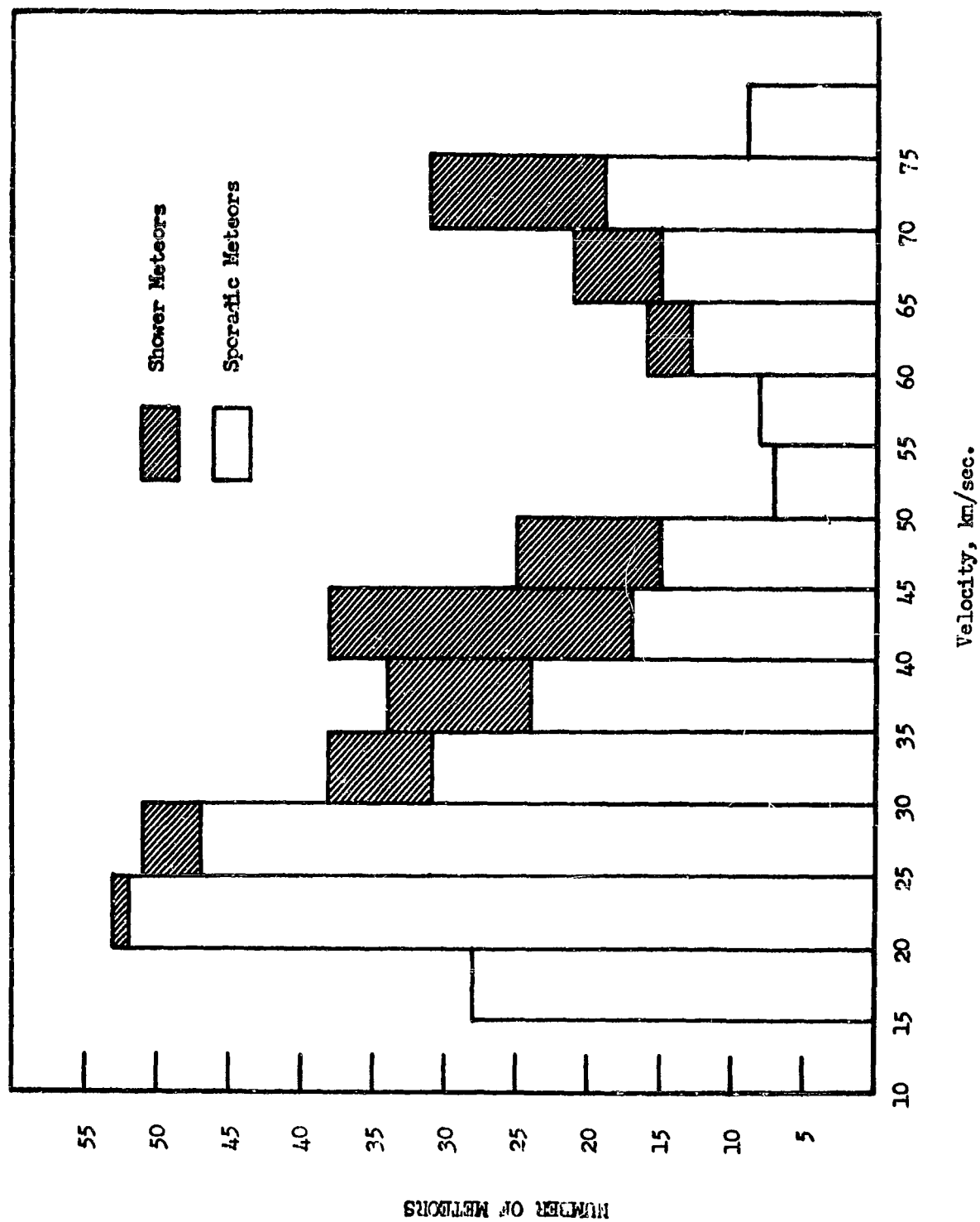


Figure 45. Distribution of Velocities for 285 Sporadic and 75 Shower Meteors.

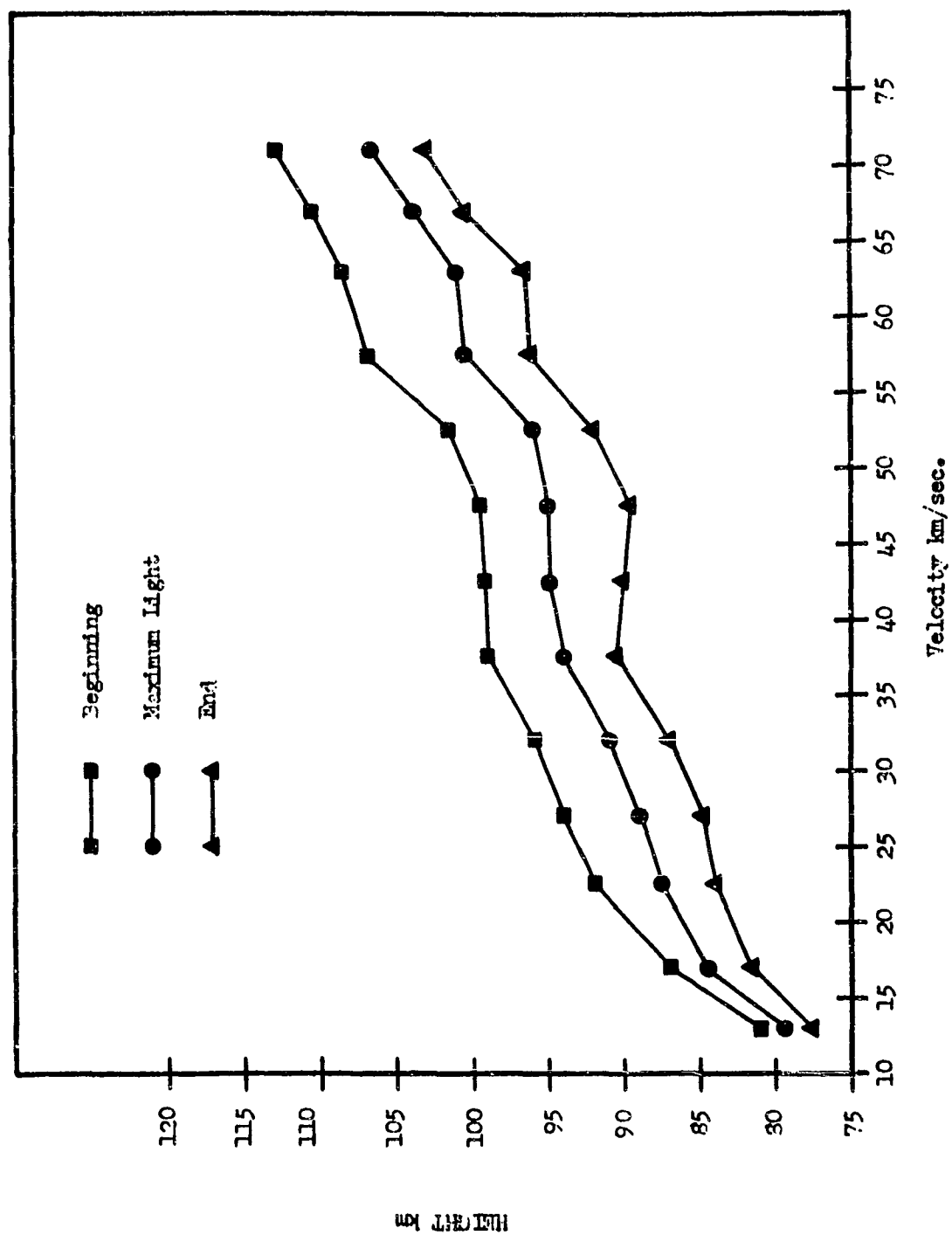


Figure 46. Mean Heights of Beginning, Maximum Light, and End for Sporadic Meteors of Various Velocities.

Table II
DATA CONCERNING METEORIODS AND THEIR PENETRATING PROBABILITIES

(1) Meteor Vis. Mag. "	(2) Mass (gm)	(3) Radius (Microns)	(4) Ass. Vel. (km/sec)	(5) K.E. (ergs)	(6) Pen. in Al. (cm)	(7) No. Earth Per Day	(8) No. 3-m Sphere Per Day
0	25.0	49,200	23	1.0×10^{14}	21.3	-	-
1	9.95	36,200	23	3.98×10^{13}	15.7	-	-
2	3.96	26,600	23	1.58×10^{13}	11.5	-	-
3	1.53	19,600	23	6.31×10^{12}	8.48	-	-
4	0.623	14,400	23	2.51×10^{12}	6.24	-	-
5	0.250	10,600	23	1.00×10^{12}	4.59	-	-
6	9.95×10^{-2}	7,900	23	3.98×10^{11}	3.38	-	-
7	3.96×10^{-3}	5,740	23	1.58×10^{11}	2.48	-	-
8	1.53×10^{-3}	4,220	27	5.87×10^{10}	1.79	-	-
9	6.23×10^{-3}	3,110	26	2.17×10^{10}	1.23	-	-
10	2.50×10^{-3}	2,290	25	7.97×10^9	0.917	-	-
11	9.95×10^{-4}	1,680	24	2.93×10^9	0.656	-	-
12	3.96×10^{-4}	1,240	23	1.07×10^9	0.469	-	-
13	1.53×10^{-4}	910.	22	3.89×10^8	0.335	-	-
14	6.23×10^{-5}	669.	21	1.41×10^8	0.238	-	-
15	2.50×10^{-5}	492.	20	5.10×10^7	0.170	-	-
16	9.95×10^{-6}	362.	19	1.83×10^7	0.121	-	-
17	3.96×10^{-6}	266.	18	6.55×10^6	0.0359	-	-
18	1.53×10^{-6}	196.	17	2.33×10^6	0.0608	-	-
19	6.23×10^{-7}	144.	16	8.20×10^5	0.0430	-	-
20	2.50×10^{-7}	106.	15	2.87×10^5	0.303	-	-
21	9.95×10^{-8}	78.0	15	1.14×10^5	0.223	-	-
22	3.96×10^{-8}	57.4	15	4.55×10^4	0.0164	-	-
23	1.53×10^{-8}	39.8*	15	1.81×10^4	0.0121	-	-
24	6.23×10^{-9}	25.1*	15	7.21×10^3	0.00884	-	-
25	2.50×10^{-9}	15.8*	15	2.87×10^3	0.00653	-	-
26	9.95×10^{-10}	10.0*	15	1.14×10^3	0.00480	-	-
27	3.96×10^{-10}	6.30*	15	4.55×10^2	0.00353	-	-
28	1.53×10^{-10}	3.98*	15	1.81×10^2	0.00260	-	-
29	6.23×10^{-11}	2.51*	15	7.21×10	0.00191	-	-
30	2.50×10^{-11}	1.58*	15	2.87×10	0.00141	-	-
31	9.95×10^{-12}	1.00	15	1.14×10	0.00103	-	-
						2 x 10 ⁸	2.22 x 10 ⁻⁵
						5.84 x 10 ⁸	6.48 x 10 ⁻⁵
						1.47 x 10 ⁹	1.63 x 10 ⁻⁴
						3.69 x 10 ⁹	4.09 x 10 ⁻⁴
						9.26 x 10 ⁹	1.03 x 10 ⁻³
						2.33 x 10 ¹⁰	2.58 x 10 ⁻³
						5.84 x 10 ¹⁰	6.48 x 10 ⁻³
						1.47 x 10 ¹¹	1.63 x 10 ⁻²
						3.69 x 10 ¹¹	4.09 x 10 ⁻²
						9.26 x 10 ¹¹	1.03 x 10 ⁻¹
						2.33 x 10 ¹²	2.58 x 10 ⁻¹
						5.84 x 10 ¹²	6.48 x 10 ⁻¹
						1.47 x 10 ¹³	1.63 x 10
						3.69 x 10 ¹³	4.09 x 10 ²
						9.26 x 10 ¹³	1.03 x 10 ³
						2.33 x 10 ¹⁴	2.58 x 10 ³
						5.84 x 10 ¹⁴	6.48 x 10 ³
						1.47 x 10 ¹⁵	1.63 x 10 ⁴
						3.69 x 10 ¹⁵	4.09 x 10 ⁴
						9.26 x 10 ¹⁵	1.03 x 10 ⁵
						2.33 x 10 ¹⁶	2.58 x 10 ⁵
						5.84 x 10 ¹⁶	6.48 x 10 ⁵

*Minimum radius permitted by solar light pressure.

observable by visual, photographic, or radio reflection techniques. The extrapolation is a necessary consequence of the fact that for practical application of any puncture theory, one is concerned with meteoritic particles of radius much smaller than 1 cm. It follows that the term "visual magnitude" (column 1) ceases to be meaningful; however, it is used in the table as a convenient argument, based on an adapted linear relationship between the luminosity and mass.

The radii presented in Column 3 of Table II were calculated on the basis of the mass values for spherical particles of density 0.05 gm/cm^3 . In actuality, the meteoroids will vary markedly in mean density and deviate considerably from the assumed spherical symmetry.

The velocities in Column 4 have been assigned on the following basis: for photographic meteors and average velocity is 28 km/sec; for smaller meteoroids the velocity has to decrease due to the reduction of the meteoroid orbital eccentricities and dimensions by physical effects. The mean value of 15 km/sec for the smallest meteoroids as well as the gradation of velocity with magnitude have been arbitrarily chosen. It is interesting to compare the velocity for photographic meteors (28 km/sec) with the grand average velocity of 35.5 km/sec calculated in the previous section from the data found in Reference 7: use of this higher velocity would increase the kinetic energies given in Column 5, Table II, by a factor of $\frac{35.5^2}{28^2}$.

The kinetic energies (Column 5) have been calculated directed from the assumed values of mass and velocity, and the penetration distance in aluminum (Column 6) has been calculated from an assumed relation, which (admittedly) lacks justification.

Data on entry of meteors into the earth's atmosphere have been extended to estimate the number of encounters with meteoroids per day that can be expected for a three-meter sphere. This has been accomplished by comparing the surface area of the earth with that of the three-meter sphere. A vehicle traveling within the earth's sensible atmosphere would be shielded somewhat from meteoroid collision by the earth.

Column 7 of Table II gives cumulative values of strikes on the earth's surface per day. This number includes all meteoric bodies brighter than or of mass greater than the number in the line in question. For example, there are 5.84×10^{18} meteoroids per day with a mass greater than 9.95×10^{-12} grams and a visual magnitude of 31 or brighter. Column 8 shows estimated puncturing probabilities for a three-meter sphere based on the assumption that the surface area of the earth exceeds that of a three-meter sphere by a factor of 4.51×10^{12} and that the shadowing effect of the earth of a spherical body near its surface equals $1/2$. Now then, consideration must be given to the case of the vehicle moving away from the earth's protective shield. At some time during this mission an altitude will be reached where the earth's shield will provide no protection and the $1/2$ factor will no longer apply. Therefore, this altitude will provide higher puncturing probabilities. As

the vehicle continues its journey through space it will enter regions where lower gravitational fields will result in less dense concentrations of space debris and decreased probabilities of puncture.

Using the data from this table, Whipple (Reference 6) predicts the probability of striking and penetrating a three-meter sphere with aluminum skin $1/8$ inch thick which corresponds to a penetration by a meteor of the 13th visual magnitude. On this basis, the three-meter sphere should be punctured once in three weeks on the average. It should be pointed out that this high rate of risk is strictly an estimation and until empirical data are available these data should be applied with extreme caution.

FIELD DATA

Measurements obtained on the Explorer missile (Reference 8) and the Pioneer missile (Reference 9) provide some interesting values for comparison with previous estimates. Comparative data were obtained during Pioneer I and Pioneer II flights (Reference 9) wherein the number of impacts for two momentum levels were recorded on these lunar shots. The instrumentation was set to measure (1) low momentum impacts between 3×10^{-4} and 10^{-2} gram-cm/sec and (2) high momentum impacts greater than 10^{-2} gram-cm/sec. These impact measurements were obtained over an area of 0.0381 square meter. The Pioneer I data show 11 low momentum strikes and one high momentum strike during a nine hour period. The Pioneer II data show different degrees of intensity for various recording periods. For example, during one period of receiver locked signal an unusually high density of 16 strikes was observed over a one minute period and during other recording intervals four strikes and no strikes were recorded. The momentum levels for these strikes were not reported in Reference 9. It is assumed that these strikes are in the low momentum range.

Meteorite impact data was telemetered during one of the Explorer flights. The sensitivity of the instrumentation was such that impacts equal to or greater than 10^{-9} grams at 30 km/sec would be recorded. To establish a common bond between Pioneer data and Explorer data, the impact sensitivity of the Explorer may be converted to a momentum value. Thus, the Explorer sensitivity of 10^{-9} grams at 30 km/sec becomes a momentum level equal to or greater than 3×10^{-3} gram-cm/sec. This value falls within the low momentum range of the Pioneer data. The Explorer measurements were obtained over an area of 0.07 square meters. A total of 150 impacts were recorded on the Explorer during 90,000 seconds of good telemetry which is equivalent to 1.66×10^{-3} impacts per second per 0.07 square meters or 2.38×10^{-2} impacts per sec per square meter.

In order to directly compare the Pioneer data with the Explorer data, the Pioneer impacts are converted to impacts per second per square meter. Thus, the 11 strikes per nine hours per 0.0381 square meter and the 16 strikes per minute per 0.0381 square meter measured on Pioneer I and Pioneer II, respectively, are calculated to be 9×10^{-13} and 7 impacts per second per square meter. In turn, these latter two values can be compared directly with

the 2.38×10^{-2} impacts per second per square meter measured on the Explorer. The high value of 7 impacts per second per square meter of Pioneer II appears to be in disagreement with the Explorer and the Pioneer I data. Perhaps this high value may be attributed to the passing of a meteor shower or to some magnetic or gravitational effect tending to concentrate meteoric particles.

INFERENCES ON PUNCTURE AND VIBRATION

It can be seen that our present knowledge on material in space is seriously limited both by observational inaccuracies and by a lack of field data. Consideration of the potential hazards indicates a continuous risk from minute particles to large puncture type debris. Several investigators have separated space debris into the two categories of (1) puncture type elements and (2) dust particles. Various estimates have been made on the probabilities of puncture. The consensus of investigations neglects the puncture problem and appears to concentrate on the erosion of vehicle materials exposed to the final dust particles. The bulk of meteorite dust is estimated to fall in the range between 10 microns (micron = one millionth of a meter) to 300 microns in diameter with an average diameter somewhere between 200 to 300 microns.

The vibration effects produced by these hypervelocity impacts may be estimated only by intuitive analysis and certainly with no quantitative accuracy. A search of the literature has failed to display any available data that correlate meteoric impacts with vibratory response within space vehicles. Lacking these data, the next logical step is to investigate the possibility of analyzing hypervelocity impacts for the purpose of estimating resultant vibration excitations. Any assessment of induced vibrations caused by these space materials requires a thorough understanding of the complex mechanics associated with hypervelocity impact.

The physics involved with this phenomenon becomes extremely difficult to formulate. Velocities from 11 km/sec to 72 km/sec should be produced to simulate meteoric velocities. This range covers the values expected of meteors (or meteoroids) within the neighborhood of earth. However, attempts to investigate this impact problem in the laboratory have resulted in the attainment of velocities in the region of 6 km/sec (approximately 20,000 ft/sec) (Reference 10), which are well below the minimum desired velocity of 11 km/sec. Furthermore, laboratory tests using these velocities assume a stationary target, whereas to be realistic, the laboratory impact studies should include the added effect of the moving target. Thus, the transfer of momentum and/or energy should be increased almost proportionately by the additional velocity of the space vehicle. Selecting the Pioneer lunar probe as a typical case, the moving target should reach a velocity as great as 11 km/sec. On this basis, an optimum test facility would be capable of creating hypervelocity impacts proportional to particle velocities of 11-72 km/sec plus target velocities approaching 11 km/sec. Penetration data from the above experiments is available (Reference 10); however, an extrapolation of these results to the realm of cosmic velocities would be of very questionable validity.

Another approach which has been employed utilizes a "liquid model" to examine hypervelocity impacts (Reference 11). This approach stems from the observation that when a high velocity projectile hits a target the pressure in the projectile at the start of the collision is several orders of magnitude (depending on the material and velocity) greater than the ultimate strength of the projectile material; under such conditions the materials must behave as though they had no shear or tensile strength at all, i.e. as fluids. Although some qualitative statements can be made from such studies, this approach has failed to yield a rigorous theoretical analysis of impacts at such velocities. Therefore, the depth of penetration or depth of surface mass loss by meteoroid impact is still a matter of speculation.

It might be mentioned here that use of the data of Table II and an elementary analysis yields time of impact of the order of microseconds. Although this fact is not to be taken literally, it can be used together with the shock response chart in Part II to give a measure of the vibration induced in the vehicle as a result of the impact.

The transfer of energy, momentum, or possibly combinations of both may accompany meteoritic impingement on space vehicles. At these high velocities the general rules of physics are no longer valid and prevent any quantitative prediction of vibration attributed to the meteorite environment. Many factors enter into an adequate definition of the hypervelocity impact process. Concurrent with the impact, various physical reactions occur in the projectile and the target material. Variants such as temperature, pressure, density, particle velocity, internal energy fields, viscosity, heat conduction, rate of impact, etc., add to the problem of solving hypervelocity mechanics and the prediction of vibration.

Considering the magnitude of meteorites which will not puncture a vehicle, together with the impact time, it is concluded that, in general, vibrations induced by extra-terrestrial materials will be negligible in magnitude and confined to a series of discontinuous impacts rather than a continuous rain. Certainly occasional meteor showers with masses greater than normal could create damaging structural vibrations. However, these encounters may be considered exceptions to the case and extremely difficult to predict. Furthermore, it is probable that meteorites capable of producing damaging structural vibration will create an extremely severe puncture problem so that the latter problem will occur first in time and be of paramount importance.

REFERENCES

1. Whipple, F. L., Smithsonian Contributions to Astrophysics, Volume 1, Number 1, page 83.
2. Rinehart, J. S., Meteor Distribution and Cratering, Technical Report No. 3, Contract No. AF18(600)-1596, Physics Division, Air Force Office of Scientific Research, ARDC and Smithsonian Institution Astrophysical Observatory.
3. Space Handbook: Astronautics and its Applications. Staff Report of the Select Committee on Astro-nautics and Space Exploration, U. S. Govt. Printing Office, Washington 1959.
4. Rinehart, J. S., Meteorites, Smithsonian Contributions to Astrophysics, Volume 1, Number 1, page 81.
5. Robey, D. H., Ground Simulation of Meteoritic Dust Impact on High Flying Vehicles, American Rocket Society, Paper No. 465-57.
6. Whipple, F. L., The Meteoritic Risk to Space Vehicles, American Rocket Society Paper No. 499-57.
7. Hawkins, G. S. and Southworth, R. B., The Statistics of Meteors in the Earth's Atmosphere, Smithsonian Contribution to Astrophysics, Volume 2, Number 11, Smithsonian Institution, Washington, D.C., 1958.
8. Private communication between Dr. Maurice Dubin, NASA, and D. T. Egbert, Norair Division, Northrop Corporation.
9. NAS Memo, 5-25-59W, USAF Space Probe, 1958.
10. NASA Technical Note D-238, May 1960.
11. For a qualitative discussion and further references, see Scientific American, October 1960, p. 128.

VI DIRECT VIBRATION EXCITATION

ROCKET ENGINE COMBUSTION INSTABILITY

Combustion instability in a rocket engine is a potential source of considerable vibration. This vibration will endure as long as the rocket engine operates, without regard for the external ambient conditions. Thus, in outer space where most other sources of excitation have ceased to exist, operation of a rocket engine will continue to induce vibration. In general, the vibration environment will tend to be most severe at positions near the engine, and diminish in more remote locations due to the damping inherent in the vehicle structure. It should be emphasized that although the following discussion gives general relationship regarding these instabilities, there is a tremendous variability in the vibration characteristics of rocket engines of varying design. Hence, it is desirable that the designer obtain measured data pertaining to his specific design.

Liquid Rocket Engines

Two regimes of liquid rocket engine instability, directly associated with combustion phenomena of propellants in the thrust chamber, have been noted. The oscillations which occur at lower frequencies are known as "chugging," while higher frequency oscillations are termed "screaming." They will be treated separately in the discussion which follows.

Chugging

The phenomenon described as chugging is a low-frequency instability characterized by abrupt and severe variations in combustion intensity which result in loss of specific impulse. The severity is such that it can cause the distortion or rupture of the chamber or injector.

Chugging is attributed, by many authors, to hydrodynamic coupling between the combustion-chamber pressure and the flow rates of propellants in the feed lines. The instability arises from a phase difference between the oscillations of these two systems which can be visualized from the following analysis, originally presented in Reference 1. The propellant feed system and the combustion-chamber pressure are closely interdependent. This interdependence dictates that a decrease in chamber pressure below its equilibrium value will cause an increase in the propellant flow to restore equilibrium. In practice, however, the increase in propellant flow is not simultaneous with the decrease of chamber pressure. This delay results from the inertia of the fluid in the feed lines and is termed the inertia time lag. A second time lag, termed combustion time delay, is caused by the time required for injection, impingement, mixing, vaporizing, pre-ignition reactions, ignition, and combustion.

Following combustion, a third delay associated with the time required to charge the chamber with gas takes place before the required pressure rise can occur. This third and final delay is called the charging time lag. These time lags, between

the onset of increased propellant flow and the resulting increase in chamber pressure, allow an excessive amount of propellant to enter the chamber. Therefore, when the chamber pressure does rise, it exceeds the pressure required to re-establish equilibrium conditions. This overpressure then causes the propellant flow rate to drop below normal with a subsequent decrease in chamber pressure. Thus, the sustained chugging oscillations result if no devices are present to stabilize the system. Note that the coincidence of a mechanical resonance in the engine or its feed lines with the chugging frequency usually results in engine destruction.

Since chugging has been rather thoroughly investigated and is now readily eliminated in newly designed rocket engines, it is not expected to be a vibration source for operational rockets. The above discussion has been included in this report to provide the designer with an awareness and basic understanding of the chugging problem. Those who desire further information on this topic may refer to Reference 1.

Screaming

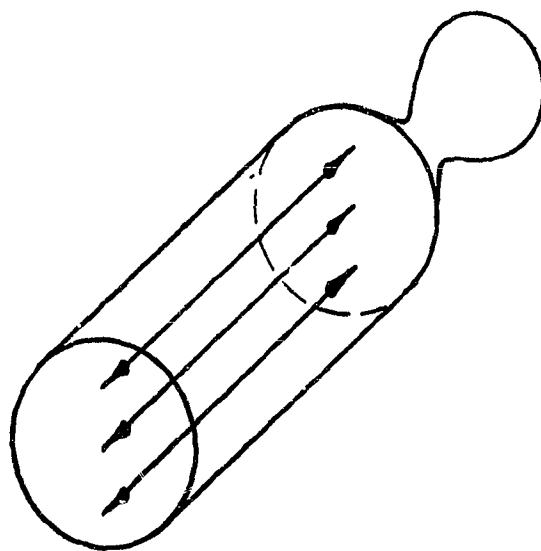
Screaming of a rocket engine is associated with acoustical resonances within the combustion chamber. Its onset is often characterized by an audible wailing sound (500-10,000 cps), a change in exhaust flame color toward blue, and oscillations of the shock positions in the exhaust wake (Reference 2). This form of instability exists in most high performance liquid rocket engines and, once initiated, will generally persist as long as the engine operates. Although screaming generates vibration excitation and results in increased heat transfer to the chamber surfaces (which may cause chamber, injector, or nozzle burnout failure), it provides some benefits. These benefits include an increase of specific impulse and improved efficiency in the fuel-oxidizer mixing process.

Screaming is considered to result from a coupling between one or more of the acoustical modes within the combustion chamber and the energy release from the combustion process. The occurrence of screaming in an engine design depends upon many factors, including the properties of the fuel, fuel-oxidizer mixture, chamber pressure, and chamber geometry. Consequently, investigations with a particular type of engine often discover regions of stability and instability, depending on the combination of these parameters.

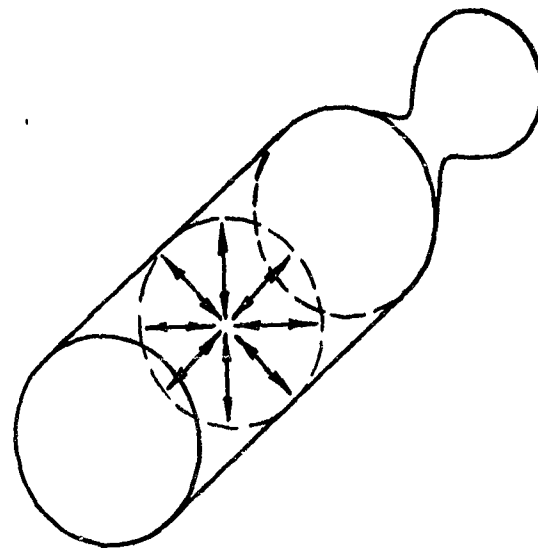
The frequency associated with screaming oscillations usually corresponds to one or more of the normal acoustical modes of the chamber (Reference 3). These basic modes include the longitudinal, transverse, and radial resonances which are sketched for a cylindrical chamber in Figure 47. The frequencies for a cylindrical chamber (Reference 4) are given by

$$f_{m,n,q} = \frac{a}{2} \left[\left(\frac{\alpha_{mn}}{R} \right)^2 + \left(\frac{q}{L} \right)^2 \right]^{\frac{1}{2}}$$

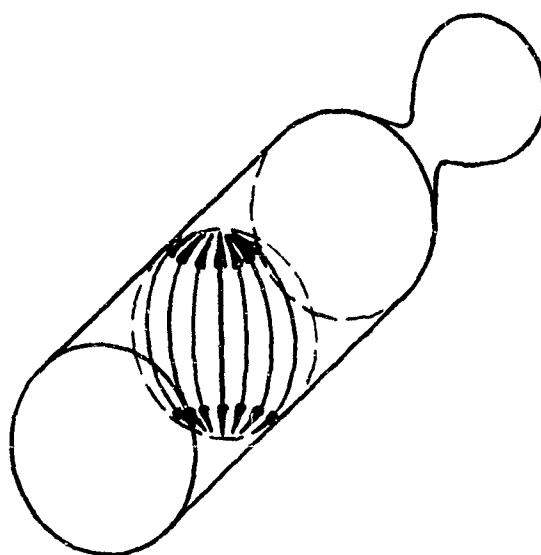
Figure 47. Normal Acoustical Modes for a Cylindrical Combustion Chamber



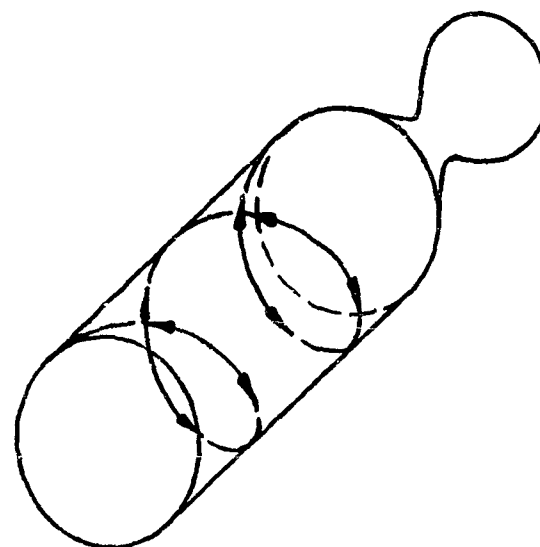
a. Longitudinal Mode
 $\begin{pmatrix} m = n = 0 \\ q = 1 \end{pmatrix}$



b. Radial Mode
 $\begin{pmatrix} n = 1 \\ m = q = 0 \end{pmatrix}$



c. Tangential, Circumferential, "Sloshing Mode", or Transverse Mode
 $\begin{pmatrix} n = q = 0 \\ m = 1 \end{pmatrix}$



d. Spinning Mode

where f = frequency, cps

a = velocity of sound in the chamber

R = chamber radius

L = chamber length

$\alpha_{m,n}$ = constant obtained from exact solution of the classical wave equation, and

m, n, q = integer wave numbers for the various modes.

$m, n, q = 0, 1, 2 \dots \infty$

If two of the three wave numbers are 0, the oscillation corresponds to a pure fundamental acoustical mode. Hence, $m = n = 0$ and $q = 1$ corresponds to the fundamental longitudinal organ pipe mode where the wavelength is twice the chamber length. Note that the choked flow condition at the nozzle acts as a reflection surface. The other combination, $m = q = 0$, and $n = 1$ gives the fundamental radial mode, and $n = q = 0$, $m = 1$ gives the fundamental transverse mode. Values of α_{mn} for the fundamental and higher modes are given below in Table III.

TABLE III

Characteristic Values of α_{mn} for the Cylindrical Chambers (Reference 4)

Values of m	0	Values of n 1	2	3
0	0.0000	1.2197	2.2331	3.2382
1	0.5761	1.6970	2.7140	3.7261
2	0.9722	2.1346	3.1734	4.1923
3	1.3373	2.5513	3.6115	4.6428

Although the velocity of sound is not constant throughout the combustion chamber, being higher in the regions of high combustion, the observed screaming frequencies are usually close to those calculated from the average velocity of sound in the chamber, which is given by

$$a = 315.5 \left(\frac{T_c}{\bar{m}} \right)^{\frac{1}{2}} \quad (\text{ft/sec})$$

where T_c is the chamber temperature ($^{\circ}\text{R}$) and

\bar{m} is the molecular weight of the combustion gases.

Thus, the expected frequencies from cylindrical combustion chambers can be calculated for a particular rocket if its chamber temperature, combustion gas molecular weight, and geometry are known.

Figure 48 gives the calculated range of frequencies for the fundamental modes as a function of chamber dimensions for a range of common propellants. This figure can be utilized for general orientation only and should not replace the more exact calculation.

A number of parameters must be considered to determine whether a rocket engine will scream in the longitudinal, the transverse, or a combination of modes. First, it appears that a given chamber tends to support the mode requiring the least amount of energy (e.g., the lowest frequency). From the equations it is seen that the longitudinal mode is the lowest mode for a chamber in which the length-to-diameter ratio exceeds 1.71. Thus, for cases where this length-to-diameter ratio is not exceeded, the first transverse mode is the lowest frequency mode for the chamber. This description, however, is an oversimplification and further considerations are necessary.

Consider the normal combustion chamber whose length is greater than 1.71 diameters. For a very low chamber pressure it may be found that no instabilities exist. Increasing the chamber pressure by the addition of greater amounts of propellant may result in the initiation of longitudinal oscillations. Further increasing the chamber pressure may provide a heat release rate sufficient to sustain a high frequency transverse mode, which will then be superimposed on the longitudinal wave. Forcing the chamber pressure still higher may cause the longitudinal wave to disappear entirely, leaving a pure transverse mode. Thus, as the energy available is increased, higher modes are seen to compete with the lower modes for prominence.

The amplitude of the pressure oscillation in a screaming thrust chamber is difficult to compute because it is affected by a multitude of parameters. The problem of analytic representation is further complicated by unknown local variations in chamber conditions. There are a number of agencies presently engaged in experimental research to further the state-of-the-art in this area.

A study was conducted by the National Advisory Committee for Aeronautics to determine the tendencies of various fuels to produce screaming (Reference 5). A 200-lb. thrust liquid-oxygen and fuel rocket engine was employed in this investigation. The fuels, in order of increasing screaming tendency, were (1) hydrazines (these did not scream at all), (2) branched-chain paraffins, aromatics and amines, and (3) straight-chain paraffins. This trend of increasing screaming tendency was noted to correlate with increasing evaporation ratio. In addition, the scream amplitude was observed to decrease slightly with increasing oxidant-fuel ratios greater than that required for peak thrust performance. However, the oscillatory pressure amplitudes were not repeatable for identical runs, indicating a rather complex mechanism.

Data from a number of experiments in rocket combustion instability (References 5 and 6) indicate that the peak-to-peak amplitude of the screaming pressures may

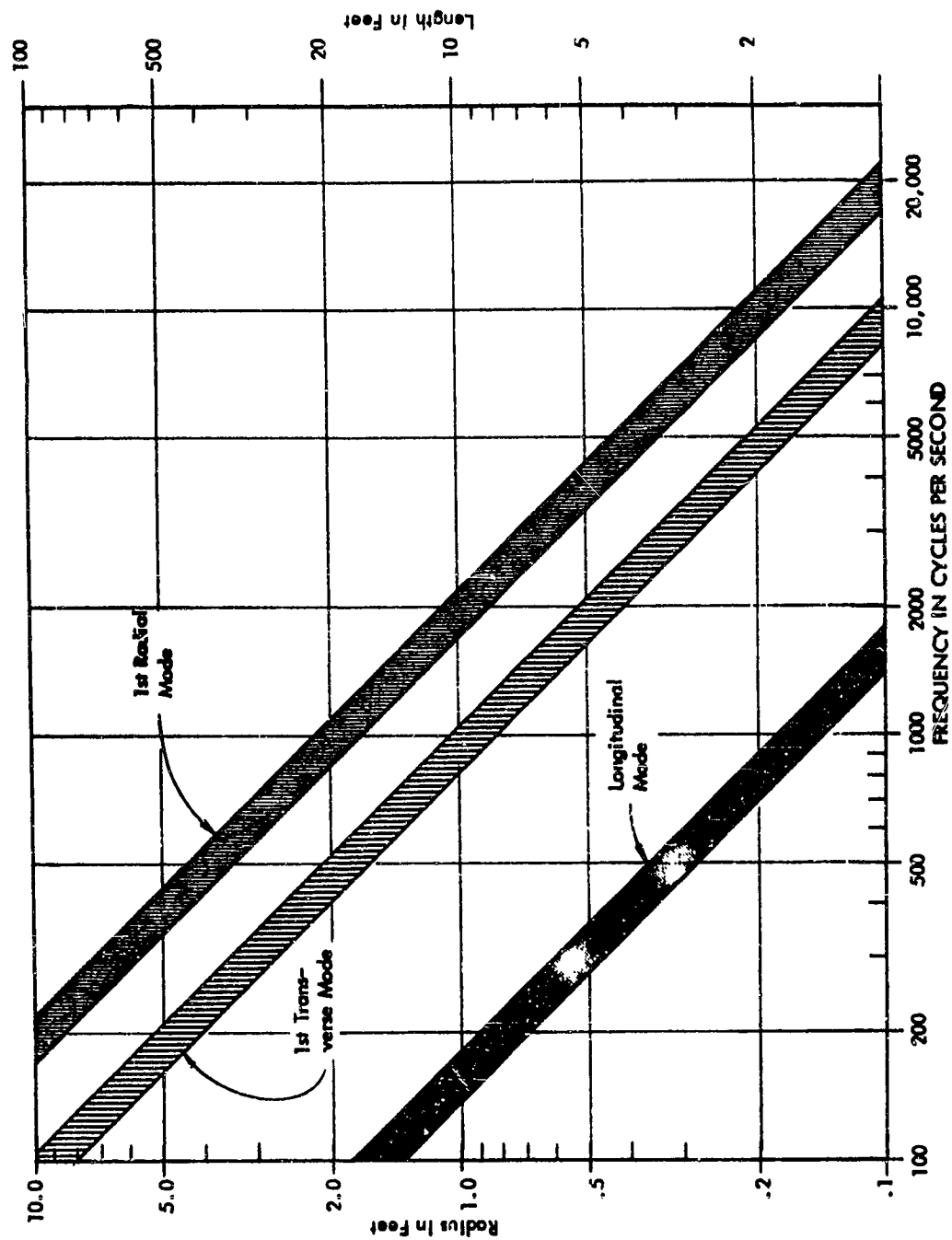


Figure 48. Calculated Range of Frequencies for the Fundamental Modes of a Closed-Cylindrical Chamber as a Function of Chamber Dimensions.

reach 75 to 100% of the mean chamber pressure. This would indicate that the total longitudinal force (rms) on the rocket motor at the longitudinal screaming frequency could be as much as 35% of the rocket's average thrust. However, because of non-linear acoustical considerations associated with high amplitude sound waves, the wave shape of the pressure oscillation becomes very steep approaching more nearly a sawtooth wave than a sinusoidal wave. Hence, the maximum rms force at the fundamental longitudinal screaming frequency is more probably on the order of 25 to 30% of the thrust.

Similar magnitudes of pressure fluctuations may occur at the fundamental transverse mode. However, in this case of the net force on the motor will be proportional to the magnitude of the pressure and the area of the chamber over which it acts. However, if the transverse mode is characterized by a spinning action, as shown by d in Figure 47, the net force vector will be materially reduced. Consequently, although screaming in the transverse mode may result in high vibrations on the chamber walls which may prove destructive, the phase relationships of these vibrations over the entire chamber often reduce their importance as a source of vehicle vibration.

Solid Rocket Engines

Solid rocket motors are often subject to the screaming oscillations previously discussed for the liquid propellant engine. The frequencies of the various modes may be calculated in the same manner as for the liquid engines (see Reference 7 for additional discussion and references). However, in general the fundamental transverse mode predominates unless the rocket burns only from the end of the propellant grain, which will excite the longitudinal mode.

From the vibration viewpoint, the major difference in the screaming characteristics of liquid and solid rockets is the variation of the frequency of the solid rocket with time from rocket ignition which contrasts with the stable frequency characteristic of the liquid motors. This variation in frequency with time reflects the increased internal dimensions within the solid rocket's combustion area which result from the burning of the grain. Hence, as burning progresses, the frequency of the transverse mode decreases.

A recent experimental series of vibration studies of a small center burning rocket used for high altitude final stage boosts, conducted by NRL (References 8 and 9) has illustrated that this decaying frequency associated with the transverse mode persists during the major portion of the burning time and is replaced at the end of the run by a short burst of high-level vibratory energy at the frequency of the fundamental longitudinal mode. Analysis of the data indicated that the net rms force from this longitudinal mode was at least 25% of the rocket thrust. This is consistent with the maximum estimates previously made for the liquid engine.

It should be noted that the NRL experiments have shown that a considerable difference in the magnitude of screaming vibration exists between supposedly identical rockets. Furthermore, rockets of a design known to scream will on occasion not scream at all during firing. Hence, if a designer is to have reasonable assurance

of the vibrations resulting from screaming for a specific type of rocket motor, it appears necessary to study the results from several firings.

Thrust Variations

Thrust variation will be important: (1) for the configuration of the vehicle which places the exhaust stream aft of all vehicle structures, (2) for the interconnecting structure between engine and vehicle, and (3) for the time following the peak of the acoustic excitation from the exhaust. It seems desirable to hold the engine peak thrust variation to a limiting value, such as three per cent or less. New design projects should give high priority to determining this quantity and to engine or propellant redesign when the thrust variations are excessive.

The basic mechanism involved in thrust variation is probably rough burning. The extreme turbulence within the combustion chamber is a result of the variable intensity of the combustion process and a result of the influence of pressure and temperature fluctuations on the rate of burning. Since the degree of roughness will not repeat itself on successive runs of the same engine, it shows the sensitivity of the burning to the internal turbulence and to the fluctuations in pressure and temperature which follow from the near explosive nature of the propellants. When the thrust variations are of the order of the three per cent, discussed previously, the variations are probably not due to acoustic vibration within the chamber or to combustion instabilities, both of which are discrete in frequency. The Rocketdyne data (References 10 and 11) shows the thrust variations to be broad band. The integral of the pressure fluctuations on the head of the case should equal the thrust variations. A large ratio of burning surface to the size of the chamber head would appear to be an alleviating parameter. The flexibility of the chamber and the damping of the combustion chamber structure might enter to a small extent.

Force variation in interconnecting structure will be loosely termed "thrust variation" in many cases. The force variation in the interconnecting structure will not be the same from case to case when the stiffness of the structure is not equivalent nor when the stiffness and mass of the back-up structure are not equivalent. The thrust variation and the dynamics of the entire system act to determine the force variations in interconnecting structure. It will be likely that broad band data contains peaks at the natural frequencies of the complete dynamic system which will often invalidate the data unless it is carefully interpreted by a vibration specialist.

It should be noted that the explosive nature of the ignition of a solid or liquid rocket engine creates a rapid build-up in thrust, with approximately a 10% overshoot in the thrust relative to the steady state thrust magnitude. The initial time lapse required for the thrust to attain its steady state magnitude is on the order of 10 or 20 milliseconds for a number of rocket engines. This time interval is very difficult to control for any engine, and therefore it is usually specified in terms of a maximum possible time lapse. This maximum time interval is a function of the type of igniter and propellants used, and the combustion chamber design. This rapid thrust rise acts as a shock-type input to the vehicle structure, and as such, is a potential source of structural vibration.

At burnout, the thrust decay is much more gradual, requiring on the order of .5 to 3 seconds. Normal burnout is therefore not expected to be of concern to the vehicle structural vibration problem.

Liquid Rocket Engine Vibration and Thrust Variations

Several excellent examples of recent liquid rocket engine data concerning vibration and thrust variations reported in References 10 and 11 were reviewed for this report. The results from the preliminary flight rating test of the Rocketdyne B2C engine are presented in Tables IV-VII. Data were recorded in three directions at each of four points: (1) The top of the adaptor flange between the 7" expansion joint and the fuel turbopump inlet, (2) the lower pillow block of the #2 thrust chamber gimbal bearing, (3) the bottom channel band of the B-2 engine, #2 thrust chamber, and the bottom reinforcing band of the B-3 engine, #2 thrust chamber, and (4) the strut attachment supporting the lube oil tank. Gulton piezos were used whose characteristics ranged as high as 35,000 cps resonance frequency, a/g range from .5 to 4,000 g's with a useful frequency response from 20 to 12,000 cps. The instrumentation is shown in Figure 49.

Reference to the high response levels shows that the many instrumentation problems which were experienced were not unexpected. Some accelerometers were damaged beyond repair and a high maintenance schedule was required. Vibration levels at ignition and cutoff were 7 to 10 times larger than vibration levels during mainstage. The high levels tended to overdrive the tape while the low levels were below the system noise. The runs were analyzed on the Panoramic Sonic Analyzer and the Tektronix Oscilloscope. The analyzer provided a frequency spectrum from 40 to 20,000 cps. The values given in the tables are approximations from the analyzer and the oscilloscope at the dominant frequencies. When the data is summarized in so brief a fashion, data concerning the non-dominant frequencies are lost. Reasonable tests of the data were made concerning a possible spurious signal and concerning acoustic coupling.

The maximum values obtained were:

	g rms	cps	E _o -peak	
Adaptor Flange to Fuel Pump Inlet	350	8000	850	vert.
Gimbal Bearing	150	1100	625	vert.
Thrust Chamber	550	2200	1850	vert.
	540	1200	2000	lat.
Lube Oil Tank	75	600	210	vert.

The time interval used to determine the peak value was 2.0 seconds for ignition and cut-off and a variable from five seconds to .5 millisecond for the mainstage.

The Rocketdyne S-3D engine has 150,000 pounds thrust and is used in Weapon System 315A, the Thor missile. The engine is attached to the vehicle structure at three attach points with a tubular truss interconnecting structure. The thrust variation (Figure 50) listed represents the maximum peak thrust variation during a time interval of .7 seconds, approximately ten seconds after ignition. The variations

TABLE IV
SUMMARY OF MAXIMUM ACCELERATION RESULTS
PFRT VIBRATION STUDY FOR THE B2C ROCKET ENGINE

ADAPTOR FLANGE VIBRATIONS				
Direction and Run Number		Panoramic Sonic Analyzer	Tektronix	
		Predominant Frequencies (cps)	Max. g^{rms}	Max. g^{pk} Peak-to-Peak
Vertical Plane	Ignition & Cutoff	8000	176	<u>Cutoff</u> 900
	Ignition	8000	350	1700
Lateral Plane	Mainstage & Cutoff	8000	176	680
	Cutoff	8000	147	645
Longitudinal Plane	Ignition	4000-5500 8000	40 90	660

TABLE V
SUMMARY OF MAXIMUM ACCELERATION RESULTS
PFRT VIBRATION TEST FOR THE B2C ROCKET ENGINE

GIMBAL BEARING VIBRATIONS				
Direction and Run Number		Panoramic Sonic Vibrations		Tektronix
		Frequencies (cps)	Max. "g" rms	Max. "g" Peak-to-Peak
Vertical Plane	Ignition Mainstage	900	42	<u>Ignition</u> 255
	Cutoff	1100	184	520
	Cutoff	1100	150	1250
Lateral Plane	Mainstage Cutoff	1600-2200	3	<u>Cutoff</u> 133
	Cutoff	1200	94	430
	Cutoff	1100	56	695
		1200-4000	19	
Longi- tudinal Plane	Cutoff	50	53	320
		500-2200	8-23	
	Ignition	40	240	1100
		60-200	64-160	
	Cutoff	1100	42	250
		2500	18	
		5500-8000	12	

TABLE VI

SUMMARY OF MAXIMUM ACCELERATION RESULTS
PFRT VIBRATION TEST FOR THE B2C ROCKET ENGINE

THRUST CHAMBER VIBRATIONS				
Direction and Run Number		Panoramic Sonic Analyzer		Tektronix
		Predominant Frequencies (cps)	Max. "g" rms	Max. "g" Peak-to-Peak
Vertical Plane	Ignition	550	100	540
	Cutoff	800	216	3280
		1200	270	
		1600-1800	216	
		2200	440	
	Cutoff	1100-2000	220-275	3700
		2200	550	
Lateral Plane	Ignition & Cutoff	800-1000	75	570
	Cutoff	800	270	4000
		800-1100	320	
		1200	540	
	Ignition & M. S.	500-1800	30-70	760
Longitudinal Plane	Ignition	50	53	220
		500-2200	8-23	2600
	Cutoff	1200	460	
	Cutoff	1100	340	3400

TABLE VII

SUMMARY OF MAXIMUM ACCELERATION RESULTS

PFRT VIBRATION TEST FOR THE B2C ROCKET ENGINE

LUBE OIL TANK VIBRATIONS					
Direction and Run Number		Panoramic Sonic Analyzer			Tektronix
		Predominant Frequencies (cps)	Max. "g" rms		Max. "g" Peak-to-Peak
Vertical Plane	Ignition M.S. Cutoff	500-7000	5-25		220
	M.S.	600	75		425
	M.S.	600 1800	50 35		280
Lateral Plate	Ignition M.S. Cutoff	500-4500	5-20		180
	M.S.	600	100		360
	M.S. Cutoff	400-4500	10-50		230-300
Longitudinal Plane	Ignition M.S. Cutoff	450-7000	5-20		<u>Cutoff</u> 190
	M.S.	400	50		215
		No Records Available			

ORIENTATION OF ACCELEROMETERS LOCATED ON THE B2C ROCKET ENGINE

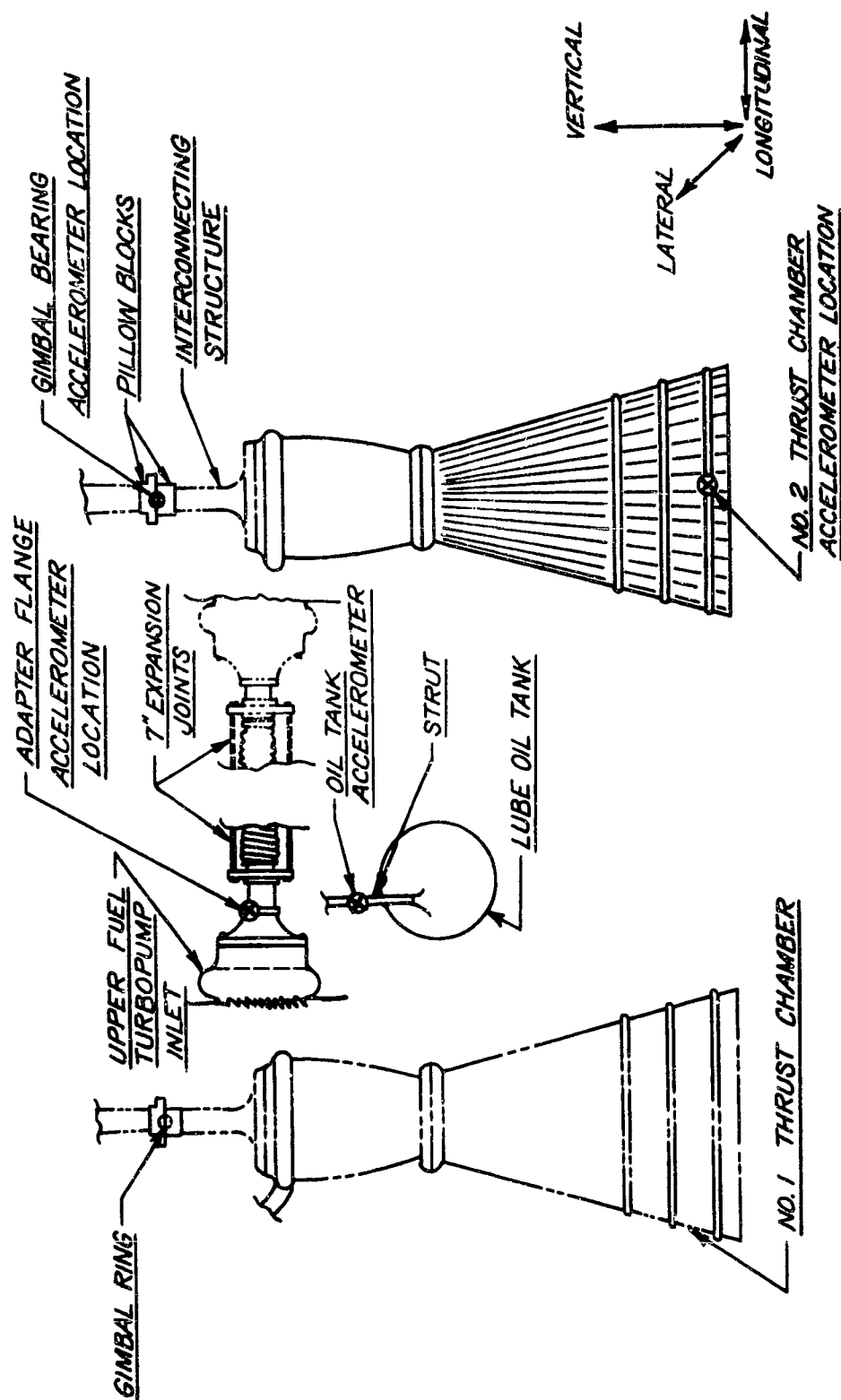


Figure 49. Sketch of Rocketdyne B2C Rocket Engine Vibration Instrumentation

Notes:

1. Maximum peak thrust variation occurring in .7 seconds of mainstage burning, 10 seconds following ignition.
2. Predominant frequencies were 500 and 650 cps.
3. No significantly greater thrust variation appeared to exist during ignition and cutoff.

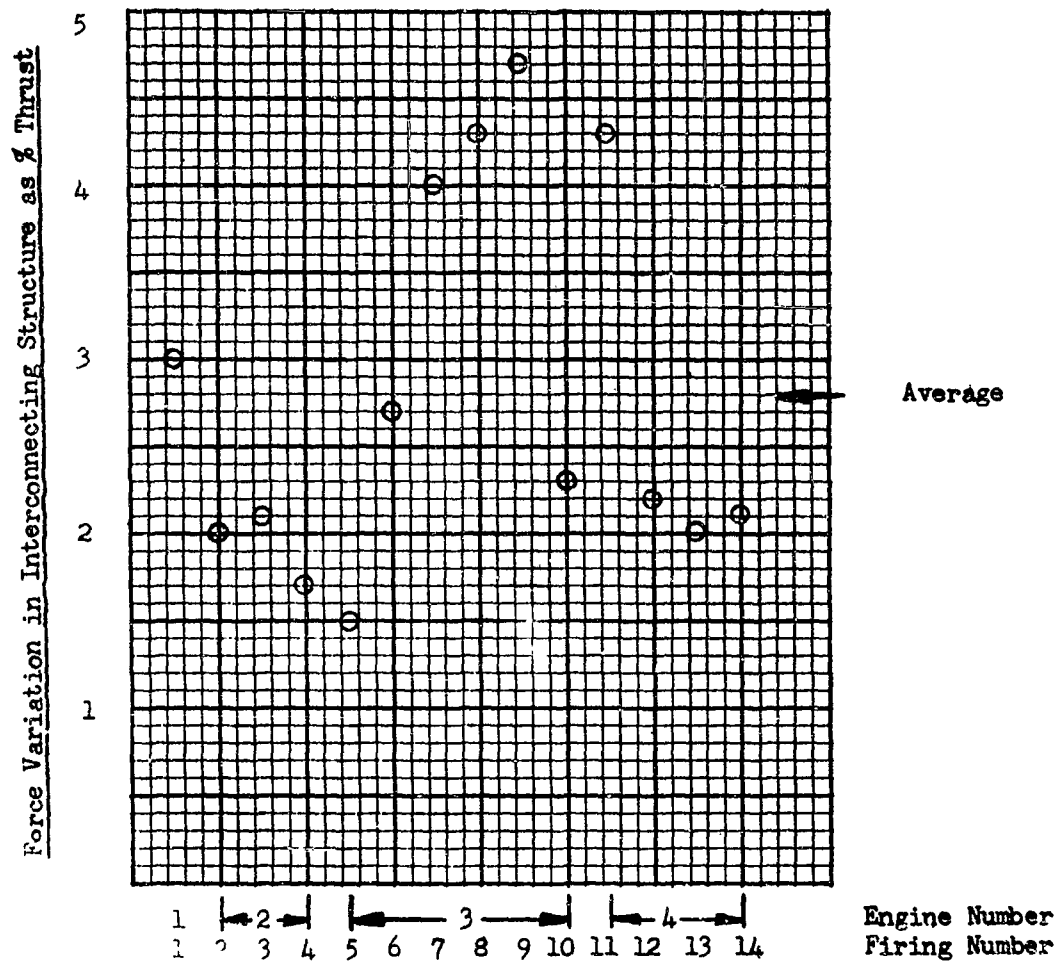


Figure 50. Thrust Variation During Mainstage Burning - S-3D Rocketdyne Engine 150,000 lbs. Static Thrust.

describe the mainstage burning and do not include the periods of ignition and cut-off. For thrust variations, the frequency range is 2 to 1250 cps. For all firings, the predominant frequencies were 500 and 650 cps. A low frequency instrumentation system covered thrust frequency bands of 0 to 200 cps. There were no predominating frequencies less than 40 cps. Frequencies between 40 and 80 were present during ignition and cut-off on one firing and are shown in Figure 51. The other twenty firings did not have frequencies less than 110 cps during ignition and the mainstage. Frequencies of 80, 100, and 1100 cps were present during cut-off at all three attachment points. A high frequency instrumentation system covered the band 250 to 10,000 cps. A rough combustion cut-off accelerometer monitors the engine operation over the frequency band 40 to 3,500 cps. The vibration on either side of the attachment points (engine side or upstream structure) was approximately equal in each case. The vibration data was taken at seven points: (1) The three attachment points, vertical direction, (2) lateral motion along the axis about which the missile pitches, (3) lateral motion along the axis about which the missile yaws, (4) lox injector flange, the vertical direction, (5) rough-combustion cut-off accelerometer on the head of the engine, vertical direction. The latter two pickups are very close and a photo suggests the two should read nearly equal amplitudes which is borne out by the majority of the data but not by the extreme values.

Maximum values recorded were

± 4.7 per cent variation in total thrust

± 6.5 per cent variation at any one attachment point

However, the arbitrary restriction to reading data at a point ten seconds following ignition was responsible for ignoring a thrust variation equal to twice the value used. For this one case, the maximum values are then.

± 6 per cent vibration in total thrust

± 7.4 per cent variation at any one attachment point

Maximum vibration acceleration g rms in low frequency region less than 150 cps were

1.1 g rms, ignition, 55 cps

8.1 g rms, cut-off, 100 cps

6 ϵ_{o-p} , ignition

30 ϵ_{o-p} , cut-off. See Figures 51 and 52.

Maximum values of the high frequency vibrations (predominant frequencies 500 and 600 cps) were

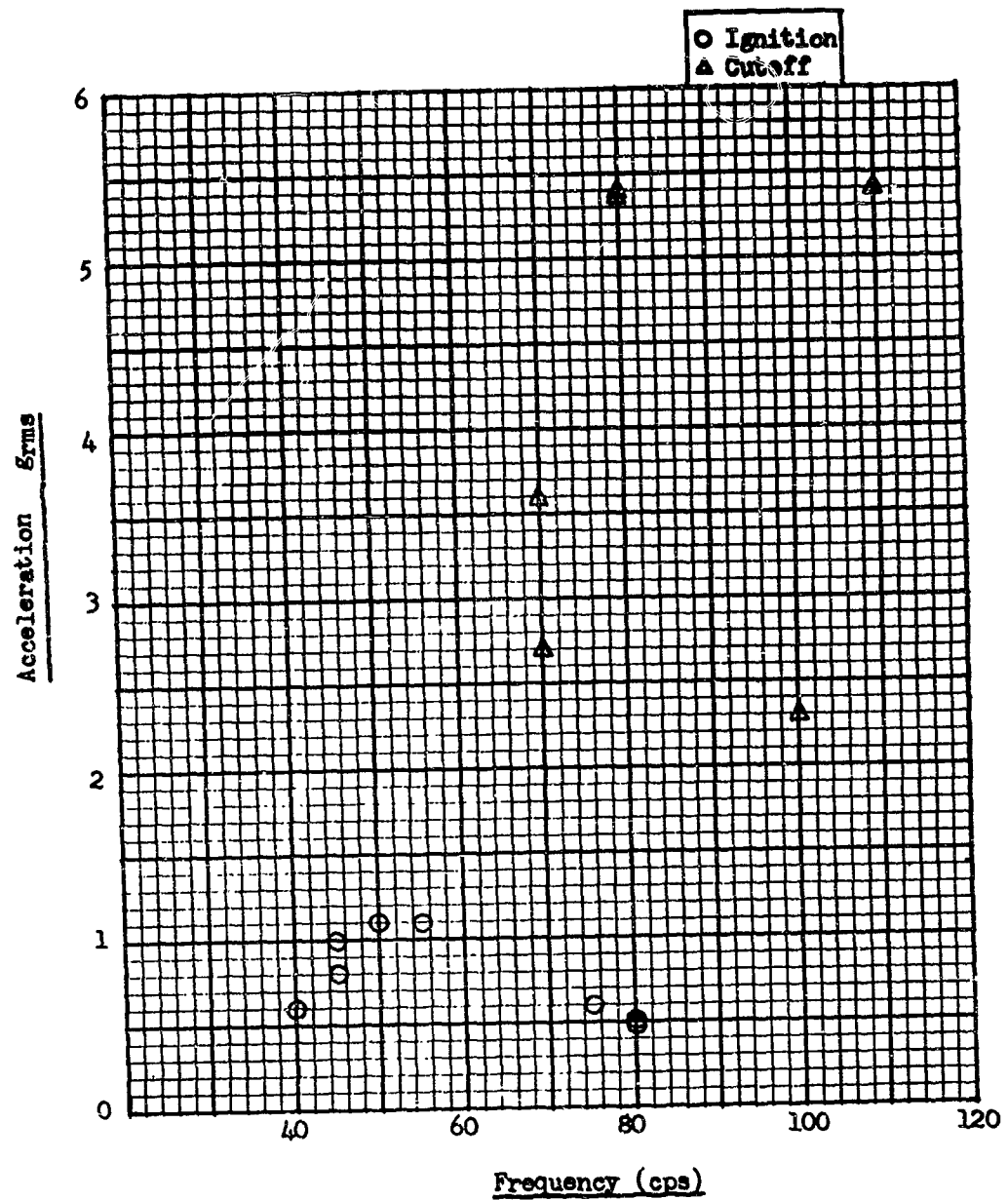


Figure 51. Low Frequency Vibration of Attach Points - S-3D Rocketdyne Engine Frequency Analysis.

	g rms	g ₀ -peak	Figure
Attachment points, vertical	27	87.5	53
Attachment points, lateral along pitch	40	80	54
Attachment points, lateral along yaw	28	105	55
Lox flange, vertical	32	127	56
Rough combustion cut-off accelerometer, vertical	68	200	57

A very interesting example of direct vibration from solid rocket boosters is given in the following:

Early reliability failures on the Snark missile led to ground firings of the large solid-propellant booster rocket which are used to zero launch the missile. The missile is launched in horizontal flight at an acceleration of 4 g's under the combined 260,000-pound thrust of these two boosters. For these ground firings, the boosters were detached structurally from the missile to determine the importance of the acoustic environment. For the purposes of this report, an opportunity existed to determine if an increment in response were present which should be ascribed to thrust variations transmitted directly to structures. A drawing and some of the characteristics of the booster bottles are shown in Figure 92. The nozzle is canted down and away from the fuselage, with a 26-degree angle between the thrust centerline and the bottle centerline. A pick-up on basic structures at Fuselage Station 600 near the main guidance equipment rack is within a few feet of the nozzle. Instead of the vibration being lessened with bottles detached, it was increased by approximately 1/3 over the whole frequency spectrum, although the variation at individual 1/3 octave bands was large.

During the "acoustic firings" the missile and the rocket are within a few feet of the ground giving a ground plane effect which is not present in an actual launching. A 3 db increase in the environment is probable which yields, according to Figures 93 - 98, a 21 to 40 per cent increase in response acceleration depending on the frequency band. This coincidence of the two increments suggests there was no effect on the response created by thrust variations.

Assuming the increase in total response would have to be 10 to 15 per cent to be noticeable, the response due to thrust variation would need to be .3 to .57 of the response due to the acoustic environment because of the way in which random traces are added. The ability to detect small thrust variation by response comparisons is negligible.

An important deduction was responsible for identifying the domination of the Snark acoustic environment from some of the available oscillograph data. A nose pick-up at the instant of launch presented the data shown in Figure 58. Structural-borne vibration proceeds through structures at a speed which varies from 15,000 ft. per second for plane waves transmitted longitudinally in the material to only 2,400 ft. per second at 1,200 cps and 600 ft. per second at 100 cps for skin waves transmitted longitudinally in the cylindrical fuselage. The smooth build-up to 4 g's horizontal acceleration is shown on the Statham, identifying the instant of build-up

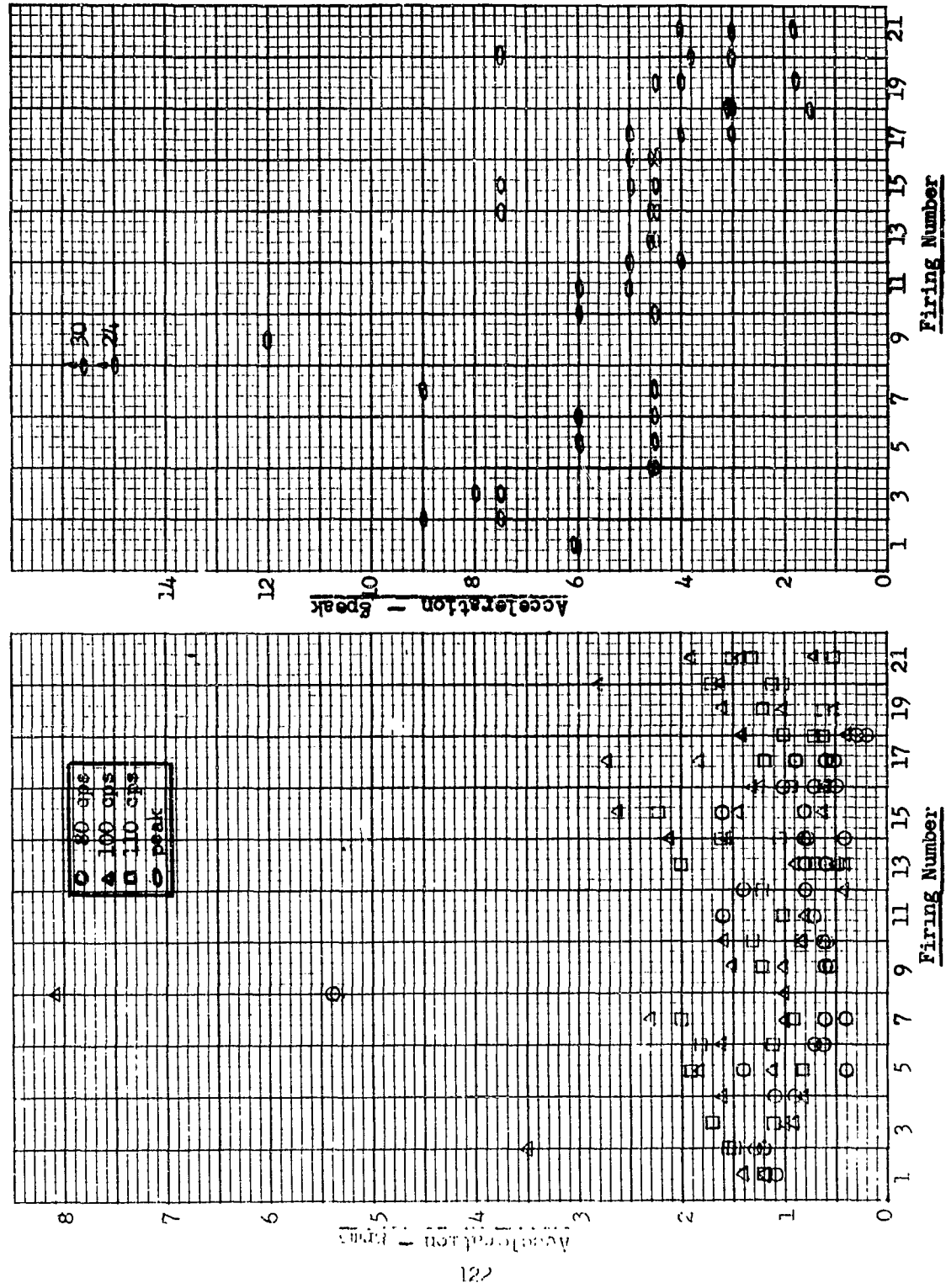


Figure 52. Variation in Cutoff Vibration During Separate Firings at the Three Attach points, (S-3D Engine)

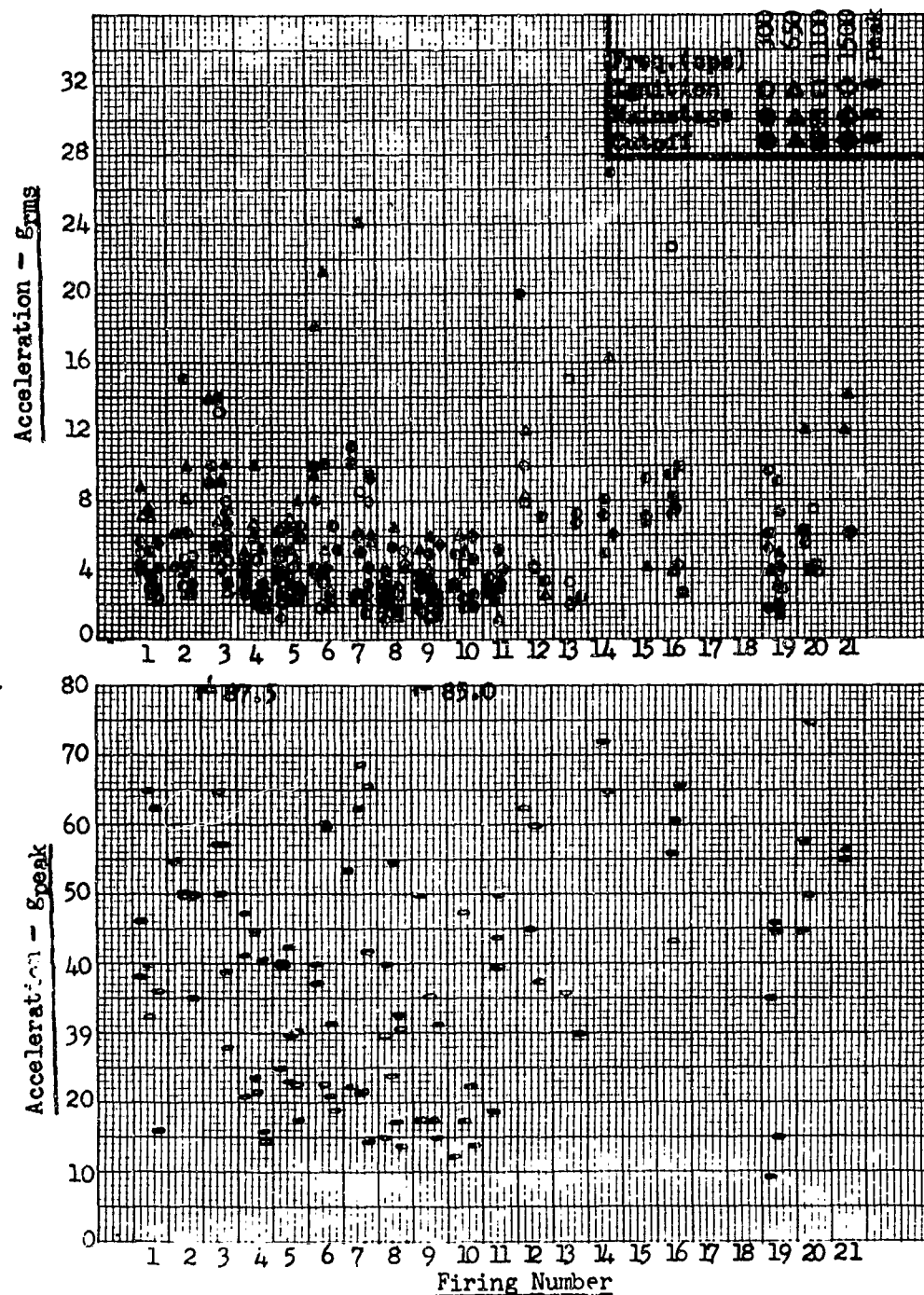


Figure 53. Vibration at the Attach Points in the Thrust Direction. Only the amplitudes of the Most Dominant Frequencies are Shown (S-3D Engine)

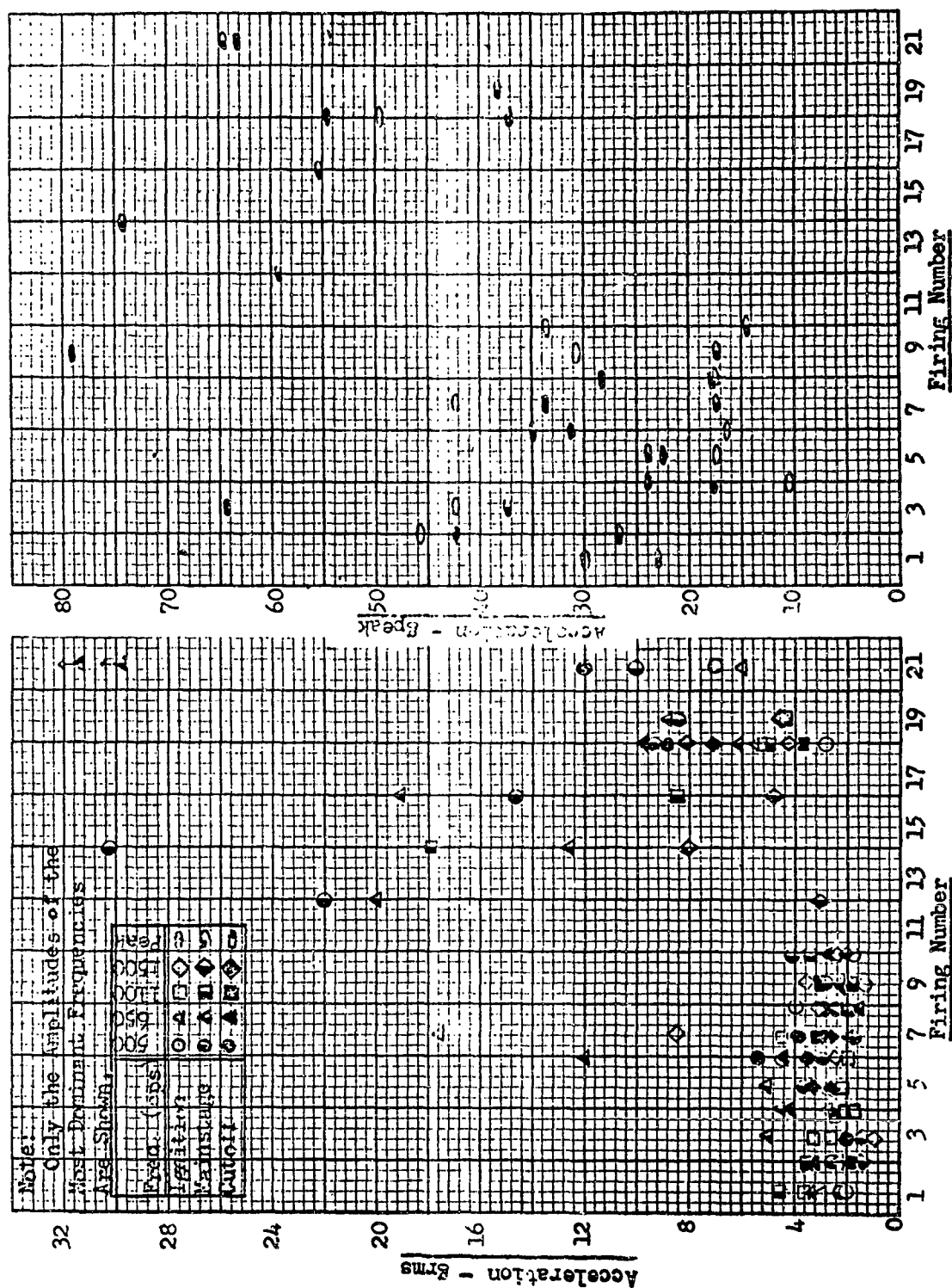


Figure 54. Vibration at the Attach Points Perpendicular to the Thrust Direction - S-3D

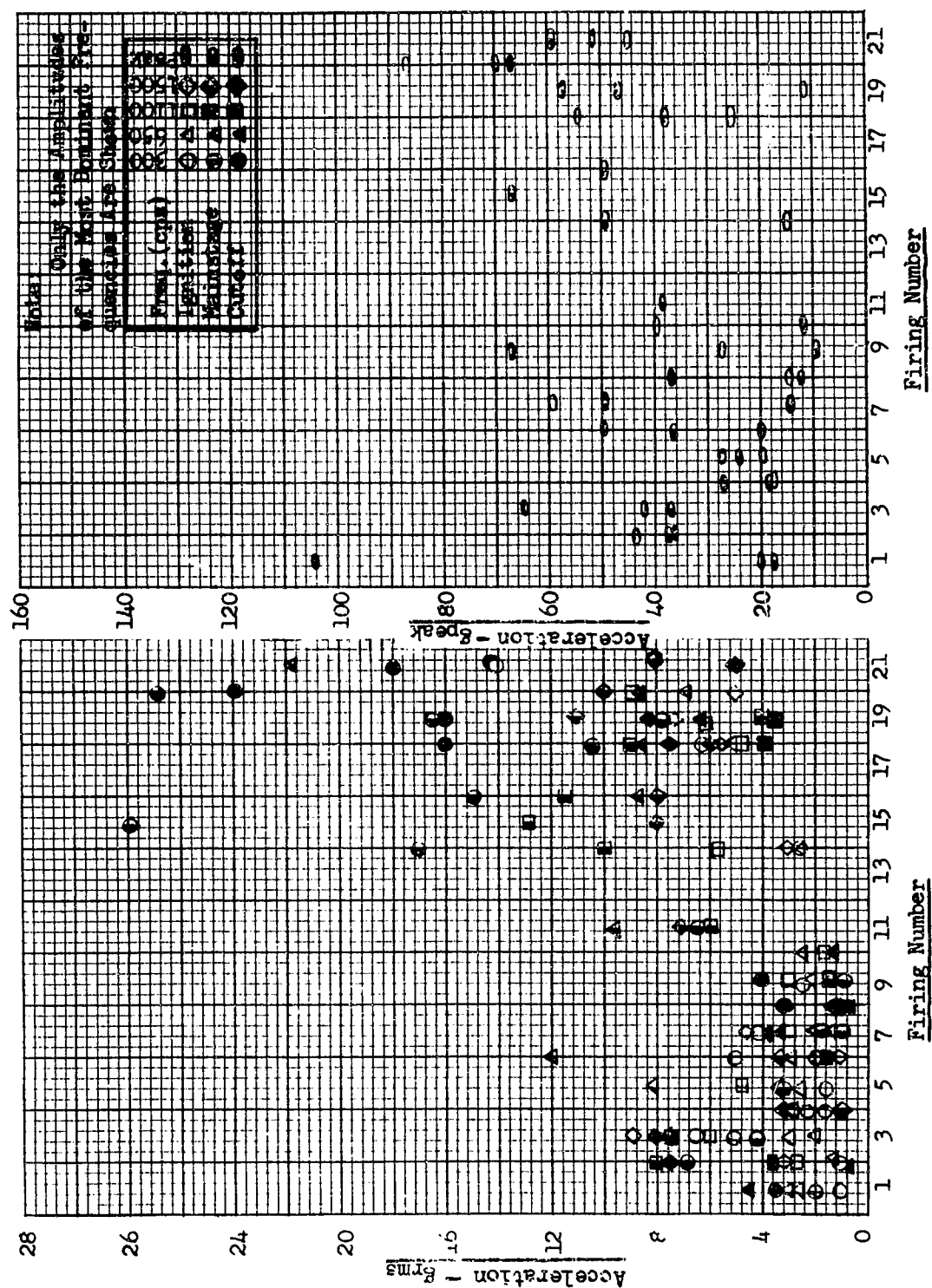


Figure 55. Vibration at the Attach Points Perpendicular to the Thrust Direction - S-3D Engine

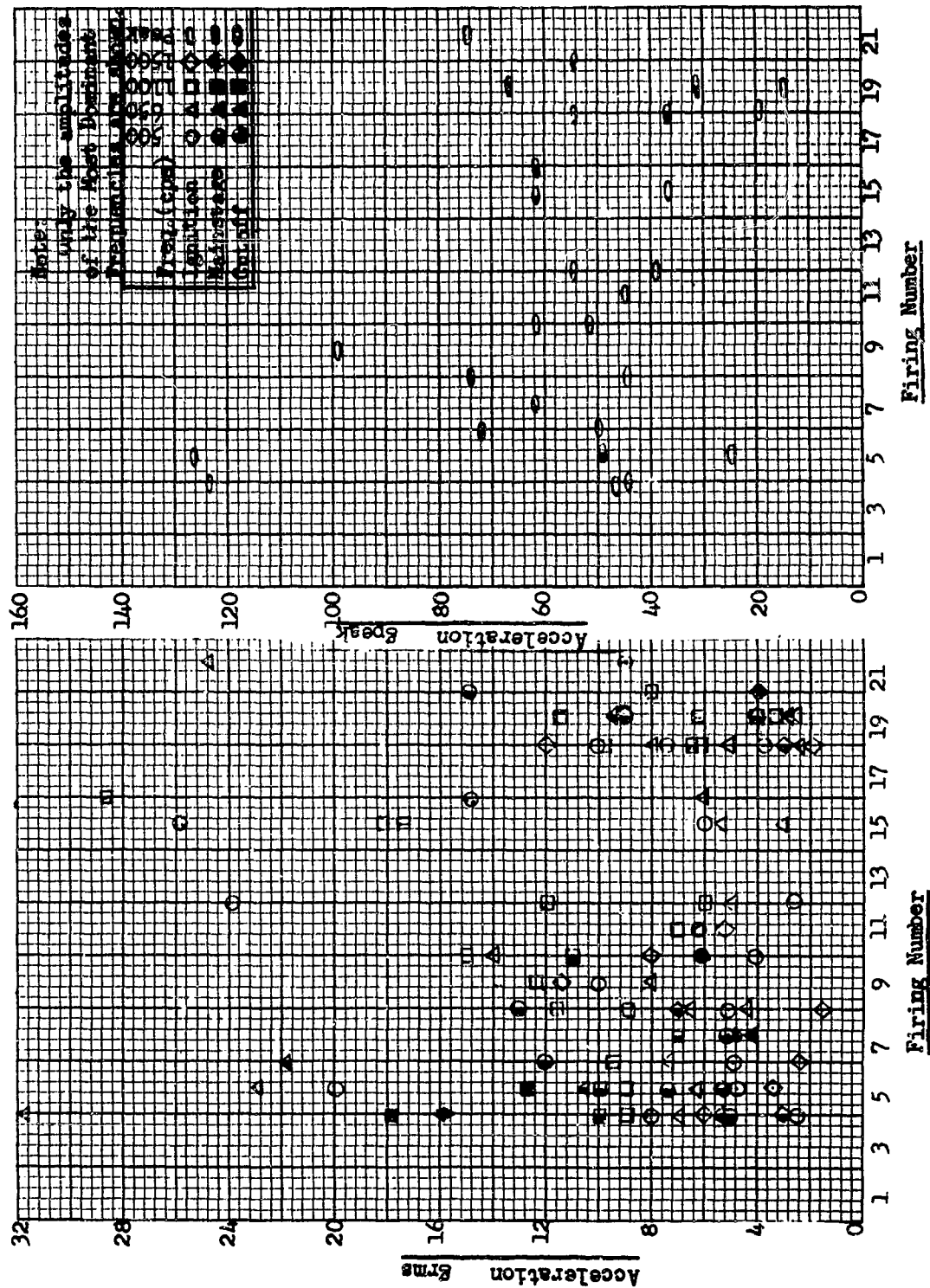


Figure 56. Vibration at the Lox Injector in the Thrust Direction (S-3D Engine)

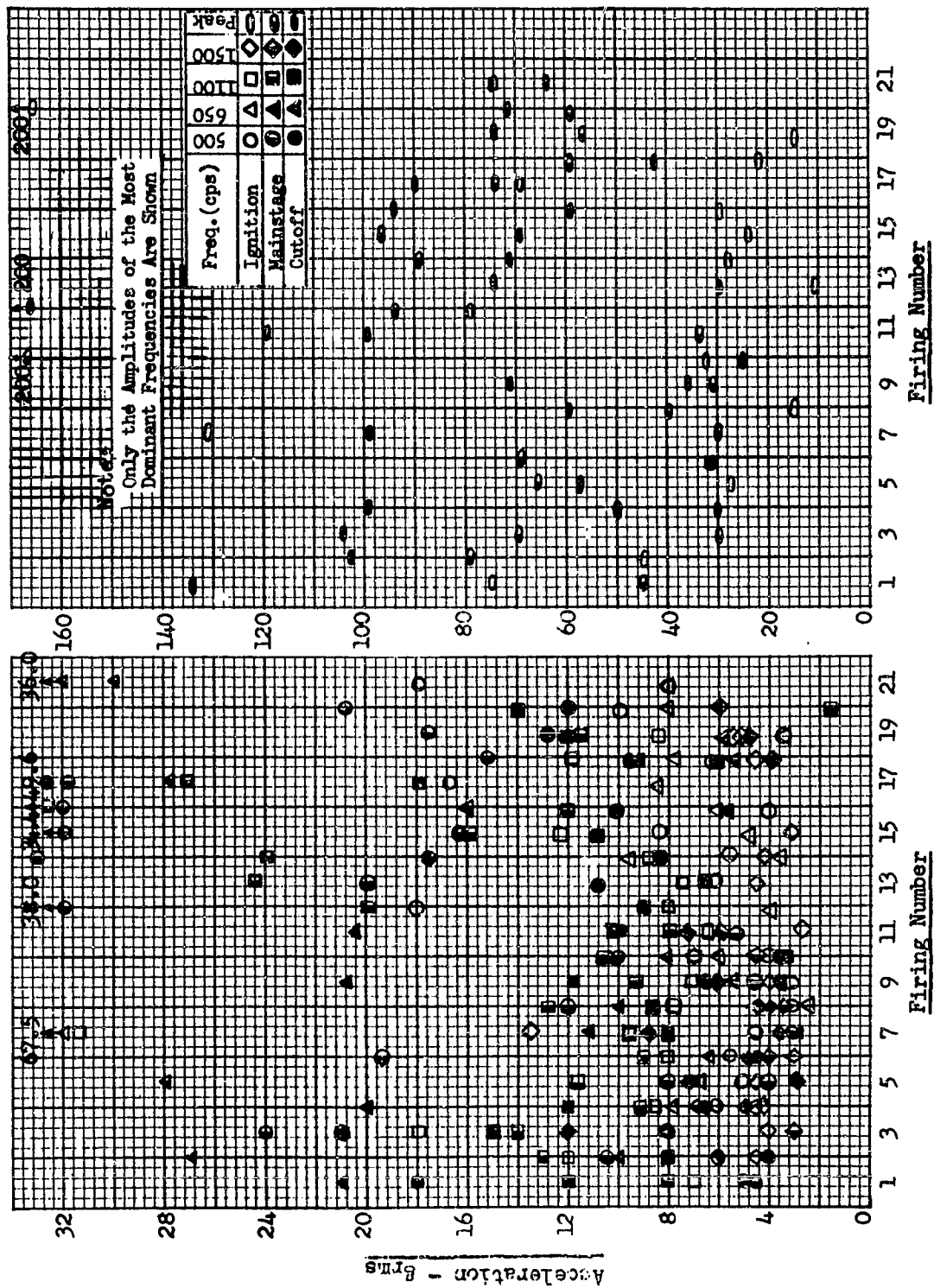
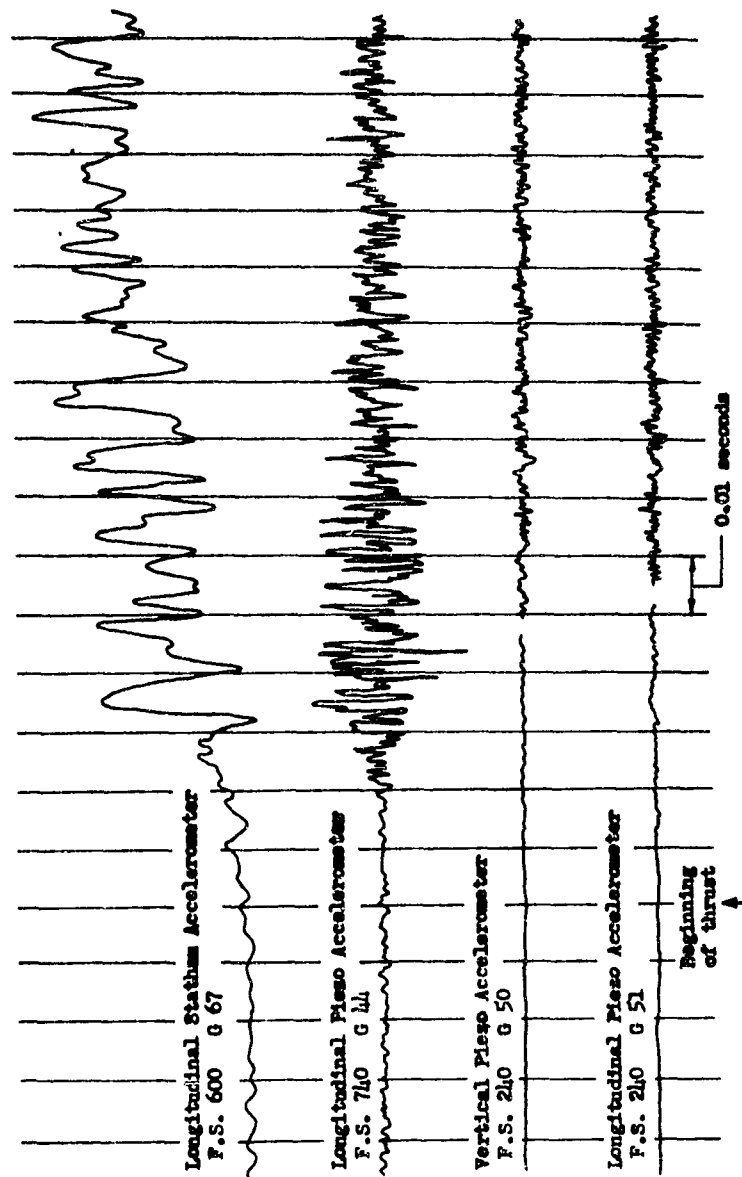


Figure 57. Vibration on the Head of the Combustion Chamber in the Thrust direction - S-3D Engine



1. Nozzle exit at Fuelage Station 640.
2. Structural bornvibrations at F.S. 240 arrives 0.03 seconds ahead of acoustic excitation.
3. Absence of shock associated with ignition and thrust build up is apparent.
4. Vibration component in longitudinal direction at F.S. 600 is equal during and after ignition and thrust build up.

Figure 58. Snark Launch Vibration Measurement During 1st 0.2 Secs. taken by a Trailing Wire.

of thrust, the point of maximum variation of thrust variation .03 seconds later and maximum thrust at .11 seconds. The piezos at fuselage station 240 show the structural borne vibration which precedes the arrival of the acoustic excitation to be a minor component of the order of 20 per cent of the response following the arrival of the airborne excitation. The manifold increase in structural response following the arrival of the acoustic excitation provided the most important evidence of the domination of the acoustic environment. The ability of the structure at the nose of the fuselage to act as a measure of thrust variation is certainly limited, but it is reasonable to infer from the data that the Snark thrust variation is responsible for no more than 10 per cent of the total response.

A third feature from the Snark program to be related concerned the program to reduce booster excitation. One example was a reignition inhibitor, 2 per cent potassium sulfate, added to the booster propellant. Figure 59 shows the influence on the external microphone showing the greatest reduction compared to a firing without the inhibitor. Unfortunately, these gains in lowered external environment were not reflected in lowered response, possibly because the gain can be characterized as a low frequency gain where the slope of the response to environment, Figures 94, 99, & 100, is small. This failure of structural vibration to lessen following a sizable reduction in the environment is also reported in Reference 27.* On the test stand a 30 to 40 per cent reduction in vibratory loads in the thrust direction for structure upstream of the isolation material was determined. Acceleration measurements on missile structures showed loads as high as $\pm 27,000$ pounds in the upstream structure. The peak vibratory load in the interconnecting structure was reduced to $\pm 4,000$ pounds for a later version of the same booster. This reduced level in a solid propellant booster of ± 3 per cent of the total thrust corresponds to that shown in Figure 10 for a liquid rocket and also to the limiting value of allowable thrust variation in many liquid rocket engineering specifications.

The swiftness of the decay in time of structural response to an acoustic environment is shown in Figure 60 of the acceleration at fuselage station 204 in the Snark as a result of two influences of the increasing speed of the vehicle. First, the noise generation depends on the difference between the exhaust velocity and the vehicle velocity and second, the noise which reaches the vehicle from an aft source is diminished.

* Section III Part II Page 239

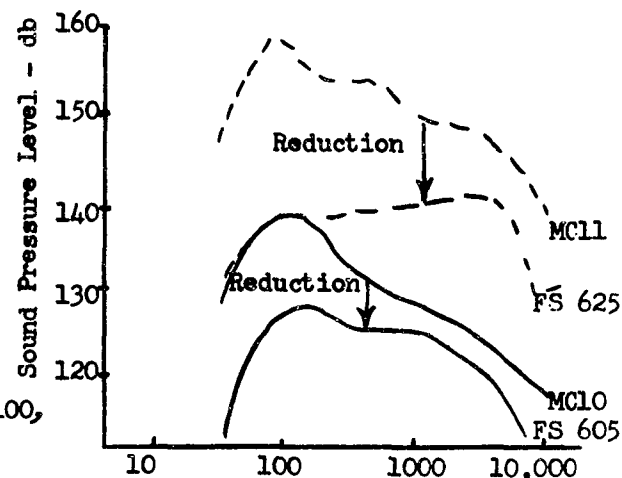


Fig. 59 - Frequency-cps
Reduction in Noise Due to the
Use of a Reignition Inhibitor

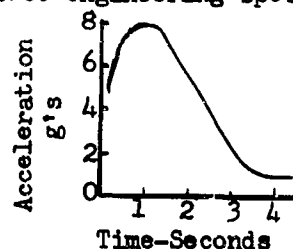


Fig. 60 - Variation of Amplitude with
Time During Launch at FS. 204

ADVANCED PROPULSION SYSTEMS AND POWER UNITS FOR SPACE

There are a large number of devices which have been conceived for eventual use in space propulsion and/or providing auxiliary power for space vehicles. Many of these are classified as "exotic" systems and only a few are past the conceptual stage and transferred to the experimental research phase. However, it is possible to evaluate the potential utility of the majority of these conceptual devices for space flight and, in a limited way, to assess their potential as vibration sources.

Table VIII gives an overall view of the various types of propulsion units, which may become practical, together with their thrust weight ratio, specific impulse, advantages, disadvantages and possible applications. This material has been taken from Reference 12. In addition, the table gives the author's assessment of the categories of vibration sources which will accompany each type of propulsion engine together with an estimate of present knowledge of these problems.

It is clear from Table VIII that the major sources of vibratory energy from these propulsion engines will be from auxiliary electrical power generators, pumps, compressors, and smaller auxiliaries. Thus, for the majority of the proposed systems, vibratory problems will be of the conventional types associated with rotating machinery. However, for many of the electrical engines (Ion and Plasma Drives) the thrust will be either pulsed or follow a full wave rectified alternating current signal. The frequencies which will be encountered range from a few pulses per day to the order of 10,000 per second. Although the electric engines will be utilized (if they become practical in the distant future) primarily for very low thrust inter-space acceleration. Hence, the vibratory forces involved are expected to be small. It is expected that the thermal engine will be the mainstay of space research for the next decade at least, with a transition occurring from primary reliance on chemical fuels to reliance on nuclear fuels.

It should be noted that the thermal engines will all produce jet noise which will be important during the boost phase at vehicle velocities below Mach 1. Although the magnitude of this noise can be evaluated from Section II, the velocities expected for nuclear rockets utilizing hydrogen as a propellant are of the order of 20,000 feet per second. This is approximately three times exit velocities for conventional chemical rockets and, hence, prediction of noise should be supplemented by measurement at the earliest practicable date.

The source of power for auxiliary functions and propulsion on the space vehicle will depend upon the length of the mission and the total power requirements. In general, conventional rotating machinery is preferable for conversion of energy to electrical power at powers over 100 kilowatts, whereas direct conversion (solar cells, fuel cells, chemical batteries) are generally preferable for powers less than 1 kilowatt. For long duration, solar energy collectors appear desirable for powers less than 10 kilowatts, but at powers above 100 kilowatts nuclear heat sources have superiority. Thus, it is probable that all but the smallest unmanned probes will have turbine-generating machinery for electrical power and will also probably have numerous auxiliaries as part of a nuclear energy source.

TABLE VIII. SUMMARY OF PROPULSION ENGINES FOR SPACE VEHICLES (Based on information from reference 12, with exception of Vibratory Potential)

CLASS	TYPE	VIBRATORY POTENTIAL		THRUST WEIGHT RATIO	SPECIFIC IMPULSE (sec)	MAJOR ADVANTAGES	MAJOR DISADVANTAGES	MISSION APPLICATIONS		
		Present Knowledge	Types of Vibratory Sources					Surface	Interplanetary	Satellite Maneuvering
Thermal Engines	Jet/Jetjet	Good	Noise in atmosphere; large compressor plus auxiliary machinery	>1	1500	Well developed; air breathing; may be waste	Complex when clustered	x		
	Recombination Ramjet	Fair	Auxiliary machinery	10^{-3} - 10^{-4}	oo	Energy & per-pellet extracted; must be from environment	Not well understood; locked to high speeds			x
	Chemical Rocket	Fair	Noise in atmosphere; liquids have turbo pumps and other auxiliary machinery; both liquids and solids have rough burning, scorch and other instabilities	10	240 (new) to 480	Well developed; cheap to manufacture	Low specific impulse; fair reliability	x	x	x
	Nuclear Heat Transfer Rocket	Fair	Turbopumps and auxiliary machinery; noise in atmosphere	2	to 1500		Nuclear radiation; cryogenic fuel storage problems	x	x	x
	Consumable Nuclear Rocket	Poor	Turbopumps and auxiliary machinery; noise in atmosphere	10	to 3000		Conceptual only; expels radioactive propellant; high cost	x	x	x
Electrical Engines	Nuclear Bomb Propulsion	Poor	Extreme shock environment	10	1000-300		Conceptual only; contamination and radiation	x	?	x
	Thermoelectric Rocket	Poor	Large electrical generator and auxiliaries; noise in atmosphere	10^{-1}	to 3000	High performance; cheap fuel	Conceptual	x	x	
	Plasma Jet	Poor	Electrical generator and aux.	10^{-3}	to 2500		Short operating lifetimes	?		x
	Ionotive	Poor	Large generator can operate either DC or AC; in latter case the thrust is modulated by the electrical frequency; also pumps and other aux.	10^{-3} - 10^{-4}	to 25,000		Erosion of electrodes requires very long time; reliability to be useful	(Unmeasured)		x
	Plasma Acceleration (magnetohydrodynamic devices)	Poor	Sims devices are steady flow; however most are alternating with frequencies to 10000 cps; large gen. and aux.	5×10^{-5} - 2×10^{-4}	to 10,000		Not well understood	(Unmeasured)		x
	Solar Sail	Poor	Should require little aux. machinery	10^{-4}	to oo	Energy obtained from environment	May be sensitive to environment; not well known	x	(Unmeasured)	

It should be emphasized again that control of the vibration for most of the auxiliary equipment discussed is in the hands of the designer. In addition, since the major source of vibratory energy from a majority of types of machinery under consideration is unbalanced, serious consideration should be given to the provision of portable balancing capability. This technique allows the ultimate in balance to be obtained by balancing the machine in its own bearings at its operating rpm, thus balancing out any manufacturing or assembly eccentricities.

AUXILIARY EQUIPMENT VIBRATION EXCITATION

Auxiliary equipment will be a source of vibration in space vehicles. This source of excitation will ordinarily be of secondary importance with the main power plant operating. However, its long time operation in a space environment can lead to fatigue problems in the immediate area of such equipment. It is also possible that the dominant vibration in the immediate area of the equipment would originate mechanically in the equipment even with the main power plant operating.

Mechanical vibration sources originate in the acceleration of moving parts and in the periodic variations of gas forces, electrical forces or other energy sources. Rotation alone serves to generate the sinusoidal forces coming from static or dynamic unbalance. The periodic nature of the inertia forces is apparent in eccentric parts, linkages, cams, wobble plates, and gear teeth. The fundamental frequency associated with the forces is that determined by the apparent frequency of the motion. Frequencies which are integral multiples of the fundamental frequencies are also present when the motion is not perfectly sinusoidal. These mechanical vibration forces act both as forces within the equipment and as external forces.

The band of frequencies over which the equipment operates should be compared to the various translational and rotational natural frequencies of the system. The natural frequencies are the resonant frequencies at which an applied periodic force creates relatively large response.

The ideal solution to the problem of vibrational forces is to design the equipment free of such forces. This freedom from vibration can never be completely accomplished as long as motion is present. Where these vibrational forces must exist due to the function of the equipment, the adjacent structure can be protected by vibration mountings which diminish the transmitted forces. The equipment may also benefit by the soft mounting if the lowered natural frequencies of the overall dynamical system are sufficiently removed from the exciting frequencies.

The many ways in which mechanical vibration is troublesome should be considered. The list includes wear out, malfunction, fatigue and comfort problems. Emphasis will be required on the fatigue problem. The performance demands on space systems will require relatively low structural weight and greater structural efficiency. The final limit in these attempts to obtain lower structural weight will be determined by fatigue. Detailed knowledge of the loading history will be required. It is interesting to note the rapidity with which large numbers of cycles are accumulated in certain fatigue problems. In cases where vibrations are induced by acoustic phenomena and high speed machinery a million cycles per hour are possible. The allowable stress for design purposes must be less than the endurance limit in these cases. In the acoustic fatigue problems the allowable rms stress level is only a small fraction of the endurance limit stress. New military specifications, Reference 13, will require vibration mapping of the expected vibration environment in the design stage. When this is done, one portion of the many inputs required for the fatigue analysis will be available.

The role of freeplay and tolerances defining bearings, hole sizes, and shafts, should be noted. The eccentricities which generate the mechanical vibration forces associated with rotating parts are the same order of magnitude as these tolerances. Freeplay at these rotation points will need careful control in many cases. In many cases design provision for portable balancing of the assembled machine running under its own power will give the minimum vibration.

The designer will find it desirable to use the specified vibration limit noted in the applicable equipment specification for use in calculating forces. Experience shows that equipment vibration is in the near proximity of these limits.

Self excited vibration instabilities also present complex mechanical vibration problems. In this case the oscillatory motion is sustained by a force which is created or controlled by the motion itself.

The study of several examples will be beneficial. The following problems demonstrate the ease with which an understanding of the forces and moments can be gained from calculations.

The engine installed in the Northrop T-38 airplane provides a suitable example for the calculation of normal vibratory forces and amplitude. The rigorous solution to this problem is quite complex but this presentation is in a simplified method to illustrate the ease with which analytical techniques can be applied to the problem of unbalanced rotating equipment.

The engine rotor has two main bearings; the aft bearing located at the turbine section and the forward bearing located toward the aft portion of the compressor section. This arrangement causes the forward portion of the compressor section to be cantilevered from the front bearing producing a critical speed at approximately 72% of engine maximum speed. The acceleration measured at the front frame on one particular engine at this critical speed was 22 "g's" which can be considered roughly equivalent to a sinusoidal single amplitude of .006 inches. Other measurements are summarized in Figure 61.

If it is assumed that the engine centerline describes a conical shape with the apex of the cone in the vicinity of the main trunnion mounts, the force at the front vertical engine support may be approximately in the following simplified analysis.

The angular acceleration, α , of the complete engine projected in the vertical plane is:

$$\alpha = \frac{a_n}{L} = \frac{22 \times 386 \text{ in/sec}^2}{42 \text{ in.}} = 202 \text{ rad/sec}^2$$

where, a_n = vertical linear peak acceleration

L = distance from main trunnion mounts to front frame.

Notes: 1. All Readings at Military Power.

2. As a Measure of Service Acceptability, Periodic Vibration Measurements Were Made on the Bulk of the Early T-38 Engines. The Average Number of Readings Available Per Engine was Eleven (11), Varying from Three (3) to Twenty Nine (29). Readings were Taken in an Engine Test Stand and Part Installed in the T-38 Aircraft. Consecutive Readings in the Aircraft and in Test Stand Showed no Variation Due to Mounting. This Figure Presents the Range of those Readings.

3. Response Frequency was 275 cps Due to Compressor Unbalance.

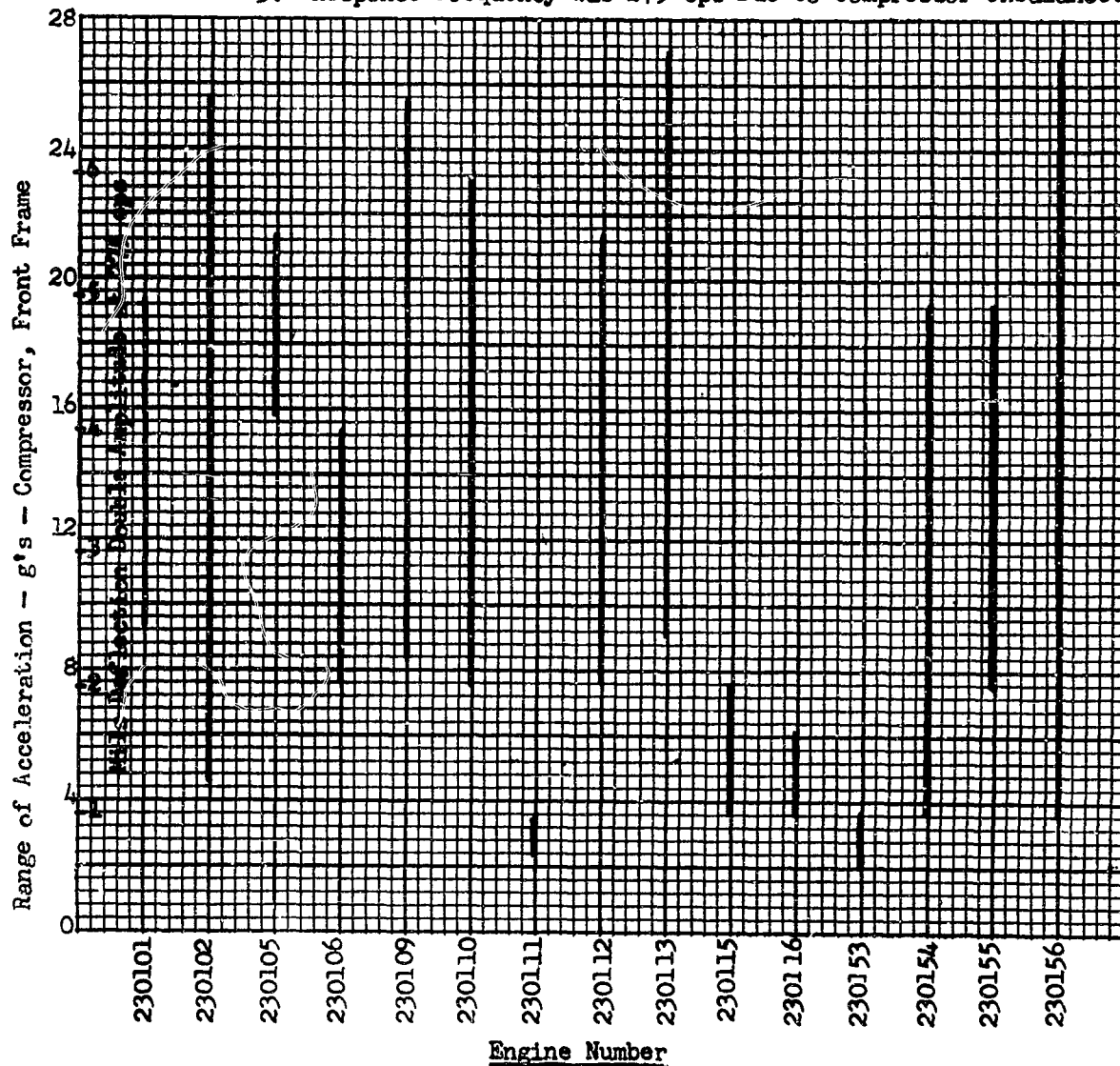


Figure 61. Vibration Ranges on XJ85-5 Engines used in the T-38

The torque, T , required to produce the above angular acceleration is:

$$T = I_p \alpha = 1040 \text{ lb-in-sec}^2 \times 202 \text{ rad/sec}^2 = 210,000 \text{ in-lb.}$$

where, I_p is the pitch moment of inertia of the complete engine about the axis through the main trunnions

α = angular acceleration

The force, F , exerted at the front support is:

$$F = \frac{T}{r} = \frac{210,000 \text{ in-lb}}{30 \text{ in}} = 7,000 \text{ lb.}$$

where, r = distance between the main trunnion mounts and the forward vertical engine support.

Since this force must come from the unbalanced rotor, the radius, e , of the circle described by the rotor center of gravity is:

$$e = \frac{F}{m \omega^2} = \frac{7000 \text{ lb}}{\frac{100 \text{ lb}}{386 \text{ in/sec}^2} (192 \times 2\pi)^2 \text{ rad/sec}^2} = .0185 \text{ in}$$

It should be noted that an additional bearing has been incorporated in the latest engine design which has reduced this vibratory force considerably.

It should not be considered that troublesome vibrations must originate with masses as large as an engine rotor. On the contrary, small motors on rotary equipment with masses in the order of one or two pounds and an unbalance measured in inch ounces can create a large oscillating force when the rotation speed is high. For example, consider an unbalanced rotor weighing two pounds having an unbalance of one inch ounce or an eccentricity of .031 inches. The oscillating force, F , at 10,000 RPM is:

$$F = m r \omega^2 = \frac{2 \text{ lb} \times .031 \text{ in}}{386 \text{ in/sec}^2} \left(\frac{10,000 \times 2\pi}{60} \right)^2 \text{ rad}^2/\text{sec}^2$$

$$= 175 \text{ lb}$$

The magnitude of the oscillating force estimated in the above simplified manner tends to be high due to the assumption that all masses and attachments are rigid. They are of course elastic.

If the nature of the rotary equipment is such that it cannot be balanced, then an isolation system should be considered. The transmitted force, F_{TR} , through a single degree of freedom isolation system (i.e. center of gravity system) is:

$$\frac{F_{TR}}{F_0 \sin \omega t} = \frac{1}{\sqrt{\left[1 + \left(\frac{\omega}{\omega_n}\right)^2\right]^2 + \left(2 \frac{c}{c_c} \frac{\omega}{\omega_n}\right)^2}}$$

where, $F_0 \sin \omega t$ = oscillating force of the unbalanced rotor.

c/c_c = ratio of actual damping of the isolation system to a critically damped system.

ω = frequency of oscillating force.

ω_n = natural frequency of isolating system.

In order to accomplish any reduction in the transmitted force, the frequency ratio, n , of the forcing frequency to the natural frequency of the isolation system must be at least 1.5. As n increases above 1.0, the transmitted force decreases. For example, an isolation system with ten percent of critical damping will transmit 34 percent of the oscillating force when n is two, whereas when n is six, the transmitted force is only three percent of the oscillating force.

High speed rotary equipment which is to be used in space vehicles should be controlled in regard to the vibratory forces originating within them. Some vendors have measured data which describe these forces. Care should be exercised that these data are applicable to the proposed equipment installation because the transmitted force is dependent upon the mounting system as well as the originating oscillating force.

Other rotary equipment is controlled by specification which limits the force or amplitude of motion of the rotary equipment. An example of this is the jet engine which is usually limited to five to eight mils double amplitude.

Another type of vibratory force originating within equipment is that of a self-excited nature. The oscillating force is not attributed to an unbalance but develops from the function of the equipment.

As an example, the following equation is derived from data taken from turbo-pumps used on current liquid fuel rockets. The energy inherent in the cavitation at the impeller blades is not of an alternating nature but is a relatively constant source of energy for the vibrating system. The vibration spectrum is typified by a relatively low level broad band random vibration upon which is superimposed spectral peaks at multiples of the impeller rotary speed. The overall root mean square

Vibration is roughly proportional to the thrust of the rocket motor being fed by the pump, Figure 62.

An approximate expression for the overall g_{rms} accelerations originating at the pump is:

$$g_{rms} = 2.5 \times 10^{-5} T$$

where: T is the thrust of the rocket motor.

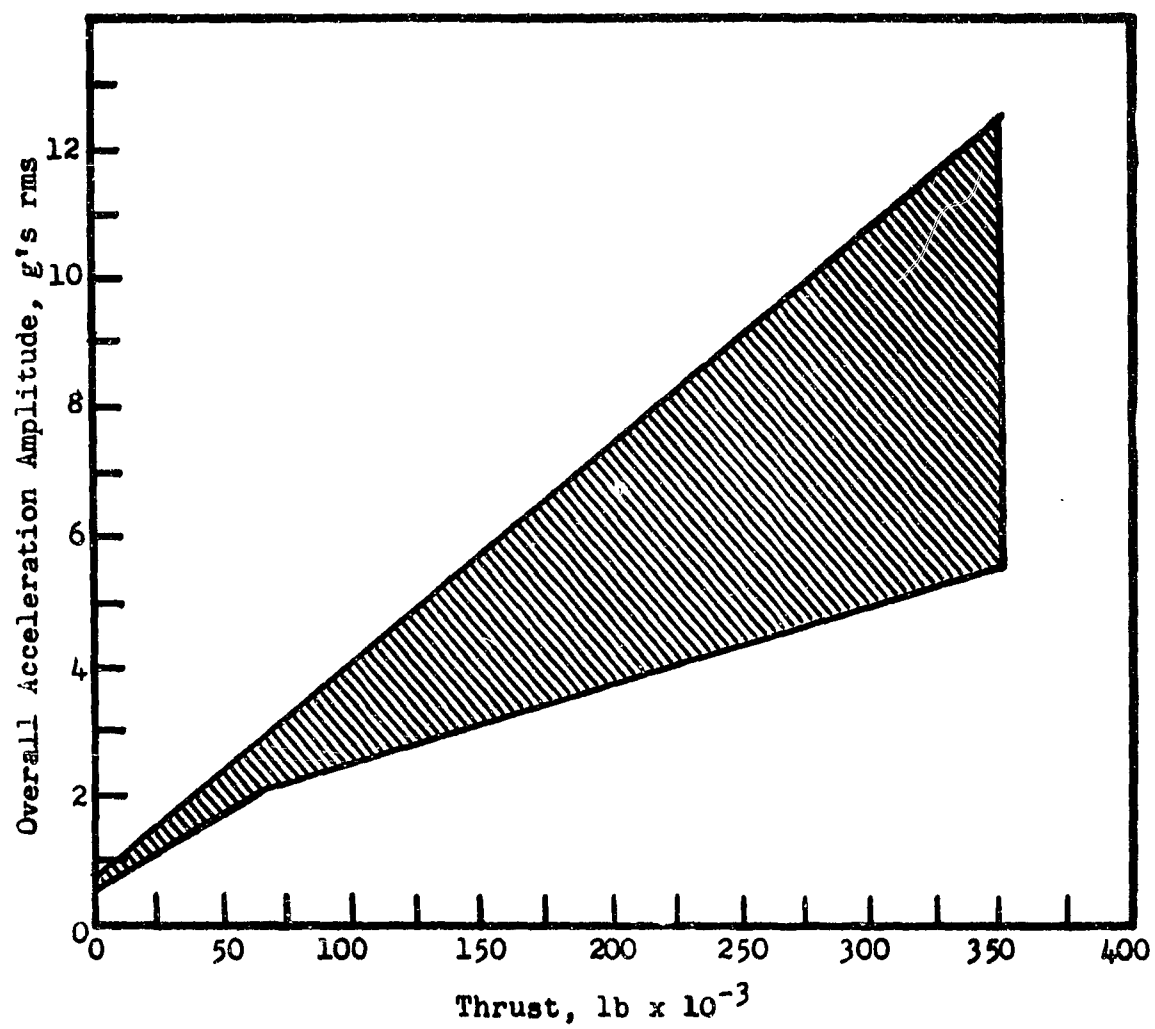


Figure 62. Range of Turbopump Vibrations

REFERENCES

1. Tischler, A. O., and Bellman, D. R., "Combustion Instability in an Acid-Heptane Rocket with a Pressurized Gas Propellant Pumping System", NACA TN 2936 Lewis Flight Propulsion Laboratory, May 1953.
2. Tischler, A. O., Massa, R. V., and Mantler, R. L., "An Investigation of High Frequency Combustion Oscillations in Liquid Propellant Rocket Engines", NACA RM E53B27, Lewis Flight Propulsion Laboratory, June 26, 1953.
3. "Basic Considerations in the Combustion of Hydrocarbon Fuels in Air", Propulsion Chemistry Division, NACA Report 1300, 1957.
4. Morse, Philip M., "Vibration and Sound", McGraw-Hill Book Company, Inc. 1948.
5. Pass, Isaac and Tischler, Adelbert O., "Effects of Fuels on Screaming in 200-Pound-Thrust Liquid-Oxygen-Fuel Rocket Engine", NACA RM E 56C10, Lewis Flight Propulsion Laboratory, June 22, 1956.
6. Osborn, J. R. and Pinchak, A. C., "Investigation of Aerothermodynamic Interaction Phenomena in Combustion Pressure Oscillations", Interim Report No. I 59-2, Jet Propulsion Center, Purdue University, June 1959.
7. Zucrow, M. J., "Aircraft and Missile Propulsion", Vol. II, John Wiley & Sons, New York, 1958.
8. NRL Memo 6261-109A of 27 February 1959.
9. Blake, R. E. and Olson, M. W., NRL Report 5102 dated 13 May 1958.
10. C. Lemons, PRFT Vibration Test for the B2C Rocket Engine, Rocketdyne Technical Report 57-32, 24 May 1957.
11. C. Lemons, Vibration and Thrust Variation on the S-3D Engine, Rocketdyne Technical Report 58-50, 22 July 1958.
12. Corliss, W. R., "Propulsion Systems for Space Flight", McGraw-Hill Book Company, Inc., New York, 1960.
13. Military Specification MIL-A-8870 (ASC), "Airplane Strength and Rigidity Vibration, Flutter, and Divergence", March 1959.

VII NOISE EXPOSURE FOR HYPOTHETICAL VEHICLE AND MISSION

The characteristics of the majority of the sources of vehicle vibration which have been discussed in this report depend on a myriad of design and mission parameters. Many will never be encountered except by vehicles with unusual design features or unusual mission profiles. Others, such as motor vibration and thrust variation, depend on specific hardware which is utilized. However, the launch noise and the boundary layer pressure fluctuations are common to all contemporary vehicles operating from earth.

Therefore, it is interesting to examine the characteristics of these two vibration sources in terms of a hypothetical vehicle and mission profile. Figure 63 illustrates a hypothetical three-stage vehicle intended to launch the third stage and payload into a recoverable orbit. Figure 64 gives a possible exit profile for this vehicle, specifying both altitude and velocity as a function of time from launch. Figure 65 gives a possible re-entry profile for the nose and first-stage section of the vehicle assuming a high drag device is used to decelerate this section during the re-entry. Note that this re-entry deceleration duration, approximately suitable for a manned re-entry, is on the order of ten times longer than in a ballistic re-entry.

Calculations have been made for the variation of rocket noise and boundary layer pressure fluctuations at two positions along the vehicle. For those calculations it was assumed that the vehicle was launched at sea level from a vertical position just above a flat ground plane.

The variation in over-all sound pressure level at the two positions during the initial launch period is illustrated in Figure 66a. As can be seen, the increase of rocket noise, resulting from the change in the directional radiation characteristics of the flow impinging on the ground plane, controls the noise exposure for the first 1.5 - 2 seconds of flight until the nozzles reach an altitude of the order of 50 nozzle diameters. By this time the noise exposure has been decreased to that anticipated directly forward of an unobstructed rocket flow. However, because the vehicle is in motion, the rocket noise continues to decrease. Note that the level at position A, which is well forward of position B, is considerably less than the level at position B.

Figure 66b, which has a more condensed time base, illustrates the continued decrease of rocket noise at both positions. However, this increase in vehicle velocity through the atmosphere brings an attendant increase in freestream dynamic pressure (q_∞). Hence, as the q_∞ is increased, the boundary layer pressure fluctuations increase and begin to assume importance. Thus, at the end of the first ten seconds for this hypothetical vehicle and mission, the external noise ceases to decrease and begins to increase. In this example, the maximum over-all level of the boundary layer pressure fluctuation approximately equals the maximum launch noise at position B and exceeds the launch noise at position A. However, the relative magnitudes of the levels from the two sources will vary with many factors, including

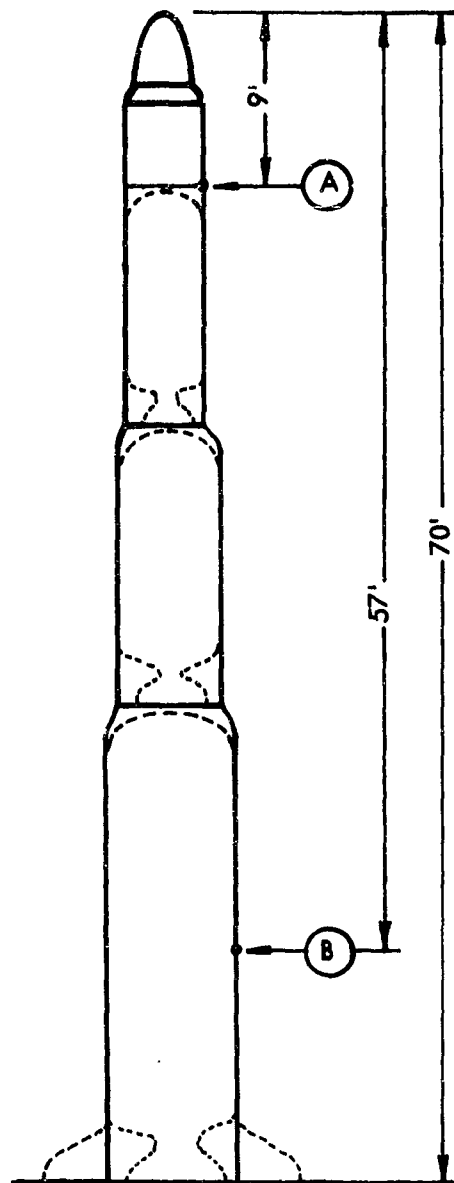


Figure 63. Sketch of Hypothetical Three-Stage Vehicle.

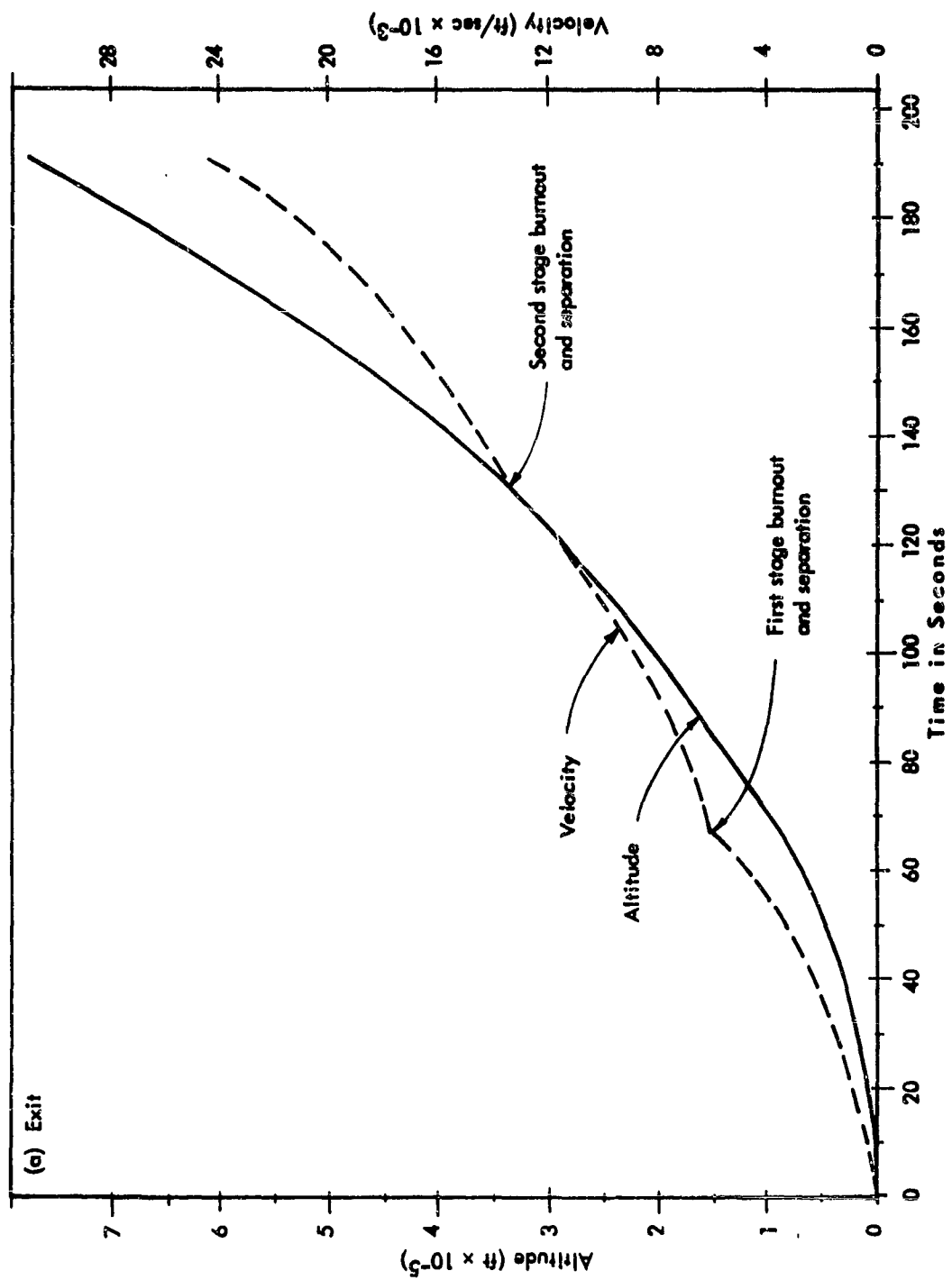


Figure 64. Exit Profile for Hypothetical Vehicle Showing Velocity and Altitude as a function of time.

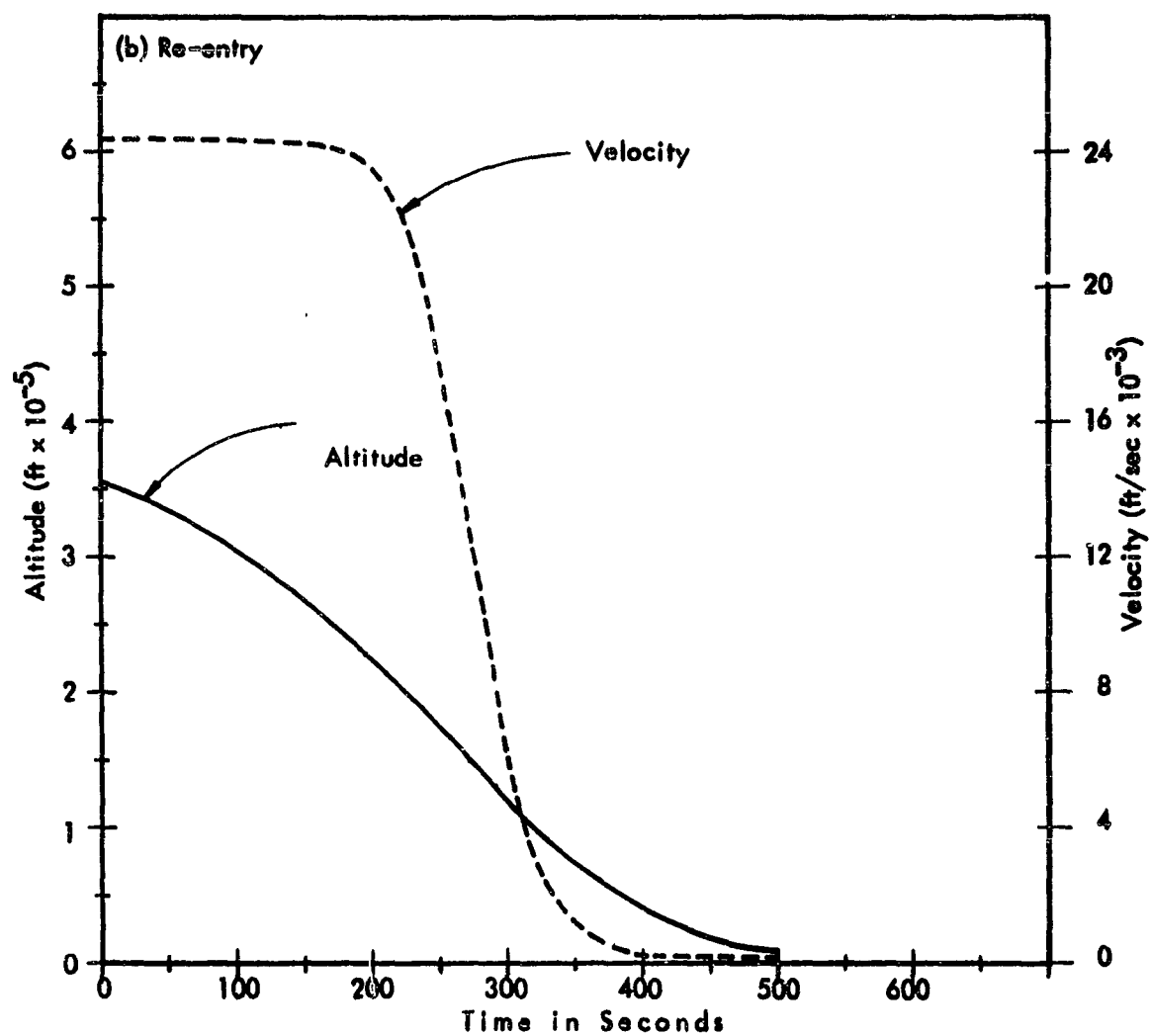


Figure 65. Re-Entry Profile for Hypothetical Vehicle Showing Velocity and Altitude as a Function of Time.

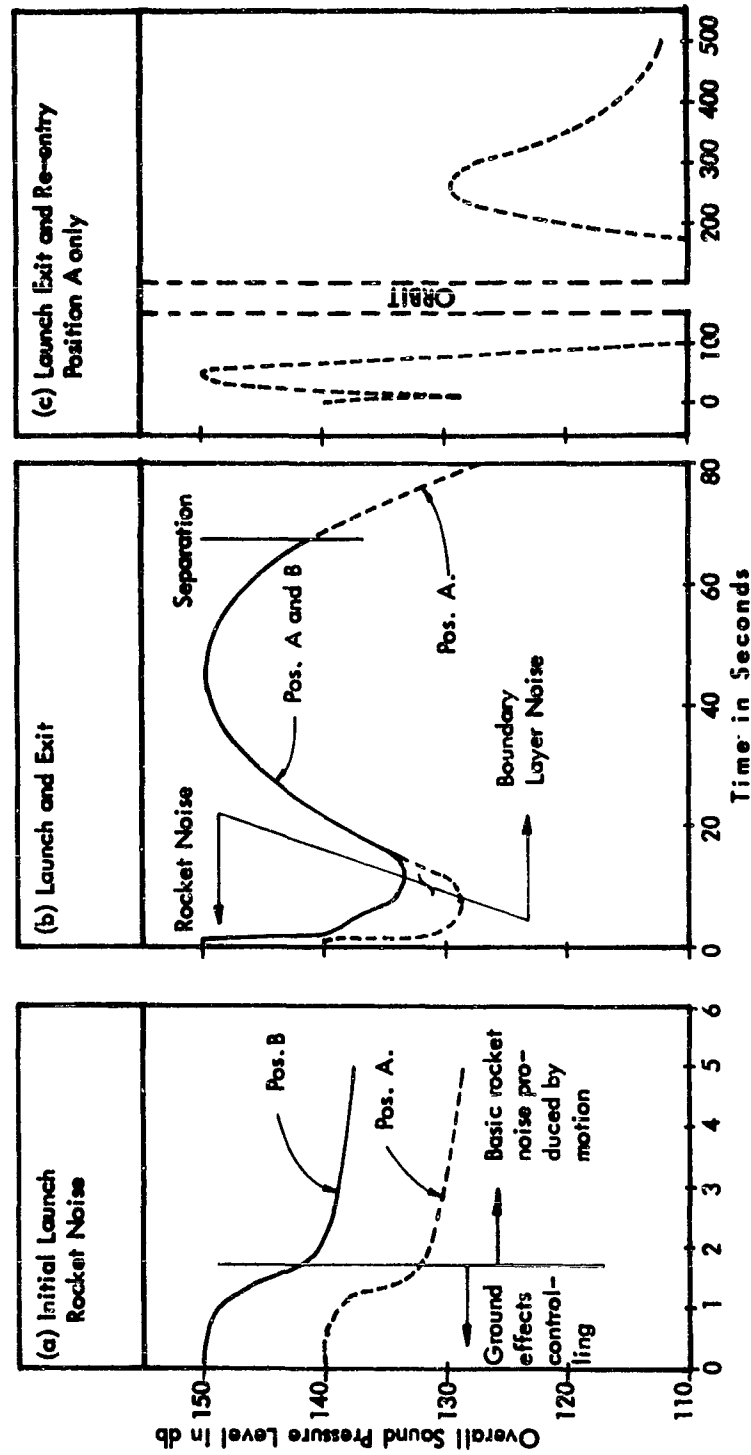


Figure 66. Estimated Variation in Overall Sound Pressure Level for two positions on Hypothetical Three-Stage Vehicle as a Function of Mission Time (from Figures 64 & 65).

position along the vehicle, mission profile, parameters of the boost rocket motor, and launch configuration.

Figure 66c illustrates the variation in over-all sound pressure level at position A throughout important portions of the mission when the vehicle is in the atmosphere. It is obvious that the maximum level during re-entry is on the order of 20 db less than that obtained during exit. However, calculations based on a possible ballistic re-entry where the maximum deceleration occurs at much lower altitude than in Figure 65 give exterior over-all levels on the order of 165 db, 35 db greater than illustrated in Figure 66c. Here it should be noted that this higher value will only result if the re-entry vehicle has a fully developed turbulent boundary layer.

Figure 67 gives a similar presentation of the variation of the level in several frequency bands at position A. As can be seen, the relative spectra are continuously changing during the flight. For this particular example, the middle frequency region is predominant during launch, the higher frequencies during exit and all frequencies are approximately equal during re-entry. It is noted that the calculation of the position A boundary layer pressure fluctuations assumed that the boundary layer was fully turbulent aft of the shoulder of the third stage, and that the flow external to this boundary layer had expanded to freestream condition aft of the shoulder.

Figure 68 gives a similar analysis of the variation with time of the spectra at position B prior to the first stage burnout. Comparison of the spectra of the boundary layer fluctuations at the two positions illustrates the greater relative energy at the lower frequencies at the aft position B. Typical mean square pressure spectra for this hypothetical vehicle at various mission phases are given for two positions in Figures 69 and 70.

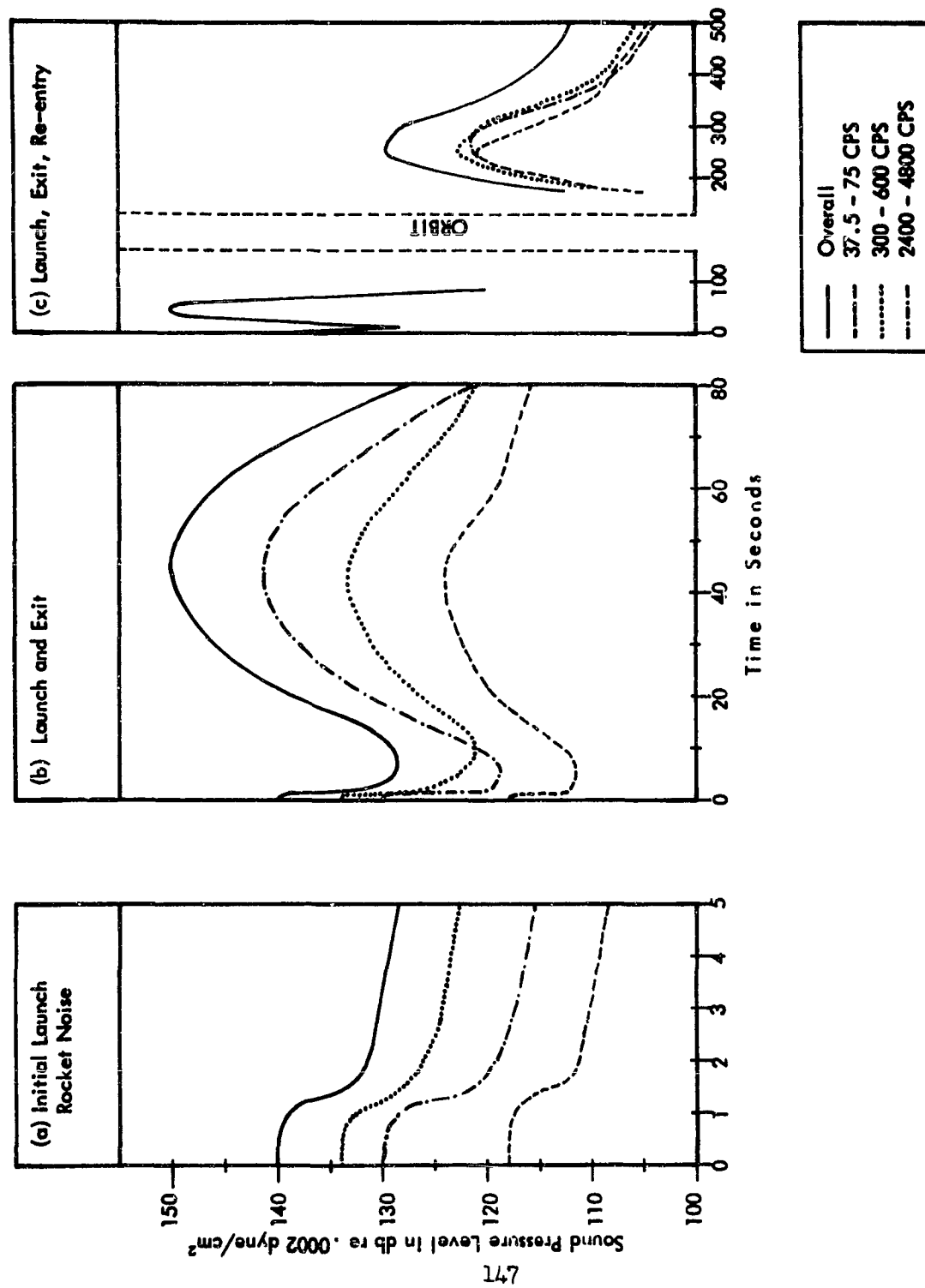


Figure 67. Estimated Variation in Overall Sound Pressure Level and the Level in Three Octave Bands as a Function of Time (from Figure 66) at Position A on the First Stage of the Hypothetical Vehicle

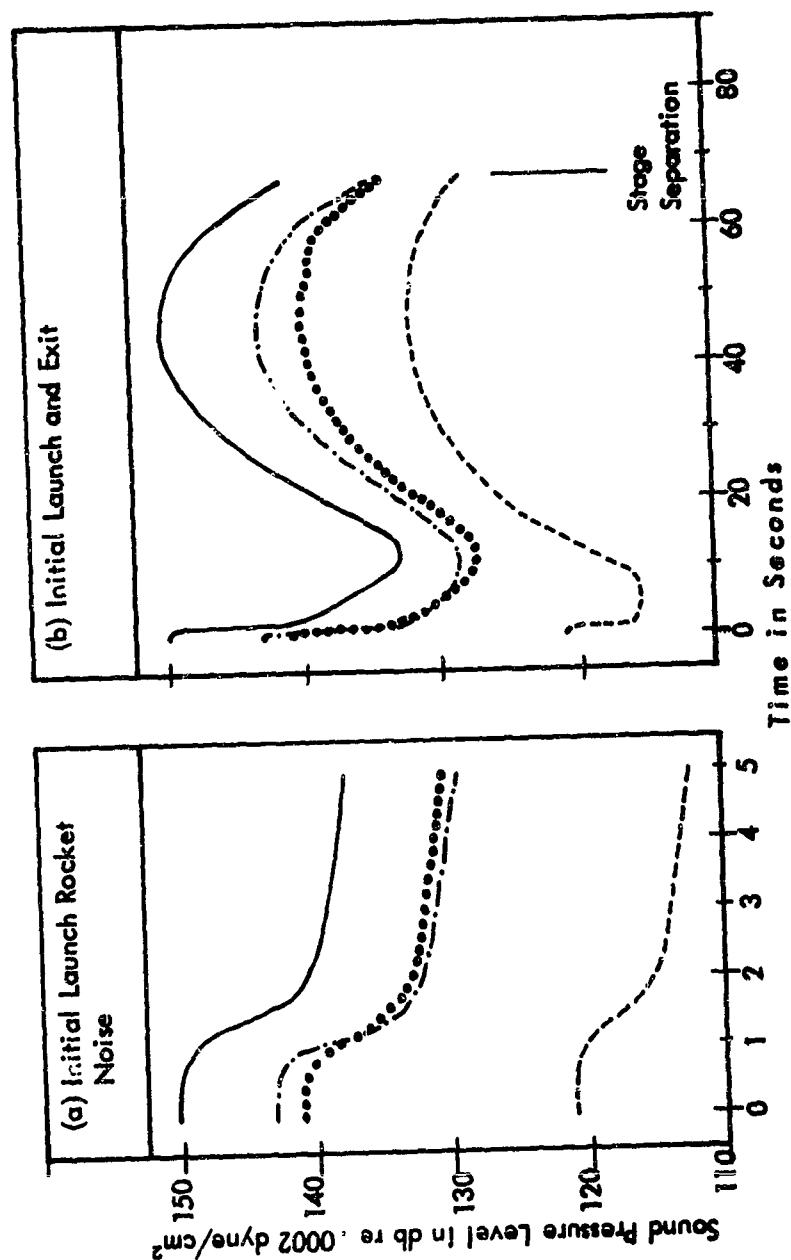
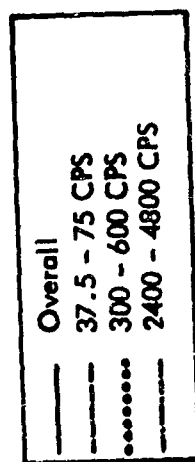


Figure 68. Estimated Variation in Overall Sound Pressure Level and Level in Three Octave Bands as a Function of Time (from Figure 66) at Position B on the First Stage of the Hypothetical Vehicle.

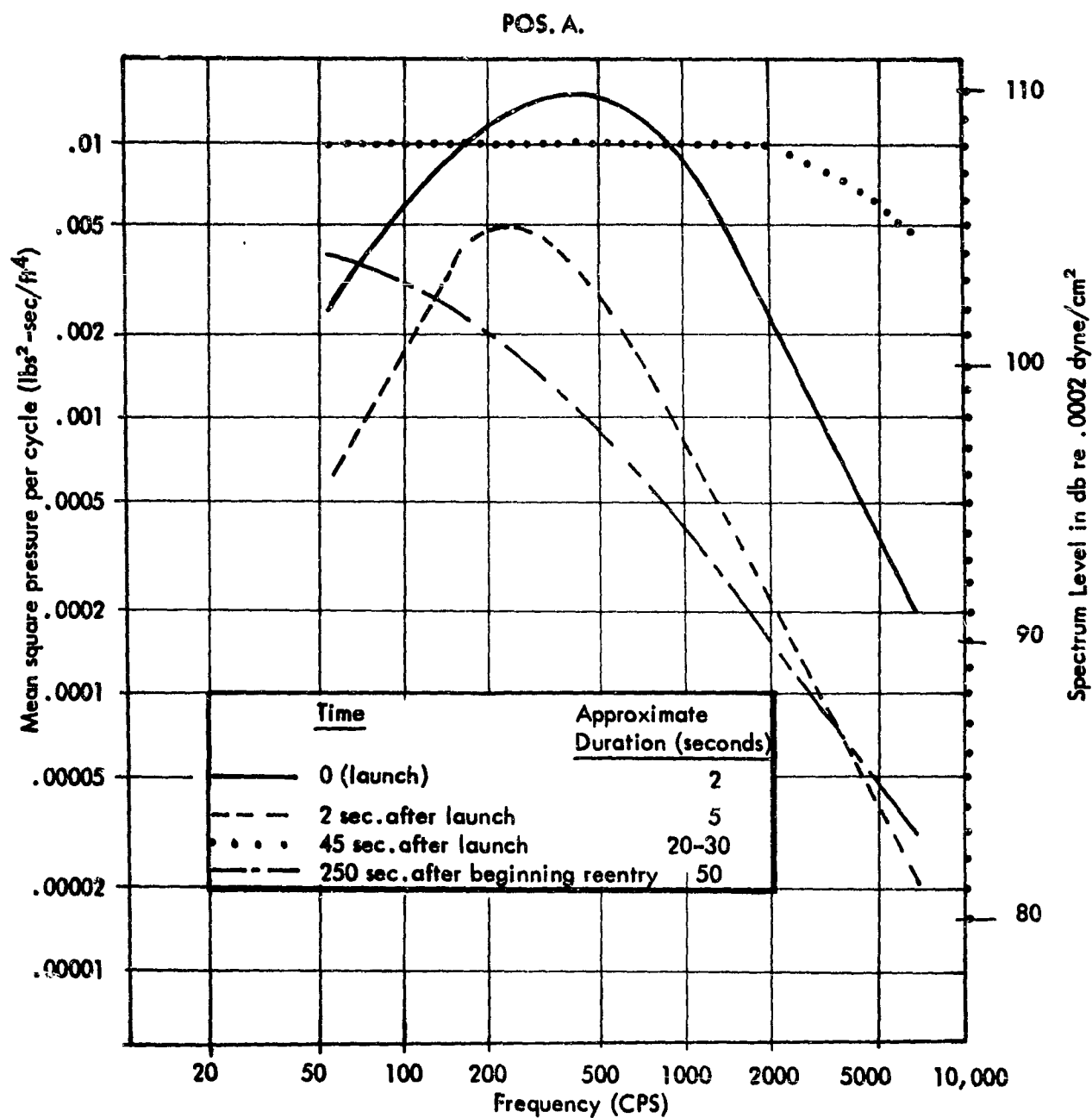


Figure 69. Estimated Mean Square Pressure Per Cycle at Several Times During Mission for Position A.

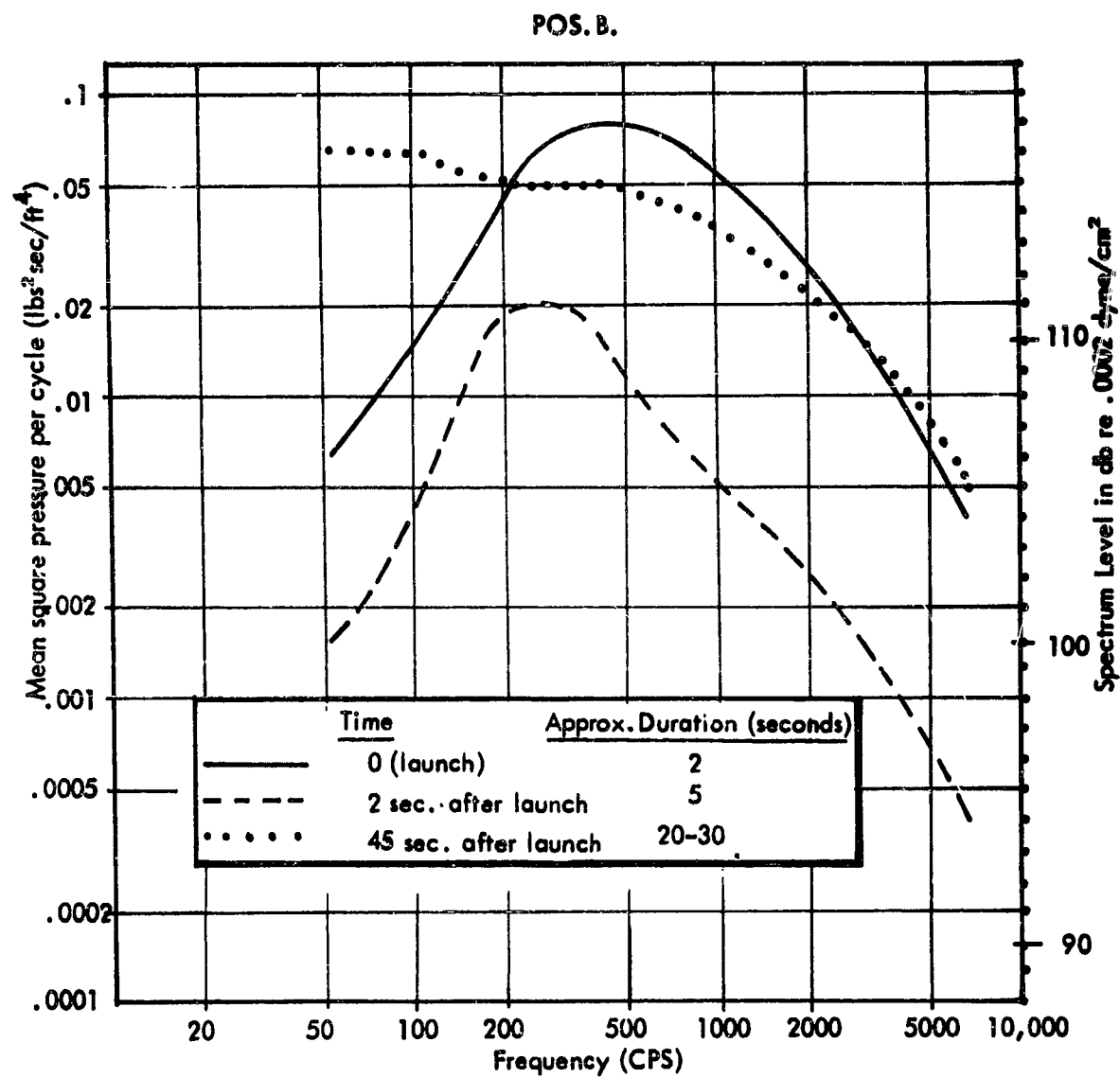


Figure 70. Estimated Mean Square Pressure Per Cycle at Several Times During Mission for Position B.

BIBLIOGRAPHY

Rocket Noise Excitation

von Gierke, H. E., "Aircraft Noise Sources," Chapter 33 of "Handbook of Noise Control," edited by Cyril Harris, McGraw-Hill Book Company, Inc., New York, 1957.

Aerodynamic Excitation

von Karman, "Significant Developments in Aeronautics," Journal of Aero/Space Sciences, March 1959.

Liepmann, "Aspects of Turbulence Problem," Zamp, Vol. III, 1952.

Kryzwoblocki, "Remarks on an Analytic Approach to Fuel Slosh and Buffet Problem of Aircraft," Journal of Aero/Space Sciences, October 1952.

Luskin, Lapin, "Remarks on an Analytic Approach to Fuel Slosh and Buffet Problem of Aircraft," Journal of Aero/Space Sciences, April 1952.

Howarth, "Modern Developments in Fluid Dynamics."

Hewson, "International Symposium on Atmospheric Turbulence," MIT AFRC TR 53-9, 1951.

Brogle, "On Frequency Spectrum Generated by a Maneuvering Aircraft," Journal of Aero/Space Sciences, July 1957.

Coles, "Remark on Equilibrium Turbulent Boundary Layer," Journal of Aero/Space Sciences, July 1957.

Batchelor, "Recent Developments in Turbulence Research," 7th International Congress for Applied Mechanics, TA 350, 1948.

Batchelor, "The Singularity in the Spectrum of Homogeneous Turbulence," Symposium in Applied Math Proceedings, Vol. 7.

Charwat and Yakura, "An Investigation of Two-Dimensional Base Pressure," Journal of Aero/Space Sciences, Feb. 1958.

Chang, "On Unsteady Interaction between a Weak Thermal Layer and a Strong Plane Oblique Shock," Journal of Aero/Space Sciences, May 1958.

Hammit, "Interaction of Shock Waves and Turbulent Boundary Layer," Journal of Aero/Space Sciences, June 1958

Honda, "The Investigation of the Interaction Between Shock Waves and Boundary Layer," Journal of Aero/Space Sciences, November 1958.

Kendall, "Experimental Investigation of Leading Edge Shock Wave Boundary Layer Interaction at $M = 5.8$," Journal of Aero/Space Sciences, January 1957.

"Turbulence in the Wake of a Thin Airfoil at Low Speeds," NACA TM 1427, January 1957.

Butchart, "Flight Studies of Problem Pertaining to High-Speed Operation of Jet Transports," NASA Memo 3-2-59H, March 1959.

Duncan, "Buffeting," British R & M, May 1943.

Huston, "Probability and Frequency Characteristics of Some Flight Buffet Loads," NACA TN 3733, August 1956.

Liepmann, "Extension of the Statistical Approach to Buffeting and Gust Response of Wings of Finite Span," Journal of Aero/Space Sciences, March 1955.

Liepmann, "On the Application of Statistical Concepts to the Buffeting Problem," Journal of Aero/Space Sciences, December 1952.

Luskin, "Analytical Approach to Fuel Slosh and Buffeting Problem of Aircraft," Journal of Aero/Space Sciences, April 1952.

Miles, "An Approach to the Buffeting of Aircraft Structure by Jets," Douglas Aircraft, SM 14795, Also IAS 435, June 1953.

"Limited Analysis of Buffeting Experienced in Flight by F-86 with and without Large External Fuel Tanks," NACA RM L54J22.

"On the Spectrum of Natural Oscillations of Two-Dimensional Laminar Flow," NACA TM 1417, December 1957.

Love, "Base Pressure at Supersonic Speeds," NACA TN 3819, January 1957.

Gadd, "Base Pressure in Supersonic Flow," BR CP271, 1956.

von Karman, "Fundamentals of the Statistical Theory of Turbulence," Journal of Aero/Space Sciences, 1937.

Goldstein, "Modern Developments in Fluid Dynamics," Vol. I, 1938.

Ryder and Zaid, "Shimmy Landing Gear Vibration Instability," Journal of Aero/Space Sciences, May 1959.

Batchelor, "Sound in Wind Tunnels," Australian Council for Aeronautics, Report 18 1945.

Batchelor, "Theory of Homogeneous Turbulence," Cambridge University Press, 1953.

Kimbro, "The Stability of Highly Accelerated Rockets During Burning," BRL 672, April 1953.

Wilmarth, "Space Time Correlation of Fluctuating Wall Pressures in a Turbulent Boundary Layer," January 1958.

Coe, "A Study of the Local Pressure Fluctuations of Two-Dimensional Airfoils," NACA RM A55J11, 1955.

Fradenburgh, "Influence of Fuselage and Canard-Type Control Surfaces on the Flow Field at $M = 2.0$," NACA RM E51K05, January 1952.

Atmospheric Wind and Turbulence Environments

Sasaki, Yoshikazu, "A Theory and Analysis of Clear-Air Turbulence," Scientific Report No. 1, Texas A & M Research Foundation, May 1958.

Liepmann, H. W., Laufer, J., Liepmann, K., "On the Spectrum of Isotropic Turbulence," NACA TN 2437, November 1951.

Schubauer, G. B., Klebanoff, P. S., "Investigation of Separation of Turbulent Boundary Layer," NACA Report 1030, 1951.

Dryden, H. L., Schubauer, G. B., Mock, W. C., Jr., Skramstad, H. K., "Measurements of Intensity and Scale of Wind-Tunnel Turbulence and Their Relation to the Critical Reynolds Number of Spheres," NACA Report 581, 1937.

Hewson, E. W., "International Symposium on Atmospheric Turbulence in the Boundary Layer," Massachusetts Institute of Technology, Geophysical Research Papers No. 19, December 1952.

Crane, H. L., Chilton, R. G., "Measurement of Atmospheric Turbulence over a Wide Range of Wave Lengths for one Meteorological Condition," NACA TN 3702, June 1956.

Court, A., "Vertical Correlation of Wind Components," AFCRC-TN-57-292, 29 March 1957.

Bieber, R. E., "Missile Structural Loads by Non-Stationary Statistical Methods," LMSD-497031, Lockheed Missiles & Space Division, 29 April 1959.

Panofsky, H. A., "Statistical Properties of the Vertical Flux and Kinetic Energy at 100 Meters," Scientific Report No. 2 (Contract AF 19(604)-166), Division of Meteorology, Pennsylvania State College, July 1953.

Shaffer, P. A., Jr., Kerr, R. E., Jr., Helfand, B., "Wind Structural Study for Rockets," North American Instruments, Inc., 8th Quarterly Report for Period 20 January 1955 to 20 April 1955, and Biennial Summary for Period 20 April 1953 to 20 April 1955, ASTIA Document No. AD-159970.

Direct Vibration Excitation

Baker, Louis, Jr., and Steffen, Fred W., "Screaming Tendency of the Gaseous-Hydrogen-Liquid-Oxygen Propellant Combination," NACA RM E58EO9, Lewis Flight Propulsion Laboratory, 30 September 1958.

Berman, Kurt, and Cheney, Samuel H., Jr., "Combustion Studies in Rocket Motors," Journal of the American Rocket Society, Vol. 23, No. 2, March-April 1953.

Berman, Kurt, and Cheney, Samuel H., Jr., "Rocket Motor Instability Studies," Jet Propulsion, Vol. 25, No. 10, October 1955.

Crocco, L., and Cheng, S., "Theory of Combustion Instability in Liquid Propellant Rocket Motors," AGARDograph No. 8, Butterworth Scientific Publications, 1956.

Lee, T. C., Gore, M. R., and Ross, C. C., "Stability and Control of Liquid Propellant Rocket Systems," Journal of the American Rocket Society, Vol. 23, No. 2, March-April 1953.

Marble, Frank E., and Cox, Dale W., "Servo-Stabilization of Low Frequency Oscillations in a Liquid Bipropellant Rocket Motor," Journal of the American Rocket Society, Vol. 23, No. 2, March-April 1953.

Osborne, J. R., and Shiewe, R. M., "An Experimental Investigation of High Frequency Combustion Pressure Oscillations in a Gaseous Bipropellant Rocket Motor," Interim Report No. I 58-1, Jet Propulsion Center, Purdue University, June 1958.

Penner, S. S., and Datner, P. P., "Combustion Problems in Liquid-Fuel Rocket Engines," California Institute of Technology, Technical Report No. 7, August 1954.

Rosenblum, M. H., Rienhart, W. T., Thompson, T. L., "Rocket Propulsion with Nuclear Energy," ARS 559-57, December 1957.

Struhlinger, E., "Design and Performance Data of Space Ships with Ionic Propulsion Systems," ARS 509-5, October 1957.

Felix, B. R., "Dynamic Analysis of a Nuclear Rocket Engine System," ARS 693-58, November 1958.

Bussard, R. W., "Some Boundary Conditions for the Use of Nuclear Energy in Rocket Propulsion," ARS 690-58, November 1958.

Kraemer, R. S., Larson, V. R., "Comparison of Several Propulsion Systems for a Mars Mission," ASME Publication No. 59-A-46, March 1959.

Edwards, R. N., Kuskevics, G., "Cesium-Ion Rocket Research Studies," ASME Publication No. 59-AV-32, March 1959.

Boden, R. H., "Recent Developments in Ion Propulsion Systems for Space Travel,"
ASME 59-AV-45, April 1959.

Den Hartog, J. P., "Mechanical Vibrations," Third Edition, McGraw-Hill Book
Company, Inc., 1947.

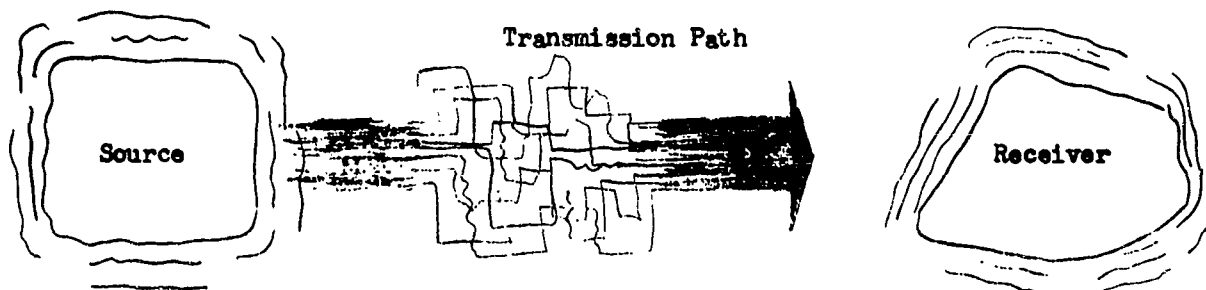
Timoshenko, S., "Vibration Problems in Engineering," Third Edition,
D. Van Nostrand Company, Inc., 1955.

PART II
RESPONSE TO VIBRATIONS

I. INTRODUCTION

The prediction of the vibratory responses and stresses in aircraft and space vehicles resulting from the various sources discussed in Part I of this report is a most formidable task. When the exciting forces were primarily sinusoidal in nature, as is the case with propeller aircraft and helicopters, the problem of predicting response is somewhat simpler, if only for the fact that the number of possible major exciting frequencies is finite. However, for space vehicles and high performance aircraft, the major excitation results from jet or rocket noise, boundary layer and base pressure fluctuations and other phenomena which are characterized by continuous frequency spectra and random amplitudes. Furthermore, although structural fatigue is predominant at frequencies below 500 cps, equipment malfunction and electronic component fatigue extend the frequency range of concern to at least 10,000 cps. Hence, for many cases, the prediction of vibration response for advanced aircraft and space vehicles, must include concern for all frequencies below 10,000 cps.

The vibration of any portion of the vehicle resulting from a source of energy depends on characteristics of the source, the path between the source and the receiver and the characteristics of the receiver itself, as illustrated in the following sketch.



At low frequencies, the response of the entire vehicle is maximum at the basic body modes, and the magnitude of the response depends primarily upon the location relative to the body mode shape, the magnification factor for the mode, the magnitude of the forcing function over the entire vehicle. At higher frequencies the maximum responses occur at the resonances of the various panels and the magnitude of the response depends on the characteristics of the source, the panel, the transmission path between panel and receiver, and upon the receiver. At frequencies above the panel fundamental resonances the factors influencing response become very complex and the possibility of resonances along the path becomes sufficiently high as to suggest that the path be treated as a transmission line with lumped parameters which, in addition to source and receiver characteristics, determine the vibration response.

From this brief discussion, it is clear that a detailed stepwise approach for the prediction of vibration for any general case would be exceedingly complex and cumbersome. Further, it is clear that a practical analytical solution of the

vibration characteristics of a mechanical system must lie in judicious simplification of the system to a series of sub-systems whose solutions are known.

The following sections begin with an analysis of the simplest vibratory system - a single degree of freedom system. This discussion is followed by an examination of vibration response data obtained in both aircraft and missiles, illustrating broad trends in the data. Successive sections give the fundamental factors which must be considered in the analysis of the vibration of a system, and discuss the natural vibratory characteristics of mechanical systems encountered in aircraft and missiles and the fatigue which can result from excessive vibration.

II. PROPERTIES OF THE SINGLE DEGREE OF FREEDOM SYSTEM

As noted in the Introduction, the understanding and solution of the complex vibration phenomena in aircraft and missiles requires great sophistication in both the methods and concepts utilized by the engineer. Whereas, in the past the engineer was confronted with relatively well-behaved sinusoidal forcing functions resulting from rotating machinery, it is now necessary to be concerned with random forcing functions, space and time correlations, and the statistical properties of random phenomena. Furthermore, the responses to these random forcing functions are complicated by the properties of the missile structure, to the point where the resulting vibration almost defies analysis. However, as will be seen in subsequent sections, many complex problems can be approached analytically if the problem can be simplified to an extent that it becomes a series of smaller problems, each capable of direct solution.

The purpose of this section is to study the most fundamental vibratory system which is a basic building block in the analysis of more complex systems. This basic building block is the single degree of freedom system which, when idealized to a lumped parameter system, includes a spring, a viscous damper and a mass which is constrained to move in one coordinate. This constraint is essential if the idealized system is to have a single degree of freedom since each additional axis of linear motion or plane of rotation permitted adds an additional degree of freedom to the system. Although the restriction of motion to only one degree of freedom is unrealistic in many cases, it often serves in the estimate of the lowest resonant frequency of more complex systems. Consequently, since vibratory motion of a system generally has its maximum amplitude, and hence maximum stress within the system at its lowest resonant frequency, the single degree of freedom approach often has great practical utility.

A detailed discussion is given below of the vibration characteristics of this idealized lumped parameter single degree of freedom for transient excitation, forced sinusoidal excitation, sinusoidal foundation motion excitation, transmissibility between the mass and the foundation for sinusoidal excitation, followed by a discussion of the vibration characteristics for random excitation, and a discussion of the electrical analogies and impedance concepts often used to more easily understand this system. In order to show how continuously distributed systems can be analyzed by single degree of freedom concepts, a mathematical derivation of the most general single degree of freedom system equations is presented next, showing the equivalence to lumped parameter systems and introducing the concept of mode shape. Finally, for convenient reference, the mathematical steps used to solve the governing differential equation are given along with a summary of the various response functions obtained for several sinusoidal and random excitations of the system.

FREE VIBRATION AND TRANSIENT EXCITATION

The general equation for the lumped parameter single degree of freedom system of Figure 71 is developed directly from Newton's second law: Force equals mass times acceleration. Therefore, following References 1 and 2,

$$\begin{array}{ccccccc} \text{inertia force} & + & \text{damping force} & + & \text{spring force} & = & \text{exciting force} \\ m\ddot{x} & + & c\dot{x} & + & kx & = & F(t) \end{array} \quad (1)$$

where m = mass
 c = viscous damping constant
 k = spring constant
 $F(t)$ = exciting force as a function of time
and x , \dot{x} , \ddot{x} = displacement, velocity, and acceleration, respectively.

If the mass is displaced to the right of its equilibrium position by an amount x_0 and then released, its motion will be given by a solution of (1) as:

$$x = x_0 e^{\left[\frac{-c}{2m} + i \sqrt{\frac{k}{m} - \frac{c^2}{4m^2}} \right] t} \quad (2)$$

Note that the general solution for free vibration is of the form

$$x = Ae^{s_1 t} + Be^{s_2 t} \quad (3)$$

$$\text{where } s_1, s_2 = \frac{-c}{2m} \pm i \sqrt{\frac{k}{m} - \frac{c^2}{4m^2}}$$

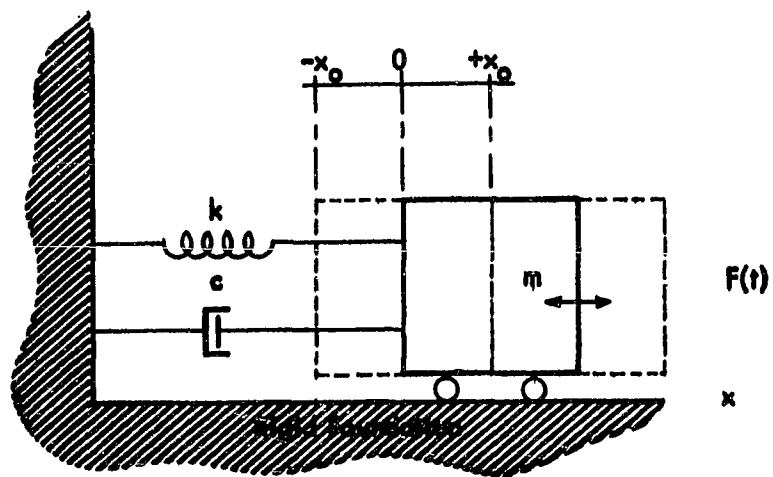
and where the constants A and B are dependent on the initial conditions.

If the damping, c , is zero, then (2) reduces to

$$x = x_0 e^{i \sqrt{\frac{k}{m}} t} = x_0 e^{i \omega_n t} \quad (4)$$

where $\omega_n^2 = \frac{k}{m}$ is the undamped natural frequency in radians per second.

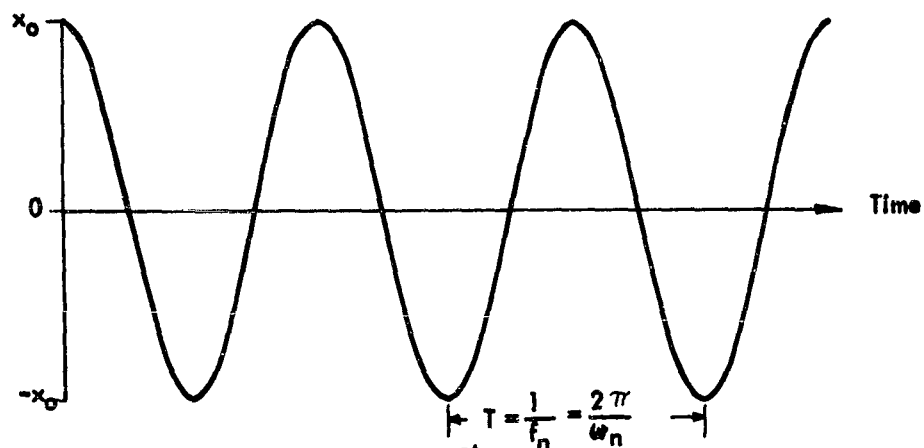
The resulting motion is sinusoidal and, because $c = 0$, continues indefinitely as illustrated in Figure 72a. It should be noted that the undamped natural frequency



Force Excitation of a Single Degree of Freedom System

Figure 71

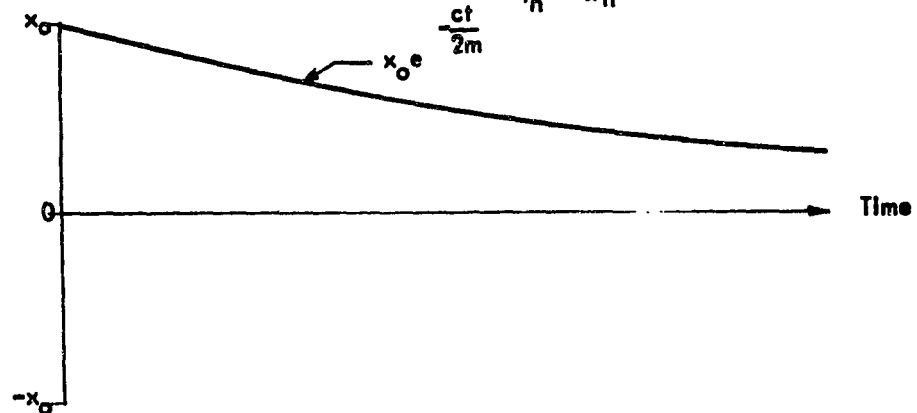
(a)



Undamped
 $c = 0$

$$x = x_0 \cos \omega_n t$$

(b)



Critically Damped

$$\frac{k}{m} - \frac{c^2}{4m^2} = 0$$

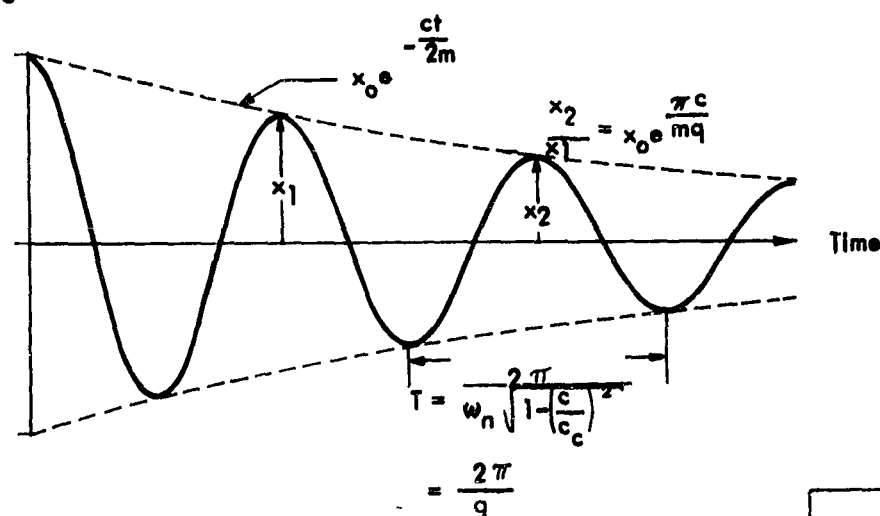
or

$$c = c_c = 2 \sqrt{km} = 2m\omega_n$$

and

$$x = x_0 e^{-\frac{ct}{2m}}$$

(c)



Damping Less
Than Critical

$$c_c > c > 0$$

$$\text{or } \frac{c}{c_c} = g < 1$$

Logarithmic decrement

$$\ln \frac{x_2}{x_1} = \delta = \frac{\pi c}{mq}$$

and for small damping
($\omega_n \approx q$), $\delta \approx 2\pi g$

$$x = x_0 e^{-\frac{ct}{2m}} \cos qt$$

Figure 72. Vibration Response for Various Damping

can be simply obtained from energy considerations where the maximum potential energy

$$\int_0^{x_0} kx dx = \frac{1}{2} kx_0^2 \text{ when the mass is at rest, equals the maximum kinetic energy,}$$

$$\int_0^{\dot{x}_0} m\dot{x} d\dot{x} = \frac{1}{2} m\dot{x}_0^2 \text{ when the mass passes through its equilibrium position. Since}$$

$\dot{x}_0 = \omega_n x_0$ for sinusoidal motion, then $\omega_n^2 = \frac{k}{m}$, as before. However, when $\frac{c^2}{4m^2}$ is

greater than $\frac{k}{m}$, both terms in the exponent of Eq. (2) are real and negative. Therefore, the motion is an exponential decay toward the equilibrium position. The amount of damping required to just prevent oscillatory motion or crossing of the $x = 0$ axis as shown in Figure 72b, is the value of c which makes the radical in (2) equal to zero. This value of damping, called the critical value of damping, c_c , also is given by

$$c_c = 2 \sqrt{mk} = 2m\omega_n \quad (5)$$

When the value of the damping constant is less than the critical value, the motion resulting from release from position x_0 is a damped cosine wave, as illustrated in Figure 72c. The damped natural frequency, q , is less than the undamped natural frequency, as shown by

$$q = \sqrt{\frac{k}{m} - \frac{c^2}{4m^2}} = \omega_n \sqrt{1 - \zeta^2}, \text{ where } \zeta = \frac{c}{c_c} \quad (6)$$

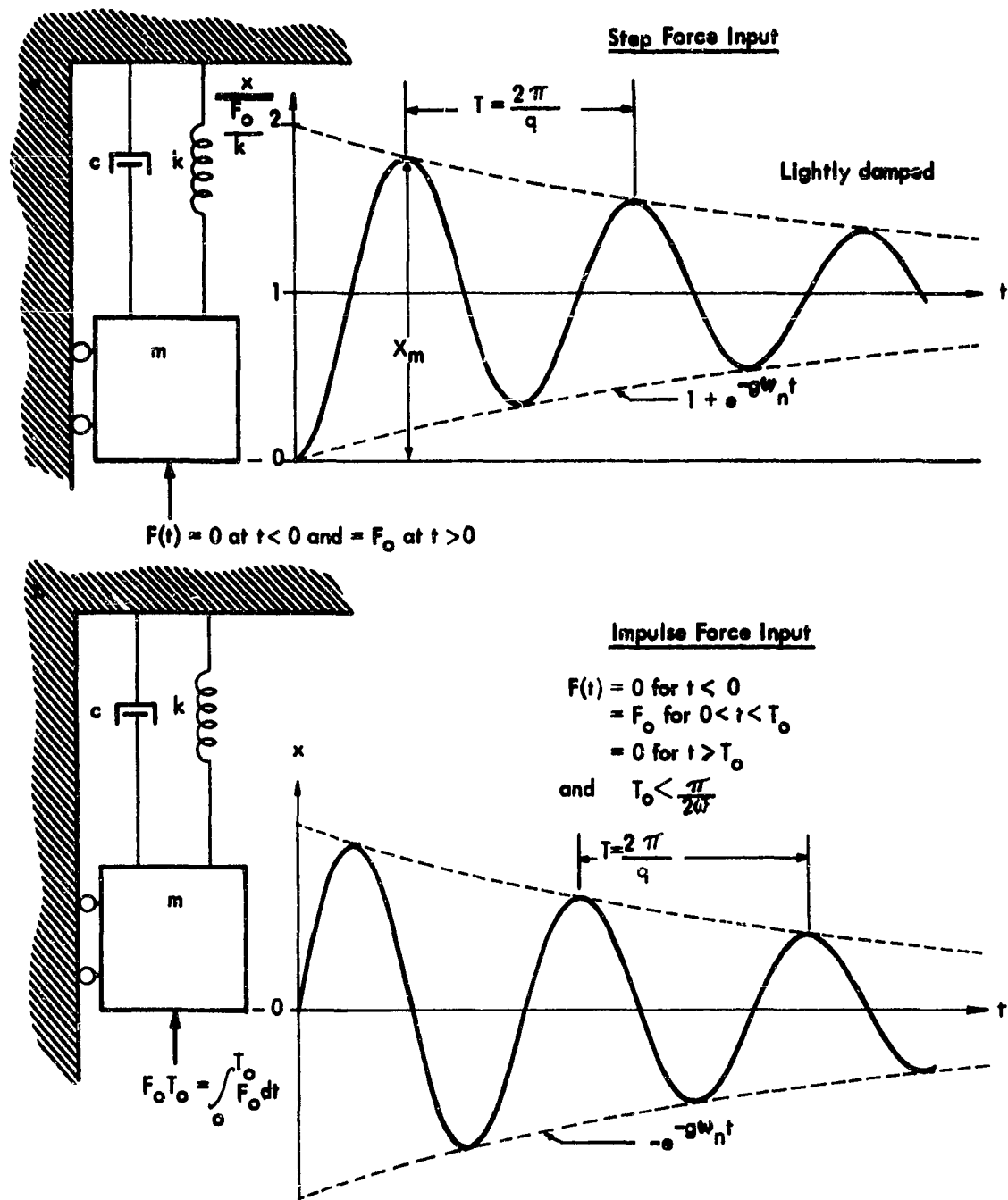
The final motion, substituting (6) and $\zeta = \frac{c}{c_c} = \frac{c}{2m\omega_n}$ into (2) becomes

$$x = x_0 e^{[-\zeta + i \sqrt{1 - \zeta^2}] \omega_n t} \quad (7)$$

There are two limiting cases of transient excitation which can be easily visualized from the preceding discussion. The first case is the sudden application of a constant force, or a step forcing function, such as the sudden release of a missile at liftoff after the engines have come up to full thrust. The second case is the application of a force for a very short time, an impulsive force, such as the explosive separation of missile stages.

The maximum response of an undamped system to the sudden application of a steady force, F_0 , can be seen easily from energy considerations. The net energy input accomplished by F_0 in Figure 73a occurs in the initial one-half cycle and equals $F_0 x_m$. The potential energy stored in the system when the mass is brought to rest at x_m is

$$\frac{1}{2} kx_m^2$$



Response to Step and Impulse Forcing Functions

Hence, the maximum displacement of the mass is equal to $\frac{2F_0}{k}$, or twice the static displacement which would result from a very slow application of F_0 . For the damped system, it follows from (7):

$$x = \frac{F_0}{k} \left[1 - e^{[-\zeta + i \sqrt{1-\zeta^2}] \omega_n t} \right] \\ = \frac{F_0}{k} \left[1 - e^{-\zeta \omega_n t} \cos \omega_d t \right] \quad (8)$$

It should be noted that the response is essentially unaltered if the total force is not applied instantaneously but is increased from 0 to F_0 in any time which is less than the time (t_0) required for a one-quarter cycle of the free vibration ($t_0 \leq \frac{\pi}{2\omega_n}$).

When the time required for the force to reach its constant value, F_0 , exceeds one-quarter cycle, the maximum response is less than that given by (8). (See Reference 3 for several examples.)

The response to an impulse is illustrated in Figure 73b. The response equation is derived from (1) assuming that the momentum acquired by the system equals the impulse $F_0 t_0$. The resulting motion (see Reference 4) is,

$$x = \frac{F_0 t_0}{\sqrt{1-\zeta^2}} \omega_n e^{-\zeta \omega_n t} \sin \omega_d t \quad (9)$$

This solution is valid for any force input (F_0) whose duration is less than one-quarter cycle of the free vibration ($T_0 \leq \frac{\pi}{2\omega_n}$).

FORCED SINUSOIDAL VIBRATION

When the damped single degree of freedom system is driven by a sinusoidal forcing function, $F(t) = F_0 \sin \omega t$, the response consists of two parts, an initial decaying transient response which depends upon the starting conditions, and a steady state or continuous forced vibration. The steady state motion is given by

$$x = x_0 \sin(\omega t - \phi) = \frac{F_0}{k} |H(\omega)| \sin(\omega t - \phi)$$

and

$$\frac{x_0}{\frac{F_0}{k}} = \frac{x_0}{x_s} = \left[\frac{1}{\left[1 - \left(\frac{\omega}{\omega_n} \right)^2 \right]^2 + 4 \left[\frac{c}{c_c} \frac{\omega}{\omega_n} \right]^2} \right]^{\frac{1}{2}} \quad (10)$$

where $|H(w)| = \left[\left[1 - \left(\frac{w}{w_n} \right)^2 \right]^2 + 4 \zeta^2 \left(\frac{w}{w_n} \right)^2 \right]^{-\frac{1}{2}}$ is the absolute value of the magnification factor,

ϕ is the phase angle between the force and displacement,

$$\phi = \tan^{-1} \frac{cw}{k - w^2 m} = \tan^{-1} \frac{2 \zeta \frac{w}{w_n}}{1 - \left(\frac{w}{w_n} \right)^2}$$

and $x_s = \frac{F_0}{k}$ is the static displacement resulting from a static force equal to F_0 . The absolute value of the magnification factor is given for several damping ratios in Figure 74. It can be interpreted as either the ratio of the maximum spring force to the exciting force or as the ratio of the maximum displacement of the mass to the displacement which would result from a static force F_0 . It is clear that very little magnification occurs when the frequency of the applied force is less than one-half of the undamped natural frequency. In this low frequency region, the system is stiffness-controlled; hence, the maximum spring force is approximately equal to and opposed by the driving force, $F_0 \approx kx$, since the driving force and the displacement are in phase, as seen in Figure 75.

However, as the frequency of the exciting force approaches the natural frequency of the system, the spring force and the inertia force begin to cancel each other, and a very considerable magnification can occur, depending upon the damping. Note that the damped natural frequency, q , is within one per cent of the undamped natural frequency for all damping ratios less than 0.14. At $w = w_n$, the magnification factor is inversely proportional to twice the damping ratio, and its value is often denoted as Q . Hence,

$$Q = \frac{1}{2\zeta} = \frac{1}{\frac{2c}{mw_n}} = \frac{mw_n}{c} \quad (11)$$

For all lightly damped systems, Q is the maximum value of the magnification factor, as can be seen in Figure 74, and the motion at the natural frequency is controlled by the damping force ($w_n c x_0 = F_0$).

When the frequency of the driving force exceeds the undamped natural frequency, amplitude of the motion of the mass becomes, approximately, inversely proportional to the square of the forcing frequency and hence, decreases asymptotically as the forcing frequency increases. In this frequency region, the motion is inertia controlled and the maximum inertial force of the mass is approximately equal to the driving force ($mw^2 x_0 \approx F_0$).

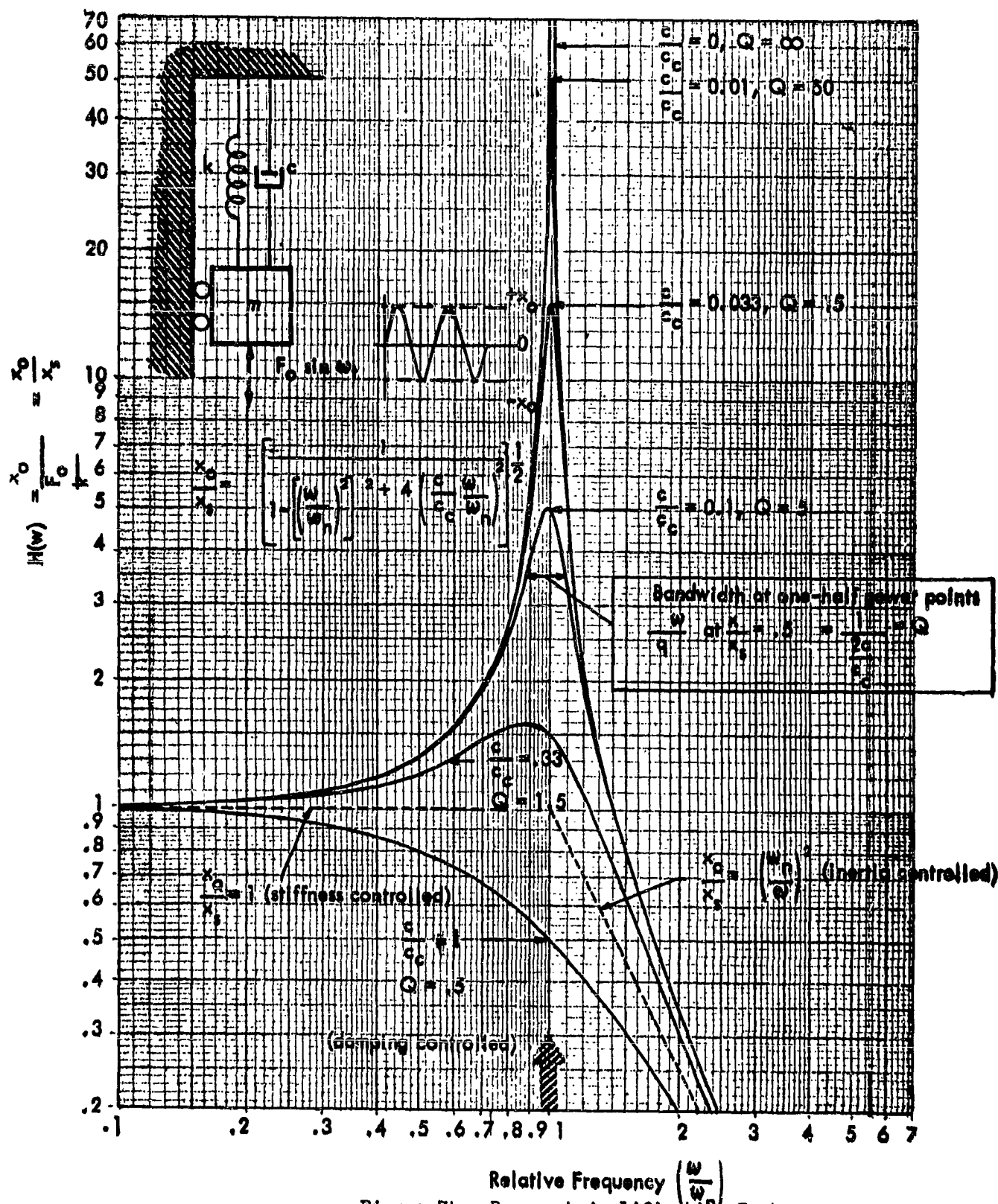
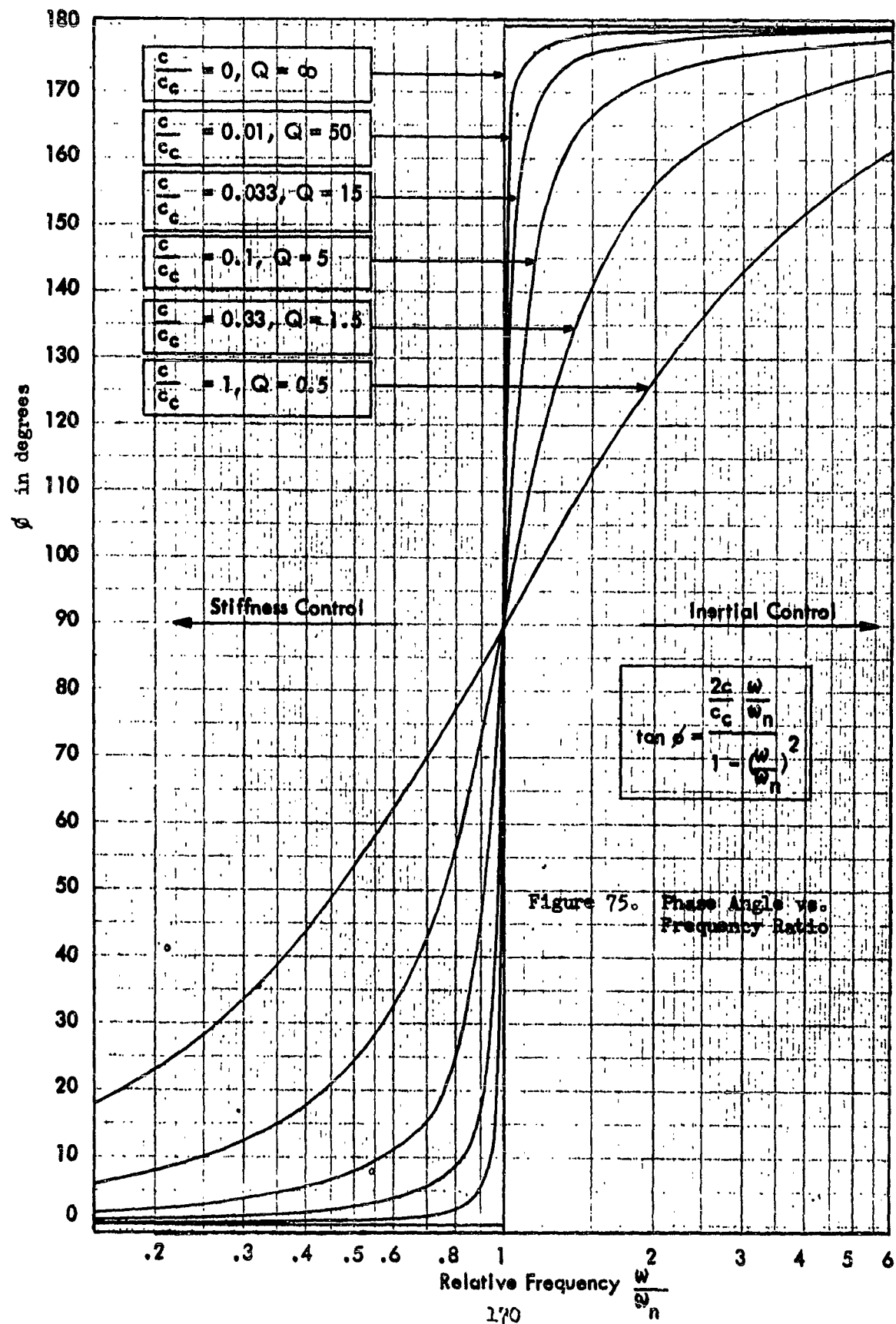


Figure 74. Resonant Amplification Factor



It should be noted that the resonant amplitude for the lightly damped system can be readily calculated by equating the power input to the system with the power dissipated in damping. It can be shown that the power input (P_i) for a sinusoidal forcing function is given by

$$P_i = w \frac{F_o x_o}{2} \sin \phi, \text{ where at resonance, } \sin \phi = 1,$$

and the power dissipated in damping (P_d) is

$$P_d = \frac{cw^2 x_o^2}{2} = \frac{mw^3 x_o^2}{2Q} \quad (12)$$

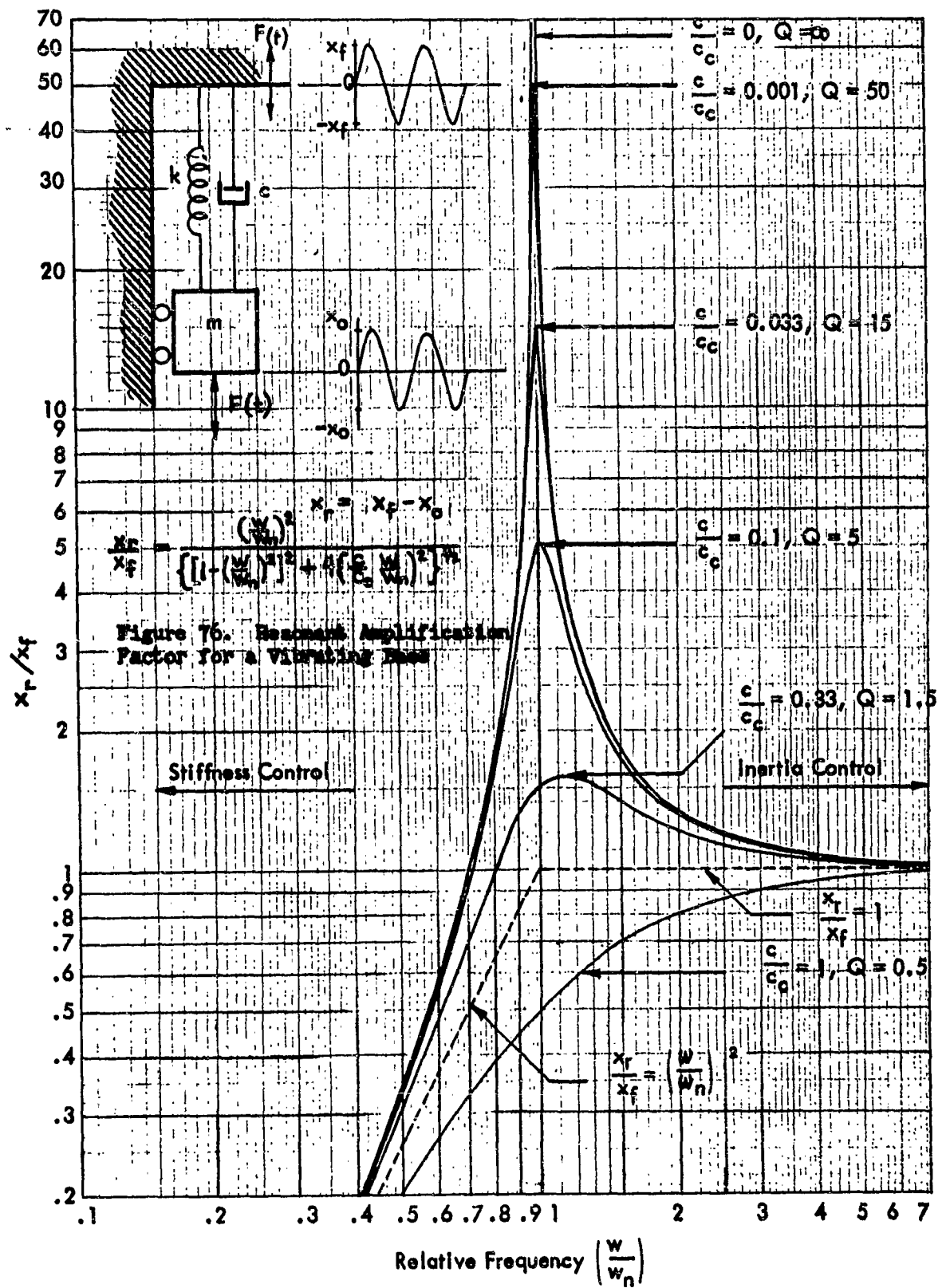
Hence,
$$x_o = \frac{F_o Q}{mw^2} = \frac{F_o Q}{k}$$

MOTION EXCITATION

The preceding solutions of equation (1) have been concerned with the response of a single degree of freedom system attached to a rigid foundation excited by a force which drives the mass. However, when equipment are mounted on vibrating structure, the motion of the foundation provides the excitation and the force $F(t)$ in equation (1) is provided by the inertia of the mass. If x_f is the foundation displacement, x_o the magnitude of the mass displacement, and x_r is the relative motion between the mass and the foundation, equation (1) becomes $m\ddot{x}_r + c\dot{x}_r + kx_r = m\ddot{x}_f$ and the solution for ($x_f = x_f \sin wt$) is:

$$\frac{x_r}{x_f} = \frac{\left(\frac{w}{w_n}\right)^2 \sin (wt - \phi)}{\left[1 - \left(\frac{w}{w_n}\right)^2\right]^2 + 4\left(\frac{c}{c_c} \frac{w}{w_n}\right)^2}^{\frac{1}{2}} = |H(w^2)| \sin (wt - \phi) \quad (13)$$

Note that this is identical with equation (10), except that F_o has been replaced by the inertia force of the mass ($mw^2 x_f$). The ratio of the magnitude of the relative displacement to the foundation displacement, x_r/x_f , is given in Figure 76 for several values of damping, and the phase relationships of Figure 75 also apply. At frequencies below resonance, the motions of the foundation and mass are in phase and for $\frac{w}{w_n} < .5$ the relative displacement is proportional to the foundation displacement



times the square of frequency, which is simply the acceleration of the foundation. This frequency region is utilized for the operation of most accelerometers.

At resonance the relative motion is 90 degrees ahead of the motion of the foundation and the magnitude of the relative motion is controlled by damping, equalling, for the lightly damped system, Qx_f , as before. Above resonance the relative motion leads the motion of the foundation by 180 degrees and the ratio $\left(\frac{x_r}{x_f}\right)$

approaches unity. Hence, the mass remains nearly motionless in a fixed coordinate system. Both displacement and velocity vibration transducers, which operate on the seismic principle, are designed to operate in this frequency range above resonance. It might be noted that the amount of damping in the transducer determines its accuracy at frequencies near resonance.

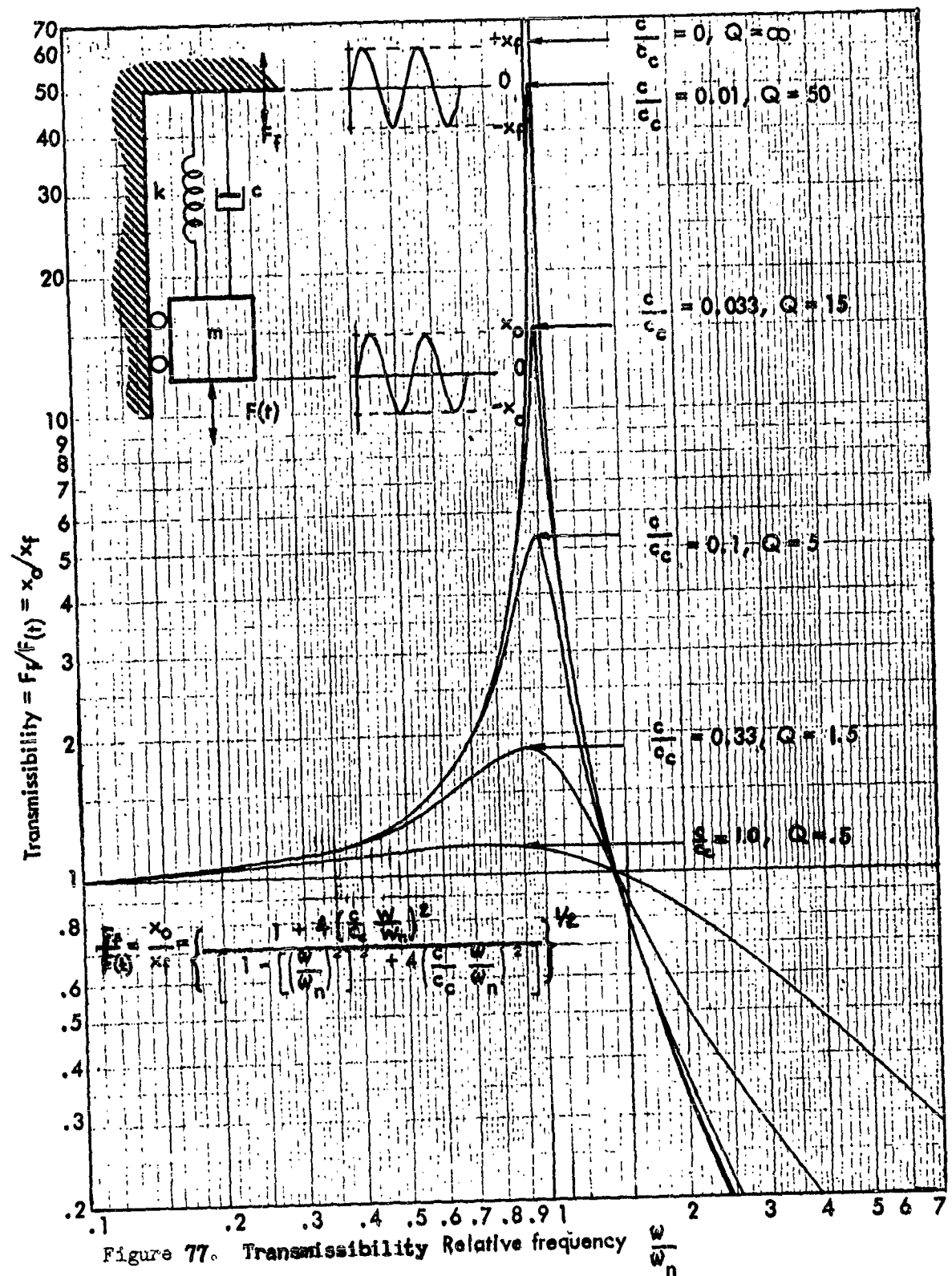
TRANSMISSIBILITY

When a spring is used for the isolation of delicate equipment from vibrating structure, or the isolation of the foundation from vibrating machinery, it is desirable to determine the degree of isolation. One measure of the isolation provided between the foundation and the mass is known as the transmissibility. For motion excitation it is the ratio of the absolute displacement of the mass to the displacement of the foundation, whereas for force excitation it is the ratio of the force transmitted to the foundation divided by the external force driving the mass. Thus the transmissibility is given from (10) and (13) by:

$$T = \left[\frac{1 + 4 \left(\frac{c}{c_c} \right)^2 \left(\frac{w}{w_n} \right)^2}{\left[1 - \left(\frac{w}{w_n} \right)^2 \right]^2 + 4 \left(\frac{c}{c_c} \right)^2 \left(\frac{w}{w_n} \right)^2} \right]^{1/2} \quad (14)$$

This relationship is illustrated in Figure 77 for several values of damping. Note that in the stiffness-controlled range below the natural frequency, the transmissibility is approximately unity, indicating small isolation. Near resonance the transmissibility equals Q . In this region the motion, or the force, is amplified by the single degree of freedom system. However, above resonance the transmissibility decreases below unity becoming nearly proportional to $\left(\frac{w_n}{w}\right)^2$, and decreasing asymptotically to zero, indicating an increasing degree of isolation.

It should be emphasized that these relationships can be directly applied only to a single degree of freedom system. If the mass is free to move along another axis or to rotate in a plane, or if the foundation is flexible, additional degrees of freedom are added which influence the solution. These more complex situations are considered in later sections.



RANDOM EXCITATION

Many of the most severe vibration environments encountered in current aircraft and missiles result from noise generated aerodynamically by the interaction of the propulsion jet with the atmosphere and from pressure fluctuations in the turbulent boundary layer which surrounds the vehicle during flight. Both of these forcing functions contain energy at all frequencies throughout a relatively wide frequency range of at least several octaves and the amplitudes of both vary in a random fashion. It is therefore, instructive to examine the response of the single degree of freedom system to a random force or motion input, in addition to its response to a single transient and a sinusoidal input which have been considered.

It is usually assumed that the amplitude probability distribution in a random noise forcing function follows the normal or Gaussian probability law. This assumption has been generally supported by analysis of the two forcing functions mentioned above. Further, it is assumed that the random forcing function is both stationary and ergodic. The assumption of stationarity requires that the statistical properties of the function do not vary with time, so that any two samples taken from a single continuous record of the function must appear statistically equivalent. The assumption of ergodicity requires further that any sample taken from a single continuous record of the function be statistically equivalent to the entire record of the function. When these requirements are fulfilled, the average properties of each sample of any record are similar and do not vary with time. This permits the use of the time averages in lieu of the more awkward sample or ensemble averages. Further, fulfillment of these requirements enables use of Fourier transforms to relate the statistical auto-correlation of the forcing function with its frequency spectrum, as will be seen in later sections.

It should be noted that many of the random forcing functions which are encountered during launch and flight do vary with time and are, therefore, neither stationary nor ergodic. However, in many cases the time history function can be divided into several shorter time periods within which the function is reasonably stationary. When the length of these shorter time periods is not sufficiently large compared to the time period of the response, large variations can be expected between the responses at differing times, because the sample length is not sufficiently long to give the true averages. This factor is undoubtedly responsible for much of the variation that is often found in missile vibration data when comparisons are made between the vibrations of individual missiles, belonging to a group of similar missiles, occurring during similar flight periods.

When the force input to a linear single degree of freedom system is random the response is also random. If the force contains energy at all frequencies over a relatively wide frequency range which includes the resonant frequency of the system, the energy at frequencies near the resonant frequency will be magnified, as in Figure 74. Therefore, the response will appear to be approximately sinusoidal with an amplitude which varies randomly with time. Figure 78 illustrates a sample of the response of a panel to jet noise excitation. The instantaneous amplitudes are distributed normally about a zero mean. The normal probability density is shown at the bottom of Figure 78. The probability, or the proportion

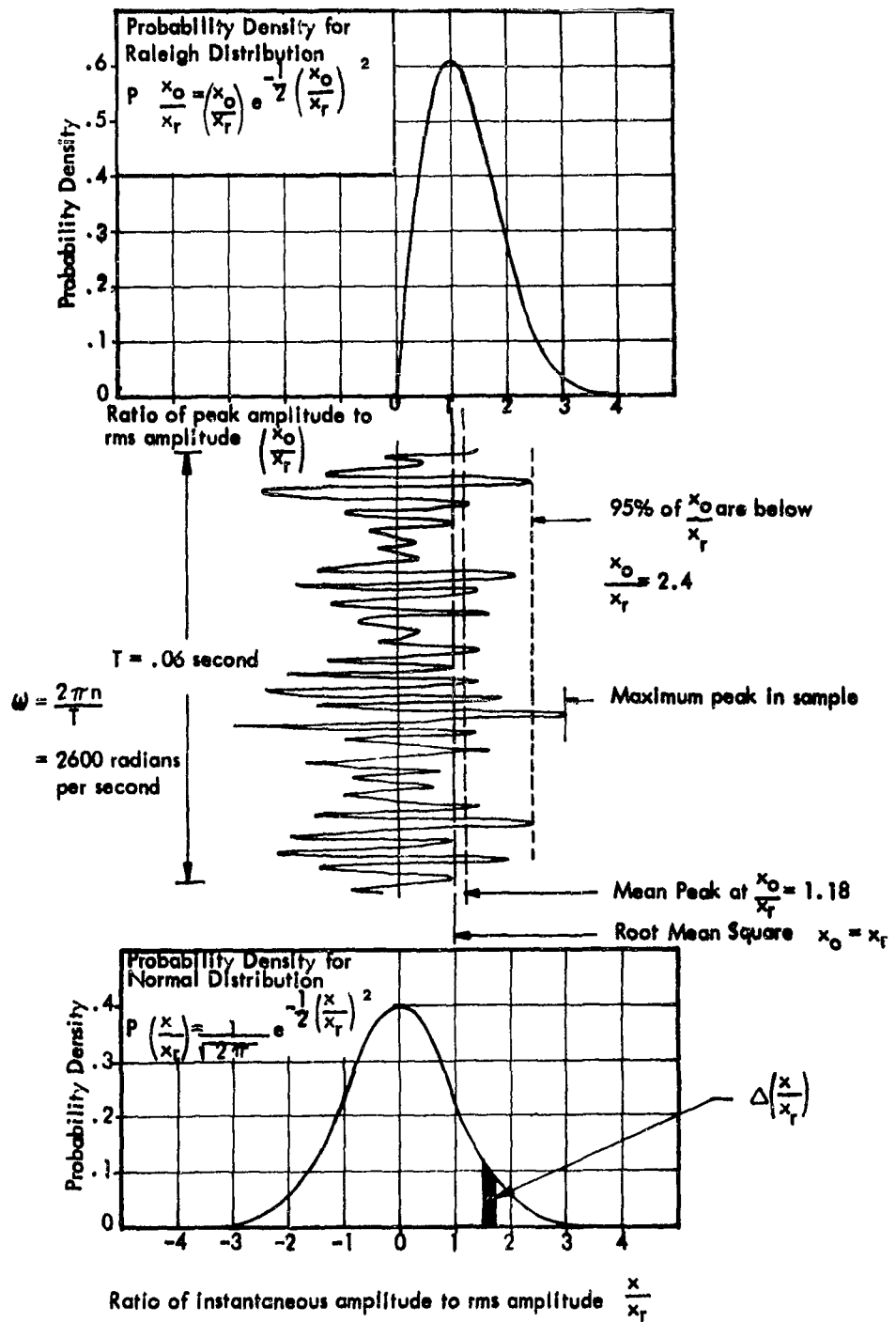


Figure 78

of time that $\frac{x}{x_r}$ is between $\frac{x_1}{x_r}$ and $\left(\frac{x_1}{x_r} + \Delta \frac{x}{x_r}\right)$ is the product of the probability density at $\frac{x_1}{x_r}$ and the interval $\Delta \frac{x}{x_r}$.

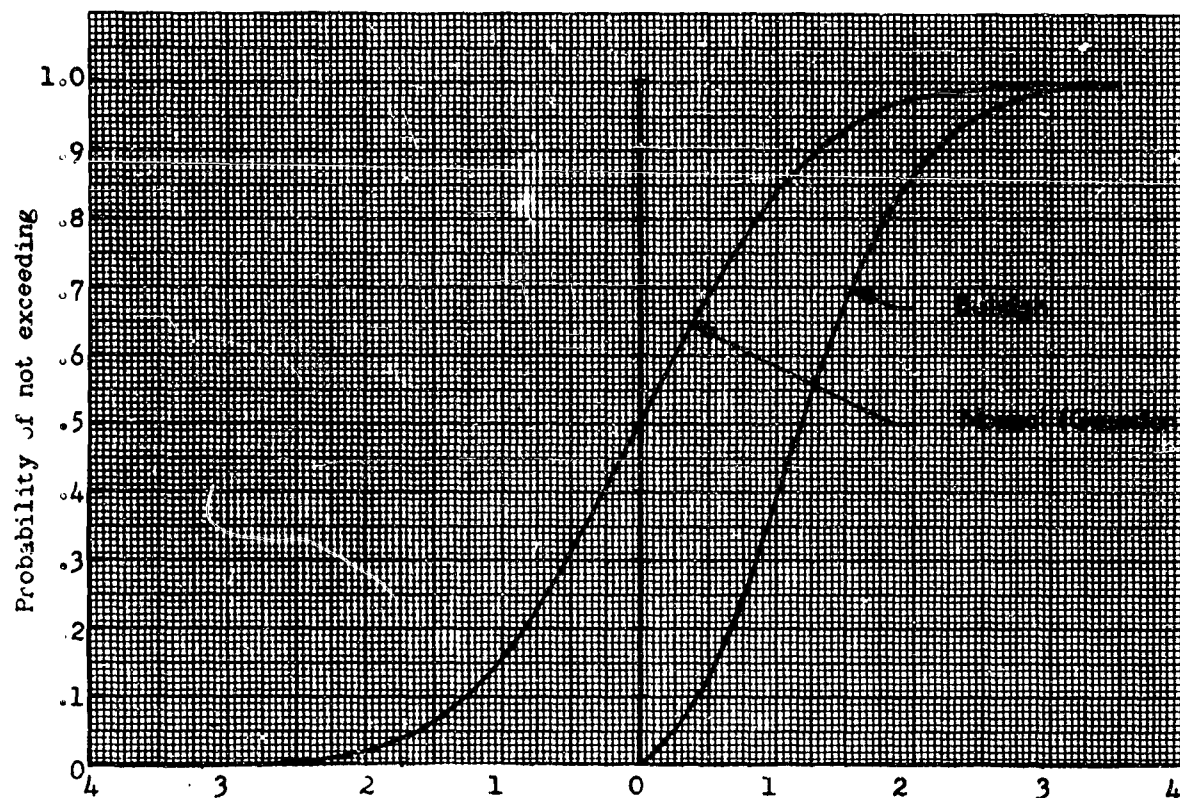
The probability density for the peak responses of the lightly damped single degree of freedom system are distributed in accordance with the Rayleigh distribution illustrated in the upper portion of Figure 78. Comparing these two probability density functions, it is clear that the probability of a zero instantaneous amplitude is higher than the probability of any other value as illustrated by the normal probability density function. However, it is improbable that the peak amplitude in any cycle equals zero, as illustrated by the Rayleigh probability density function where the most probable peak amplitude is seen to be the rms amplitude, $\frac{x}{x_r} = 1$.

The probability distribution functions for these two distributions are given in Figure 79. The probability distribution is the integral of the probability density and gives the probability that the amplitude ratio is less than or equal to any value of the ratio. Thus, for the normal distribution of amplitudes, it is equally probable that the instantaneous amplitude be positive or negative relative to the mean of zero. Further, 68% of the instantaneous amplitudes are less than the root mean square value. For the Rayleigh distribution, 39% of the peak amplitudes are less than the rms amplitude, 50% are less than 1.18 times the rms value, 86% are below 2.0 times the rms value, and 99% are below 3.0 times the rms value. As can be seen in the sample response shown in Figure 78, the maximum peak amplitude occurred at the 99% level and three peaks equal or exceed the 95% level.

It should be noted that the Rayleigh distribution will be expected only in the single degree of freedom system. When additional degrees of freedom exist in the system, additional resonant frequencies will exist. The response will be more complex and the peak amplitudes will tend to be more normally distributed about the mean amplitude. However, when the response is analyzed through a filter with a narrow bandwidth, the peak amplitudes from the filter will tend toward the Rayleigh distribution.

It is clear that the distribution of amplitudes in a random forcing function or response can be conveniently described in terms of the root mean square amplitude. However, the importance of the distribution of amplitudes relative to the rms amplitude cannot be overemphasized for the vibration engineer. In comparison with the steady state sinusoidal case, this distribution adds another dimension to the analysis of vibration data, the evaluation of a vibration environment for either equipment or structure, and the selection of test methods for the determination of equipment or structural reliability. The necessity of this added dimension results directly from the fact that the majority of equipment malfunctions occur at the maximum peak amplitudes and, as will be seen later, a disproportionate amount of the fatigue damage to structure is caused by the relatively infrequent peaks.

In order to determine the response of the single degree of freedom system to a random forcing function, it is necessary to define the frequency distribution



Normal: Ratio of instantaneous amplitude to rms amplitude.
 Raleigh: Ratio of peak amplitude to rms amplitude.

Figure 79: Normal and Rayleigh Probability Distribution Functions

as well as the amplitude distribution of the random input. It was noted in the discussion of forced sinusoidal vibration that the amplitude at resonance could be determined by equating the power input to the system with the power dissipated by damping within the system. Now the instantaneous power dissipated by damping equals the instantaneous damping force times the instantaneous velocity of the motion. Therefore, the average damping power (P_d) which is dissipated between time t_1 and t_2 is the integral of the instantaneous power during the time interval, divided by the duration of the interval, or

$$P_d = \frac{1}{t_2 - t_1} \int_{t_1}^{t_2} c \dot{x}^2 dt \quad (15)$$

where $c \dot{x}$ is the instantaneous damping force and \dot{x} is the instantaneous velocity.

Since c is a constant (when viscous damping can be assumed), the damping power equals c times the average or mean value of the square of the velocity during the time interval. Hence (15) could be written

$$P_d = c \overline{\dot{x}^2} \quad (16)$$

where $\overline{\dot{x}^2}$ is the mean square velocity (or the square of the rms velocity). It is convenient to utilize the concept of damping power in the definition of the frequency distribution of the random forcing function or response. For example, consider a random forcing function which contains force components at all frequencies within the frequency region between f_1 and f_2 , and which excites a single degree of freedom system consisting of only a viscous damper. If the damper were separated from the forcing function by a series of unity gain filters covering the frequency range between f_1 and f_2 , each with bandwidth Δf , the power dissipated in the damper resulting from the portion of the forcing function passed through the filter of frequency f_a is:

$$\Delta P_a = c \Delta \overline{\dot{x}_a^2} \quad (17)$$

where $\Delta \overline{\dot{x}_a^2}$ is the mean square velocity resulting from the portion of the forcing function of bandwidth Δf centered on frequency f_a .

The Power Spectral Density (PSD) is simply the damping power per cycle per second, or

$$PSD = \frac{\Delta P_a}{\Delta f} = \frac{c \Delta \overline{\dot{x}_a^2}}{\Delta f} = c \overline{\dot{x}^2}(f)$$

and the total power P_d between frequencies f_1 and f_2 is the sum of the mean square velocity per cycle per second times the bandwidth Δf and the damping constant c throughout the frequency range:

$$P_d = \sum_{f_1}^{f_2} (\text{PSD}) \Delta f = \sum_{f_1}^{f_2} \overline{c \dot{x}^2(f)} \Delta f \quad (18)$$

Because of the convenience of the power spectral density approach, the term is often applied to accelerations or displacements as well as velocities. Further, when applied to these other quantities, it is tacitly assumed that the value of c is unity and the result becomes the power spectral density of the function (either in displacement, x , or velocity, \dot{x} , or acceleration, \ddot{x} .) To avoid confusion, it is often preferred to speak of mean square (displacement, velocity, or acceleration, depending on the quantity used) per cycle per second rather than power spectral density. This distinction allows the reservation of the word "power" for actual mechanical power.

The response of a single degree of freedom system to an applied random forcing function which is characterized by a continuous distribution of mean square force per cycle per second, $\overline{F^2(f)}$, is given by the sum of the mean square responses associated with each narrow frequency band Δf . However, since the response functions derived earlier for the sinusoidal case were given in terms of w in radians per second, it is desirable to use the mean square force per radian per second, which is $\frac{\overline{F^2(f)}}{2\pi}$ and the band width (Δw).

$$\text{Then from (10)} \quad \overline{x^2(f)} = \frac{1}{2\pi} \frac{\overline{F^2(f)}}{k^2} |H(w)|^2 \Delta w \quad (19)$$

and the total mean square response, $\overline{x^2}$, is the sum of the responses in each Δw , from w_1 to w_2 :

$$\overline{x^2} = \frac{1}{2\pi} \sum_{w_1}^{w_2} \frac{\overline{F^2(f)}}{k^2} |H(w)|^2 \Delta w$$

and when the forcing function is continuous throughout the resonant frequency range, it can be shown (see Reference 4) that the total mean square response is

$$\overline{x^2} = \frac{Q w_n \overline{F^2(f)}}{4k^2} = \left(\frac{\pi}{2} \frac{f_n}{Q} \right) Q^2 \frac{\overline{F^2(f)}}{k^2} \quad (20)$$

where the response equals an effective bandwidth $\frac{\pi f_n}{2Q}$ times Q^2 and times the mean square force per cycle per second divided by the square of the stiffness. It should be noted that the mean square resonant response to a random forcing function of constant $\overline{F^2(f)}$ differs from its mean square response to a sinusoidal forcing

function of $\overline{F_n^2}$, which coincides with the natural frequency and has the same magnitude as $F^2(f)$, simply by the effective response bandwidth $\frac{\pi}{2} \frac{f_n}{Q}$.

Hence, the mean square resonant response to a random forcing function is proportional to Q times the mean square per cycle value of the forcing function, whereas in the sinusoidal case, the mean square response is Q^2 times the mean square value of the forcing function.

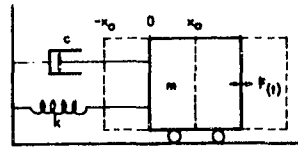
DYNAMIC ANALOGIES

The vibration characteristics of many complex mechanical systems can often be determined by applying electrical network theory to the interrelationships between the various mechanical elements rather than attempting the solution of the appropriate differential equations. The applicability of this technique results directly from the similarity between the basic differential equations for the electrical circuit and those for the mechanical system.

Figure 80 illustrates two types of electrical analogies for the single degree of freedom system. The impedance analogy, where the mechanical impedance is the ratio of the exciting force to the velocity of the mass, is seen to be equivalent to the electrical concept of impedance which is the ratio of voltage to current. The mobility analogy is the inverse of the impedance analogy and the mechanical mobility is the ratio of the velocity of the mass to the exciting force. For the majority of mechanical systems, the mobility analogy is far easier to apply than is the impedance analogy. This results directly from the ease of measuring velocities at various points in a mechanical system and voltages at various points in an electrical circuit. On the other hand, the impedance analogy requires measurement of mechanical force, which necessitates breaking into the system or circuit.

The use of these analogies permits both the direct calculation of response to applied force or motion through the standard electrical network solutions. However, in addition it offers the possibility of physically constructing an electrical analog of the mechanical system under study, and actually measuring the responses at desired points in the circuit to an applied electrical signal which simulates the expected mechanical exciting function.

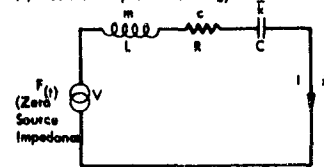
(a) Mechanical Single Degree of Freedom System



Force Equation:

$$\begin{array}{ccccccc} \text{Inertia} & & \text{Damping} & & \text{Spring} & & \text{Exciting} \\ \text{Force} & + & \text{Force} & + & \text{Force} & = & \text{Force} \\ m\ddot{x} & + & c\dot{x} & + & kx & = & F(t) \end{array}$$

(b) Electrical Impedance Analogy



Mechanical	analogous to	Electrical
Force $F(t)$		Voltage V
Velocity \dot{x}		Current i
Mass m		Inductance L
Compliance $\frac{1}{k}$		Capacitance C
Damping Constant c		Resistance R
Mechanical Impedance Z_m		Impedance Z

Network Voltage Equation:

$$\begin{array}{ccccccc} \text{Inductive} & & \text{Resistive} & & \text{Capacitive} & & \text{Applied} \\ \text{Voltage} & + & \text{Voltage} & + & \text{Voltage} & = & \text{Voltage} \\ \text{Drop} & & \text{Drop} & & \text{Drop} & & \\ L \frac{di}{dt} & + & Ri & + & \frac{1}{C} \int i dt & = & V \end{array}$$

Equivalent Mechanical Equation:

$$m \frac{dx}{dt} + cx + k \int x dt = F(t)$$

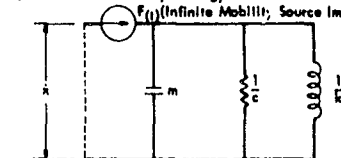
Electrical Impedance:

$$Z = \frac{V}{i} = j\omega L + R + \frac{1}{j\omega C}$$

Mechanical Impedance:

$$Z = \frac{F(t)}{\dot{x}} = j\omega m + c + \frac{k}{j\omega}$$

(c) Electrical Mobility Analogy



Mechanical	analogous to	Electrical
Force $F(t)$		Current i
Velocity \dot{x}		Voltage V
Mass m		Capacitance C
Compliance $\frac{1}{k}$		Inductance L
Damping Constant c		Conductance $\frac{1}{R}$
Mechanical Mobility M		Mobility α

Network Current Equation:

$$\begin{array}{ccccccc} \text{Current in} & & \text{Current in} & & \text{Current in} & & \text{Total} \\ \text{Capacitor} & + & \text{Conductance} & + & \text{Inductance} & = & \text{Current} \\ m \frac{dv}{dt} & + & \frac{1}{R} V & + & \frac{1}{L} \int V dt & = & i \end{array}$$

Equivalent Mechanical Equation:

$$m \frac{dx}{dt} + cx + k \int x dt = F(t)$$

Electrical Mobility:

$$\alpha = \frac{1}{V} = \frac{1}{j\omega L + R + \frac{1}{j\omega C}}$$

Mechanical Mobility:

$$M = \frac{\dot{x}}{F(t)} = \frac{1}{j\omega m + c + \frac{k}{j\omega}}$$

Figure 80. Mechanical - Electrical Analogies for the Single Degree of Freedom System

MATHEMATICAL DERIVATION AND SUMMARY OF THE RESPONSES OF A SINGLE DEGREE OF FREEDOM SYSTEM

The discussions presented heretofore on the characteristics and responses of the single degree of freedom system have been somewhat intuitive in order to emphasize the physical concepts involved and to show the precise relationships between the various engineering parameters used in vibrations and their corresponding mathematical expressions. The vibration engineer's understanding of the characteristics of such systems, his ability to skillfully apply these concepts to solving actual vibration problems, and his understanding of the limitations of such systems and the restrictive assumptions often imposed, are enhanced by a knowledge of the mathematical steps used to derive the response solutions of the governing differential equations of motions, especially when random excitations and random responses occur. Also, a better understanding of the methods for solving more complex problems, which may be mathematically tractable, and the meanings of the various response functions obtained, can be gained from a knowledge of the mathematics of the most fundamental of vibration systems. In addition, the single degree of freedom system analyzed above was a lumped parameter system, consisting of a single lumped mass, a single lumped spring, and a linear viscous dashpot. It is desirable to broaden the discussion to include also continuous systems, such as beams, plates, shells, etc., which, in many cases, have responses which are characteristic of the response of a single degree of freedom lumped parameter system.

The present discussion is therefore concerned first with a presentation and discussion of the governing differential equations of the general single degree of freedom system; secondly, the derivation of the steady state solutions of these equations for periodic forcing functions; thirdly, the derivation of the expressions for the power spectral density (psd) functions of response in terms of the psd and cross-psd functions of the excitation, or forcing functions, and finally the derivation of expressions for the over-all rms response to Gaussian white noise excitation. The solutions of the various cases considered are presented in Table IX for convenient reference.

EQUIVALENCE OF LUMPED PARAMETER AND CONTINUOUSLY DISTRIBUTED SINGLE DEGREE OF FREEDOM SYSTEMS

The vibratory motion of any volume or mass of elastic material is classified as single degree of freedom type oscillation if the response of the material can be defined everywhere by the product of a time function, $\varphi(t)$, and a space function, $h(x,y,z)$, so that at any point (x,y,z) in the material and at any time t , the total oscillatory motion is expressible by the function $H(x,y,z,t)$ where

$$H(x,y,z,t) = \varphi(t) \cdot h(x,y,z) \quad (21)$$

The function $h(x,y,z)$ is called the mode shape of the vibration and in general defines curves or surfaces of constant phase in the material, thus describing the relative phasing of the vibration at any two points in the material. If the material is a volume-type body, such as a block of rubber or a complex three-dimensional airframe, the function h will in general depend upon three coordinates, x , y , and z . If the material is essentially two-dimensional, such as a flat plate

or curved shell, the function may depend only on x and y , or r and θ in polar coordinates. For such configurations as a bar vibrating longitudinally where the motion is rectilinear, the function may depend upon only one independent variable, say x . The function $\psi(t)$ merely expresses the time variation of this mode shape at any point.

It is to be noted that the oscillatory motion may be quite general, and may consist of bending, twisting, and expansion or compression of the material simultaneously, so long as the net motions are defined by a single mode shape and a single time function. Such a general type motion is called a coupled response, characterized by a coupled mode shape, consisting possibly of several distinct types of uncoupled motions, each having the same mode shape and frequency response characteristics. A two degree of freedom system is characterized as one requiring two mode shapes, h_1 and h_2 , and two corresponding time functions, ϕ_1, ϕ_2 , to completely define the motion so that

$$H(x,y,z,t) = \phi_1(t) \cdot h_1(x,y,z) + \phi_2(t) \cdot h_2(x,y,z) \quad (22)$$

Similarly for an n -degree of freedom system.

The governing differential equation for the undamped vibratory motion is easily obtained by use of Lagrange's equation of motion

$$\frac{d}{dt} \left(\frac{\partial T}{\partial \dot{\phi}} \right) + \frac{\partial V}{\partial \phi} = \mathcal{F}(t) \quad (23)$$

where

T = total kinetic energy of the material

V = total potential energy of the material

ϕ = generalized coordinate

$\mathcal{F}(t)$ = generalized force acting on the material

The total kinetic energy is given by the expression

$$T = \frac{1}{2} \int_{\text{Vol.}} \dot{\phi}^2(t) \cdot h^2(x,y,z) \cdot \rho(x,y,z) \cdot dx \, dy \, dz$$

or

$$T = \frac{1}{2} \dot{\phi}^2(t) M \quad (24)$$

$$M = \int_{\text{Vol.}} h^2(x,y,z) \cdot \rho(x,y,z) \cdot dx \, dy \, dz = \text{generalized mass} \quad (25)$$

ρ = density of the material.

The equation for potential energy is in general not simply expressed as an integral over the volume, and it is sufficient here to express V as

$$V = \frac{1}{2} \varphi^2(t) \cdot K \quad (26)$$

where K is the generalized stiffness of the material, found by integrating over the volume the product of the virtual displacements and the elastic forces which must be overcome in producing those displacements. The generalized force $\mathcal{F}(t)$ is expressed as

$$\mathcal{F}(t) = \int_{Vol} F(x,y,z,t) \cdot h(x,y,z) \cdot dx \, dy \, dz \quad (27)$$

where $F(x,y,z,t)$ equals the applied force per unit volume acting at (x,y,z) . Substituting (24) and (26) into (23) gives immediately

$$M \ddot{\varphi}(t) + K \varphi(t) = \mathcal{F}(t) \quad (28)$$

A dissipative term is generally introduced (for linear damping) by analogy with the differential equation for a lumped parameter single degree of freedom system. Thus,

$$M \ddot{\varphi}(t) + C \dot{\varphi}(t) + K \varphi(t) = \mathcal{F}(t) \quad (29)$$

M = generalized mass

C = generalized damping = $2\mathfrak{J} M \omega_0$

K = generalized stiffness

$\mathcal{F}(t)$ = generalized force

ω_0 = natural frequency of the system = $\sqrt{K/M}$

\mathfrak{J} = (actual damping)/(critical damping)

Thus, (29) may be written as

$$\ddot{\varphi}(t) + 2\mathfrak{J}\omega_0 \dot{\varphi}(t) + \omega_0^2 \varphi(t) = \frac{\mathcal{F}(t)}{M} \quad (30)$$

which is the standard equation defining the single degree of freedom system, and is seen to be equivalent to (1) when (5) and (6) are introduced.

It is of interest to note that if the density of the material is constant and the force applied per unit volume, F , varies with time but is invariant spatially (i.e., $F(x,y,z,t) = F(t)$), then

$$M = \rho \int_{\text{Vol.}} h^2(x,y,z) dx dy dz = m \frac{\int_{\text{Vol.}} h^2(x,y,z) dx dy dz}{\int_{\text{Vol.}} dx dy dz}$$

$$\mathcal{F}(t) = F(t) \int_{\text{Vol.}} h(x,y,z) dx dy dz = F_0(t) \frac{\int_{\text{Vol.}} h(x,y,z) dx dy dz}{\int_{\text{Vol.}} dx dy dz}$$

where

$$m = \rho \int_{\text{Vol.}} dx dy dz = \text{total mass of material}$$

$$F_0(t) = F(t) \int_{\text{Vol.}} dx dy dz = \text{total applied force acting on the material}$$

so that

$$\frac{\mathcal{F}(t)}{M} = \eta \frac{F_0(t)}{m}$$

where

$$\eta = \frac{\int_{\text{Vol.}} h(x,y,z) dx dy dz}{\int_{\text{Vol.}} h^2(x,y,z) dx dy dz} = \text{factor accounting for the fact that the system is continuously distributed.}$$

Thus, (30) becomes, for a continuously distributed system of constant mass and applied force density:

$$\ddot{\varphi}(t) + 2 \gamma \omega_0 \dot{\varphi}(t) + \omega_0^2 \varphi(t) = \frac{\eta}{m} F_0(t) \quad (31)$$

For a lumped parameter system, such as that shown in Fig. 71, it is clear that $\eta = 1.0$ since $h = 1.0$.

Now that the equivalence between continuously distributed and lumped parameter single degree of freedom systems has been established, it is convenient in the mathematical solution of this equation to use the more standard terminology of the previous discussion; namely,

$$m\ddot{x} + c\dot{x} + kx = F(t) \quad (32)$$

where

$$c = 2\gamma\omega_0 m = J.C \text{ critical}$$

The solutions of this equation for various types of steady state excitation are derived below and presented in summary form in Table IX, using the terminology appearing in (1). It is important to note that these summarized response functions correspond to a lumped parameter system so that in applying these results to continuously distributed systems, the response functions must be multiplied by the factor n above.

DERIVATION AND SUMMARY OF RESPONSES OF THE LUMPED PARAMETER SINGLE DEGREE OF FREEDOM SYSTEM

Table IX presents a summary of steady state responses of the single degree of freedom system, shown in this table, to both sinusoidal and random excitations. Both the rms absolute response of the mass m and rms relative response of this mass with respect to the massless "base," or "foundation," are listed along with other important response parameters such as phase angle, probability density of the instantaneous amplitudes and peak amplitudes, average power developed in damping, work done in time Δt , and the number of response cycles in time Δt .

The rms responses to sinusoidal inputs are easily obtained from the differential equations presented in the table by substituting the following steady state excitation and response equations:

1. Sinusoidal $F(t)$, with no base motion

$$F(t) = F_0 e^{i\omega t}$$

$$Y(t) = \dot{Y}(t) = \ddot{Y}(t) = 0$$

$$x_{\text{rel.}} = x_{\text{abs.}} = x_0 e^{i(\omega t + \phi)}$$

$$\ddot{x}_0 = i\omega \dot{x}_0 = -\omega^2 x_0$$

$$\left\{ \begin{array}{l} (\text{rel.} = \text{relative response}) \\ (\text{abs.} = \text{absolute response}) \end{array} \right.$$

2. Sinusoidal $\ddot{Y}(t)$ with no applied force $F(t)$

$$\ddot{Y}(t) = \ddot{Y}_0 \cdot e^{i\omega t}$$

$$F(t) = 0$$

$$x_{\text{rel.}} = x_{0\text{rel.}} e^{i(\omega t + \phi)}$$

$$x_{\text{abs.}} = x_{0\text{abs.}} e^{i(\omega t + \theta)}$$

3. Sinusoidal $F(t)$ of frequency ω_1 , and $Y(t)$ of frequency ω_2

$$F(t) = F_0 e^{i\omega_1 t}$$

$$\ddot{Y}_0 = \ddot{Y}_0 e^{i(\omega_2 t - \lambda_3)}$$

λ_3 = phase angle of \ddot{Y} relative to $F(t)$

$$x_{\text{rel.}} = x_{0\text{rel.}} e^{i\omega t}$$

$$x_{\text{abs.}} = x_{0\text{abs.}} e^{i\omega t}$$

The phase angles for this case and for the case where $\omega_1 = \omega_2 = 0$ were not determined.

For each of these inputs, solving for $x_{0\text{rel.}}$ and $x_{0\text{abs.}}$ produces complex algebraic expressions. These expressions are then used to determine the complex expressions for $x_{\text{rel.}}$ and $x_{\text{abs.}}$. The mean square value of the response is determined by averaging the square of the real parts of $x_{\text{rel.}}$ and $x_{\text{abs.}}$ over one, or several complete response cycles according to the equations:

$$\overline{x_{\text{rel.}}^2} = \frac{1}{T} \int_0^T [\text{Real}(x_{\text{rel.}})]^2 dt$$

$$\overline{x_{\text{abs.}}^2} = \frac{1}{T} \int_0^T [\text{Real}(x_{\text{abs.}})]^2 dt$$

The root mean square response magnitudes are then found by taking the square root of the mean square responses. Similarly, the rms response velocities and accelerations can be determined by averaging $[\text{Real}(\dot{x}_{\text{rel.}})]^2$, $[\text{Real}(\dot{x}_{\text{abs.}})]^2$, etc.

$$\overline{\dot{x}_{rel.}^2} = \frac{1}{T} \int_0^T [\text{Real}(\dot{x}_{rel.})]^2 dt, \quad \overline{\ddot{x}_{rel.}^2} = \frac{1}{T} \int_0^T [\text{Real}(\ddot{x}_{rel.})]^2 dt$$

$$\overline{\dot{x}_{abs.}^2} = \frac{1}{T} \int_0^T [\text{Real}(\dot{x}_{abs.})]^2 dt, \quad \overline{\ddot{x}_{abs.}^2} = \frac{1}{T} \int_0^T [\text{Real}(\ddot{x}_{abs.})]^2 dt$$

The average power developed by the damper is easily determined from the equation

$$P_{ave.} = \frac{c}{g} \cdot \overline{\dot{x}_{rel.}^2}$$

and the work done in time (Δt) is then

$$\text{Work} = P_{ave.} \cdot (\Delta t)$$

Note that Δt is assumed to be much greater than the period of the response.

For the cases of combined sinusoidal input $F(t)$ and $\ddot{Y}(t)$, the expressions are lengthy and these appear in the table below the array of response equations. In these equations, the Kronecker delta function is used and is defined as follows:

$$\delta(\omega_2 - \omega_1) = 1, \quad \omega_2 = \omega_1$$

$$\delta(\omega_2 - \omega_1) = 0, \quad \omega_2 \neq \omega_1$$

The rms responses of the SDF system, shown in Table .IX, to random Gaussian white noise type force and base accelerations, are easily constructed. First consider the relative deflection x_r of the mass m with respect to the massless base, or foundation. The differential equation of motion governing this response is

$$\begin{aligned} \text{or} \quad m\ddot{x}_r + c\dot{x}_r + kx_r &= F(t) - m\ddot{Y}(t) \\ \ddot{x}_r + 2\zeta\omega_0\dot{x}_r + \omega_0^2 x_r &= \frac{F(t)}{m} - \ddot{Y}(t) \end{aligned} \quad (33)$$

The steady state solution of this equation (33) is given by the equation

$$x_r(t) = \frac{1}{\omega} \int_0^t e^{-\zeta\omega_0(t-\tau)} \cdot \sin \omega(t-\tau) \cdot \left[\frac{F(\tau)}{m} - \ddot{Y}(\tau) \right] \cdot d\tau \quad (34)$$

where

$$\omega = \omega_0 \sqrt{1 - \zeta^2} = \text{damped natural frequency}$$

This equation (34) can be written in the following more convenient form, preparatory to taking the Fourier transform of the equation:

$$x_r(t) = \int_0^t h(t-\tau) \cdot \left[\frac{F(\tau)}{K} - \frac{\ddot{Y}_0(\tau)}{\omega_0^2} \right] \cdot d\tau \quad (35)$$

$$h(t) = \frac{\omega_0}{\sqrt{1 - \zeta^2}} e^{-\zeta \omega_0(t)} \cdot \sin \omega t \quad (36)$$

Denoting the Fourier transforms of the quantities, $x_r(t)$, $h(t)$, $F(t)$, and $\ddot{Y}(t)$ by $X_r(\omega)$, $H(\omega)$, $F(\omega)$, $\ddot{Y}(\omega)$ and applying the Fourier convolution theorem, the associated Fourier transform of equation (35) is:

$$X_r(\omega) = \left[\frac{F(\omega)}{K} - \frac{\ddot{Y}(\omega)}{\omega_0^2} \right] H(\omega)$$

where the Fourier transform of $h(t)$, Eq. (36), is

$$H(\omega) = \frac{1}{\left\{ \left[1 - \left(\frac{\omega}{\omega_0} \right)^2 \right]^2 + \frac{1}{Q^2} \left(\frac{\omega}{\omega_0} \right)^2 \right\}^{\frac{1}{2}}} ; \quad Q = \frac{1}{2\zeta} \quad (37)$$

The power spectral density $\Phi_{X_r}(\omega)$ of the relative response is defined by the equation:

$$\Phi_{X_r} = \lim_{T \rightarrow \infty} \frac{|X_r(\omega)|^2}{T} = \lim_{T \rightarrow \infty} \frac{X_r(\omega) \cdot X_r^*(\omega)}{T}$$

where

$$X_r^*(\omega) = \text{complex conjugate of } X_r(\omega).$$

Now $X_r(\omega)$ and $X_r^*(\omega)$ are given by the equations:

$$X_r(\omega) = \left[\frac{F(\omega)}{K} - \frac{\ddot{Y}(\omega)}{\omega_o^2} \right] \cdot H(\omega)$$

$$X_r^*(\omega) = \left[\frac{F^*(\omega)}{K} - \frac{\ddot{Y}^*(\omega)}{\omega_o^2} \right] \cdot H^*(\omega)$$

so that

$$\begin{aligned} |X_r(\omega)|^2 &= \left[\frac{F(\omega) F^*(\omega)}{K^2} + \frac{\ddot{Y}(\omega) \ddot{Y}^*(\omega)}{\omega_o^4} - \frac{F^*(\omega) \ddot{Y}(\omega)}{K \omega_o^2} - \frac{F(\omega) \ddot{Y}^*(\omega)}{K \omega_o^2} \right] H(\omega) H^*(\omega) \\ &= \left[\frac{|F(\omega)|^2}{K^2} + \frac{|\ddot{Y}(\omega)|^2}{\omega_o^4} - \frac{F^*(\omega) \ddot{Y}(\omega)}{K \omega_o^2} - \frac{F(\omega) \ddot{Y}^*(\omega)}{K \omega_o^2} \right] |H(\omega)|^2 \end{aligned} \quad (38)$$

Dividing (38) through by the time duration, T , and performing the limiting process, ($T \rightarrow \infty$) gives the equation

$$\Phi_{X_r}(\omega) = \left[\frac{1}{K^2} \Phi_F(\omega) + \frac{1}{\omega_o^4} \Phi_{\ddot{Y}}(\omega) - \frac{\Phi_{F\ddot{Y}}(\omega) + \Phi_{\ddot{Y}F}(\omega)}{K \omega_o^2} \right] |H(\omega)|^2 \quad (39)$$

where

$\Phi_{X_r}(\omega)$ = PSD of the relative response

$\Phi_F(\omega)$ = PSD of the force input

$\Phi_{\ddot{Y}}(\omega)$ = PSD of the base acceleration input

$\Phi_{\ddot{Y}F}(\omega), \Phi_{F\ddot{Y}}(\omega)$ = cross PSD functions of the force and acceleration inputs

Note that if $F(t)$ and $\ddot{Y}(t)$ are completely uncorrelated, then these cross PSD functions (defined more precisely in Section IV) are equal to zero.

The mean square relative displacement response, $\overline{X_r^2}$, to random excitation is defined by the equation

$$\overline{X_r^2} = \int_0^\infty \Phi_{X_r}(\omega) \cdot d\omega = \frac{1}{2\pi} \int_0^\infty \Phi_{X_r}(\omega) \cdot d\omega \quad (40)$$

where all PSD functions are in terms of "per cps" units. Substituting the above expression (39) for $\Phi X_r(\omega)$ in this integral and taking the square root of the mean square displacement response gives the rms relationships shown in Table IX

The rms relative velocity and acceleration response can be obtained by replacing $\Phi X_r(\omega)$ by $\Phi \dot{X}_r(\omega)$ and $\Phi \ddot{X}_r(\omega)$ according to the following relations:

$$\Phi \ddot{X}_r(\omega) = \omega^2 \Phi \dot{X}_r = \omega^4 \Phi X_r$$

Performing the integration over the entire frequency band as before gives the results shown.

The absolute response is easily determined from the following equation:

$$\begin{aligned} X_{abs.}(t) &= X_r(t) + Y(t) \\ &= X_r(t) - \frac{\ddot{Y}(t)}{\omega^2}, \end{aligned}$$

the Fourier transform of which is

$$X_{abs.}(\omega) = X_r(\omega) - \frac{1}{\omega^2} \ddot{Y}(\omega)$$

and hence

$$\Phi X_{abs.}(\omega) = \Phi X_r(\omega) - \frac{1}{\omega^2} \Phi \ddot{Y}(\omega).$$

Substituting for $\Phi X_r(\omega)$ gives the PSD of the absolute response, the equations for which are as follows:

$$\Phi X_{abs.}(\omega) = \left[\frac{1}{K^2} \Phi F(\omega) + \frac{1}{\omega_o^4} \Phi \ddot{Y}(\omega) - \frac{\Phi F \ddot{Y}(\omega) + \Phi \dot{Y} F(\omega)}{K \omega_o^2} \right] |H(\omega)|^2 - \frac{1}{\omega^2} \Phi \ddot{Y}(\omega)$$

The PSD functions $\Phi \dot{X}_{abs.}(\omega)$ and $\Phi \ddot{X}_{abs.}(\omega)$ are then determined according to the relations:

$$\Phi \ddot{X}_{abs.}(\omega) = \omega^2 \Phi \dot{X}_{abs.}(\omega) = \omega^4 \Phi X_{abs.}(\omega).$$

As before, integration of the entire frequency band gives the results shown in Table

The rms responses for a constant spectral base velocity $\dot{\Phi}_Y(\omega)$ and a constant spectral base deflection $\Phi_Y(\omega)$ can be derived from the preceding equations by the use of the following relationships:

$$\Phi_{\ddot{Y}}(\omega) = \omega^2 \Phi_{\dot{Y}}(\omega) = \omega^4 \Phi_Y(\omega)$$

$$\dot{\Phi}_{F\dot{Y}}(\omega) = -i\omega \dot{\Phi}_{FY}(\omega) = -\omega^2 \Phi_{FY}(\omega)$$

$$\Phi_{\ddot{Y}F}(\omega) = i\omega \Phi_{\dot{Y}F}(\omega) = -\omega^2 \Phi_{YF}(\omega).$$


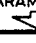
In order to obtain the rms response to either a random force excitation or a random base excitation, it is merely necessary to drop the PSD functions, for which there is no corresponding excitation, in the general expression derived above.

It is noted that in performing the above integrations, the integrals I_{-4} , I_{-3} , ..., I_{-8} , defined in Table IX, must be evaluated. Unfortunately, all of these integrals, except I_0 , I_1 , and I_2 , are infinite for the frequency range from $\omega = 0$ to $\omega = \infty$. Upper and lower cutoff frequencies, ω_U and ω_L , for the excitation spectra, Φ_F , $\Phi_{\dot{Y}}$, $\Phi_{\ddot{Y}}$, and Φ_Y , are therefore defined in order to obtain more practical finite responses for the SDF system. The approximate expressions for these integrals are presented in Table IX, and, whereas the solutions of the integrals are exact for I_{-3} , I_{-1} , I_0 , I_1 , I_2 , I_3 , and I_5 , the solutions are only approximate for I_{-4} , I_{-2} , I_4 , I_6 , and I_8 , the latter being obtained by contour integration. For the approximate solutions, it was assumed that the cutoff frequencies were well outside of the bandwidth of the SDF system, say by 2 to 4 bandwidths. The higher the Q of the system (i.e., the lower the damping), the better these approximations become. Approximate and simpler expressions for these integrals can be obtained by imposing the assumption that the excitation spectra are constant in the neighborhood of the system natural frequency and zero elsewhere, thus eliminating (approximately) the effect of either ω_L or ω_U .

In order that the expressions appearing in Table IX may be more readily used in engineering, a consistent set of units, or dimensions, for all quantities in the table is presented below.

m	:	lb-sec ² /in
c	:	lb-sec/in
k	:	lb/in
F_0	:	lb
X	:	in
\dot{X}, \dot{Y}	:	in/sec

\ddot{X}, \ddot{Y}, g : in/sec²
 ω : rad/sec
 Work : lb-in
 Power : lb-in/sec
 Φ_F : lb²/cps
 $\Phi_{\ddot{Y}}$: (in/sec²)²/cps
 $\Phi_{\dot{Y}}$: (in/sec)²/cps
 Φ_Y : in²/cps
 $\Phi_{\ddot{Y}F}, \Phi_{F\ddot{Y}}$: (lb-in/sec²)/cps
 $\Phi_{\dot{Y}F}, \Phi_{F\dot{Y}}$: (lb-in/sec)/cps
 Φ_{YF}, Φ_{FY} : (lb-in)/cps

INPUT 	SINUSOIDAL F(t) OF AMPLITUDE F ₀ AND FREQUENCY ω; ȳ(t)=0		SINUSOIDAL F(t) OF AMPLITUDE F ₀ AND FREQUENCY ω ₀ ; ȳ(t)=0		SINUSOIDAL ȳ(t) OF AMPLITUDE ȳ ₀ AND FREQUENCY ω; F(t)=0		SINUSOIDAL ȳ(t) OF AMPLITUDE ȳ ₀ AND FREQUENCY ω ₀ ; F(t)=0		COMBINED SINUSOIDAL INPUTS			
	FORCE F(t; F ₀ , ω) ACCELERATION ȳ(t; ȳ ₀ , ω ₀)		FORCE F(t; F ₀ , ω ₀) ACCELERATION ȳ(t; ȳ ₀ , ω ₀)		FORCE F(t; F ₀ , ω) ACCELERATION ȳ(t; ȳ ₀ , ω ₀)		FORCE F(t; F ₀ , ω ₀) ACCELERATION ȳ(t; ȳ ₀ , ω ₀)		FORCE F(t; F ₀ , ω ₀) ACCELERATION ȳ(t; ȳ ₀ , ω ₀)			
EXCITATION SPECTRUM	• ∞ at ω • 0 elsewhere		• ∞ at ω ₀ • 0 elsewhere		• ∞ at ω • 0 elsewhere		• ∞ at ω ₀ • 0 elsewhere		• ∞ at ω ₀ • 0 elsewhere			
RESPONSE PARAMETERS 	RMS ABS. RESPONSE	RMS REL. RESPONSE	RMS ABS. RESPONSE	RMS REL. RESPONSE	RMS ABS. RESPONSE	RMS REL. RESPONSE	RMS ABS. RESPONSE	RMS REL. RESPONSE	RMS ABS. RESPONSE	RMS REL. RESPONSE	RMS ABS. RESPONSE	RMS REL. RESPONSE
DISPLACEMENT	$\frac{H F_0}{\sqrt{2} K}$		$\frac{Q F_0}{\sqrt{2} K}$		$\frac{H}{\sqrt{2} \omega^2} \ddot{y}_0$	$\frac{H}{\omega_0^2 \sqrt{2}} \ddot{y}_0$	$\frac{1}{\sqrt{2} \omega_0^2} \ddot{y}_0$	$\frac{Q}{\omega_0^2 \sqrt{2}} \ddot{y}_0$	1	4	7	10
PHASE ANGLE	-φ		$-\frac{\pi}{2}$		-π - θ	-π - φ	-π - tan ⁻¹ Q	$\frac{\pi}{2}$				
VELOCITY	$\frac{\omega H F_0}{\sqrt{2} K}$		$\frac{\omega_0 Q F_0}{\sqrt{2} K}$		$\frac{H}{\sqrt{2} \omega} \ddot{y}_0$	$\frac{H}{\omega_0^2 \sqrt{2}} \ddot{y}_0$	$\frac{1}{\sqrt{2} \omega_0} \ddot{y}_0$	$\frac{Q}{\omega_0^2 \sqrt{2}} \ddot{y}_0$	2	5	8	11
PHASE ANGLE	$\frac{\pi}{2} - \phi$		0		$-\frac{\pi}{2} - \theta$	$-\frac{\pi}{2} - \phi$	$-\frac{\pi}{2} - \tan^{-1}Q$	-π				
ACCELERATION	$\frac{\omega^2 H F_0}{\sqrt{2} K}$		$\frac{\omega_0^2 Q F_0}{\sqrt{2} K}$		$\frac{H}{\sqrt{2}} \ddot{y}_0$	$\frac{H}{\omega_0^2 \sqrt{2}} \ddot{y}_0$	$\frac{1}{\sqrt{2}} \ddot{y}_0$	$\frac{Q}{\sqrt{2}} \ddot{y}_0$	3	6	9	12
PHASE ANGLE	π - φ		$\frac{\pi}{2}$		-θ	-φ	-tan ⁻¹ Q	$-\frac{\pi}{2}$				
RESPONSE AMPLITUDE PROBABILITY DENSITY FUNCTION	$\frac{1}{\pi \sqrt{X_0^2 - X^2}}$ X ₀ = peak response displacement, either relative (REL.) or absolute (ABS.)											
PEAK RESPONSE AMPLITUDE PROBABILITY DENSITY FUNCTION	• ∞ at X = ±X ₀ • 0 at X ≥ X ₀											
AVERAGE POWER DISSIPATED	$\frac{\omega^2 H^2 F_0^2}{2 K \omega_0 Q}$		$\frac{\omega_0^2 Q F_0^2}{2 K}$		$\frac{K \omega^2 H^2 \ddot{y}_0^2}{2 Q \omega_0^5}$		$\frac{K Q \ddot{y}_0^2}{2 \omega_0^3}$		$\frac{K}{\omega_0 Q}$ (5)		$\frac{K}{\omega_0 Q}$ (11)	
WORK DONE IN TIME (Δt)	$\frac{\omega^2 H^2 F_0^2}{2 K \omega_0 Q} (\Delta t)$		$\frac{\omega_0^2 Q F_0^2}{2 K} (\Delta t)$		$\frac{K \omega^2 H^2 \ddot{y}_0^2}{2 Q \omega_0^5} (\Delta t)$		$\frac{K Q \ddot{y}_0^2}{2 \omega_0^3} (\Delta t)$		$\frac{K}{\omega_0 Q} (\Delta t)$ (5)		$\frac{K}{\omega_0 Q} (\Delta t)$ (11)	
NUMBER OF RESPONSE CYCLES IN TIME (Δt)	$\frac{\omega}{2\pi} (\Delta t)$		$\frac{\omega_0}{2\pi} (\Delta t)$		$\frac{\omega}{2\pi} (\Delta t)$		$\frac{\omega_0}{2\pi} (\Delta t)$		$\frac{\omega_0}{2\pi} (\Delta t)$		$\frac{\omega_0}{2\pi} (\Delta t)$	

$$1 = \left[\frac{F_0^2}{K^2} + \frac{\ddot{y}_0^2}{\omega_0^4} - \frac{2F_0\ddot{y}_0}{K\omega_0^2} \cos \lambda_3 \right] \frac{Q^2}{2} + \left[\frac{F_0}{K} \sin \lambda_3 + \frac{\ddot{y}_0}{\omega_0^2} \cos \lambda_2 \right] \frac{Q\ddot{y}_0}{\omega_0^3} - \frac{\ddot{y}_0^2}{2\omega_0^2}$$

$$2 = \left[\frac{F_0^2}{K^2} + \frac{\ddot{y}_0^2}{\omega_0^4} - \frac{2F_0\ddot{y}_0}{K\omega_0^2} \cos \lambda_3 \right] \frac{Q^2 \omega_0^2}{2} + \left[\frac{F_0}{K} \sin \lambda_3 + \frac{\ddot{y}_0}{\omega_0^2} \cos \lambda_2 \right] Q\ddot{y}_0 - \frac{\ddot{y}_0^2}{2\omega_0^2}$$

$$3 = \left[\frac{F_0^2}{K^2} + \frac{\ddot{y}_0^2}{\omega_0^4} - \frac{2F_0\ddot{y}_0}{K\omega_0^2} \cos \lambda_3 \right] \frac{Q^2 \omega_0^4}{2} + \left[\frac{F_0}{K} \sin \lambda_3 + \frac{\ddot{y}_0}{\omega_0^2} \cos \lambda_2 \right] Q\ddot{y}_0 \omega_0^2 - \frac{\ddot{y}_0^2}{2}$$

$$4 = \left[\frac{F_0^2}{K^2} + \frac{\ddot{y}_0^2}{\omega_0^4} - \frac{2F_0\ddot{y}_0}{K\omega_0^2} \cos \lambda_3 \right] \frac{Q^2}{2}$$

$$5 = \left[\frac{F_0^2}{K^2} + \frac{\ddot{y}_0^2}{\omega_0^4} - \frac{2F_0\ddot{y}_0}{K\omega_0^2} \cos \lambda_3 \right] \frac{Q^2 \omega_0^2}{2}$$

$$6 = \left[\frac{F_0^2}{K^2} + \frac{\ddot{y}_0^2}{\omega_0^4} - \frac{2F_0\ddot{y}_0}{K\omega_0^2} \cos \lambda_3 \right] \frac{Q^2 \omega_0^4}{2}$$

$$7 = \frac{H_1^2 F_0^2}{2 K^2} + \frac{H_2^2 \ddot{y}_0^2}{2 \omega_0^4} + \frac{\ddot{y}_0^2}{2 \omega_0^2} - \frac{H_1 H_2 \ddot{y}_0}{K \omega_0^2} \cos \lambda_3 \cdot \delta(\omega_2 - \omega_1) - \frac{H_1 F_0 \ddot{y}_0}{K \omega_0^2} \cos(\lambda_1 + \lambda_3) \cdot \delta(\omega_2 - \omega_1) + \frac{H_2 \ddot{y}_0^2}{\omega_0^2 \omega_0^2} \cos \lambda_2$$

$$8 = \frac{\omega_0^2 H_1^2 F_0^2}{2 K^2} + \frac{\omega_0^2 H_2^2 \ddot{y}_0^2}{2 \omega_0^4} + \frac{\ddot{y}_0^2}{2 \omega_0^2} - \frac{\omega_1 \omega_2 H_1 H_2 \ddot{y}_0}{K \omega_0^2} \cos \lambda_3 \cdot \delta(\omega_2 - \omega_1) - \frac{\omega_1 H_1 \ddot{y}_0}{K \omega_0^2} \cos(\lambda_1 + \lambda_3) \cdot \delta(\omega_2 - \omega_1) + \frac{H_2 \ddot{y}_0^2}{\omega_0^2} \cos \lambda_2$$

$$9 = \frac{\omega_1^2 H_1^2 F_0^2}{2 K^2} + \frac{\omega_1^2 H_2^2 \ddot{y}_0^2}{2 \omega_0^4} + \frac{\ddot{y}_0^2}{2} - \frac{\omega_1^2 \omega_2 H_1 H_2 \ddot{y}_0}{K \omega_0^2} \cos \lambda_3 \cdot \delta(\omega_2 - \omega_1) - \frac{\omega_1^2 H_1 \ddot{y}_0}{K} \cos(\lambda_1 + \lambda_3) \cdot \delta(\omega_2 - \omega_1) + \frac{\omega_2^2 H_2 \ddot{y}_0^2}{\omega_0^2} \cos \lambda_2$$

$$10 = \frac{H_1^2 F_0^2}{2 K^2} + \frac{H_2^2 \ddot{y}_0^2}{2 \omega_0^4} - \frac{H_1 H_2 \ddot{y}_0}{K \omega_0^2} \cos \lambda_3 \cdot \delta(\omega_2 - \omega_1)$$

$$11 = \frac{\omega_1^2 H_1^2 F_0^2}{2 K^2} + \frac{\omega_1^2 H_2^2 \ddot{y}_0^2}{2 \omega_0^4} - \frac{\omega_1 \omega_2 H_1 H_2 \ddot{y}_0}{K \omega_0^2} \cos \lambda_3 \cdot \delta(\omega_2 - \omega_1)$$

$$12 = \frac{\omega_1^2 H_1^2 F_0^2}{2 K^2} + \frac{\omega_1^2 H_2^2 \ddot{y}_0^2}{2 \omega_0^4} - \frac{\omega_1^2 \omega_2 H_1 H_2 \ddot{y}_0}{K \omega_0^2} \cos \lambda_3 \cdot \delta(\omega_2 - \omega_1)$$

$$I_8 = \int_0^{\omega_1/\omega_0} \left[\frac{\omega}{\omega_0} \right]^8 H^2(\omega) \cdot \omega d\omega$$

$$I_6 = \int_0^{\omega_1/\omega_0} \left[\frac{\omega}{\omega_0} \right]^6 H^2(\omega) \cdot \omega d\omega$$

$$I_5 = \int_0^{\omega_1/\omega_0} \left[\frac{\omega}{\omega_0} \right]^5 H^2(\omega) \cdot \omega d\omega$$

$$I_4 = \int_0^{\omega_1/\omega_0} \left[\frac{\omega}{\omega_0} \right]^4 H^2(\omega) \cdot \omega d\omega$$

$$I_3 = \int_0^{\omega_1/\omega_0} \left[\frac{\omega}{\omega_0} \right]^3 H^2(\omega) \cdot \omega d\omega$$

$$I_2 = \int_0^{\infty} \left[\frac{\omega}{\omega_0} \right]^2 H^2(\omega) \cdot \omega d\omega$$

$$I_1 = \int_0^{\infty} \left[\frac{\omega}{\omega_0} \right]^1 H^2(\omega) \cdot \omega d\omega$$

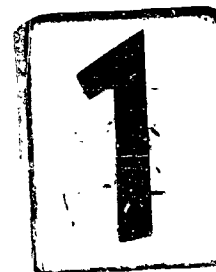
$$I_0 = \int_0^{\infty} H^2(\omega) \cdot \omega d\omega$$

$$I_{-1} = \int_{\omega_1/\omega_0}^{\infty} \left[\frac{\omega_0}{\omega} \right]^1 H^2(\omega) \cdot \omega d\omega$$

$$I_{-2} = \int_{\omega_1/\omega_0}^{\infty} \left[\frac{\omega_0}{\omega} \right]^2 H^2(\omega) \cdot \omega d\omega$$

$$I_{-3} = \int_{\omega_1/\omega_0}^{\infty} \left[\frac{\omega_0}{\omega} \right]^3 H^2(\omega) \cdot \omega d\omega$$

$$I_{-4} = \int_{\omega_1/\omega_0}^{\infty} \left[\frac{\omega_0}{\omega} \right]^4 H^2(\omega) \cdot \omega d\omega$$



SINUSOIDAL $\dot{Y}(t)$ OF AMPLITUDE \ddot{Y}_0 AND FREQUENCY ω_0 ; $F(t) = 0$		COMBINED SINUSOIDAL INPUTS FORCE $F(t; \ddot{Y}_0, \omega_0)$ ACCELERATION $\ddot{Y}(t; \ddot{Y}_0, \omega_0)$				GAUSSIAN WHITE NOISE FORCE $F(t)$; $\ddot{Y}(t) = 0$		GAUSSIAN WHITE NOISE ACCELERATION $\ddot{Y}(t)$; $F(t) = 0$		GAUSSIAN WHITE NOISE VELOCITY $\dot{Y}(t)$; $F(t) = 0$		GAUSSIAN WHITE NOISE DISPLACEMENT $Y(t)$; $F(t) = 0$		COMBINED GAUSSIAN WHITE NOISE INPUTS FORCE $F(t)$ ACCELERATION $\ddot{Y}(t)$		COMBINED GAUSSIAN WHITE NOISE INPUTS FORCE $F(t)$ VELOCITY $\dot{Y}(t)$			
∞ at ω_0 0 elsewhere		∞ at ω_0 0 elsewhere				$\Phi_F = \text{constant}$		$\Phi_{\ddot{Y}} = \text{constant}$		$\Phi_{\dot{Y}} = \text{constant}$		$\Phi_Y = \text{constant}$		$\Phi_F = \text{constant}$ $\Phi_{\ddot{Y}} = \text{constant}$		$\Phi_F = \text{constant}$ $\Phi_{\dot{Y}} = \text{constant}$			
RMS ABS. RESPONSE	RMS REL. RESPONSE	RMS ABS. RESPONSE	RMS REL. RESPONSE	RMS ABS. RESPONSE	RMS REL. RESPONSE	RMS ABS. RESPONSE	RMS REL. RESPONSE	RMS ABS. RESPONSE	RMS REL. RESPONSE	RMS ABS. RESPONSE	RMS REL. RESPONSE	RMS ABS. RESPONSE	RMS REL. RESPONSE	RMS ABS. RESPONSE	RMS REL. RESPONSE	RMS ABS. RESPONSE	RMS REL. RESPONSE		
$\frac{1}{\omega_0^2} \alpha \ddot{Y}_0$	$\frac{Q}{\omega_0^2 \sqrt{2}} \ddot{Y}_0$	$\sqrt{1}$	$\sqrt{4}$	$\sqrt{7}$	$\sqrt{10}$	$\frac{1}{2K} \sqrt{Q \omega_0^3 \Phi_F}$		$\sqrt{\frac{I_2^2 + I_4^2}{2\pi \omega_0^3}} \ddot{Y}$	$\frac{1}{2} \sqrt{\frac{Q}{\omega_0^3}} \ddot{Y}$	$\sqrt{\frac{I_2^2 + I_4^2}{2\pi \omega_0}} \dot{Y}$	$\frac{1}{2} \sqrt{\frac{Q}{\omega_0}} \dot{Y}$	$\sqrt{\frac{I_2^2 + I_0}{2\pi \omega_0^{-1}}} Y$	$\sqrt{\frac{4b}{2\pi}} I_4 \ddot{Y}$	$\sqrt{\frac{13}{2\pi}}$	$\sqrt{\frac{16}{2\pi}}$	$\sqrt{\frac{19}{2\pi}}$	$\sqrt{\frac{22}{2\pi}}$		
$-\tan^{-1} Q$	$\frac{\pi}{2}$							RANDOM											
$\frac{1}{\omega_0} \alpha \ddot{Y}_0$	$\frac{Q}{\omega_0 \sqrt{2}} \ddot{Y}_0$	$\sqrt{2}$	$\sqrt{5}$	$\sqrt{8}$	$\sqrt{11}$	$\frac{1}{2K} \sqrt{Q \omega_0^3 \Phi_F}$		$\sqrt{\frac{I_2^2 + I_4^2}{2\pi \omega_0}} \ddot{Y}$	$\frac{1}{2} \sqrt{\frac{Q}{\omega_0}} \ddot{Y}$	$\sqrt{\frac{I_2^2 + I_0}{2\pi \omega_0^{-1}}} \dot{Y}$	$\sqrt{\frac{4b}{2\pi}} I_4 \dot{Y}$	$\sqrt{\frac{I_2^2 + I_4^2}{2\pi \omega_0^{-3}}} Y$	$\sqrt{\frac{\omega_0^3}{2\pi}} I_6 \ddot{Y}$	$\sqrt{\frac{14}{2\pi}}$	$\sqrt{\frac{17}{2\pi}}$	$\sqrt{\frac{20}{2\pi}}$	$\sqrt{\frac{23}{2\pi}}$		
$\frac{\pi}{2} - \tan^{-1} Q$	$-\pi$							RANDOM											
$\frac{1}{2} \alpha \ddot{Y}_0$	$\frac{Q}{\sqrt{2}} \ddot{Y}_0$	$\sqrt{3}$	$\sqrt{6}$	$\sqrt{9}$	$\sqrt{12}$	$\frac{1}{K} \sqrt{\frac{4b^2}{2\pi}} I_4 \Phi_F$		$\sqrt{\frac{I_2^2 + I_0}{2\pi \omega_0^{-1}}} \ddot{Y}$	$\sqrt{\frac{4b I_4}{2\pi}} \ddot{Y}$	$\sqrt{\frac{I_2^2 + I_4^2}{2\pi \omega_0^{-3}}} \dot{Y}$	$\sqrt{\frac{4b^3}{2\pi}} I_6 \dot{Y}$	$\sqrt{\frac{I_2^2 + I_4^2}{2\pi \omega_0^{-5}}} Y$	$\sqrt{\frac{\omega_0^5}{2\pi}} I_8 \ddot{Y}$	$\sqrt{\frac{15}{2\pi}}$	$\sqrt{\frac{18}{2\pi}}$	$\sqrt{\frac{21}{2\pi}}$	$\sqrt{\frac{24}{2\pi}}$		
$-\tan^{-1} Q$	$-\frac{\pi}{2}$							RANDOM											
α = peak response displacement, either relative (REL.) or absolute (ABS.)						$\frac{1}{Q \sqrt{2\pi}} \exp \left[-\frac{1}{2} \frac{X^2}{\sigma^2} \right]$ X = response displacement { either relative (REL.) or absolute (ABS.) σ = RMS response displmt.													
						$\frac{X}{\sigma^2} \exp \left[-\frac{1}{2} \frac{X^2}{\sigma^2} \right]$ X = peak response displacement { either relative (REL.) or absolute (ABS.)													
$\frac{K Q \ddot{Y}_0^2}{2 \omega_0^3}$	$\frac{K (5)}{\omega_0 Q}$	$\frac{K (11)}{\omega_0 Q}$	$\frac{\omega_0^2 \Phi_F}{4 K}$	$\frac{K \Phi_{\ddot{Y}}}{4 \omega_0^2}$	$\frac{K I_4 \ddot{Y}}{2\pi Q}$	$\frac{K \omega_0^2 I_6 \ddot{Y}}{2\pi Q}$	$\frac{K (17)}{2\pi \omega_0 Q}$	$\frac{K (23)}{2\pi \omega_0 Q}$											
$\frac{K Q \ddot{Y}_0^2}{2 \omega_0^3} (\Delta t)$	$\frac{K (5)}{\omega_0 Q} (\Delta t)$	$\frac{K (11)}{\omega_0 Q} (\Delta t)$	$\frac{\omega_0^2 \Phi_F}{4 K} (\Delta t)$	$\frac{K \Phi_{\ddot{Y}}}{4 \omega_0^2} (\Delta t)$	$\frac{K I_4 \ddot{Y}}{2\pi Q} (\Delta t)$	$\frac{K \omega_0^2 I_6 \ddot{Y}}{2\pi Q} (\Delta t)$	$\frac{K (17)}{2\pi \omega_0 Q} (\Delta t)$	$\frac{K (23)}{2\pi \omega_0 Q} (\Delta t)$											
$\frac{\omega_0}{2\pi} (\Delta t)$	$\frac{\omega_0}{2\pi} (\Delta t)$	$\frac{\omega_0}{2\pi} (\Delta t)$						$\frac{\omega_0}{2\pi} (\Delta t)$	{ low damped system, $Q \geq 5$										

$$\begin{aligned}
 I_8 &= \int_0^{\omega_u/\omega_b} \left[\frac{\omega}{\omega_b} \right]^8 H^2(\omega) \cdot d(\omega/\omega_b) = \frac{\pi \cdot 0}{2} \left[1 - \frac{13}{2Q^2} + \frac{12}{Q^4} - \frac{3}{2Q^6} \right] + \frac{1}{4} \left[\frac{\omega_u}{\omega_c} \right]^5 \\
 I_6 &= \int_0^{\omega_u/\omega_b} \left[\frac{\omega}{\omega_b} \right]^6 H^2(\omega) \cdot d(\omega/\omega_b) = \frac{\pi \cdot 0}{2} \left[1 - \frac{3}{Q^2} + \frac{1}{Q^4} \right] + \frac{1}{3} \left[\frac{\omega_u}{\omega_0} \right]^3 \\
 I_5 &= \int_0^{\omega_u/\omega_b} \left[\frac{\omega}{\omega_b} \right]^5 H^2(\omega) \cdot d(\omega/\omega_b) = \frac{1}{2} \left[\frac{\omega_u}{\omega_0} \right]^2 - \left[1 - \frac{1}{Q^2} \right] \text{LN}(\text{H}(\omega_u)) + \frac{0}{2} \frac{2 \left[1 - \frac{1}{2Q^2} \right]^2 - 1}{\sqrt{1 - \frac{1}{4Q^2}}} \left[\pi - Z(\omega_u/\omega_b) \right] \\
 I_4 &= \int_0^{\omega_u/\omega_b} \left[\frac{\omega}{\omega_b} \right]^4 H^2(\omega) \cdot d(\omega/\omega_b) = \frac{\pi \cdot 0}{2} \left[1 - \frac{1}{Q^2} \right] + \frac{\omega_u}{\omega_0} \\
 I_3 &= \int_0^{\omega_u/\omega_b} \left[\frac{\omega}{\omega_b} \right]^3 H^2(\omega) \cdot d(\omega/\omega_b) = -\frac{1}{2} \text{LN}(\text{H}(\omega_u)) + \frac{0}{2} \frac{1 - \frac{1}{2Q^2}}{\sqrt{1 - \frac{1}{4Q^2}}} \left[\pi - Z(\omega_u/\omega_0) \right] \\
 I_2 &= \int_0^{\omega_u/\omega_b} \left[\frac{\omega}{\omega_b} \right]^2 H^2(\omega) \cdot d(\omega/\omega_b) = \frac{\pi \cdot 0}{2} \\
 I_1 &= \int_0^{\omega_u/\omega_b} \left[\frac{\omega}{\omega_b} \right]^1 H^2(\omega) \cdot d(\omega/\omega_b) = \frac{0}{2 \sqrt{1 - \frac{1}{2Q^2}}} \left[\frac{\pi}{2} + \text{TAN}^{-1} \left\{ 0 \frac{1 - \frac{1}{2Q^2}}{\sqrt{1 - \frac{1}{4Q^2}}} \right\} \right] \\
 I_0 &= \int_0^{\omega_u/\omega_b} H^2(\omega) \cdot d(\omega/\omega_b) = \frac{\pi \cdot 0}{2} \\
 I_{-1} &= \int_{\omega_l/\omega_b}^{\omega_u/\omega_b} \left[\frac{\omega_b}{\omega} \right]^1 H^2(\omega) \cdot d(\omega/\omega_b) = -\frac{1}{2} \text{LN}(\text{H}(\frac{1}{\omega_l})) + \frac{0}{2} \frac{1 - \frac{1}{2Q^2}}{\sqrt{1 - \frac{1}{4Q^2}}} \left[\pi - Z(\omega_0/\omega_l) \right] \\
 I_{-2} &= \int_{\omega_l/\omega_b}^{\omega_u/\omega_b} \left[\frac{\omega_b}{\omega} \right]^2 H^2(\omega) \cdot d(\omega/\omega_b) = \frac{\pi \cdot 0}{2} + \frac{\omega_b}{\omega_l} \\
 I_{-3} &= \int_{\omega_l/\omega_b}^{\omega_u/\omega_b} \left[\frac{\omega_b}{\omega} \right]^3 H^2(\omega) \cdot d(\omega/\omega_b) = \frac{1}{2} \left[\frac{\omega_b}{\omega_l} \right]^2 - \left[1 - \frac{1}{Q^2} \right] \text{LN}(\text{H}(\frac{1}{\omega_l})) + \frac{0}{2} \frac{2 \left[1 - \frac{1}{2Q^2} \right]^2 - 1}{\sqrt{1 - \frac{1}{4Q^2}}} \left[\pi - Z(\omega_0/\omega_l) \right] \\
 I_{-4} &= \int_{\omega_l/\omega_b}^{\omega_u/\omega_b} \left[\frac{\omega_b}{\omega} \right]^4 H^2(\omega) \cdot d(\omega/\omega_b) = \frac{\pi \cdot 0}{2} \left[1 - \frac{3}{Q^2} + \frac{1}{Q^4} \right] + \frac{1}{3} \left[\frac{\omega_b}{\omega_l} \right]^3
 \end{aligned}$$

$$H(\omega) = \left\{ \left[1 - \left(\frac{\omega}{\omega_0} \right)^2 \right]^2 + \frac{1}{Q^2} \left[\frac{\omega}{\omega_0} \right]^2 \right\}^{-1}$$

$$\phi(\omega) = \tan^{-1} \left[\frac{\left(\frac{\omega}{\omega_0} \right)}{Q \left[1 - \left(\frac{\omega}{\omega_0} \right)^2 \right]} \right]$$

$$\theta = \tan^{-1} \left[\frac{\frac{1}{\alpha} \left(\frac{\omega}{\omega_0} \right)^3}{1 - \left(\frac{\omega}{\omega_0} \right)^2 \left(1 - \frac{1}{\alpha^2} \right)} \right]$$

$$Z(\omega/\omega_0) = \tan^{-1} \left[\frac{\left(\frac{\omega}{\omega_0}\right)^2 \frac{1}{Q} \sqrt{1 - \frac{1}{4Q^2}}}{-1 + \left(\frac{\omega}{\omega_0}\right)^2 \left[1 - \frac{1}{2Q^2}\right]} \right]$$

$$Q = \frac{\sqrt{km}}{c} \quad \omega_0^2 = \frac{k}{m}$$

$$H_1 = H(\omega_1)$$

$$H_2 = H(\omega_2)$$

$$\bar{\lambda}_1 = \phi(\omega_1)$$



$$i = \sqrt{-1}$$



GAUSSIAN WHITE NOISE VELOCITY $\dot{Y}(t); F(t) = 0$				GAUSSIAN WHITE NOISE DISPLACEMENT $Y(t); F(t) = 0$		COMBINED GAUSSIAN WHITE NOISE INPUTS			
				FORCE $F(t)$ ACCELERATION $\ddot{Y}(t)$		FORCE $F(t)$ VELOCITY $\dot{Y}(t)$		FORCE $F(t)$ DISPLACEMENT $Y(t)$	
$\dot{\Phi}_Y = \text{constant}$		$\dot{\Phi}_Y = \text{constant}$		$\dot{\Phi}_F = \text{constant}$ $\dot{\Phi}_Y = \text{constant}$		$\dot{\Phi}_F = \text{constant}$ $\dot{\Phi}_Y = \text{constant}$		$\dot{\Phi}_F = \text{constant}$ $\dot{\Phi}_Y = \text{constant}$	
ABS. RESPONSE	RMS REL. RESPONSE	RMS ABS. RESPONSE	RMS REL. RESPONSE	RMS ABS. RESPONSE	RMS REL. RESPONSE	RMS ABS. RESPONSE	RMS REL. RESPONSE	RMS ABS. RESPONSE	RMS REL. RESPONSE
$\frac{1}{\omega_0} \dot{\Phi}_Y$	$\frac{1}{2} \sqrt{\frac{Q}{\omega_0}} \dot{\Phi}_Y$	$\sqrt{\frac{I_1 + I_0}{2\pi\omega_0^2}} \dot{\Phi}_Y$	$\frac{\omega_0}{2\pi} I_0 \dot{\Phi}_Y$	$\sqrt{\frac{13}{2\pi}}$	$\sqrt{\frac{16}{2\pi}}$	$\sqrt{\frac{19}{2\pi}}$	$\sqrt{\frac{22}{2\pi}}$	$\sqrt{\frac{25}{2\pi}}$	$\sqrt{\frac{28}{2\pi}}$
RANDOM									
$\frac{1}{\pi\omega_0^2} \dot{\Phi}_Y$	$\frac{\omega_0}{2\pi} I_0 \dot{\Phi}_Y$	$\sqrt{\frac{I_1 + I_2}{2\pi\omega_0^2}} \dot{\Phi}_Y$	$\frac{\omega_0^3}{2\pi} I_0 \dot{\Phi}_Y$	$\sqrt{\frac{14}{2\pi}}$	$\sqrt{\frac{17}{2\pi}}$	$\sqrt{\frac{20}{2\pi}}$	$\sqrt{\frac{23}{2\pi}}$	$\sqrt{\frac{26}{2\pi}}$	$\sqrt{\frac{29}{2\pi}}$
RANDOM									
$\frac{1}{\pi\omega_0^2} \dot{\Phi}_Y$	$\frac{\omega_0^3}{2\pi} I_0 \dot{\Phi}_Y$	$\sqrt{\frac{I_1 + I_4}{2\pi\omega_0^2}} \dot{\Phi}_Y$	$\frac{\omega_0^5}{2\pi} I_0 \dot{\Phi}_Y$	$\sqrt{\frac{15}{2\pi}}$	$\sqrt{\frac{18}{2\pi}}$	$\sqrt{\frac{21}{2\pi}}$	$\sqrt{\frac{24}{2\pi}}$	$\sqrt{\frac{27}{2\pi}}$	$\sqrt{\frac{30}{2\pi}}$
RANDOM									
X = response displacement { either relative (REL.) or absolute (ABS.) O = RMS response displmt. }									
X = peak response displacement { either relative (REL.) or absolute (ABS.) }									
$\frac{K I_1 \dot{\Phi}_Y}{2\pi Q}$	$\frac{K \omega_0^2 I_0 \dot{\Phi}_Y}{2\pi Q}$	$\frac{K (17)}{2\pi \omega_0 Q}$	$\frac{K (23)}{2\pi \omega_0 Q}$	$\frac{K (29)}{2\pi \omega_0 Q}$					
$\frac{K I_4 \dot{\Phi}_Y}{2\pi Q} (\Delta t)$	$\frac{K \omega_0^2 I_6 \dot{\Phi}_Y}{2\pi Q} (\Delta t)$	$\frac{K (17)}{2\pi \omega_0 Q} (\Delta t)$	$\frac{K (23)}{2\pi \omega_0 Q} (\Delta t)$	$\frac{K (29)}{2\pi \omega_0 Q} (\Delta t)$					
$\frac{\omega_0}{2\pi} (\Delta t)$	{ low damped system , $Q \geq 5$								

$$+ \frac{1}{4} \left[\frac{\omega_u}{\omega_0} \right]^5$$

$$2 \left[1 - \frac{1}{2Q^2} \right]^{-1} \left[\pi - Z(\omega_u/\omega_0) \right]$$

$$\sqrt{1 - \frac{1}{4Q^2}}$$

$$- Z(\omega_u/\omega_0)$$

$$\left. \right\}$$

$$\frac{2}{Q^2} \left[\pi - Z(\omega_0/\omega_u) \right]$$

$$+ \frac{Q}{2} \frac{2 \left[1 - \frac{1}{2Q^2} \right]^{-1}}{\sqrt{1 - \frac{1}{4Q^2}}} \left[\pi - Z(\omega_u/\omega_u) \right]$$

$$\frac{4}{\omega_u^3}$$

$$H(\omega) = \left\{ \left[1 - \left(\frac{\omega}{\omega_0} \right)^2 \right]^2 + \frac{1}{Q^2} \left[\frac{\omega}{\omega_0} \right]^2 \right\}^{-1/2}$$

$$\phi(\omega) = \tan^{-1} \left[\frac{\left(\frac{\omega}{\omega_0} \right)}{Q \left[1 - \left(\frac{\omega}{\omega_0} \right)^2 \right]} \right]$$

$$\theta(\omega) = \tan^{-1} \left[\frac{\frac{1}{Q} \left(\frac{\omega}{\omega_0} \right)^3}{1 - \left(\frac{\omega}{\omega_0} \right)^2 \left(1 - \frac{1}{Q^2} \right)} \right]$$

$$Z(\omega/\omega_0) = \tan^{-1} \left[\frac{\left(\frac{\omega}{\omega_0} \right)^2 \frac{1}{Q} \sqrt{1 - \frac{1}{4Q^2}}}{-1 + \left(\frac{\omega}{\omega_0} \right)^2 \left[1 - \frac{1}{2Q^2} \right]} \right]$$

$$Q = \frac{\sqrt{K/m}}{c} \quad \omega_0^2 = \frac{K}{m}$$

$$H_1 = H(\omega_1) \quad H_2 = H(\omega_2)$$

$$\beta_1 = \phi(\omega_1) \quad \beta_2 = \phi(\omega_2)$$

$$I = \sqrt{-1}$$

$$(13) = \omega_0 \left[\frac{\Phi_F I_0}{K^2} + \frac{i \omega_0}{K O \omega_0} [\Phi_F \dot{Y} - \dot{\Phi}_F Y] I_1 + \left\{ \frac{\Phi_Y}{Q^2 \omega_0} - \frac{1}{K \omega_0} [\Phi_F \dot{Y} + \dot{\Phi}_F Y] \right\} I_2 + \frac{1}{\omega_0} \Phi_Y I_4 \right]$$

$$(14) = \omega_0^3 \frac{\Phi_F I_2}{K^2} + \frac{i \omega_0}{K O} [\Phi_F \dot{Y} - \dot{\Phi}_F Y] I_1 + \left\{ \frac{\Phi_Y}{Q^2 \omega_0} - \frac{\omega_0}{K} [\Phi_F \dot{Y} + \dot{\Phi}_F Y] \right\} I_2 + \frac{1}{\omega_0} \Phi_Y I_4$$

$$(15) = \omega_0^5 \frac{\Phi_F I_4}{K^2} + \frac{i \omega_0^3}{K O} [\Phi_F \dot{Y} - \dot{\Phi}_F Y] I_3 + \left\{ \frac{\omega_0 \Phi_Y}{Q^2} - \frac{\omega_0^3}{K} [\Phi_F \dot{Y} + \dot{\Phi}_F Y] \right\} I_2 + \omega_0 \Phi_Y I_0$$

$$(16) = \omega_0 \left[\frac{\Phi_F}{K^2} + \frac{\Phi_Y}{\omega_0^2} - \frac{1}{K \omega_0^2} [\Phi_F \dot{Y} + \dot{\Phi}_F Y] \right] I_0$$

$$(17) = \omega_0^3 \left[\frac{\Phi_F}{K^2} + \frac{\Phi_Y}{\omega_0^2} - \frac{1}{K \omega_0^2} [\Phi_F \dot{Y} + \dot{\Phi}_F Y] \right] I_2$$

$$(18) = \omega_0^5 \left[\frac{\Phi_F}{K^2} + \frac{\Phi_Y}{\omega_0^2} - \frac{1}{K \omega_0^2} [\Phi_F \dot{Y} + \dot{\Phi}_F Y] \right] I_4$$

$$(19) = \omega_0 \left[\frac{\Phi_F}{K^2} + \frac{\Phi_Y}{Q^2 \omega_0^2} + \frac{1}{K O \omega_0} [\Phi_F \dot{Y} + \dot{\Phi}_F Y] \right] I_0$$

$$(20) = \omega_0^3 \left[\frac{\Phi_F}{K^2} + \frac{\Phi_Y}{Q^2 \omega_0^2} + \frac{1}{K O \omega_0} [\Phi_F \dot{Y} + \dot{\Phi}_F Y] \right] I_2$$

$$(21) = \omega_0^5 \left[\frac{\Phi_F}{K^2} + \frac{\Phi_Y}{Q^2 \omega_0^2} + \frac{1}{K O \omega_0} [\Phi_F \dot{Y} + \dot{\Phi}_F Y] \right] I_4$$

$$(22) = \omega_0 \frac{\Phi_F I_0}{K^2} + \frac{1}{K} [\Phi_F \dot{Y} - \dot{\Phi}_F Y] I_1 + \frac{1}{\omega_0} \Phi_Y I_2$$

$$(23) = \omega_0^3 \frac{\Phi_F I_2}{K^2} + \frac{i \omega_0^2}{K} [\Phi_F \dot{Y} - \dot{\Phi}_F Y] I_3 + \omega_0 \Phi_Y I_4$$

$$(24) = \omega_0^5 \frac{\Phi_F I_4}{K^2} + \frac{i \omega_0^4}{K} [\Phi_F \dot{Y} - \dot{\Phi}_F Y] I_5 + \omega_0^3 \Phi_Y I_6$$

$$(25) = \omega_0 \left\{ \frac{\Phi_F}{K^2} + \frac{\Phi_Y}{K} + \frac{1}{K} [\Phi_F \dot{Y} - \dot{\Phi}_F Y] \right\} I_0 - \frac{i \omega_0}{K O} [\Phi_F \dot{Y} - \dot{\Phi}_F Y] I_1 + \frac{\omega_0}{Q^2} \Phi_Y I_2$$

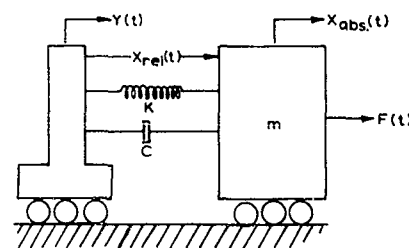
$$(26) = \omega_0^3 \left\{ \frac{\Phi_F}{K^2} + \frac{\Phi_Y}{K} + \frac{1}{K} [\Phi_F \dot{Y} - \dot{\Phi}_F Y] \right\} I_2 - \frac{i \omega_0^3}{K O} [\Phi_F \dot{Y} - \dot{\Phi}_F Y] I_3 + \frac{\omega_0^3}{Q^2} \Phi_Y I_4$$

$$(27) = \omega_0^5 \left\{ \frac{\Phi_F}{K^2} + \frac{\Phi_Y}{K} + \frac{1}{K} [\Phi_F \dot{Y} - \dot{\Phi}_F Y] \right\} I_4 - \frac{i \omega_0^5}{K O} [\Phi_F \dot{Y} - \dot{\Phi}_F Y] I_5 + \frac{\omega_0^5}{Q^2} \Phi_Y I_6$$

$$(28) = \omega_0 \frac{\Phi_F I_0}{K^2} + \frac{\omega_0}{K} [\Phi_F \dot{Y} - \dot{\Phi}_F Y] I_2 + \omega_0 \Phi_Y I_4$$

$$(29) = \omega_0^3 \frac{\Phi_F I_2}{K^2} + \frac{\omega_0^3}{K} [\Phi_F \dot{Y} - \dot{\Phi}_F Y] I_4 + \omega_0^3 \Phi_Y I_6$$

$$(30) = \omega_0^5 \frac{\Phi_F I_4}{K^2} + \frac{\omega_0^5}{K} [\Phi_F \dot{Y} - \dot{\Phi}_F Y] I_6 + \omega_0^5 \Phi_Y I_8$$



3

TABLE IX

$$m \ddot{X}_{rel} + c \dot{X}_{rel} + K X_{rel} = F(t) - m \ddot{Y}(t)$$

$$m \ddot{X}_{abs} + c \dot{X}_{abs} + K X_{abs} = F(t) + c \dot{Y} + K Y$$

REFERENCES

1. Hartog, Den, "Mechanical Vibration", McGraw-Hill Book Company, 1956.
2. Timoshenko, S., "Vibration Problems in Engineering," D. Van Nostrand, January 1955.
3. Frankland, J. M., "Effects of Impact on Simple Elastic Structures," Taylor Model Basin Report 481, April 1942.
4. Grandall, Stephen H. (ed), "Random Vibration," Technology Press, Cambridge, 1958.
5. Bendat, Julius, "Principles and Applications of Random Noise Theory," John Wiley & Sons, 1958.
6. Rayleigh, Lord, "Theory of Sound," Vol. 1, Dover Publications, 1877.
7. Beranek, L., "Acoustics," McGraw-Hill Book Co., 1954.
8. Firestone, F. A., "Twixt Earth and Sky with Rod and Tube, the Mobility and Classical Impedance Analogies," Journal of the Acoustical Society of America, 28, 1117-1153, 1956.

III. SUMMARY OF VIBRATION DATA FROM JET AIRCRAFT AND MISSILES

INTRODUCTION

The vibration engineer's "right arm" is most often his "data" which he has collected from his own experiments and from the experiments of others. This reliance on data does not necessarily imply a distrust of calculation or theory, rather it signifies the necessity for a reference frame which can be used to place the results of analytical endeavors in a proper order of magnitude. Further, this data supplies the necessary empirical constants for the analytical equations and is often useful in providing a first guess or estimate of the probable vibration environment for a new and untried aircraft or space vehicle.

This section is concerned with the vibration data which have been measured on a variety of aircraft and missiles and which have been made available to the authors by the efforts of engineers of both industry and government laboratories. It is well known that the majority of measured data are never published but, rather, due to the urgency of each successive project, lie in the rear of desk drawers and in the minds of individual engineers. This unfortunate situation is particularly prevalent in the vibration field because the majority of vibration engineers are primarily responsible for the solution of immediate and pressing problems. Therefore, once the data, which have been obtained in the analysis of a problem together with the analytical calculations which assist in obtaining solutions, have served their foremost purpose, they often become dormant, and known only to those who performed the actual work. However, if vibration analysis is to progress as a science, at the rate demanded by the new challenges which face the vibration engineer, much greater dissemination of data, together with pertinent analysis of its import, is required.

The purpose of this section is the presentation of vibration data, the comparison of data obtained in different classes of vehicles and different flight phases, and an analysis of the broad trends which can be of assistance in the prediction of vibration environments. However, before discussing the data themselves, it is necessary to consider some of the circumstances regarding the measurements and analysis.

ORIGIN OF VIBRATION DATA

The nature and quality of reported vibration data is profoundly influenced by the techniques employed in selecting, locating and mounting the vibration transducers, and by the recording and analysis of the data, in addition to the procedures utilized in designing and specifying the test conditions. These many requirements regarding measurement procedures are not always simultaneously attainable and consequently, much data must be obtained under less than desirable circumstances.

Historically, the methods of obtaining and analyzing vibration data have revolved about available instrumentation and the nature of individual problems. Prior to the 1930's most data were acquired by mechanical gadgets such as vibrating reeds, direct mechanical oscillographs and light beam indicators. As the electronic capabilities increased, the multi-channel ink and photographic oscillographs gained favor, tracing the amplified electronic signal generated in strain gauge accelerometers and moving coil velocity pickups. The analysis of these oscillograms was simple for relatively pure sinusoids but became rather tedious when visual and mechanical methods were required to obtain a Fourier analysis of a complex trace composed of many sinusoids. However, although the electrical output of the transducers was occasionally recorded on film soundtracks, as in the Mirrograph or on record disks, it was not until the development of magnetic tape, that the oscillograph had a serious competitor. It is fortunate that magnetic tape development preceded today's random vibration phenomena, for it is difficult to imagine the analysis of random vibration without sophisticated electronic filters, distribution analyzers, correlators, and the many associated graphic recording devices.

There are many factors which determine the selection of the transducers which are installed in aircraft or space vehicles to determine the vibration environment. These factors include, besides availability: frequency range, vibration sensitivity, weight, linearity, etc. The locations of the transducers are determined by the type of information desired, the availability of space, recording or telemetering channels, convenience of mounting, and a host of other practical considerations. The validity and applicability of the recorded data clearly depend upon the proper consideration of all of these factors and the thorough calibration of the entire system to insure that the final data has been appropriately corrected.

In this sequence of over-all system calibration, it is often tacitly assumed that the electrical signal from the transducer, after correction for the various transducer response characteristics, represents the vibration environment at the locations of the transducer. The validity of this assumption depends upon the vibratory characteristics of the bracket or structure on which the transducer is mounted. Naturally, when a transducer weighing only a few ounces or less is firmly attached to a piece of heavy machinery, the transducer mass cannot influence the machine's vibration. Further, since it is well known that even this lightweight transducer should not be mounted on a lightweight panel because it might influence the panel's vibration, the extremely lightweight strain gauge is often more appropriate.

Although for many practical situations these rough rules of thumb give adequate guidance, the problems in the provisions of suitable mounting for pickups on lightweight structure can be quite subtle. These subtleties result from the desire to extend the frequency range of vibration data to several thousand cycles per second, and at the same time utilize a transducer whose mass can resonate in this frequency range on its bracket or with a portion of the lightweight structure to which it is supposedly attached. These often unexpected mechanical mounting resonances, if not determined prior to the measurement, can cause large distortions in the final data and its interpretation.

The seriousness of possible mounting resonances is illustrated in Figure 8A, where most significant vibration amplitudes appearing in the reduced acceleration data are shown to result from resonances of the transducers on the mounting bracket. The corrections which were applied to the data by Blake (Reference 1) resulted from his method for finding the natural vibration characteristics of the "installed" transducer. His technique consists of the application of a standardized shock to the case of the transducer by a small portable shock device. The device produces a known force for the pulse time which can be varied between 10 and 30 milliseconds. An analysis of the resulting transient output from the transducer defines the transducer-mount transfer function, including a definition of the generalized mass of the local structure.

A paper by Boulton (Reference 2) on the measurement of rocket thrust variations to frequencies of 4,000 cps is another fine example of the explicitness needed in differentiating between the casual output of a pickup and the desired quantity. In this case it was shown how the thrust variations over a broad frequency band were obtained from a strain gauge located at a point in the interconnecting structure between the rocket and its base. The entire dynamic system was analyzed and revised to finally yield a design for the interconnecting and base structure with sufficient stiffness to provide meaningful high frequency data. The upper limiting frequency of this system was defined by calibration and analysis, and its natural frequencies were never in danger of being interpreted as excitation frequencies. The resulting mechanical system allowed only one natural frequency in the band of interest and the response was quite flat except for the one sharp resonance.

Although a detailed discussion of vibration measurement and analysis procedures is beyond the scope of this section (see for example References 3 and 4 for additional discussion), the discussion of the data which follows must be preceded by brief consideration of the filter bandwidths employed in the data analysis and the final form of data presentation.

In the past, the form of data presentation has been predicated on the type of transducer and the analysis procedure. Therefore, most early vibration data are reported in terms of the displacement of the motion which was the quantity most often obtained from mechanical vibration pickup. This trend continued, even with the development of velocity transducers and electronic recording oscillographs, often by employing electronic integration of the transducer output, so that the

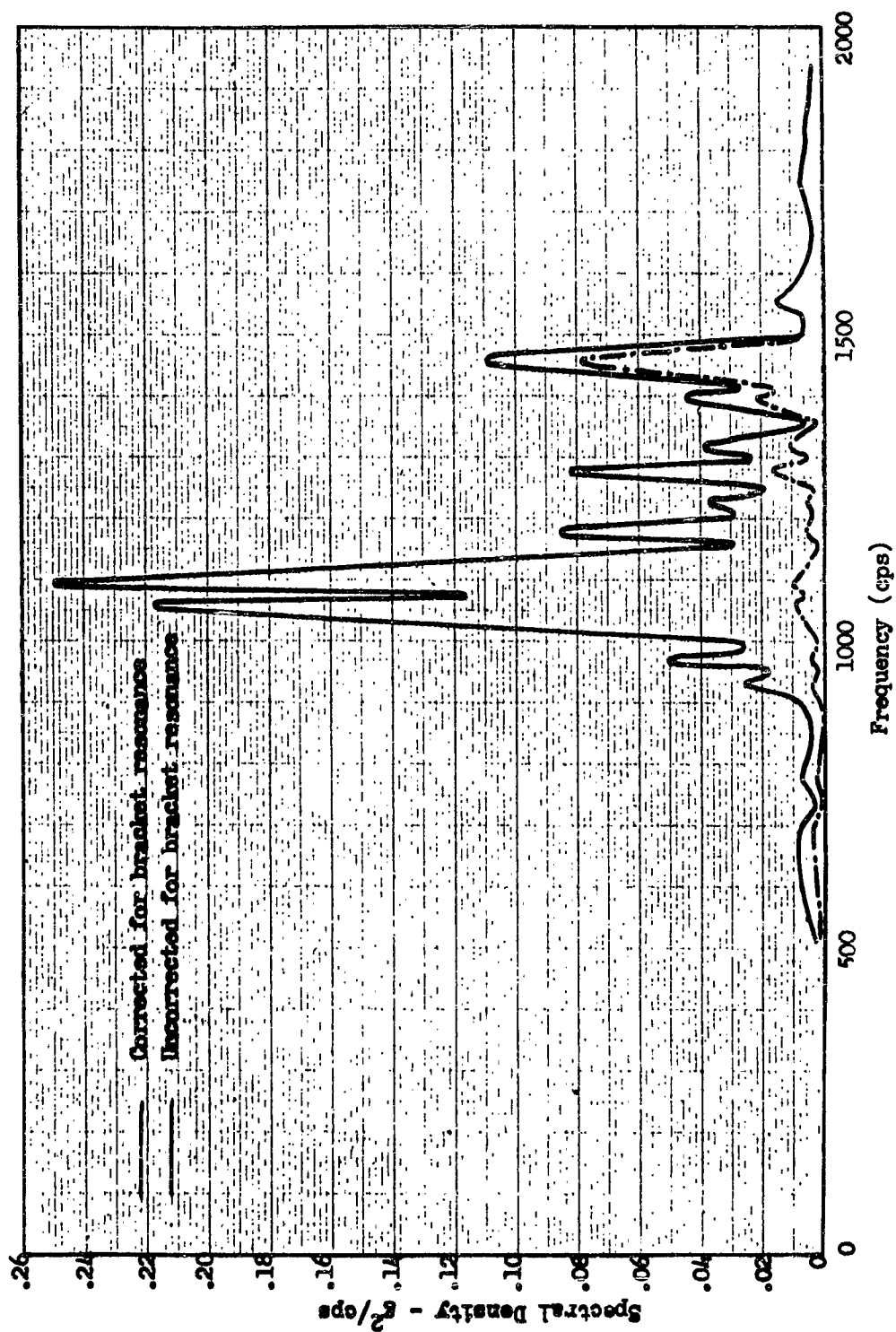


Figure 81. Example of Missile Vibration Data Without and With Correction for Bracket Resonance from Blake, Ref. 1.

recording was made directly in terms of displacement. Various methods were utilized in the description of the displacement trace, double amplitude, peak-to-peak amplitude, single amplitude, etc. These descriptions were very usable for sinusoidal and complex sinusoidal motion and were directly available to the engineer who analyzed the oscillogram.

However, the use of displacement as the primary quantity for final data presentation has been gradually superseded in the aircraft and missile industry by the use of quantities related to the acceleration of the motion. This transition appears to result from the widespread popularity of accelerometers for most measurements which involve an extended frequency range. Accelerometer data which are readout from oscillograms, usually previously filtered through electronic filters, are most often reported as peak acceleration ratio in a/g units, mean peak and, occasionally, in the terms of the peak distribution. However, acceleration data which are readout on vacuum tube voltmeters are given as root mean square or mean square per cycle, and in some cases a complete distribution of either the instantaneous amplitudes or the peak amplitudes are given.

Obviously, there are a multitude of quantities which can be utilized for data presentation. Unfortunately, few of these quantities can sufficiently specify the actual vibration to enable accurate comparison with other vibration data which are presented in other terms, except where actual statistical distributions are presented.

Furthermore, the form of data presentation and its interpretation is intimately linked with the bandwidth of the filter utilized during analysis. Filter bandwidth is particularly important when data are reported in terms of "Power Spectral Density," which has become a popular practice. In most cases "Power Spectral Density" refers to mean square acceleration per cycle; however, it may refer to velocity or displacement, as discussed in Section II. The spectral density concept is very convenient in defining random processes, as will be seen in Section IV where the mathematical implications of this concept are made clear. However, when data are reduced to mean square values per cycle, the usual data reduction procedure is the measurement of the mean square or root mean square amplitude in a finite bandwidth and the reduction of this mean square value to the "per cycle" basis by dividing by the bandwidth. This simple arithmetic procedure may be very misleading if the filter bandwidth is too wide for the phenomenon under analysis. Since data are often analyzed in either octave, one-half, one-third and one-sixth octave bandwidths, as well as 100 cps, 50 cps, 20 cps, 5 cps and 2 cps bandwidths, etc., many problems may occur.

The potential difficulties can be readily seen in the example of Figure 82, which was taken from reference 5. Here, a recorded signal from an accelerometer is analyzed by three filters, each having differing bandwidths; one cps, one octave, and 100 cps. In each case the data have been converted to mean square acceleration ratio per cycle (Power Spectral Density). The actual acceleration consists of several interrelated sinusoidal components, superimposed on a continuous random acceleration, and is accurately portrayed by the one cycle bandwidth filter.

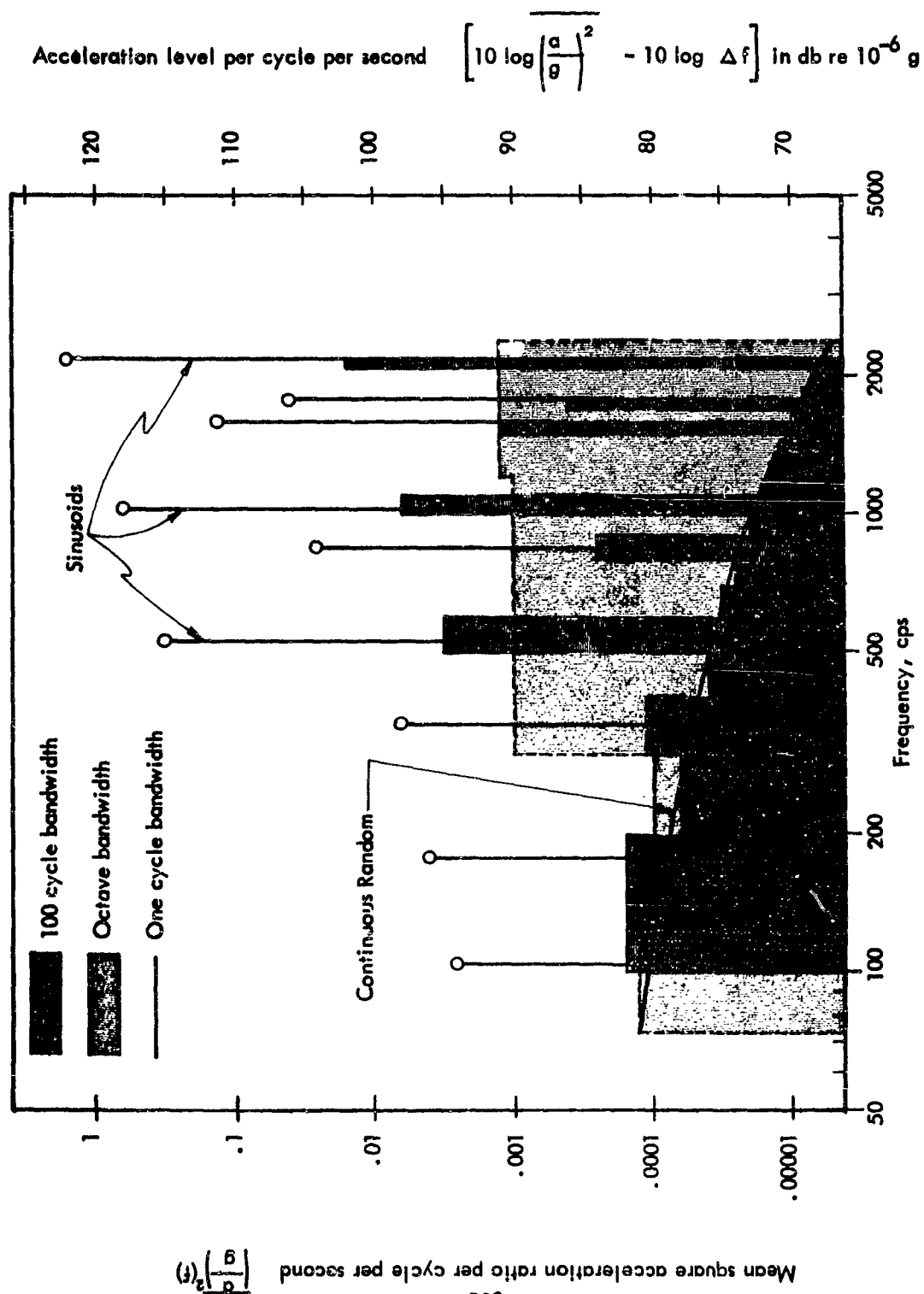


Figure 82. Comparison of Analysis of a Spectrum with Filters having Different Frequency Bandwidths and Reduction to a Per-cycle Basis.

However, when either the octave band or 100 cps bandwidth levels are reduced to mean square acceleration ratio per cycle, they indicate an amplitude intermediate between the actual continuous random mean square acceleration per cycle and the mean square amplitude of the sinusoidal components. For the 100 cps bandwidth filter, this discrepancy is most severe at the low frequencies and less severe at the high frequencies. The converse is true for the octave bandwidth. Now, it is recognized that the example shows sinusoids, rather than resonant peaks of random vibration, superimposed on the continuous random level. However, the problem of analysis bandwidth is similar for both cases.

Another illustration of this situation can be seen in Figure 83 which gives the mean square acceleration ratio for the data of Figure 82 as directly measured by the filter prior to dividing by the bandwidth. It is clear that large discrepancies between the various results still exist, although the one-sixth octave appears to give a usable, or interpretable, result with this particular spectrum and at the higher frequencies the 100 cps bandwidth becomes fairly accurate.

Although the purpose of this discussion is to illustrate the analysis problem, rather than to discuss its solution in the necessary detail, a few general comments are appropriate. First, the use of a broad band filter for final analysis of vibratory phenomena is justified only when similar data have been found to have continuous spectra, or when the actual vibration amplitudes are too small to be of concern. If neither of these criteria is met, it is normally preferable to sample the vibration recordings, with filters whose bandwidths is of the order of, or less than, the bandwidths of the vibration phenomena, to distinguish discrete frequency components, resonant peaks excited by random forcing functions, and continuous random vibration. Second, it appears misleading to reduce data analyzed through the wide band filters to a spectral density basis unless, and only unless, the vibration is known to be of a continuous spectral distribution. Third, it is advisable to determine the distribution of peaks for all important frequency regions in the vibration spectra, such as the resonance peaks, since the availability of a distribution enables comparison of data which are read out in differing fashions as, for example, an oscillograph and a voltmeter, and is of importance for both the fatigue and equipment malfunction problem areas.

The various major difficulties which arise in the comparison of vibration data taken by several organizations, assuming all data have been corrected for the usual response factors, stem directly from the three problem areas discussed in this sub-section. In fact, comparison of much of the valuable data presently available is only possible when the data are transferred to an arbitrary standardized presentation form. For this standardization certain ground rules were followed which were felt to introduce the least error in determining and comparing the various empirical trends. The data which are available had been reduced by filters of one-half octave, 100 cps bandwidth and a series of smaller bandwidths ranging down to 2 cps. The results were reported as displacement or acceleration in terms of mean square per cycle, rms for the bandwidth, mean peak, etc. Statistical distributions of either peak amplitude or instantaneous amplitude were also occasionally presented.

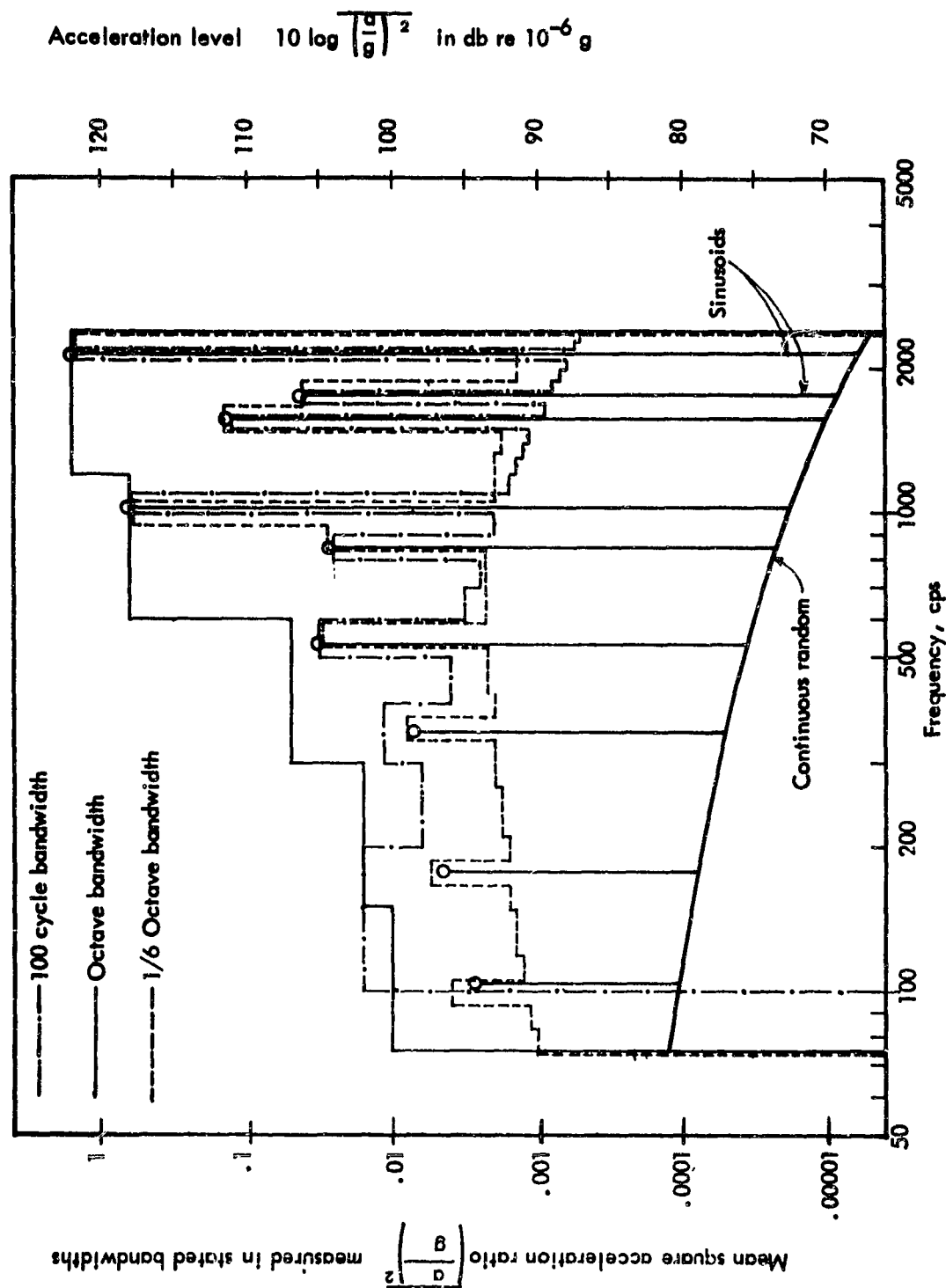


Figure 83. Comparison of the Analysis of a Spectrum with Filters Having differing Frequency Bandwidths, and presentation of the Data as the Mean Square Amplitude for the Total Bandwidth.

To obtain standardization, all acceleration data were converted to the rms amplitude for the original bandwidth. Where the analysis bandwidth was narrower than the bandwidth of the resonance phenomena, the energy under the particular resonance was summed and the result reduced to the rms amplitude which is associated with the single resonance. Sinusoids, where identifiable, were considered separately as appropriate to each of the summary figures. Where only the maximum mean square amplitudes per cycle of resonant peaks were reported, the rms value for the total resonant vibration associated with each peak was estimated over the resonance bandwidth associated with a Q of 15, which seems typical of many missile structures. Where mean peak data were given for the value of resonance vibration it was assumed that the resonant peak amplitudes would follow a Rayleigh peak distribution and the rms amplitude was computed by dividing the mean peak amplitude by 1.19.

VIBRATION IN JET AIRCRAFT

Although the major emphasis throughout this report is on space vehicles, the examination of empirical vibration data for the space vehicle is assisted by direct comparison with the more familiar aircraft vibration environment. For this reason, the summary of aircraft vibration presented by Crede and Lunney (Reference 6) is duplicated here. The data have been converted from displacement amplitude, as given originally, to root mean square acceleration ratio to be consistent with other data in this section.

Figure 84 gives the summary of jet fighter data which were gathered at various flight conditions and from many locations on structures in the respective aircraft. Although the details regarding each of these data are not precisely known (see Reference 6), they are considered representative of the vibration environment in the conventional jet fighter aircraft.

It is interesting to note that the median line fitted to the data almost represents a line of constant velocity, which is proportional to the acceleration divided by the frequency. Further, when these data were examined to determine the median and the 85% limit, it was found that their logs are almost distributed normally, whereas the distribution of the linear amplitudes was very skewed. It might be presumed that that data were acquired from several transducers randomly located on each aircraft, and recorded at random portions of the flight profile. It may be also assumed that the maximum amplitudes represent the more severe flight conditions, say takeoff jet noise and maximum dynamic pressure (q) flight, and the lower amplitudes represent less severe flight conditions. The tendency in the data toward a log normal distribution suggests that the duration of the more severe vibration occupies a significantly shorter period of time during a typical mission than does the duration of the lower amplitude vibrations. This might be anticipated from direct observation during flight, and it is similar to the log normal distributions found in gust fatigue problems.

Figure 85 gives similar data from Crede and Lunney for the B47 and B52 aircraft. As can be seen from the medians for these two aircraft, the B52 vibration environment is significantly higher than that measured for the B47. Although this difference may result from the positions of the transducers, which are not known

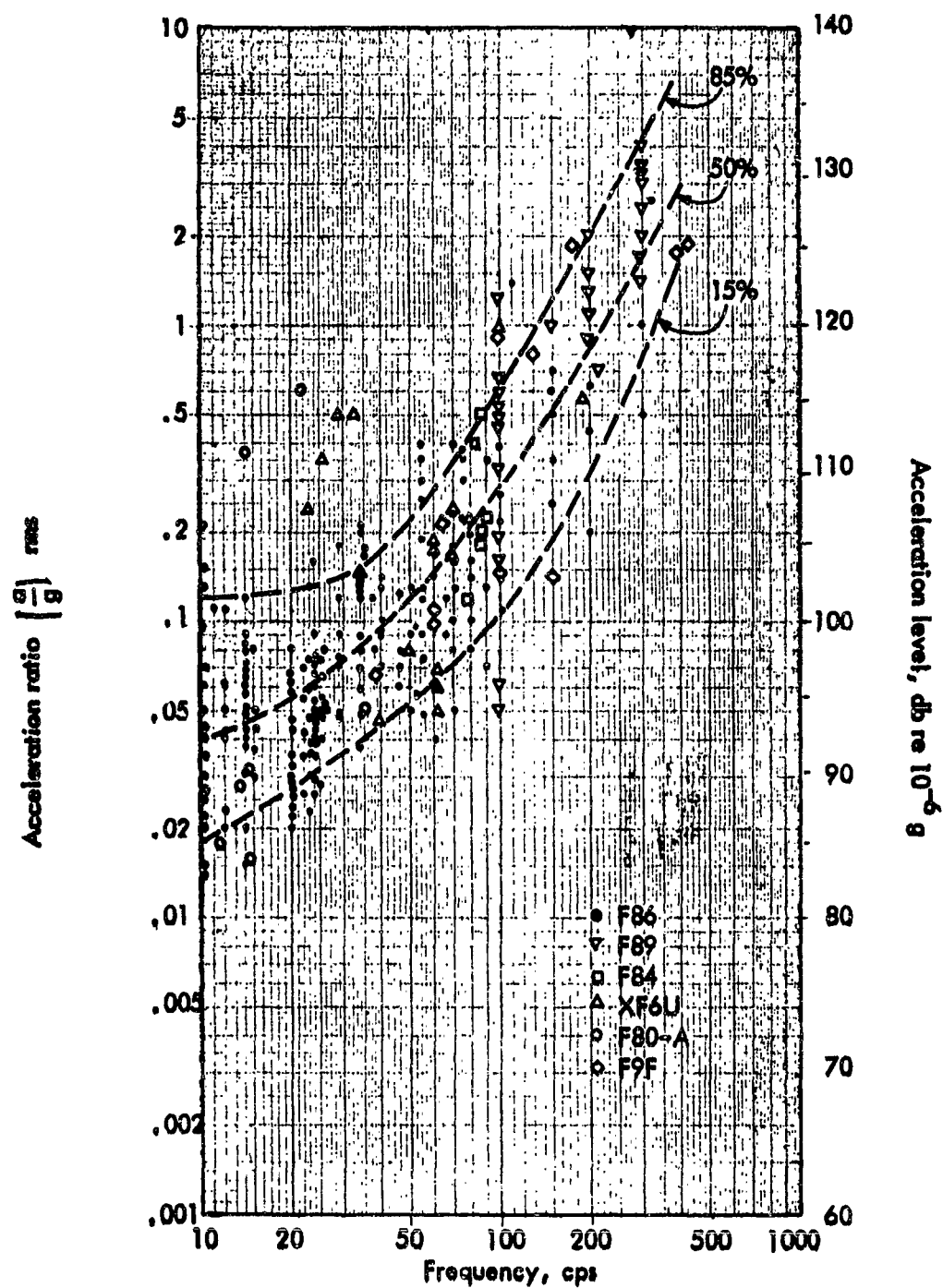


Figure 84. Acceleration in Jet Fighter Aircraft (After Crede & Lunney, Ref. 6).

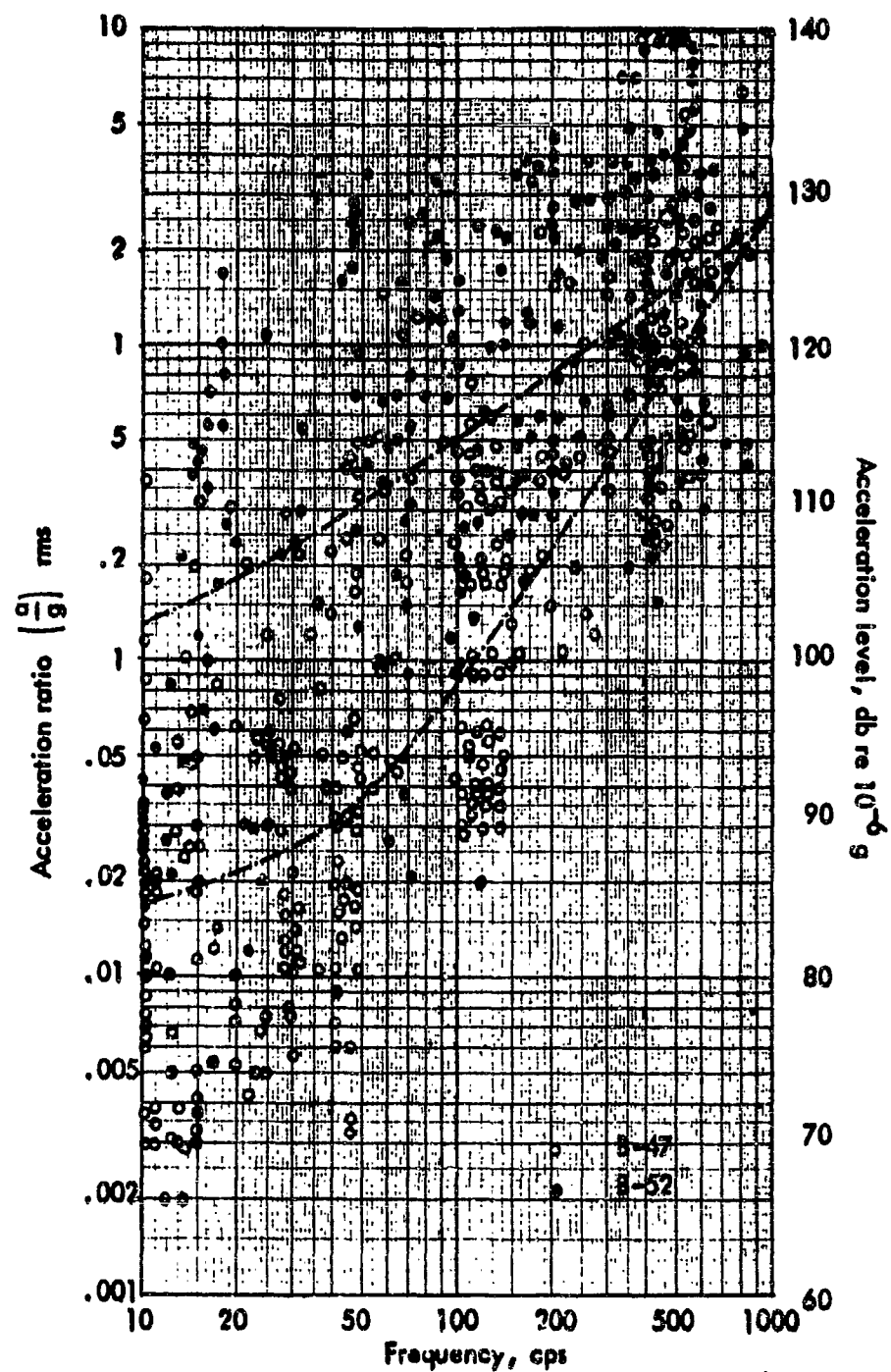


Figure 85. Acceleration in Jet Bomber Aircraft (After Crede and Lunney, Ref. 6).

to the authors, it may also be the logical result of the higher noise exposure of the B52, particularly in the near field of the engines under the wing, and from the higher maximum flight performance for the B52. Again, the data for each of these aircraft tend to follow the log normal distribution and appear to represent, more nearly, constant velocity amplitude rather than constant acceleration or displacement.

VIBRATION IN MISSILES

The vibration environment in a missile varies rapidly with time during a typical flight profile. This rapid variation can be illustrated by the continuous recording of the noise in a forward compartment of a small ground-to-ground missile. It might be noted that a recording of noise is illustrated rather than a recording of vibration simply because of the availability of the former.

Figure 86 from Reference 7 illustrates the several phases of noise or vibration environment which are usually found in missile flight data. The rocket noise at launch provides a high level of vehicle response, which decreases rapidly as the vehicle leaves the pad and accelerates. However, as vehicle velocity increases, the pressure fluctuations in the turbulent boundary layer increases, the pressure in magnitude and the vehicle response begins to increase. The transients shown on the graphic level recording represent a shock as the vehicle velocity exceeded Mach 1 and a second shock when the sustainer engine was ignited. As can be seen, the response continued to increase until the maximum dynamic pressure was reached, at which time in the flight profile the boundary layer pressure fluctuations are maximum. As the vehicle continued to accelerate into less dense atmosphere, the q decreased, as did the response. However, when the vehicle descended into more dense atmosphere in the terminal portion of the flight, the vehicle q and response both increased.

It was evident from Figure 86 that the two most severe vibration environments are a result of rocket noise at launch, and aerodynamic phenomena at maximum q . The relative severity of these two forcing functions and their responses in a specific vehicle depends on many factors, including the flight profile and the launch configurations, as discussed in Part I of this report. It should be noted that, for some vehicle types, other forcing functions may also be of comparative severity.

The quest for missile vibration data which has general application toward empirical correlation studies is very laborious and difficult. This difficulty results from the problems encountered by vibration engineers in industry when they are forced to compete with other important groups for the assignment of telemetering channels. In most cases, this competition severely limits the number of transducers which can be utilized and requires commutation of the various transducers. Furthermore, these limitations require that potential problem areas and important equipment receive priority for transducer locations, so that ideal surveys, which phase vibration at various structural locations throughout the vehicle, are seldom realized.

Figure 87 presents data obtained at the launch of rocket powered ballistic missiles from transducers located on structure in the middle and forward positions of the

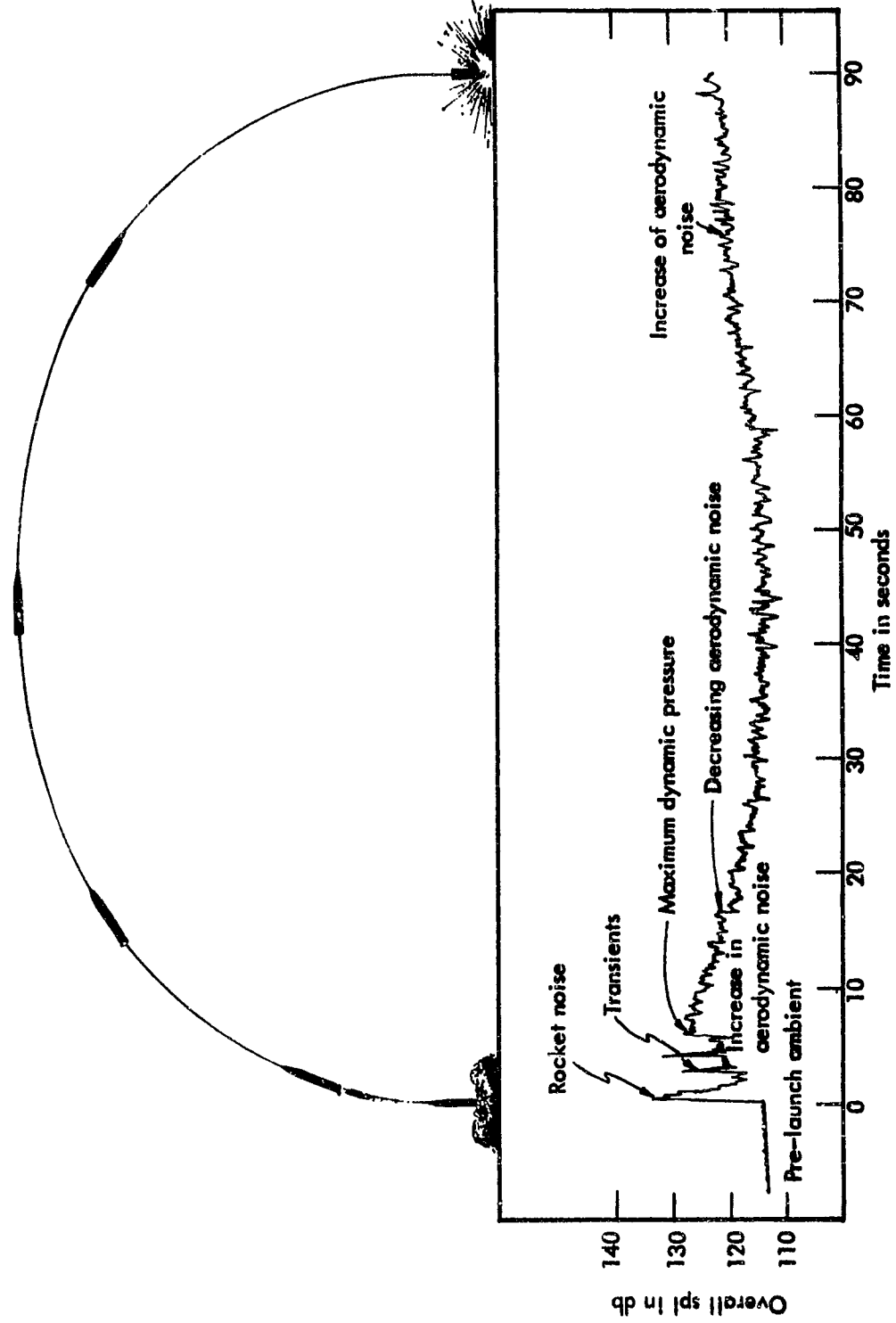


Figure 86. Graphic Level Recording of Variation of Overall Noise Level Inside Forward Compartment of a Small Missile During its Flight.

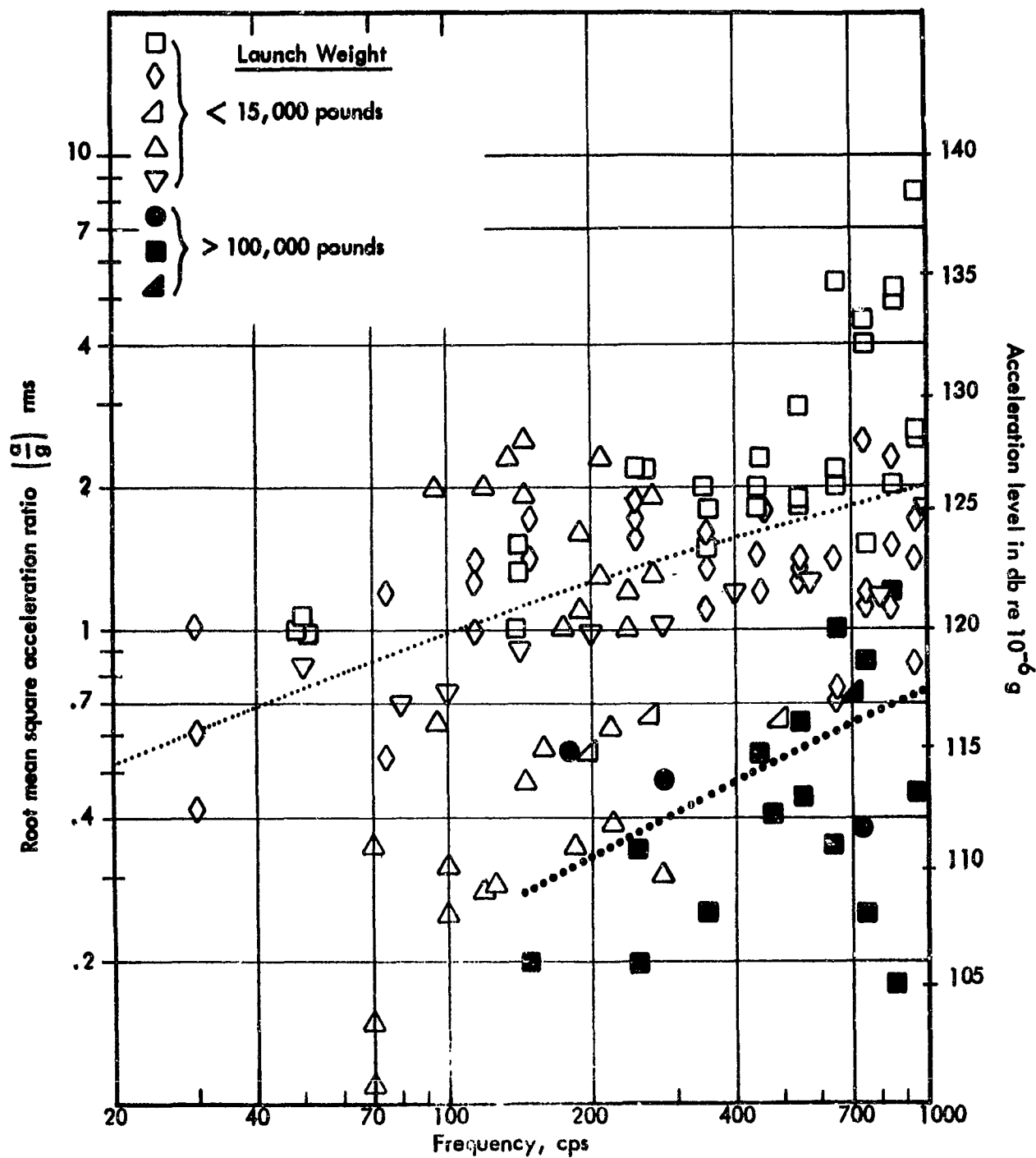


Figure 87. Missile Launch Accelerations Obtained on Structure in Forward Half of Vehicle.

vehicles. The data were obtained from References 8 - 23, which include five missiles which have gross launch weights less than 15,000 lbs., and three missiles which have gross launch weights in the 100,000 - 300,000 lb. range. The lightweight vehicles are denoted by open symbols and the heavier missiles by the solid symbols. It is evident from the figure that the vibration amplitudes in the heavy missiles are on the order of 20 to 25% of the amplitudes measured in the lightweight vehicles.

Figure 88 gives similar data for the vibration at maximum q flight phase for six missiles, four of which are lightweight and two of which are in the heavyweight class. Again, it is clear that the vibration of the heavy missile is significantly lower than the vibration of the light missiles. It is noted that the vibrations given in the figure are thought to result only from pressure fluctuations in the boundary layer along the vehicle's skin. Thus, the figure does not include the data from a missile which responded to the high turbulence created by the wakes of its dive brakes or another vehicle which was excited by base pressure fluctuations. These two known special cases of aerodynamic excitation are discussed in Part I.

Figure 89 presents available data for vibration of missile structure located near the engine. There is a rather large scatter in the data, but no consistent division is seen between light and heavy missiles. Rather, it appears that much of the data represents high level vibration and a smaller proportion of the data represents lower level vibration. This is not at all unexpected because of the large variability in structure for the various locations, as well as the variability of the vibratory energy output of different types of rocket engines.

Figure 90 summarizes the data obtained on four pieces of equipment, two of which are located in each of two types of the heavy missiles. The range of data represents many repeat flights with the transducers located at the same positions. In general, the vibration appeared to be sinusoidal at several harmonically related frequencies which were generated by the particular equipment. Obviously, these data represent specific cases and are included here only because of the large amount of data measured on each of these equipments, and to give a feeling for the amplitudes which might be encountered on or near equipment vibratory sources. However, the prediction of vibration near any equipment vibratory source should be predicated on measurements of the specific type of equipment.

COMPARISON OF AIRCRAFT AND MISSILE VIBRATION TRENDS

In each of the figures in the preceding discussion of aircraft and missile vibration a median curve was fitted to the data. These curves, taken from Figures 84, 85, 86, 87, and 88, are summarized in Figure 91. As was shown in the original data figure, the median of the data for the B52 exceeds that for the B47, whereas the median for the jet fighter vibration data lies between the medians of the two bombers. The medians for light missile launch and maximum q flight are generally higher than those for the aircraft, whereas the medians for the heavy missiles are significantly lower and are of the same order as the jet fighter and B47 vibration. Note that the vibration on structure located near the rocket engine is considerably higher. Thus, this figure clearly demonstrates that the severe portions of the

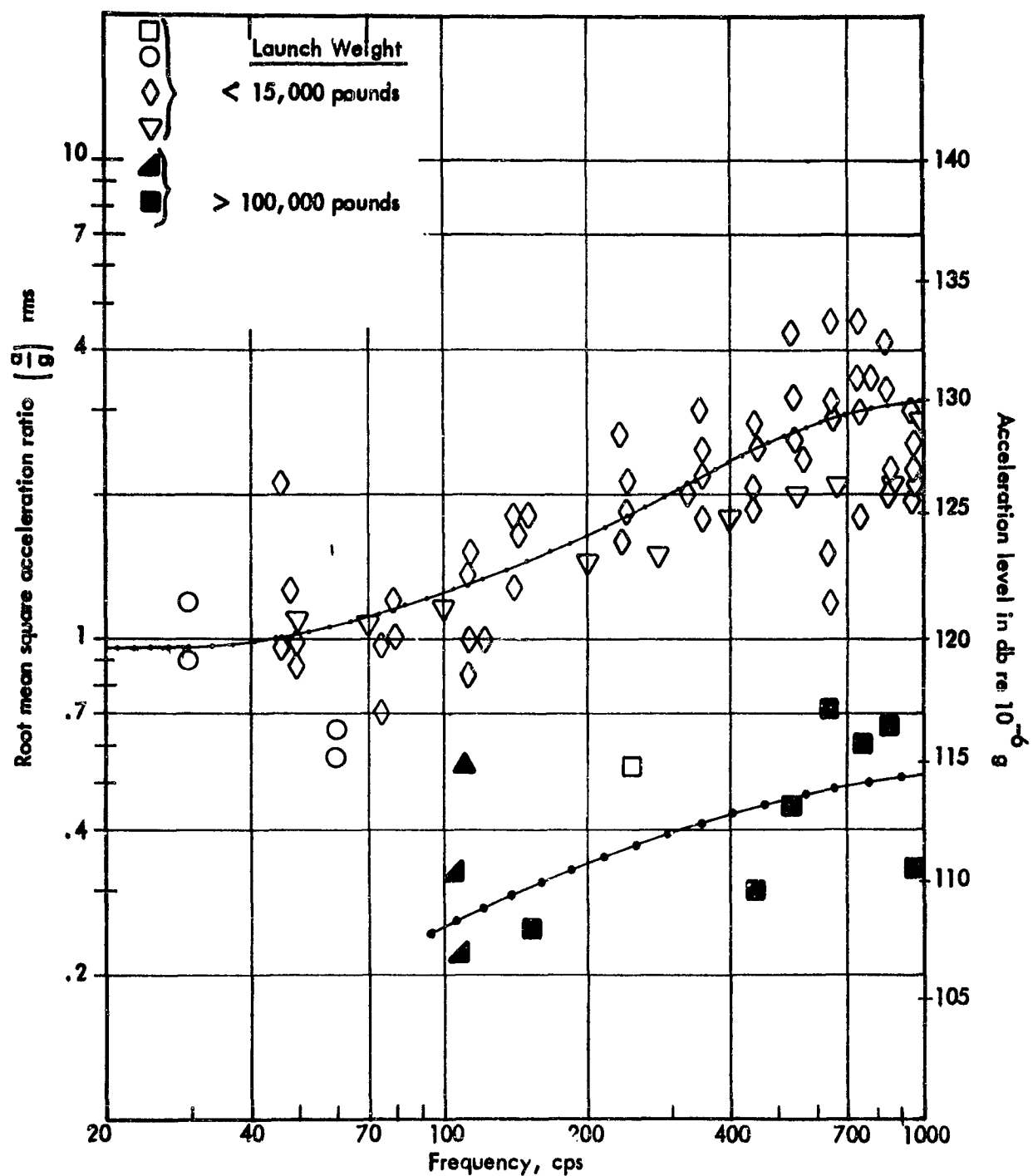


Figure 88. Missile Flight Accelerations on Structure in Forward Half of Vehicle and Obtained Near Maximum Dynamic Pressure, Flight Phase.

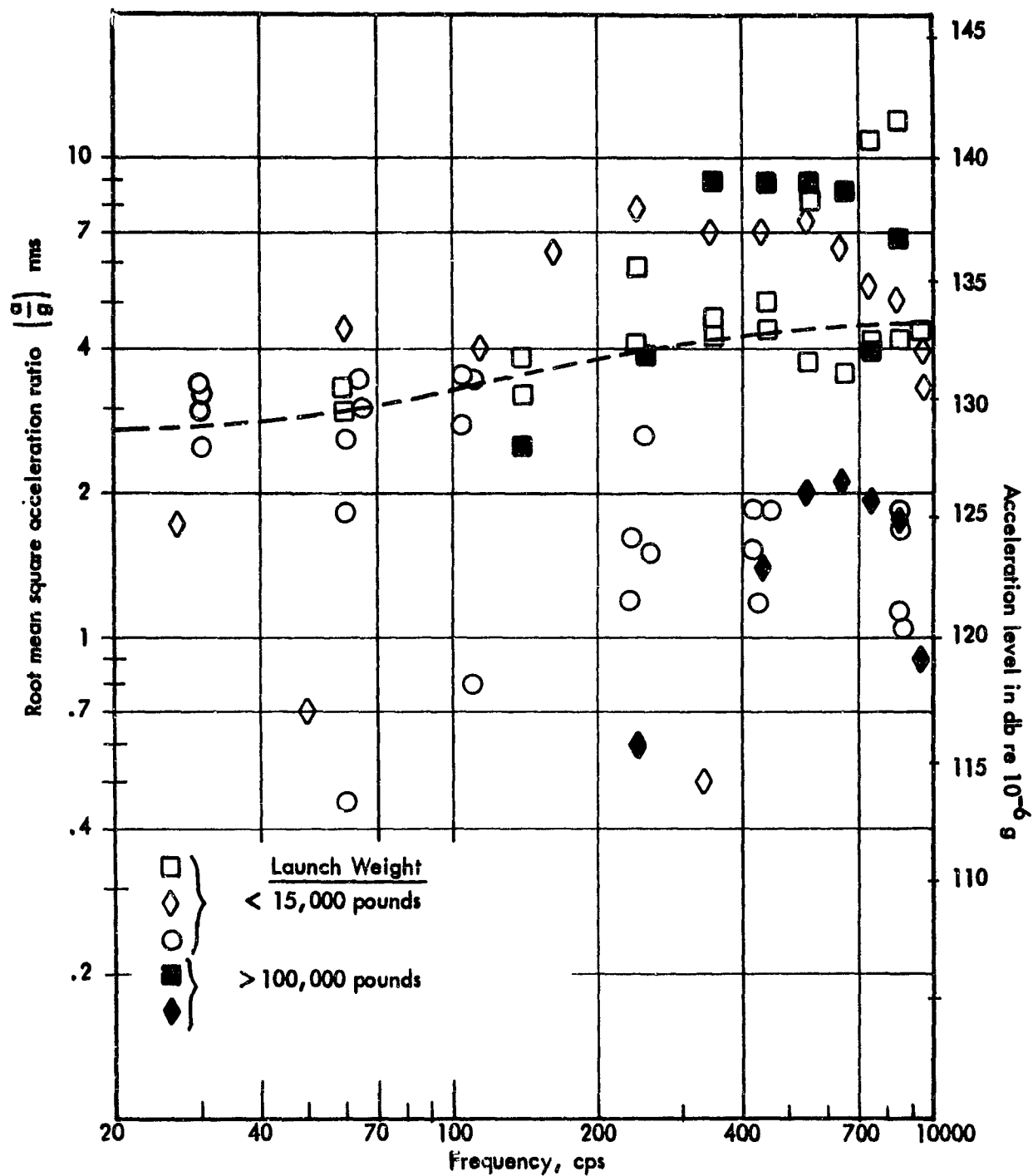


Figure 89. Missile Flight Accelerations on Structure Adjacent to Rocket Engine.

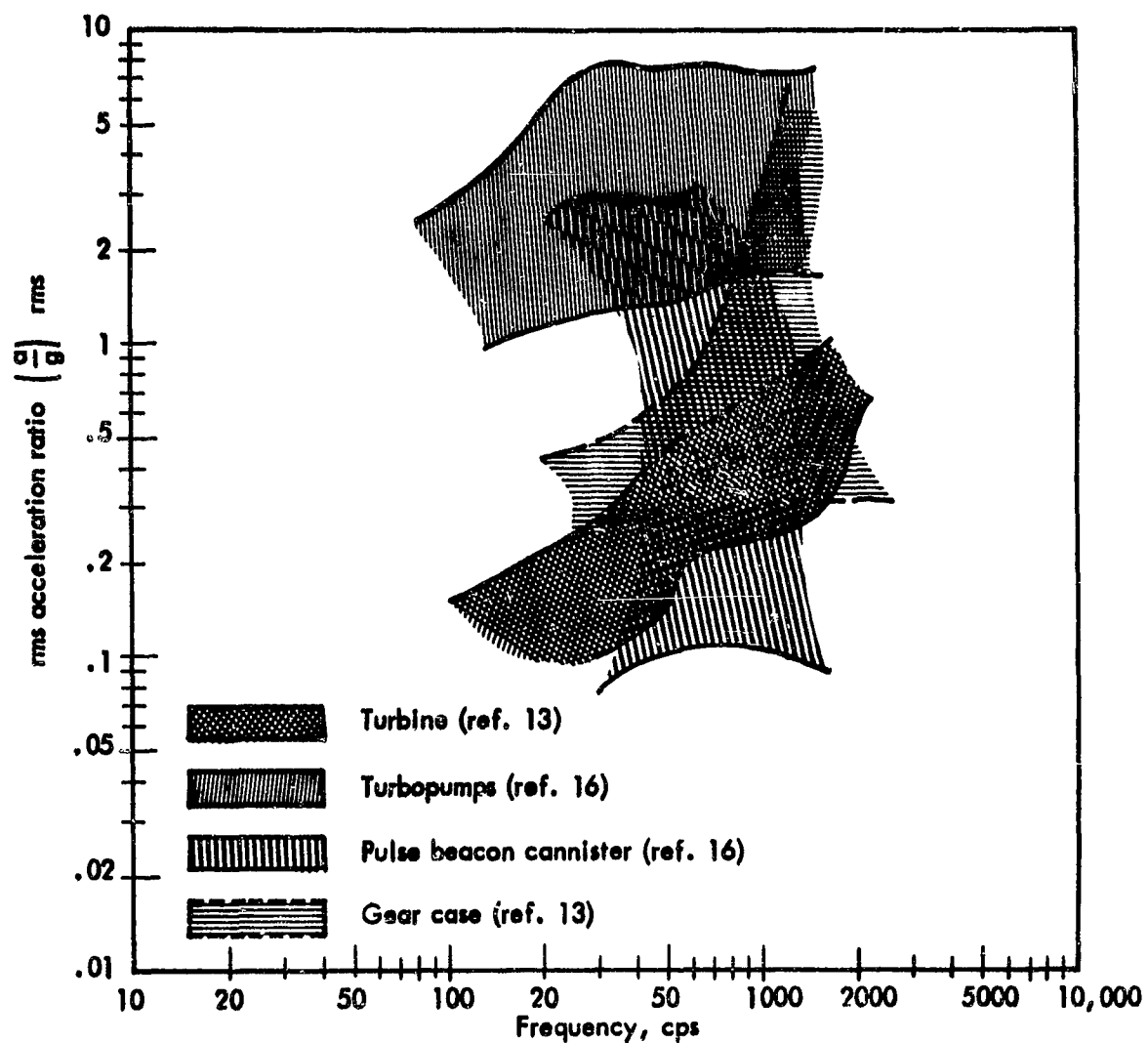


Figure 90. Range of Accelerations for Four Types of Self-Excited Missile Equipment.

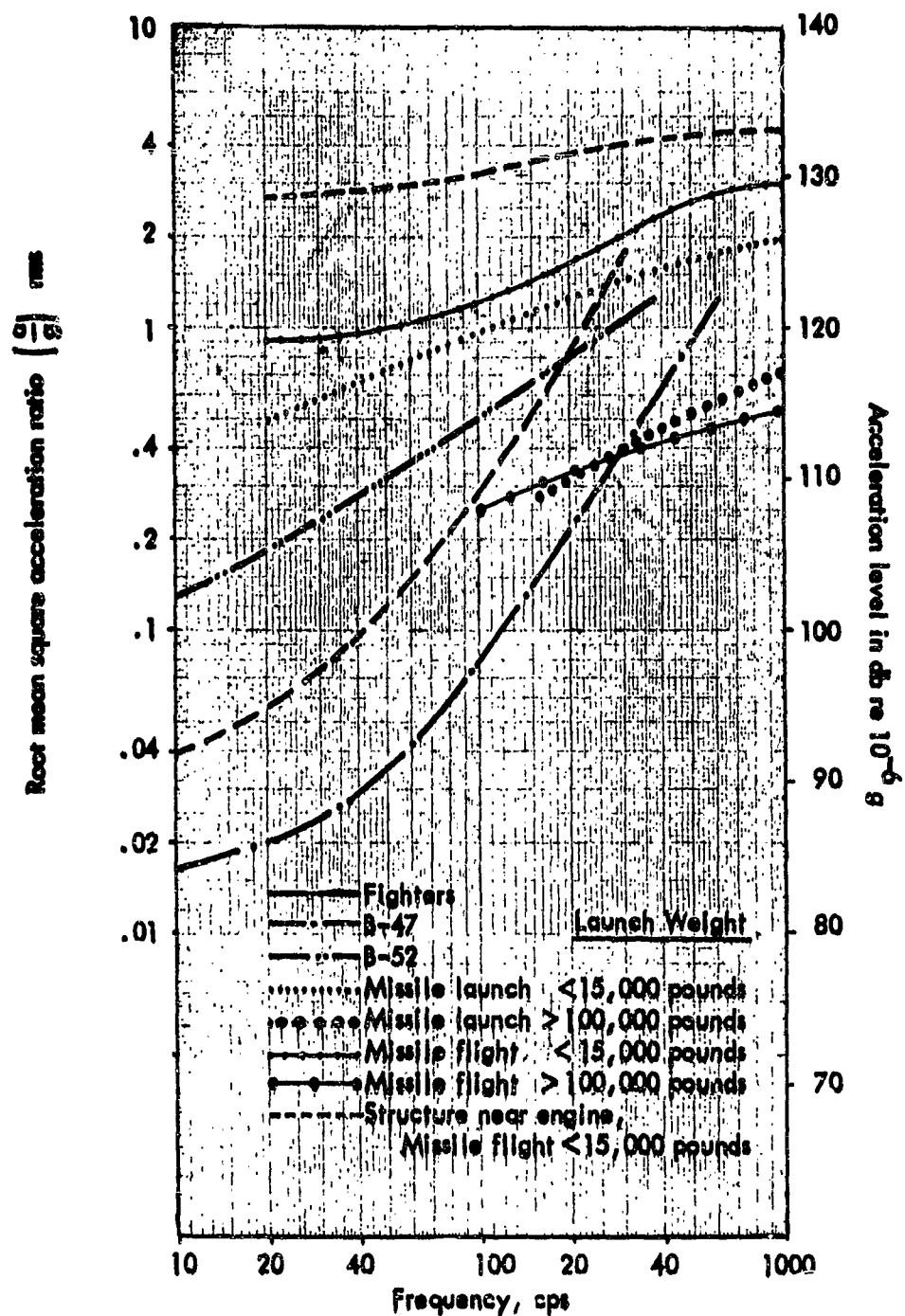


Figure 91. Summary of Median Curves for Aircraft and Missile Accelerations

vibration environment in the light missiles generally exceeded those experienced in high performance jet aircraft. However, the vibrations in the heavy missiles of the IREM and ICM category, have been generally of the same order as those of the aircraft.

It should be noted again that the relative severity of launch and maximum q flight phase vibration depends upon both the flight profile and the launch configuration. For example, all of launch data result from surface launches rather than silo launches. A comparison of the surface launch noise environment with the silo launch noise environment based on the information in Part I, Section II, indicates that the magnitude of vibration might be on the order to 3 to 5 times greater in a silo than on the surface. Thus, the silo launch vibration equipment for heavy missiles might be expected to approach the surface launch vibration environment in the light missiles.

The median curves in Figure 91 indicate that the aircraft acceleration data increase proportionately with increasing frequency. This indicates that the median vibration has essentially constant velocity, regardless of frequency. This constant velocity characteristic has considerable implication if one considers the total rms vibration over the entire bandwidth of the measurement. For example, when the aircraft data are recorded in terms of acceleration, the total acceleration measured by a meter over the entire bandwidth is predominantly determined by the high accelerations which occur at the higher frequencies. Thus, the total rms acceleration for a measurement will be significantly higher if the upper limit of the measurement is 1000 cps rather than, say, 500 cps. On the other hand, since the vibration is characterized by constant velocity, a meter reading of total velocity over the entire bandwidth from a signal proportional to velocity, would be less affected by the high frequency cutoff of the measurement system than would the total measured rms acceleration. Consequently, comparisons of total velocities over the measurement bandwidth for different aircraft tend to be more meaningful than comparisons of total acceleration. However, the missile vibration seems to increase with increasing frequency at a rate intermediate between constant acceleration and constant velocity. Hence, use of acceleration as the final form of data presentation tends to emphasize the amplitudes at high frequencies, whereas use of velocity would similarly emphasize the lower frequencies.

EMPIRICAL PREDICTION OF VEHICLE VIBRATION

The ultimate objective of this report is to assist the engineer in his understanding of the phenomena which are responsible for, or control, the vibration in a space vehicle, and to assist him in the prediction of the resulting vibration environment. As is the case in many young technologies, where the state of the art is not sufficiently complete to enable direct analytical solutions of specific problems, or when the analytical approach involves excessive complexity, it is desirable to attempt to derive direct empirical correlations which may be utilized as predictive tests and which define apparent trends.

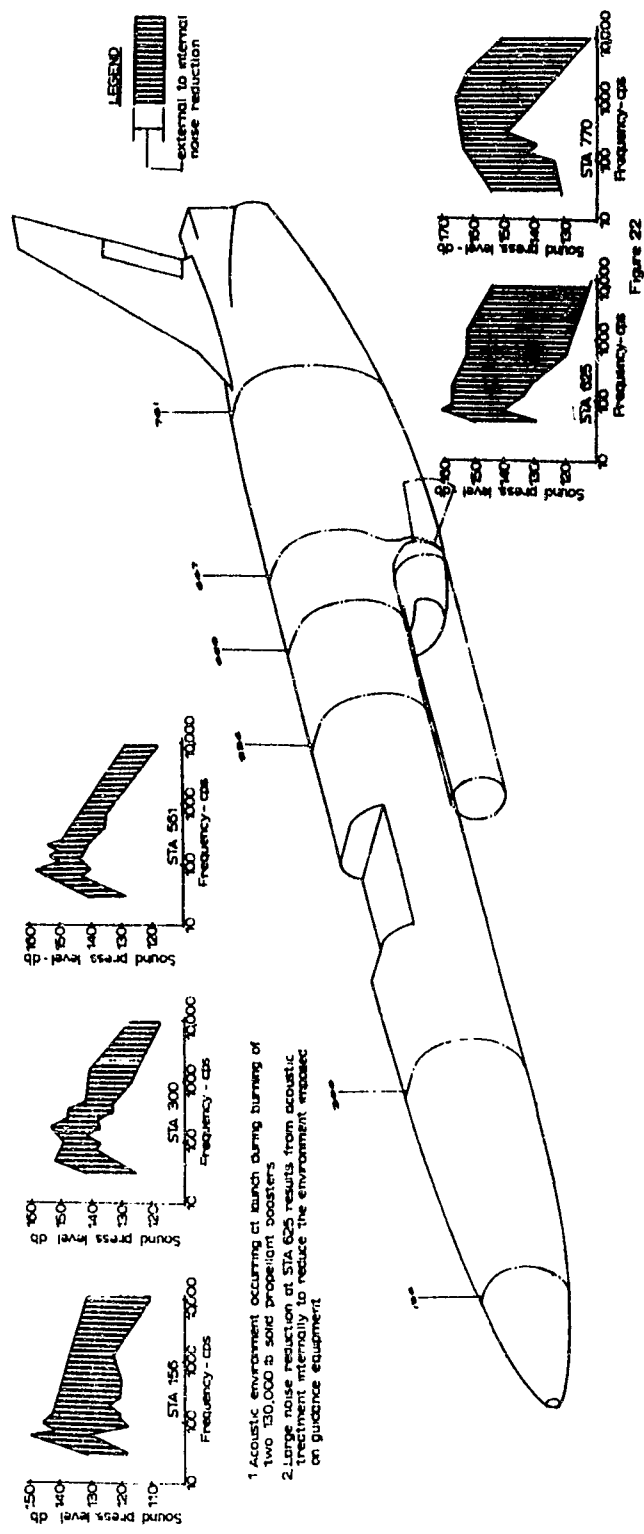
The success of these empirical correlations generally depends upon the degree with which the correlating parameters represent the actual physical phenomena under study, and their actual scaling laws. In addition, the development of an empirical correlation which will stand the test of time often depends upon the relationship between the presently available range of each of the parameters and the range of the parameters which will eventually be encountered. For example, empirical correlation of jet noise from data which represents only a small range of jet velocities would, in all probability, not result in a proper scaling law for the velocity parameter, and in consequence, be a very inaccurate predictive tool for velocities which differ significantly from those considered. The preceding cautionary factors represent the basic hazards of the empirical approach, and suggest that empirical correlations be re-examined constantly to assure that they remain consistent with advances in the general "state of the art."

Direct Correlation of Noise and Adjacent Structural Vibration in Aircraft

One approach to the correlation of vibration response of aircraft with external noise has been previously suggested by Convair (References 24-26). This correlation was obtained by directly comparing the external sound pressure level on the B-58, resulting from jet engine noise, to the vibratory response of adjacent internal structure. Thus, vibration measurements in the nose of the aircraft were compared directly to sound pressure levels measured on the external skin of the nose section, and vibration measurements in the aft end of the aircraft were compared to sound pressure levels measured on the external skin of the aft skin, etc. Since the external noise environment on the B-58, and other types of jet aircraft, varies considerably from the relatively low noise levels forward to the very high levels toward the aft end, a comparison of this type includes a range of external noise levels of the order of approximately 30 db.

As an example of this direct approach, consider the noise exposure of the Snark missile illustrated in Figure 92. The external noise level at launch results from two rocket boosters which are mounted beside the fuselage and exhaust alongside the after portion of the fuselage. As can be seen from the octave band sound pressure levels (spl), the noise environment at the fuselage stations aft of the nozzles is very high.

It might be noted that the Snark noise environment is the most severe of any aircraft type missile and is certainly comparable to the most severe environment that



1. Acoustic environment occurring at launch during burning of two 150,000 lb solid propellant boosters
 2. Large noise reduction at STA 605 results from acoustic treatment internally to reduce the environment imposed on guidance equipment

Figure 92: Internal and External Acoustic Environment of the Snark Missile

would be expected for any ballistic missile utilizing present engine and launch concepts. Of course, this severity results from the positioning of the nozzles alongside the fuselage, rather than at the aft end. Incidentally, this location was not selected in ignorance of potential noise problems, but rather as a necessary location for boosters which were added to a weapons system to give it a zero launch capability after the airframe had been designed for conventional takeoff. Therefore, the location of the boosters and their thrust axes were determined by the center of gravity and aerodynamic characteristics of an existing airframe. The ensuing severe acoustic environment resulted in a very extensive test program which has been described in References 27 and 28.

At the time when this work was undertaken, it was not universally recognized that the vibration response at launch was the result of the external noise rather than the result of vibration transmitted directly to the structure from the engine or booster. Consequently, one of the more interesting phases of the Snark test program was the comparison of vibration response for two series of restrained firings, one series with the boosters normally attached to the airframe, and the second series with the boosters completely detached, but in their normal position relative to the airframe. The tests conclusively proved that the vibration response resulted from acoustic excitation only, and that response to direct engine vibration was not significant in comparison. It might also be noted that the noise reductions shown on Figure 92 in the forward compartments, which have no internal acoustical absorption, are typical for a lightweight external skin (.19 in. magnesium). The higher reductions illustrated for the after compartments are the result of added internal acoustical absorption material.

If the response of the internal structure is directly proportional to the adjacent external noise field, it should be possible to obtain the constant of proportionality by comparing the responses measured near a given station with the external noise at that station. Furthermore, if the structure is similar throughout the fuselage, it would be expected that the constant relating external noise with adjacent response would be unchanged as a function of position and, hence, noise level along the fuselage, as proposed by Convair.

This comparison has been made for several frequency bands, including the over-all noise and vibration levels and five octave frequency bands in Figure 93 through 96. Note that the slight differences in noise level represent different firings, whereas each group of data associated with a given noise level represents a specific fuselage station. In addition, the acceleration data include transducers oriented in various directions, but all attached to actual airframe structure.

As might be expected, the data exhibit considerable scatter, so that it is possible only to estimate a trend line through the points. However, more significant than the scatter is the slope of the trend line. Note that if the acceleration amplitude increases by a factor of ten for an increase of 20 db sound pressure level, a direct linear relationship exists between the internal structural vibration amplitude and the adjacent external sound pressure amplitude. In this event, the trend line through the data gives the constant of proportionality between external sound and internal vibration.

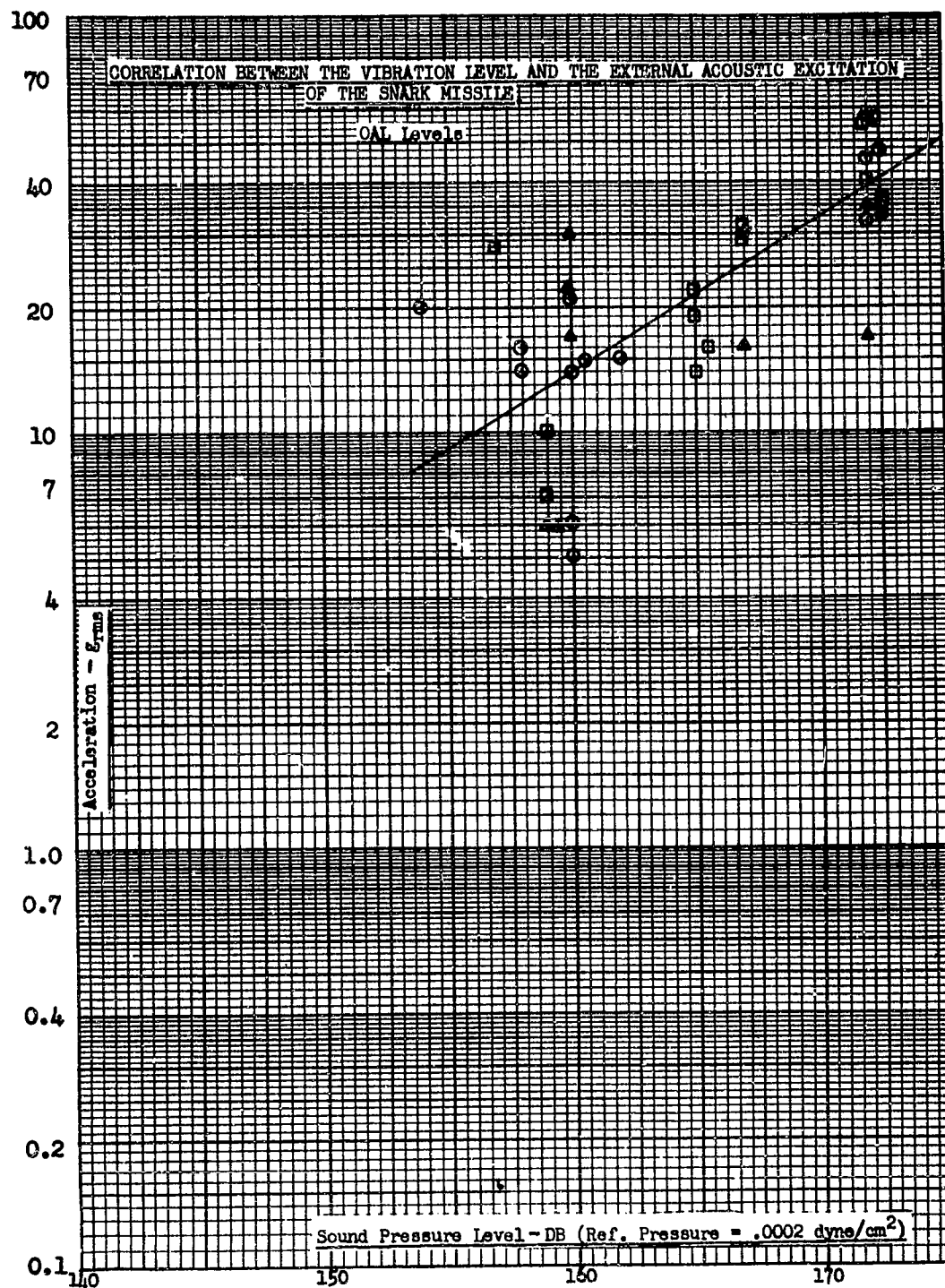


Figure 93. Correlation Between the Vibration Level and the External Acoustic Excitation of the Snark Missile - OAL Levels.

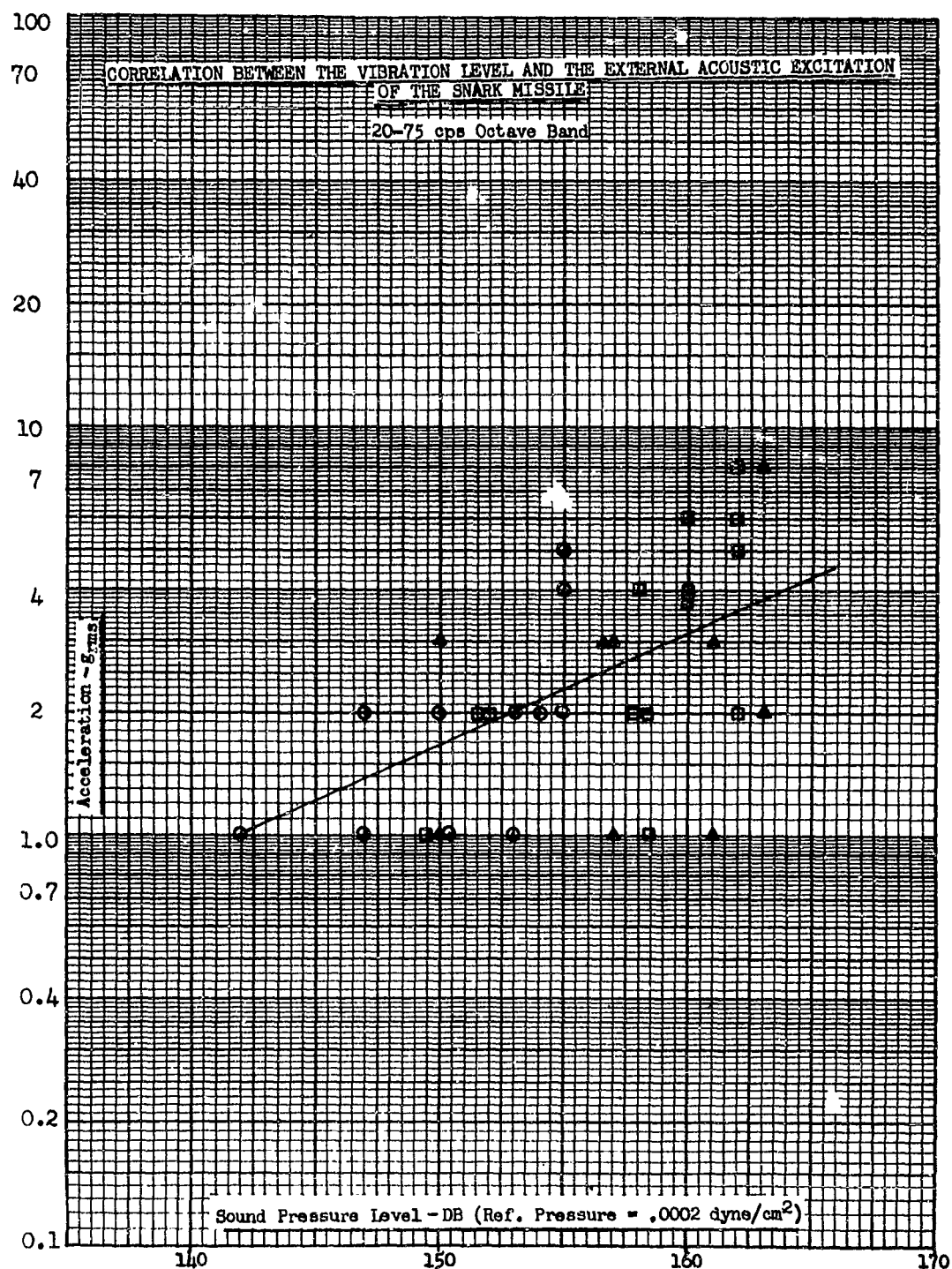


Figure 94. Correlation Between the Vibration Level and the External Acoustic Excitation of the Snark Missile - 20-75 cps Octave Band.

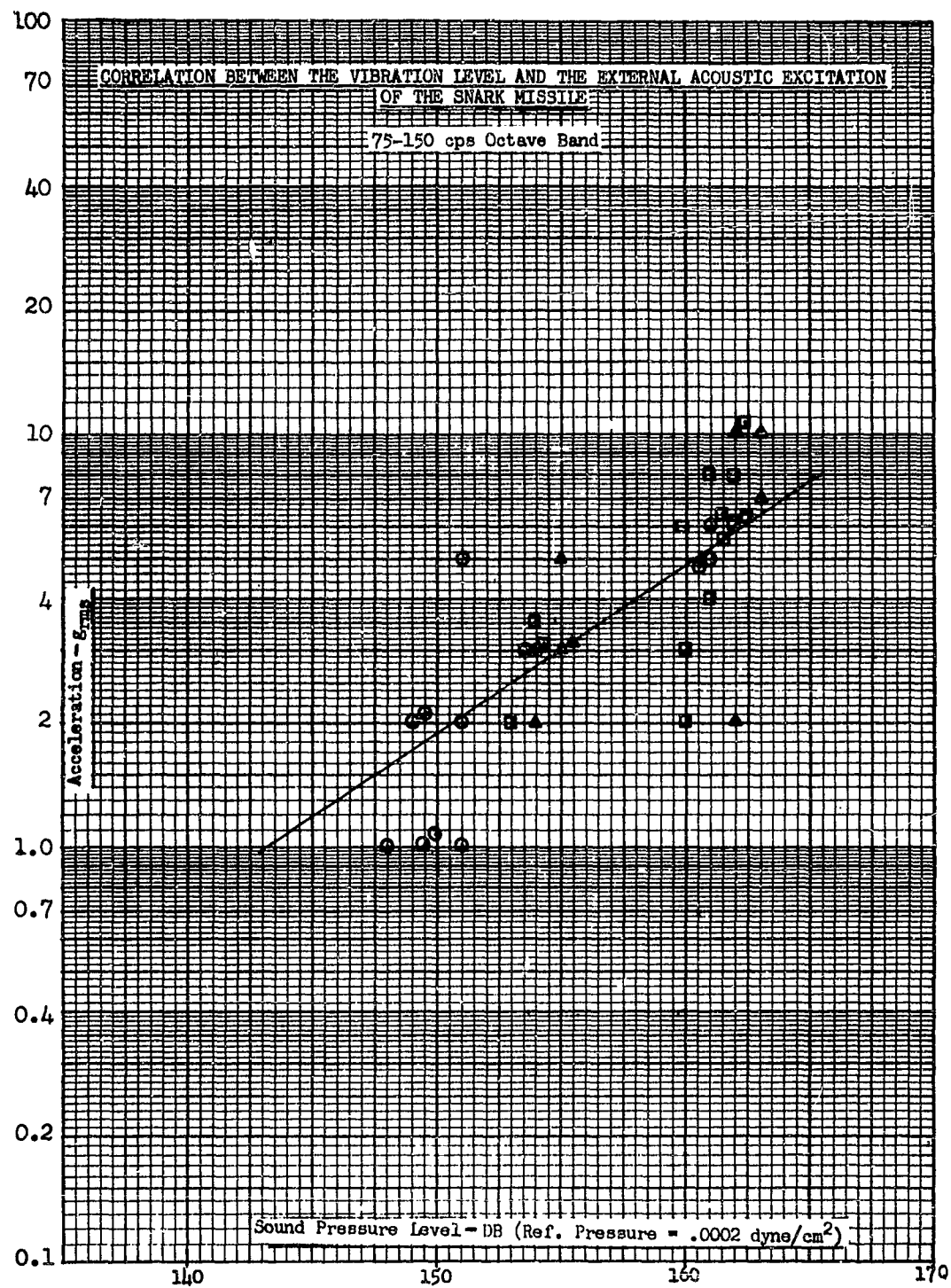


Figure 95. Correlation between the Vibration Level and the External Acoustic Excitation in the Snark Missile - 75-150 cps Octave Band.

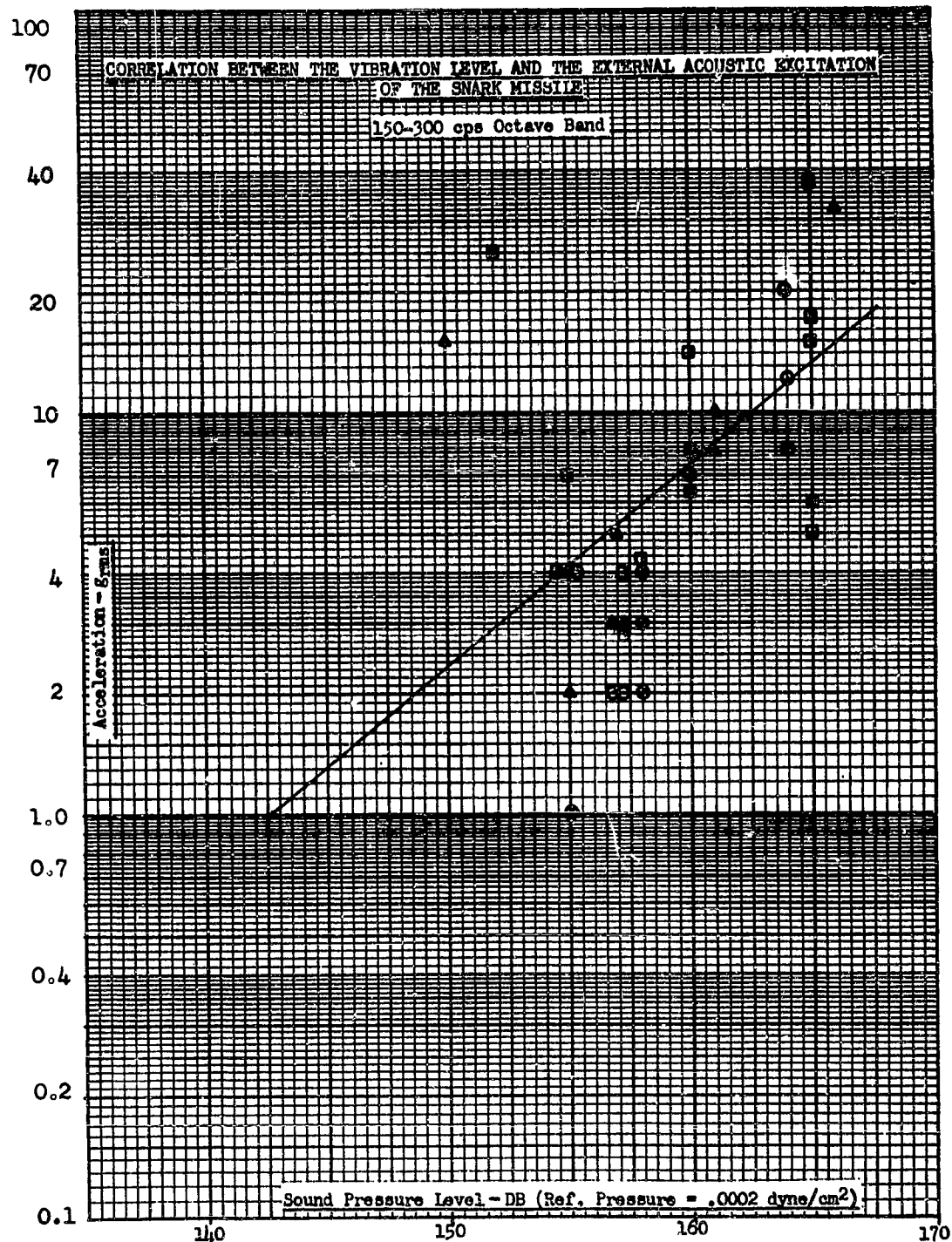


Figure 96. Correlation Between the Vibration Level and the External Excitation of the Snark Missile - 150-300 cps Octave Band

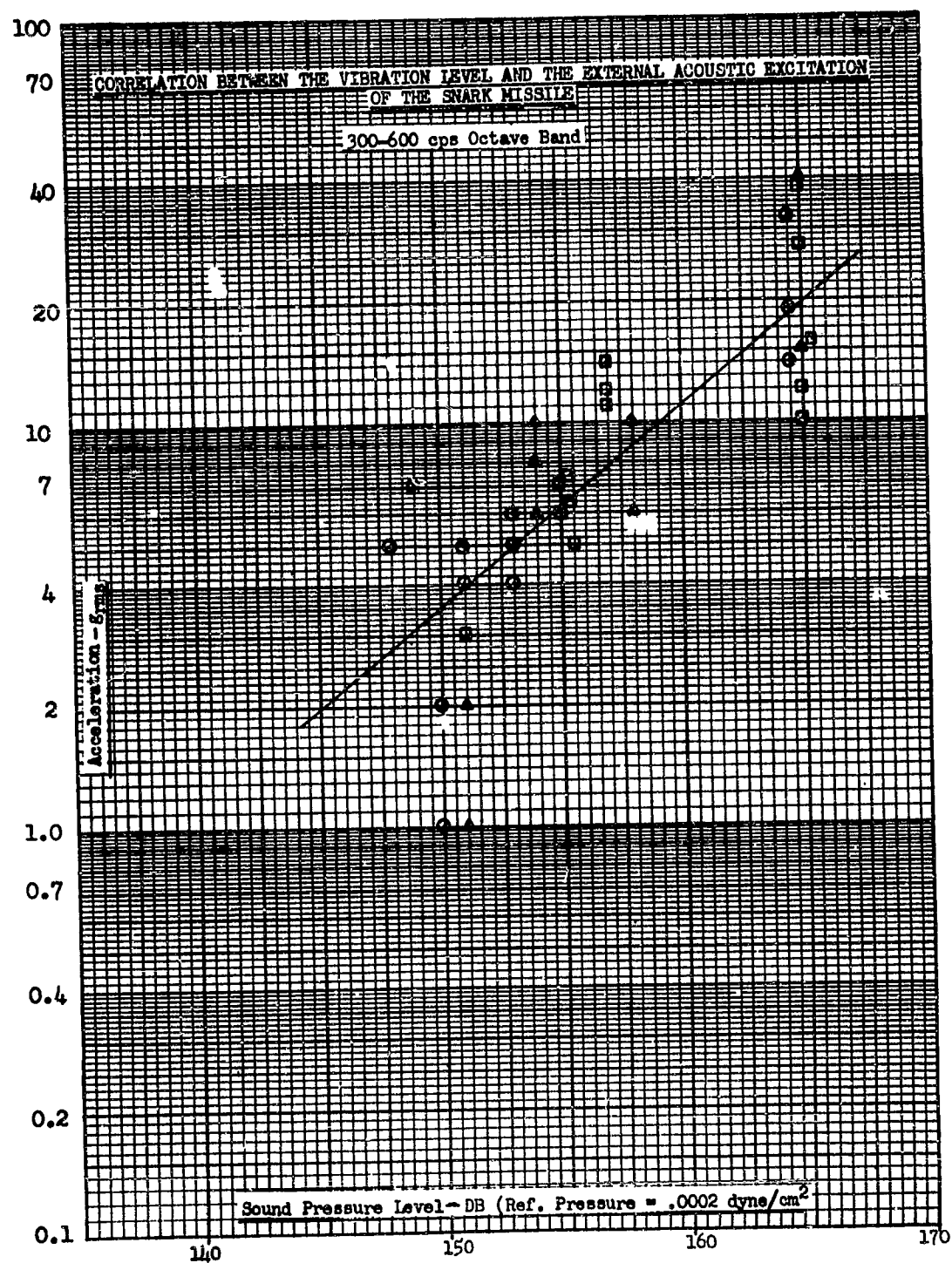


Figure 97. Correlation Between the Vibration Level and the External Acoustic Excitation of the Snark Missile - 300-600 cps Octave Band.

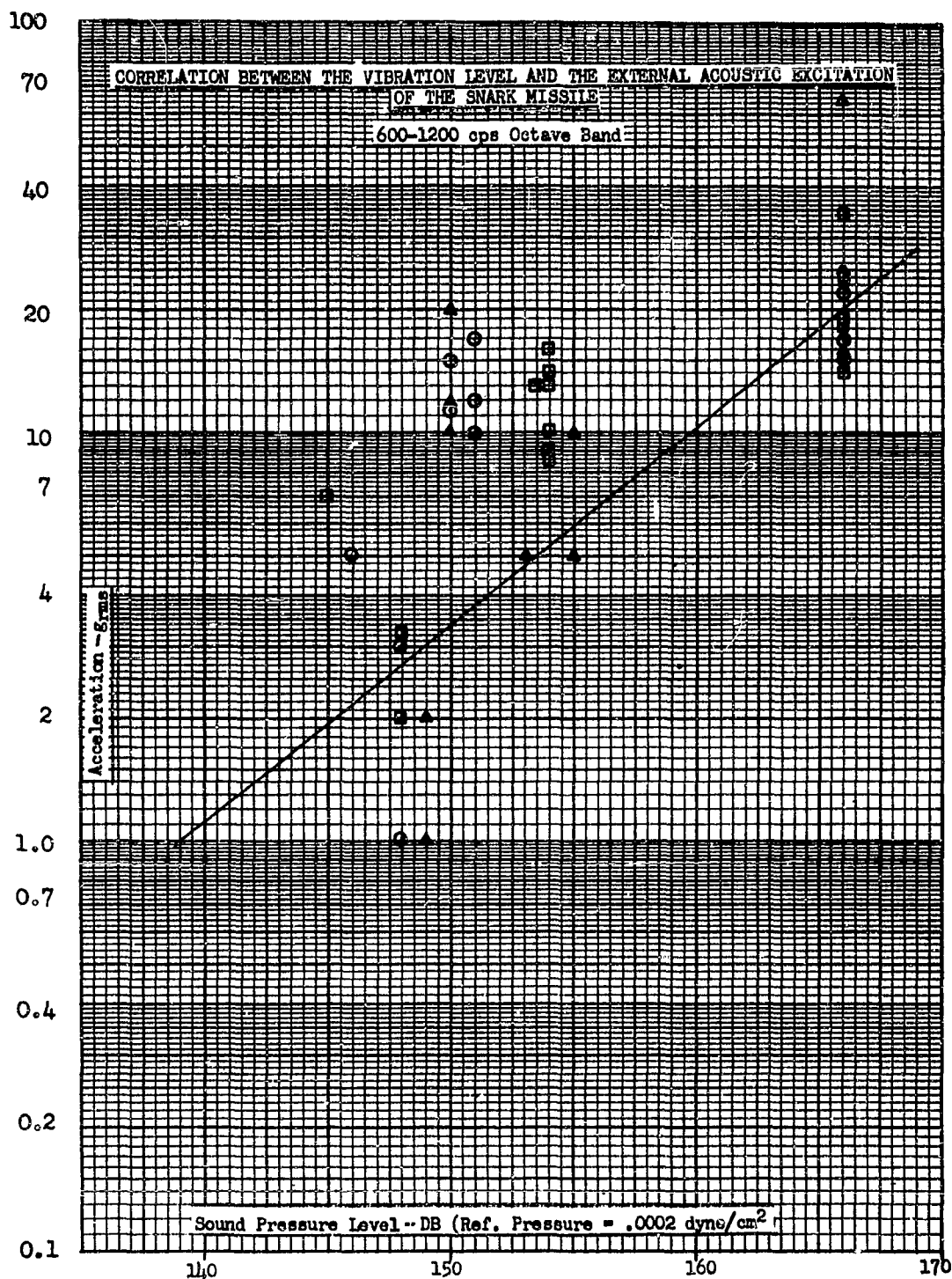


Figure 98. Correlation Between the Vibration Level and the External Acoustic Excitation of the Snark Missile - 600-1200 cps Octave Band.

However, if the trend line has a slope of less than unity, as is the case of the low frequency data for the Snark in Figures 93 through 95 and for the low frequency Convair data in Figure 99, a direct linear relationship between internal vibration and adjacent external sound pressure cannot be proved by the correlation. Several factors might, individually or collectively, be responsible for slopes less than unity. These factors include:

- (a) Structure borne transmission of vibration from high external noise level areas to those of lower external noise level.
- (b) Non-uniform structure throughout the fuselage (which undoubtedly contributes to scatter.
- (c) Non-linear response of the structure.
- (d) Unfortunate selection of transducer location with respect to modal response.

Before considering any of these factors in more detail, it is helpful to examine the slopes of the trend curves as a function of frequency. Figure 100 summarizes the results of this type of direct correlation for four aircraft-type structures, including the B-66 of Reference 29 together with Snark, B-58, and B-52. The upper portion of the figure gives the slopes of the trend curves and the lower portion of the figure gives the average rms acceleration for each octave band when the adjacent external octave band sound pressure level is 150 db. It is clear from Figure 100 that some correlation between adjacent external noise may exist above 150 cps for the Snark and at the higher frequencies for the other aircraft where the slopes of the trend curves approach unity. Since a large number of randomly selected transducer locations are included in the various surveys, it is doubtful that the accidental location of transducers with respect to the various vibration modes accounts for the lower slopes at the lower frequencies. Similarly, since several experiments give the same general conclusion with regard to the trend curves, it is not felt that structural non-uniformity is a particular factor in the determination of the slope of the trend curve, although it undoubtedly is a most significant factor in the scatter of the individual data.

The role of nonlinear behavior in the structure cannot be evaluated with respect to the trend curves from the available data. However, it is considered to be less important than the fact that the response at any general position in the structure is given by the sum of the noise energy transmitted directly to adjacent structure, plus the noise energy received at more remote locations and transmitted as vibratory energy through the structure to the position. Thus, at higher frequencies better correlation would be expected between adjacent acoustical excitation and response because the vibrational energy transmitted through the structure from remote locations has been attenuated and makes only a minor contribution. Conversely, at low frequencies the vibrational energy transmitted from the areas which have the highest external noise levels to those with lower external noise levels would be expected to exceed the local excitation. This general result might be anticipated since the attenuation of vibratory energy transmitted by bending waves

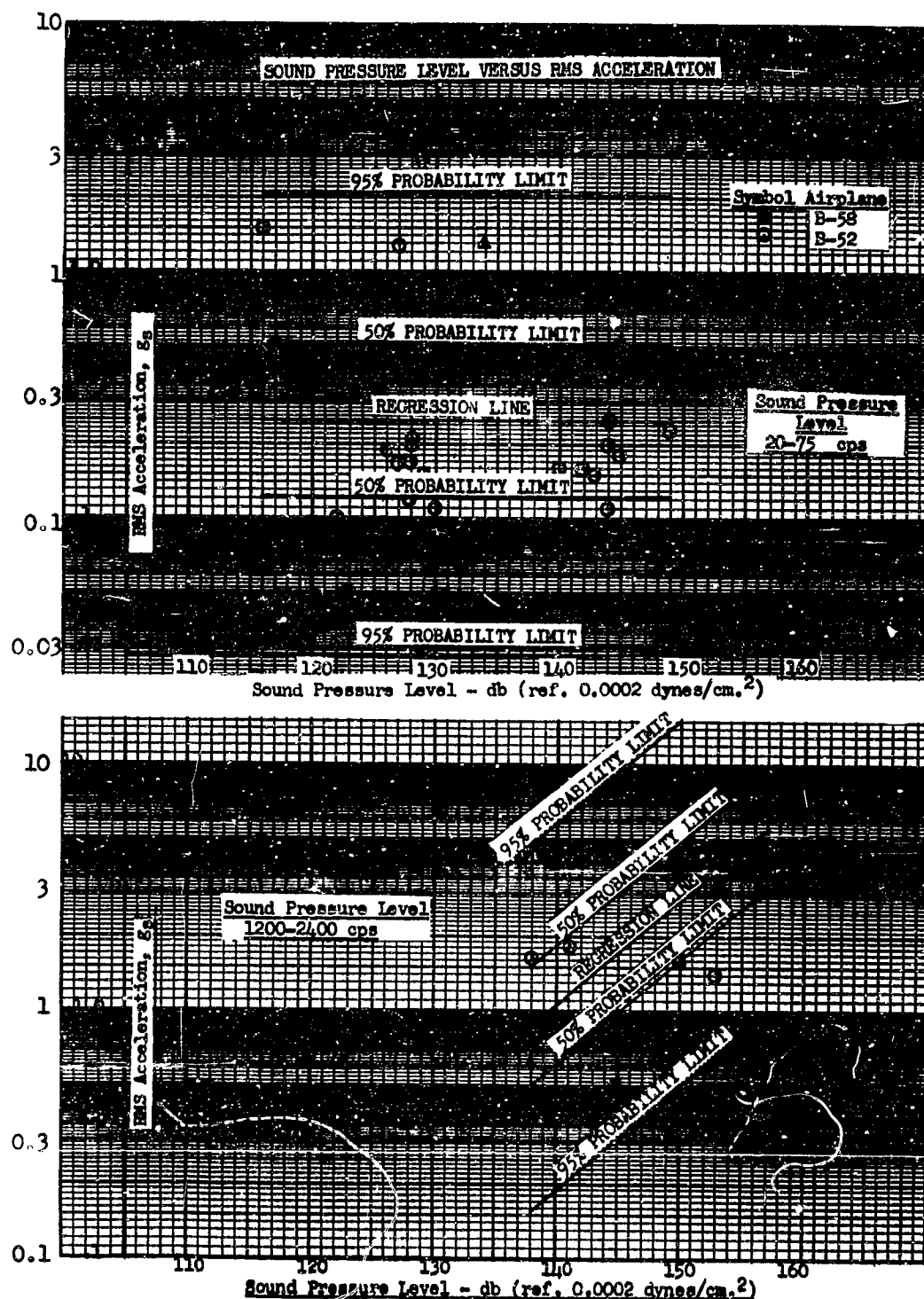


Figure 99. Sound Pressure Level vs. RMS Acceleration for Two Frequency Bands.

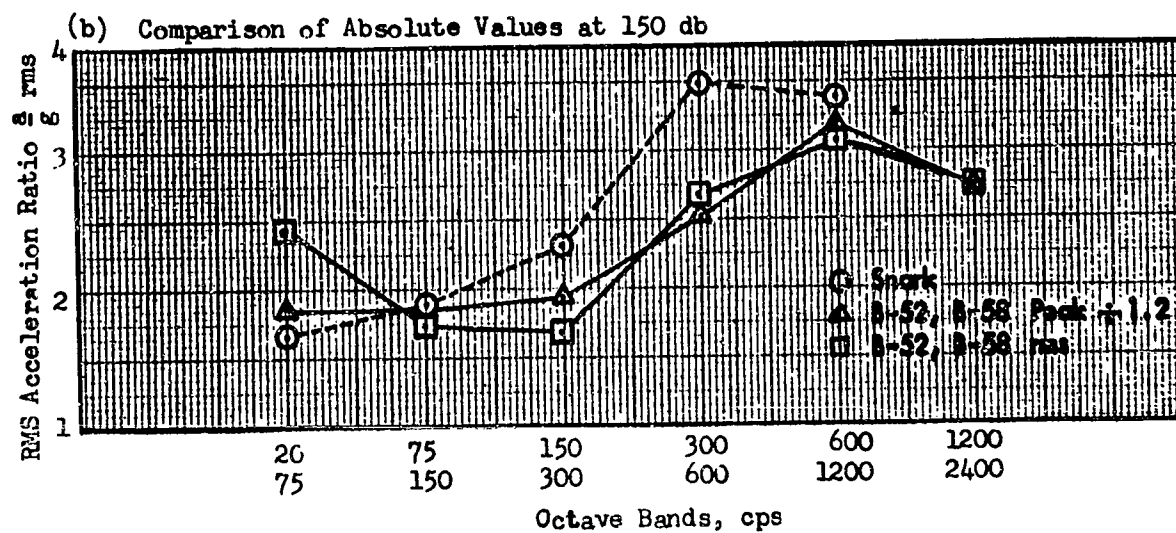
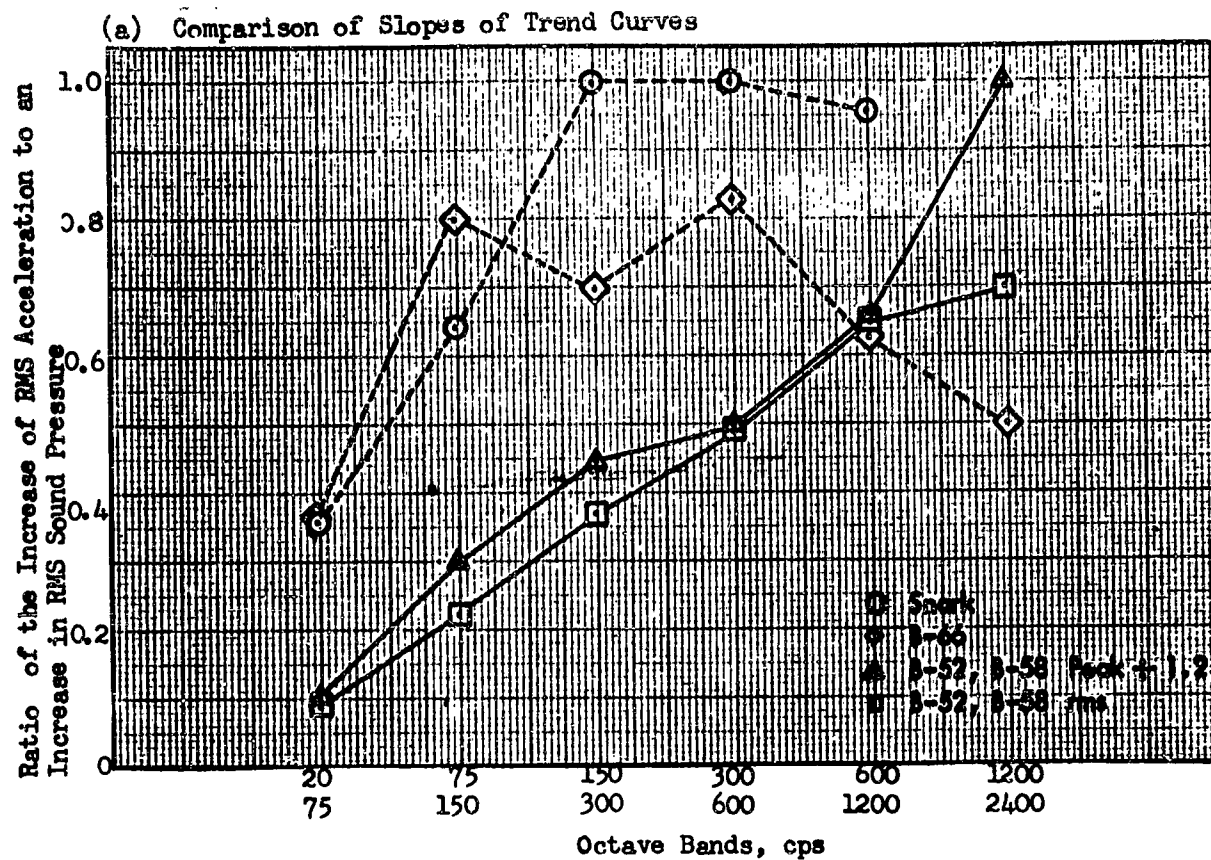


Figure 100. Summary of Aircraft Empirical Correlation of External Noise with Acceleration of Adjacent Structure.

along the fuselage is essentially constant per wavelength, as shown in Section IV from measured Snark data. Thus, the high frequency energy suffers considerably more attenuation than does low frequency energy when both are transmitted for the same distance through the fuselage.

It is felt that the results of this direct correlation technique are encouraging in the higher frequency range where a measure of correlation is achieved. Furthermore, the results point toward a method of summing the contribution to the response from local external excitation and remote external excitation. However, in the lower frequency range the results are essentially negative. Consequently, any application of these results in the prediction of aircraft vibration should proceed with great caution.

Correlation of Ballistic Missile Launch Noise and Response

The vibration data given in Figures 87 and 88 for structure forward of the engine area of ballistic missiles during both launch and maximum dynamic pressure flight, consistently showed that the vibration environment of the large and heavy missiles was significantly less than the vibration of the smaller and lighter missiles. This suggests that the next generation of space vehicle launch platforms which are anticipated to be considerably larger than the present ICBM's, might have even less severe vibration. On the other hand, changes in launch configuration, engine parameters, or maximum q could result in increases. It is, therefore, desirable to determine an empirical relationship between the response and the forcing function, appropriately modified by the vehicle's structural parameters.

It is believed that an empirical correlation can be found by equating the available energy of the forcing function with the mechanical energy of the resulting vibration. It is fundamental that these two quantities are related since all of the incident acoustical energy which is absorbed by the vehicle must result in vibration and be dissipated through damping. Unfortunately, the results of this approach have been inconclusive, probably indicating insufficient sophistication in the definition of one or more of the pertinent parameters.

However, an alternative approach to the correlation of the launch acoustical forcing with vehicle response appears to give encouraging results, and will be discussed in detail. As will be shown in subsequent sections, complicated (and even simple) structure has many resonances, distributed throughout the frequency range, which occur at frequencies above its fundamental resonance frequency. Consequently, the response of structure to a random forcing function, which has energy approximately equally distributed over a broad frequency range, exhibits many resonant peaks. Similarly, the majority of the missile launch data in Figure 87 is representative of the vibration amplitudes associated with one or more of the many resonances which occur in the missile.

It is well known that the natural vibration characteristics of many complex structures can be approximated by individual consideration of each resonance or mode of vibration, assuming it to be essentially unaffected by, or decoupled from, any other mode. The response of the vehicle in any one of these modes can be obtained

from expressions similar to those developed for the single degree of freedom if an appropriate definition can be obtained for the amount of the total mass which is involved in actual vibratory motion, and for the effective or "generalized force" on the vehicle. Viewed in this perspective, the total response of the vehicle at any location is simply the sum of the contributions from all of the vehicle's vibratory modes.

In Section II it was stated that the mean square displacement response of a single degree of freedom system to a continuous random forcing function was given by:

$$\overline{x^2} = \frac{Q w_n \overline{F^2(f)}}{4k^2}$$

where

$\overline{x^2}$ is the mean square displacement,

Q is one divided by twice the damping ratio,

w_n is the natural frequency in radians/second

$\overline{F^2(f)}$ is the mean square force per cycle per second, and

k is the stiffness of the system.

The mean square acceleration ratio $\left(\frac{a}{g}\right)^2$ associated with this response can be readily derived from (1) to give:

$$\left(\frac{a}{g}\right)^2 = \frac{w_n Q \overline{F^2(f)}}{4W^2}$$

where

W is the weight of the mass.

In order to apply this simple concept of the single degree of freedom system to the empirical correlation of multi-mode missile vibration, it is necessary to consider the relationship between the generalized force and generalized mass of the vehicle with the single forcing function and single mass in the single degree of freedom solution. As shown in Section IV, the generalized force on a panel in a space vehicle resulting from acoustic excitation depends, in addition to the actual magnitude of the sound pressure, primarily upon the spatial correlation of the sound pressure, or the distances over which the pressure is in phase, in relationship to the distance between nodes in the panel's bending response. It is also known that when acoustic phenomena are similar, except for a scale factor, their spatial correlations are similar when compared on a wave number basis. Here the nondimensional wave number ($k*r$) is equal to the number of radians per unit distance $\left(\frac{W}{a_0} = k^*\right)$ times

a distance characteristic of the size of the object or missile. Here, k^* equals the wave number ($1/\lambda$, λ = wave length), w equals the frequency, (rad/sec), and a_0 equals the speed of sound. For the purpose of this correlation, r is defined as the radius of the vehicle, and it is assumed that the spatial correlation is essentially similar at launch for geometrically similar vehicles and similar launch configurations when compared at equal values of k^*r .

Continuing with the panel, the natural frequency of any mode of two geometrically similar panels varies inversely with the ratio of the panel dimensions (or the scale factor). Consequently, since the distance between nodes on the panel varies directly with the scale factor, the relationship between the scaled spatial correlation of the sound pressure and the scaled shape of the bending panel remain unaltered when compared on a constant kr basis. It can also be shown that the generalized mass of the scaled panel would be the same proportion of the total mass for the same mode of vibration. Hence, it would be expected that any empirical correlation for geometrically similar structures would be a function of (k^*r) and that for this purpose, (2) should be written

$$\left(\frac{a}{g}\right)^2 = \frac{\beta^2 w_n Q F^2(r)}{k W^2}$$

where β^2 represents the constant of proportionality for all factors in Eq. (2) and is a function of (k^*r) .

It is clear that both the damping in the structure and the type of structure will affect any correlation of response with forcing function, as both additional damping or additional stiffness in a specific vehicle will reduce the response for a fixed forcing function. Therefore, in absence of sufficient data describing these two factors for the various missiles of Figure 87, a constant Q of 15 was assumed for all missiles and all natural frequencies. The missile weight (W) was taken as the gross launch weight, but the stiffness variable remains in the correlation as an additional unknown.

The forcing functions were calculated for surface launch of each of the eight missiles represented in Figure 87, utilizing Figures 8 and 13 from Part I, together with the appropriate engine parameters. The actual value of mean square force per cps was obtained by integrating the predicted mean square pressure per cps over the entire vehicle to determine the average mean square pressure per cps on the vehicle and multiplying this result by the square of the vehicle's surface area. It is obvious that this quantity cannot represent the true generalized force on the vehicle, but it should be proportional to the generalized force for constant values of k^*r . Eq. (3) was then solved for β for each of the $(\frac{a}{g})$ data points in Figure 87.

The results are given as a function of k^*r in Figure 101 and as a function of frequency in Figure 102. The correlation appears only slightly better when compared with wave number rather than frequency, but certainly cannot lead to a definite preference.

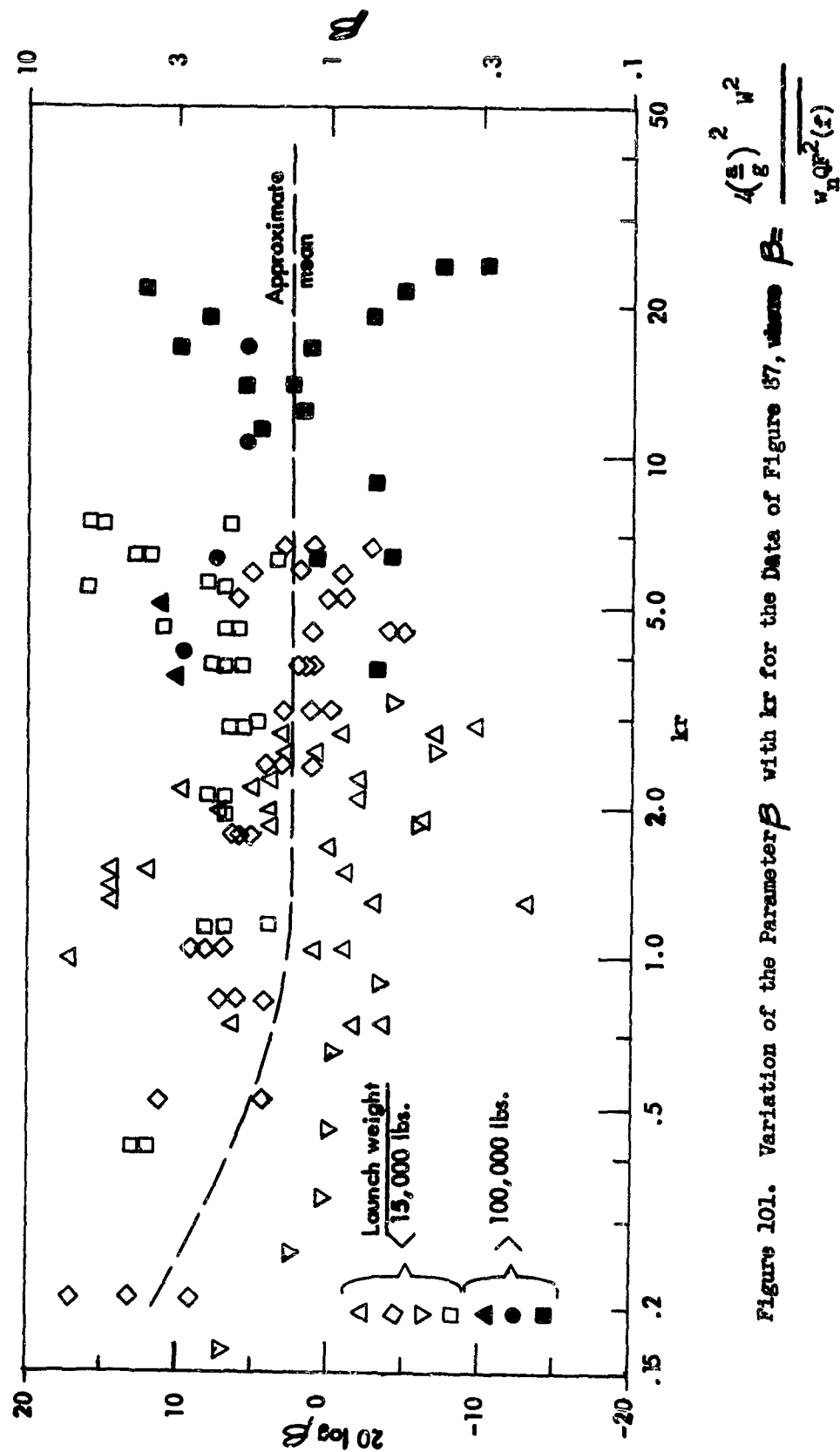


Figure 101. Variation of the Parameter β with kr for the Data of Figure 87, where $\beta = \frac{4 \left(\frac{\pi}{g}\right)^2 w^2}{v Q R^2 (x)}$

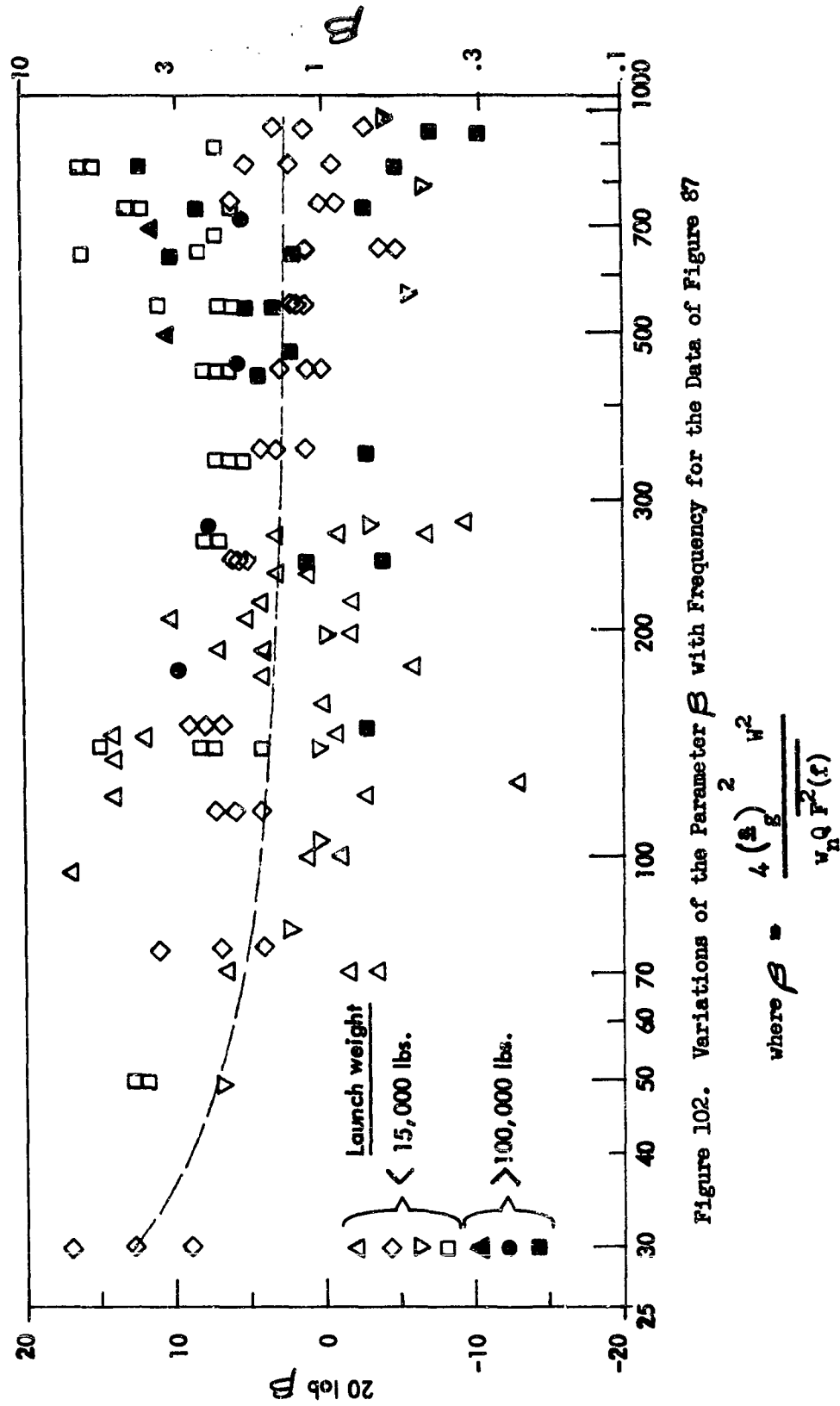


Figure 102. Variations of the Parameter β with Frequency for the Data of Figure 87

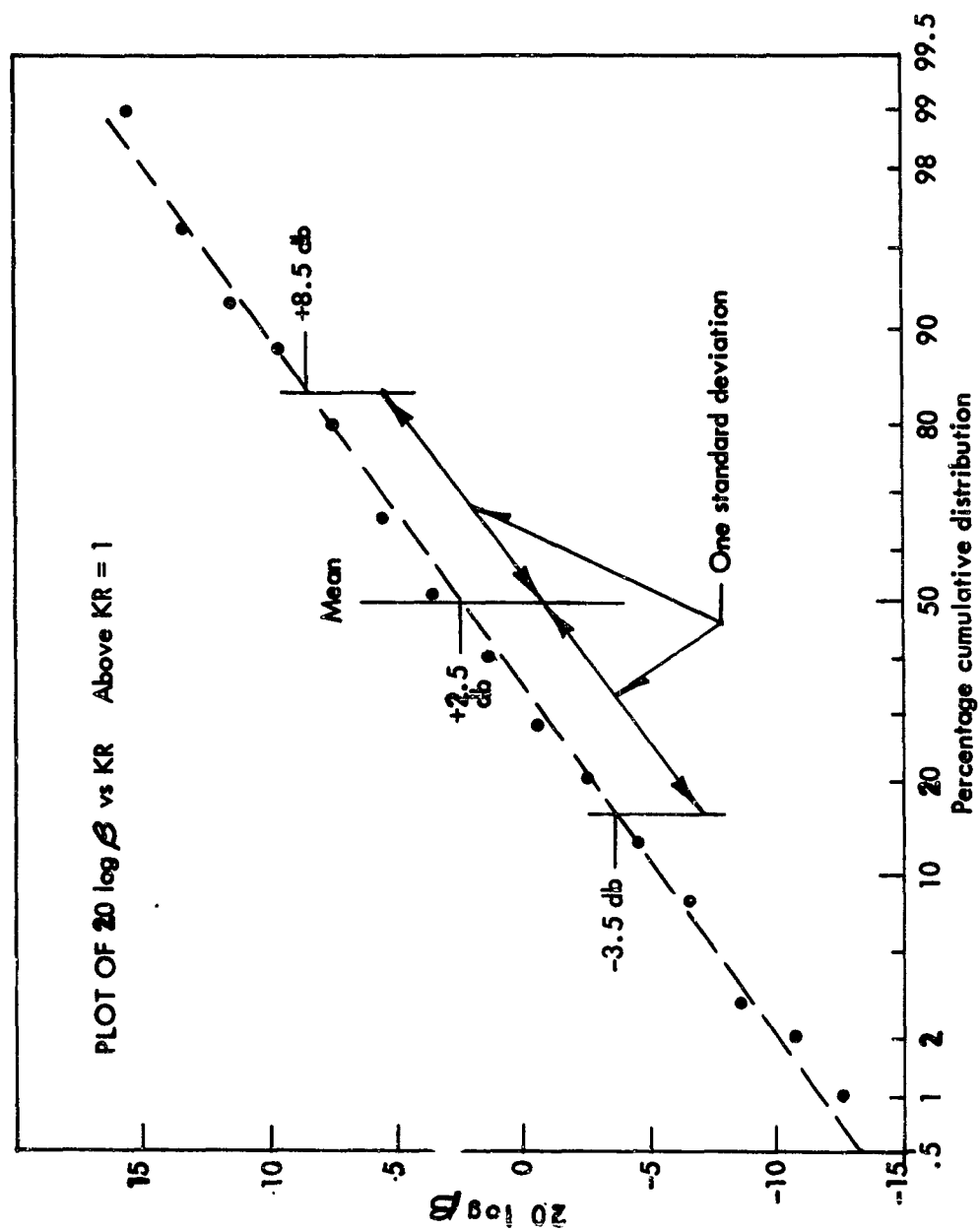


Figure 103. Cumulative distribution of data from figure 101 for $KR \geq 1$.

Considering Figure 101 β appears to be almost constant, slowly decreasing with increase wave number. The standard deviation of $20 \log \beta$ is approximately 6 db, which indicates that 68% of the values of β are between .5 and 2.0, as seen in the histogram of Figure 103. Although it would be desirable to effect a reduction in the scatter of the values for β , it is actually somewhat surprising that the scatter is so small when all the assumptions are considered. Several comments are pertinent, including:

First, it is improbable that all of these missiles are dynamically similar, since a wide variety of structural design concepts are represented.

Second, the forcing functions have been estimated through necessity, as insufficient measured launch noise data has been made available. While it might be thought that the use of an estimator rather than measured data would help to insure consistency, the estimation did not consider minor and largely unknown variations in rocket deflectors and other configuration details.

Third, it was assumed that Q has a constant value of 15 for all missiles and all frequencies where Q probably varies between one-half and twice this value.

Fourth, it is well known that the launch noise environment has a relatively short duration and that the response cannot always be considered stationary from the statistical viewpoint. Consequently, variation in response can be expected at the same location for different launches or short duration engine runups.

Fifth, the scatter at various transducer locations and various flights of one missile is seen to be almost as great as the total scatter in the figure.

When these and other factors are considered, the results of this correlation are encouraging. Perhaps the most startling result is the fact that the mean value of β is approximately one, as in the single degree of freedom case. This indicates that the ratio of generalized force to generalized mass remains constant with wave number, and that the method of obtaining the forcing function fortuitiously gives the ratio exactly equivalent to the single degree of freedom case.

It would be highly desirable to test this empirical correlation with additional data and, wherever possible, substitute measurement for calculation and assumption. It would be desirable also to test an extension of these concepts to the maximum dynamic pressure portion of flight; however, the necessary flight parameters were not available for such an extension. In lieu of this test, it appears that the value of β in Figure 101 could be utilized, together with the boundary layer pressure fluctuation forcing function in Section III of Part I, to estimate this response.

As a final note on the broad trend exhibited between vibration amplitude and weight of missile, the data obtained in the calculations indicated that the mean square acceleration at a constant value of kr varies roughly inversely with the square of the radius of the missile, or inversely with the two-thirds power of the gross weight. This relationship, illustrated in Figure 104, is subject to innumerable

restrictions and should be interpreted only in this vein. For example, a change in launch configuration to a silo might bring a five-fold increase in the vibration, or less, depending upon the acoustical treatment in the silo. Also, a change in the thrust-weight ratio, mass-stiffness ratio, damping, type of rocket stream, etc., can each affect this generalization, and should be interpreted analytically with Figure 101 as a possible guide or reference.

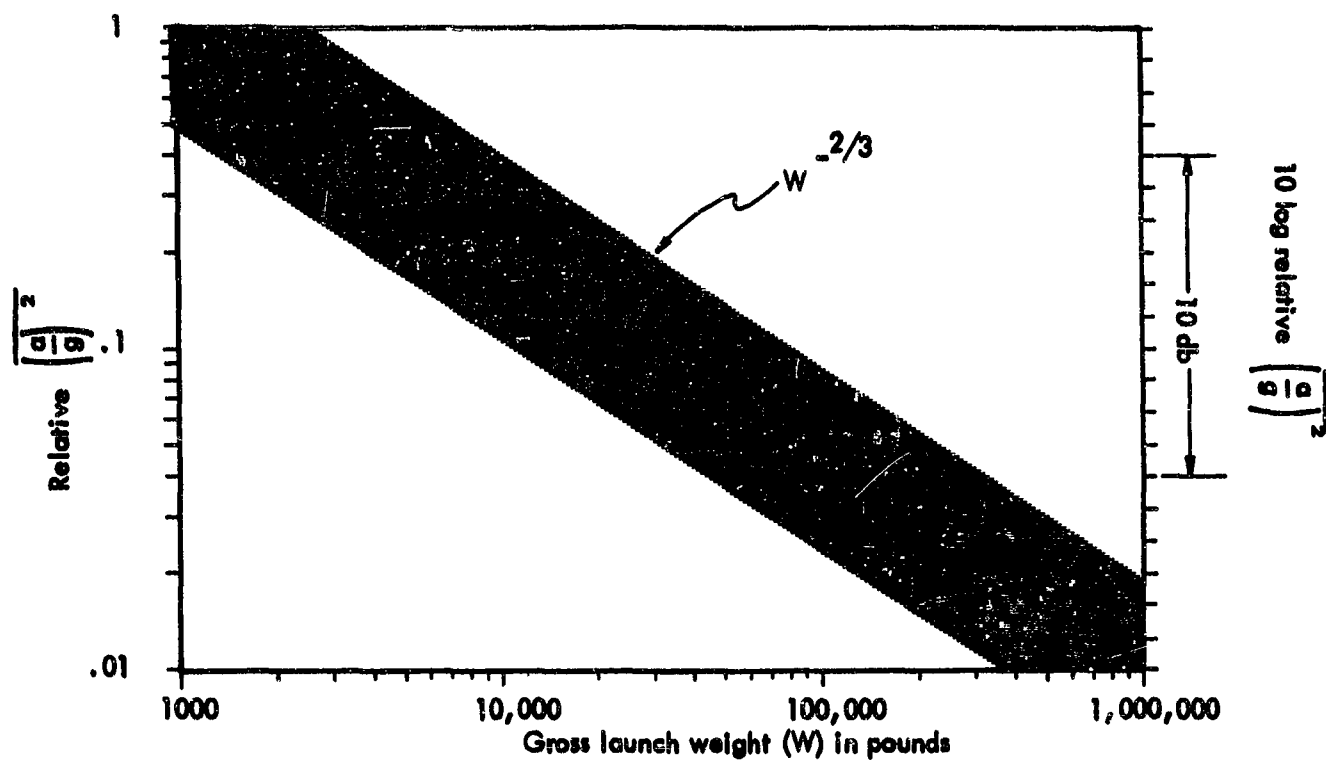


Figure 103a. Approximate Trend for Surface Launch Acceleration as a Function of Gross Launch Weight Based on Present Vehicles and Engines.

REFERENCES

1. Blake, R., and Paul, V., "Experimental Method of Determining Dynamic Response Characteristics of Missile Structure," Lockheed, LMSD-2955.
2. Boulton, V. R., "Measurements of Rocket Thrust at Frequencies to 4000 cps" SVB #20, May 1953.
3. Crandell, Measurement Chapter, "Random Vibration." Technological Press, 1958.
4. Symposium on High Intensity Noise Measurement, Acoustical Society of America Fall Meeting, San Francisco, 1960.
5. Gold, P. D., Francis, J. J., and Eldred, K. M., "Resume of Application of Vibration Engineering to the Solution of Marine Operational Problems Encountered by Naval Vessels," 1953 Transaction of Society of Naval Architects and Marine Engineers.
6. Lunney, E. J., and Crede, C. E., "Establishment of Vibration and Shock Tests for Airborne Electronic Equipment," WADC TR57-75, January 1958.
7. Eldred, K. M., "Analysis of Noise Data for Convair, Pomona, Tartar LTV-1, SN-3 and SN-6," P. S. Veneklasen & Associates report dated 10 September 1958.
8. Gates, C., "Environment of Corporal Missile XSSM-A-17," JPL Progress Report 20-185, April 1953.
9. Blake, R., and Oleson, M., "Vibration Data Obtained During Firings of Vanguard," NRL Report 5102, plus memos 6261-292, -315, and -46 from October 1957 to February 1958.
10. Beckwith, H., and Douglas, D., "Vibration Data on Thor," Space Technology Labs, TR-59-0000-00566, January 1959.
11. Morrison, S., Beckwith, H., Vargas, R., Douglas, D., "Vibration Data for Thor," No's. 112, 114, 115, 117, 118, 119, 123, 126, 138, 140, 146, 164, and 176 STL Reports.
12. Douglas, D., "Quick Look," Vibration Report of Titan A-5, STL Report, March 1959.
13. Mains, R., "Flight Vibration Measurements from Talos," Johns Hopkins Report APL/JHV, CF-2284.
14. Kuoppamaki, K., Burns, L., Lewis, R., "Program for Determination of Polaris Vibration Environment," Lockheed LMSD 480002, May 1959.

15. Cameron, B., "Report of Polaris FTV-1 Series Vibration Environment," Lockheed LMSD 460029, September 1958.
16. Blake, R., "Report of Polaris FTV-1 Series Vibration Environment," Part II, January 1959.
17. Paul, V., "Predicted Flight Vibration and Acoustic Environment of Polaris," Lockheed LMSD 461291, October 1958.
18. Cameron, B., "Preliminary Analysis AX-6 Structure," Lockheed DD 16920, July 1959.
19. Beckwith, H., "Vibration Data on Atlas Series A," STL GM-TR-0165-0048, September 1959.
20. Hines, M., Beckwith, H., and Douglas, D., "Vibration Data for Atlas #3B, 4B, 5B, 8B, 9B, 11A, 11B, 13A, 15A, 16A," STL Reports October 1958 to November 1959.
21. Fine, A., and Bell, D., "Captive Firings of Terrier," NOLC Report 215, September 1955.
22. Tatum, G., and Delaney, B., "Review of Shock and Vibration Test Requirements for Terrier," Vitro TR-34, February 1952.
23. Beckwith, H., "Vibration Data on Final Stage Able-1," STL Report, July 1958.
24. Convair Report FZS-4-149, "Method for Predicting B-58 Vibration Environment," October 1957.
25. Convair Report FZM-4-803, "B-58 Environmental Vibration Qualification Tests," February 1958.
26. Convair Report FZS-4-160, "B-58 Predicted Vibration Environment and Vibration Range Curves for Environmental Test," February 1958.
27. Egbert, D. T., and Harter, W. W., "Vibration and Acoustic Environment Measurements as Applied to Snark Missile Equipment," SVB #24, February 1957.
28. Mustain, R., and Vernier, B., "Snark Acoustic and Vibration Data Analysis," Northrop Report NAI-56-686, Vol. I & II, 1956; N69D Missile N3305, November 1956; NAI-57-583, November 1957; NAI-57-582, "Internal Acoustical Treatment," January 1958; NAI-57-584, "Salted Grain Booster Bottles," July 1958; NAI-59-25, "Summary of Acoustic and Pressure Data Booster Blast Off Program," December 1958.
29. Kennard, D. C., Jr., "Some Vibration as Exemplified by the RB-66B Airplane," WADC Technical Note 59-158, May 1959.

IV GENERAL CONCEPTUAL APPROACH TO STRUCTURAL VIBRATIONS

INTRODUCTION

The purpose of any investigation of the structural vibration of space vehicles is ultimately to determine the reliability of the structure and the on-board equipment through the prediction of fatigue life and load carrying capacity of the structural elements and the ability of equipment to properly function under the induced vibration. Both engineering analysis and direct testing are used to supply the needed information to determine this reliability. Analysis is generally used where relatively simple mathematical models of the structure and the applied forces provide sufficiently accurate results. Tests are used where such ideal models fail to account for certain significant parameters which involve complexities in the structure and the vibration stimulus. It is generally more desirable to have analysis and test complement each other by providing an independent check over common areas. This adds to the reliability, and often to the accuracy of the data obtained. Analysis further provides a basic insight into the physical character of a given problem area, thus providing a basis for developing still better prediction methods and also providing for the improvement of testing procedures. It is felt, therefore, that the breadth of prediction by analytical techniques should be increased to account more accurately for the various parameters affecting structural response.

It is intended in this chapter to consider the structural response problem from a conceptual approach, and thereby to show what information generally is required to predict response and to present in a broad form the equations that should be used to obtain this result. A flow diagram has been constructed in Figure 104 which contains, in block form, a summary of the specific type of data that would be available at each step of an ideal vibration analysis. Also included in this diagram are the symbols chosen to represent each block of data and the general relationships which exist between the various groups of data.

For most engineering vibration problems, a complete knowledge and description of the source of excitation, the applied force, and the structural mobility will not be available, nor will the actual mathematical relationships be as simple as those shown—these may not even be defined mathematically. However, the diagram and the discussion have been made sufficiently general to cover most of the significant vibration problems of concern, and they are further made fairly complete so as to permit a better assessment of how far some present analyses are forced to deviate from an accurate prediction method.

A short discussion of excitation sources is given which essentially discusses the distinction between the actual disturbance source and the applied forces and pressures acting on the structure, showing the need, in some problem areas, for defining a transfer function relating these two. This is felt to be important since during flight the characteristics of the mechanism of transfer may change. A discussion is then given of the forcing function used to define these applied forces and pressures. Since these forces are generally random in nature, the statistical

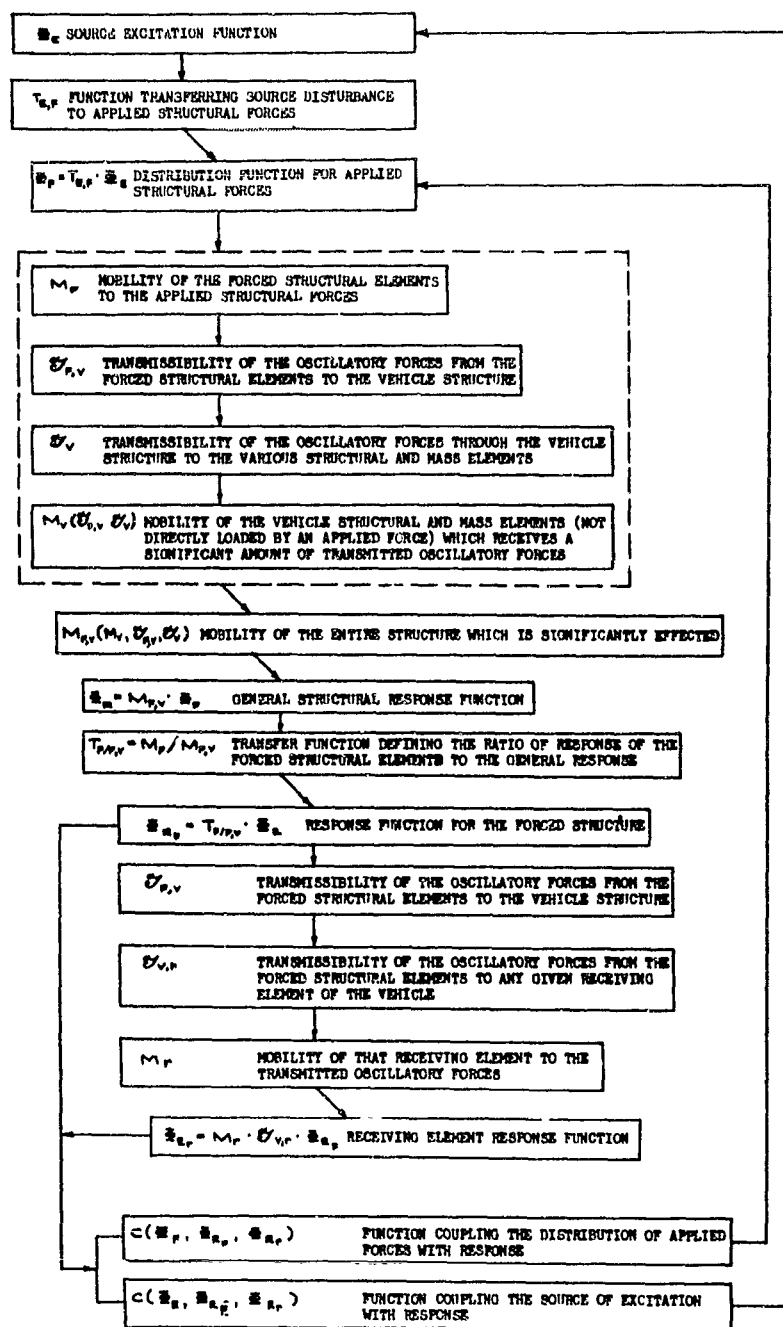


Figure 104. General Vibration Flow Diagram From the Source of Excitation to Final Response.

properties of the forcing function are discussed in detail in order to show generally what information is required to define the forces and how this information may be obtained. The physical interpretations of the various statistical parameters used, such as power spectral density functions, mean square averages, auto- and cross-correlation functions, are discussed which lead to a derivation of the equations for the time correlation coefficient. The next discussion considers the interpretations of space-time correlation coefficients for fluctuating pressures over the surface of the vehicle. Equations are then presented for the generalized force input to the structure in terms of these space-time correlation coefficients which lead naturally to the definition and equation for the commonly used quantity called joint acceptance. The joint acceptance of a panel acoustically excited is presented. Once the applied forces are fully defined, it is possible to discuss the mobility of the structure to these forces and the general problem of determining structural response, which discussion is presented next. In order to bring these various concepts into focus on an actual problem, the vibrations of a panel to far-field acoustic excitation are discussed along with a derivation of the governing equations. The discussion in this section is then concluded with the presentation of a special case of the two degree of freedom problem--resonance-on-resonance.

EXCITATION SOURCES

Vibration excitation sources and their characteristics are discussed in detail in Part I report and are considered here only in a general fashion to show their role in the over-all vibration problem and to indicate possible areas of difficulty.

These sources of excitation can be divided into four major categories: acoustic noise, various types of aerodynamic disturbances, free atmospheric disturbances, and mechanical disturbances. Each of these categories consists of essentially different types of disturbances which create a wide variety of forces on the structure, and may include localized forces acting at fixed points, pressure disturbances over areas of the structure ranging from the relatively small to those of the entire vehicle external skin, and forces and pressures which are essentially stationary (spatially) or propagating over the structure.

Excitation sources are often defined by quasi-source parameters which do not always define the actual source phenomenon, but which partly describe the effects which these stimuli create on the structure. As an example, rocket engine acoustic excitation is often defined in terms of the distribution of sound pressure level over the skin. Also, rocket engine combustion instabilities are defined in terms of the force acting on some structural link attached to the engine.

Figure 104 shows a more detailed breakdown of the process which actually occurs. The phenomena causing the excitation are generally located either in the medium surrounding the vehicle or within on-board equipment and thus seldom occur directly on the structure. A propagation, or transfer, is required between the source and the structure in order for these to produce actual forces on the structure. The parameters presently being used to define a number of sources must therefore account for both of these effects. When more detailed information and a better understanding of the excitation sources are available, it may ultimately be desirable, where

practical, to separate the source parameters from the propagation or transfer parameters. As shown in Figure 104, Φ_E symbolizes very generally the function or functions which define the actual source, and $T_{E,F}$ represents the function, or functions which transfer the disturbance, defined by Φ_E , to forces on the structure.

It is usually assumed that the various sources of excitation can be considered as independent in predicting structural response. However, for similar types of sources, such as aerodynamic sources, coupling may occur which, because of nonlinearities, will produce a combined source whose characteristics are different from those of the original sources. For example, coupling may occur between attached shock waves, boundary layer disturbances, base pressure fluctuations, and acoustic noise. For refined predictions, such coupling effects may be of considerable interest.

The response of certain structural elements of the vehicle constitutes a second type of coupling which can alter the characteristics of the excitation source. This coupling is shown symbolically in Figure 104. Burning instabilities of liquid rocket engines, for example, may induce excitation of the fuel feed lines which in turn cause pressure fluctuations in the combustion chamber. Mechanically-induced vibrations originating within certain equipment items will feed back through the equipment and may, under some circumstances, alter the internal unbalanced forces causing the response. Skin panel response to boundary layer disturbances form another example of this type of coupling by altering the shape and thickness of the boundary layer and also by producing additional pressure fluctuations which travel downstream to further alter the boundary layer.

Response of the structure is also important in the production of new sources of excitation. The additional sources may in some cases be of secondary importance such as the acoustic noise generated within the closed pressurized vehicle by skin response to external acoustic excitation. On the other hand, response of the entire structure to free atmospheric disturbances can produce significant aerodynamic forces resulting from angle of attack changes which clearly are not part of the original source of excitation.

It is desirable therefore to isolate the source parameters from those of the propagation or excitation-to-force transfer parameters, and also to determine the source-to-source coupling, the response-to-source coupling, and the response-to-source initiation parameters. This may be very difficult to do at the present time and for many types of excitation and structures this may never be feasible. However, conceptually this does represent a more systematic approach to the over-all description of what is generally classified as excitation sources.

Since the sources of excitation often consist of random-type phenomena, the description of Φ_E must be statistical. For these cases, the transfer function, $T_{E,F}$, must carry the excitation statistical parameters over to the statistical description of the applied random forces. Since the statistical definitions used for different types of sources vary widely and since these are discussed in generalities in the Part I report, they are not discussed here.

STRUCTURAL FORCING FUNCTION

The purpose of Part I of this report, in addition to the general description of various sources of excitation, was to define as well as possible the actual applied forces on the structure. The present section is chiefly concerned with the parameters used to define the general force function, the statistical description of random forces, and possible response-to-force coupling that may occur.

The general forcing function, denoted by Φ_F , is shown in Figure 1Q as the product of the excitation function, Φ_E , and the excitation-to-force transfer function, $T_{E,F}$. This is a symbolic equation which merely indicates the combined effect of these two functions, and will not always be mathematically separable into the product form, except for very special cases.

The parameters used to define the general force function, Φ_F , are spatial distribution over the structure (including position, x , and direction, ψ), and the distribution with respect to time, t , of the oscillatory force (or pressure) amplitude, F , frequency, ω , and phasing, ϕ . Φ_F may therefore be represented as

$$\Phi_F(x, \psi, F, t, \omega, \phi)$$

The actual form used for Φ_F , in practice may vary, depending upon the definable properties of the applied force. If the applied force is random, Φ_F may be in the form of some statistical average such as the power spectral density function or correlation function. If the force amplitude, F , is definable in terms of position, x , direction, ψ , and time, t , then the more convenient mathematical form can be used,

$$F(x, \psi, t)$$

where the frequency, ω , and the phasing, ϕ , are implicit properties of this function.

The force function, Φ_F , may be well defined in terms of each of the above parameters, such as that shown in the following diagram, and expressed by the accompanying equation:



$$F(x, \psi, t) = \sum_{n=1}^n A_n(x, \psi) \cdot \cos(\omega_n t + \phi_n)$$

$A_n(x, \psi)$ = known functions of position, x , and direction, ψ .

If the force acts at a discrete set of points on the structure, then the functions, $A_n(x, y)$, will be discrete in the variables x and y . Such a force distribution may be due to the internally-generated vibrations of on-board equipment mounted at multiple attach points. If the force acting is in the form of a pressure over an area, then $A_n(x, y)$ will be continuous functions of x and y .

Generally, however, the force function is not well defined, and it is often known to be random in one or more of the parameters, since the excitation source phenomena causing the forces are usually random in nature. Random forces, or force components, are definable only in terms of the statistical averages of estimated or measurable properties of the force, such as the mean, mean square, correlation functions, and power spectral density functions. Well defined forces do not, in themselves, present any difficulty in the vibration response problem, and can usually be treated separately from the random forces. The remainder of this section is therefore concerned with the statistical description of applied random forces and/or pressures. The form of the force function, \hat{F} , that is used in the following discussion is $F(x, y, t)$ and other forms are presented in the terms of this one.

The force amplitude, $F(x, y, t)$, may have a random variation with respect to time, t , and with respect to its spatial distribution over the structure in terms of position x , and direction, y . Numerous examples of random variation with time and position exist among the various acoustic and aerodynamically generated forces acting on the vehicle surface. Random variation with direction, y , is not so common, since fluid media applied pressures act normal to the surface skin. If, however, the pressures are integrated over the surface to produce a net force, as in the case of lift and drag due to atmospheric gusts, the resulting force vector may have a random variation with direction. The statistical description of $F(x, y, t)$ must therefore consist of both time and space averages.

At the present time, only the first few time and space averages are used because of the limited quantity of accurate data available for a statistical analysis. A complete description of $F(x, y, t)$ can be given, however, only when all of the corresponding joint probability distribution functions and their dependence upon time are known. It would seem that such a complete description of random force functions will never be attained under any circumstances and fortunately, for practical engineering applications this will be unnecessary. However, improvements can and should be made to advance the state-of-the-art by investigating more statistical averages than are presently used. Justification for this lies in the fact that the accurate prediction of structural fatigue life depends upon the accuracy of response predictions, which can be made with no greater degree of certainty than that of the information used to describe the stimulus.

Statistical Properties of the Random Force, $F(t)$

Of the statistical averages presently used, the most common are concerned with the amplitude, $F(t)$, of an oscillatory, unidirectional random force acting at a fixed point, and which contains a continuous spectrum of frequencies with arbitrary phasing. Although the statistical averages are difficult and time consuming to obtain in practice (unless electronic computing devices are used), the necessary expressions and concepts are easily established.

Statistical averages must be determined from a sample of data obtained from repeated experiments or trials of the same random process. For the case being discussed, these sample data would consist of a set of N records, $F_k(t)$, ($k = 1, 2, 3, \dots, N$), obtained from measurements of $F(t)$ at some fixed point, x , and direction, γ , on the vehicle over the same time period for repeated flights of the same type vehicle. For example, a flush-mounted microphone located at a given position on the vehicle skin could record the amplitude variation of sound pressure level at x during numerous launchings or flights. Different vehicles (even the same type of vehicle in design and performance) will have slightly different characteristics and will often be launched under varying conditions of thrust, trajectory, weather, etc. The characteristics of the random process causing $F(t)$ will thus change from record to record and it may be impossible to obtain two records of the same random process. Unless the variation between the different records is very significant, the individual random processes occurring during each flight could be thought of as being part of a more general random process whose variation is sufficiently broad to include the variations between the different force amplitude—time records.

By knowing the time scale equivalence between the various $F_k(t)$ records, and by aligning these time coordinates along a vertical scale, the force amplitudes, $F_k(t)$, as shown below in Figure 105, constitute an "ensemble." This ensemble statistically represents the random process which characterizes $F(t)$.

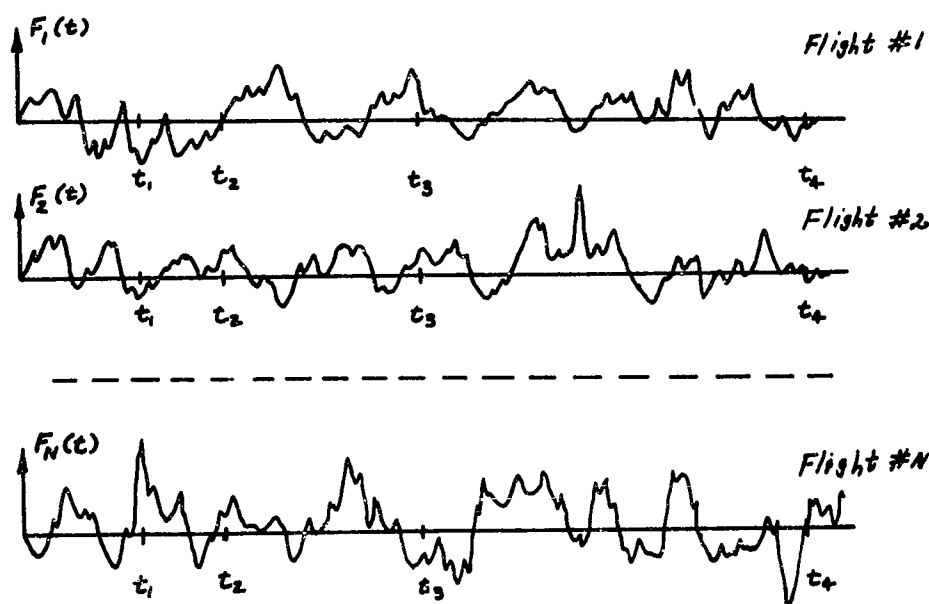


Figure 105: An Ensemble of Measured Time Histories of Force

Unless the simplifying assumptions of stationarity and ergodicity (discussed below) are imposed on this random process, the statistical averages of $F(t)$ will vary with time and hence must be determined from this ensemble by averaging over the amplitudes $F_k(t)$ for each fixed time, t_1 , say t_1, t_2, t_3, \dots . The mathematical expressions for the mean, mean square, standard deviation, autocorrelation function, and power spectral density function are listed below for a general nonstationary, non-ergodic force function $F(t)$. These expressions are given for the exact case in terms of known probability density functions, $P_F(\cdot)$, and for the approximate case where these are not known. The symbol $E[A]$ is used here to denote the expected or mean value of the random variable, A .

$$\text{Mean: } E[F(t_1)] = \overline{F(t_1)} = \int_{-\infty}^{\infty} z \cdot P_F(z, t_1) \cdot dz \approx \frac{1}{N} \sum_{k=1}^N F_k(t_1)$$

$$\text{Mean Square: } E[F^2(t_1)] = \overline{F^2(t_1)} = \int_{-\infty}^{\infty} z^2 \cdot P_F(z, t_1) \cdot dz \approx \frac{1}{N} \sum_{k=1}^N F_k^2(t_1)$$

$$\text{Standard Deviation: } \sigma(t_1) = \sqrt{\overline{F^2(t_1)} - \{\overline{F(t_1)}\}^2}$$

$$\begin{aligned} \text{Autocorrelation: } E[F(t_1) \cdot F(t_j)] &= \overline{F(t_1) \cdot F(t_j)} = \int_{-\infty}^{\infty} \int_{-\infty}^{\infty} z_1 \cdot z_2 \cdot P_F(z_1, t_1; z_2, t_j) \cdot \\ &\quad dz_1 \cdot dz_2 \approx \frac{1}{N} \sum_{k=1}^N F_k(t_1) \cdot F_k(t_j) \end{aligned}$$

$$\text{Power Spectral Density: } S_F(\omega) = \lim_{T \rightarrow \infty} 2 \int_{-\infty}^{\infty} e^{-i\omega\tau} \left[\frac{1}{2T} \int_{-T}^T F(t) \cdot F(t+\tau) \cdot dt \right] \cdot d\tau,$$

where t_1 corresponds to t , and t_j corresponds to $t+\tau$.

$P_F(z, t_1)$ is the probability density function for the amplitude, $F(t)$, at time $t=t_1$, and equals the probability that at $t=t_1$ the amplitude F lies in the interval

$$z < F < z + dz$$

$P_F(z_1, t_1; z_2, t_1)$ is the joint probability density function for $F(t)$, which equals the probability that F lies in both of the intervals,

$$z_1 < F < z_1 + dz \quad \text{at} \quad t = t_1$$

$$z_2 < F < z_2 + dz \quad \text{at} \quad t = t_1$$

The $P_F(\)$ functions are obtained by sampling the various $F_k(t)$ records for fixed values of $t = t_1$, and constructing the usual relative frequency-of-occurrence graphs. Such a graph is shown in Figure 106 below for approximating $P_F(z, t_1)$.

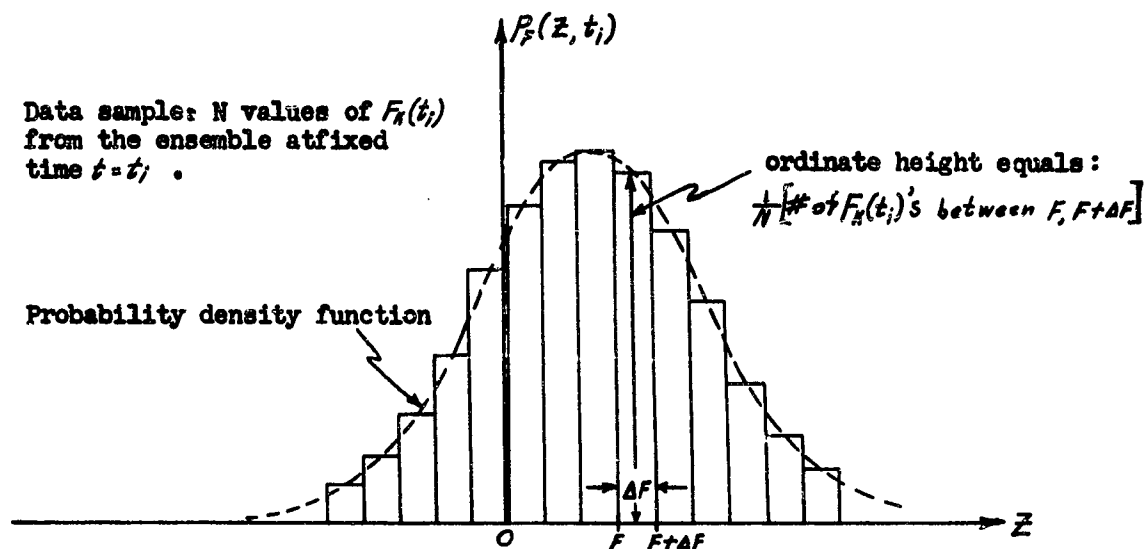


Figure 106: Histogram for Approximating the First Probability Density Function

The joint probability density function, $P_F(z_1, t_1; z_2, t_1)$, is a function of two variables, z_1 and z_2 , and hence is geometrically described by a surface. This surface is approximated in the same manner as the curve shown above, except that the increment ΔF must be replaced by the area increment $\{\Delta F, \Delta F'\}$ as shown in Figure 107.

The larger the data sample size, N , and the smaller the amplitude intervals tested (i.e., the smaller the ΔF or the smaller the $\Delta F \cdot \Delta F'$ area) the more accurately the force probability density functions can be determined.

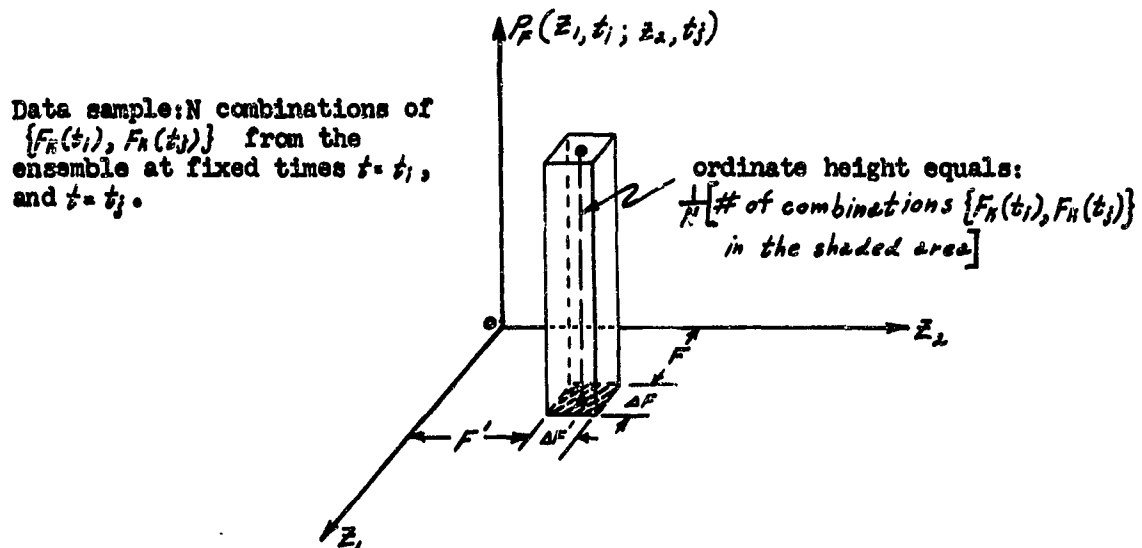


Figure 107: Method for Determining the First Joint Probability Density Function

It is clear from the above discussion how the higher order ensemble statistical averages of $F(t)$ can be obtained. The mathematical expressions for a few of these are:

$$E[F^n(t_1)] = \int_{-\infty}^{\infty} z^n \cdot P_F(z, t_1) \cdot dz \propto \frac{1}{N} \sum_{k=1}^N F_k^n(t_1), \quad n = 1, 2, 3, 4, \dots$$

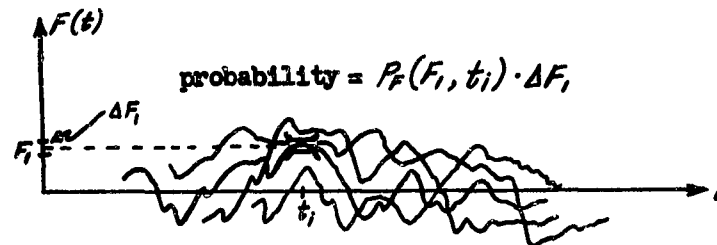
$$E[F^n(t_1) \cdot F^m(t_2)] = \int_{-\infty}^{\infty} \int_{-\infty}^{\infty} z_1^n \cdot z_2^m \cdot P_F(z_1, t_1; z_2, t_2) \cdot dz_1 \cdot dz_2$$

$$\approx \frac{1}{N} \sum_{k=1}^N F_k^n(t_1) \cdot F_k^m(t_2), \quad n, m = 1, 2, 3, 4, \dots$$

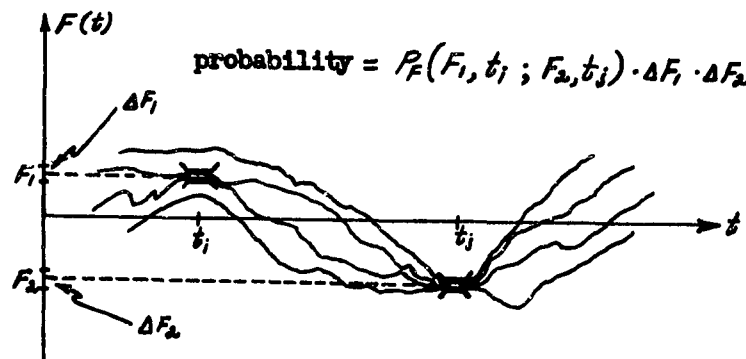
$$E[F^n(t_1) \cdot F^m(t_2) \cdot F^r(t_3)] = \int_{-\infty}^{\infty} \int_{-\infty}^{\infty} \int_{-\infty}^{\infty} z_1^n \cdot z_2^m \cdot z_3^r \cdot P_F(z_1, t_1; z_2, t_2; z_3, t_3) \cdot dz_1 \cdot dz_2 \cdot dz_3$$

$$\approx \frac{1}{N} \sum_{k=1}^N F_k^n(t_1) \cdot F_k^m(t_2) \cdot F_k^r(t_3), \quad n, m, r = 1, 2, 3, 4, \dots$$

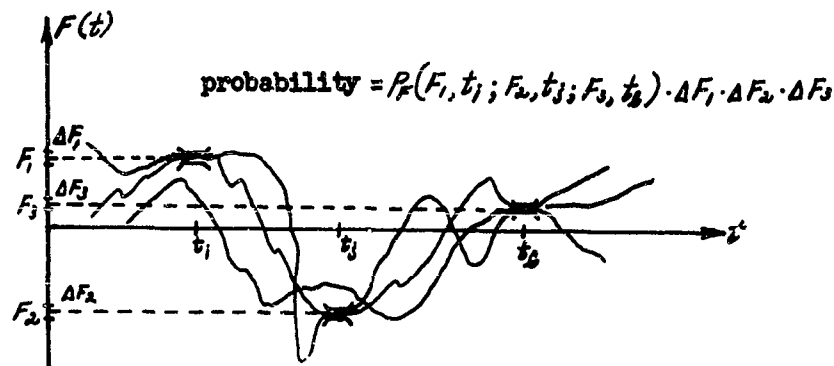
A very simple interpretation of these probability density functions can be given which shows how the statistical properties of $F(t)$ are defined in increasing detail with a knowledge about the higher order joint probability density functions, Reference 1. The following diagram illustrates the probability, $P_F(F_1, t_1) \cdot \Delta F_1$, that $F(t)$ passes through the narrow slit, $(F_1, F_1 + \Delta F_1)$ at $t = t_1$. For a complete description of $F(t)$, this information will be known for each value of t .



The next diagram illustrates the probability that $F(t)$ passes through two slits, $(F_1, F_1 + \Delta F_1)$, $(F_2, F_2 + \Delta F_2)$ at $t = t_1$ and $t = t_2$ respectively.



Similarly, for the third order joint probability density function.



The more joint probability density functions that are evaluated and the more combinations of times used in this evaluation, the more accurately Φ_F will be defined.

In order to simplify the problem of obtaining the above ensemble statistical averages, it is often assumed that the random process which it characterizes is stationary. This implies that the averages are invariant with respect to time. Thus, the ensemble mean, $\overline{F(t)}$, and mean square, $\overline{F^2(t)}$, may be determined at any time, t . All of the force amplitudes, $F_k(t)$, used to obtain these averages must correspond to the same value of T . The autocorrelation function which generally depends upon two values of t , say t_1 and t_2 , will now depend only upon the time difference, τ , between t_1 and t_2 . The mathematical expressions for the first few statistical averages, shown above, reduce to the following simpler forms for a stationary random process:

Letting t_0 be equal to any time,

$$\text{Mean: } E[F] = \overline{F} = \int_{-\infty}^{\infty} z \cdot P_F(z, t_0) \cdot dz \approx \frac{1}{N} \sum_{k=1}^N F_k(t_0)$$

$$\text{Mean Square: } E[F^2] = \overline{F^2} = \int_{-\infty}^{\infty} z^2 \cdot P_F(z, t_0) \cdot dz \approx \frac{1}{N} \sum_{k=1}^N F_k^2(t_0)$$

$$\text{Standard Deviation: } \sigma = \sqrt{\overline{F^2} - \{\overline{F}\}^2}$$

$$\text{Autocorrelation: } E[F(t_0) \cdot F(t_0 + \tau)] = R_F(\tau) = \int_{-\infty}^{\infty} \int_{-\infty}^{\infty} z_1 \cdot z_2 \cdot P_F(z_1, t_0; z_2, t_0 + \tau) \cdot$$

$$dz_1 \cdot dz_2 \approx \frac{1}{N} \sum_{k=1}^N F_k(t_0) \cdot F_k(t_0 + \tau)$$

$$\text{Power Spectral Density: } S_F(\omega) = 2 \int_{-\infty}^{\infty} e^{-i\omega\tau} \cdot R_F(\tau) \cdot d\tau$$

The more familiar symbol, $R_F(\tau)$, is used here for the autocorrelation function in place of $F(t_0) \cdot F(t_0 + \tau)$. Since the autocorrelation function, $R_F(\tau)$, of the stationary random process is independent of time, t , the time integral found in the expression for power spectral density, page 248, becomes:

$$\lim_{T \rightarrow \infty} \frac{1}{2T} \int_{-T}^T \overline{F(t) \cdot F(t+\tau)} \cdot dt = \lim_{T \rightarrow \infty} \frac{1}{2T} \int_{-T}^T R_F(\tau) \cdot dt = R_F(\tau),$$

thus giving the much simpler expression for power spectral density shown here.

With the assumption of stationarity, the higher order statistical averages shown on page 249 become:

$$E[F^n] = \int_{-\infty}^{\infty} z^n \cdot P_F(z, t_0) \cdot dz \approx \frac{1}{N} \sum_{k=1}^N F_k^n(t_0), n=1, 2, 3, 4, \dots$$

$$\begin{aligned} E[F^n(t_0) \cdot F^m(t_0+\tau)] &= \int_{-\infty}^{\infty} \int_{-\infty}^{\infty} z_1^n \cdot z_2^m \cdot P_F(z_1, t_0; z_2, t_0+\tau) \cdot dz_1 \cdot dz_2 \\ &\approx \frac{1}{N} \sum_{k=1}^N F_k^n(t_0) \cdot F_k^m(t_0+\tau), n, m = 1, 2, 3, 4, \dots \end{aligned}$$

$$\begin{aligned} E[F^n(t_0) \cdot F^m(t_0+\tau_1) \cdot F^r(t_0+\tau_2)] &= \int_{-\infty}^{\infty} \int_{-\infty}^{\infty} \int_{-\infty}^{\infty} z_1^n \cdot z_2^m \cdot z_3^r \cdot P_F(z_1, t_0; z_2, t_0+\tau_1; \\ &\quad z_3, t_0+\tau_2) \cdot dz_1 \cdot dz_2 \cdot dz_3 \\ &\approx \frac{1}{N} \sum_{k=1}^N F_k^n(t_0) \cdot F_k^m(t_0+\tau_1) \cdot F_k^r(t_0+\tau_2), n, m, r = 1, 2, 3, 4, \dots \end{aligned}$$

If the ensemble is composed of time records of $F(t)$ which are sufficiently long, the ensemble statistical averages may change significantly with time, such as that shown in Figure 108 for a single time record. The random process associated with this $F(t)$ is clearly nonstationary; however, it may be segmented into time intervals, $(0, t_1)$, (t_1, t_2) , (t_2, \dots) , such that during each interval the random process can be assumed stationary. Stationary statistical averages can then be determined for each segment. Only one record of the ensemble is shown here, but it is assumed that this one is typical of most of the $F_k(t)$ records in the ensemble, with respect to the locations

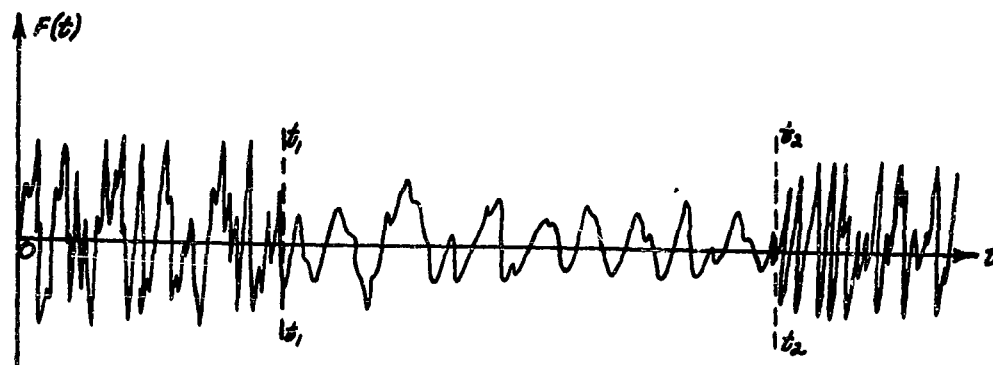


Figure 108: Time Record of a Nonstationary Random Force Function

of the ends of the stationary segments. If this record is not typical of all but a negligibly small number of the N ensemble records, then considerable error may be introduced by assuming stationarity over these segments.

A further simplifying assumption is usually made—that the random process which characterizes $F(t)$ is ergodic. The combined assumptions of stationarity and ergodicity imply, in addition to the invariance of the ensemble statistical averages with time, that any one of the $F_k(t)$ samples of $F(t)$ is statistically equivalent to the entire ensemble. Thus, the statistical averages defining the random force function, $F(t)$, may be obtained by timewise integrations, thereby eliminating the immediate requirement for the probability density functions. The mathematical expressions for the statistical averages then become:

$$\text{Mean: } E[F] = \bar{F} = \lim_{T \rightarrow \infty} \frac{1}{2T} \int_{-T}^T F(t) \cdot dt$$

$$\text{Mean Square: } E[F^2] = F^2 = \lim_{T \rightarrow \infty} \frac{1}{2T} \int_{-T}^T F^2(t) \cdot dt$$

$$\text{Autocorrelation: } E[F(t) \cdot F(t+\tau)] = R_F(\tau) = \lim_{T \rightarrow \infty} \frac{1}{2T} \int_{-T}^T F(t) \cdot F(t+\tau) \cdot dt$$

$$\text{Power Spectral Density: } S_F(\omega) = 4 \int_0^{\infty} R_F(\tau) \cdot e^{-i\omega\tau} \cdot d\tau$$

The higher order statistical averages can also be obtained from time averages under the assumptions of stationarity and ergodicity. Expressions for these are given below:

$$E[F^n(t)] = \lim_{T \rightarrow \infty} \frac{1}{2T} \int_{-T}^T F^n(t) \cdot dt$$

$$E[F^n(t) \cdot F^m(t+\tau)] = \lim_{T \rightarrow \infty} \frac{1}{2T} \int_{-T}^T F^n(t) \cdot F^m(t+\tau) \cdot dt$$

$$E[F^n(t) \cdot F^m(t+\tau_1) \cdot F^{\sim}(t+\tau_2)] = \lim_{T \rightarrow \infty} \frac{1}{2T} \int_{-T}^T F^n(t) \cdot F^m(t+\tau_1) \cdot F^{\sim}(t+\tau_2) \cdot dt$$

(etc.)

where $n, m, \sim = 1, 2, 3, 4, \dots$

Although the probability density functions are not required in obtaining the statistical averages of $F(t)$ for a stationary and ergodic random process, these functions are of importance, as discussed in Section II, and should be determined. A method has already been outlined for approximating these functions from ensemble samplings. Time averages are often used when an adequate and representative ensemble is not available. Hence, when the assumptions of stationarity and ergodicity are imposed, the probability density functions may have to be obtained from a single time record of $F(t)$. The diagram presented in Figure 106 for approximating $P_F(z, t)$ is still valid, except that $P_F(z, t)$ becomes $P_F(z)$, and the data sample would consist of say N^1 values, $F(t_k)$, ($k = 1, 2, \dots, N^1$), of $F(t)$ measured at even intervals of time as shown in Figure 10 below. It is important that Δt be sufficiently small to ensure

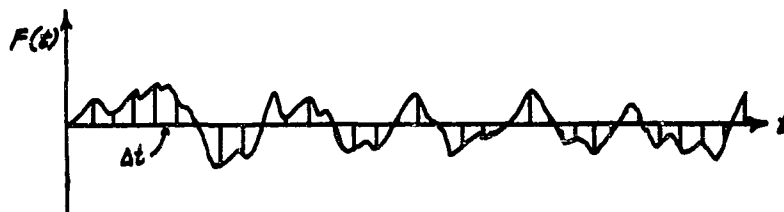


Figure 109: Amplitude Sampling of $F(t)$ at Even Intervals of Time.

that the highest frequency amplitude variations are weighted equally with those of the lower frequencies. Bendat, Reference 2, indicates that at least two sample readings per cycle should be made for the highest frequencies and that 10 to 20 sample readings per cycle might be practical estimates. The joint probability

density functions, $P_F(z_1, t; z_2, t + \tau)$ would be calculated as indicated in Figure 107 except that the data samples would consist of pairs of readings in Figure 109, each element of any pair being spaced at τ = time apart. A different distribution conceivably could be obtained for each different τ . It is now quite clear how any higher order joint probability density functions can be obtained for a single record, $F(t)$, in view of the expressions presented on pages 252 and 253.

The mathematics required to establish the expressions which have been presented thus far for the statistical averages of $F(t)$ and the intricate mathematical implications of the above assumptions, such as ergodicity, are beyond the scope of this report. Detailed derivations and descriptions of these are presented in a number of text books on the statistical analysis of random processes, such as References 1, 2, 3, and these should be consulted for more detailed information. Only a few brief comments are made here concerning the practical engineering aspects of the statistical description of $F(t)$ in terms of the above mathematical expressions.

All of the above expressions for time averages involve integrations over negative time and, because of the limiting process, require infinitely long records. These restrictions are of a theoretical nature and although these will never be satisfied in practice, they may be closely approximated. Stationarity of the random process assumes, by definition, that the effects of all starting transients can be neglected and hence, that the process has always occurred with no changes in its statistical properties (i.e., it began at $t = -\infty$). Also, the exact statistical averages of the random process can only be obtained if the sample size is infinite, which necessitates infinitely long records. For practical applications, this type of precision is unwarranted and sufficiently accurate results can be obtained for finite, but large, data samplings. All of the above analytical expressions for time averages may therefore be replaced by expressions of the form

$$\frac{1}{T_2 - T_1} \int_{T_1}^{T_2} \{ \quad \} . dt$$

Some degree of non-stationarity exists in most random processes which have a physical origin, so that ensemble averages should be used in determining the statistical properties of $F(t)$. This, however, is undesirable at the present time for a number of reasons. First, the quantity of data generally available for statistical analysis, in practice, is often meager and of limited accuracy. This is due, in part, to the difficulties encountered in duplicating any given random process, which thus restricts the number of ensemble sample records that accurately represent the particular random process being investigated. It is important to note that even though numerous records and/or long time records may be available, they may contain spurious information introduced by the influence of other random or non-random physical processes.

Secondly, when adequate and accurate representative samplings are available, the data reduction can be a heavy task. As shown above, it is necessary to obtain statistical averages for many times, t_1, t_2, t_3, \dots (theoretically an infinite

number) and all combinations of these times, (t_1, t_2) , (t_1, t_3) , (t_2, t_3) , ..., (t_1, t_2, t_3) , (t_1, t_3, t_4) , etc. It would thus certainly be necessary to use high speed digital computers if a statistical analysis of any quality were to be made.

Finally, there is a great desire on the part of analysts to take full advantage of the simpler time averaging expressions which are valid for stationary and ergodic random processes. Analog computing techniques are readily available, and relatively easy to program, which can efficiently determine at least the first few, and most important, statistical averages. The assumptions of stationarity and ergodicity are therefore widely used with segmented time records, as a first approximation of the statistical averages.

The following block diagrams show the simple procedure for obtaining the mean, mean square, autocorrelation function, and power spectral density function for a single time record $F(t)$ by means of electronic analog techniques. The function $F(t)$ must be fed into the circuitry from magnetic tape.

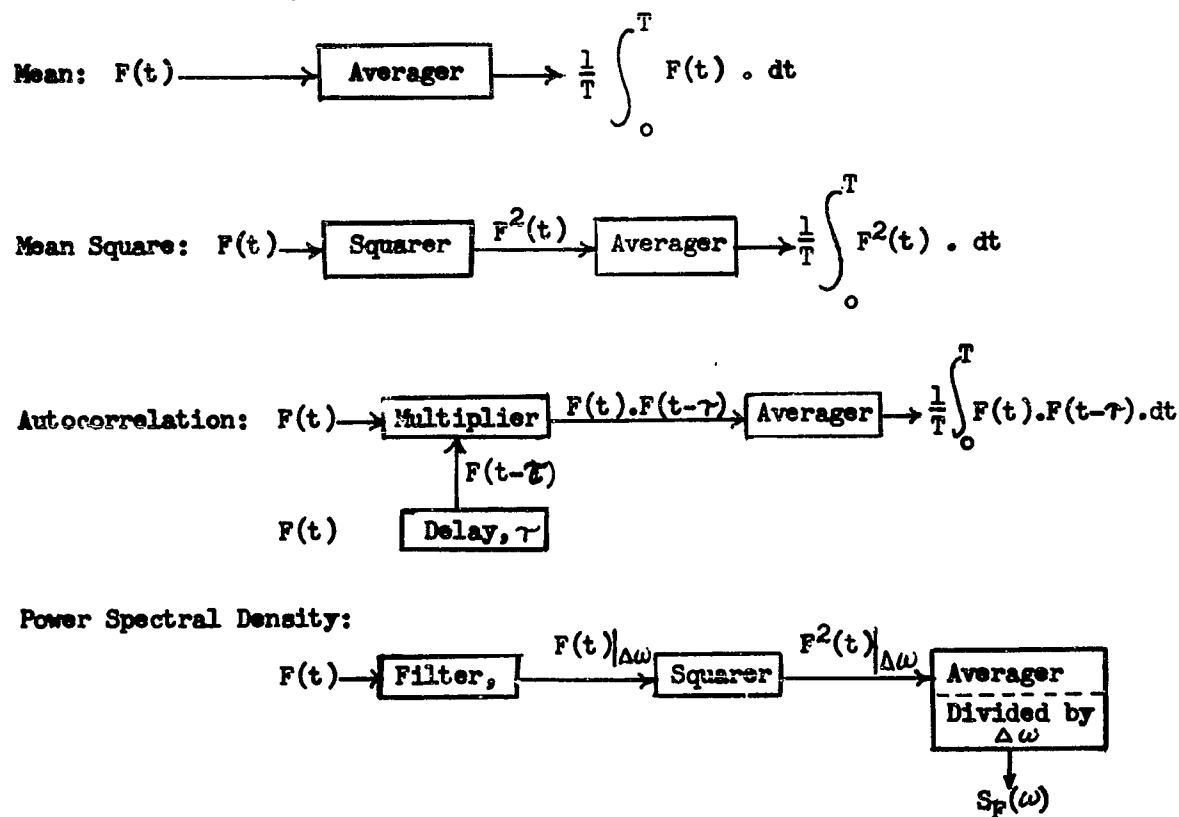


Figure 110: Block Diagrams of Electronic Analog Circuits for Computing Statistical Averages

In practice, the length of the time records of $F(t)$ may be relatively short, and in real time may contain only one second or less of recorded data. In order to increase the sample size, the ends of the magnetic tape may be joined, forming a loop, which can then be repeatedly analyzed electronically many times as a continuous uninterrupted $F(t)$ signal. This effectively increases the time duration of the random process and assumes that the process is stationary.

If a number of representative samples of $F(t)$ are available, and if electronic analog techniques are to be employed, the statistical averages may be evaluated as time averages for each record and the set of statistical results obtained from all of the samples may then be further averaged as an ensemble. For example, if the mean value, \overline{F}_k , has been determined for each of N records ($k = 1, 2, 3, \dots, N$), by the expression,

$$\overline{F}_k = \frac{1}{T} \int_0^T F_k(t) \cdot dt$$

the ensemble mean \overline{F} , of all the N records is given by the expression,

$$\overline{F} = \frac{1}{N} \sum_{k=1}^N \overline{F}_k$$

Similarly for the mean square, and autocorrelation function:

$$\overline{F_k^2} = \frac{1}{T} \int_0^T F_k^2(t) \cdot dt \quad R_{F_k}(\tau) = \frac{1}{T} \int_0^T F_k(t) \cdot F_k(t+\tau) \cdot dt$$

$$\overline{F^2} = \frac{1}{N} \sum_{k=1}^N \overline{F_k^2} \quad R_F(\tau) = \frac{1}{N} \sum_{k=1}^N R_{F_k}(\tau)$$

The ensemble power spectral density function would then be most conveniently determined from the resultant autocorrelation function $R_F(\tau)$ using the expression

$$S_F(\omega) = 4 \int_0^\infty R_F(\tau) \cdot e^{-i\omega\tau} \cdot d\tau$$

If in future analyses, computing equipment and programs become available to determine both ensemble and time averages for segmented records, the choice of the proper method to use should be based upon the number of samples available and the length of these samples. Bendat, Reference 2, indicates that many samples of short records are more efficiently analysed by ensemble techniques, with time averages employed for a small number of long records.

Interpretation of the Statistical Averages of $F(t)$

It should be noted that all of the above expressions for the mean, mean square, and autocorrelation function are independent of frequency, and therefore represent the statistical averages of $F(t)$ over all frequencies that are contained in $F(t)$. This type of information is of limited value as it does not show the relative importance of possible high amplitude persisting frequency components of $F(t)$, nor the general distribution of power throughout the frequency range of $F(t)$. Since structural response is strongly dependent upon the frequency of excitation, it is necessary to determine these statistical averages for certain discrete frequencies and frequency bands. The power spectral density function for example is one of the statistical averages used to describe the mean square of $F(t)$ in terms of its frequency components. In the following discussion of the properties of the statistical averages of $F(t)$, particular attention will be given to spectral characteristics of these averages.

The components of $F(t)$ contained within certain frequency bands or at discrete frequencies are obtained in practice by filtering techniques. If $F(t)$ is stored on magnetic tape, it can be passed through a set of electrical filters which transmit only those frequencies within the bandwidth of the filter. The action of these filters is closely associated with the Fourier series and Fourier transform which display the theoretical frequency components of a function. The convenient mathematical forms provided by Fourier methods are very useful in explaining the actual frequency content of $F(t)$ and in the interpretation of results obtained by filtering. It is important to consider briefly the spectral properties of $F(t)$ itself and the problem of filtering before considering the spectral properties of the statistical averages of $F(t)$. It is not intended that the following discussion be mathematically rigorous or sufficiently precise to include all possible types of functions. The arguments presented are directed towards the practical aspects of the problem.

Consider first that the function $F(t)$ is well defined of period $2T$ and contains a finite number of constant peak amplitude frequency components which remain unchanged for all time (i.e., from $t = -\infty$ to $t = +\infty$). Such a function is stationary and can be expressed by the finite Fourier series,

$$F(t) = \frac{a_0}{2} + \sum_{n=1}^N (a_n \sin \omega_n t + b_n \cos \omega_n t) = c_0 + \sum_{n=1}^N c_n \cos(\omega_n t - \phi_n)$$

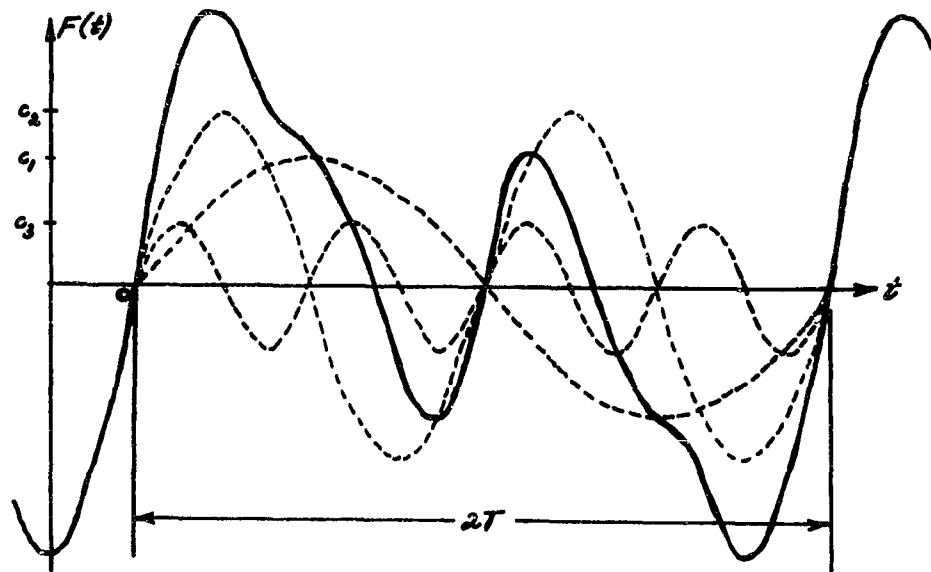
$$c_n = \sqrt{a_n^2 + b_n^2} = \text{peak amplitude of the } n\text{-th frequency component; } c_0 = a_0/2$$

$\phi_n = \tan^{-1}(b_n/a_n)$ = phase angle of the n-th frequency component

$$a_n = \frac{1}{T} \int_{-T}^T F(t) \cdot \cos \omega_n t \cdot dt \quad b_n = \frac{1}{T} \int_{-T}^T F(t) \cdot \sin \omega_n t \cdot dt$$

$$\omega_n = n\omega_0, \quad \omega_0 = \frac{2\pi}{2T} = \text{basic Fourier frequency}$$

All of the a_n 's, b_n 's, and c_n 's will be zero except for those which correspond to values of ω_n which appear as discrete frequencies in $F(t)$. Figure 111 shows an example of such a function for three frequency components.



$$F(t) = c_1 \sin \frac{\pi}{T} t + c_2 \sin \frac{2\pi}{T} t + c_3 \sin \frac{4\pi}{T} t$$

Figure 111: Periodic Time Function with Three Sinusoidal Components

The amplitudes of the various frequency components are easily obtained for an $F(t)$, known to contain only discrete frequencies, by electrically filtering $F(t)$ through a variable frequency band pass filter of bandwidth $\Delta\omega_b$. The block diagram in Figure 110 shows the essential equipment required for this process and Figure 112 shows a plot of the typical characteristics of such a filter relative to some center band frequency ω_c .

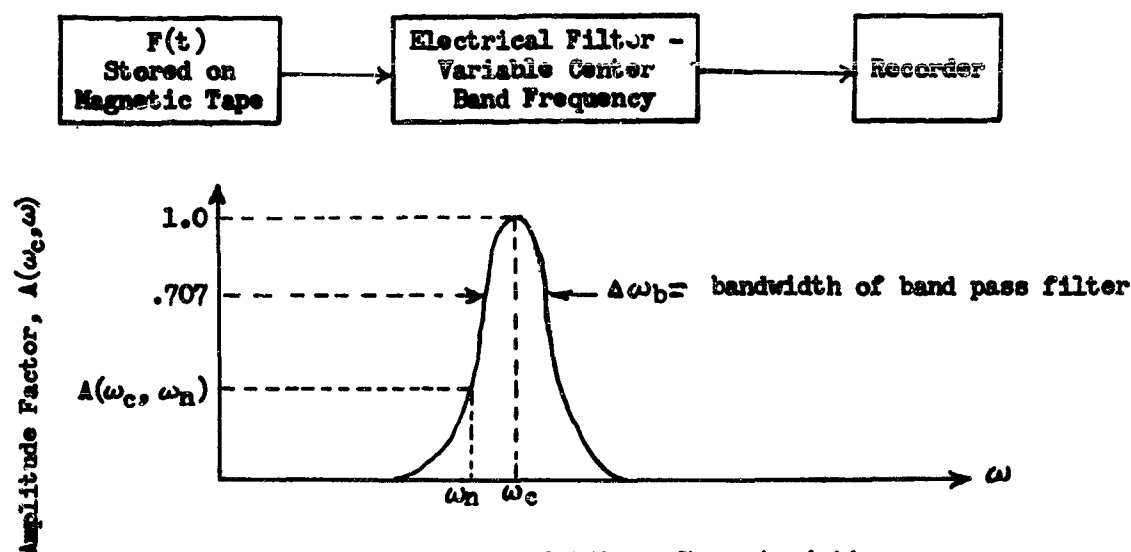


Figure 112: Typical Filter Characteristic

The amplitude of each filtered frequency component of $F(t)$ is given by the product,

$$c_n \text{ (filtered)} = A(\omega_c, \omega_n) \cdot c_n$$

Thus each unfiltered amplitude, c_n , may be obtained by sweeping ω_c through the entire frequency range of interest so that ω_c is made to coincide, one at a time, with each of the frequencies, ω_n . If the bandwidth is sufficiently narrow, only one frequency component will be transmitted to the recorder for each fixed ω_c , and the filtered wave in each case will be a pure sinusoid of constant peak amplitude. If, however, more than one frequency component is transmitted as shown in Figure 113, the filtered wave will be modulated as shown in Figure 114 and the individual amplitudes of the unfiltered wave may be more difficult to obtain. It may therefore be desirable to use narrower bandwidth filters in order to separate close frequencies. A lower practical limit to the bandwidth does exist, but these limitations are not discussed here.

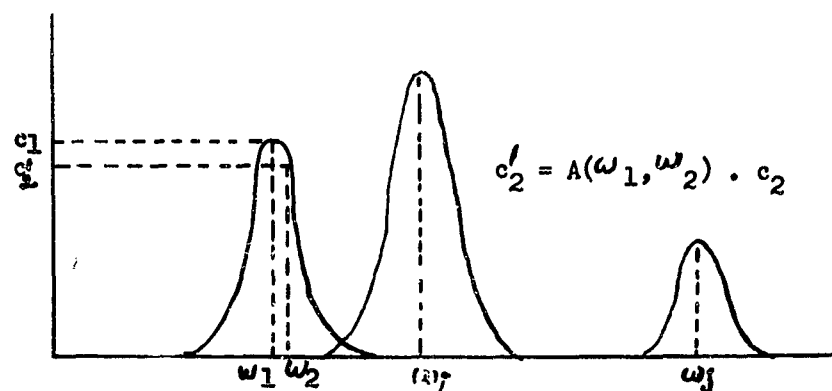


Figure 113: Amplitudes of Filtered Frequency Components of $F(t)$.

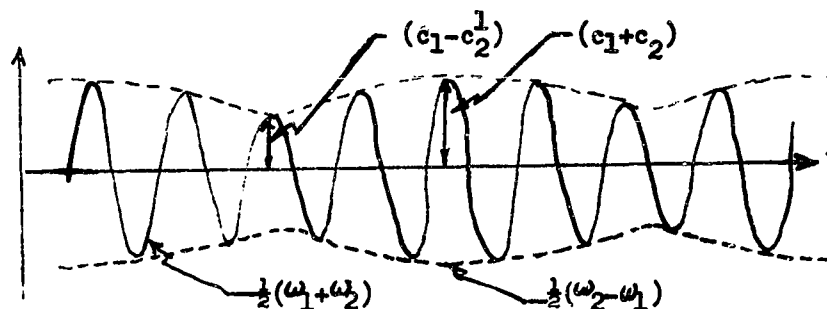


Figure 114: Modulated Wave Obtained When Two Discrete Frequency Components Lie Within the Bandwidth of the Filter.

Finally, the information obtained by filtering out the discrete frequency components of $F(t)$ can be presented in the form of a bar graph, as in Figure 115. It is to be noted that only the component amplitudes, c_n , are shown, as phase data are generally not obtained in present data reduction systems. For many dynamic problems, it is important that the phasing be known, and in the future it will be desirable to measure this quantity. This phasing, for a periodic function, can be obtained from the above time integrations for a_n and b_n .

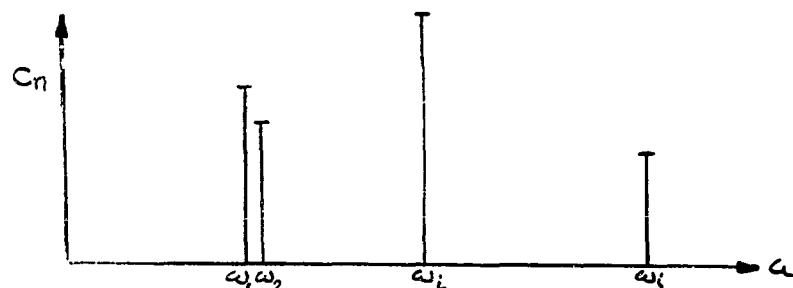


Figure 115: Bar Graph of the Amplitudes of Filtered Discrete Frequency Components.

The above finite Fourier series can be extended to include functions, having period $2T$, which contain an infinite number of frequencies which are all multiples of the basic frequency, π/T . Such a function and corresponding amplitude bar graph are shown in Figure 116 below.

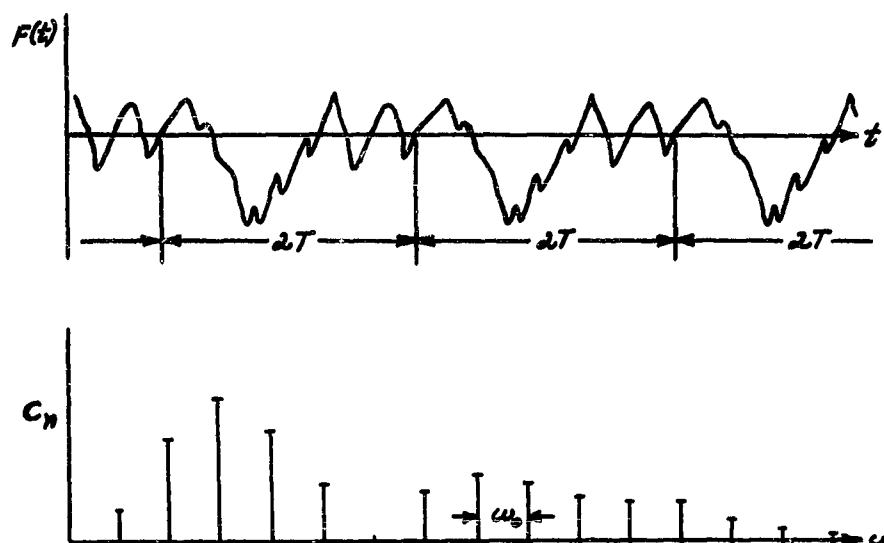


Figure 116: Time Function, $F(t)$, and a Bar Graph of the Discrete Frequency Components of $F(t)$.

Generally, the function $F(t)$ is random and has no finite period (i.e., $T \rightarrow \infty$). This is true for both stationary and nonstationary random functions. Such functions cannot be represented by the Fourier series as they contain a continuous band of frequencies which are not multiples of some basic frequency. (For an infinite period, this basic frequency is zero.) The spectral characteristics of the function must be described by either its Fourier transform or by its power spectral density function, but not both. It is assumed here that neither the transform nor the spectrum function are trivially zero or infinite in amplitude.

Following the approach used by Bendat, Reference 2, the above Fourier series ($N \rightarrow \infty$) can be rewritten in the complex form

$$F(t) = \sum_{n=-\infty}^{\infty} A_n \cdot e^{i\omega_n t}$$

$$A_n = \frac{\omega_0}{2\pi} \int_{-T}^T F(t) \cdot e^{-i\omega_n t} \cdot dt = \frac{1}{2}(a_n - ib_n), \quad n \neq 0$$

$$A_n = a_0/2, \quad |A_n|^2 = \frac{1}{2} c_n^2$$

where ω_0 is shown in Figure 116 above and equals π/T , where $F(t)$ is of period $2T$.

As the period T approaches infinity, $T \rightarrow \infty$, the basic frequency, ω_0 , approaches zero, which shows that more and more frequencies are contained in $F(t)$. Thus, the coefficient A_n , and hence a_n and b_n , approach zero, which implies that the amplitudes, c_n , of the individual frequency components also approach zero. However, as $T \rightarrow \infty$, the ratio A_n/ω_0 becomes the Fourier transform,

$$\lim_{\omega_0 \rightarrow 0} \frac{A_n}{\omega_0} = \frac{1}{2\pi} \int_{-\infty}^{\infty} F(t) \cdot e^{-i\omega t} \cdot dt = \mathcal{F}_F(\omega)$$

The Fourier transform of $F(t)$, when it exists, may therefore be used to describe the frequency characteristics of nonperiodic functions. This transform exists for a limited case of nonstationary functions, where the total energy associated with these functions is finite. Typical examples of these functions are isolated pulses of various shapes, or a finite train of pulses. Examples of the Fourier transform for three types of pulses are presented in Figure 117 below.

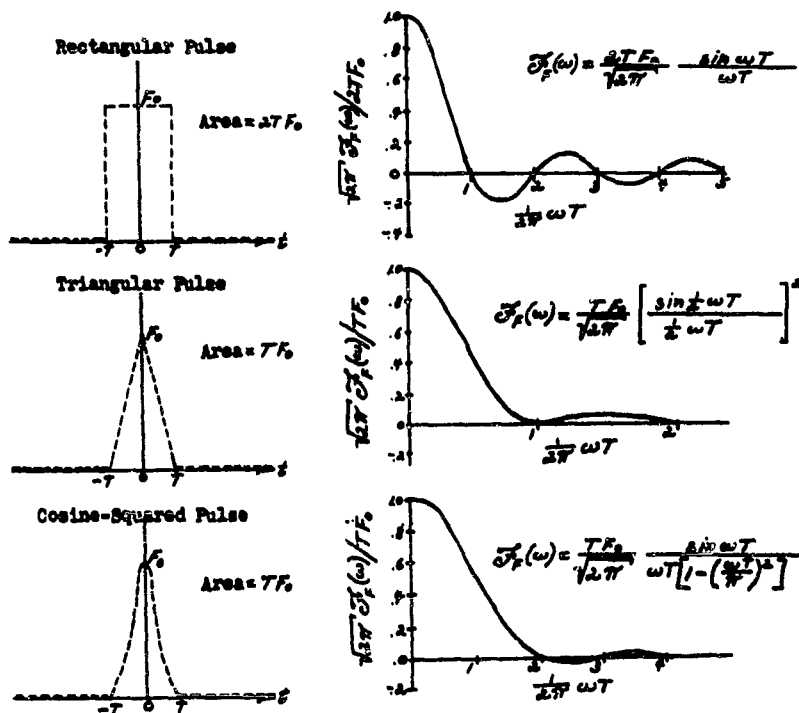


Figure 117: Finite Isolated Pulses and Their Fourier Transforms

If $F(t)$ contains a sinusoidal component of nonzero amplitude at some frequency, $\bar{\omega}$, then the Fourier transform, $\mathcal{F}_F(\omega)$, will exhibit an infinite spike at $\bar{\omega}$.

For stationary non-periodic random processes, the total energy associated with $F(t)$ is infinite and the above Fourier transform is also infinite. In this case the spectral properties of $F(t)$ are displayed by the use of the power spectral density function, $S_F(\omega)$. Formally, this function is defined as

$$S_F(\omega) = \lim_{T \rightarrow \infty} \frac{|\mathcal{F}_F(\omega)|^2}{T}$$

Although $|\mathcal{F}_F(\omega)|$ is infinite, this ratio exists and is finite (for non-periodic $F(t)$). If $F(t)$ contains a sinusoidal component at frequency, $\bar{\omega}$, then $S_F(\omega)$ will exhibit an infinite spike at that frequency. It should be noted that for non-stationary functions where the Fourier transform exists, the power spectral density function will be zero except for periodic components where it will exhibit infinite spikes. Since well-defined oscillatory functions contain periodicities, it is not possible to show a diagram of some analytical function and its corresponding power spectral density. Such spectrums must be determined from a statistical analysis of a recorded function resulting from some physical random phenomenon. The power spectral function is further discussed below.

It is now clear that the filtering techniques used for functions which contain a continuous band of frequencies must be altered somewhat from those discussed above for periodic functions. Because the amplitude of each frequency component is zero, for such functions (except for additional discrete sinusoids), it is necessary to filter a narrow band of frequencies and determine the statistical averages of the amplitude of the filtered signal over all frequencies in that narrow band. Since it is more desirable to use electrical filters, with the function, $F(t)$, stored on magnetic tape, the time averages associated with stationary and ergodic processes are preferred over ensemble averages because of available electronic analog methods for determining these averages. From the above discussion, it is seen that the non-stationary functions which are of practical interest (i.e., those containing a finite amount of energy) are transients that appear in the form of isolated pulses and shocks. These are difficult to filter because of the small sample sizes available—usually one or two records which are small fractions of a second in length. The following discussion of the statistical averages of the frequency components of $F(t)$ will then be confined to stationary and ergodic random process, or those processes for which the assumptions of stationary and ergodicity closely approximate the actual conditions.

It has been observed that in many random processes occurring in nature, the mean value of the oscillating amplitude of a random variable, say $F(t)$, is approximately equal to zero. Also, the time variation of the amplitudes of the individual frequency components of $F(t)$ will have a near zero mean value. The assumption that the mean is zero therefore is widely used in practice. Whether or not this assumption is valid naturally depends upon the random variable being considered. For example, the distribution of the amplitude peaks of $F(t)$ may be Rayleigh, which cannot have a

zero mean as shown on page 176.

The mean square value, $\overline{F^2}$, of $F(t)$ has a special physical interpretation that is fundamental in spectral analyses. The instantaneous power developed by a resistor, R , in an electrical network equals I^2R or E^2/R , where E is the voltage drop across the resistor and I is the resistor current. Analogously, the instantaneous power, $P(t)$, dissipated in a structure having viscous damping, c , and vibratory velocity, v , equals cv^2 or $AF^2(t)$, where A is a constant of proportionality. The average power, P_{ave} , is the time average (mean) of the instantaneous power,

$$P_{ave} = \frac{1}{T} \int_{-T}^T P(t) \cdot dt = \frac{A}{T} \int_{-T}^T F^2(t) \cdot dt$$

and hence is proportional to the mean square value, $\overline{F^2}$, of $F(t)$.

$$P_{ave} = A \overline{F^2}$$

That is, a knowledge of over-all mean square value of the applied force $F(t)$ indicates the amount of power being dissipated in a linear structure, to within a constant of proportionality.

In order to broaden the use of the power concept so that the techniques which have been developed for its application can be extended to include random variables for which true damping power does not exist, the proportionality constant, A , is dropped and the mean square value of the random variable is called the total average power of the variable. As mentioned in Section II, it may be more appropriate for such cases to retain the "mean square" terminology. Both of these will be used here in order to avoid possible confusion with existing terminology used in the referenced literature.

The mean square value is particularly useful in dealing with near discrete frequency, random amplitude, components of $F(t)$. For the well-behaved periodic function, the discrete frequency components have constant peak amplitudes and can be defined by a bar graph of c_n versus frequency. For a near discrete frequency with random amplitude, it is not practical to determine all of the many Fourier coefficients, c_n , required to define this component. Instead, a narrow band filter is used to obtain these near discrete components and the mean square value of the amplitude of each such frequency is obtained and presented in the form of a bar graph as shown in Figure 118.

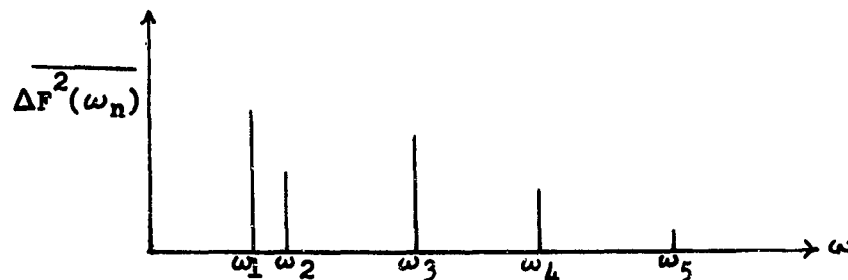


Figure 118: Bar Graph of the Mean Square Amplitudes of Discrete Frequency Components of $F(t)$.

The equivalent sinusoidal amplitude in terms of the Fourier coefficients is given by the relation

$$\overline{\Delta F^2(\omega_n)} = \frac{1}{2} c_n^2 = \text{mean square value of a true sinusoid with amplitude equal to } c_n.$$

The total average power, P_{ave} , for all of the near discrete components, is equal to the arithmetic sum of the power, $\Delta P(\omega_n)$, of each component.

$$P_{\text{ave}} = \sum_n \Delta P(\omega_n) = \sum_n \overline{\Delta F^2(\omega_n)}$$

The above bar graph of the mean square value of the individual frequency components is similar to that of Figure 115 where the Fourier amplitude coefficients are displayed for each sinusoidal component of $F(t)$. Just as did these Fourier coefficients, the mean square value of each frequency component, and hence the power in each component, decreases to zero when the number of frequencies contained in $F(t)$ increases to a continuous band of frequencies. This assumes, of course, that no finite amplitude discrete frequencies are present. In order to eliminate this difficulty, it is usual to consider the mean square value over a finite frequency range of continuous frequency components, and to divide this quantity by the frequency band. In the limit, as the frequency band decreases to zero, this ratio becomes a mean square density function with respect to frequency and is usually called the power spectral density function, $S_F(\omega)$. Mathematically expressed:

$$S_F(\omega) = \lim_{\Delta \omega \rightarrow 0} \frac{\overline{F^2(\Delta \omega)}}{\Delta \omega} = \lim_{\Delta \omega \rightarrow 0} \frac{P_{\text{ave}}(\Delta \omega)}{\Delta \omega}$$

$\overline{F^2(\Delta\omega)}$ = mean square amplitude over all frequencies in $\Delta\omega$

$P_{ave}(\Delta\omega)$ = total average power over all frequencies in $\Delta\omega$

The total average power contained in all frequency components in $F(t)$ is therefore given by the equation

$$P_{ave} = \overline{F^2} = \int_0^{\infty} S_F(\omega) \cdot d\omega$$

The physical interpretation of the mean square statistical average of $F(t)$ is now evident in terms of the definition of power presented above.

The power spectral density function, $S_F(\omega)$, is also related to the autocorrelation function, $R_F(\tau)$, as shown in the previous expressions for the statistical averages. For a stationary and ergodic process, reciprocal relations exist in terms of the Fourier transform. These convenient mathematical relations are as follows:

$$S_F(\omega) = 4 \int_0^{\infty} R_F(\tau) \cdot e^{-i\omega\tau} \cdot d\tau$$

$$R_F(\tau) = \frac{1}{2\pi} \int_0^{\infty} S_F(\omega) \cdot e^{i\omega\tau} \cdot d\omega$$

The relationships are not easily explained by physical arguments and are not discussed further in this report.

The autocorrelation function, $R_F(\tau)$, of a single time function, $F(t)$ also has a special interpretation which is important in determining response of the structure. Basically, this function shows quantitatively the agreement between the function $F(t)$ at time t and at time $t + \tau$ (i.e., between the functions $F(t)$ and $F(t + \tau)$). When $\tau = 0$, the two functions are in perfect agreement at every point and the correlation between the two is as large as possible. Thus,

$$|R_F(0)| \geq |R_F(\tau)|$$

It is to be noted that $R_F(0)$ is equal to the mean square value, $\overline{F^2}$, of $F(t)$. A correlation coefficient, $C_F(\tau)$, is a convenient measure of the relative correlation of $F(t)$ with itself. This coefficient is defined here as follows:

$$C_F(\tau) = \frac{R_F(\tau)}{R_F(0)}$$

Thus, $C_F(\tau)$ may have any value between 0 and 1. $C_F(\tau) = 1$ indicates perfect correlation, $C_F(\tau) = 0$ indicates no correlation, and values of $C_F(\tau)$ between 0 and 1 indicate partial correlation.

The validity of this concept of correlation is easily shown by considering a simple sine wave of the form,

$$F(t) = C \cdot \sin(\omega t + \phi)$$

The correlation coefficient, $C_F(\tau)$, for this case is,

$$C_F(\tau) = \frac{\left| C^2 \int_{-T}^T \sin(\omega t + \phi) \cdot \sin(\omega t + \omega\tau + \phi) \cdot dt \right|}{\left| C^2 \int_{-T}^T \sin^2(\omega t + \phi) \cdot dt \right|}$$

$$= \left| \frac{\frac{1}{2} C^2 \cos \omega\tau}{\frac{1}{2} C^2} \right| = |\cos \omega\tau|$$

A plot of $C_F(\tau)$ is presented in Figure 119, and it will be valuable to compare this ideal coefficient with those obtained in practice for random functions.

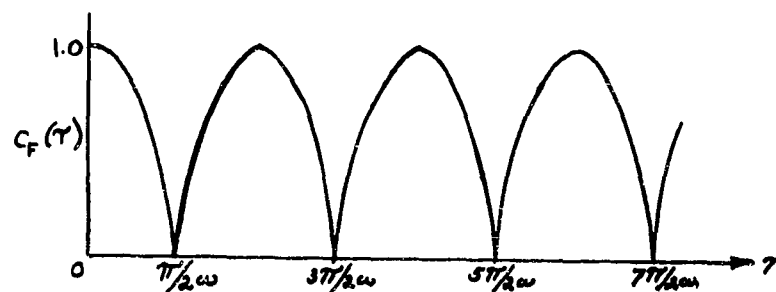


Figure 119: Time-Correlation Coefficient for a Pure Sinusoidal Function

In contrast to a well-behaved periodic function, the correlation coefficient for random "white noise" is zero for all $\tau > 0$.

As a final property of the correlation function, $R_F(\tau)$, to be considered here, it is not difficult to show mathematically or physically that the correlation function is symmetric with respect to $\tau = 0$, i.e.,

$$\begin{aligned} R_F(\tau) &= \frac{1}{T} \int_{-T}^T F(t) \cdot F(t + \tau) \cdot dt \\ &= \frac{1}{T} \int_{-T}^T F(s - \tau) \cdot F(s) \cdot ds \\ &= R_F(-\tau). \end{aligned}$$

Space-Time Correlations

In addition to the time averages of a force acting at a fixed point, spatial averages are required to completely define, statistically, the applied forces on the structure. Only one spatial average seems to have significant physical interpretation -- the space correlation function, $R_F(X)$. This function and the time correlation function $R_F(\tau)$, are very important to the description of the generalized force i.e., the effective force felt by the structure. When space correlations must be considered, $R_F(\tau)$ and $R_F(X)$ are generally not separable, except in elementary cases, and must be considered as a single, space-time correlation function, $R_F(x, \tau)$. It is also possible to have a three parameter correlation function, $R_F(x, \psi, \tau)$, which involves the direction, ψ , of the applied force, but this is generally not of interest since for those forces which require description by correlation functions, the direction of the force will be known.

The direction, ψ , is defined as the direction of a force acting at a point and should therefore not be confused with angular coordinates used to describe the position, X . Thus, for example, it is possible to have time correlation at a fixed point, space-time linear correlation on the surface of a missile parallel to the centerline axis of the missile, and space-time angular correlation around the circumference of the missile, the latter two correlations being defined by $R_F(x, \tau)$.

Space-time correlations arise when dealing with random acoustic or hydrodynamic pressure waves which are propagated over the surface skin of a vehicle. Although these pressure fluctuations are of a random nature, it has been observed that for short periods of time and for short distances over the surface, the pressure waves exhibit a certain degree of regularity in phasing within narrow frequency bands. At a given point on the surface, the pressure fluctuations occurring at one time are nearly in phase with those occurring at a short τ -time earlier or later. This phasing steadily changes with time, in keeping with the random nature of the excitation phenomenon, but the change is sufficiently slow to permit these fluctuations to appear steady and unchanging for this short time. For $\tau = 0$ the correlation is perfect, and for τ very nearly equal to zero the correlation coefficient may be relatively high. As the time difference, τ , increases, the shift in phasing increases and the correlation drops off, eventually to zero. The rate at which the correlation decreases depends upon the rate at which the phasing changes. For a theoretical "white noise" type fluctuation, the correlation drops immediately to zero for any time difference $\tau > 0$.

The same observations have been made spatially by comparing the pressure fluctuations at two points on the structure. When the separation distance between the points is small, the propagating waves will move from one point to the next with relatively little change so that the relative phase between the waves at the two points will be small. As the separation distance increases, the phase shift increases and the correlation decreases. Considering both space and time, it would seem that if τ were the time required for a wave to move between the two points the correlation of the force, $F(x_1, 0)$, at the one point and the force, $F(x_2, \tau)$ at the second point would be highest for small distances of separation.

The distance over which the propagating pressures are essentially in phase is called the correlation length. This length is a function first of the direction between the two points in relation to the direction of propagation over the surface, and secondly of the angle of incidence of the wave fronts relative to the surface. If the correlation length is determined for every direction through a given point on the surface, it is possible to define a correlation area, as shown in Figure 120. The shape of this correlation area is therefore dependent upon the direction at which the wave fronts impinge on the surface.

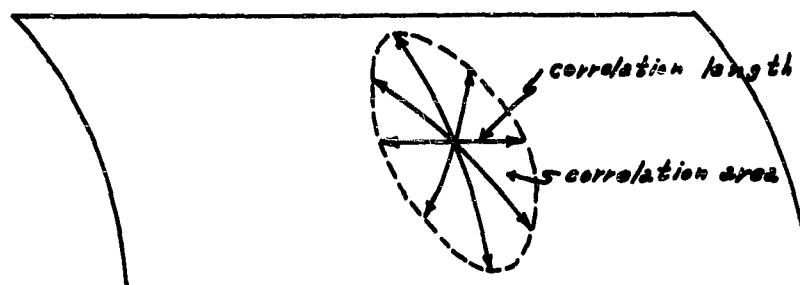


Figure 120: Correlation Length and Correlation Area on Vehicle Surface Associated with Surface Pressure Fluctuations

Figure 121 shows a cross section of the vehicle with a pressure wave incidence angle of θ . In flight this angle will be approximately 90 degrees for all wave fronts, but may have a smaller angle when the missile is sitting on the launch pad and the acoustic waves are generated away from the base of the vehicle. It is to be noted in Figure 120 that the correlation length is greater around the circumference of the surface. This is the condition which should exist in flight, where $\theta \approx 90$ degrees, indicating that the phase distortion along the wave front is less than that which occurs in the direction of propagation.

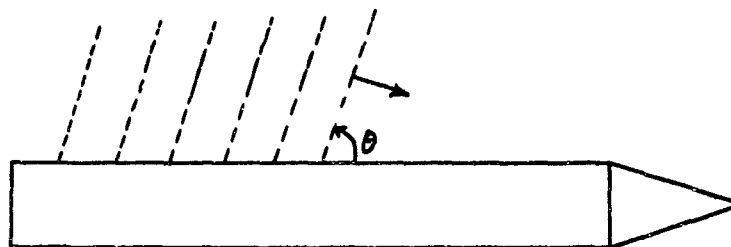


Figure 121: Propagations of Acoustical Pressure Waves Over Surface of a Missile

The time-correlation functions obtained in practice will differ from the simple periodic case shown in Figure 119. The first zero point in the curve of Figure 119 corresponds to a 180 degree phase shift of the sine wave and thereafter the correlation coefficient returns to unity when the phasing reaches 360 degrees. Figure 122 below shows a typical correlation coefficient obtained for a random acoustic pressure fluctuation. The first zero point in this case also corresponds to a 180 degree phase shift, but thereafter increases to only small values, indicating that the phasing never returns to the initial state, at $\tau = 0$, and the phase difference steadily changes as τ increases for random forces and pressures so that the correlation diminishes to zero.

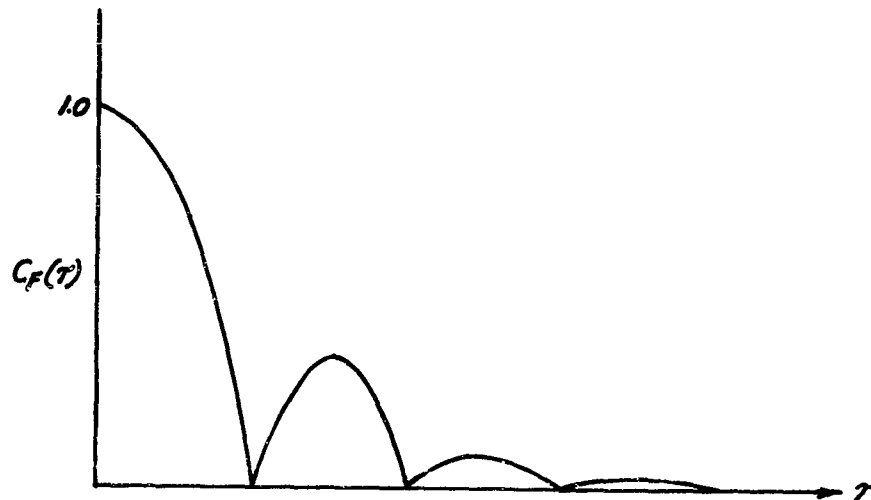


Figure 122: Typical Time-Correlation Coefficient Obtained in Practice

The curve in Figure 122 is also typical of the correlation of pressure, at two points where τ is replaced by the separation distance. For a zero time delay, $\tau = 0$, there exists a distance at which the phase difference between the fluctuating pressures is 180 degrees. As the separation distance further increases, more time is required for the waves to propagate between the points which permits a longer phase shift to occur. In this case the correlation also decreases with distance and approaches zero correlation.

The magnitudes of both the time and space correlations are dependent upon the frequency of the pressure fluctuations. A low frequency pressure fluctuation propagating past a fixed point on the vehicle surface will present a high correlation at that point for a longer period of time, by virtue of its long wave length, than the high frequency, low wave length, fluctuations. It is clear that the same is true for space correlations. A rather simple physical interpretation of the frequency effect is possible by considering a train of periodic pressure waves of some frequency propagating over the structure. There is a continuous phase and

frequency shift between successive cycles, so that the larger the number of cycles occurring at a point during a time interval and the larger the number of cycles existing between two points on the structure, the larger the phase and frequency shift. Thus the higher frequencies will have the least correlation. This is seen to be the case in Figure 123, Reference 4, for the space correlation function of jet acoustic noise. The absolute value signs of the correlation coefficients may be dropped so that the coefficients may range from -1 to +1. This is done in Figure 123 for convenience.

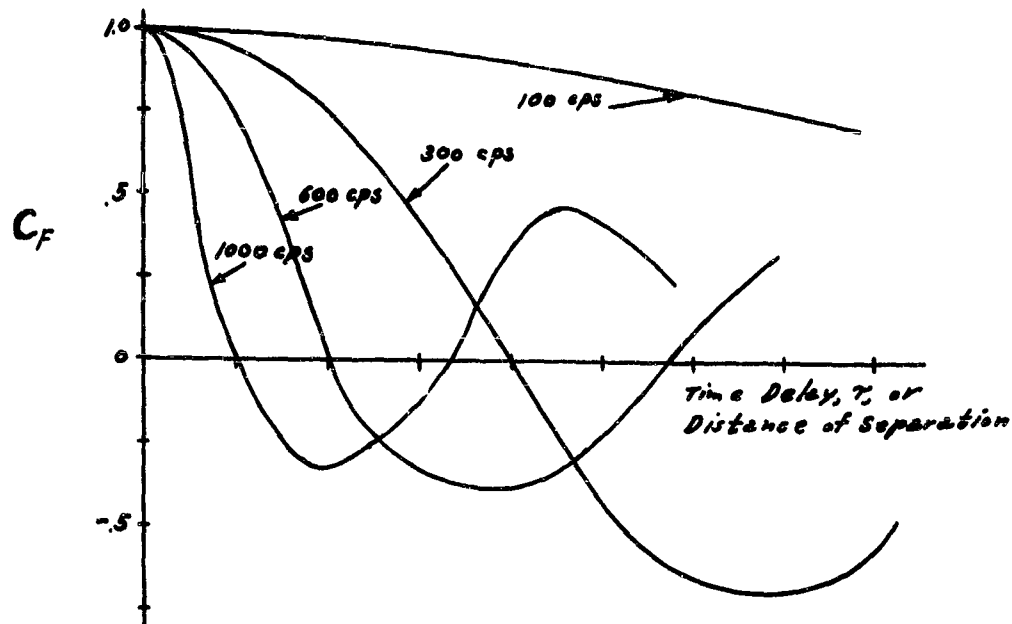


Figure 123: Variation of Correlation Coefficient with Frequency

Mathematically the space-time correlation function can be expressed as:

$$R_F(x_1, x_2, \tau) = \frac{1}{2T} \int_{-T}^T F(x_1, t) \cdot F(x_2, t + \tau) \cdot dt$$

where

$$F(x_1, t) = \text{Pressure at Position } x_1 \text{ and time } t$$

$$F(x_2, t + \tau) = \text{Pressure at Position } x_2 \text{ and time } t + \tau$$

The position is symbolically indicated by x , but the position of any point will actually be defined in terms of any coordinate system which is convenient for the geometry of the structure. $R_F(x_1, x_2, \tau)$ is called a cross-correlation

function, and reduces to the previously discussed auto-correlation function, $R_F(\tau)$, when the two points χ_1 , and χ_2 coincide.

Generalized Force

The generalized force input to the structure represents the effective force causing vibration and is dependent upon the distribution of external force over the structure and the natural vibration characteristics of the structure. Expressed mathematically the generalized force F_G , is

$$F_G(t) = \int_A F(\chi, t) \cdot \frac{\partial x}{\partial q} \cdot dA$$

$F_G(t)$ = generalized force

$F(\chi, t)$ = applied pressure over the element of area,

x = displacement of the structure

q = generalized displacement coordinate

A = area

If the structure is nonlinear, the derivative $\partial x / \partial q$ may have a complex form which depends upon the type of nonlinearity involved and must be handled by special methods. For a linear structure, this derivative can be replaced by any one of the natural mode shapes, $Y_n(\chi)$, of the structure that will be excited by the applied force, $F(\chi, t)$. The following discussion is confined to the linear case, for which the generalized force takes the form

$$F_G(t) = \int_A F(\chi, t) \cdot Y_n(\chi) \cdot dA$$

If the applied force, $F(\chi, t)$ is well defined, then F_G will be used in the form shown here and then presents no analytical difficulties. However, when the applied force is random, $F(\chi, t)$ is known only in terms of the statistical averages discussed above, so that the generalized force, F_G , must also be described in terms of statistical averages. For this purpose, the power spectral density function is preferred especially when dealing with broad band acoustic or hydrodynamic excitation. When the power spectral density of the generalized force is known, the power spectral density of response can be determined as the product of this function and the structural transfer function, defined in terms of the mobility of the structure.

Based upon the discussion and the mathematical expressions presented above, the power spectral density function $S_{F_G}(\omega)$, of the generalized force is easily obtained in terms of the applied force power spectral density, $S_F(\chi_0, \omega)$ at some reference point, χ_0 , and a space correlation coefficient over a narrow frequency band $\Delta\omega$

centered around the frequency, ω . The time correlation function, $R_{F_G}(\tau)$, of the generalized force is given by

$$R_{F_G}(\tau) = \frac{1}{2T} \int_{-T}^T F_G(t) \cdot F_G(t + \tau) \cdot dt$$

and with the above expression for F_G , this becomes,

$$\begin{aligned} R_{F_G}(\tau) &= \int_A \int_A \left\{ \frac{1}{2T} \int_{-T}^T F(x_1, t) \cdot F(x_2, t + \tau) \cdot dt \right\} \cdot Y_n(x_1) \cdot Y_m(x_2) \cdot dA \cdot dA' \\ &= \int_A \int_A R_F(x_1, x_2, \tau) \cdot Y_n(x_1) \cdot Y_m(x_2) \cdot dA \cdot dA' \end{aligned}$$

Here $R_{F_G}(\tau)$ is the correlation of F_G over a narrow frequency band $\Delta\omega$, and $R_F(x_1, x_2, \tau)$ is the space-time correlation function over the same frequency band. Let $R_F(x_0, 0)$ be the mean square value, over $\Delta\omega$, of $F(x_0, t)$, where x_0 is some convenient reference point on the structure. The above expression can be written as

$$\frac{R_{F_G}(\tau)}{\Delta\omega} = \frac{R_F(x_0, 0)}{\Delta\omega} \cdot \int_A \int_A \left\{ \frac{R_F(x_1, x_2, \tau)}{R_F(x_0, 0)} \right\} \cdot Y_n(x_1) \cdot Y_m(x_2) \cdot dA \cdot dA'$$

which gives, for $\tau = 0$,

$$S_{F_G}(\omega) = S_F(x_0, \omega) \int_A \int_A C_F(x_1, x_2, \omega) \cdot Y_n(x_1) \cdot Y_m(x_2) \cdot dA \cdot dA'$$

$$C_F(x_1, x_2, \omega) = \frac{R_F(x_1, x_2, 0)}{R_F(x_0, 0)} = \text{space correlation coefficient}$$

This correlation coefficient must be determined experimentally. It is to be noted that $S_{F_G}(\omega)$ is the power spectral density function corresponding to the modes of vibration whose mode shapes are $Y_n(x_1)$ and $Y_m(x_2)$. This quantity must then be determined for all significant modes of vibration.

The generalized force power spectrum can be written in terms of the "joint acceptance," $j_{n,m}^2(\omega)$, defined by Powell, Reference 4,

$$S_{F_G}(\omega)_{n,m} = S_F(x_0, \omega) \cdot A^2 \cdot j_{n,m}^2(\omega)$$

where

$$j_{n,m}^2(\omega) = \int_A \int_A C_F(\chi_1, \chi_2, \omega) \cdot Y_n(\chi_1) \cdot Y_m(\chi_2) \cdot \frac{dA}{A} \cdot \frac{dA'}{A}$$

Joint acceptance is a non-dimensional term which must be determined from the space correlation coefficient and the modes of deflection of the structure.

It is often assumed that there is no coupling between different modes of the structure, so that

$$S_{FG}(\omega)_{n,m} = 0, \quad n \neq m$$

In this case the joint acceptance becomes,

$$j_n^2(\omega) = \int_A \int_A C_F(\chi_1, \chi_2, \omega) \cdot Y_n(\chi_1) \cdot Y_n(\chi_2) \cdot \frac{dA}{A} \cdot \frac{dA'}{A}$$

A further simplifying assumption is possible when the correlation length is small compared with the half wave length of the structural mode. The expression for joint acceptance for this case is similar to that given in Reference 5 and is

$$j_n^2(\omega) = \frac{Y_n^2(\chi)}{A^2} \int_A C_F(\chi_1, \chi_2, \omega) \cdot dA$$

where χ is the location of the correlation area, say in the center of such an area. This, for example, would be the joint acceptance of a panel in the near field of a jet or rocket exhaust.

Two very interesting examples of the joint acceptance of panels appear in References 4, 5, and 6, which show the physical significance of joint acceptance.

The first example consists of a panel, of length b , vibrating as a rigid body, so that $Y_n(x)=1$, with pressure loads on the panel due to incident sound waves generated in the far field of a jet or rocket exhaust. Figure 124 shows these sound waves at the incidence angle θ , velocity of propagation C , and trace wave length λ . The velocity of the trace waves along the panel is given by $c/\sin \theta$. The joint acceptance for this panel is given by

$$j^2(\omega) = \left[\frac{\lambda}{\pi b} \cdot \sin \frac{\pi b}{\lambda} \right]^2$$

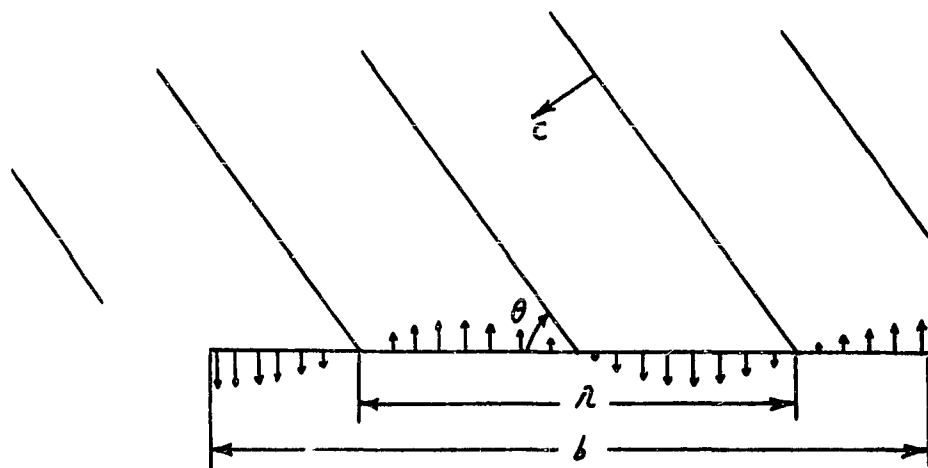


Figure 124: Rigid Panel with Propagating Acoustical Pressures Over the Surface

The curve of $j^2(\omega)$ versus b/λ is shown in Figure 125. As the angle θ approaches zero, the trace wave length becomes very long in proportion to the panel length b , and the correlation coefficient over the panel is near unity. In this case

$b/\lambda = 0$ and $j^2(\omega) = 1$. When $b/\lambda = 1$, the total integrated pressure on the panel is zero, being positive on one-half of the panel and negative on the other half.

b/λ represents the number of full trace wave lengths over the panel, and the larger the number of wave lengths the greater the pressure cancellation over the surface from the positive and negative pressures. Thus, the length of the panel over which unbalanced pressure forces exist becomes smaller as b/λ increases, so that the joint acceptance of the panel to the applied pressure decreases, eventually to zero.

The second example consists of an elastic panel vibrating in the same pressure field, but with a sinusoidal mode having n half-waves of wavelength b . The joint acceptance for this case is given by the following expression, the complete curve of which is shown in Figure 126.

$$j^2(\omega) = \frac{2}{\pi^2 n^2} \left[\frac{1}{1 - b^2/\lambda^2} \right]^2 \left\{ 1 - (-1)^n \cdot \cos \frac{n\pi b}{\lambda} \right\}$$

When $n = 1$, the only nodes are located at the ends of the panel, and it is clear that $\theta = 0$ or $b/\lambda = 1$ will produce the maximum joint acceptance and hence the maximum excitation. For all other values of n , the excitation is a maximum when the applied pressures are in phase, at all points on the panel, with the mode shape. This occurs when $b/\lambda = 1$ as indicated by the curve in Figure 126. A flexible panel therefore acts as a wavelength filter which becomes increasingly more selective as the number of modal half wavelengths on the panel increases. Although the example presented is for panels, the same concepts are valid for other vehicle structure, but it is felt that panels will exhibit the greatest response to this type of excitation. The resonance and coincidence conditions associated with this panel are further discussed on page 286.

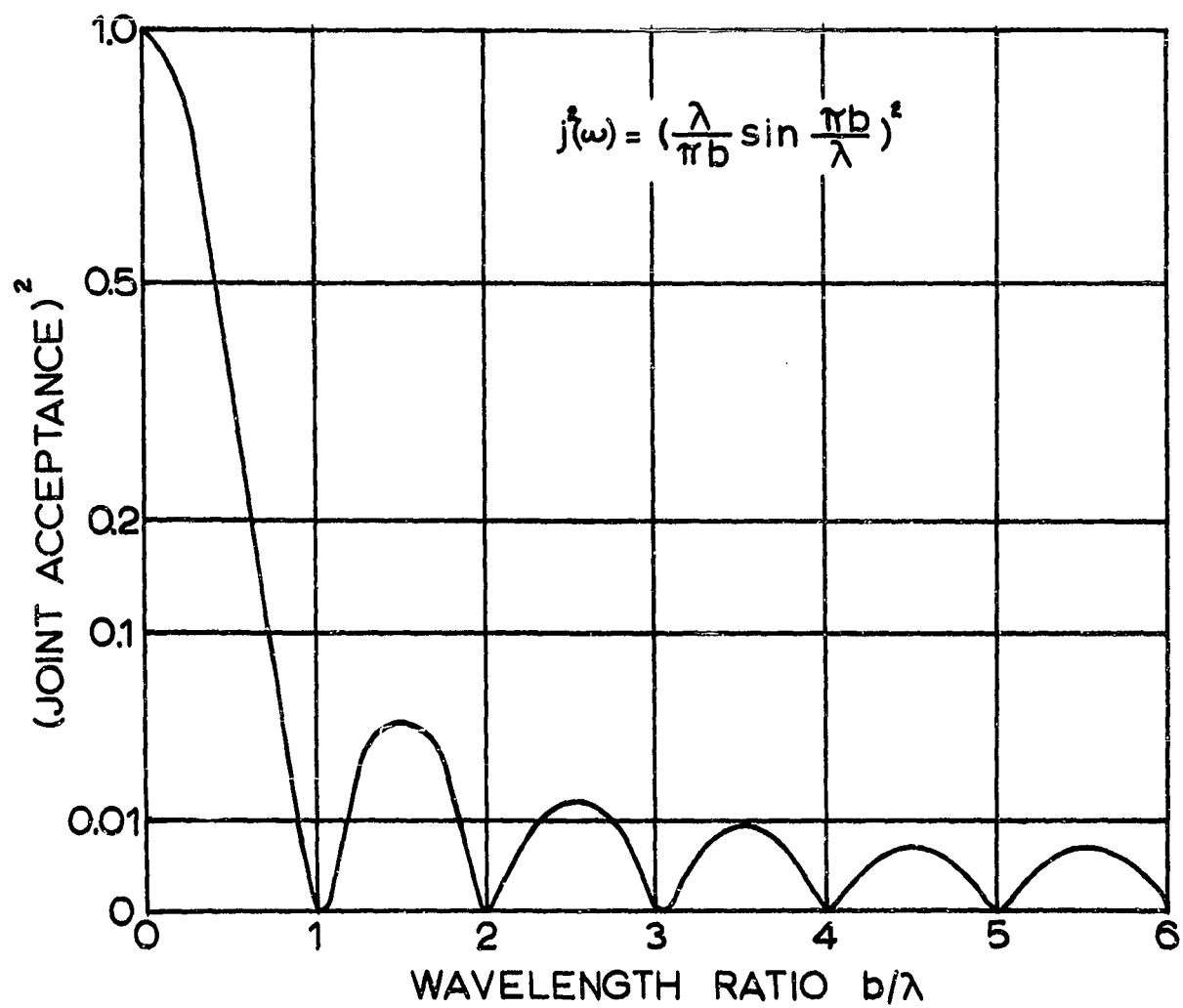


Figure 125 Joint Acceptance of a Rigid Panel to Far Field Acoustic Pressure Fluctuations.

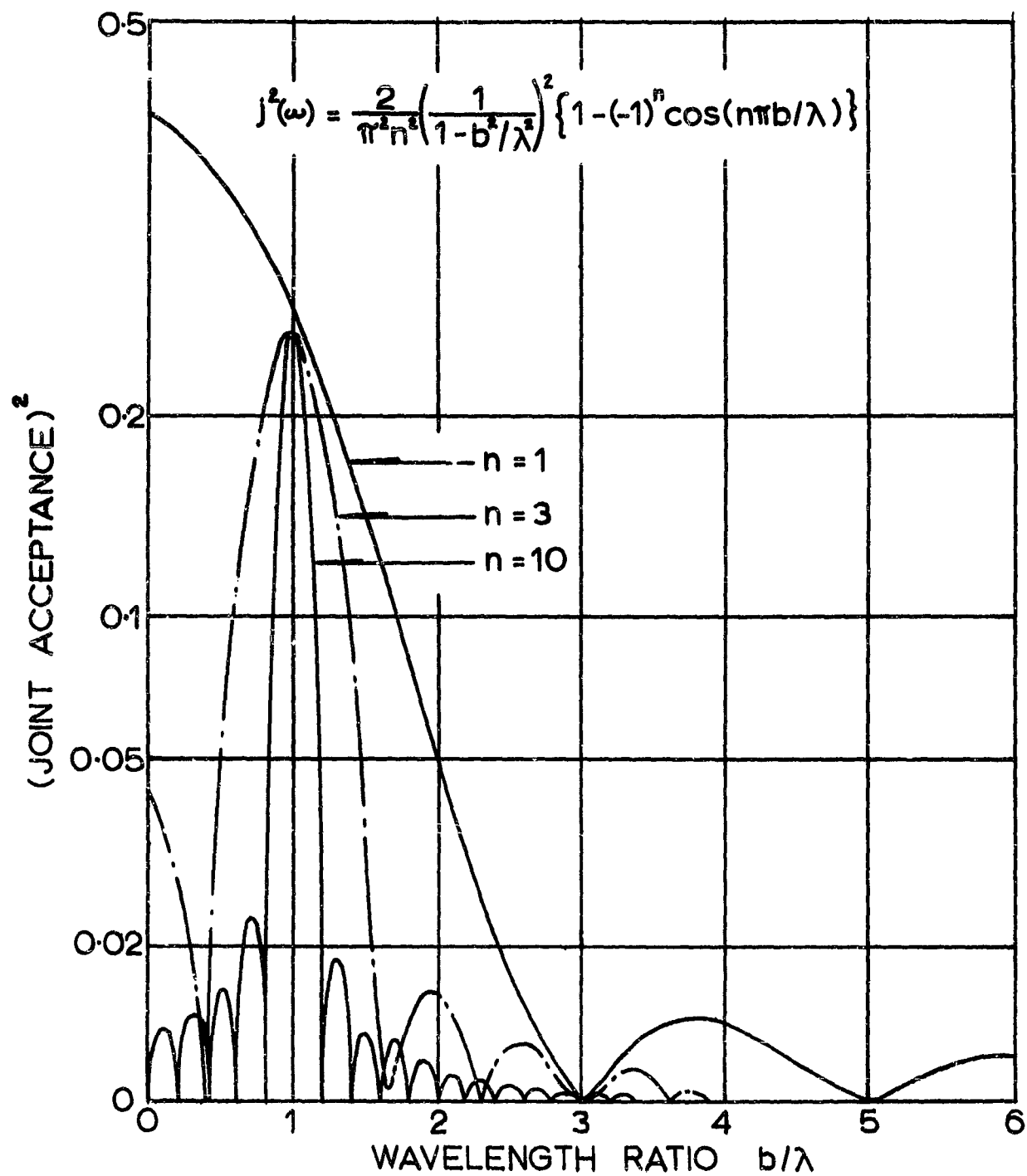


Figure 126. Joint Acceptance of Flexible Panel to Far Field Acoustical Pressure Fluctuations.

MOBILITY OF THE STRUCTURE

The term mobility is used in mechanical network theory to define the ratio of the response of simple mechanical elements, such as a mass, spring or damper, to the force acting on these elements when the response and the applied force are simple harmonic functions of time having the same frequency. Equivalent mobilities of series and parallel combinations of these simple mechanical elements can also be defined as the ratio of the total response of the entire network of elements to the total external applied force acting across the network. In certain limited cases, space vehicle structures can be approximated by such ideal networks; but, for structures which are excited by wave type phenomena, such as the flexible panel discussed in the previous section, or those which exhibit two- or three-dimensional response properties, the simple mobility concept is not valid. However, the most systematic approach to structural vibration problems, and the one that is now widely used, consists in defining a force function of some form, say Φ_F , and then multiplying this function by a second function, say M , to obtain a response function, Φ_R .

$$\Phi_R = M \cdot \Phi_F$$

It is desirable therefore to extend the simple concept of mobility to include all steady state vibration problems which may be so formulated, and to let M denote the mobility of the structure. It is not necessary to include transient vibrations due to nonstationary forces as these may be obtained from the Fourier transform of solutions to the stationary vibration problem, as discussed in Reference 7. Figure 127 shows a convenient summary of responses that can be obtained from transient shock inputs.

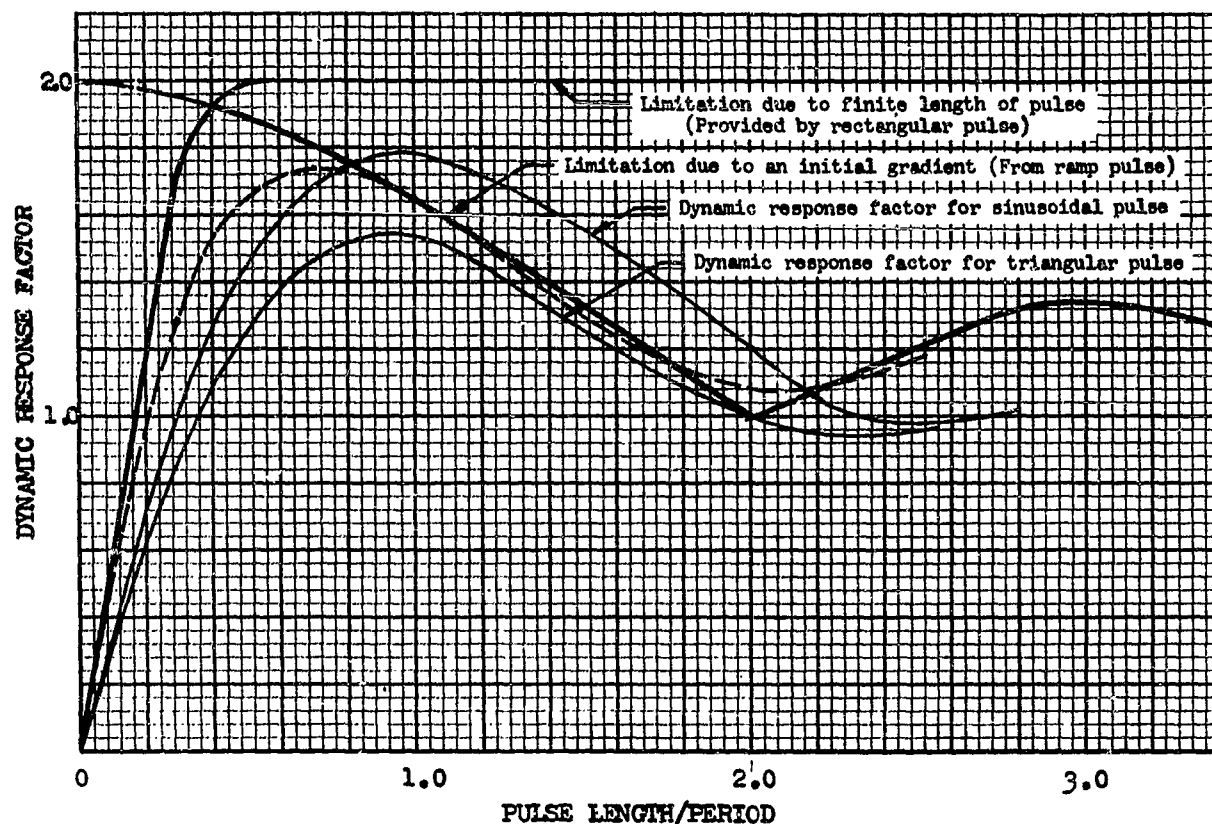
As shown in the previous sections of this chapter, the force function, Φ_F , may be well defined or it may necessarily be a statistical description of the applied force, such as mean square spectral distribution function for near discrete frequency components or a power spectral density function for broad band random forces. The response function, Φ_R , then has the same form, statistical or otherwise, as Φ_F , and the mobility, M , is merely their ratio

$$M = \Phi_R / \Phi_F$$

The mobility, M , will vary with the type of structure being excited and with the type of excitation force being applied to the structure. For a linear structure then, the response function, Φ_R , will be the linear sum of such products,

$$\Phi_R = M_1 \Phi_{F1} + M_2 \Phi_{F2} + M_3 \Phi_{F3} + \dots$$

where M_1 is the mobility of the structure corresponding to the force function which in turn corresponds to the applied force F_1 .




1. If pulse has both finite length and an initial gradient, both limits apply
 2. The 1/2 sine pulse appears to violate the limits due to an initial gradient until an equivalent ramp time is defined. Using the equivalent pulse length the curve shifts to the limit as the dotted version suggests.
- 
3. The dynamic response factor is the ratio of the response of a dynamic system to the response of the same system to the maximum impulsive load slowly applied.
 4. At small times, the response is proportional to the area under the pulse and independent of the shape of the pulse.
 5. Significant transient response occurs only for a ratio of pulse length/period ≤ 2 .
 6. Pulse length is twice the rise time for a ramp pulse.
 7. The results presented are appropriate to any small damping ordinarily present in structure.

Figure 127. Dynamic Response Factor for Transient Response of Linear Structures to Shock Excitation.

For structures which exhibit non-linearities, these linear forms will not accurately describe the response, and the mobility of the structure and the force function will not be mathematically separable into a single product. In this case, the response will be some more complex function of M and Φ_F which will have a different form for each different type of nonlinearity. It might be argued that even this more general concept of mobility has little value when nonlinearities are present and of significance. However, even for this case, there always exists some ratio between the response and the excitation force. The description of mobility is more complex, however, and depends upon more parameters, some of which are parameters normally found in and isolated to the forcing function, such as the amplitude of the force. For example, if it is known that the response amplitude for a given input force varies as the n -th power of the input amplitude, A , thus

$$\Phi_R = \{M \cdot A^n\} \Phi_F = M' \Phi_F$$

where the mobility M' of the structure is dependent upon the forces applied to it. It should be further noted that the assumption of linearity of the structure, for which the mobility concept is valid, is often a good first approximation to the actual solution so that it is merely necessary to correct the linear mobility to include certain nonlinear effects.

The term "transfer function" has sometimes been used in the above expressions instead of mobility. This term should not be used here as it is the Laplace transform of the response to an impulsive force applied to a linear system. Transfer functions may be used correctly, however, to define the ratio of response at one point in the structure to the response at some other point of the structure. The term transmissibility is used to define the ratio of the forces acting at two points of the structure.

Physically, mobility represents the ease with which a structure accepts and responds to the vibratory energy supplied by the applied force. If the mobility of a given structural element or group of elements to a given force is small, the element or elements transmit a high percentage of this force to the foundation, whereas for high mobility, a higher percentage of the energy supplied is accepted by the element or elements in the form of kinetic energy and less is transmitted to the foundation. Thus, the mobility of an element is highest, and the energy acceptance is therefore highest, when the element is in a state of resonance under the action of the applied force. Consistent with this simple physical concept, it was shown in Section II that the power developed by a simple harmonic damped oscillator (single degree of freedom system) is highest at resonance.

The input energy is supplied to relatively small portions of the over-all structure, such as engine mounts, equipment mounts, and skin panels. The elements being forced directly are denoted in Figure 104 as the forced structural elements. The mass-stiffness coupling of the various structural elements provide numerous transmission paths whereby this energy is distributed throughout the structure. For a given energy input, the energy density and hence the response level could be locally very high if only a few elements accepted this energy with little or no transmission to

their foundation. If instead the forced elements transmit part of this input energy through their foundation to other parts of the structure, the energy density drops, reducing the response of the forced elements and the increase in response of other structural elements. Hence, it is important that in order to determine the structural response level to any given applied force, the total mobility be known for all structural elements and on-board equipment which accepts a significant amount of the vibratory energy supplied by the applied force.

From Figure 104, the mobility of the entire structure which is significantly affected, depends upon the mobility of the elements being forced, the transmissibility of the element foundation mounts, the transmissibility of the vehicle structure to the numerous mass elements throughout the vehicle, and finally the mobility of the structural and mass elements which receive the transmitted oscillatory energy.

It was shown in the previous section that panels exhibit a selectivity to acoustic and hydrodynamic surface pressure waves. The relationship between mobility and transmissibility discussed above can be used to show that other structural elements, or in fact the entire structure, has a wave-type selectivity to the input energy and the vibratory energy transmitted throughout the vehicle. For very low frequency inputs which have wave lengths longer than the longest natural wave lengths of the entire vehicle, such as those often associated with atmospheric winds, any resultant vibration will be of the rigid body type since the mobilities of all individual structural elements will be negligibly small and transmission from element to element will be high. For input wave lengths on the order of over-all vehicle wave lengths, such as those associated with atmospheric turbulence, the transmissibility of each individual structural element is also very high, with low mobility, but the mobility of the entire vehicle may be high. As the frequencies of the applied forces increase, the shorter wave lengths correspond more nearly to the natural wave lengths of the individual structural elements. The mobilities of the forced structural elements increase, becoming highest at resonance, and the distribution of energy throughout the structure is highly dependent upon the distribution of high acceptance resonant structural elements in the vehicle at the surface or internal structure and equipment.

Damping is an important factor in determining the transmission and distribution of vibratory energy throughout the structure. It has been shown experimentally that damping of vibration waves in the structure is on a per-cycle basis. Thus, the longer wave lengths of the low frequencies experience little damping with distance and are easily transmitted to all parts of the structure. However, the very short wave lengths of the high frequencies experience considerable damping with distance, so that high frequency vibrations are generally localized to small areas near the input.

Structural mobility may be determined by different methods, each of which will have its own particular advantages in dealing with different types of structures and structural geometries, different types of applied forces, and even for different modes of vibration of a given structure. These methods can be broadly divided into three separate categories: (1) analytical techniques where the structural properties of mass, stiffness, and damping distribution are known or can be adequately approximated; (2) direct testing of the structure; and, (3) an empirical approach which represents a combined analytical and test approach with the use of scaling laws from analysis and correlation of measured data.

Within each of these general categories there exist a number of quite distinct methods that can be used to attack this problem. Analyses may be performed with the assumption that the structure, or portions thereof, are continuous such as for beams, plates, and shells. For more complex structures, lumped parameters may be used to approximate the structures which may then be analyzed by techniques developed for mechanical and electrical networks. Direct tests may be performed on the full-scale structure or scaled models where the forces applied to these structures may be simulated by mechanical shakers, wind tunnels, acoustical sirens, jet and rocket engines, etc. Empirical scaling laws may be derived in a multiplicity of ways by combining information obtained from various types of analyses, full scale tests, model tests into simple mathematical expressions that can be used for prediction of structural vibration.

Structural tests have the advantage of including the many complexities and nonlinearities which may be difficult to handle by analytical methods, but because of the limitations on measuring devices and because of the money and time required to reduce large quantities of data, the results must be limited to essential data so that all of the desired results are generally not obtained. Analytical attacks on the problem can produce, on the other hand, quite accurate results and rather complete information about a problem if the simplifying assumption that must be made adequately describes the true situation. This, of course, is a great restriction; and although complete results can be obtained, their accuracy is often limited. For many vibration problems, and especially those which are complex problems, it is therefore often desirable to attack the problem from quite different approaches using a number of different methods and converging to the true solution.

It is not intended that a detailed discussion be given of the various methods available for determining the mobility of the structure. Standard engineering texts fully describe the techniques used in the mechanical network analysis of lumped parameter multi-degree of freedom systems. These lumped parameter systems may also be conveniently handled by constructing equivalent electrical networks and using four-pole parameter techniques as discussed in Reference 8. The latter approach is particularly useful in showing the transmission characteristics of the structure. Both of these methods represent powerful analytical tools for vibration analyses as the system parameters can be lumped into quantities which are physically measurable.

Determination of structural mobility by solving the complete equations of motion of the structure is also very useful in certain frequency ranges and for certain types of structures. If the frequencies of the input are low so as to excite the basic body modes, the structure may be assumed to act as a beam and the complete equations are easily solved by standard methods. For higher frequencies, the complexities of the structure in geometry and mass and stiffness distribution limit the desirability of this approach to ideal structures such as shells and plates. A fairly comprehensive treatment of the latter problem is given in the next section in terms of mode shapes and frequencies which are the essential parameters used to define mobility when solving the equations of motion.

RESPONSE OF THE STRUCTURE

The general response function, \bar{F}_R , is shown in Figure 104 as the product of the vehicle mobility, $M_{s,F}$, and the force function, \bar{F}_F . The definition is consistent with the definition of mobility given in the previous section and although the mobility of the entire structure may be difficult to obtain, this equation does show conceptually the combined effect of these two important quantities. For linear structures this response function may have the following form for multiple force functions:

$$\bar{F}_R = M_1 \bar{F}_{F1} + M_2 \bar{F}_{F2} + \dots$$

The parameters used to define the force function, \bar{F}_F , are the same as those used to define response, i.e., amplitude, frequency, and phasing as a function of position on the structure and the direction. As with the applied force function, the response is most conveniently expressed as $R(\lambda, \psi, t)$ where R is the response amplitude in the direction, ψ , and position, x , on the structure and the frequency, ω , and phasing, ϕ , are implicit in the functional form of $R(\lambda, \psi, t)$.

The direction, ψ , in the response function has more importance than it does in the force function, $F(\lambda, \psi, t)$, described in the previous sections. Although such forces as the acoustical and hydrodynamic surface pressures create forces normal to the surface skin, the resulting internal vibrations in the vehicle may be in quite different directions for different structural elements. It has been observed experimentally that very high frequency vibrations are nearly homogeneous in direction, i.e., the amplitude of vibration is approximately the same in all directions.

The response function, $R(\lambda, \psi, t)$, defines the response of the structure at convenient reference points. For modal analyses, these reference points are those at which the normalized modes are taken as unity. When network analyses are used the response will also be given at some point in the network, often at the point of application of the force. It is generally required however that the response of a particular structural element or item of equipment be determined. The structural elements to which the forces are applied are often of particular interest, such as panels, since they may be subjected to the highest stresses caused by the excitation. When the complete mode shapes of the structure are known or when the network response transfer functions are known between any two points, the response of any piece of structure or equipment is easily determined from the general response function, $R(\lambda, \psi, t)$. The chart shown in Figure 104 shows a systematic approach to determining the response of the forced structural elements and any other element, denoted in the chart as a receiver of vibratory energy. The more detailed approach taken in Figure 104 is to emphasize the flow of energy through the forced structural elements to their foundation, then through the many structural load paths to the receiving elements, and finally the acceptance of the receiving elements

for the transmitted energy. For complex structures which defy analysis either by modal methods or by mechanical and electrical network methods, this flow diagram should be carefully considered in predicting or estimating structural response.

The vibration response of the vehicle, like the forcing function, may or may not be well defined, depending upon the information available for describing the applied forces and the mobility in terms of the natural vibration characteristics of the structure. The response cannot, therefore, be defined with any greater certainty than either of these, and will usually have a more inaccurate description than the applied forces.

It is clear from the definition of mobility that if the applied forces are random or contain random components, the statistical description used for \bar{F}_F will be the same as that used for response \bar{F}_R . As shown in the discussion of the generalized force, the power spectral density function is preferred for statistically describing the effective force acting on the structure for random pressures and forces. Thus, the response to these random forces and pressures are most generally described in terms of the power spectral density of response. It is to be noted that response may be given in terms of deflection, velocity, or acceleration. The units of the spectrum function corresponding to each of these are,

$$(\text{rms Deflection})^2/\text{cps}$$

$$(\text{rms Velocity})^2/\text{cps}$$

$$(\text{rms Acceleration})^2/\text{cps}$$

As discussed in the previous section, the structure acts as a filter so that structural response of the forced elements will generally contain a broader band of significant frequency components than those elements within the structure that are further removed from the areas of force application. Also, a high frequency force applied to the vehicle is not expected to induce a significant response at a distance very far removed from the point of application because of the structural damping.

VIBRATIONS OF A PANEL DUE TO FAR FIELD ACOUSTIC EXCITATION

In order to show how the response function, \bar{F}_R , can be determined from a knowledge of the mobility of the structure and the force function, \bar{F}_F , the case of uniform, flat, rectangular panel with acoustic pressure loading on one side is briefly discussed.*

*Note that this assumes that the flat panel represents a portion of an infinite wall (infinite baffle) in that the effects of diffraction of the pressure waves around the free edges of the panel are ignored. It should be emphasized that diffraction phenomena be considered for panel configurations dealt with in practice. See References 9, 10, and 11.

Assume that the panel is simply supported along two opposing edges a distance, b' , apart, on a massive, rigid framework which does not deflect significantly under the applied acoustic loading. Assume that the other two opposing edges, a distance, L , apart, are free. As a result of the last assumption, it can further be assumed without great error that the modes of vibration of the panel are two-dimensional and the mode shapes are simple waves of the form

$$\sin \frac{n\pi x}{b'}$$

where n is the number of half wave lengths over the length of the panel. Figure 128 shows the configuration being considered. b = wave length of the panel sinusoidal vibration modes.

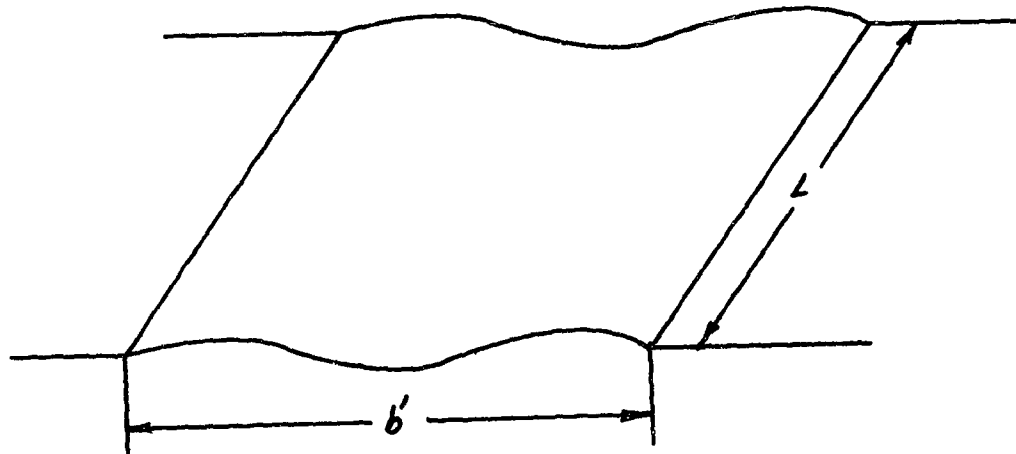


Figure 128: Flexible Panel Excited by Propagating Acoustic Pressure Waves

It is easily shown from Lagrange's equations of motion that if the different natural modes of vibration do not interact, then the equation of motion for the panel is given as:

$$M_{G_n} \cdot \ddot{\xi}_n(t) + \mathcal{L}_{G_n} \cdot \dot{\xi}_n(t) + \omega_n^2 \cdot M_{G_n} \cdot \xi_n(t) = F_{G_n}(t)$$

where $M_{G_n} = \int_0^b m \cdot \sin^2 \frac{n\pi x}{b'} \cdot dx$ = generalized mass for n -th mode.

$$C_{Gn} = \int_0^b c \cdot \sin^2 \frac{n\pi x}{b'} \cdot dx = \text{generalized damping for } n\text{-th mode.}$$

$$F_{Gn}(t) = \int_0^b F(x, t) \cdot \sin \frac{n\pi x}{b'} \cdot dx = \text{generalized force for } n\text{-th mode.}$$

$F(x, t)$ = surface pressure at point x and time t .

m = mass per unit length of the panel.

c = viscous damping constant.

ω_n = natural frequency of the n -th mode.

$\xi_n(t)$ = deflection of the panel, in the n -th mode, at the point or points where the n -th mode shape equals unity.

For a constant m and c , this equation is rewritten as

$$\ddot{\xi}_n(t) + \frac{c}{m} \dot{\xi}_n(t) + \omega_n^2 \xi_n(t) = \frac{1}{M_{Gn}} \cdot F_{Gn}(t)$$

and as shown in Section II this equation has the form,

$$\ddot{\xi}_n(t) + 2\zeta \omega_n \dot{\xi}_n(t) + \omega_n^2 \xi_n(t) = \frac{1}{M_{Gn}} F_{Gn}(t)$$

where

$$\zeta = c/c_{\text{critical}}$$

The pressure loading is that shown in Figure 124, and corresponds to acoustic pressures generated in the far field of a jet or rocket engine. If these pressure waves propagate over the structure so as to approximate a stationary random process, then the response in each n -th mode of vibration can be considered as stationary. If ω is the frequency of the pressure fluctuations at a point on the structure, then

$$\ddot{\xi}_n(t) = -\omega^2 \xi_n(t)$$

$$\dot{\xi}_n(t) = i\omega \xi_n(t)$$

so that the above equation takes the form,

$$(-\omega^2 + 2j\omega_n\omega + \omega_n^2) \cdot \ddot{y}_n(t) = \frac{1}{M_{G_n}} \cdot F_{G_n}(t)$$

The time correlation function can now be determined for both sides of this equation in exactly the same manner used to determine $R_{F_{G_n}}(\tau)$ on page 276.

The resulting equation can be written as:

$$R_{\ddot{y}_n}(\tau) = \frac{1}{M_{G_n}^2 \cdot |H_n(\omega)|^2} \cdot R_{F_{G_n}}(\tau)$$

where

$$|H_n(\omega)|^2 = (\omega_n^2 - \omega^2)^2 + 4\zeta^2\omega^2\omega_n^2$$

and where $R(\tau)$ in both cases is the time correlation over a narrow frequency band $\Delta\omega$ centered around the frequency, ω . Dividing both sides by $\Delta\omega$, setting $\tau = 0$ to obtain the mean squared value, this expression takes the form,

$$S_{\ddot{y}_n}(\omega) = \frac{1}{M_{G_n}^2 \cdot |H_n(\omega)|^2} S_{F_{G_n}}(\omega)$$

where $S_{\ddot{y}_n}(\omega)$ = power spectral density function of the deflection, \ddot{y}_n , in the n-th mode.

$S_{F_{G_n}}(\omega)$ = power spectral density function of the generalized force input to the n-th mode.

$S_{F_{G_n}}(\omega)$ can be given in terms of the joint acceptance of the panel as defined on page 277.

$$S_{\ddot{y}_n}(\omega) = \frac{A^2 \cdot j_n^2(\omega)}{M_{G_n}^2 \cdot |H_n(\omega)|^2} \cdot S_F(x_0, \omega)$$

where $S_F(x_0, \omega)$ = power spectral density function of the surface acoustic pressures at the reference point x_0 .

x_0 = reference point, most conveniently taken at the same point as \ddot{y}_n ; i.e., where the mode shape equals unity.

A = area of the panel.

The joint acceptance curve is that shown in Figure 126.

This equation may now be written in more convenient terms which will be consistent with those used in the flow chart of Figure 104 and in the discussion of mobility:

$$\Phi_R(x_o, \omega) = M \cdot \Phi_F(x_o, \omega)$$

$\Phi_R(x_o, \omega)$ = response function at the reference point x_o . (In this case, the power spectral density function of panel deflection.)

$\Phi_F(x_o, \omega)$ = force function at the reference point x_o . (In this case, the power spectral density function of the applied pressure.)

$M = \sum_n M_n$ = total mobility of the panel (equals the linear sum of the individual mobilities of each n-th mode of vibration).

M_n = mobility of the n-th mode of vibration.

$$= \frac{A^2 j_n^2(\omega)}{M_{Gn}^2 [(\omega_n^2 - \omega^2) + 4\zeta^2 \omega^2 \omega_n^2]}$$

For the case being considered,

$$M_{Gn} = \frac{mb}{2} = \frac{1}{2} \mathcal{M}, \text{ for all } n$$

where

$$\mathcal{M} = \text{total mass of panel.}$$

Thus

$$M_n = 4 \left(\frac{A}{\mathcal{M}} \right)^2 \frac{j_n^2(\omega)}{[(\omega_n^2 - \omega^2)^2 + 4\zeta^2 \omega^2 \omega_n^2]}$$

It should be noted that the response function could have been given in terms of velocity, acceleration, or stress spectral density. Acceleration spectral density, $\Phi_R(x_o, \omega)$, (the derivative is symbolic) is given by

$$\ddot{\Phi}_R(x_0, \omega) = \omega^4 \cdot \Phi_R(x_0, \omega)$$

$$= 4 \left(\frac{A}{M}\right)^2 \cdot \Phi_F(x_0, \omega) \cdot \sum_n \frac{j_n^2(\omega)}{\left[1 - \frac{\omega_n^2}{\omega^2}\right]^2 + 4\zeta^2 \left(\frac{\omega_n}{\omega}\right)^2}$$

In order to obtain stress spectral density, it is necessary to determine a constant of proportionality, K, which relates stress and deflection at the reference point,

$$(\text{Stress at } x_0) = (K) (\text{total deflection at } x_0),$$

and the stress spectral density becomes:

$$\frac{\ddot{\Phi}_R(x_0, \omega)}{(\text{Stress})} = 4 K^2 \left(\frac{A}{M}\right)^2 \cdot \Phi_F(x_0, \omega) \sum_n \frac{j_n^2(\omega) \cdot \omega^2}{\left[1 - \frac{\omega_n^2}{\omega^2}\right]^2 + 4\zeta^2 \left(\frac{\omega_n}{\omega}\right)^2}$$

It is seen from the above equations that for a nearly flat pressure spectrum, $\Phi_F(x_0, \omega)$, the response will be relatively large when the frequency of the pressure fluctuations at any point on the panel equals the natural frequency, ω_n , of one of the natural modes of vibration. This condition is known as resonance, and the denominator of the n-th term in the above series expression equals $4\zeta^2$, for resonance in the n-th mode of vibration. Clearly, if the panel damping is small, the response could be quite large. Considering once again the n-th mode, it is seen from the curve of joint acceptance shown in Figure 126, that the response is highest for any input frequency, ω , when the ratio, b/λ , equals unity, except the first mode of vibration, ω_1 . When $b/\lambda = 1$, the pressure variation over the surface of the panel is in phase with the deflection shape of the panel. This condition is known as coincidence (i.e., coincidence between the panel shape and the pressure shape). When $b/\lambda = 0$, the waves are propagated perpendicular to the surface of the panel, and if the frequency of these incoming waves equals the natural frequency, ω_n , then the response of the panel will be larger than for any other mode of vibration and for any other type of pressure variation over the surface. For all other frequencies of the panel, the response is largest whenever both resonance and coincidence occur simultaneously. The latter phenomenon is discussed in greater detail in Reference 13.

RESONANCE ON RESONANCE

INTRODUCTION

The response of primary vehicle structure to random excitation is highly concentrated at the few natural frequencies of the structure. This concentration is easily noticed on a frequency response analysis of vibration pickups mounted directly to structure. If a small part were mounted directly to structure the question arises under what conditions the resonant response of primary structure might act as an input to the small part. The response of the small item would then be doubly amplified when its natural frequency agrees with one of the natural frequencies of primary structure. The probability of frequency agreement will increase as the number of secondary items increases.

A general feeling for the coupling between the masses of a two-degree-of-freedom system suggests that when the masses are of the same size two distinct coupled modes appear sufficiently separated in frequency that the modes act independently in their response to random excitation. The suggestion was made, however, that when the secondary mass was small compared to the primary mass resonance on resonance might exist.

The hypothesis was tested through a general study of the complete two-degree-of-freedom system shown in Figure 59. The primary structure is given by mass M and the secondary item by mass m . The mathematical work is presented by means of appendix A. Generality was maintained throughout. The particular conditions under study were equal uncoupled frequency and an exciting frequency which agrees with the lower coupled frequency. As the secondary mass becomes smaller relative to the primary mass the coupled frequencies converge. Damping normally possessed by structure, 3.3% of critical damping or a resonant amplification factor of 15, was used. Effects of both sinusoidal and random excitation were studied.

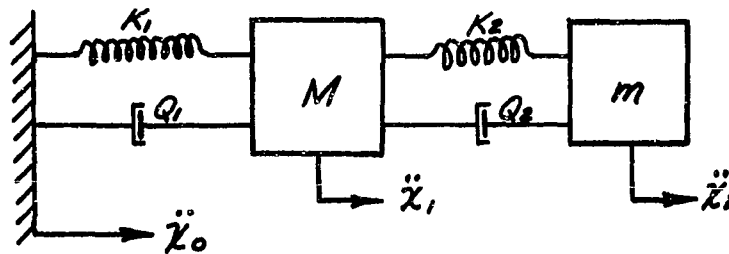


FIGURE 129 Two-Degree-of-Freedom System

DISCUSSION

The two-degree-of-freedom system with and without damping for sinusoidal excitation has been studied extensively. However, the literature does not contain a satisfactory discussion of the random case with damping. The case is studied here in detail with the results presented as a function of the mass ratio.

The results are presented in figures 130-132. The results reflect excitation at the lower coupled frequency since it was shown that response to excitation at the higher coupled frequencies led to a lesser response. A comparison of the responses to white noise excitation is shown in figure 132 although the input conditions are slightly different from those used in the remaining analysis. The response of both the primary and secondary masses to sinusoidal and random excitation is presented in figures 130 and 131. The results demonstrate the phenomenon of resonance on resonance as the mass ratio becomes large. The small mass approaches the asymptote Q^2+1 in the sinusoidal case and $.6 Q^{3/2}$ in the random case. These are the expected values except for the factor 0.6 in the random case. The deviation in the random case may be due to introducing the excitation to the secondary mass in an indirect way through the primary mass. The response frequency is the lower coupled frequency as expected and this frequency converges to the equal uncoupled frequencies as the mass ratio increases. The amplitude of response of the small mass is a smoothly varying envelope influenced once again by the filtering of the primary mass. This deviation from random response may also partially account for the less than expected response of the small mass in the random case.

The theoretical results are presented in figure 130 and 131 as solid lines with the analog results shown by the circled points. In addition, the random response case was given an additional check through the use of normal mode response analyses. Good agreement between the various approaches is shown. Appendix A contains the detailed mathematical derivations.

The original hypothesis of resonance on resonance is correct when near coincident natural frequencies exist between the modes of primary and secondary structure and when high mass ratios occur. Thus the two-degree-of-freedom system has been shown to respond in different ways depending on the mass ratio. Either the system acts as independently coupled modes for mass ratios near unity or as a resonating primary mass causing the secondary mass to resonate doubly for high mass ratios. The phenomenon explains one of the major causes of the failure of small parts mounted directly to primary structure. The phenomenon appears to be unavoidable when black box equipment containing a great number of small parts is mounted to primary structure without vibration isolators.

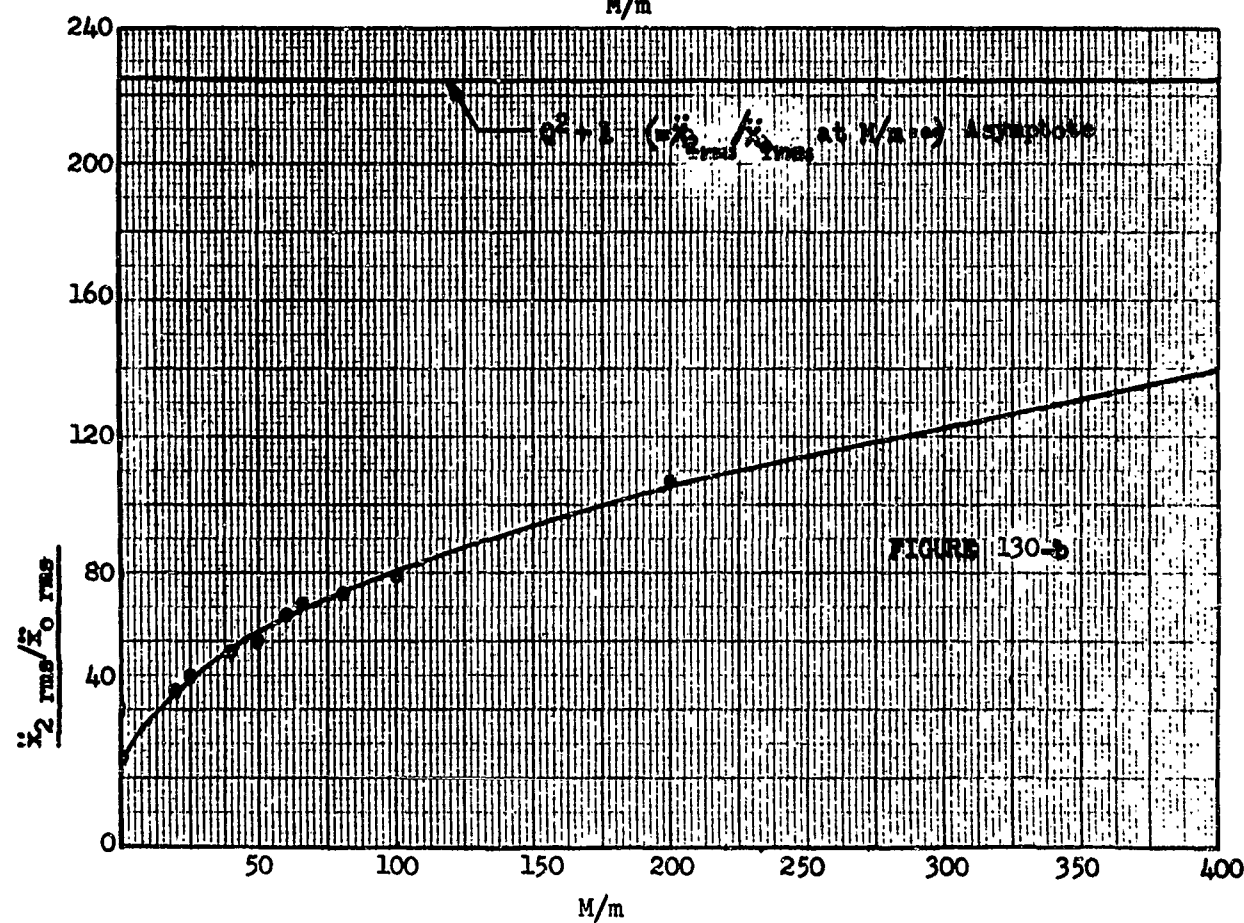
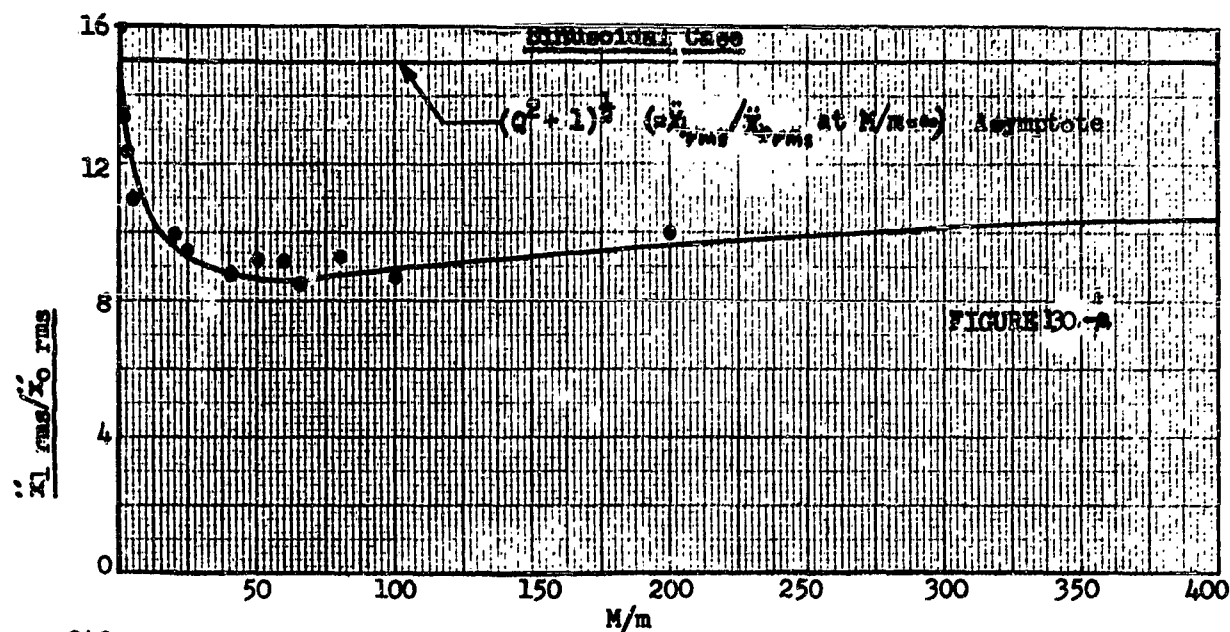


Figure 130-a 130-b. Response of Primary Structure and Secondary Items as a Function of the Mass Ratio.

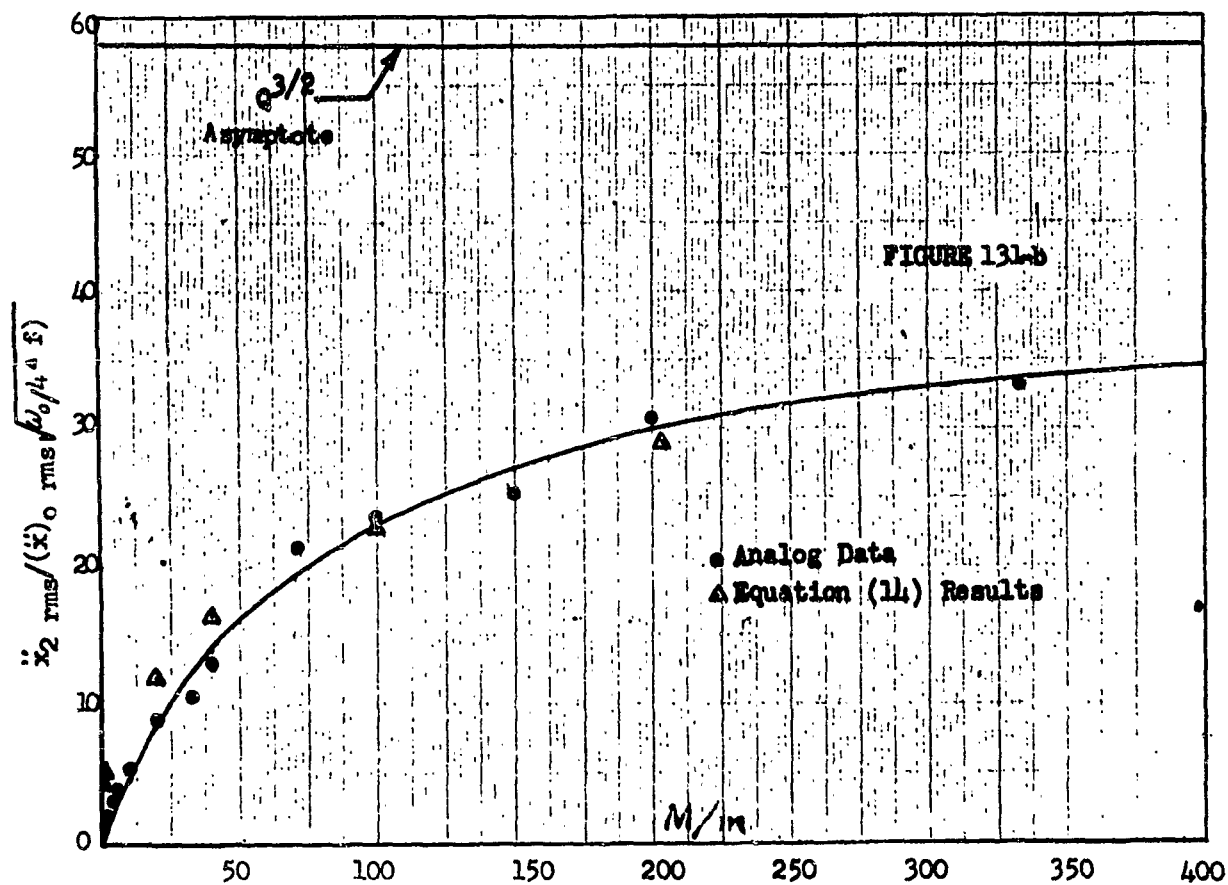
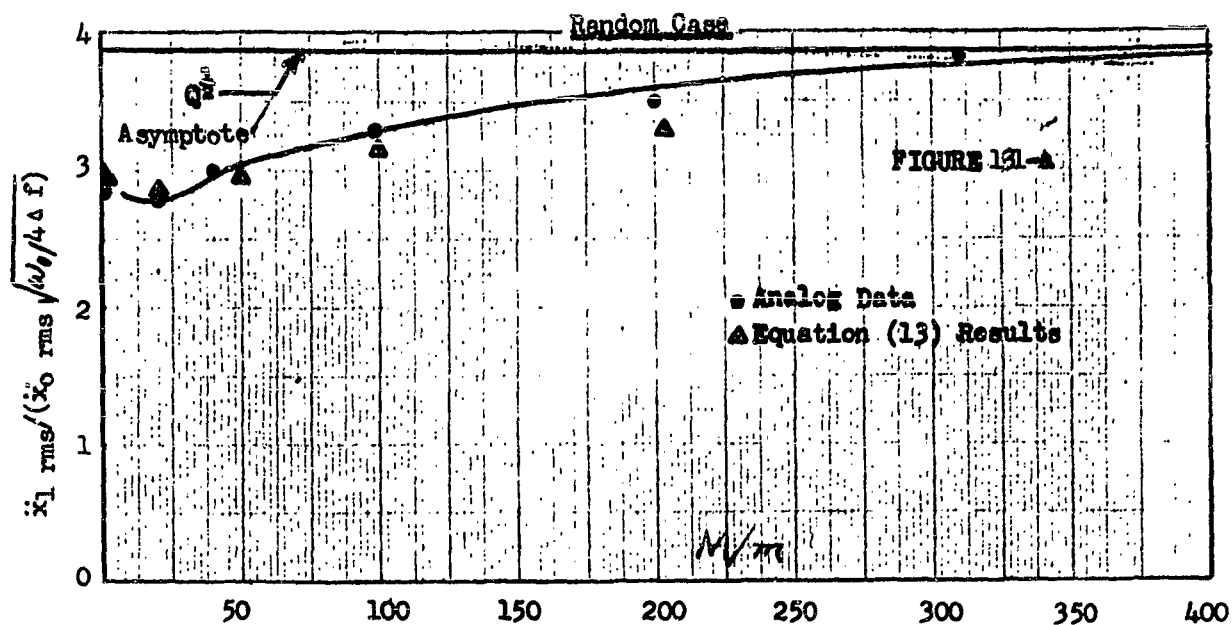


Figure 131-a 131-b. Response of Primary Structure and Secondary Items as a Function of the Mass Ratio.

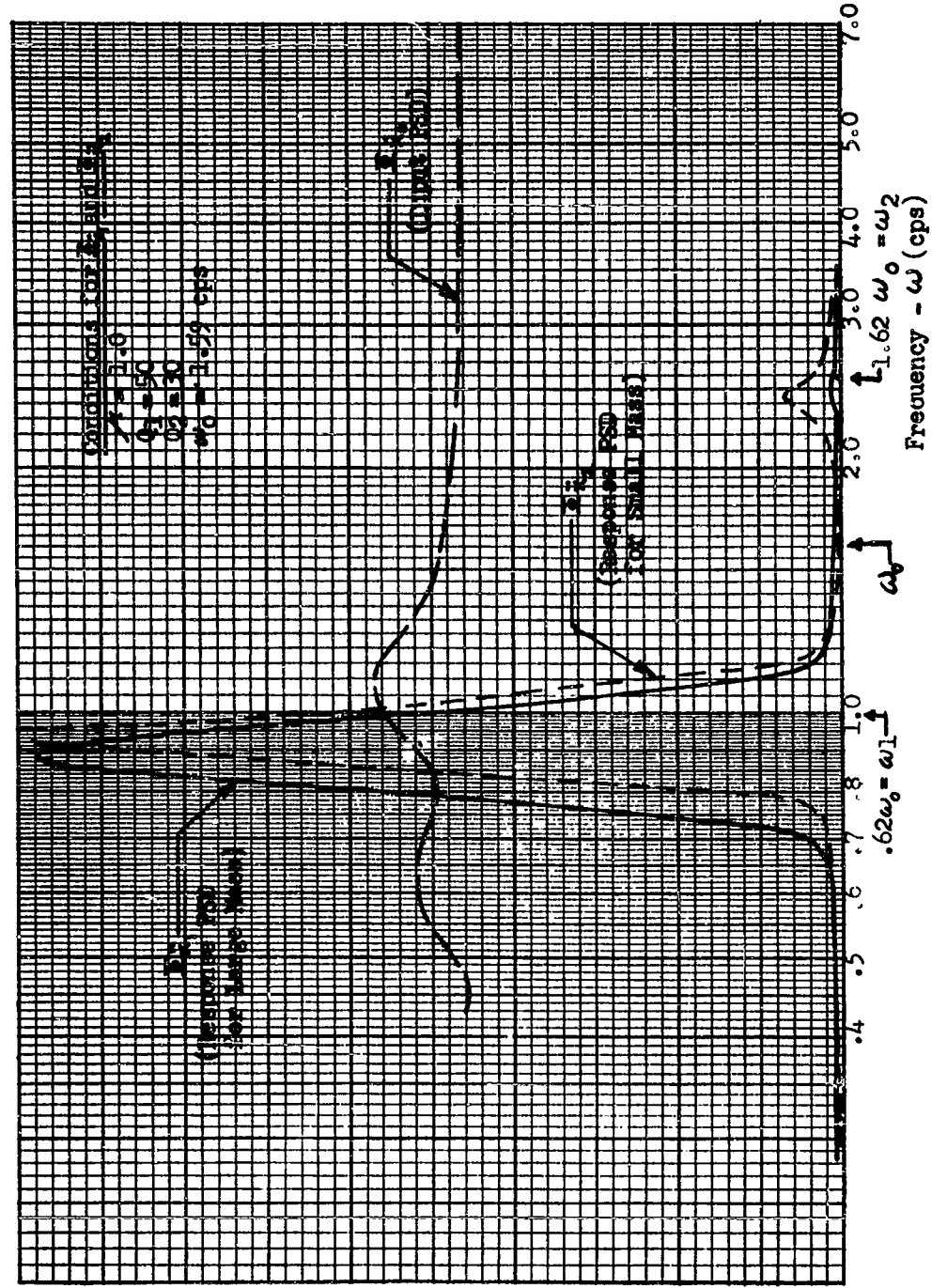


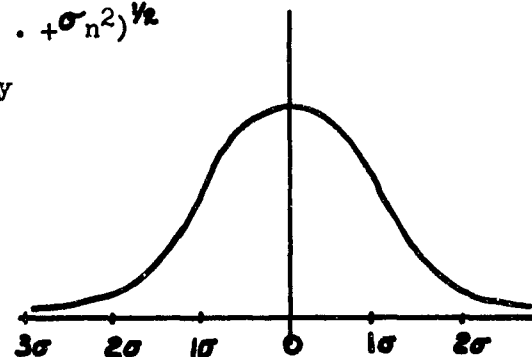
Figure 132. Power Spectral Density of the Input and Response.

RULES OF ADDITION FOR RANDOM PROCESSES

The addition of a number of sine waves is a vector addition which accounts for both magnitude and phase. An independent random process is described by its statistical characteristics because its future value is not predictable. Both the amplitude and phase are random and only certain conjectures are possible regarding future expected values. The statistical properties which define a random process are the mean value or d.c. component, the rms value of the a.c. component, the probability density function and the power spectral density. The same statistical characteristics which define a single random process also describes a sum of several processes. The probability density function defines the probability of occurrence of amplitudes greater or less than a given value. The area under any segment of the probability density function is the probability that the instantaneous amplitude of the time function is between the amplitudes bounding the area. The power spectral density is the distribution in frequency of the power of the signal, i.e., the a.c. component. The area under any segment of the power spectral density curve is the mean square value of the function between the frequencies which bound the area. The following equation defines the rms value of the sum of a number of components.

$$\sigma_{\text{TOTAL}} = (\sigma_1^2 + \sigma_2^2 + \dots + \sigma_n^2)^{1/2}$$

It is not necessary that the two waves have any common frequency content for the sum to exist. The sum is also independent of the probability density function of the components. The power spectral densities are directly additive over the common frequency band.



Probability Density Function

Figure 133

Many of the vibration and acoustic phenomena are closely described by the Gaussian or Normal amplitude probability density:

$$p(s) = \frac{e^{-(s-m)^2/2\sigma^2}}{\sigma\sqrt{2\pi}}$$

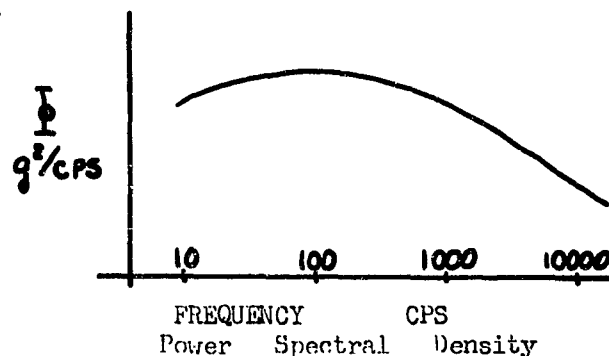


Figure 134

The parameters m and σ are the mean and rms values of the process. If the time function were Gaussian random noise, σ^2 is the total area under the power spectral density curve; a point of interest since it represents the only connection between the density function and the frequency distribution of the power. The sum of the mean values is

$$m_{\text{TOTAL}} = m_1 + m_2 + \dots + m_n$$

If $p_1(s)$ and $p_2(s)$ are the amplitude probability density functions of two component processes associated with two time functions $F_1(t)$ and $F_2(t)$

$$p_{\text{TOTAL}}(s) = \int_{-\infty}^{\infty} p_1(x) p_2(s-x) dx$$

This integral is the convolution integral of the function $p_1(s)$ and $p_2(s)$, and results in a Gaussian density function for the total when the components are Gaussian. An example calculation is given in Appendix B for the sum of a narrow band Gaussian component with a sinusoidal component. The resulting distributions are plotted on page 457 for various ratios of the sinusoidal amplitude to the random rms amplitude. When the sine components drop out, the familiar Rayleigh distribution of peaks results. It should be emphasized that the above remarks are applicable to stationary processes - i.e., to processes having statistical properties which are time invariant. In practical cases the environment of structure and equipment changes during the progress of the mission, but the excitation or response can usually be broken into segments which can be considered as stationary processes.

METHOD OF ESTIMATING VIBRATION RESPONSE TO MANY SOURCES

The above rules of addition for random processes define at any point in the vehicle the composite response resulting from many sources. The composite is a variable in its amplitude, frequency spectra, and probability density function over the whole vehicle and in addition, each of these quantities also vary with time. The manner in which changing conditions throughout a mission and during the service life of the vehicle may be accounted for, will be considered in Part 3. Coalescing of the composite responses into single simplified process will be discussed in the light of the nonlinearities, intermixing of the load levels and equivalent damage concepts.

REFERENCES

1. Lanning, J. H., Jr., and Patten, R. H., Random Processes in Automatic Control. McGraw Hill, 1956.
2. Bendat, J. S., Principles and Applications of Random Noise Theory. John Wiley and Sons., Inc., 1958.
3. Miller, K. S., Engineering Mathematics. Rinehart and Co., Inc., 1956.
4. Powell, A., "On the Response of Structures to Random Pressures and to Jet Noise in Particular", Chapter 8 of Random Vibrations by Stephen Crandall. Technology Press of M.I.T., 1958.
5. Clarkson, B. L., "The Effect of Jet Noise on Aircraft Structures", The Aeronautical Quarterly, Vol. X, May 1959.
6. Powell, A., "The Problem of Structural Failure Due to Jet Noise", British Report, ARC 17, 514.
7. Crandall, S. H., "Mechanical Vibrations with Deterministic Excitation". Chapter I of Random Vibrations, Technology Press of M.I.T., 1958.
8. Kriewall, T. E., and Johnson, J. C., "A Network Approach to Vibration Analysis", ASTIA AD No. 14915, August 1957.
9. Sivian, L. J., and O'Neil, H. T., "On Sound Diffraction Caused by Rigid Circular Plate, Square Plate, and Semi-Infinite Screen", JASA 3, 483-510, 1932.
10. Wiener, F. J., "Sound Diffraction by Rigid Spheres and Circular Cylinders", JASA 19, 444-451, 1947.
11. Wiener, F. M., "Sound Diffraction of Disks in Square Plates", JASA 1949.
12. Shock and Vibration Bulletin No. 24, "Vibration and Acoustic Environmental Measurements as Applied to Snark Equipment in an Experiment Using Isolation Material Between the Boosters and the Missile".
13. Dyer, Ira, "Estimation of Sound-Induced Missile Vibration", Chapter 9 of Random Vibrations, edited by Stephen H. Crandall, Technology Press of M.I.T. 1958.

V PANEL VIBRATIONS

The purpose of this section is to consider the dynamics of those structural elements which are most likely to have their greatest response in the frequency range just above that of the basic body modes. Although a variety of structural elements may have resonances in this region, it is felt that panels constitute the largest and, except for isolated cases, the most important class of such elements. Of primary interest are the exterior panels which are exposed to the intense acoustic environment of the jet and rocket engine exhaust noise and the boundary layer noise. However, since various types of structural elements exhibit panel vibration characteristics in response to oscillatory excitation caused either by changing surface pressures or by foundation motion, it is expedient to consider the general problem of panel vibrations in this section. The term "panel" is used here in the broad sense in that certain structures not having the immediate appearance of a panel may actually have response properties which are much like those of normal panels.

The first section consists of a brief description of panels, with examples, in an attempt to show the wide variety of structural types that may be classified as such. The second section deals with the problem of the determination of panel natural frequencies and mode shapes showing the sensitivity of these to parameters such as mass and stiffness distribution, edge fixity conditions, foundation flexibility, and certain nonlinearities such as membrane stresses. In the third section, the important factor of panel damping is considered. This includes material, acoustic, coulomb and visco-elastic damping and the nonlinearities introduced by each.

GENERAL DESCRIPTION OF PANELS

Panels might be broadly characterized by structural elements which have surface dimensions which are large in proportion to their thickness and which are weakly supported over their surfaces, except at the boundaries or portions thereof, for certain frequency ranges and applied loads so that their greatest degree of freedom in deflection generally lies normal to their surface. For the obvious cases of panels for which geometry alone dictates the boundaries of the panels this is a trivial comment. However, this description has been made sufficiently broad to include such cases as groups of normal panels acting jointly as one single isolated panel or sections of a large stiffened panel which respond individually as isolated panels.

No clear-cut rule can be given for defining the boundaries of a panel, as defined here, and must rest upon experience and engineering judgment. The parameters which must be considered are geometry, distribution of structural mass and stiffness, and the distribution, phase, frequency, and direction of the applied loads. For example, a thin flat plate with no added stiffness, except at

the edge, mounted on a massive rigid frame certainly will have panel response to applied pressure loads of any sort. Consider next a group of such flat plates mounted on a flexible framework and loaded with oscillating acoustic pressures. The effective panel boundaries of the latter system are very likely to be determined by the area or region over which the acoustic pressures are in phase, or nearly so, i.e., over the system area where some degree of pressure correlation exists. Finally, for panels of different surface densities and different stiffnesses mounted adjacent to each other, the distribution of mass and stiffness of the system may dictate panel boundaries by indicating the amount of dynamic coupling between the adjacent panels.

Examples of typical structural elements exhibiting panel characteristics are: external fuselage or main body skin, body cylindrical shells or portions thereof, nose cones or portions thereof, wing flaps, control fins or their surface skins, exhaust nozzles of rocket or jet engines, bulkheads, blunt trailing edge cover plates, flat panel type equipment racks, portions of fuel tanks, flat equipment mounting brackets, etc.

The construction of structural panel type elements have a wide variation. These may consist of sheets of material which may or may not be uniform in surface mass and stiffness and may or may not have additional stiffeners attached to the surface. For certain applications, sandwich type of construction may be used such as honeycomb and other laminated materials. Composite structures of ribs, longerons and thin skin are also used, particularly for control surfaces. These built-up structures may definitely experience vibrations of a type other than panel response, such as the vibration of a single component of this structure. The latter is not discussed in this section. When considering panel type response of surface stiffened or built-up structural elements, which display panel response properties, sufficient engineering accuracy is usually attained (for purposes of determining the response characteristics of a panel) by replacing the actual structure by an equivalent uniform panel having the same surface density and stiffness.

With this equivalence, many geometrical shapes are possible. These include flat plates, cylindrical and conical shells or portions thereof, and shells with double and compound curvatures such as spherical and parabolic sections. In addition, these shapes may have a variety of peripheral geometries, of which the rectangular and circular boundaries are the most common. Multiple disconnected boundaries may be encountered in cases of cut-outs in a structural element responding as a panel.

In any practical case, boundary or edge fixity conditions are seldom ideal. Panels such as exhaust nozzles, some bulkheads, and panels with cut-outs have a free edge. The other edge or edges of these panels and the edges of most other panels will be characterized by some degree of edge fixity between the conditions of pinned and fully clamped edges and even vertical mount flexibility. In addition, the edge fixity is not always uniform along the entire edge as the panel may be attached to stiffeners or primary structure having different masses and stiffnesses along different edges of the panel, say of a rectangular plate.

NATURAL RESPONSE CHARACTERISTICS OF PANELS

As with any dynamical system, the response of panels to applied oscillatory forces depends upon the magnitudes and distributions of these forces, the mode shapes of the panels which are a factor in determining the effective or generalized force input, the ratios of the forces and natural frequencies, and the amount of inherent damping in the panel and the amount of damping provided by the surrounding medium. This section deals with the mode shapes, natural frequencies, and damping in the panel system. The discussion is divided into two parts: consideration is first given to the undamped modes and frequencies, and secondly to the effects of panel damping. This division follows the method of analysis generally used for dynamics problems; i.e., first the modes of vibration and their corresponding frequencies are determined by assuming no damping in the system and then the panel frequency response function is determined in terms of these undamped natural frequencies and the panel damping. (See for example the one degree of freedom system discussed in Section II.) This approach has the advantage that the mode shapes considered are invariant with time, a condition which would fail to exist if damped mode shapes were used.

Mode Shapes and Natural Frequencies of Panels

A rigorous determination of the undamped mode shapes and natural frequencies of panels is a difficult procedure analytically for all except very special cases where ideal conditions such as panel uniformity in mass and stiffness, simply supported or clamped edges, and simple surface and peripheral geometries are assumed to be valid. Fortunately, for practical applications in engineering, this rigour is unwarranted because the forcing functions are generally crude approximations of the actual inputs which are often random in nature, and because the exact response has little value in other than defining the overall stress level of the panel for fatigue and reliability analyses and the overall acceleration level as might effect neighboring structures and equipment. However, in order to minimize the accumulation of error in design and dynamic analysis, every reasonable effort should be made to determine these mode shapes and panel natural frequencies as closely as possible. In view of the fact that actual panels are seldom ideal and since available solutions to this problem are generally ideal solutions, it is especially important that the dependence upon sensitive parameters of geometry, edge fixity, non-uniformity, etc., be determined, even if these dependencies are of the single parameter type where coupling of parameter changes is neglected.

Essentially three methods may be used for determining panel mode shapes and frequencies; analytical, empirical, and by direct testing. The analytical approach consists essentially of solving a boundary value problem in which the unforced equations of motion of the panel or the expressions for its kinetic and potential (strain) energies are made to satisfy certain assumed geometric or natural boundary conditions along the edges of the panel. The empirical determination of panel mode shapes and frequencies can be performed with the

use of scaling laws, the functional forms of which are usually based upon frequency equations derived analytically, which show the variation of mode shapes and frequencies with parameters such as size, shape, edge fixity, etc., and which can be used to adjust the known frequency, say, of one panel to that of the desired panel. Direct testing of panels for the natural response characteristics is performed by a laboratory duplication of the manner in which the panel is to be mounted and then applying a frequency sweeping sinusoidal force to the panel by means of a shaker or by means of a monochromatic acoustic noise. Which method is to be used in any situation depends upon the accuracy required, the computing equipment available for analysis, the ability for the laboratory to duplicate the actual mounting conditions, the degree of geometric complications of shape of the panel, the degree of non-uniformity of the mass and stiffness of the panel and of its edge fixity, and the number of natural frequencies required. A few of the most important aspects of these three methods are discussed below.

The analytical equations used for the mathematical model of the panel may be obtained from the partial differential equations of motion for panel deflection in which all forces external to the panel are neglected along with the panel damping constants. They may also be obtained in integral form from the expressions of the maximum kinetic and potential, or strain, energies of the plate in terms of the panel deflection function, which of course is unknown. In either case, the deflection is assumed in the form of a series of known functions which satisfy the natural boundary conditions of deflection and slope at the edges of the panel. These functions for example may be trigonometric (sines and cosines) or uniform beam modes. Many others are also possible. The series assumed will involve constant coefficients as factors with the known functions. These must then be determined from orthogonality relations of the assumed functions, if they exist, or from the minimization of the frequency, or certain energy relations or from the minimization of functions which express the error in the approximation being used with respect to the exact solution. Many such methods are used in this problem and they are too numerous to mention here, and the mathematical complications involved in each are beyond the scope of this report. It is necessary here to merely appreciate the general approach used in the analytical method in order to understand why certain simplifying assumptions are made in theory.

Since the simplifying assumptions often made in theoretical work of this nature are generally based upon sound engineering judgment, it is necessary at this point to understand the nature of the complications which arise in the mathematical model discussed above. The origins of a number of these complications are as follows:

- (1) coordinate geometry required for defining the middle surface of the panel and its edges
- (2) functionally satisfying simultaneously the natural boundary conditions of deflection and slope at all edges of the panel and at other restrained points on its surface

- (3) coupling of the motions of the panel in different directions, such as the radial, circumferential and axial motions of a cylindrical surface
- (4) combined effect of bending flexure (inextensional motion) of the middle plane of the panel and the membrane-like stretch (extensional motion) of this plane
- (5) non-uniformity in panel mass and stiffness distribution
- (6) nonlinearities resulting from the change in stiffness, damping and mass (apparent mass due to gas or liquid medium) with the maximum deflection amplitude of the panel
- (7) foundation flexibility, which may be non-uniformly distributed along the boundaries in linear and rotational deflection
- (8) thick panels which permit extensional vibrations between the two faces of the panel
- (9) large deflections of the panel which greatly distort the panel from its equilibrium position

No analyses are available in which the combined effects of the above situations are accounted for. Further, there are but a few analyses which involve the combined effects of more than two and at most three of the above. Unless large scale computer programs are developed and made available to the engineer, the effects of the above conditions on the frequencies and mode shapes of panels must be taken individually, i.e., a single parameter at a time and even then the analysis will be somewhat ideal. Digital computer programs may be set up to solve the difference equations for the equations of motion, where effectively the panel is subdivided into a lattice of mass points and springs as an approximation to the actual panel. Pages 30 through 35 contain a list of a few equations for panel frequency taken from available literature which will be used in an attempt to show the variation in frequency with certain parameters. Volumes of literature have been published on the subject of mode shapes and frequencies of panels. Included in the bibliography are a few references of analyses of flat plates and curved shells for special cases of surface and peripheral geometries.

Fortunately, as will be seen later on, the lowest frequencies are predominant in response level, especially when rather broad band excitation is applied to the panel. Thus, only the first and possibly the second mode of vibration of a panel need be determined especially for deflections normal to the panel surface. It is possible, however, that inputs with essentially high frequency content, such as shocks, could cause significant response at higher resonance frequencies, so that from a fatigue standpoint these could be important.

The above discussed analytical methods, except for computer programs, will yield expressions which approximate the panel frequencies for various small ranges of parameters such as size, geometry, fixity, etc. Equations for mode shapes are

not readily available since they are far too complex for practical usage. These frequency equations may be used for scaling laws where only the functional form of the equations are maintained and the constants are supplied from measured full scale or model type test data. It is important to note that these scaling laws used for the empirical determination of panel frequencies are seldom sufficiently general to accurately predict frequencies over other than a narrow range of panel variables because of changing physical phenomena in the panel over large variations in such things as curvature, length, thickness, fixity, etc.

From what has already been discussed, it is seen that the direct testing of full scale panels clearly has an advantage over the theoretical approach in being able to more realistically account for the effects of geometry, mass and stiffness distribution, edge fixity, etc. They have the disadvantage, however, of being both time consuming and costly, especially when the conditions of edge fixity are to be closely duplicated with those corresponding to actual usage of the panel. For panels which are clearly defined by their geometric boundaries, the isolated panel characteristics will not be difficult to obtain as a massive and rigid mounting may be used. However, if the effects of the elastic support are to be considered, or in the case of a group of panels acting jointly as a single panel, the direct test of the panel may become quite involved.

Because of the high intensity broad band acoustical noise associated with space vehicles, the natural response characteristics of the thin cylindrical body shells which are exposed to this excitation should be of greatest interest. The nature of these random acoustical inputs is such that only portions of these cylindrical shells are expected to display panel-like vibrations, the entire shell being seldom excited at frequencies above the basic body frequencies. These sections of the cylindrical shell are expected to exist between ring type circumferential stiffeners or between sections of the middle which are very massive, such as fuel tanks and bulkheads. The end fixity conditions for these shells may vary from fully clamped ends to simply supported ends, where the fixity at both ends need not be the same.

The natural frequencies of these cylindrical shells including the effects of pressure may be determined from the approximate frequency equations given on page 310 and the nomographs presented in Figures 138 through 141. These were nomographs obtained from Reference 61. These equations and nomographs cover a wide frequency range including beam, ring and flat plate type cylinder vibration modes, and can, therefore, be used for obtaining the fundamental body frequencies of an entire uniform (in thickness, density, and stiffness) cylindrical body. Caution must be used here for the fundamental modes since the presence of large masses such as fuel tanks attached to the skin will greatly alter these fundamental uniform cylinder frequencies.

These equations, given in terms of the free flexural wave velocity on the surface of the cylinder, are only approximate for $q = 1$ and $q = 2$, but are very nearly exact for $q > 2$. It is to be noted from the nomographs that the effect of internal pressure, $\Omega = (1+2) \frac{pR}{Eh}$, is negligible for the lower modes corresponding to $n=0$, but has a considerable effect for $n=3$. The general effect of internal

pressure is to effectively increase the surface stiffness of the cylinder and to thus raise the cylinder natural frequencies. The mode shapes corresponding to various values of n and q are shown on page 315.

When only the transverse surface vibrations of the cylinder are of interest, the frequency equation given on page 311 can be used, and this equation more clearly shows the effect of internal pressure on the natural frequencies. This equation which was derived under the assumption that the axial and circumferential inertial forces could be neglected for transverse vibrations, Reference 17, has the additional advantage of showing the relative contributions of the middle plane inextensional flexural motion and the membrane-like stretch of the middle plane extensional motion. The mode shapes corresponding to this equation are also shown on page 311, where m corresponds to q , in the first frequency equation, page 310.

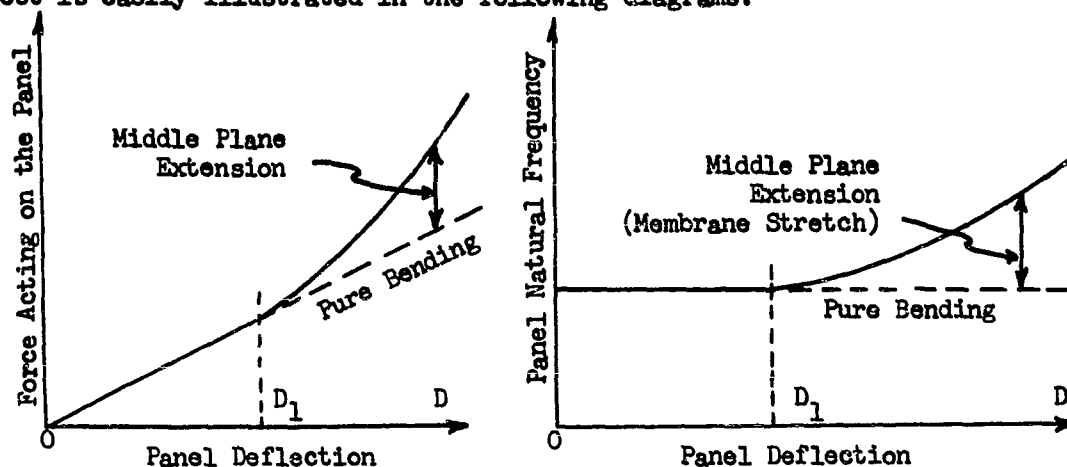
Figure 139 shows a comparison of the exact cylinder frequencies for a number of different modes of vibration with those approximated by using the equation given on page 311. Figure 140 shows the number of circumferential waves that might exist at the lowest natural frequency of vibration, for values of internal pressure. A plot of a typical frequency response curve is presented in Figure 141 for a thin pressurized cylindrical shell.

The concept of inextension and extension is important in dealing with panel vibrations for any shaped panel. Aside from the assumptions that (1) the vibrations in different directions in a uniform panel may often be uncoupled and (2) that certain inertial forces may be neglected, the greatest simplification in the frequency equations for panels is effected when the energies developed by either extensional or by inextensional motion can be neglected, i.e., when the motion is purely extensional or purely inextensional. Pure inextensional or flexural modes are proportional to the thickness of the panel whereas pure extensional or stretching modes are independent of this thickness. Higher energies are required to excite the extensional modes than are required for the inextensional modes. Therefore, the lowest frequencies are associated with inextension so that the higher frequencies of extension are often of little importance. The importance of each, however, is dependent upon the type of excitation applied. For example, if only radial forces of uniform intensity and phasing are applied to a uniform circular cylinder, the frequencies of interest will be those of extension. In any actual structure both extensional and inextensional effects will be present. For a circular cylinder fixed at both ends (zero deflection), pure inextensional or flexural vibration cannot exist as the boundary conditions are not satisfied. However, as discussed in Reference 34, the condition of pure flexure does exist over most of the cylinder with extension being confined to a narrow "boundary layer" at the ends of the cylinder, the length of which is on the order of the cylinder thickness. In this case the energy developed by extension is negligibly small. On the other hand, for such panel shapes as cones, spheres, etc., the inextensional frequencies are infinitely large so that the fundamental frequencies will be those corresponding to extension. Simple examples of pure extensional vibration are longitudinal vibration of rods and cylinders and the torsional vibrations of cylinders.

The frequency equations for pure inextension shown on page 318 for a uniform circular cylinder are derived in Reference 62. The two dimensional vibration equation corresponds to that flexure term in the equation on page 311. These are included here in order to show the effect of considering the vibration of the cylinder as being three dimensional. Also shown on page 318 are the frequency equations for pure extensional cylinder vibrations, which for special cases reduce to the frequency equation for pure radial motion, longitudinal motion and torsional motion.

A majority of the panels encountered in space vehicles will be curved in the form of cylindrical sections with some having double curvature. The curvatures of these are such that they may often be adequately approximated as flat panels. As will be shown, the effect of this curvature is to increase the stiffness so that the comparable flat plate frequencies will be lower than the actual frequencies of the curved panels. Numerous examples of flat panels are also available in the form of bulkheads, fins, etc. Since flat panels are much simpler to analyze theoretically, the effects of changes in edge fixity and peripheral geometry are best evaluated for flat panels. Although flat panel frequency equations are available from various references, a fairly complete list is compiled here and given on pages 319 through 321 for the cases having known solutions. Frequency equations for rectangular panels mounted on elastic foundations are also included. These are presented for ready availability in making comparisons.

The geometry of flat panels is such that the transverse vibration modes are, for all practical purposes, essentially inextensional for small deflection amplitudes. Extension of the middle plane in the form of biaxial tension occurs, however, when the center deflection of the panel exceeds approximately two panel thicknesses. This increases the effective panel stiffness and thus increases the natural frequency. This effect on the natural frequency is a progressively non-linear effect as the panel frequency is dependent upon the amplitude, whereas for small deflections the frequency is independent of this amplitude. This effect is easily illustrated in the following diagrams:



Using the assumption that the load versus deflection curve can be approximated by the expression, $(\alpha_0 D + \beta_1 D^3)$, a method is developed in Reference 15 for computing the natural frequency of a clamped rectangular panel in terms of the panel's center deflection. The equations required for this computation are presented on page 322 and the necessary curves taken from Reference 9 are shown in Figure 143. A relatively simple expression for frequency has been developed by Timoshenko, Reference 64, which accounts for the middle plane extension of a thin clamped circular flat plate. This equation is shown on page 326.

As an example of these membrane effects, measured test results for clamped plates, taken from Reference 1, are presented in Figures 145a and 146 which show respectively the static stress versus static pressure for four flat plate thicknesses (.032, .040, .064, .081 inches), and the peak amplitude stress versus frequencies for the .040 inch thick flat panel for three different pressure levels (.00184, .00366, .0147 psi). The increase in frequency with amplitude is clearly shown. Figures 145b and 147 show similar data for cylindrically curved panels with clamped edges. It is to be noted in Figure 150 that for relatively low peak stress amplitudes (relatively low deflection), the panel stiffness increases, with applied load, thus increasing the panel natural frequency. But, as the amplitude further increases, the stiffness is reduced which lowers the natural frequency. As explained in Reference 1, this effect is most likely due to panel dimpling for high loads. In addition, it should be noted by comparing Figures 146 and 147, that since the over-all panel dimensions were the same for the flat and curved panels, the effect of curvature is to generally increase the panel stiffness; the effect here was to roughly double the panel natural frequency.

The combined effect of panel thickness and panel deflection upon the middle surface extension is shown in Figure 148. It is seen that for decreasing thickness and/or increasing deflection (or stress), the energy absorbed in extension becomes relatively greater. The effect of membrane deflection on the amplification factor at the panel natural frequency is shown in Figure 149 for one flat panel.

It has been shown above for one test condition how a single curvature of a panel affects the natural frequency. The effect of double curvature of thin shells is shown in Figure 150, Reference 35. Here the lowest axi-symmetric vibration frequencies of shallow spherical shells are plotted in terms of the fundamental frequencies for the equivalent flat circular plate with zero Poisson's ratio, for various ratios of center depression depth, H , of the shell to the shell thickness, h , and for various values of Poisson's ratio, ν . The frequency equations for these shells are not presented here as they involve parameters which are not easily defined. It is of interest to note, however, that the inextensional frequencies of very shallow shells are independent of the curvature when the circular edge of the panel is free. As the depth increases, the curvature becomes more important. As this occurs, the inextensional frequencies increase and the vibration becomes more predominantly extensional, and in the limit, for a closed spherical shell, the vibration is pure extensional.

The storage of fuels in some space vehicles requires that the inner surfaces of certain panels be in direct contact with large volumes of liquid. This liquid loading will certainly influence the natural vibration characteristics of such panels. Although the liquid volume will have resonances of its own, these are not expected to occur in the range of panel natural frequencies. Reference 61 describes the effect of the liquid on panels as being one of an added surface mass m to the panel, since pressures induced by the panel on the liquid during vibration are quickly dissipated in the volume of liquid due to the relatively high speeds of sound in a liquid which cause rapid concentrations of the pressure induced in the liquid; i.e., any vibratory forces existing between the panel and the liquid caused only a non-resonant forced vibration in the liquid. The liquid being neither very compressible nor dissipative in the sense of damping, the liquid must act like mass attached to the panel. The amount of mass to be added is a function of the type of panel vibration, the uncoupled panel frequency, and the density of the liquid and the geometry of the liquid volume. Figure 151, Reference 61, shows that for a cylindrical shell the added mass is larger for the lower frequencies and low circumferential order n , and that this mass may be very large in comparison with the surface mass of the panel. The effect of liquid loading is, therefore, to reduce the panel natural frequencies.

Equation for the natural frequency of uniform thin cylindrical shells having either beam, ring or flat plate type of vibration: (Ref. 61)

$$f_{nq} = \frac{Q c_n}{2l} = (K_L \omega)_{nq} \cdot \left(\frac{c_L}{2\pi a} \right)$$

$Q = q$: cylinder simply supported at both ends

$Q = q + 1/2$: cylinder clamped or free at both ends

$Q = q - 1/2$: cylinder cantilevered from one end, free at other end

a = radius of cylinder

l = length of cylinder

n = 0, 1, 2, ... = number of circumferential waves

($2n$ = number of circumferential nodes)

c_n = flexural wave velocity for n circumferential waves

c_L = speed of sound in the material composing the cylinder

q = 1, 2,, = order number of the resonance

Q = number of axial half-waves with $1/4$ -wave assumed for free and clamped ends

$k_L = 2\pi f/C_L =$ wave number for frequency f in the material

$k_n = 2\pi f_n/C_n =$ flexural wave number

$f_n =$ frequency of vibration for n circumferential waves

$h =$ cylinder thickness

Procedure for calculating cylinder natural frequencies:

1. Choose integer q and computer (Qa/L) .
2. Choose integer n and draw dashed line (which corresponds to the value of (Qa/L) on nomograph (Figures 139, 140, and 141) corresponding to n .
3. Intersection of this dashed line with solid line determines a value of $(k_L a) = (k_L a)_{nQ}$.
4. Compute $(C_L/2\pi a)$.
5. With the computed value of $(C_L/2\pi a)$ and the value of $(k_L a)_{nQ}$, compute the frequency f_{nq} by the above equation.

$n = 0$ implies expansion and contraction of cylinder cross-section.

$n = 1$ implies translation of cylinder cross-section without deformation.

$n \geq 2$ bending or corregation of cross-section perimeter.

Frequency equation for the transverse vibrations of the surface of a pressurized thin cylindrical shell when the circumferential and axial inertial forces are negligibly small: (Reference 17)

$$f_{mn} = \frac{1}{2\pi} \frac{1}{a} \sqrt{\frac{E}{\rho}} \sqrt{\underbrace{\frac{\lambda^4}{(n^2 + \lambda^2)^2}}_{\text{Extension}} + \underbrace{\frac{(h/a)^2}{12(1-\nu^2)}}_{\text{Inextension}} (n^2 + \lambda^2)^2 + \underbrace{\frac{Pa}{Eh} (n^2 + \frac{1}{2}\lambda^2)}_{\text{Internal Pressure}}}$$

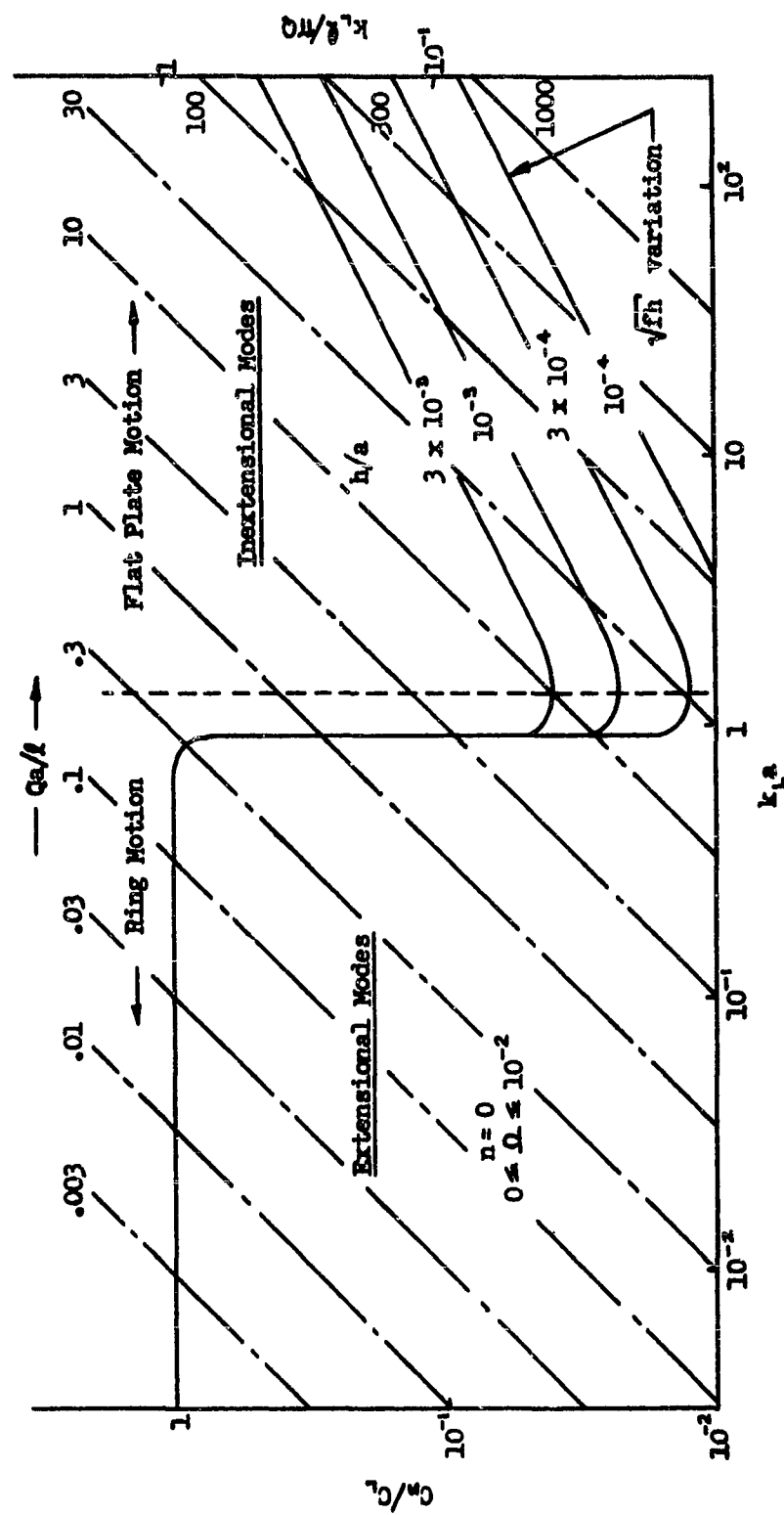
$$\lambda = \frac{m\pi a}{L}, \quad m \geq 1, \quad n \geq 2, \quad L/a \geq 5, \quad a/h \geq 10$$

$m =$ number of axial half-waves

$m + 1 =$ number of axial node points

$n =$ number of circumferential waves

$2n =$ number of circumferential node points.

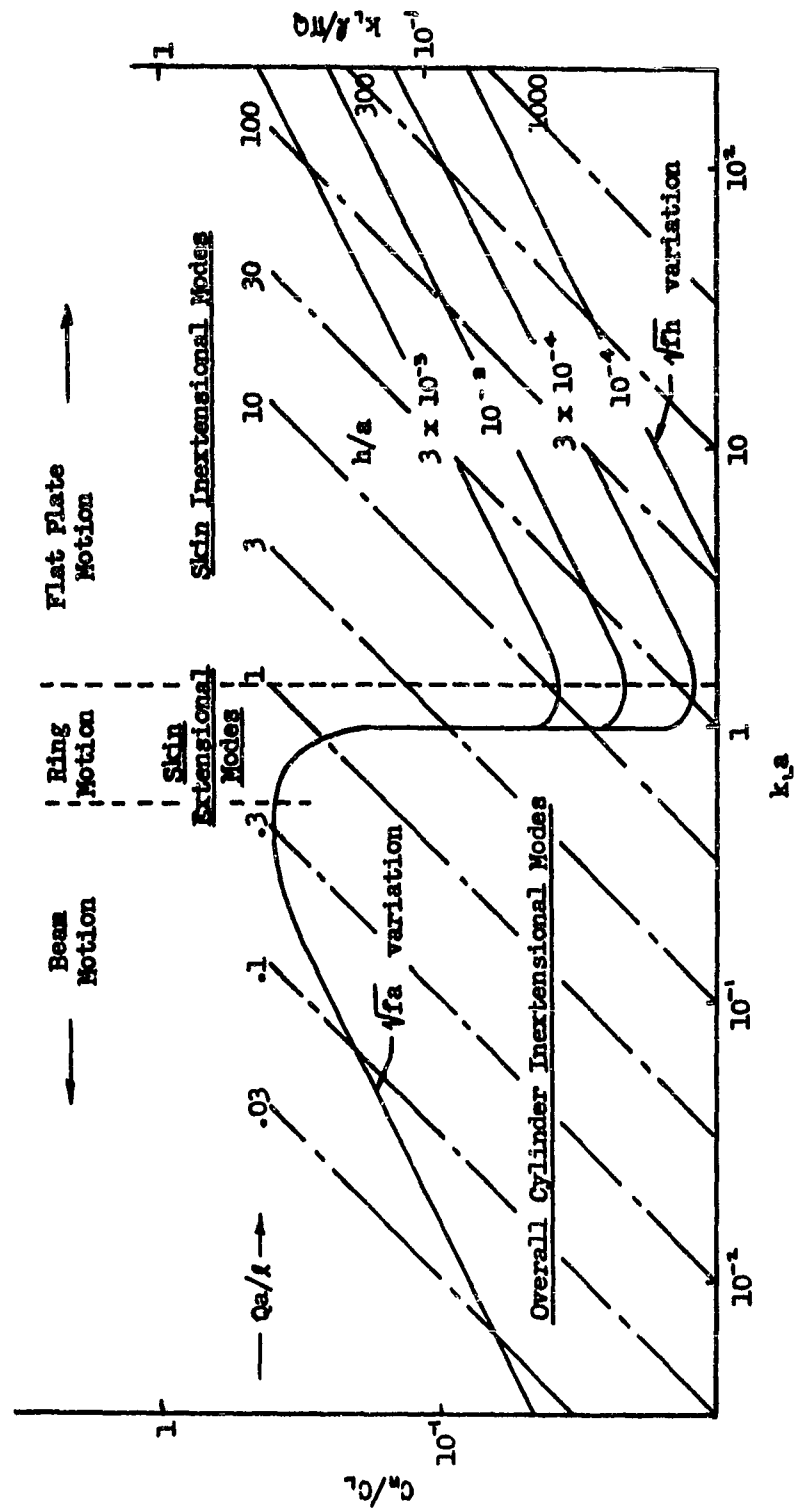


— C_o/C_o vs $k_{1,a}$ for various h/a
 --- $k_{1,l}/k_{1,q}$ vs $k_{1,a}$ for various Qa/l

Figure 135. Free Flexural Velocity, C_o ; Pressurized Cylinder not Loaded by a Liquid

$$n = 1$$

$$0 \leq n \leq 10^{-2}$$



- C_n/C_1 vs k_{1a} for various h/a
- k_{1a}/k_Q vs k_{1a} for various Qa/h

Figure 136. Free Flexural Velocity, C_0 ; Pressurized Cylinder Not Loaded by a Liquid

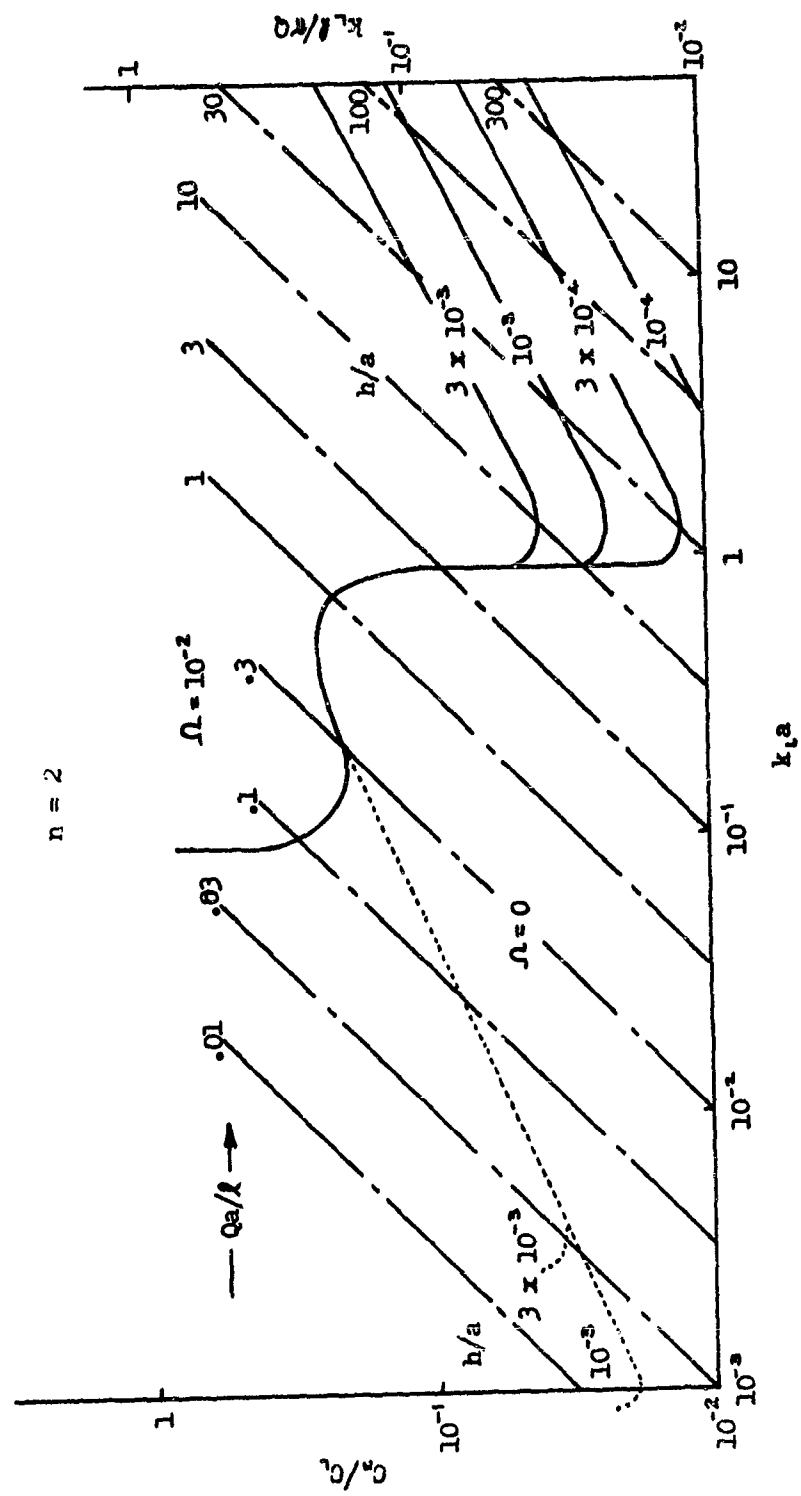


Figure 137: Free Flexural Velocity, C_0 ; Pressurized Cylinder Not Loaded by a Liquid
 — C_n/C_v vs $k_1 a$ for various h/a
 --- $k_1 l / Q$ vs $k_1 a$ for various Qa/l






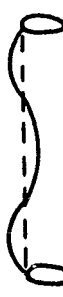

Circumferential Modes	Pure Radial	Translation Without Distortion	Corrugated or Bending		
					
Axial Modes		$(n,q)=(0,1)$	$(1,1)$	$(2,1)$	$(3,1)$
		$(0,2)$	$(1,2)$	$(2,2)$	$(3,2)$
		$(0,3)$	$(1,3)$	$(2,3)$	$(3,3)$
		$(0,4)$	$(1,4)$	$(2,4)$	$(3,4)$

Figure 138. Axial and Circumferential Mode Shapes of a Uniform, Thin, Circular Cylinder.

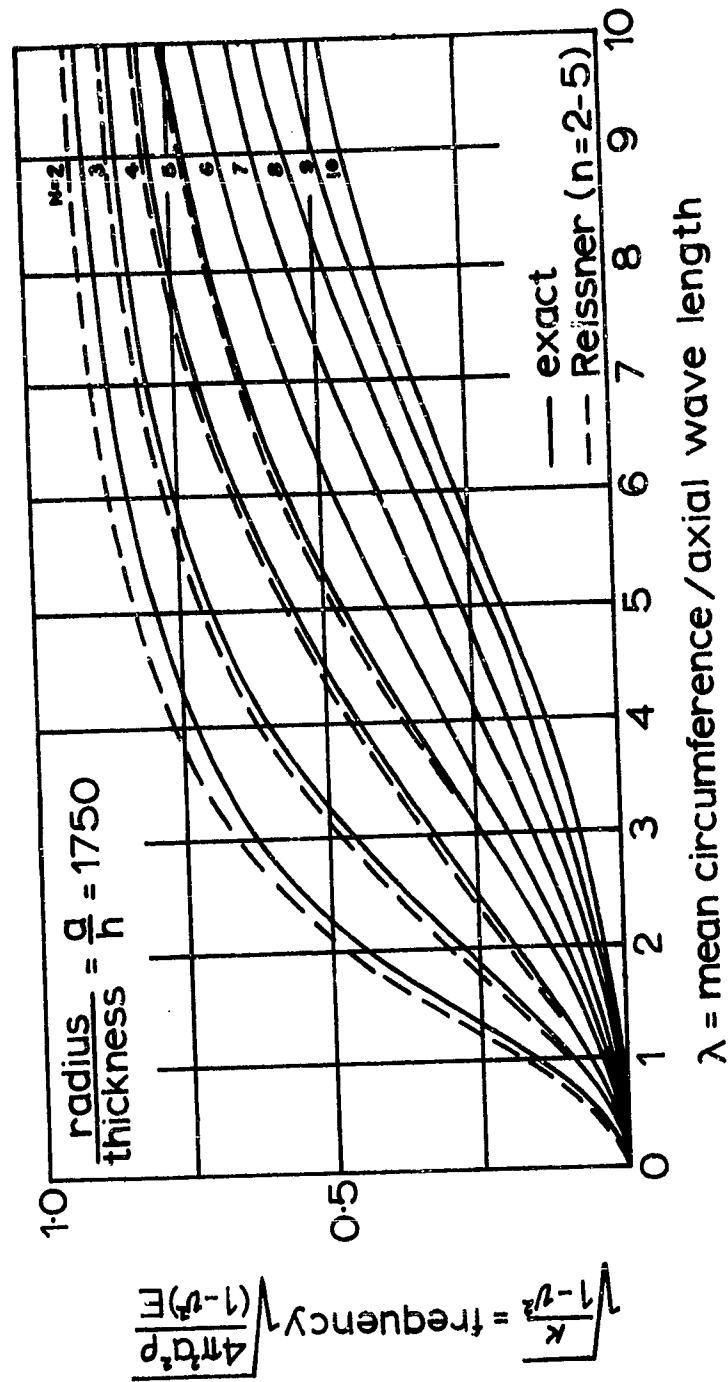


Figure 139. Comparison of Frequencies Predicted by Exact and Approximate Shell Theories

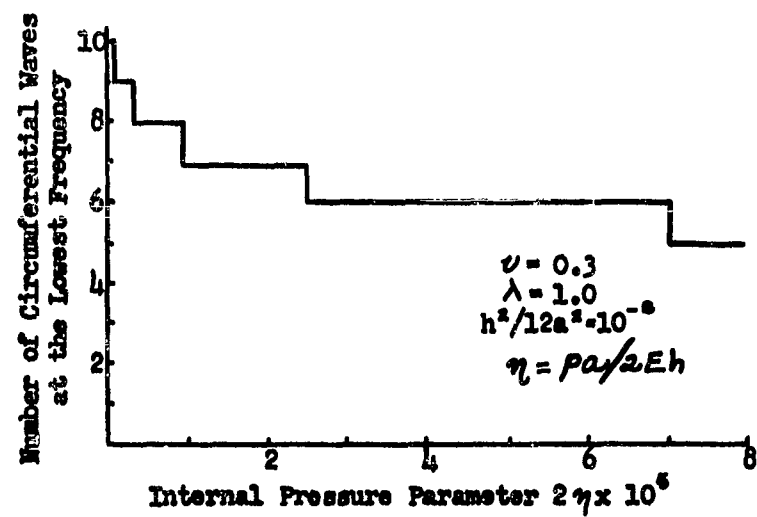


Figure 140. Conditions at the Lowest Frequency

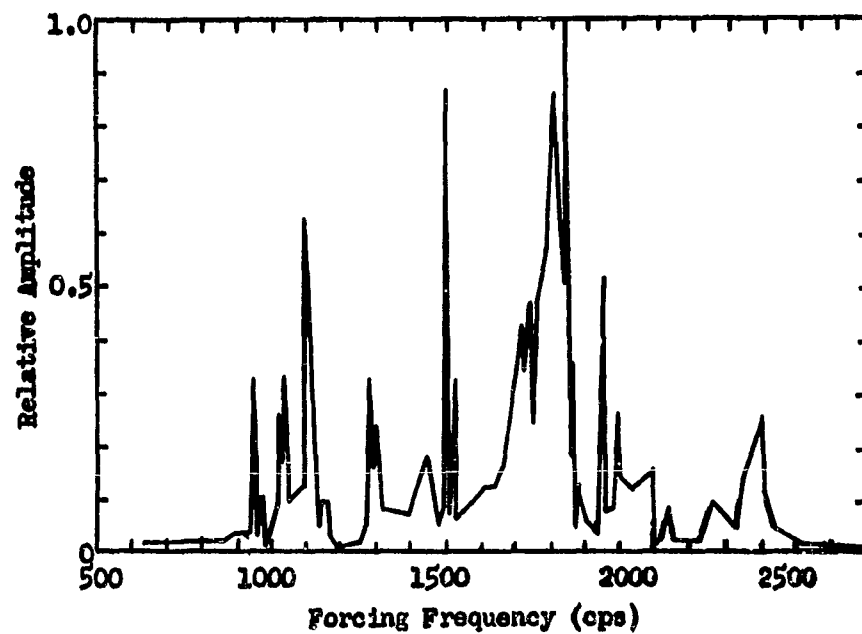


Figure 141. Typical Frequency Response Curve of a Thin Pressurized Cylindrical Shell

Equation for the pure inextensional natural frequency of a uniform, thin cylindrical shell of radius, a , length, L , thickness, h , and density, ρ . E is equal to the modulus of elasticity of the material, ν is Poisson's ratio. Reference 62, page

Two-Dimensional Vibration Perpendicular to the Surface

$$\omega_n^2 = \frac{E h^2}{12 \rho (1 - \nu^2) a^4} \cdot \frac{n^2 (n^2 - 1)^2}{n^2 + 1}, \quad n = 2, 3, \dots$$

Note that this equation is independent of length, L .

Approximate Equation for Three-Dimensional Vibration
(Radial, axial, circumferential)

$$\omega_n^2 = \frac{E h^2}{12 \rho (1 - \nu^2) a^4} \cdot \frac{n^2 (n^2 - 1)^2}{n^2 + 1} \cdot \frac{1 + 2\nu (1 - \nu) a^2 / n^2 L^2}{1 + 12 a^2 / [n^2 (n^2 + 1) L^2]}$$

Equations for the pure extensional natural frequencies of a uniform, thin cylindrical shell. Note that these equations are independent of thickness, h . Reference 62, page 546.

$$f_n^4 - f^2 \frac{E}{\rho (1 - \nu^2)} \left[\frac{1}{a^2} + \frac{4n^2 \pi^2}{L^2} \right] + \frac{4 E^2 n^2 \pi^2}{\rho^2 (1 - \nu^2) a^2 L^2} = 0$$

$$\omega_n = 2\pi f_n$$

Pure Radial Vibration: $a/L \approx 0$

$$\omega_n^2 = \frac{E}{\rho (1 - \nu^2) a^2}$$

Longitudinal Vibration: $a/L \approx 0$

$$f_n = \frac{n}{L} \sqrt{E/\rho}$$

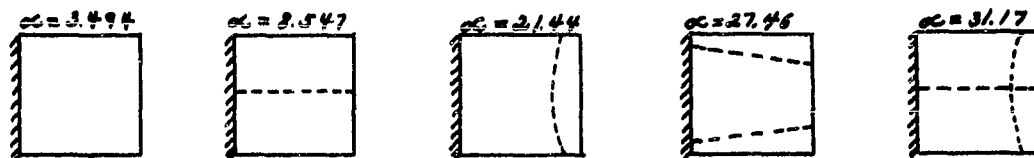
Torsional Vibration: $a/L \approx 0$

$$f_n = \frac{n}{L} \sqrt{\frac{E}{2\rho(1-\nu)}}$$

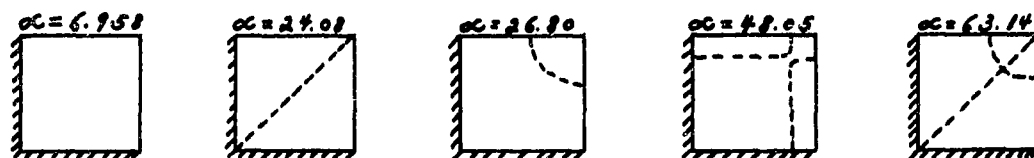
Fig. 142. Natural Frequencies of Square Flat Plate with Various Edge Conditions:

$$f = \frac{\alpha}{2\pi} \sqrt{\frac{E h^4}{12 \rho (1 - \nu^2) a^4}}$$

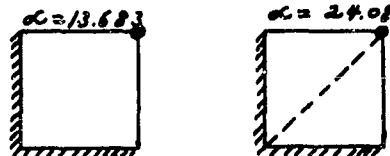
Cantilevered Plate



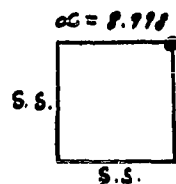
Two Clamped Adjacent Edges
Two Free Adjacent Edges



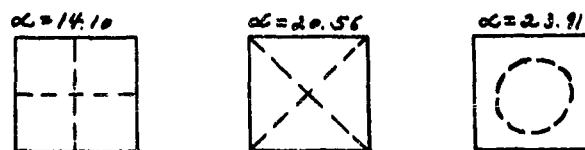
Same as Previous Case with
Pin Added at the Free Corner



Two Simply Supported Adjacent Edges
Two Free Adjacent Edges
Pinned at the Free Corner



All Edges Free



Natural Frequencies of a Thin Circular Flat Plate with Various Boundary Conditions:


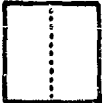
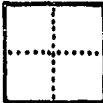


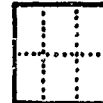
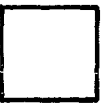
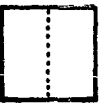

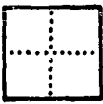
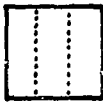
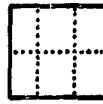
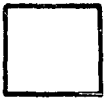
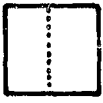

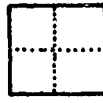
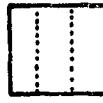
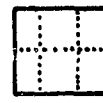

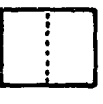

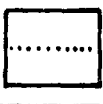
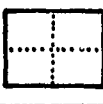



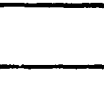
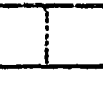
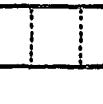
$$f = \frac{\alpha}{2\pi a^2} \sqrt{\frac{E h^4}{12 \rho (1 - \nu^2)}}$$

Table X: Values for α

Boundary Conditions		0	1	2	3
Clamped Edge	0	10.21	39.78	88.90	
	1	21.22			
	2	34.84			
Free Edge	0		9.076		
	1		20.52		
	2	5.251	35.24		
	3	12.23	52.91		
Center Simply Supported (Node Point at Center) Axial Symmetric Vibrations	0	3.75	20.91	60.68	119.7
	1				
	2	5.251			
	3	12.23			

S = number of nodal circles.

n = number of nodal diameters.

b/a	ξ	The mode number					
		1	2	3	4	5	6
1.0	0 20 ∞	19.74 31.09 35.99 	49.35 64.31 73.41 	78.96 95.85 108.3 	98.70 117.3 131.6 	98.70 116.8 132.3 	128.3 147.6 165.2 
0.9	0 20 ∞	17.86 28.21 32.67 	41.85 54.57 62.29 	47.47 61.97 70.76 	71.46 86.85 98.14 	81.82 97.03 109.4 	111.4 123.0 143.5 
0.8	0 20 ∞	16.19 25.80 29.08 	35.14 46.02 52.52 	45.79 59.98 68.52 	64.74 79.06 89.40 	66.72 79.24 89.29 	96.33 111.2 124.5 
0.6	0 20 ∞	13.42 22.30 25.90 	24.08 32.58 37.28 	41.85 50.48 56.93 	43.03 56.97 65.18 	53.69 66.96 75.94 	
0.4	0 20 ∞	11.45 20.30 23.65 	16.19 24.15 27.81 	24.08 31.20 35.45 	$f = \frac{\omega}{2\pi a^2} \sqrt{\frac{E h^3}{12 \rho (1-\nu^2)}}$ <p>Table XI Values For ω.</p> <p>a, b = dimensions of the plate. β = foundation elasticity coefficient for homogeneous foundation rotation along all four edges $\beta = 0$, pinned edges $\beta = 20$, partially clamped edges $\beta = \infty$, fully clamped edges. Reference 44. $\frac{\partial^2 w}{\partial x^2} = \frac{\beta}{2} \frac{\partial w}{\partial x}$ at edges.</p>		
0.2	0 20 ∞	10.26 19.38 22.64 	11.45 20.15 23.45 	13.42 21.52 24.89 			

The following equations, in conjunction with the curves of Figures 146 and 147, may be used to determine the frequency response function and the associated stress of a flat clamped-clamped rectangular plate when the extension of the middle plane of the plate is significant. It is assumed that the plate is uniformly loaded by an oscillating pressure having a single frequency and normal incidence to the plate.

$$K_3 \Delta^3 + K_2 \Delta^2 + K_1 \Delta + K_0 = 0 \quad (41)$$

$$K_3 = \frac{9}{16} \rho^2$$

$$K_2 = \frac{3}{2} \omega_0^2 \rho \left[1 - \left(\frac{\omega}{\omega_0} \right)^2 \right]$$

$$K_1 = \omega_0^4 \left\{ \left[1 - \left(\frac{\omega}{\omega_0} \right)^2 \right]^2 + \frac{1}{Q^2} \left(\frac{\omega}{\omega_0} \right)^2 \right\}$$

$$K_0 = - \left(\frac{P}{\rho h} \right)^2$$

$$\rho = \frac{\delta D}{b^4 h^3}$$

$$\omega_0^2 = \frac{\eta r D}{b^4 h}$$

$$D = \frac{E h^3}{12(1 - \nu^2)}$$

$$\eta = \left[\int_0^a \int_0^b \varphi(x,y) dx dy \right] \div \left[\int_0^a \int_0^b \varphi^2(x,y) dx dy \right] \begin{matrix} \approx 1.3 \text{ at } b/a=0 \\ \text{to} \\ 1.5 \text{ at } b/a=1.0 \end{matrix}$$

$$Q = \frac{1}{2\zeta}$$

$$\Delta = \left[\text{Maximum amplitude of oscillation of center of plate} \right]^2 \equiv A^2$$

γ, ζ = Nondimensional parameters obtained by curve-fitting the equation

$$\frac{Pb^4}{Dh} = \gamma \left(\frac{A}{h} \right) + \delta \left(\frac{A}{h} \right)^3 \quad (42)$$

to the curves in Figure 146.

a, b = edge dimensions of panel ($a \geq b$).

D = plate bending stiffness

E = Young's modulus of material in plate

ρ = density of material in plate

h = total plate thickness

ν = Poisson's ratio

ζ = ratio of actual damping to critical damping

ω_0 = plate natural frequency in bending

ω = frequency of applied pressure

P = maximum amplitude of applied pressure

$\varphi(x, y)$ = mode shape of panel

η = dynamic factor accounting for the effect of the mode shape on the effective mass and effective applied force.

Procedure for calculation:

1. Specify: $a, b, E, \rho, h, \nu, \zeta, P, \omega$.
2. Fit Equation (42) to appropriate curve in Figure 146 and determine γ and δ .
3. Compute: $D, \beta, \omega_0, Q, K_3, K_2, K_1$, and K_0 .
4. Solve Equation (41) for Δ and compute A by relation $A = \sqrt{\Delta}$.
5. Compute A/h from the value of A given by step 4.
6. In Figure 146 determine, from appropriate b/a curve, a value for $\frac{P(b)^4}{Dh}$ for A/h computed in step 5; the value of P in this expression is the equivalent static pressure on the plate, and differs from the P given above because of the dynamic plate response. In order to avoid confusion, this value of P is denoted by P_e and the original value of P is denoted by P_s . Thus, $\frac{P_e(b)^4}{Dh}$ is now known. Also, let $\frac{A}{h}$ corresponding to

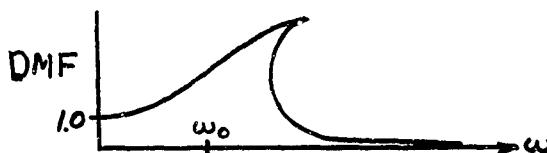
$\frac{P_e(b)^4}{Dh}$ be denoted by $\frac{A_e}{h}$. Thus, $\frac{A_e}{h}$ is known from Step 5.

7. Compute $\frac{P_s(b)^4}{Dh}$ and find $\frac{A_s}{h}$ from Figure 146 using the appropriate b/a curve. P_s and A_s are assumed to correspond to static values of the pressure and center plate deflection.
8. Dynamic magnification factor for deflection = A_e/A_s .
9. With the two values, $\frac{P_e(b)^4}{Dh}$ and $\frac{P_s(b)^4}{Dh}$, enter Figure 147 and from the appropriate b/a curve determine the corresponding dynamic and static stress factors, S_e and S_s respectively.
10. The stress σ at the long edge of the plate can be found from the expression

$$\sigma = S \frac{E h^2}{(1-\nu^2)(b/2)^2}$$

and thus σ_e and σ_s corresponding to S_e and S_s can be computed.

11. Dynamic magnification factor for stress = $\sigma_e/\sigma_s = S_e/S_s$. (Note that due to the nonlinearities introduced by the membrane extensional stresses, the dynamic magnification factors for amplitude and stress are different.)
12. The above process can be repeated for the same value at P (or P_s) for different values of ω , and frequency response curves can be constructed for the amplitude and stress dynamic magnification factors. These curves will appear to have the following form:



Different values of P (or P_s) generate different response curves. The above procedure is taken from Reference 15 and Figures 146 and 147 were taken from pages 348 and 349 of Reference 9.

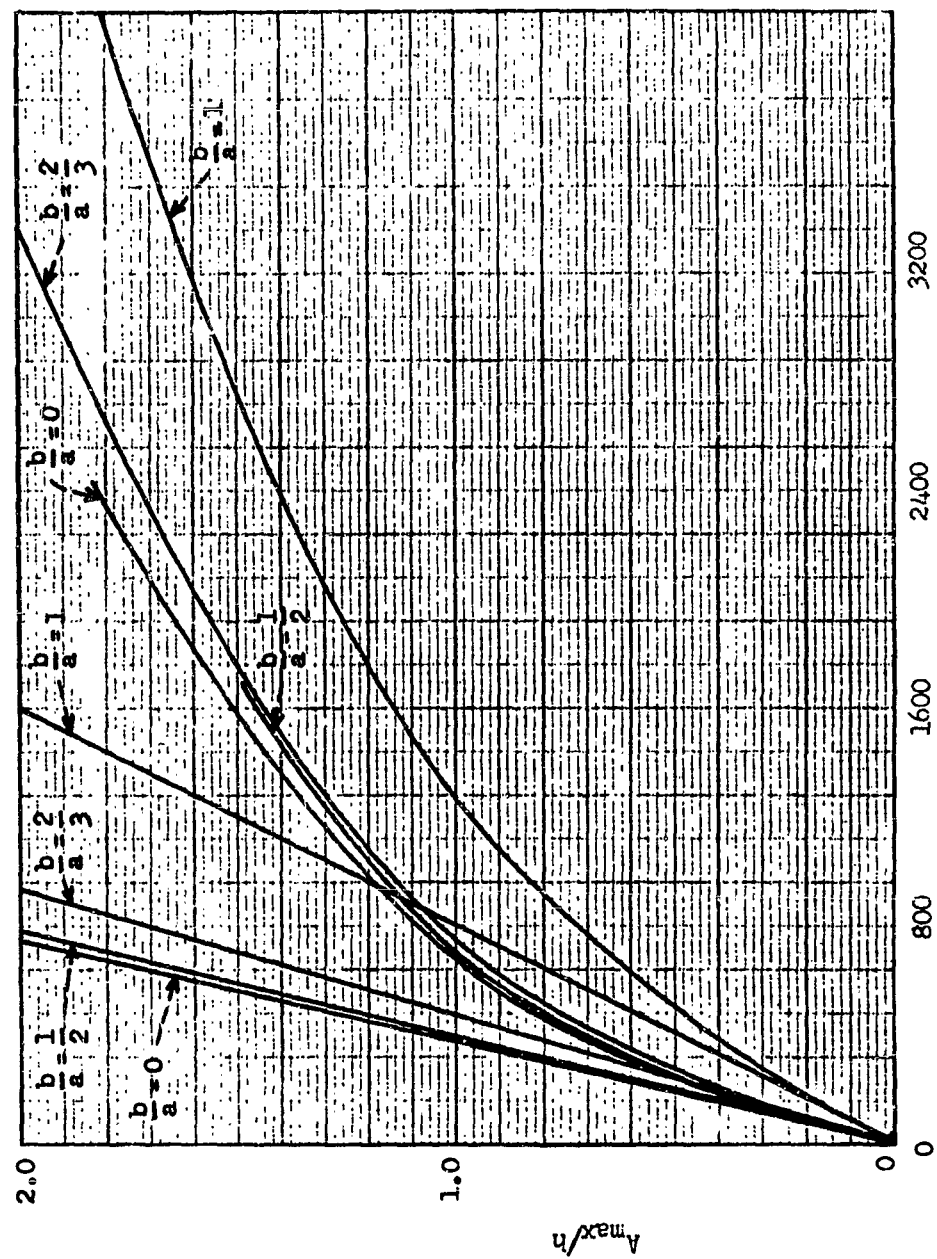


Figure 143 Large Static Deflections of Flat Rectangular Panels for a Uniform Surface Pressure, P. Ref.64, Page 350.

Equation for the fundamental frequency of vibration for a thin, circular, clamped, flat plate experiencing middle plane extension. Reference 64, Page 433,4.

$$f = \frac{10.21}{2\pi a^2} \sqrt{\frac{Eh^2}{12\rho(1-\nu^2)}} \sqrt{1 + 1.464 \frac{\mathcal{B}^2}{h^2}}$$

$$\mathcal{B} = \frac{3Pa^4(1-\nu^2)}{16Eh^3} \frac{1}{1 + .488 \mathcal{B}^2/h^2}$$

\mathcal{B} = Deflection at the center of the circular plate

P = Uniformly distributed pressure loading over the plate

h = Plate thickness

a = Radius of the plate

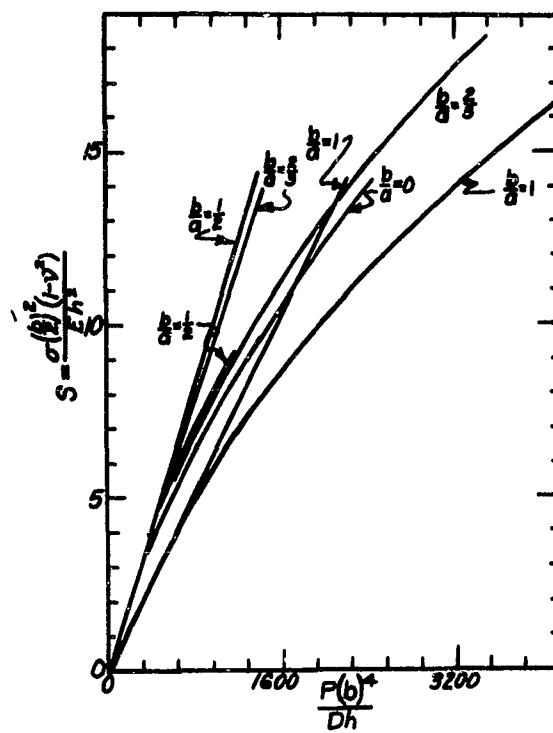
ρ = Mass density

E = Young's Modulus

ν = Poisson's ratio

f = Frequency

Figure 144. Stress Factor for Large Static Deflection of Flat Rectangular Panel with Uniform Surface Pressure P ; Stress for Longest Edge of Panel



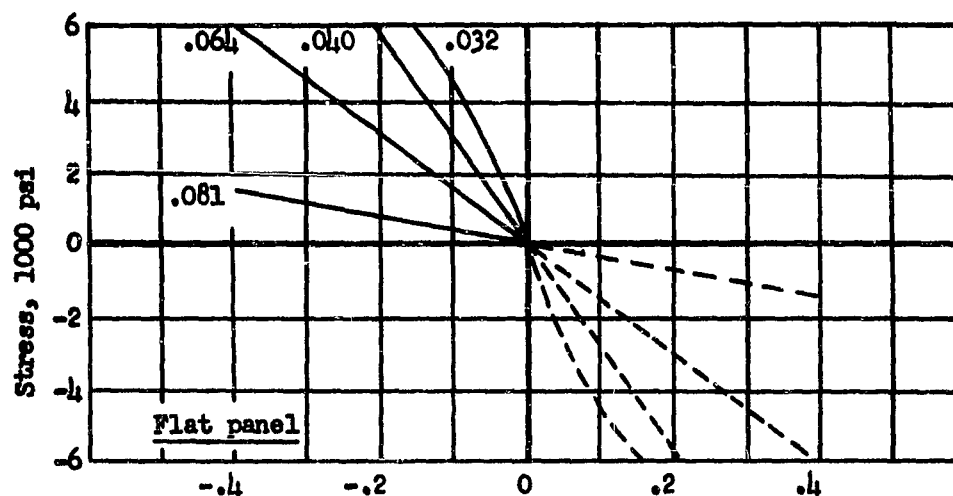


Figure 14.5a: Static Stress vs. Static Pressure for 11" x 13" Flat Rectangular Aluminum Panels of Thicknesses .032, .040, .064, and .081 Inches.

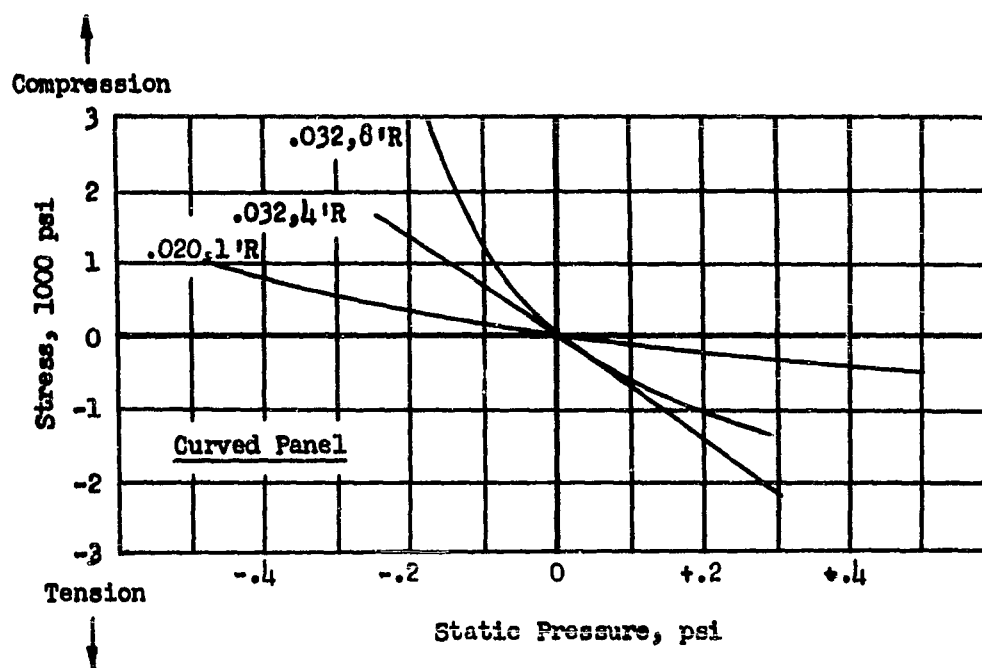


Figure 14.5b: Static Stress vs. Static Pressure for Curved Panels with 11" x 13" Rectangular Base with Various Radii of Curvature.

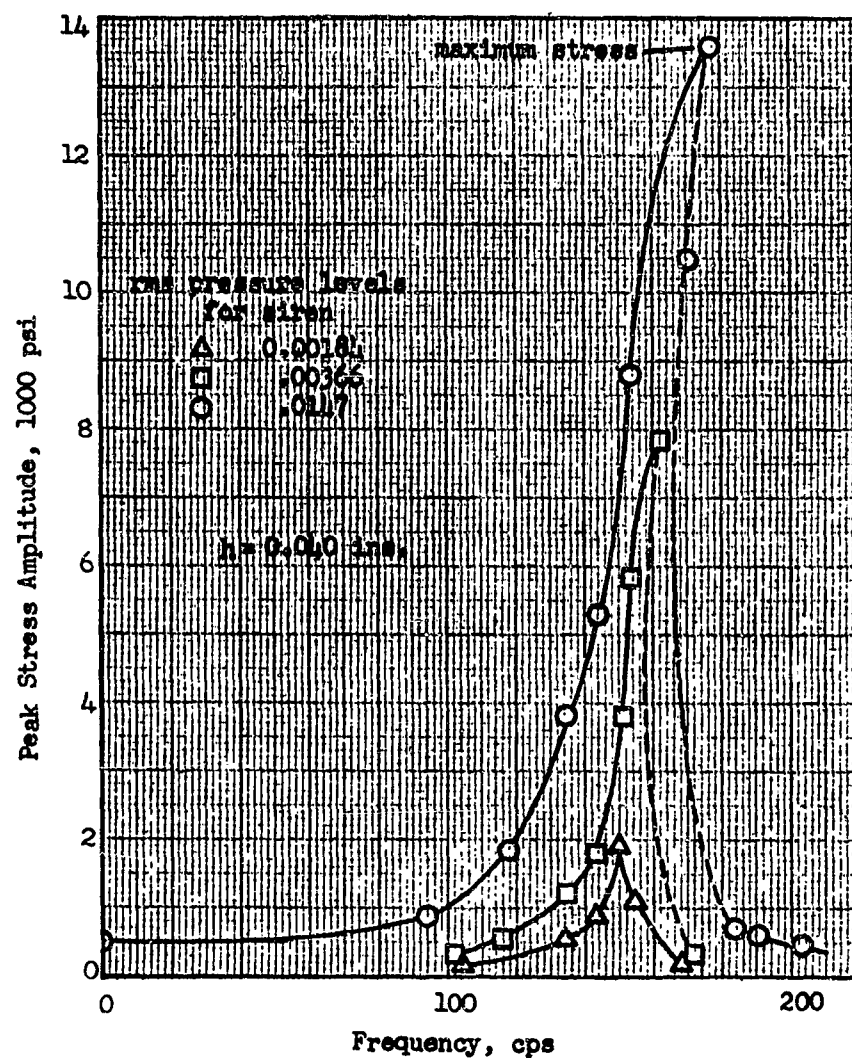


Figure 146. Peak Stress Amplitude vs. Frequency for .040 Inch Thick Flat Panel with Acoustical Siren Normal Pressure Loading

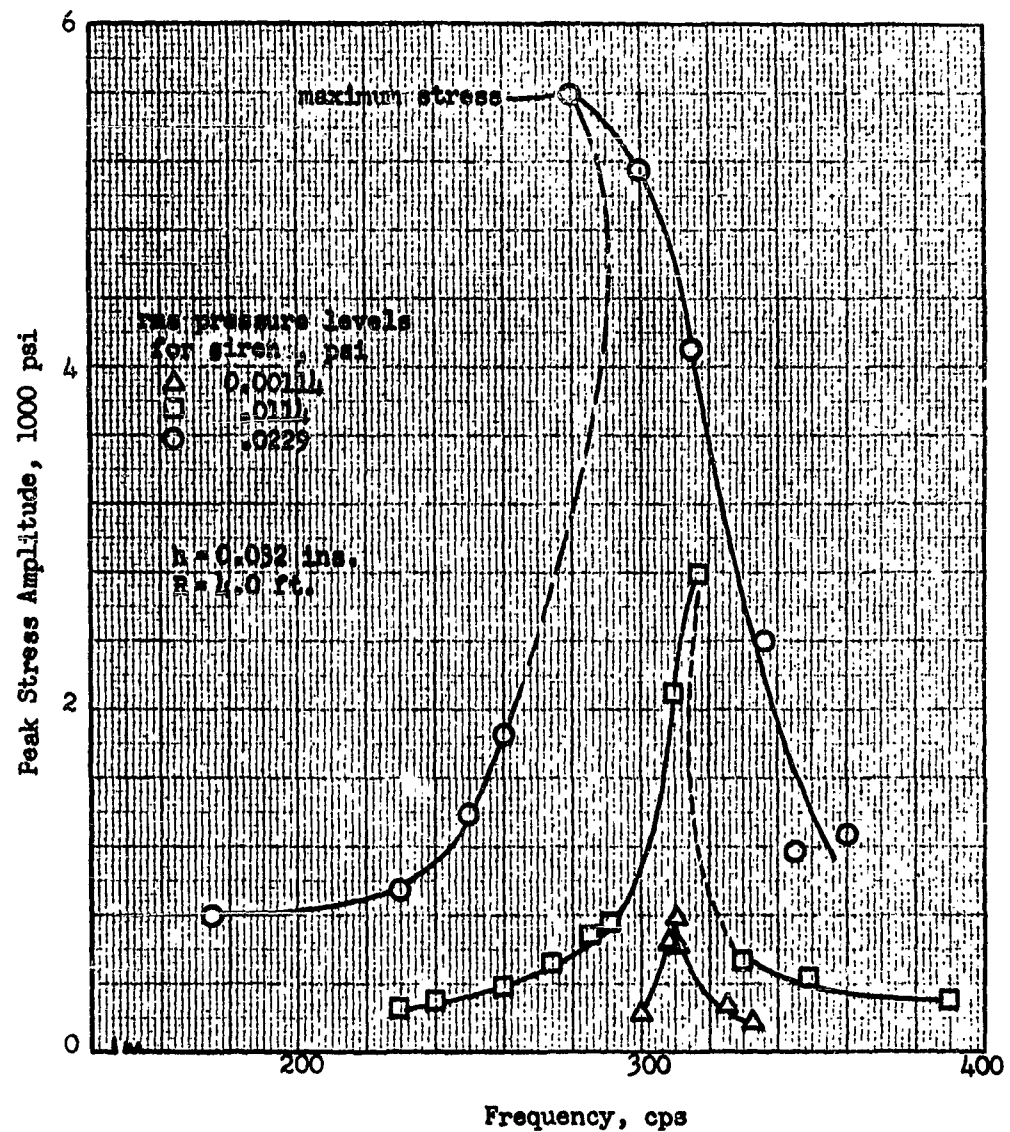


Figure 147. Peak Stress Amplitude vs. Frequency For a Curved Panel with Acoustical Siren Normal Pressure Loading.

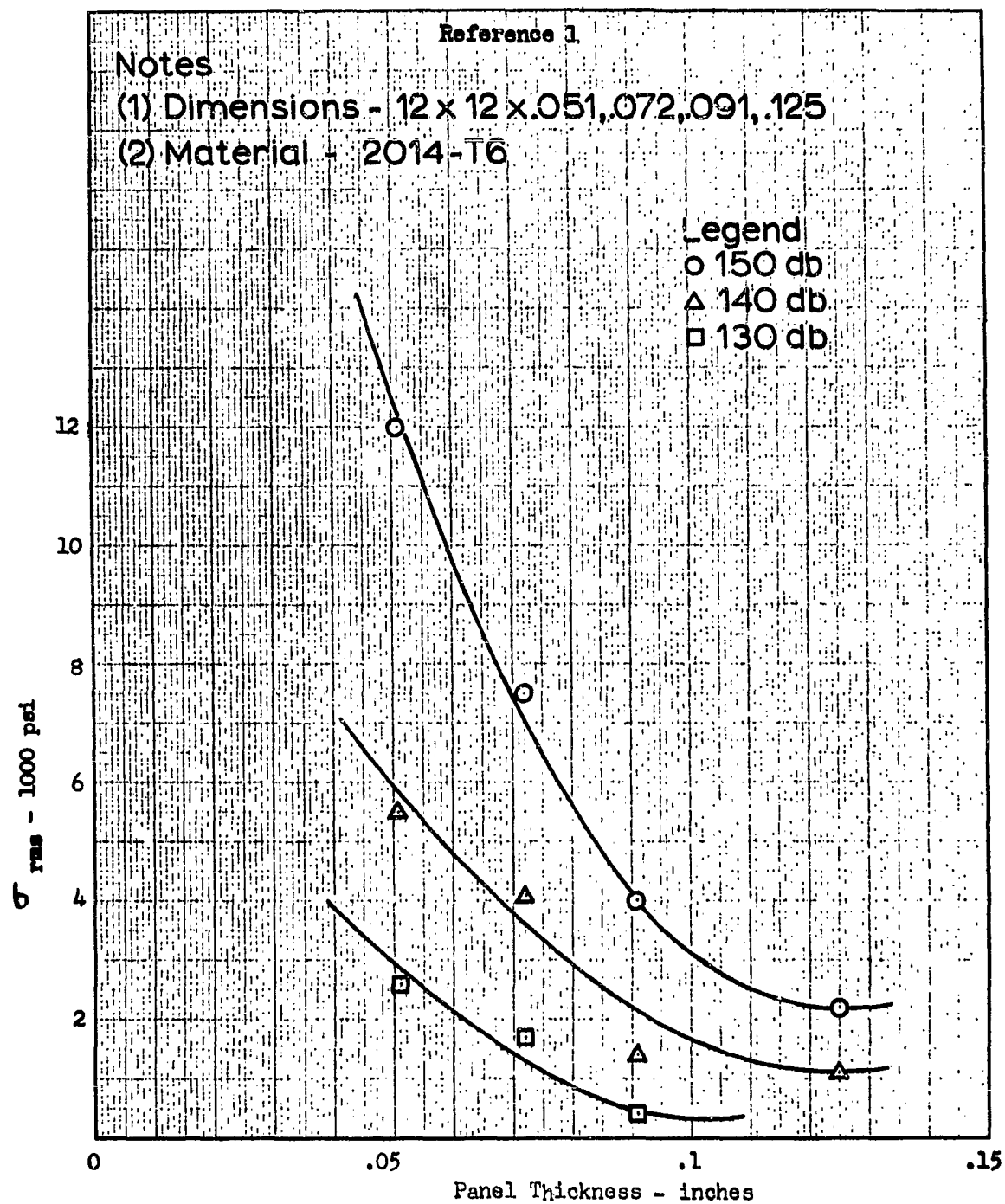


Figure 148. Maximum Stress vs. Panel Thickness.

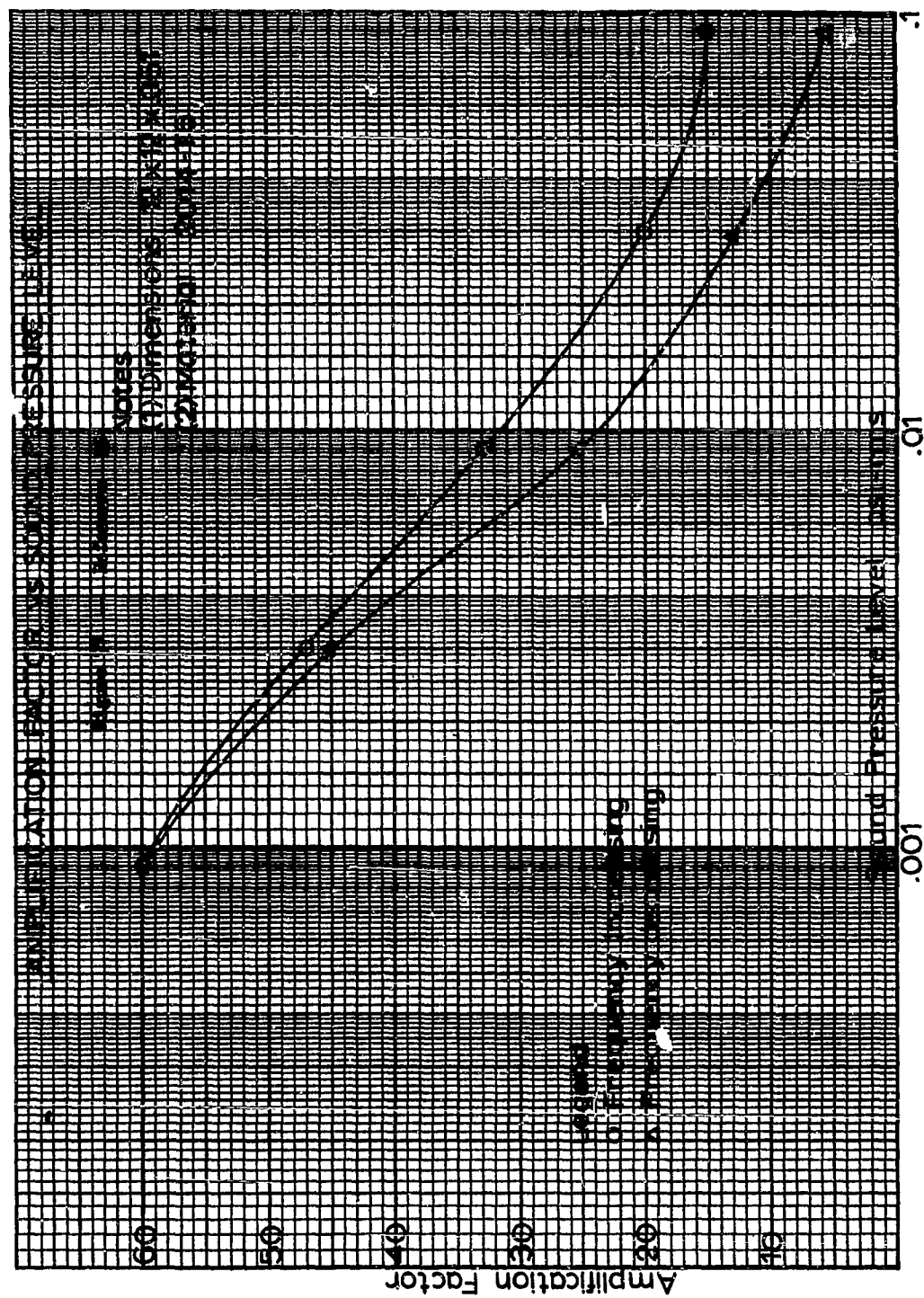


Figure 149 Amplification Factor vs. Sound Pressure Level

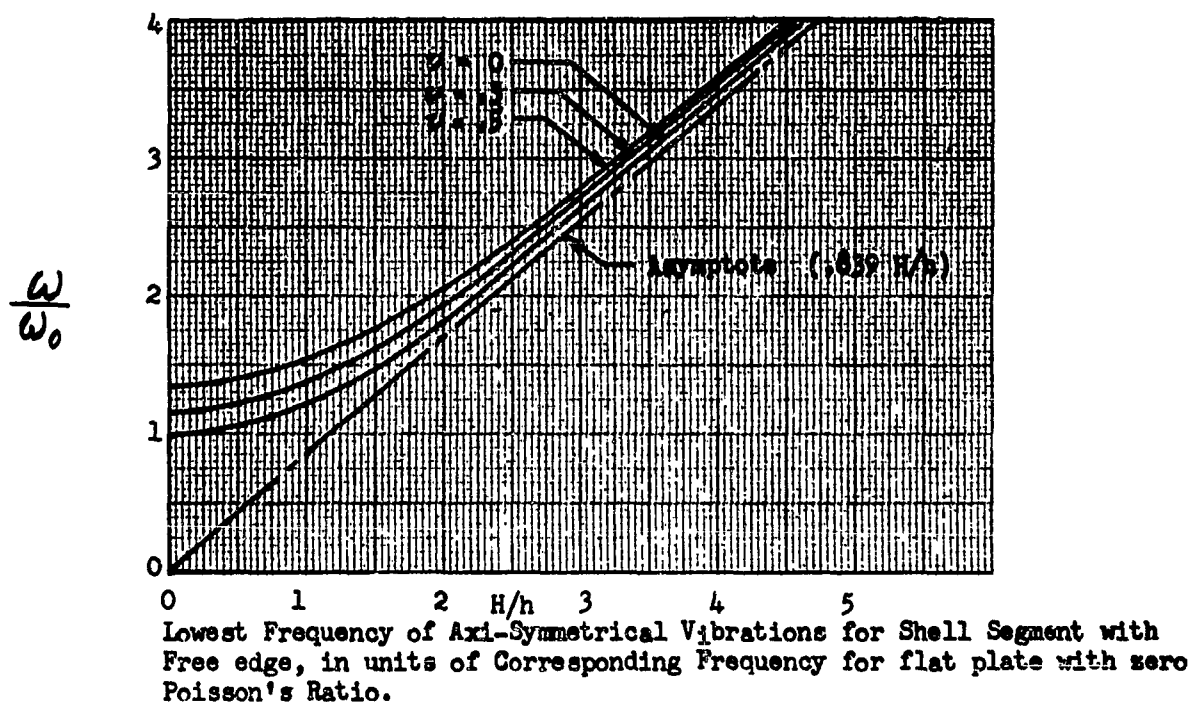
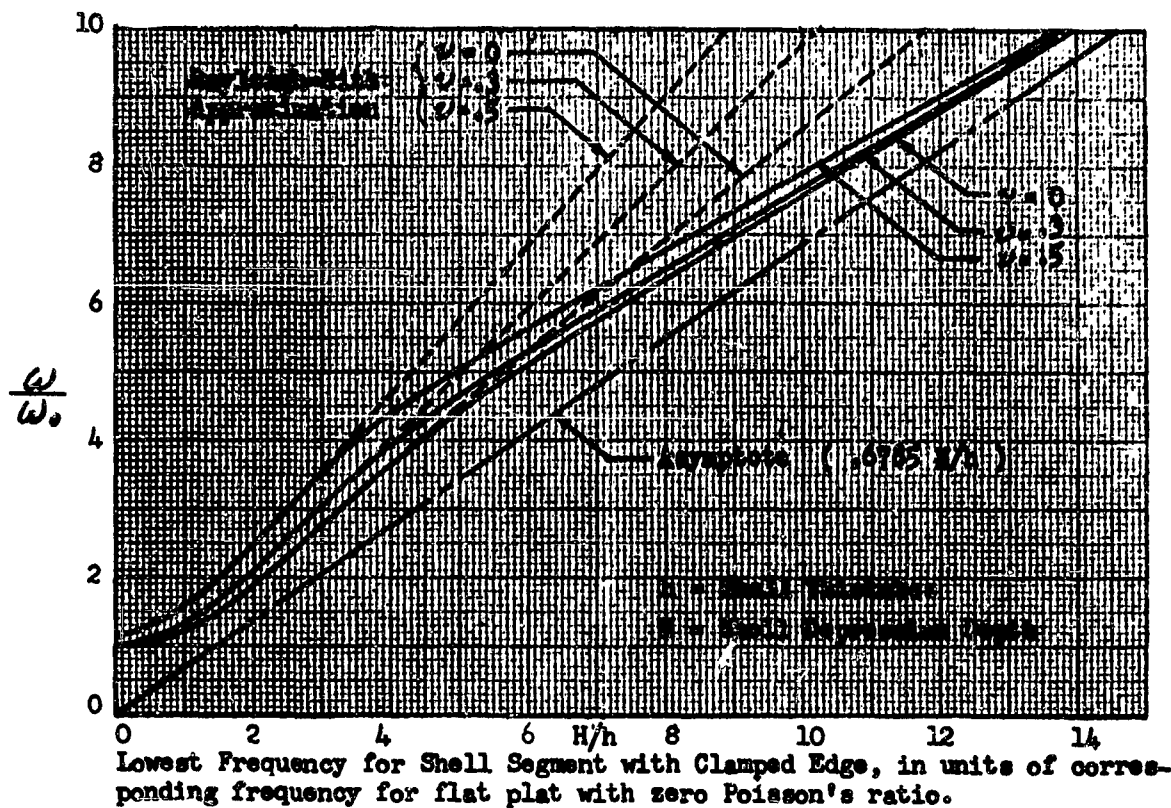


Figure 150. Fundamental Axi-Symmetric Vibration Frequencies of Shallow Spherical Shells, Ref. 35.

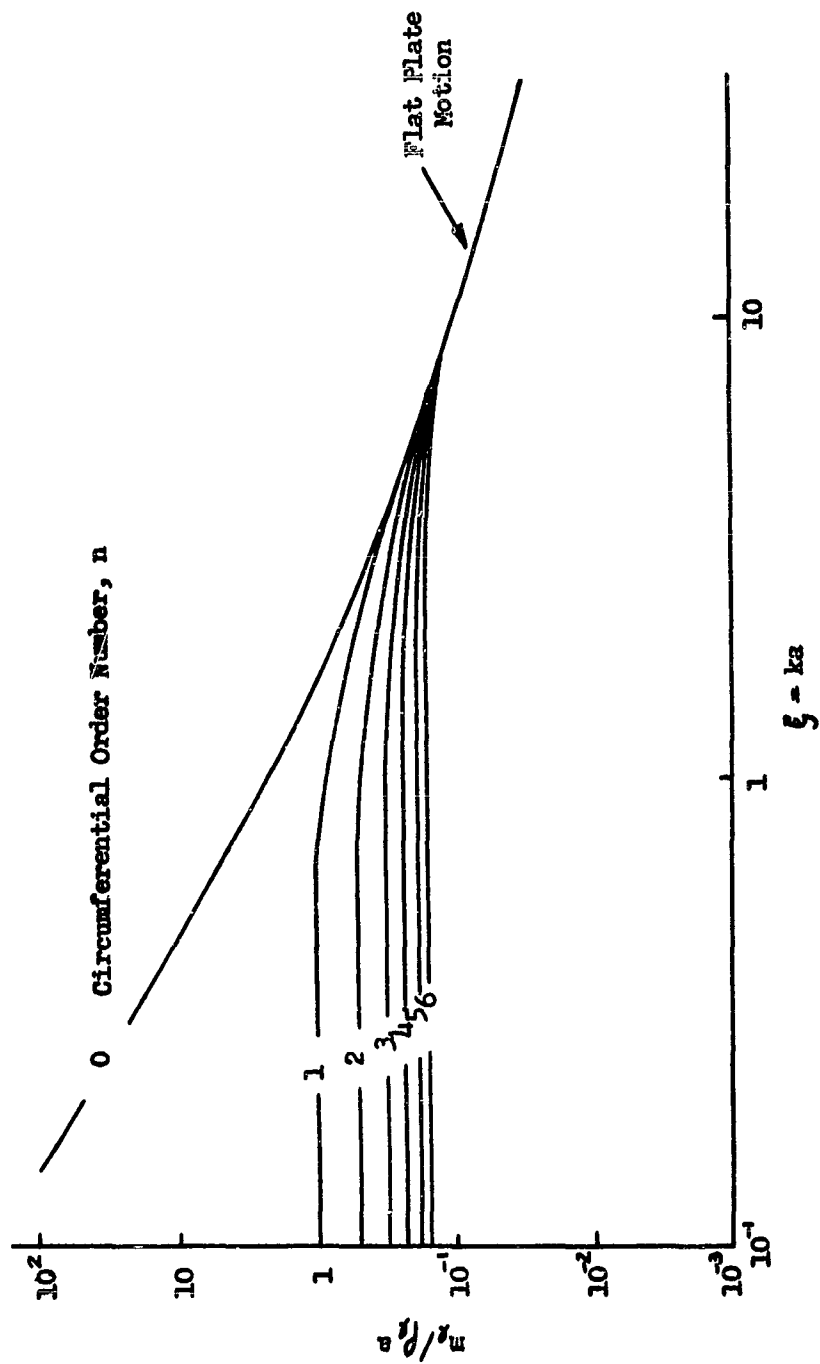


Figure 151. Added Surface Mass of a Liquid in a Cylinder (Reference 61)

Panel Damping

The damping of vibrations in panel structures is a composite of several types of damping from different sources and having different characteristics. The major constituents are listed here:

1. Material damping of the structure.
2. Coulomb (friction due to slip) damping in the joints at the fixed panel boundaries, or in the joints of panel structure itself in the case of panels which are built-up from several elements.
3. Viscoelastic damping in the joints at the boundaries of the panel or in the joints within the panel proper for built-up panels.
4. Viscoelastic damping of additive panel surface damping materials.
5. Acoustical radiation damping into the medium surrounding the panel.
6. Aerodynamic damping.

Material damping of the panel structure is highly dependent upon the state of stress which exists in the panel; i.e., upon the magnitude and distribution of stress throughout the panel. According to Pian, Ref. 65, at very low stress levels, the damping is governed by the thermoelastic properties of the material. A varying low magnitude stress, or strain, which has a uniform stress distribution throughout the material, leads to a uniform low stress level, the distribution of stress is nonhomogeneous, temperature gradients are set up which produce energy losses at intermediate frequencies. For very low or very high frequencies, little or no damping occurs because the temperature gradients have time to level-off at low frequencies and the process is essentially adiabatic at high frequencies. At higher stress levels a different material damping process occurs. The stress strain relationships become multiple valued leading to hysteresis loop because of plastic action, or internal friction, within the material. The area of this loop, for any fixed stress level equals the amount of energy damped per cycle.

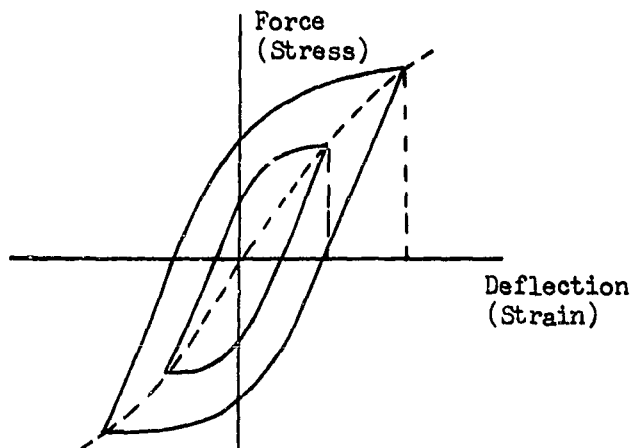


Figure 152. Hysteresis Loop for Two Stress Levels

Material damping at these higher stress levels is independent of frequency since the hysteresis loop for a particular case is the same for a static as well as a dynamic state of stress and strain. This damping is, however, dependent upon the stress amplitude and hence, for panels upon the surface, deflection of the panel. The most common expression used for measuring damping is the energy dissipated by the material per cycle of harmonic loading. This quantity is related to stress according to the relationship, Reference 16,

$$\Delta E = (\Delta E)_0 \cdot S^m$$

where

ΔE = damping energy dissipated per cycle for stress amplitude S .

$(\Delta E)_0$ = damping energy dissipated per cycle for a stress level of 1 psi.

m = real positive number.

In the intermediate stress range, above the very low stresses and below a certain critical stress level, the value of m lies generally between 2 and 3 for most structural materials. (Note: $m = 2$ implies linear damping). A critical stress value exists for all materials, called the "cyclic stress sensitivity limit," or the fatigue strength point, Reference 16, above which the value of m increases markedly and may attain magnitudes of from 3 to 20, depending upon the material involved. Reference 16 states that this range is probably from 3 to 13 for aircraft structures with an average value of 8. This may be shown in the following diagrams in terms of the panel deflection rather than panel stress:

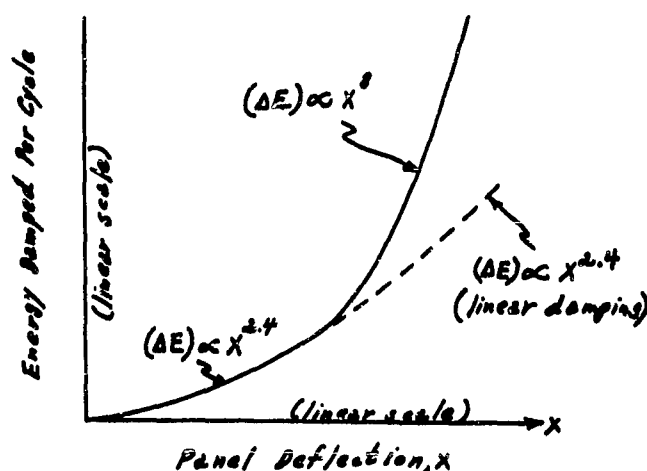


Figure 153. Damping Energy vs. Panel Deflection

True coulomb friction is a kinetic frictional force which is characteristic of the force existing between dry sliding surfaces. The energy damped per cycle for such a damping action is proportional to the first power of the deflection. The type of damping occurring at riveted or bolted joints at the boundaries of the panel or of any built-up panel structure is better characterized as "slip" damping. Although this is essentially coulomb in nature, "slip" differs from coulomb in that energy dissipation per cycle is not in general proportional to the first power of the amplitude of the deflection. The following graph shows a probable variation of damped energy versus deflection for plates with riveted or bolted edge support:

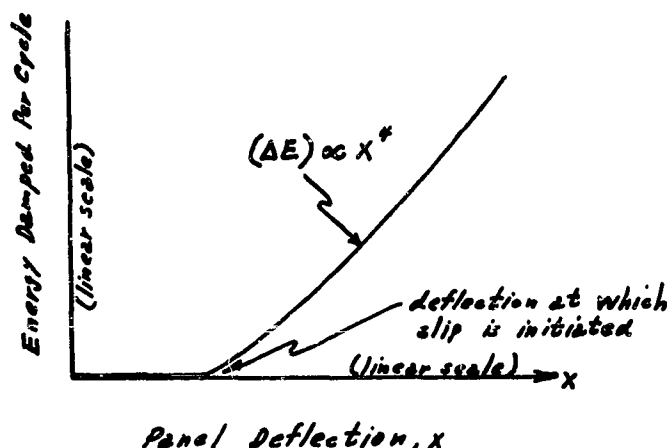


Figure 154.

Slip Damping

Slip occurs at joints when the stress around rivets and bolts reaches a magnitude greater than or equal to that which produces a force between the plate and rivet (or bolt) equal to the maximum static friction force in the joint. Since the latter tangential force depends upon the normal pressure in the joint, the deflection (or stress) at which slip initiation occurs, this deflection will vary with the tightness of the joint. The tightness of the joint also determines the amount of damping obtainable from sliding friction, and has a variation like that shown in Figure 155.

Only a brief mention is made here of the damping effect of viscoelastic materials since these are not at present widely used in space vehicle structural design. This does not imply, however, any lack of importance for such materials, since these may significantly add to the damping of panel vibrations. Viscoelastic materials, such as Poly-iso-butylene, are used at the interfaces between the panel and the supporting frame such as is shown in Figure 156, Reference 16. Deflections of the panel surface produce small deflections at the edges causing cyclic shearing stresses in the viscoelastic material. In addition to the damping properties of these materials, they also produce elastic restoring forces on the deflected panel. A three dimensional plot, shown in Figure 157, shows the variation in energy dissipated per cycle with the elastic and viscous shear forces G_1 and G_2 . In terms of panel stress the dissipation equation given above generally has an $m = 4$ for interface damping so that $(\Delta E) = (\Delta E)_0 \cdot S^4$.

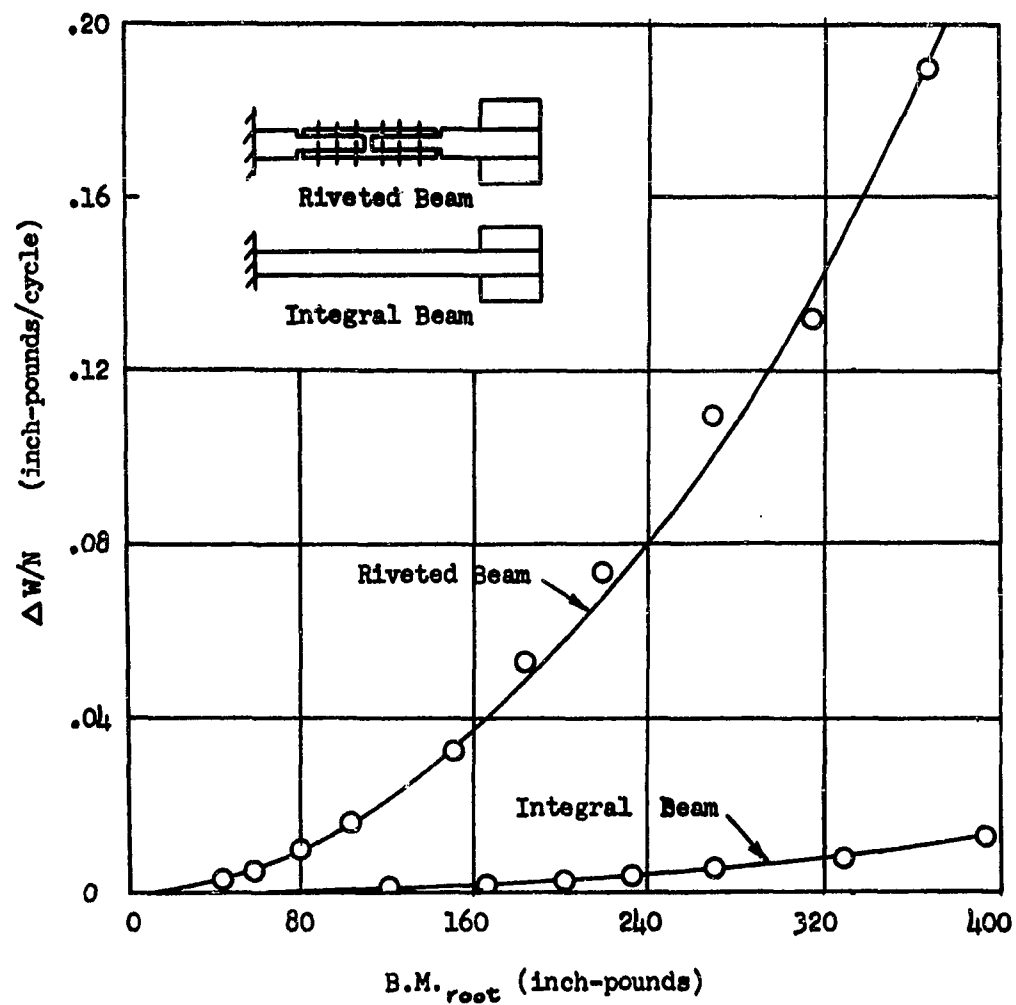


Figure 155. Energy loss per Cycle for Various Loadings of A Riveted and Integral Beam

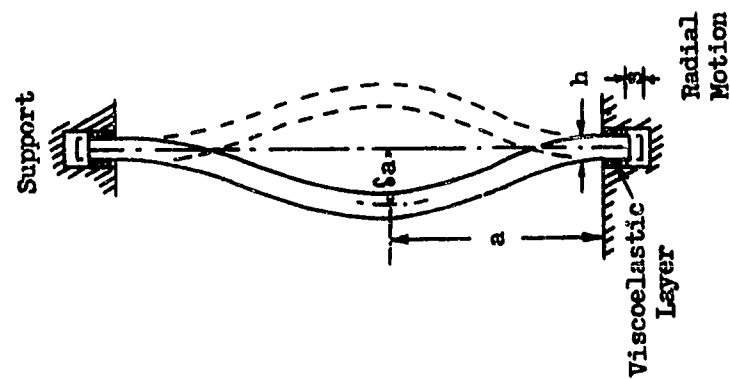


Figure 156. Beam with Visco-Elastic Layer

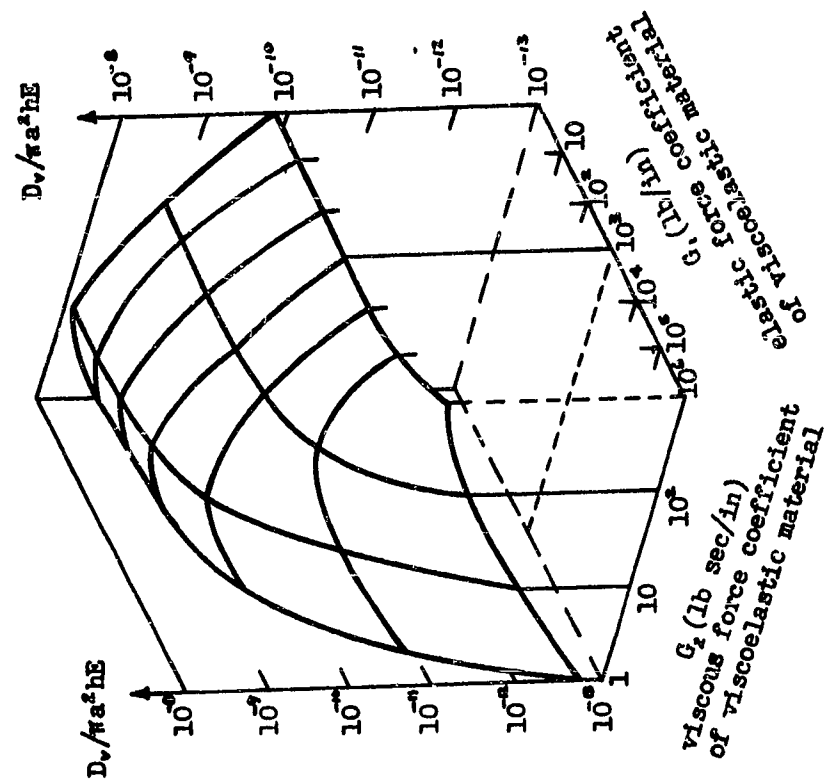


Figure 157. Elastic and Viscous Energy Dissipation

A second type of viscoelastic material may be used to dampen panel vibrations. These are in the form of overlays on the panel surface. Figure 159 shows the ratio of composite damping, γ , of a plate with such an overlay, to the damping γ_1 , of the viscoelastic material itself. This graph shows the dependence of the damping ratio on the thickness and elastic modulus ratios of the plate and the overlay.

A vibrating panel immersed in a fluid medium, such as air, induces pressure waves in that medium which are propagated away from the panel surface. In doing so, the panel gives up a certain amount of its kinetic energy, with the resultant effect on the panel being the same as damping. In Reference 55, the equation of motion is derived for a single degree of freedom rigid plate surrounded by a fluid medium and attached to a foundation through a spring and upon which acts a force $F(t)$. ρ is the density of the surrounding medium and c is the speed of sound in that medium. The effective damping provided by the fluid medium is seen to be $2\rho c$. [$Q = \frac{1}{2}\gamma = K/2\rho c\omega$.] The effect of this damping for such fluids as air is very small except at resonance of the system. At resonance, the motion of the plate is actually limited by this effect so that: $\frac{x}{x_{static}} = \frac{K}{2\rho c\omega_0}$; $\omega_0^2 = K/M$.

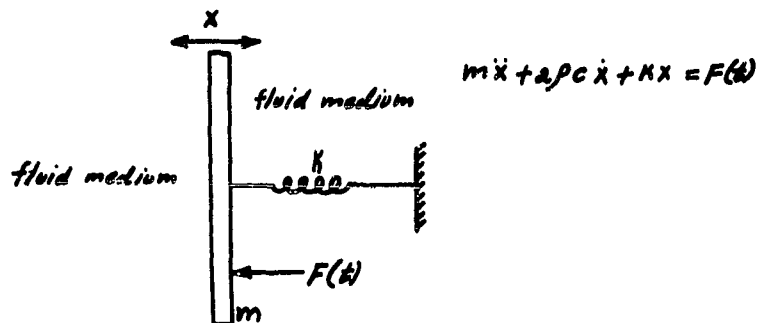


Figure 158. Schematic for Showing Fluid Damping

It has been assumed above that the propagated waves are not reflected back to the vibrating plate. In the case of a panel at the surface of a closed cylindrical shell, standing wave patterns may be set up in the contained fluid causing this fluid to become reactive as well as dissipative, thus changing the panel natural frequencies from their "in vacuo" magnitudes. This is quite a complex problem, beyond the scope of this report, and reference is made to 56, 66, and 67 in the bibliography for further discussion of this problem.

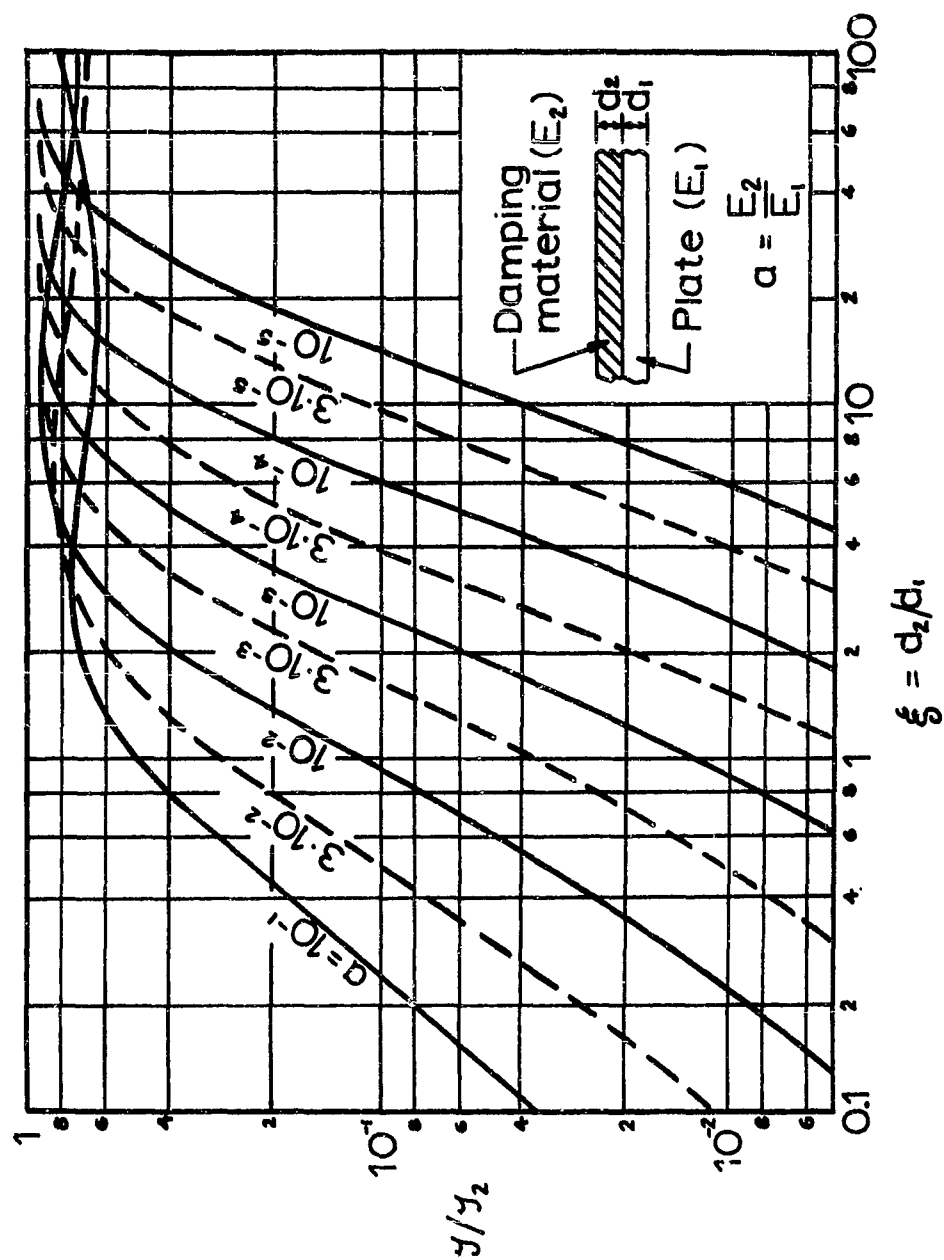


Figure 159: Ratio of Total Damping to Viscoelastic Material Damping for a Viscoelastic Overlay on a Plate.

ATTENUATION OF VIBRATION WITH DISTANCE IN TYPICAL STRUCTURE

The vibration at point A may be due to the local environment at point A or it could be due to the environment at point B, inducing sufficient response at point B which is transmitted thru structure to point A. The gradient of the environment and the vibration attenuation characteristics of the structure would appear to be governing factors. Fortunately, an experiment was conducted some years prior to this contract which provided the raw data to determine the attenuation of typical structures. A 300-inch length of Snark fuselage structure on a soft suspension was vibrated at one end and the structural response measured as a function of distance from the source. The input was normal to the fuselage centerline and the responses were measured in the same distance. The vibration was a sinusoidal input at discrete frequency from 20 cps to 1200cps. A random input was used but no complete analyses were made of this output. The Snark fuselage is 60 inches in diameter and made up of constant .190 magnesium skins.

The analysis was an attempt to answer the question whether a constant attenuation between successive cycles might describe the attenuation independently of frequency. Data from Reference 61 (S. Crandall, Random Vibrations, Technology Press) was used to determine the velocity of surface waves being transmitted longitudinally thru the skin. The velocity of these surface waves varied from 2700 fps at 1200 cps to 715 fps at 100 cps as compared to the speed of sound in magnesium of 15,100 fps. The results presented in Figure 161 show that the attenuation per cycle is indeed a constant independent of frequency. The constant is .72 for the ratio of successive peaks or .515 for successive peaks of amplitude squared.

In the plots of Snark response during launch, Figures 93-98, an anomaly in the data exists on Figure 98 in that a bulge in the response data suggests a locally high response in the area immediately forward of the rocket nozzle. Structural borne transmission from areas of still higher structural response do not account for all of the exceedance, and it may be possible that part is coming from a resonance effect of the local fuselage panels or substructure. This one case is an exception, however, and the success of the correlations presented in general shows that the vibration at any given point is in general determined by the local environment. This is particularly true for frequencies above 100-200 cps and not directly true at frequencies below these values, except as one integrates the excitation over the whole vibration and correspondingly obtains an integral measure of the deflections and generates a correlation on this basis. The significance of the frequency which divides the correlations into direct and integral correlations is the agreement of this frequency with the upper limit of the gross vehicle natural frequency considered significant and worthy of measurement on a ground vibration test and its agreement with the lower bound of frequency representing structural panels and substructure.

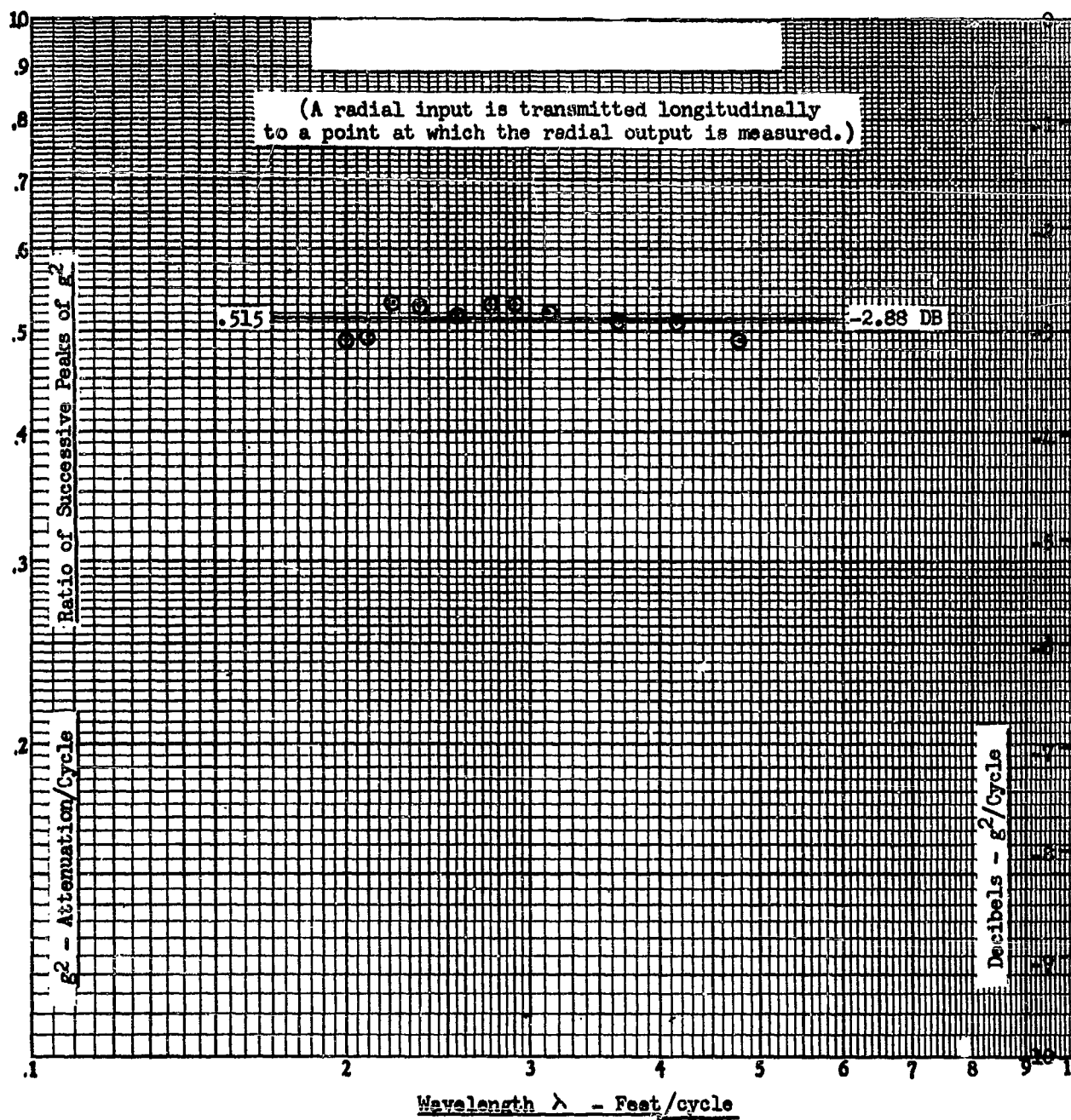


Figure 160. Vibration Attenuation in Snark Fuselage

STRUCTURAL DAMPING

A summary of the available damping data is presented in Figure 161 to help in the estimation of transfer functions and to obtain a general feel for the structural damping of the gross vehicle modes. Transfer functions may be estimated knowing the natural frequency, mode shape, generalized force and mass for each mode, if an estimate of the damping is also available. The damping for aircraft modes is higher than expected due possibly to an incomplete definition of the response curves. The damping was estimated from the width of the resonant peak. In transient analysis of complete structural response, it is common to use 5 per cent of critical damping as an estimate.

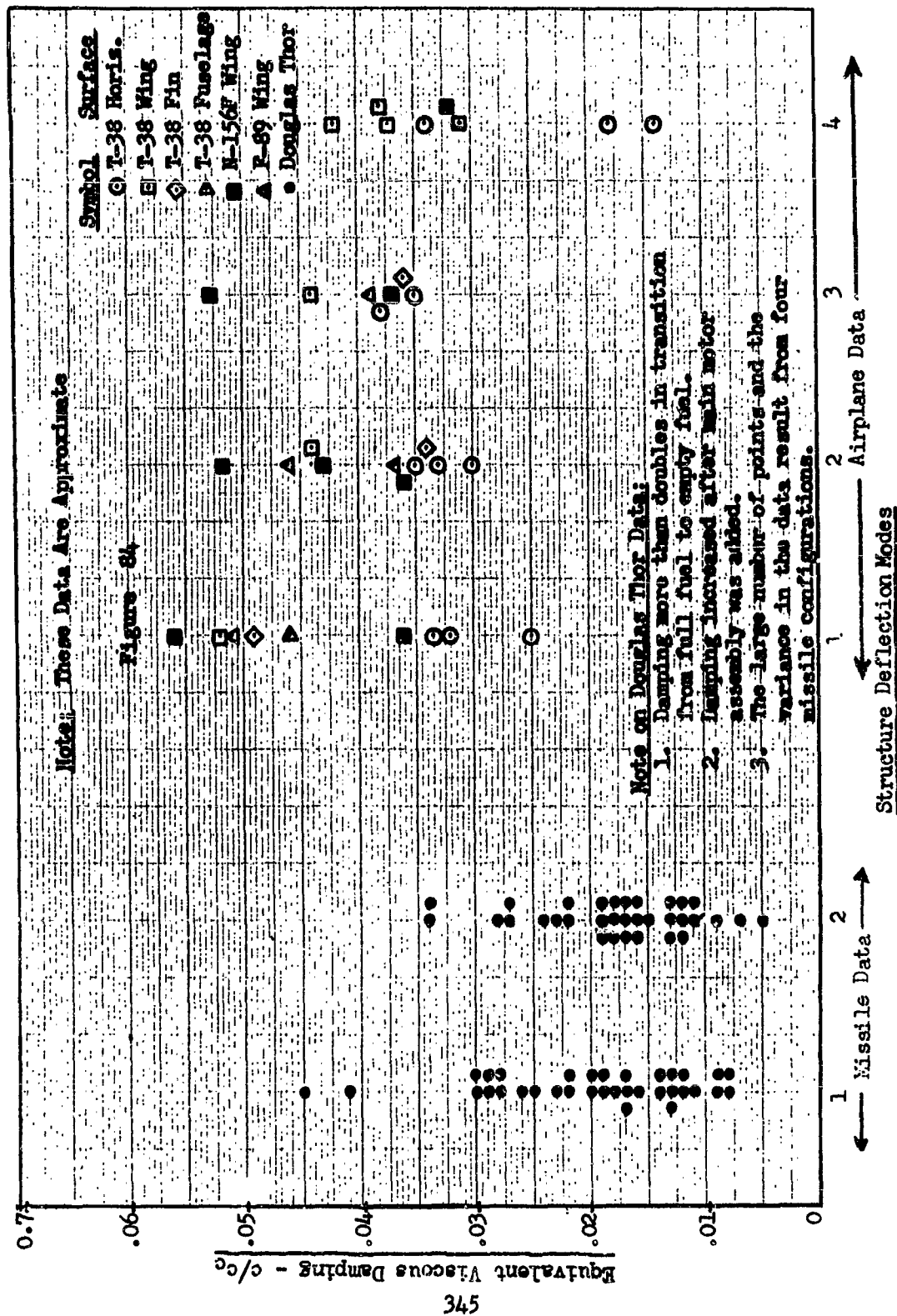


Figure 161. Compilation of Structural Damping Data - Equivalent Viscous Damping of Primary Structural Modes of Completed Vehicles.

REFERENCES

1. Lassiter, L. W., Hess, R. W.: Calculated and Measured Stresses in Simple Panels Subject to Intense Random Acoustic Loading Including the Near Noise Field of a Turbojet Engine. NACA TN 4076 September 1957.
2. Wang, Chi-Teh: Bending of Rectangular Plates with Large Deflections. NACA TN 1462, April 1948.
3. Hess, R. W., Lassiter, L. W., and Hubbard, H. H.: A Study of the Response of Panels to Random Acoustic Excitation. NACA RM L55E13c, 1955.
4. Lassiter, L. W., Hess, R. W., and Hubbard, H. H.: An Experimental Study of the Response of Simple Panels to Intense Acoustic Loading. Jour. Aero. Sci., vol. 24, no. 1, Jan. 1957, pp. 19-24, 80.
5. Callaghan, E. E., Howes, W. L., and Coles, W. D. (with appendix by Channing C. Conger and Donald F. Berg): Near Noise Field of a Jet-Engine Exhaust. II. Cross Correlation of Sound Pressures. NACA TN 3764, 1956.
6. Miles, John W.: On Structural Fatigue Under Random Loading. Jour. Aero. Sci., vol. 21, no. 11, Nov. 1954, pp. 753-762.
7. Wang, Chi-Teh: Nonlinear Large-Deflection Boundary-Value Problems of Rectangular Plates. NACA TN No. 1425, 1948
8. Ramberg, Walter, McPherson, Albert E., and Levy, Samuel: Normal-Pressure Tests of Rectangular Plates. NACA TN No. 849, 1942.
9. Timoshenko, S.: Theory of Plates and Shells. McGraw-Hill Book Co., Inc. 1940.
10. Houbolt, J. C.: On the Response of Panels Subject to a Flow Field Containing Random Disturbances. Shock and Vibration Bulletin, Part II, No. 26, December 1958.
11. Houbolt, J. C.: A Study of Several Aerothermoelastic Problems of Aircraft Structures in High-Speed Flight. Thesis presented to the Swiss Federal Institute of Technology, Zurich, for the degree of Doctor of Technical Sciences, Prom. Nr. 2760 (1958)
12. Press, H., and Tukey, J. W.: Power Spectral Methods of Analysis and Application in Airplane Dynamics, Bell Telephone Systems Tech. Pub., Monograph 2606; or AGARD Flight Test Manual, Vol. IV, Part IVC.
13. Press, H., and Houbolt, J. C.: Some Applications of Generalized Harmonic Analysis to Gust Loads on Airplanes, J. Aero. Sci., Vol. 22, No. 1 (1955)

14. Houbolt, J. C.: On the Response of Structures Having Multiple Random Inputs, presented before the meeting of the Wissenschaftliche Gesellschaft fur Luftfahrt W. V. (WGL), Essen, Germany, April 9-12, 1957.
15. Kirchman, E. J.; Thomas, D.; Greenspon, J.: Panel Excitation by Acoustic noise. Progress Report, Engineering Report No. 8637, The Glenn L. Martin Co., September 1956.
16. Lassen, B. J., Trapp, W. J.: Acoustic Fatigue and Damping. Shock and Vibration Bulletin, Part II, No. 26, December, 1958.
17. Anderson, Oiva R.: Some Considerations of Structural Design Criteria for Guided Missiles. Allied Research Associates, Inc. Report, Air Force Report WADC Technical Report 58-196, ASTIA Document No. AD, January 1958.
18. Budiansky, Bernard, Fralich, Robert W.: Effects of Panel Flexibility on Natural Vibration Frequencies of Box Beams. NACA TN 3070, March 1954.
19. Ungar, Eric E.: Free Oscillations of Edge-Connected Simply Supported Plate Systems, Bolt Beranek and Newman, Inc. Report No. 721, January 11, 1960.
20. Hahne, H. V.: Oscillations of Pressurized Cylindrical Shells. Lockheed Aircraft Corporation Report LMSD-2355, 5 March 1958.
21. Grigolyuk, E. I.: Small Oscillations of Thin Resilient Conical Shells. NASA TT F-25, May 1960.
22. Movchan, A. A.: On Vibrations of a Plate Moving in a Gas. NASA RE 11-22-58W January 1959.
23. Klosner, J. M., and Pohle, F. V.: Natural Frequencies of an Infinitely Long Noncircular Cylindrical Shell. Polytechnic Institute of Brooklyn, PIBAL Report No. 476, July 1958.
24. Lieber, P., and Yenik, K. T.: A Theoretical Investigation of Periodic Aerodynamic Forces and Fuselage Vibration Caused by Propellers, Part II - Vibration of Thin Curved Plates, Navy Department Bureau of Aeronautics, Contract No. a(S) 9652, September 25, 1949.
25. Mindlin, R. D., and Medick, M. A.: Extensional Vibrations of Elastic Plates. Columbia University Report done for the Naval Research Dept., April 1958.
26. Lassiter, L. W., and Hess, R. W.: Calculated and Measured Stresses in Simple Panels Subject to Intense Random Acoustic Loading Including the Near Noise Field of a Turbojet Engine. NACA TN 4076, September 1957.

27. Greenspon, J. E.: Vibrations of Thick Shells in a Vacuum and in an Acoustic Medium, Part II - Axially Symmetric Vibrations of a Thick Cylindrical Shell in an Acoustic Medium. J. G. Engineering Research Associates Report for Naval Research Dept., November 1959.
28. Yu, Yi-Yuan: Simple Thickness-Shear Modes of Vibration in Infinite Sandwich Plates. Polytechnic Institute of Brooklyn Report for AF Contract 49(638)-453, Tech. Note No. 2, ASTIA No. AD 204 132. October 1958.
29. Foxwell, J. and Franklin, R. E.: Acoustic Effects in the Vibrations of Structures. Aeronautical Research Council Report, ASTIA Document No. 161 225, 29 August 1957.
30. Kirchman, E. J., Thomas, D., and Greenspon, J.: Panel Excitation by Acoustic Noise. Progress Report Engineering Report No. 6637 for the Glenn L. Martin Company, ASTIA Document No. 150 890. 14 September 1956.
31. Yu, Yi-Yan: Flexural Vibrations of Elastic Sandwich Plates. Air Force Research Contract AF 49(638)-453, ASTIA Document No. 211 219. March 1959.
32. Proceedings of the National Specialists Meeting on Dynamics and Aeroelasticity, held at Fort Worth, Texas, November 6 - 7, 1958.
33. Mead, D. J.: The Internal Damping Due to Structural Joints and Techniques for General Damping Measurement. A.R.C. Technical Report C.P. No. 452, 1959.
34. Reissner, Eric: On Transverse Vibrations of Thin, Shallow Elastic Shells. Quarterly of Applied Mathematics, Vol. XIII, No. 1, April 1955, pp. 169-176.
35. Reissner, Eric: On Axi-Symmetrical Vibrations of Shallow Spherical Shells. Quarterly of Applied Mathematics, Vol. XIII, No. 1, April 1955, pp. 279-290.
36. Martin, A. I.: On the Vibration of A Cantilever Plate. The Quarterly Jour. of Mechanics and Applied Mathematics, Vol. IX, 1956, pp. 94-102.
37. Buchwald, T., and Tiffen, R.: Boundary-Value Problems of Simply-Supported Elastic Plates, Vol. IX, 1956, pp. 489-498, The Quarterly Jour. of Mechanics and Applied Mathematics.
38. Pursey, H.: The Launching and Propagation of Elastic Waves in Plates. The Quarterly Jour. of Mechanics and Applied Mathematics, Vol. X Part 1, February 1957, pp. 45-62.
39. Ashwell, D. G.: The Equilibrium Equations of the Inextensional Theory for Thin Flat Plates. The Quarterly Jour. of Mechanics and Applied Mathematics, Vol. X Part 1, February 1957, pp. 169-182.

40. Buchwald, V. T.: A Mixed Boundary-Value Problem in the Elementary Theory of Elastic Plates. The Quarterly Jour. of Mechanics and Applied Mathematics, Vol. X Part 1, February 1947, pp. 183-190.
41. Fung, Y. C., and Wittrick, W. H.: A Boundary Layer Phenomenon in the Large Deflexion of Thin Plates. The Quarterly Jour. of Mechanics and Applied Mathematics, Vol. VIII Part 2, June 1955, pp. 191-210.
42. Cox, H. L.: Vibration of Certain Square Plates Having Similar Adjacent Edges. The Quarterly Jour. of Mechanics and Applied Mathematics, Vol. VIII Part 2, June 1955, pp. 454-456.
43. Klumpp, J. H., and Laman, B. J.: Frictional Damping and Resonant Vibration Characteristics of an Axial Slip Lap Joint. WADC Technical Report 54-64, ASTIA Document No. 31155. March 1954.
44. Carmichael, T. E.: The Vibration of a Rectangular Plate with Edges Elastically Restrained Against Rotation. The Quarterly Jour. of Mechanics and Applied Mathematics, Vol. XII Part 1, February 1959, pp. 29-42.
45. Morley, L. S. D.: An Improvement on Donnell's Approximation for Thin-walled Circular Cylinders. The Quarterly Jour. of Mechanics and Applied Mathematics, Vol. XII Part 1, February 1949, pp. 89-99.
46. Haywood, J. H.: Response of an Elastic Cylindrical Shell to a Pressure Pulse. The Quarterly Jour. of Mechanics and Applied Mathematics, Vol. XI Part 2, May 1958, pp. 129-141.
47. Gladwell, G. M. L.: Some Mixed Boundary Value Problems in Isotropic Thin Plate Theory. The Quarterly Jour. of Mechanics and Applied Mathematics, Vol. XI Part 2, May 1958, pp. 159-171.
48. Johnson, M. W. and Reissner, E.: On Inextensional Deformations of Shallow Elastic Shells. Journal of Mathematics and Physics, Vol. XXXIV, Number 4, January 1956, pp. 335-346.
49. Duffin, R. J. and Schild, A.: On the Change of Natural Frequencies Induced by Small Constraints. Journal of Mathematics and Mechanics, Vol. 6, Number 6, November 1957, pp. 731-758.
50. Thomas, T. Y.: The Decay of Waves in Elastic Solids. Journal of Mathematics and Mechanics, Vol. 6, Number 6, November 1957, pp. 759-768.
51. Morse, P. M.: Vibration and Sound. McGraw-Hill Book Company, Ind. Second Edition, 1948.

52. Smith, P. W., Jr.: Minimum Axial Phase Velocity in Shells. The Journal of the Acoustical Society of America, Vol. 30, No. 2, February 1958, pp. 140-141.
53. Kraichnan, R. H.: Noise Transmission from Boundary Layer Pressure Fluctuations. The Journal of the Acoustical Society of America, Vol. 29, No. 1, January 1957, pp. 65-80.
54. Herrmann, G. and Mitzky, I.: Monaxially Symmetric Motions of Cylindrical Shells. The Journal of the Acoustical Society of America, Vol. 29, No. 10, October 1957, pp. 1116-1123.
55. Haskins, J. F. and Walsh, J. L.: Vibrations of Ferroelectric Cylindrical Shells with Transverse Isotropy. I. Radially Polarized Case. The Journal of the Acoustical Society of America, Vol. 29, No. 6, June 1957, pp. 729-734.
56. Cosces, G. M. and Liepmann, H. W.: On The Transmission Through a Fuselage Wall of Boundary Layer Noise. Douglas Report No. SM-19570, Santa Monica Division, December 1955, TL 25,991-C. 1.
57. Blake, R. E. and Paul, V. R.: Three Experimental Methods of Determining Dynamic Response Characteristics of Missile Structures. Lockheed Aircraft Corporation Report No. LMSD 2955, August 1958.
58. Ungar, E. E.: Free Oscillations of Edge-Connected Simply Supported Plate Systems. ONR Contract Nonr 2322(00), BBN Job. No. 5156, Report No. 721, Bold Beranek and Newman Inc., 11 January 1960.
59. Young, D.: Vibration of Rectangular Plates by the Ritz Method. T. L. 38, 570-C. 1.
60. Podnieks, E. R. and Lazan, B. J.: Effect of Material Damping and Stress Distribution on the Resonant Fatigue Strength of Parts. WADC Technical Note 55-284, August 1955.
61. Dyer, Ira: Estimation of Sound-Induced Missile Vibration; Chapter 9 of Random Vibrations by S. H. Crandall; Technology Press of MIT, 1958.
62. Love, A.E.H.: The Mathematical Theory of Elasticity. Dover Publications.
63. Rayleigh, J.W.S.: The Theory of Sound Volumes I and II. Dover Publications.
64. Timoshenko, S.: Vibration Problems in Engineering. D. Van Nostrand Co. Inc.
65. Pian, T.H.H.: Structural Damping; Chapter 5 of Random Vibrations edited by Stephen H. Crandall, Technology Press of MIT.
66. Faxwell, J., Franklin, R.E.: Acoustic Effects in the Vibrations of Structures. ASTIA AD No. 161225., August 1957.

67. Smith, P. W., Jr.: Sound Transmission Through Thin Cylindrical Shells. JASA Vol. 29, No. 6, June 1957, Page 721.

VI FATIGUE

INTRODUCTION

The mechanism of vibration and acoustic failure is fatigue. Although a working knowledge of fatigue exists in every design and structures group, the recent developments in this problem area have been unusually worthwhile as a result of more effort and emphasis. Approximately 300 papers per year are produced on this subject. The nature of the damage within the crystal is more thoroughly understood and a usable mathematical base for analysis and prediction is approaching. The knowledge to optimize solutions of the fatigue problem is not available and reliance is placed mainly on testing and the margin of safety.

Past experience was concerned with failure of equipment and secondary structures. Primary structural failures were exceedingly rare until the last few years. Acoustic fatigue of jet engine inlet ducts and gust induced fatigue of primary structure are important and costly examples. A failure existed due to acoustic fatigue in the internal structure of the main box of the horizontal stabilizer of the B45 aircraft. It is unfortunate that the more common failure in the acoustic fatigue problem involves substructure which is difficult if not impossible to inspect. All aspects of the contributions of dynamic stressing of primary structure must now be provided for. Both economic reasons and weapon system effectiveness support this conclusion.

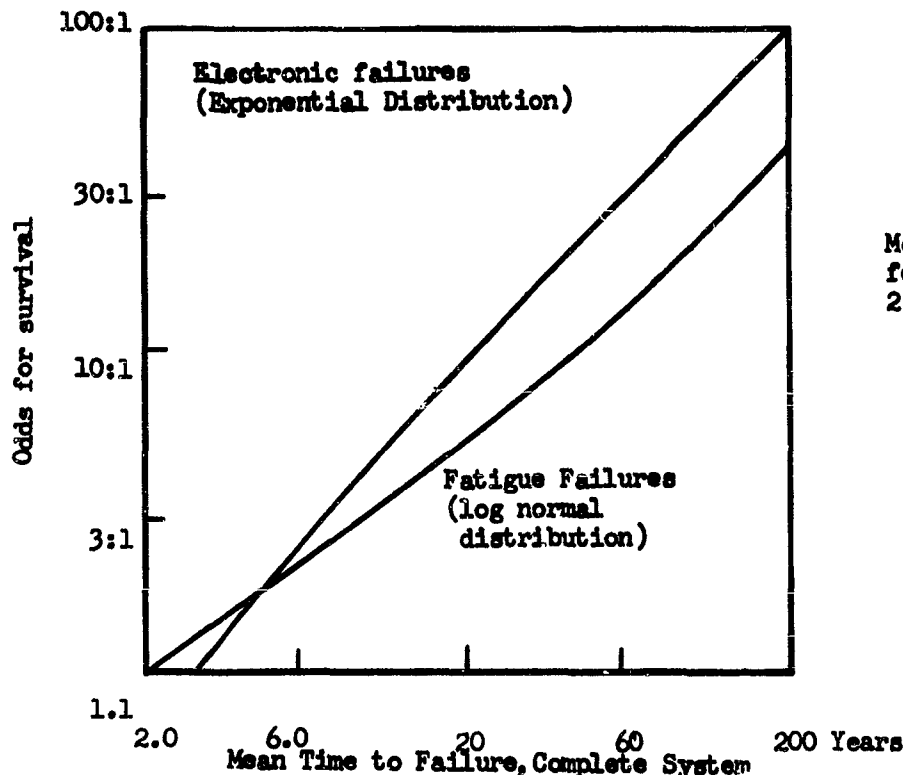


Figure 162

Mean Time to Failure
for Complete System for
2 Year Mission Into
Space

Three reasons for the emergence of fatigue as a primary design criterion have been the requirements for greater vehicle performance, the use of more efficient concepts of structural design for problems other than fatigue, the use of optimum design principles throughout the vehicle, a general cut in design margin, and a greater number of parts arising from greater complexity.

A thought provoking illustration of the need for additional emphasis is shown, in Figure 162, taken from Reference 15.

Attaining mean times to failure for a complete system of this order will require new knowledge.

A basic presentation of the fundamentals of fatigue is given which include the important experimental results. Material of Shanley, Reference 1, and Sines, Reference 2, is used.

A conventional presentation of the S-N data for a number of different materials shows considerable variation in level, Figure 163. No basic correlation exists in the data which could be used to predict new situations. The fatigue curve may be divided into three parts, the repeated load portion similar in stress level to the strength of the material, the center of the curve which is a straight line using log-log scales, and the endurance limit region. No one set of governing parameters covers all parts of the curve.

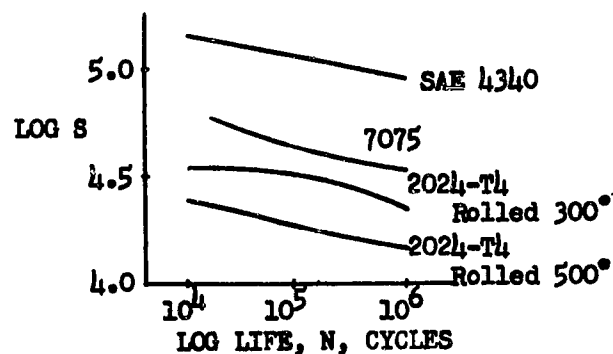


Fig. 163 Conventional Presentation of S-N Data

The failure mechanism within the crystal is due to unbonding from plastic deformation. A measure of plastic deformation occurs in the hysteresis loop. The hysteresis loop is a result of the fundamental imperfections of the material, a reflection of internal dislocations and slip. These same material characteristics which give width to the hysteresis loop are responsible for fatigue. When the hysteresis loop collapses to a straight line, perfectly elastic action is indicated and fatigue is impossible. In real material, the ideal of perfectly elastic action is approached below the endurance limit where the plastic strain is negligible.

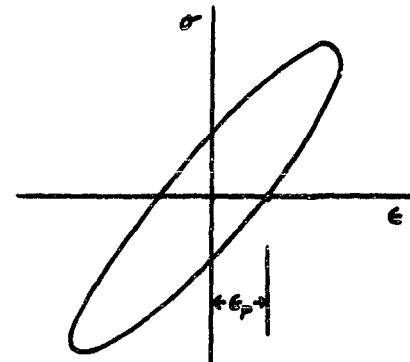


Fig. 164. Hysteresis Loop

If the hysteresis loop were to remain constant throughout the life of the part, a constant relationship would exist between the alternating values of the plastic strain, the total strain and the total stress. In Figure 165 it is shown that the bending moment required to produce constant strain is often a variable, however Strain hardening and strain softening is illustrated.

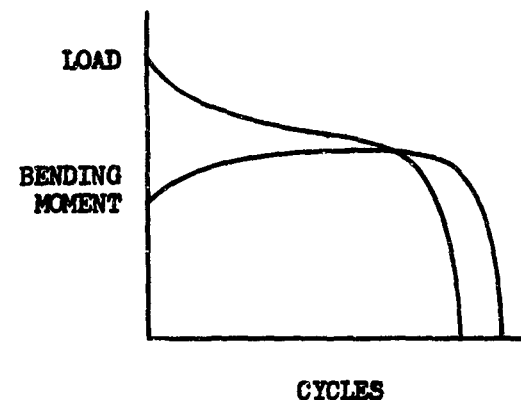


Fig. 165. Bending Moment required to Produce Constant Strain

Still a third parameter suggesting that a test should be made for correlation based on plastic strain is the fact that the damping indicated by the hysteresis loop increases radically in some materials above a stress value called the cyclic stress sensitivity limit (See Lazan¹³). This stress is very near the endurance limit.

The correlation based on plastic strain is shown in Figure 166 for steel and aluminum and for normal and elevated temperatures. Although based on limited data it appears a fundamental correlation does exist. It is worthwhile noting that the collapsing of the data to a single line based on parameters measurable in fatigue has at the same time eliminated consideration of conventional material

properties. A cause for some of the previous unwanted scatter in fatigue data is given by considering the above result. The data suggest that plastic strain is the proper quantity to measure and hold constant during testing rather than the imposed load or stress level.

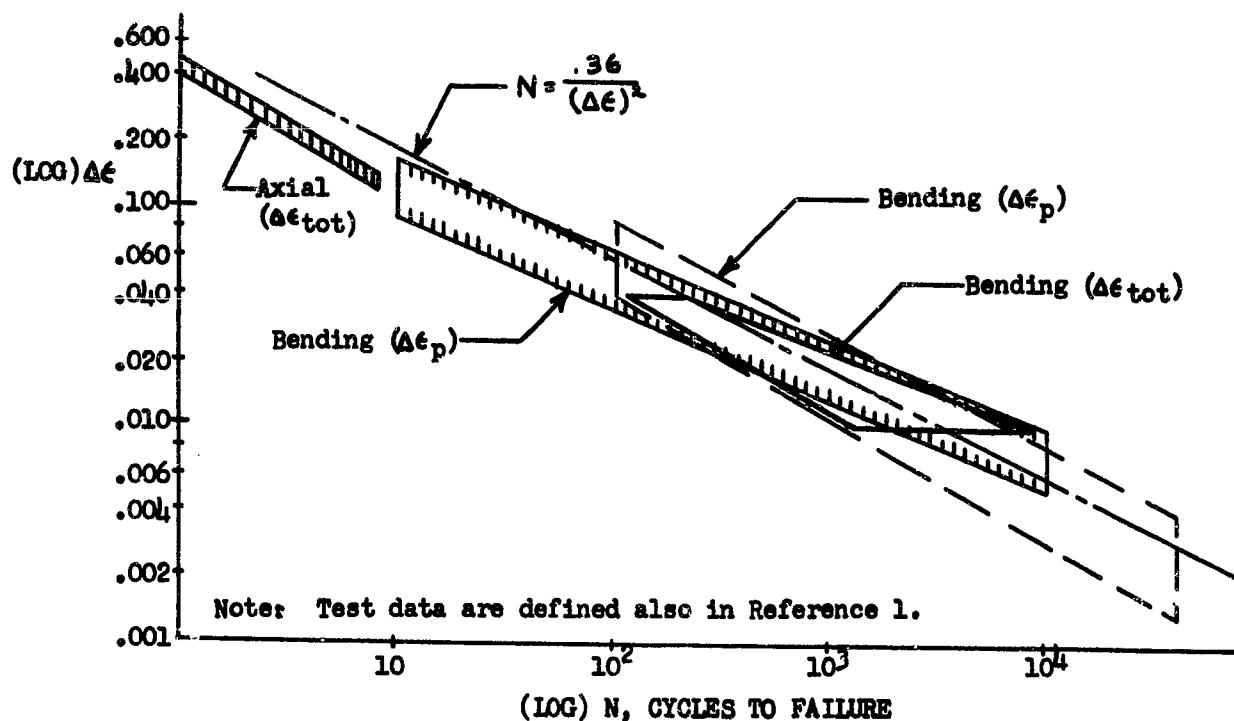


Figure 166 . Fatigue Data from Controlled Strain Tests (Reference 3)

Fatigue cracks originate at the surface. The rare exceptions are found to be concerned with internal voids which may also be looked at as free surfaces. Slip planes exist as normal flaws within the crystal in any material. With continued working, the slip planes become more prominent, allowing a reversible shearing action which causes progressive severing of the atomic bonds. A crack develops within one crystal, is temporarily delayed at the grain boundary and finally spreads to adjacent crystals. The electron microscope has identified cracks in material after only four percent of the life span.

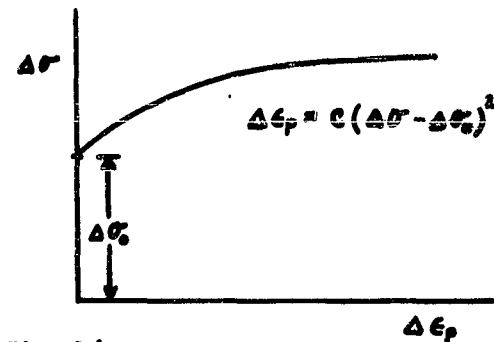


Fig. 167 Hypothetical Variation of Plastic Strain

A leverage action takes place at the edges of the unbonded area when tension stresses are present perpendicular to the unbonded area. Tension accelerates the breakdown of the material but is not a basic requirement since failure can be produced wholly in the compression range. The fundamental parameter is the amount of plastic strain imposed.

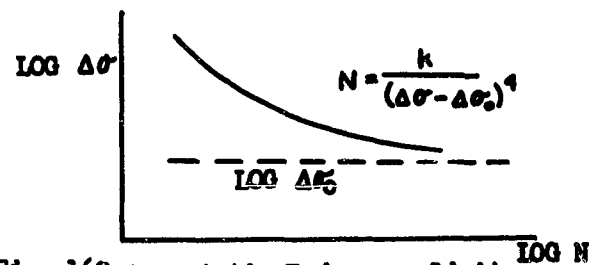


Fig. 168 Asymptotic Endurance Limit

If a value of cyclic stress amplitude $\Delta\sigma_0$ exists below which no cyclic plastic strains occur, an endurance limit will be present. Figure 167 shows the cyclic plastic strain $\Delta\epsilon_p \sim (\Delta\sigma - \Delta\sigma_0)^2$. Figure 169 shows an alternative possibility $\Delta\epsilon_p \sim \Delta\sigma^4$ with a cutoff at $\Delta\sigma_0$ and Figures 168 and 170 show the corresponding S-N curves.

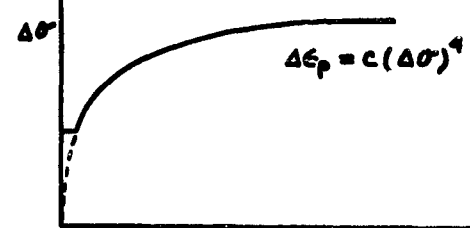


Fig. 169 Hypothetical Variation of Plastic Strain

The physical explanation of the endurance limit is that the dislocations within the crystal are pinned by mild stressing. Such locking up of the dislocations does not occur when high stress levels are intermixed with low stresses. The intermixing of high and low stresses generates more dislocations at high stress levels than can be pinned at low levels. Consequently, S-N curves for random loading are significantly below those generated at one stress level only. References 6, 17, and 18.

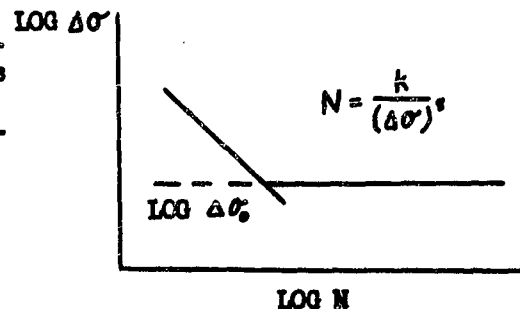


Fig. 170. Cutoff Endurance Limit

For cyclic plastic strain of constant amplitude, the rate of growth of crack area can be expressed

$$\frac{da}{dn} = c \Delta \epsilon_p^2$$

where a = crack area

n = number of cycles

$\Delta \epsilon_p$ = plastic strain

Integrating,

$$a = C \Delta \epsilon_p^2 n$$

At the point when the critical area is reached, n becomes N , a fatigue life.

$$a_{cr} = C \Delta \epsilon_p^2 N$$

$$N = \frac{C'}{\Delta \epsilon_p^2}$$

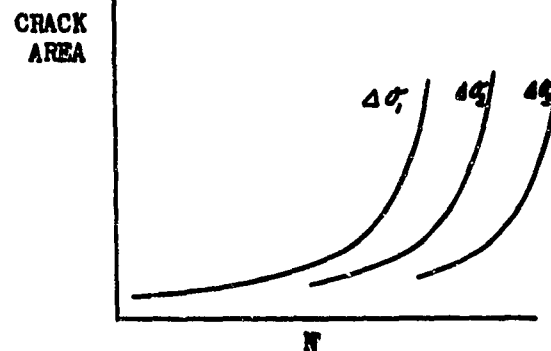


Fig. 171 Affine Crack Growth Curves

Using the experimentally determined constant from Figure 166,

$$N = \frac{.36}{\Delta \epsilon_p^2}$$

The slope obtained on log-log paper, $-1/2$, arises from the exponent of the plastic strain and agrees with measured data.

The relation between plastic strain and the stress is that shown by Figures 167 and 169.

$$\Delta \epsilon_p = f(\Delta \sigma)$$

$$\Delta \epsilon_p = (\Delta \sigma)^x$$

$$N = \frac{C}{(\Delta \sigma)^{2x}}$$

The effects of mean stress can be approximately represented by the linear interaction curve

$$\frac{\Delta \sigma}{\Delta \sigma_0} + \frac{\sigma_m}{\sigma_{m_0}} = 1$$

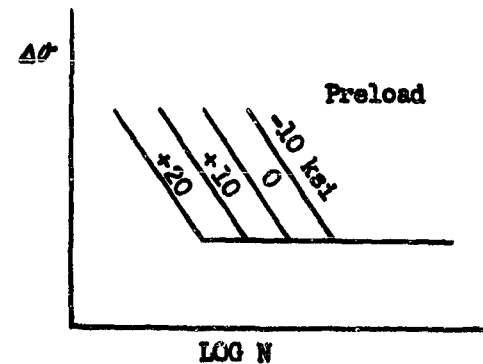
usable to the yield strength where

$\Delta \sigma$ alternating stress

$\Delta \sigma_0$ allowable alternating stress at zero mean stress

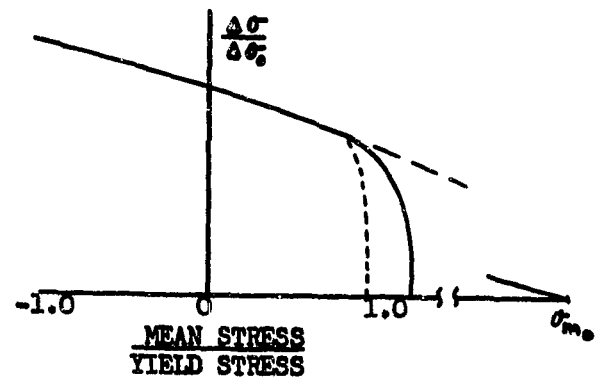
σ_m mean static stress

σ_{m_0} extrapolation of the straight line as shown to give a fictitious allowable mean stress at zero alternating stress. See Figure 173.



S-N Family to Display Preload Effect

Figure 172



Interaction between Alternating and Steady Stress

Figure 173

An interaction curve is illustrated in Figure 173. A more conventional plot is that shown in Figure 172.

Combined Stresses

The valid theoretical mechanisms which attempt to explain the mechanism of fatigue include: (1) maximum shear criterion, (2) octahedral shear stress, (3) strain energy method, (4) the principal strain, and (5) the principal stress. Concentrating on the octahedral shear stress criterion because of its support from experimental data, we describe the stresses on a small volume of material by enclosing it in a cube and defining the moment and shear stresses on the six faces. The cube can be oriented so only normal stresses result; these are extreme values called the principal stresses.

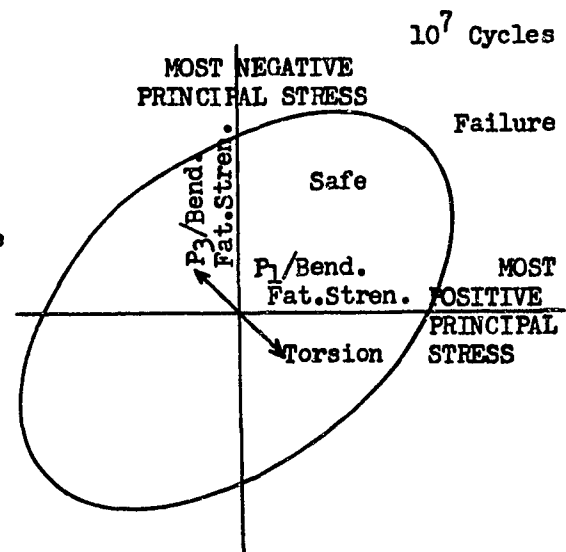
Of more interest to plastic flow problems (and fatigue is apparently in this category) are the shear stresses. The octahedral shear closely predicts plastic flow

$$\tau_{octa} = \frac{1}{3} \sqrt{(P_1 - P_2)^2 + (P_2 - P_3)^2 + (P_3 - P_1)^2}$$

where the P_i are the three principal alternating stresses.

Figure 174 is a plot of the criterion. Pure bending is a vector along one of the axes, pure torsion at 45° as indicated. Combined bending and torsion occur only in the same quadrants as pure torsion. Each principal stress oscillates from a given value in the tensile direction to an equal value in the compressive direction on the other half cycle. The diagram is applicable to a free surface, $P_2 = 0$. In the first and third quadrants, the principal stresses are in phase.

The common problem is not alone one of combined alternating stresses but also includes an array of static stresses as well; all combinations of axial bending or torsional stresses must be considered. Common engineering practice presents these data in the form of the Goodman diagram, but this procedure fails when the static stress is not the same kind as the alternating stress. The very interesting summaries of the results of the interactions are given in Figures 175 and 176. The ordinate is the alternating stress; the abscissae, the static stress. The data shows no interaction of (1) static torsion on alternating torsion, nor (2) static torsion on alternating bending as long as the static torsion stress is less than the yield strength.



Octahedral Shear Failure Criterion

Figure 174

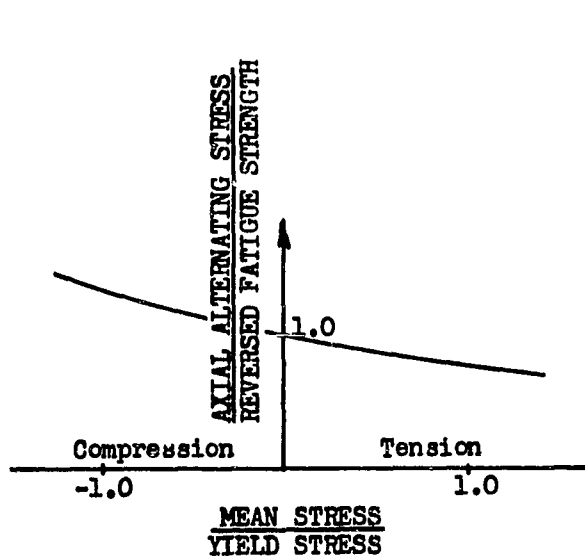
The permissible alternation of the octahedral shear stress is a linear function of the orthogonal normal static stresses (at a given life)

$$\tau_{\text{octa}} \leq \frac{\sqrt{2}}{3} f_0 - \alpha (s_1 + s_2 + s_3)$$

where f_0 = alternating uniaxial fatigue strength at zero mean stress at the desired life

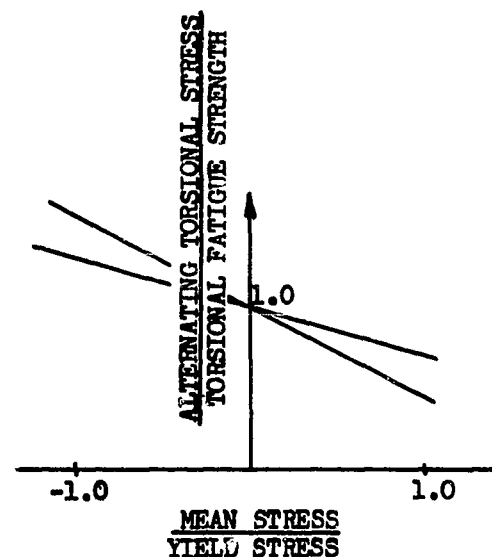
$$\alpha = \frac{\sqrt{2}}{3} \left(\frac{f_0}{f_1} - 1 \right)$$

f_1 = alternating uniaxial fatigue strength centered on a mean stress of the same value, at the desired life.



Effect of Mean Axial Stress on Axial Fatigue

Figure 175



Effect of Static Normal Stress on Torsional Fatigue

Figure 176

Yielding must be prevented to provide a design which is at all conservative. A simple conservative criterion, in lieu of the longer and more exact method above, is that the maximum local shear stress must not exceed one-half the yield strength.

$$\frac{P_1 - P_3}{2} = t_{\max} \leq \frac{Y.S.}{2}$$

Wang¹⁰ shows that the octahedral shear stress can be calculated without knowing the principal stresses. In an elastic solid there are three mutually perpendicular planes with no shear stress. The normal stresses are the principal stresses. With the cube oriented in an arbitrary direction, three linear simultaneous homogeneous equations must be solved to find the principal stresses and directions. The secular determinant is set equal to zero, yielding:

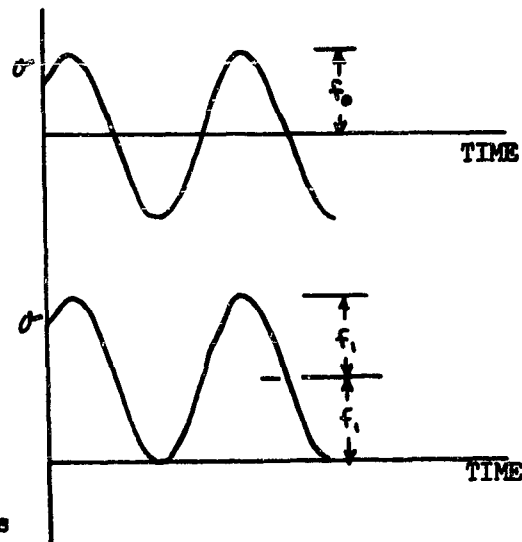


Figure 177. Definitions of f_0 and f_1

$$S^3 - J_1 S^2 - J_2 S - J_3 = 0$$

$$J_1 \equiv \sigma_{xx} + \sigma_{yy} + \sigma_{zz}$$

$$J_2 \equiv -(\sigma_{xx}\sigma_{yy} + \sigma_{yy}\sigma_{zz} + \sigma_{zz}\sigma_{xx} - \sigma_{xy}^2 - \sigma_{yz}^2 - \sigma_{zx}^2)$$

$$J_3 \equiv \sigma_{xx}\sigma_{yy}\sigma_{zz} + 2\sigma_{xy}\sigma_{yz}\sigma_{zx} - \sigma_{xx}\sigma_{yz}^2 - \sigma_{zz}\sigma_{xy}^2 - \sigma_{yy}\sigma_{zx}^2$$

The solution of this equation is independent of the choice of coordinates and the J_j are called stress invariants. Expressed in terms of the principal stresses

$$J_1 = S_1 + S_2 + S_3$$

$$J_2 = -(S_1 S_2 + S_2 S_3 + S_3 S_1)$$

$$J_3 = S_1 S_2 S_3$$

If the hydrostatic pressure is subtracted from each of the principal stresses, one of the invariants obtained has a number of significant physical meanings. Let $p = J_1/3$ where p , the average of the normal stresses, is called the hydro-

static pressure. Subtracting the hydrostatic pressure from the principal stresses gives the stress deviator

$$S'_1 = S_1 - p \quad S'_2 = S_2 - p \quad S'_3 = S_3 - p$$

Forming J'_2 , the second invariant of the stress deviator

$$\begin{aligned} J'_2 &= -(S'_1 S'_2 + S'_2 S'_3 + S'_3 S'_1) \\ &= 1/2 (S'^2_1 + S'^2_2 + S'^2_3) \\ &= 1/6 [(S_1 - S_2)^2 + (S_2 - S_3)^2 + (S_3 - S_1)^2] \end{aligned}$$

Starting with only the data available from an arbitrary set of coordinates at the beginning of the problem

$$\begin{aligned} J'_2 &= 1/6 \left[(\sigma_{xx} - \sigma_{yy})^2 + (\sigma_{yy} - \sigma_{zz})^2 + (\sigma_{zz} - \sigma_{xx})^2 \right. \\ &\quad \left. + 6(\sigma_{yz}^2 + \sigma_{zx}^2 + \sigma_{xy}^2) \right] \end{aligned}$$

The second invariant of the stress deviator, J'_2 , has the following physical significance:

- a. It is proportional to the mean shear stress obtained from considering planes with all possible orientations, $2 J'_2 / \sqrt{10}$
- b. It is the shear stress on the octahedral plane, $\sqrt{2} J'_2 / 3$
- c. It is proportional to the elastic energy stored by change in shape, $(1 + \nu) J'_2 / E$
- d. It is the von Mises criterion for plastic deformation, $\sqrt{J'_2} \geq K$

A further broad general statement is possible regarding the stress invariants. The failure of all isotropic or quasi-isotropic solids may be expressed

$$F(J_1, J_2, J_3) \geq 0$$

where careful experiments must be performed to find the function F applicable to the type of failure or material under consideration.

The special case of combined stress solvable by Mohr's circle depends on knowing one principal direction. When this is not available, the stress formulas given above are required for the general case.

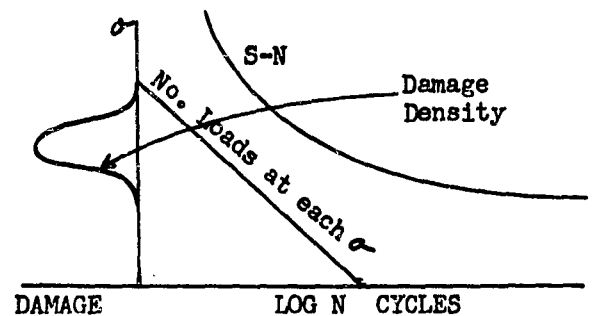
Variable Amplitude Loading

An important class of fatigue failures will result from a nearly continuous spectrum of the applied alternating loads. Loads from different stress levels will be intermixed. It is believed that an accurate picture of randomly applied loads is obtained if these loads are merely summed to form such a continuous load spectrum. To obtain the loading history from a random wave, it is necessary to know the probability density distribution of the stress amplitudes.

The simplest case is presented in Figure 178 in which the damage density (i.e., the cycle ratios) is presented. The presentation in this form is highly recommended as it gives a valuable picture of the damaging portion of the load spectrum.

Conventional S-N curves present failure data for a certain combination of mean and alternating stresses, a combination which is held constant until failure occurs. These data are not applicable to the random load case because intermixing of high and low loads allows significantly more damage to be done at low stress levels. The situation is illustrated in Figure 179. The explanation is that high stresses generate the dislocations and that when only low stresses are present, the dislocations are pinned; but when the stresses are intermixed, significant damage is done by the low stresses at and below the endurance limit.

Freudenthal⁴ has shown that the Miner fraction varies between .1 and 1.0 when intermixed stresses are used on smooth unnotched specimens of 2024 aluminum and 4340 steel, Figure 180.



A Suggested Presentation of the Damage,
the Load History, and the Strength
Figure 178

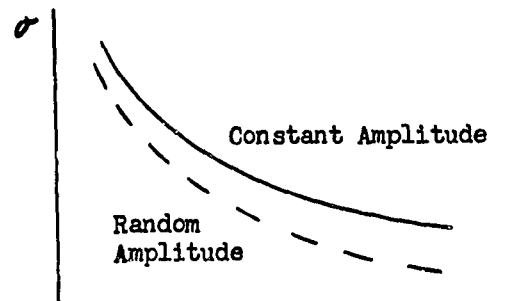


Figure 179. S-N Comparison

Miner's rule has been used as a guide on conventional built-up structure with its many stress concentrations and reasonably justified for a certain class of problems. Miner's rule was created to accumulate damage for the basic case of unnotched material. However, Freudenthal has given a fundamental demonstration of its lack of applicability to the basic case. Therefore, the future use of Miner's rule must be ringed with qualifications to prevent its use in areas unsupported by test data or previous experience.

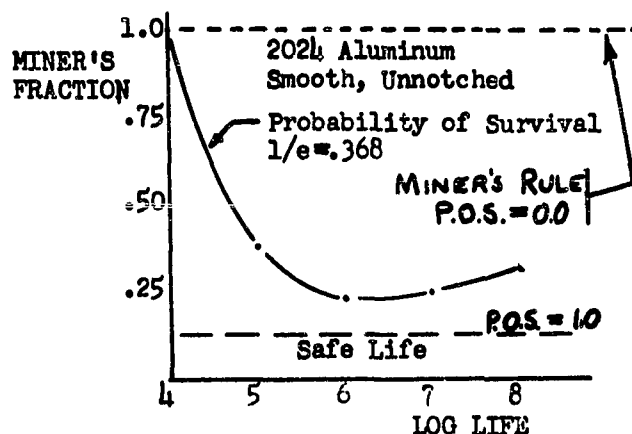


Figure 180. Influence of Stress Interaction

The Stress Concentration Factor

The usual fatigue failure is not caused by stressing an appreciable portion of the material above its endurance limit but is caused by the existence of locally high stresses around attachments, drill holes, inclusions, and surface roughnesses. If these elastic stress concentrations were removed, the number of failures would be considerably less.

The elastic stress concentration factor is the ratio of the elevation in stress predicted by the theory of elasticity for a flawless material. One would expect the S-N curve applicable to a part with a stress concentration to be the S-N curve for the unnotched material divided by the stress concentration factor, K_t . The factor K_t applies to a peak stress affecting an insignificant number of grains and in the practical case, the degradation in strength predicted by K_t is not obtained. The fatigue notch factor, K_f , is the ratio of the unnotched/notched fatigue strength and can be thought of as expressing an average increase in stress affecting a statistically significant number of grains--the number within one per cent of the peak stress, for example. Spaulding presents a chart in Reference 19 showing $K_t = 4.5$ to be representative of the best that can be depended upon in typical aircraft structure when special care is exercised in design.

The notch sensitivity factor, q , is a measure of how much K_t effect is finally exhibited in the experimental result.

Notch sensitivity is usually presented graphically as a function of the notch radius and is defined as

$$q = \frac{K_f - 1}{K_t - 1}$$

and varies between the limits of zero indicating no notch effect, $K_f = 1$; and unity, indicating full theoretical notch effect, $K_f = K_t$. As the radius approaches very low values of the order of the grain size, the sensitivity approaches zero. In the limiting case of small radius but finite notch depth, $K_t \rightarrow \infty$ & $q \rightarrow 0$ but K_f approaches finite values in the range of 2 to 4. The curve shown is expressed by an equation of the form $q = 1/(1 + a/r)$ where a is a constant peculiar to a given material but varying with its heat treatment and the size of the inclusions which may be present. A listing of the data available regarding the parameter is on page 295, Reference 16. The grain size effect shown has been hypothesized as due to (1) the number of grains in the volume of material where the stress is within one percent of the peak stress, or (2) the existence of a stress gradient which is steep in relation to the grain size.

q
Notch
Sensitivity

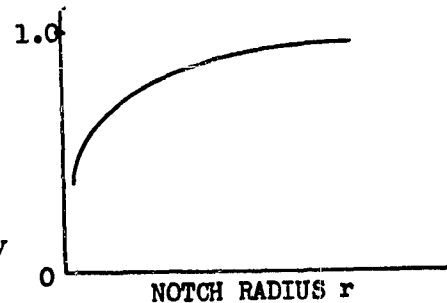


Figure 181. Notch Sensitivity

Size effect describes a variation in fatigue strength in a series of parts all of which are geometrically similar; the larger the part the lower is its fatigue strength. The greater volume of the large part which is stressed to within one percent of the maximum stress provides a greater probability of finding weak links-weak crystals.

Miles¹¹ has attempted to show the compatibility of the existing S-N data, the random response theory, and Miner's rule. The Rayleigh distribution of peaks was used to describe the loading history. There is, however, a basic incompatibility between (1), a load history which, to be consistent with S-N data, implies equal negative peaks between adjacent positive peaks and (2), the Rayleigh distribution, which does not. The use of the Rayleigh distribution for the load history may be improper. McClymonds¹² has shown that an alternative approach is possible which divides random stresses into alternating and mean stresses. Examination showed both to be normally distributed. This result would seem to require the use of the joint probability of occurrence of the mean and alternating stresses. The statement was made, however, that the effect of the mean stresses was negligible.

Further developments must be expected before an established method is available to handle random loads. The method must cover mean stresses and stress concentrations.

Referring to the random S-N curve of Figure 179, it will be possible to establish rather easily the endurance limit for the random load case. Successive failures are obtained by test using the full spectrum randomly applied, then the block containing the lowest stresses is omitted, next the lowest two levels are omitted, and so on until the comparative life begins to increase. The endurance limit for random loads is defined by this procedure. This test was suggested by Shanley.

Cumulative Damage A uniform rate of damage accumulated per cycle at constant stress level is one leg of the cumulative damage definition. The other leg of the definition is the linear rule of damage accumulation under variable stress amplitudes.

Freudenthal increased the linear damage rate per cycle $1/N_i$; by a stress interaction factor w to obtain w/N_i , $w > 1$.

Partial Damage $D = w_i n_i / N_i$

Cumulative Damage $\Sigma D = \Sigma w_i n_i / N_i$

Miner's rule is obtained when ΣD and $w = 1$. Let $n_i = p_i N$ where N is the total number of cycles to failure obtained by summing the load history at all stress levels, and p_i is the fraction of the total number of cycles at any given stress level.

$$\Sigma D = \Sigma w_i p_i N / N_i = 1$$

$$N = \frac{1}{\Sigma w_i p_i / N_i} = \frac{1}{\int_{s_e}^{s_u} \frac{w_i p_i}{N_i} ds}$$

For rms stresses low enough to result in long life, the damage is done by the few peaks appreciably in excess of the rms value, a significant conclusion.

Application to Engineering Problems

Considering the extremes in flight time and power plant operation that exist in missiles, aircraft, and spacecraft, there is a tendency to expect fatigue failures to be a remote possibility in the vehicle with the short flight times. In practice this has not proven to be true. The severity of the environment has tended to balance the duration of the exposure. Failure has moved to higher frequency bands in equipment vibration and acoustic panel fatigue problems where a million cycles of alternating load can be applied in one hour's time. The German V-2 missile suffered approximately 30 complete

structural failures following launch which were due to skin failure following panel flutter.

Failure of flat panels in the T-38 engine inlet duct took place in only 10 hours. If full power had been used continuously it was estimated that failure would have been induced in only one hour. At zero forward velocity, air is inducted with sufficient turbulence to cause pressure fluctuations at the level of 154 DB. Single skins held by countersunk rivets are inadequate for this environment. At all speeds above a low forward speed, air is smoothly inducted -- the corresponding measured pressure fluctuations drop to 139 DB. The probable mechanism of the generation of the high turbulence on the ground is the flow of air across the sharp leading edge of the duct, since a portion of the air supply is drawn from the side and from the rear. A reasonable leading edge radius on the duct inlet on subsonic vehicles has not always prevented internal duct panel damage. Extensive damage also has existed in completely circular inlets and in the case of reasonable radius and a circular inlet. That damage can occur in the circular duct with the large leading edge radius is significant because it would have been expected to be less susceptible to damage than a duct with flat panels and sharp leading edge. These parameters were insufficient to prevent damage. Very few jet intakes have escaped this type damage.

Extensive acoustic damage to secondary structures exists on many jet engined aircraft and has become so common that a satisfactory service life for fairing and ejector structures adjacent to the jet stream has proven to be as low as 500 hours. The Air Force estimates acoustic fatigue damage to have cost roughly on hundred million dollars in the last five years; (Ref.: WADC TR 59-507 Supplement #1). The initiation of studies concerned with rate of crack growth were partly the result of the need for a criterion for safe life of secondary structure containing cracks. These costs are incompatible with the expressed position of several companies that fatigue is a detail design problem and can be prevented by properly engineered details.

REFERENCES

1. Shanley, F. R.: Discussion of Methods of Fatigue Analysis. Rand Report P-1749, 6 July 1959.
2. Sines, G., and Waisman, J. L.--Editors: Metal Fatigue. McGraw-Hill Book Company, Inc. 1959.
3. Pian, T. H. H., and D'Amato, R.: Low-Cycle Fatigue of Notched and Unnotched Specimens of 2024 Aluminum Alloy Under Axial Loading. WADC Technical Note 58-27, February 1958.
4. Freudenthal, A. M., and Heller, R. A.: On Stress Interaction in Fatigue and a Cumulative Damage Rule. Jour. Aero/Space Sciences, Vol. 26, No. 7, July, 1959.
5. Fralich, R. W.: Experimental Investigation of Effects of Random Loading on the Fatigue Life of Notched Cantilever-Beam Specimens of 7075-T6 Aluminum Alloy. NASA Memorandum 4-12-59L, June 1959.
6. Hess, R. W., Herr, R. W., and Hayes, W.H.: A Study of the Acoustic Fatigue Characteristics of Some Flat and Curved Aluminum Panels Exposed to Random and Discrete Noise. NASA TN D-1, August 1959.
7. Johanson, A.: Fatigue of Steels at Constant Strain Amplitude and Elevated Temperature. Springer-Verlag, Berlin. Presented at Colloquium on Fatigue, I.U.T.A.M., Stockholm, May, 1955.
8. Schjelderup, H. C.: A New Look at Structural Peak Distributions Under Random Vibration. Presented at WADD - Minnesota Acoustical Fatigue Conference, National Engineering Science Company, 28 September 1959.
9. Schjelderup, H. C.: Prediction of Acoustic Fatigue Life. National Engineering Science Company, 15 March 1960.
10. Wang: Applied Elasticity. McGraw Hill Book Company, 1953.
11. Miles, J. W.: On Structural Fatigue Under Random Loading. Jour. of the Aeronautical Sciences, Vol. 21, No. 11, November, 1954.
12. McClymonds, J. C.: Sonic Fatigue Design Analysis. WADC TR 59-507, 11-13 August 1959.
13. Lazan, B.J.: Energy Dissipation Mechanisms in Structures, with Particular Reference to Material Damping. ASME Colloquium on Structural Damping, Section 1, December 1959.

14. Miner, M. A.: Cumulative Damage in Fatigue. Jour. of Applied Mechanics, September 1945.
15. Root, Gene: Talk delivered to IAS Channel Cities Section, March 1960.
16. WADC Symposium, Fatigue of Aircraft Structure, TR 59-507. August 1959.
17. Hess, R. W., Fralich, R. W., and Hubbard, H. H.: Studies of Structural Failure Due to Acoustic Loading, N.A.C.A. TN-4050. July 1957.
18. Hardarth, H. F., Utley, E. C., and Guthrie, D. E.: Rotating-Beam Fatigue Tests of Notched and Unnotched 7075-T6 Aluminum-Alloy Specimens Under Stress of Constant and Varying Amplitudes, N.A.S.A. TN D-210. December 1959.
19. Design for Fatigue, SAE Preprint 140, October 1953. E. H. Spaulding
Aircraft Fatigue Handbook Vol. II A.I.A.
Detail Design for Fatigue in Aircraft Wing Structure. E. H. Spaulding,
Jan. 18, 1954.

CONCLUSIONS

There are a large number of conclusions implicit within each of the sections of this report, many of which are of value only when viewed in context with the discussion. However, several general and specific conclusions can be restated here, as follows:

A.

- (1) In general, the maximum vibration in space vehicles occurs at either launch, as a result of rocket noise, or during the maximum dynamic pressure flight phase as a result of boundary layer pressure fluctuations.
- (2) The rms acceleration associated with the amplification of either of the above random noise inputs appears on the order of 2 g for light missiles, weighing less than 15,000 lbs., and on the order of .5 g for heavy missiles weighing over 100,000 lbs. Note that these amplitudes result from surface launch and present maximum q values.
- (3) These missile accelerations increase approximately in proportion to the square root of frequency.
- (4) Rms acceleration amplitudes on missile structures near operating rocket engines in both heavy and light missiles are on the order of 3-10 g independent of flight phase.
- (5) Total rms accelerations including all frequencies below 12,000 cps on rocket motors are generally of the order of 4 - 10 g with peak amplitudes during firing as much as 10 times the rms values; however, some rms values of the order of 50 to 500 g have been reported with peaks ranging to 2000 g.
- (6) Internal acoustic levels can be as high as 150 db SPL for certain configurations and must be considered in relation to electronic and other equipment.

B.

- (1) An empirical correlation of missile launch vibration data showed that prediction of resonant vibration could be made by considering the mean square force per cycle input to the vehicle, regardless of spacial correlation, the vehicle's weight, and frequency. The data indicate that the ratio of generalized force on the vehicle to the generalized mass taking part in the motion is constant for constant values of the wave number associated with the noise input.
- (2) A correlation between external noise and vibration of adjacent structure showed promise for aircraft at the higher frequencies. However, the results were negative at low frequencies, indicating that the vibration of structure in regions remote from the location of the maximum noise levels is a summation of direct local excitation and vibration transmitted through the structure from the areas of maximum noise. These results are consistent

with the concept of a constant value of attenuation per wavelength of the transmitted vibration bending wave, as demonstrated from a Snark experiment, Figure 160. The data also exhibited major differences between types of aircraft which may result from differing structures and configurations.

C.

- (1) The analytical approach for the understanding and prediction of space vehicle vibration emphasizes the use of mobility concepts, where mobility of the vehicle is defined as the ratio of the response to the generalized force input;
- (2) Computation of the generalized force, or the effective force on the vehicle, requires statistical knowledge of the spatial correlations of the forcing function, together with definition of the mode shape of the panel or shells which are exposed to the forcing function;
- (3) The definition of the mobility of the structure can be approached analytically by studying various simplified analytical models, appropriate to the geometry of the structure obtaining a series of solutions which converge towards an increasingly better approximation of the true structure.

D.

- (1) Resonance on resonance is responsible for the failure of many small parts. The two degree of freedom system has been analyzed many times in the past without noting that for the small mass of the system that a Q^2 response for sinusoidal excitation and a $Q^{3/2}$ response for random excitation is possible for large mass ratios. Hence, resonance on resonance should be prevented by proper damping of the critical items and/or vibration isolation.

E.

- (1) A fundamental correlation between strain and life is presented based on limited data from work of Shanley and Pian and D'Amato derived from several different materials, from different temperature ranges, and from the thermal fatigue problem.

PART III

SIMPLIFIED COMPOSITE RESPONSE

I. INTRODUCTION

The previous sections of this report have been concerned with the prediction of the dynamic forcing functions encountered in the operation of a space vehicle and the vehicle's responses to this environment. This section discusses the combining of the various dynamic responses encountered during the vehicle's normal service life to a simplified composite response, suitable for test specifications.

In former years, vibration test specifications for aircraft were developed for an entire class of aircraft, generally from envelopes of vibration data acquired from a large body of measurements on a variety of aircraft. In general, these specifications applied to mechanical or electronic equipment mounted within the aircraft and were intended to prevent occurrence of either malfunction or fatigue failure during the service life of the equipment. Furthermore, these specifications were tailored to available sinusoidal vibration shakers which were capable of sweeping through the frequency range at a constant amplitude or dwelling at one frequency at various amplitudes. Thus, the actual flight vibration environment which usually consisted of a super-position of many sinusoidal vibration components, resulting from both engine vibration and acoustical coupling between the propeller and the aircraft, was reproduced during test one frequency at a time. These envelope specifications were adequate for equipment in the majority of propeller aircraft, since the envelope environment was more severe than any environment encountered in an individual aircraft, and the aircraft design state of the art did not result in vibration environments for new aircraft which differed radically from the environments of their predecessors. Furthermore, although compliance with these specifications resulted in a considerable upgrading of the fragility level of many types of equipment, it did not necessitate a radical change in "good design practice" for equipment, nor did it result in equipment which became too heavy, bulky or otherwise incompatible with other aircraft requirements.

The development of modern, high performance, lightweight flight vehicles with jet or rocket propulsion has resulted in a significant change in the characteristics of vehicle dynamic environments, and in some cases the introduction of structural fatigue as a problem area of vital concern.

As shown in previous sections, the most severe vibration environments for modern vehicles generally result from external pressure fluctuations of either acoustical or aerodynamic origin. These pressure fluctuations are characterized by a distribution of energy at all frequencies throughout a wide frequency range and by gaussian amplitude distribution. Thus, mechanical energy is available to simultaneously excite many resonances in a panel, substructure component or equipment. Secondly, because of the random amplitude distribution of the forcing function, the relationships between the resulting responses at the various resonances can be described only statistically.

The general increase in the severity of the dynamic environment, coupled with this change in the nature of the exciting forces and the increasing concern with structural fatigue, has necessitated a re-evaluation of previous vibration specifications. In many cases, equipment and design techniques which were qualified for propeller aircraft have been found unsatisfactory for modern flight vehicles, necessitating major redesign and often the introduction of technological advances to the design state of the art. Equal difficulty has been encountered in determining proper laboratory test procedures which insure adequate simulation of the flight environment which results from the random external pressure fluctuations. Further, the lack of a large body of vibration data has handicapped selection of general vibration specifications, particularly with the realization that excessive conservatism in the specification often requires significant advances in both design and construction techniques, with their accompanying cost penalties. On the other hand, occasional lack of sufficient attention to qualifying flight structure or equipment for its actual service dynamic environment has resulted in serious malfunctions or failures, with their attendant cost penalties.

Thus, the dynamic environment in a space vehicle has proven more difficult to specify and simulate in the test laboratory than previous aircraft environment. These difficulties have been resolved by varying methods for each of the new vehicles after consideration of the predicted or measured environment for the particular vehicle. The following sub-sections will discuss the considerations implicit in formulating suitable test specifications for the various problem areas and time-varying dynamic environments.

II. CONSIDERATIONS IN THE DESIGN OF THE TEST

The sole reason for developing vibration specifications and test requirements for components of a space vehicle is the necessity to assure a satisfactory level of reliability for the component when it is exposed to the service operational environment. The required reliability for each component can be determined directly from the design reliability goals for the entire vehicle or system. Hence, it would appear appropriate that all judgments involving acceptable test procedures, confidence levels, safety margins, environmental predictions, etc., should be made with cognizance of and reference to the vehicle's overall reliability requirements. Further, it would seem equally appropriate that the economic aspects of these judgments be viewed in the context of the total vehicle or program reliability requirement.

This latter point should not be minimized, for once the overall program reliability requirement has been determined from consideration of personnel safety, national security or prestige and economics, the procedures required to attain these requirements must be compatible with the importance of the reliability requirements. Thus, the specifications of what to test, how to test and how long to test, depend upon the level of confidence necessary to meet the overall reliability requirement. Similarly, arbitrarily increasing the severity of the test environment relative to the expected flight environment to provide a safety factor must be weighed in terms of the possible economic or performance penalties of requiring unnecessary upgrading of a vehicle's component fragility level.

Here, it must be recognized, the emergence of space vehicles has not only been characterized by more severe vibration environments than generally encountered previously, but has also been accompanied by fantastic increases in necessary component reliability to assure even marginal mission reliability and increases in the required vehicle performance. These factors combine in emphasizing the importance of adequate test programs to assure successful missions. Hence, if these trends continue, it would be expected that environmental testing will become increasingly thorough, and occupy a more prominent part of the design process.

The environmental specialist must define the test specification to provide adequate reliability. Normally, this definition involves a preliminary specification during the preliminary design stage and one or more revisions as more detailed environmental predictions, model data and, eventually, flight data become available. The design of a test specification is subject to innumerable compromises during its evolution. Not the least of these considerations is the original concept of an ideal test for a specific component intended for use in a known environment. This concept of an ideal test necessarily involves compromises in the duration of test and the number of samples to be tested to assure a stated confidence level in the test results. Secondly, the concept of an ideal test requires definition of the allowable deviation of the laboratory simulation of environment from the actual service environment.

Each of these basic compromises involves additional risk and must therefore be related to the basic reliability objective. Hence, departures from the ideal test, which may be required because of unavailability of equipment to perform the ideal test, must be justified on an engineering basis in terms of additional risk, if any. Thus, when it can be shown that a feature of the environment is unimportant in terms of failing the component, it should be unnecessary to reproduce this feature in test. However, if it cannot be shown that a given environmental feature is definitely unimportant in the failure process, its elimination by the test method involves additional risk. Generally, this additional risk can be minimized by increasing the severity of the test.

If each compromise which involves additional risk is resolved in this manner, the combined effect may add considerably to the test severity of the component. This increased requirement may, in turn, necessitate a significant upgrading of the component involving either economic or performance penalties. Whenever this occurs, it would seem appropriate to weigh the penalties of upgrading the component versus those of upgrading the test method to a point where the compromise is not necessary.

Thus, the design of a test specification involves assessment of the overall reliability requirement and the overall economic balance, as well as engineering definition of service environment and knowledge of the mechanism of component failure.

III. THE SIMPLIFIED COMPOSITE RESPONSE

The response to various stimuli was determined in Part II. When several excitations acted simultaneously, composite responses were defined. The composite response is the sum of the separate responses combined according to the rules of addition for random processes. The result was a record as long in time as the life of the vehicle.

Processing these data into one neat bundle for cumulative damage failures is visualized in the following manner.

1. To obtain segments in time where stationarity may be assumed it is necessary to divide the life into intervals containing an approximately constant level of vibration and a constant statistical distribution of the amplitudes.
2. Time may be removed from the description of the loading history by counting within each of the above blocks the peaks at each different stress level. The number of occurrences at each different level is required to define the cumulative damage done in fatigue to equipment or structure. An analogous count for other cumulative damage problems might be the number of occurrences of each different acceleration level. The number of occurrences at each different stress level may be defined for a reference station on the part and if information is preserved in the counting process of the associated frequency, mean stress, and whether a particular occurrence takes place in the first tenth, say, of the vehicle life or a later tenth, an adequate description of the loading history has been obtained.

The fatigue process is concerned with alternating stresses mainly and to a lesser degree with mean stresses. (See Section VI.) The influence of mean stress was presented in Part II as shown in Figure 182.

The information preserved in determining the number of occurrences at each stress level may be presented in another fashion as the number of occurrences at each different stress level for a given mean stress described by whatever number of mean stress levels may be appropriate to picture the mean stress life history of the part. A loading history is presented for each mean stress and is shown in Figure 183.

In the general case, response at different frequencies will represent responses in different modes. Although the stress at an appropriate reference station might be equal at two different frequencies, the stresses at other stations in the part will not be equal. The X% response at frequency f_1 and the Y% response at frequency f_2 , and so on, is preserved therefore.

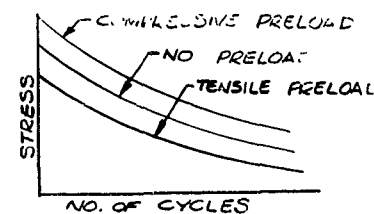
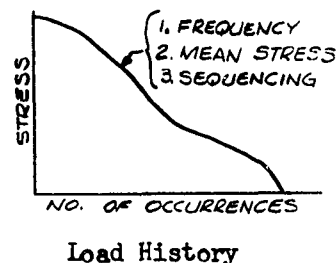


Figure 182. Effect of Preload

If, in addition, the bulk of the high stresses occur in the first tenth of the life of the vehicle, the test imposed on the part may be required to duplicate this sequencing effect.

By these means, a record in time as long as the life of the vehicle is reduced to a loading history. The loading history, in the most general case, must preserve information on frequency, mean stress and sequence. It will pay to illustrate in detail the means of transferring data from a typical random vibration trace into a load history.

Consider the cases shown in Figure 184 where an overall mean stress exists. Three cases are shown: a positive, zero and negative mean stress. Examining a random trace in detail in Figure 185, it is desired to describe the trace between points A and B as an alternating half cycle of amplitude $(A-B)/2$ and having a local mean stress of $(A+B)/2$. It is important to note that the data cannot be analyzed on the basis of its peak distribution. While a Rayleigh distribution of peaks may describe the trace very well, this distribution cannot be used as a load history on an S-N curve because the load history is a count of the alternating load in the load history, it must lie between two positive peaks of the same amplitude. The assessment of the load history by this technique was advanced by McClymonds¹ and Schelderup². The latter reference examines strain gage response data from an acoustic input to 17 structural elements for 1000 cycles each and shows the distribution of mean stress is a normal distribution while the alternating stresses were between a normal and a Rayleigh distribution. Although no definite relation between the rms stress and the normal distribution could be established, reasonable correlation was obtained by considering the rms stress equal to the mean alternating stress. The arbitrary trace analysis suggested above and shown in Figure 185 may be used for multi-mode response while the case of the single mode response appears to be satisfactorily covered by the theory.

The equivalent simplified response presented above as an integrated load history may be used to define a random trace in the time domain having the characteristics of the integrated load history. The random trace so defined would feature inter-mixing of the loads in-the-small that is, large load, small load, medium load following one another successively, and

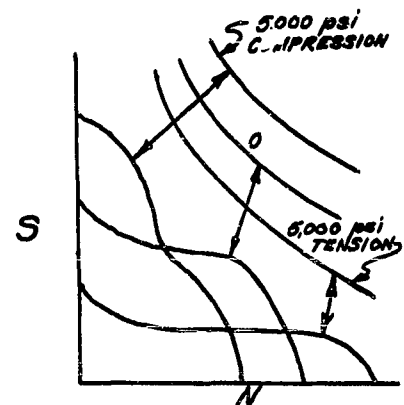


Figure 183. Load History Related to Mean Stresses.

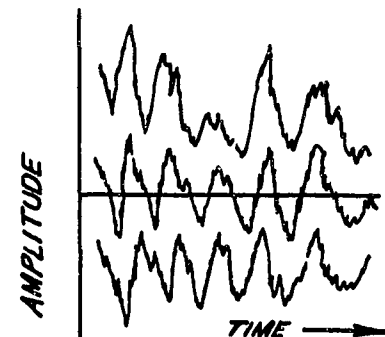


Figure 184. Overall Mean Stress.

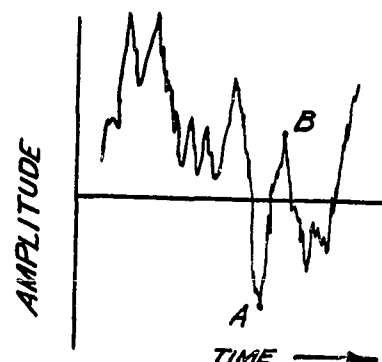


Figure 185. Alternating Stress.

would make use of the data preserved in the integrated load history:

1. mode and frequency data
2. mean stress
3. sequencing, intermixing in-the-large

This newly defined trace would differ from the original composite response record which was as long in time as the life of the vehicle in that a convenient number of discrete blocks of alternate stress and mean stress would be used, and in that the statistical distribution applicable to the original intervals of time has disappeared into the integrated load history and would be replaced by the statistical description of that integrated load history.

This reconstruction of a random trace in the time domain may not be a necessary step. The need for intermixing in-the-small will be discussed in Section V on sine-random equivalence when the present damage accumulation theory is looked at in the light of Freudenthal's work. If the need for intermixing in-the-small exists, then one method of satisfying this need will be the reconstruction of an equivalent random trace in the time domain. Other methods will be discussed in the following sections.

IV. NONLINEARITIES ASSOCIATED WITH ACCELERATED TESTING

Present practice for qualifying airplane structure and equipment consists of compliance with a group of military vibration specifications such as MIL-E-5272 which typically call for a nine hour vibration test to represent the life of military vehicles varying between 1000 and 5000 hours. These specifications contain arbitrary levels meant to approximate the damage potential of the long time environment. The maximum environment encountered in the vehicle for a significant time period is multiplied by a factor of 2 or 3 to provide the test levels. The process is arbitrary and depends on adequate feedback or monitoring to tailor the process to an acceptable reliability level. Monitoring has been carried out over a period of years and in the area of arbitrary specifications some of these are quite useful. Their main disadvantage is the inapplicability to specific items in specific locations in specific weapon systems.

The following nonlinearities will be discussed:

1. Those associated with the S-N curve
2. Nonlinear structural response
3. Nonlinear inputs
4. Nonlinear damping
5. Influence of temperature
6. Influence of frequency

An obvious nonlinearity occurs in attempting to accelerate the testing for a part whose load history lies under the endurance limit. Such a part will not fail in service but will fail in test following an increase in level. In assessing whether a load history lies below the endurance limit, it is necessary to compare a load history stress level from random response to an endurance limit obtained from similar random testing. Endurance limits from random vibration testing on parts containing stress concentrations are very low, 4000 psi rms in aluminum, for example, and do not at all compare to the endurance limit for the basic material, 15,000 psi for aluminum, for constant amplitude loading. The characteristic of the S-N curve is then that a very large number of loads approaching infinity may be applied below the endurance limit without contributing to fatigue damage. An experiment for defining the endurance limit for random loading appears on page 366, Part II.

A second nonlinearity associated with the S-N curve occurs at the yield point where damage is intensified. Good design requires that the yield stress not be reached at the location of maximum stress concentration.

In view of these nonlinearities in the S-N curve, the question arises as to what acceleration in level is acceptable? A satisfactory increase in level should not

cross the stress level defined by either of the above nonlinearities of the S-N curve. If the peak stress level at the point of maximum stress concentration is below the endurance limit, the accelerated test should stay below this limit.

Acceleration is permissible to this limit but it appears that the only advantage is in demonstrating a margin of safety. If the peak stress level at the point of maximum stress concentration is below the yield stress, acceleration is permissible to this limit provided a satisfactory damage accumulation theory is available. A discussion of the present availability of such a cumulative damage theory seemed most appropriate for the section on sine-random equivalence and is included there.

Another nonlinearity associated with accelerated testing, is nonlinear response of the test item. As the input level is increased, if the item undergoes either more or less than the expected increase in response, the test may be an unsatisfactory representation. Acoustic testing of flat panels is an example of an item which stiffens considerably under accelerated testing. If accelerated testing were undertaken with expectation of accelerated response, such accelerated response would not occur. In addition, the distribution of stresses about the rms level is altered in that all stresses above the rms level are decreased, producing less than proportionate increase of the high peaks. At high noise levels, above the order of 170 db, the nonlinear properties of air begin to affect the propagation of sound. At these high levels a sine wave becomes highly distorted after it progresses only a few wavelengths from the source. Consequently, accelerating a test by means of increasing the sound level must consider the nonlinearities present in the acoustical system and cannot assume that a 6 db increase in input to the noise transducer results in a 6 db increase in the input to the item under test. Curvature, pressure differential across a panel, and temperature differential between a panel and its supporting structure are causes of nonlinear panel responses. Membrane stress is the basic cause of the increased stiffness of flat panels. Curved panels are generally more flexible as deflection increases. Pressure differential combined with curvature would appear to stiffen the panel when acting in one direction and make it more flexible in the other. The amount of nonlinearity in a flat panel increases with a decrease in thickness. As the panel cycles once, the membrane stress cycles twice, always in tension. Difficulties in measuring the natural frequency of thin panels are associated with this nonlinear feature. Nonlinear influence from the damping should also be expected. In commenting on a paper by Galt Booth³, D. C. Kennard of WADD stated, "The resonant amplification factor "Q" in typical dynamical systems with constant acceleration input tends to increase with resonant frequency and is not constant. Also, increasing the acceleration input for a resonant frequency causes a decrease in Q. Generally speaking, there is a greater decrease in Q for highly damped systems for corresponding changes in applied acceleration."

One of the hypotheses for explaining the mechanism of fatigue damage is unbonding of the atoms along a slip plane advanced by Shanley⁴. The slip planes are merely the planes along which the crystal shows a propensity to slip, the atoms ordinarily releasing their bonds across this plane, but rebonding as neighboring unbonded atoms pass by. The crack forms at the edges of the crystal where a block of material has moved past a mating block on the other side of the slip plane. Repeated

reversals of the slip motion propagate the crack by failure of the atoms to rebond. Associated with the internal work is an appreciable release of heat but heat which is probably concentrated at the slip plane and at the edge of the unbonded region. Heat at the edges of the advancing crack may play a part in propagating the damage.

The influence of frequency of load application is discussed by N. Stephenson⁵. "Little effect of frequency in the range 16-170 cps exists on the endurance limit at room temperature provided there is negligible heating through hysteresis, corrosion is absent and the material is not in the creep range. Increase in frequency over broader frequency ranges increases the endurance but only at high stresses. Microscopic evidence of deformation is less apparent with increase in frequency. Damping capacity decreases and elastic modulus increases with increase in frequency. These changes are consistent with the decrease in plastic deformation with increase in frequency. The striations which formed at the higher frequencies often showed a granular surface film with a slightly stained appearance of the surface. This suggested that a localized increase in temperature had occurred. For an aluminum alloy at 200°C there was evidence of a small speed effect but fatigue failure depended mainly on the number of cycles applied rather than on time. The frequency of load application is important for the material of high hysteresis."

The above results which are adequately documented in the reference allow acceleration in frequency by either accounting for the increased fatigue strength or accepting the small error encountered at low frequency. Acceleration in frequency is possible, then, for parts operating well below the fundamental mode or modes where the mode shape and load distribution do not change.

In summary, the nonlinearities associated with accelerated testing are brought out. The nonlinearities associated with the S-N curve require consideration of one necessary new approach to qualifying parts. If certification can be provided that the stress level at the point of maximum stress concentration is less than the endurance limit, then that part should be considered qualified. The certification could be through analytical determination of the response of the part where methods are established and acceptable or through a test to determine the stress level in a simulated environment. This procedure is followed to some degree at present in that only equipment items expected to be critical are qualified by test and only a small number of structural items are tested.

V. SINE-RANDOM EQUIVALENCE

The simplified composite process was presented as an integrated load history which was supplemented by information on the mean stress, sequencing, and frequency or mode shape for cumulative damage failures. A sine equivalent to this random history might be formulated by dividing the load history into say 10 parts along the stress axis and 10 equal parts along the number of occurrences axis, 100 blocks in total. A sinusoidal equivalent for each of these blocks may now be constructed, and if these sinusoids are applied within the limitations of the requirements of the supplementary information regarding mean stress, sequencing, and frequency or mode shape, a satisfactory duplication of the response is obtained. In the general case, where several mode shapes and several mean stresses are involved, the number of blocks is expanded to accommodate these features. In the case of the multimode response, a complex input which excites the several modes simultaneously, could be considered. This definition of equivalence is felt to be a rigorous definition of sine-random equivalence for cumulative damage failures.

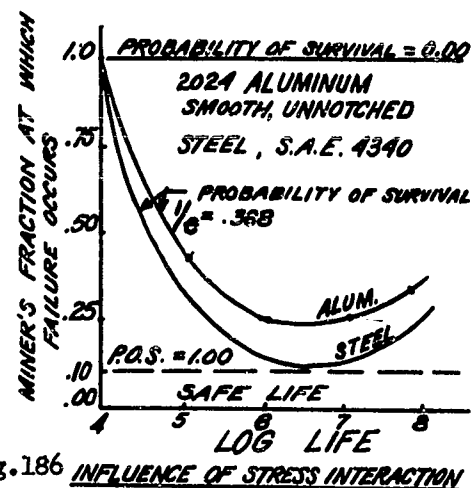
No acceleration in load level was considered in the above equivalence for the following reasons:

1. Nonlinearities are often present.
2. No cumulative damage theory exists for random vibration at present.
3. Effect of intermixing is likely to be changed.

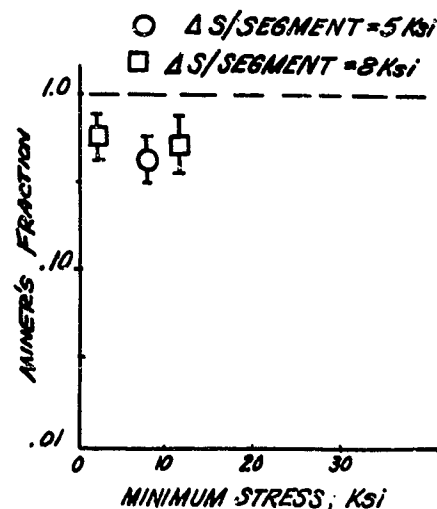
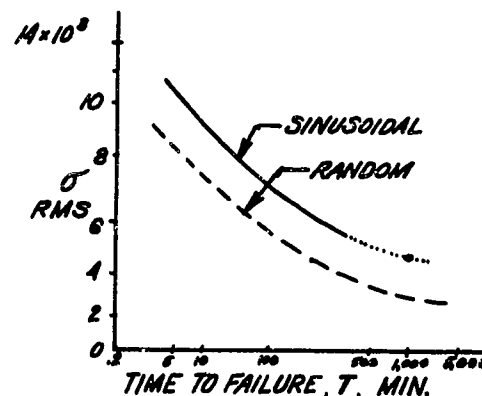
To understand these latter two points it is necessary to have an understanding of Freudenthal's work on stress interaction. He shows that the intermixing of the load levels of successive peaks has a significant influence on the damage history. With the degree of intermixing used in Freudenthal's experiments, which were tape controlled, so as to make the shortest block of the applied loads at least as long as 12 cycles, Miner's fraction at failure is as low as .2 for aluminum and .1 for steel, as shown in Figure B6. However, with random loading, the degree of intermixing may be significantly greater than the intermixing in Freudenthal's experiments. The question must be asked whether Miner's fraction at failure may not be significantly less in some cases than is indicated by Freudenthal's work with the greater intermixing appropriate to random response. This deviation from the unity constant in Miner's rule is a concise presentation of the damage done by intermixing. Therefore, the rigorous definition of sine-random equivalence must be amended with a fourth supplementary description defining the degree of intermixing. Whatever degree of intermixing in-the-small exists in the real environment, at least this much must be used in the test.

The mechanism of the damage done by the intermixing, Shanley suggests, can be explained by dislocation theory. Under constant stress amplitudes the density of the free dislocations tends to decrease because some dislocations are pinned. When intermittent high stresses are applied some of the pinned dislocations are freed and more are generated, increasing the cyclic plastic strain and reducing the life.

NASA has carried out extensive work in this problem area which is reported in References 6-12. (Lassiter and Hess⁶; Hess, Fralich and Hubbard⁷; Hess, Herr and Mayers⁸; Lip and Corten⁹; Hardrath, Utley and Guthrie¹⁰; Hess, Lassiter and Hubbard¹¹; R. W. Fralich¹². Similar work is reported by Getline¹³. The work consists of acoustic fatigue tests on panels, and variable amplitude loading tests of cantilever beams. Several interesting plots from the NASA reference are shown in Figures 187, 188 and 189. Comparisons with the Miles Theory and Miner's rule show general agreement at low stress levels and conservative at high stress levels.



A number of investigators, Freudenthal, Corten and Shanley, agree that damage is propagated at stresses below the endurance limit obtained by constant amplitude testing. It is not apparent that this effect has been accounted for in the NASA calculation as a straightforward application of Miles theory does not account for this damage nor for that done by intermixing. The NASA work includes comparisons between experiment and theory, but only for cases where stress concentrations are present. It is likely, therefore, that the agreement presented in References 1, 2 and 11 is an agreement based on the cancellation of major variables not accounted for: the damaging effect of intermixing versus the advantage of omitting the lowering of the endurance limit and a second advantage due to a favorable effect from the stress concentration. Shanley has commented on this point: "It has been found that notched specimens sometimes have a higher life under random loading than that predicted by the cumulative damage theory. This is undoubtedly caused by the building up of favorable residual stresses in the critical regions, thereby reducing the cyclic plastic strain. For design purposes, such effects should generally be ignored, because of the possibility that a particular structure might experience a less favorable loading history." The damaging effect of the intermixing probably contains two factors: that due to the lowering of the endurance limit and that due to the production of more dislocations. The favorable influence of stress concentration has not been measured, al-



though the data indicates that this influence is of similar magnitude to the influence of intermixing.

Acoustic fatigue tests which integrate the influence of a loading spectrum over a period of time cannot be used to work backwards to define the influence of a single variable such as the random endurance limit or the damage threshold in the presence of intermixed loads. A suggestion as to how the random endurance limit might be measured was made on page 366, Part II. A cumulative damage estimate cannot be made if the random endurance limit is not defined. As a loading spectrum moves to higher stresses the influence of the stress concentration will certainly vary. Freudenthal's work on stress interaction adequately covers the movement of the loading spectrum to higher stresses for smooth specimens.

For all these reasons it was stated that there is not a satisfactory damage accumulation theory available for resonant response of structure. Acceleration in test level cannot proceed without this guide in the general case. In a particular problem, for which a correlation has been established for accelerated test levels, and in which the proposed test specimen is like those used in establishing the correlation; alike in 1) same degree of intermixing 2) same kind, number and intensity of stress concentration 3) same loading spectrums 4) same material and 5) with similar nonlinearities; accelerated testing may proceed on firm ground.

Acceleration in Time

One of the nonlinearities discussed in Section IV which did not offer a serious interference was that of frequency. Therefore the speeding up of the application of a loading spectrum may be used for the particular case when the mode shapes and the load distribution are independent of frequency. This occurs when the loading frequency band in the real environment is well below the first mode or resonance. Here, acceleration in time is acceptable for either the application of the random load history or its sine equivalent.

Another possible method of time acceleration is the use of a structure model for testing, obtaining a time acceleration inversely proportional to the scale factor. In a small number of cases the modelling technique may provide a solution to the test design.

Equivalence for Two Particular Response Patterns

There are two particular response patterns for which sinusoidal equivalents may be easily specified. One case consists of damage localized to one particular strain level, as shown in Figure 189. A sinusoid at this same amplitude may be substituted with confidence. However, supplementary information about the load history regarding mean stress and frequency would be used in the most general case. This simplification will apply to any high cycle case, since the relation of the S-N

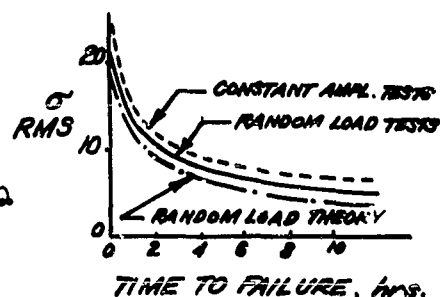


Figure 189. Typical S-N Curves.

curve to the load history must be approximately as shown. Also, the damaging effect of interaction appears to be negligible in this case.

A second case consists of a part which has a known response to a random input concentrated at two or three resonant frequencies, known in the sense that calculations or predictions had been made at an acceptable level of accuracy. Rather than simulate the actual random input, it is only necessary to simulate the resulting random responses, each of which is random in amplitude and phase but essentially constant in frequency. A number of references, Getline, Hall-14 and indirectly work done by Shanley and Lazan-15 indicate that this equivalence may be based on work equivalence. Expressing an equivalent sinusoid for each mode allows the testing to proceed either by simulating each mode separately or combined. A tape controlled electronic power supply would allow three modes to be excited simultaneously. A significant reduction in power required is an advantage of this suggestion. Alternatively, the extra power available could be used to obtain greater response.

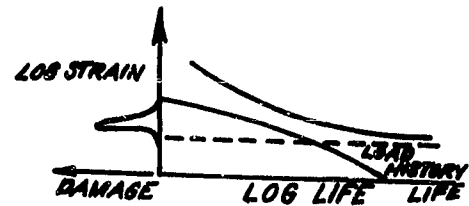


Figure 190. Cumulative Damage.

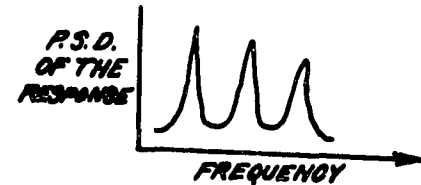


Figure 191. Response Spectrum.

Work as a Basis for Equivalence

Consideration should be given to Lazan's presentation of the variation of the internal material damping as the stress level varies, Figure 192. At a stress level called the cyclic stress sensitivity limit, the damping increases rapidly. Section VI, Part II study showed the correlation between the plastic strain and the fatigue life. The plastic strain is proportional to the width of the hysteresis loop, which in turn is a measure of both the internal work and the damping, Figure 193.

These points are indirectly tied to other of Lazan's conclusions which are of interest:

1. A typical engineering material under a uniform stress distribution (tension and compression) at its endurance stress level at 60 cps can absorb and dissipate as much as 1 HP/cu.in.
2. Damping is dependent on the prior stress history at stress levels $> \sigma_L$. As the damage progresses the damping increases.
3. In choosing materials for high resonant fatigue strength, comparisons should be made on the basis of a) damping at a given stress, b) stress for equal energy absorption and c) the proximity of this stress to the fatigue strength.

D
LOG
SPEC.
DAMPING
ENERGY
IN-LB/IN³/CYC.

DAMPING PROPERTIES OF A VARIETY OF ENGR. MATLS.

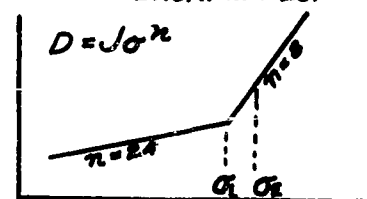


Figure 192. LOG STRESS

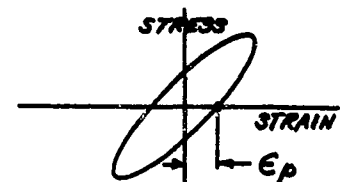


Figure 193. Hysteresis Loop.

Because of the logarithmic nature of the variation of the damping energy with stress level, the bulk of the work done on the material is work done at stresses near to or above the endurance limit and therefore the work done becomes an approximate measure of the damage.

Suggestions by Getline and Hall that sine-random equivalence be based on equivalent work for particular cases of their interest are shown here to be fundamentally sound. It has the disadvantage of failure to include intermixing and the assumption of linear damping is made, which Lasan's work contradicts. Hall attempts to find a factor between experiment and theory which accounts for the many unaccounted-for variables. It should be recognized that no such constant generally exists because of the many nonlinearities in the problem.

Why Do Random Vibration Testing

Random vibration testing is used because it is the most accurate simulation possible of a random environment. Random vibration causes simultaneous resonance throughout a dynamical system and this will often produce failure modes not present when only single resonances are excited. Simultaneous resonance of two parts which are interconnected by a third part can only be made to fail in certain cases by random excitation. Collision of two parts of a flexible system may be created by random excitation. Bingham¹⁶ states, "Failures occurring in qualified items (qualified to applicable military specification) during acoustic fatigue tests to certify hardware for major Air Force weapon systems were occasionally caused by excessive response of sensitive items but more often were caused by fasteners being shaken loose. Broad band random excitation at high frequency appears to be a more efficient means of loosening screws than sinusoidal excitation." But the major reason for the need for random vibration is stress interaction or intermixing of the loads.

The above statements are not meant to be an endorsement of random vibration testing and/or of random facilities planning and purchases. A clear statement of the problem and the nature of the correct questions to be asked and the means of obtaining the answers was attempted in Section II. Not only is random vibration testing expensive from the standpoint of facilities, but also from set-up time, fixture requirements, difficulty in equalizing the input for flatness and other operational complexities.

The question arises as to whether a preliminary study test may not be useful in some cases. Random vibration would be imposed without extensive set up to make comparative sine-random response measurements and to evaluate the possibility of modal interaction. One random vibration facility could accomplish many more tests in this way and the power requirements could be compromised. The ability to inspect for modal interference will certainly depend on the complexity of the part. The more complex the part the more necessary it is to use random vibration testing or one of the equivalences discussed below. Many presently written specifications are calling for three types of vibration input: random, sinusoidal resonant dwell, and sinusoidal sweep testing.

The search for vibration damage above 500 should not be made automatically but should depend on the characteristic of the part. Electron tubes are most sensitive in the band 2000-3000 . All equipment for the Snark missile was qualified below 600 . After the appearance of guidance system reliability problems an extended vibration environmental study was made to determine the degree of damage in the band 600-1000 . The work is reported by Mustain-17. Twenty packages of equipment likely to be the most sensitive in this frequency band were tested including a random acoustic input with only one failure resulting, it being of the type where simultaneous resonance was required. Cook-18 has further comments of interest on this point. The power requirement for random facilities are reduced whenever the frequency band of interest is reduced.

Studies Presently Completed

There have been a number of studies completed in the equivalence area. A brief review follows:

Booth suggests a sweep random test wherein a wide band low acceleration density is replaced with an intense narrow band random input. It is equivalent when the magnitude and sweep rate characteristics are chosen so the number of stress reversals in any incremental stress interval are the same. It is necessary to increase the grms with increased frequency for this test and the necessary development for making this increase automatically is shown in the paper. Figure shows a cost comparison made at MB Mfg. Co. In commenting on the technique, D. C. Kennard of WADD asks about the effect of neglecting simultaneous resonance, about the necessity of defining Q properly and allowing it to vary with frequency, and points out its nonlinearity with amplitude.

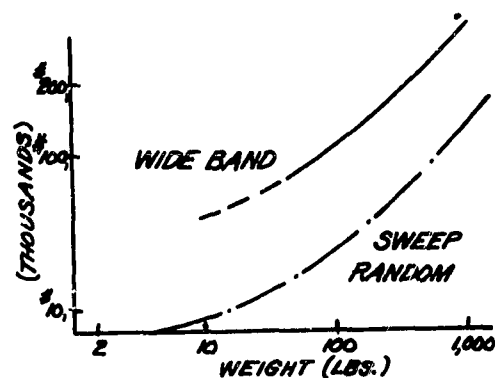


Figure 194. Cost Comparison

Spence-19 shows an equivalence based on experimental tests of four electronic packages. He applies the existing equivalence relationships for one degree freedom systems to the multi-mode resonant packages by assuming decoupled modes. For each package, vibration response measurements were made at various internal members which act to provide the structural vibration input to sensitive component parts. The data from the measurements was processed using single resonance theory resulting in showing the existence of an rms sinusoidal-random relationship for each package within a certain scatter.

Trotter-20 examines experimentally two methods for examining sinusoidal-random equivalence from References 21 and 22. Cantilever specimens, some with strong response in the fundamental mode only, some with strong response in the first two modes, and some with and without stress concentrations were tested to determine comparative fatigue failures. Complex electronic packages were tested to determine malfunction thresholds. The experimental evidence showed the two methods are unconservative, had wide scatter, and if corrections were made to render them conservative, many items would experience excessively severe tests.

Galef⁻²³ endorses the narrow band random test suggested in References 24, 25 and 26 and suggests a two-level modulated sinusoid to duplicate the Rayleigh peak distribution.

Both the above authors, References 20 and 23, express the viewpoint that a random vibration test has been compromised to a large extent by a number of practical difficulties so that it often is not a valid test. It is an envelope test, an envelope which has been smoothed, and which is difficult to duplicate by equalization. A very rigid shaker armature and fixture are required, but these cannot duplicate structural impedances at all frequencies. The complex three dimensional motion is not being simulated even in one plane.

Bingman⁻¹⁶ recommends more attention to the problem of acoustic fatigue. His paper was prompted by an indicated lack of awareness of the widespread extent and diversity of damage which occurs under noise. Acoustic fatigue is a serious problem of detail design in secondary structure and in subsystem components. Acoustic fatigue may impose an excessive maintenance burden in weapon system hardware.

The Air Force program to control acoustic fatigue is discussed in this same reference and has a three-fold objective: 1) control of the average maintenance man-hours required to repair acoustic fatigue damage, 2) determination of how and where to inspect and, 3) use of fail-safe design to prevent safety of flight problems. Past experience has shown that a final proof test of all design details is required. When the noise loading is significant over much of the entire aircraft, the final proof test is best accomplished utilizing the complete aircraft. Typical tests have consisted of operating the power plant on the ground under the most severe conditions of noise impingement for a sufficient time to indicate reasonable service life. Cycles composed of 10-30 minutes of maximum power followed by inspection have been used. An hour of ground time at maximum power may produce damage that is produced by 200-600 hours of normal service operation. It was pointed out that the rms stress in certain elements which fail later in the test may be below the endurance limit of the material and therefore, this type test cannot be sufficiently long to produce enough peak stresses to reach the knee of the S-N curve of all the structural elements. Broken clips and supporting brackets, wires, bonding cables or straps, coaxial connectors, broken hydraulic lines, failure of heat shields and insulation of air ducts, failures in bearings and rod end bearings and in fire detection systems made up the more common failures in these proof tests. Rib failures and failures in more minor structural elements such as stiffeners, gussets, shear ties and fasteners have always represented a large percentage of the failures. Stress concentrations appear to be even more critical under high frequency complex modes of response. The nominal stress level associated with acoustic fatigue failures is generally not sufficient to cause any local yielding. Fabrication and assembly is, therefore, more critical for secondary structure. The nature of the majority of failures uncovered in proof tests was such that prediction of the stresses would be nearly impossible. A lack of application of good fatigue design principles is frequently indicated. Many of the study designs and fabrication practices have been found to be unacceptable. The following design practices have been found necessary: 1) design for increased stiffness, 2) to minimize stress concentrations, 3) to increase damping and,

4) to distribute loads evenly at joints. The development program should be applied to all subsystems and not limited to structure.

The bulk of the reliability and qualification testing in the past has been concerned with equipment and to only a lesser degree with structure. Full weight must be given to qualification of all structure.

Any one of these methods has its shortcomings when compared to the requirements which are necessary to avoid interference from the nonlinearities and the necessity to be compatible with the significant parameters associated with fatigue. In line with the discussion of Section II on the statement of the problem, it is felt that the proper overall question is, "What is the cheapest way to provide a targetted level of reliability?" It may be through random vibration testing, sinusoidal testing or through new design innovations such as miniaturizing, transistorizing, potting of components, or the analogous structural advances which basically design around the problem.

VI. MALFUNCTION AND DAMAGE TO EQUIPMENT

Equipment components used in space vehicles range from relatively heavy and rugged components, such as turbopumps, plumbing valves, motors, generators and transformers to very small and fragile items such as electron tube elements, relays, optical lenses, pressure sensors, magnetic pickups, etc. The latter category are generally sensitive items having fine tolerances and requiring fine adjustments which must not be excessively disturbed. Shocks and vibration transmitted from the source through the main and secondary structure and through the equipment mounts, and the direct impingement of acoustic pressures can cause considerable vibration response of these equipment components and their internal mechanisms, thus destroying fine tolerances and adjustments. Shock and vibration environments therefore represent damage and malfunction potentials which may permanently or temporarily interrupt the normal operating and function of such equipment components.

The probability of occurrence of equipment damage or malfunction in a space vehicle is quite high because of the very large number of relatively fragile items required for instrumentation, data recording, guidance, etc. The overall reliability of the vehicle and its mission is highly dependent upon the proper functioning of each such component during at least a portion of the mission, so that acceptable overall reliability can be attained only by insuring that the reliability of each piece of equipment be as high as possible.

Equipment failures to shock and vibration environments can be broadly divided into two classes: temporary and permanent failures. Temporary failures, often called malfunctions, are characterized by out-of-tolerance performance of equipment when the shock and vibration environments are applied and by normal performance when these environments are removed. Permanent failures are characterized by breakage resulting from high amplitude overstressing associated with shocks, and cumulative damage leading to fatigue type failures associated with vibration. These two classes are not necessarily distinct since temporary failures are often accompanied by "wear" and gradual deterioration of the equipment which may promote permanent type failures under continued action of the environment. This type of "aging" of the components will often lead to conditions which could not be classed as failures, but must be classed as below normal functioning.

Before attempting to analyze the problem of equipment damage and malfunction, it is necessary to understand the various mechanisms which lead to damage. These mechanisms are easily understood from the types of failures that occur, so that the following list of examples of malfunction-and damage-type failures should well define the problem area.

EQUIPMENT FAILURES

1. Oscillations of electronic tube elements such as filaments, grids, cathodes and plates, is such that the spacing between these elements fluctuates. The relative positions of these elements are often critical and fluctuations of this nature may temporarily change the tube characteristics, increase electrical background noise in the tube such as that associated with microphonics, and where arcing or shorting of these elements occurs, temporary paralysis of the electronic circuitry can result. Conventional tube elements are often long and slender and are generally cantilevered from the base with natural frequencies ranging from 500 cps to 8000 cps. Internal damping is very low, producing high Q's resulting in high resonant responses. The mica spacers between these elements can become cracked and permanent distortion and direct shorting of the elements is a common cause of permanent tube failure. Other tube damages are open circuiting, cracked glass envelopes due to impact with neighboring components, cracked plastic bases, gassiness, pin breakage, vibration of the tube from the socket. When conventional glass envelope tubes are used, these failures are common, making the electron tube very vulnerable to serious damage, and often the most vulnerable of all components, Reference 1.
2. Acoustical excitation produces nearly uniform compression of small components: a capacitor may act as a microphone creating electrical noise in the circuit with little or no permanent damage to the capacitor; a large chassis may be excited acoustically and cause vibration of attached elements.
3. Relay chatter is a frequent type of failure in which the contacts of an open relay oscillate and accidentally close an open circuit or open a closed circuit. Oscillation of the contacts of a closed relay changes the normal pressure between the contacts so that the contact area fluctuates, changing the electrical resistance of the contact and the current flowing through the relay. Although these represent temporary malfunctions, arcing and corroding do occur leading to serious changes in circuit parameters and may eventually freeze the relay closed or permanently open. Mechanical warping and breaking may also occur, for example, in the brushes of a motor generator.
4. Resistors and capacitors are often located adjacent to a large flat surface such as a chassis and when vibration excited by the flat surface will experience numerous impacts with the surface which often leads to breakages - especially of carbon resistors.
5. Wires connected to terminal posts from resistors, tubes, capacitors and transformers experience stretching due to chassis flexures; high bending moments at the terminal posts result from this stretch and from the high amplitudes of oscillations that can be attained by these low natural frequency wires. When soft wire is used, such as hook-up wire, the wire is easily deformed so that a "flopping" action occurs along the wire between tie down points. Cumulative damage of this type leads to fatigue in a relatively few number of cycles. Wire breakage is considered to be one of the most common causes of failure in electronic equipment.

6. Vibrating wires may rub against a neighboring component so that the insulation on the wires wears away producing short circuits. This is also a common failure in multiconductor cables.
7. About 10% of the failures of electronic equipment under shock and vibration environments can be attributed to broken lock washers, loosened screws and nuts, loosening of threaded fasteners, and component mounting stud failures (Reference 1).
8. Change in alignment of optical systems.
9. Flexing of coaxial cables can produce considerable "noise" voltages in the circuit.
10. Transformers are heavy, rigid type components which experience little internal damage from vibration, but which have been known to inflict considerable breakage of the other components by breaking loose from the mountings which are sometimes made with undersized bolts and understrength mounting studs.
11. Chassis and mounting bracket fatigue failures can cause considerable malfunctioning and permanent failure of mounted components.
12. Under high acceleration peaks from shocks and random vibration, equipment components mounts may bottom and inject a shock pulse to the mounted equipment.
13. Galling of bearings and bearing races under high dynamic loading.
14. It should be noted that many good design and installation techniques have been developed recently for virtually eliminating certain types of equipment failure and greatly reducing the probability of occurrence of others. It is beyond the scope of this section to discuss these techniques, Reference 1, but the following are examples which will indicate the present approach to the problem:
 - (a) Replacement of conventional glass (and metal) envelope electronic tubes with transistors which experience very little damage and malfunction under shock and vibration environments.
 - (b) Cementing or clamping small items such as resistors, capacitors, transistors to circuit boards and chassis.
 - (c) Miniaturization of large blocks of electronic components to minimize the weight and inertia loads on individual components (i.e., increasing the natural frequencies and lowering the stress) and to obtain higher density (volume saving) packages.

- (d) Careful tie down of all wires to rigid subassemblies along the entire length of the wire.
- (e) Potting of entire electronic packages.
- (f) Mounting all components such that the strongest axis of the component is oriented parallel to the direction of greatest vibration and shock excitation.

The ultimate goal of any engineering discussion of equipment failures should be the establishment of either improved equipment design techniques or better laboratory methods for qualification testing. The present discussion is primarily concerned with testing and the problems associated with providing for realistic but practical criteria for assessing the damage potential of the in-service shock and vibration environment to on-board equipment components. Practical criteria are often dependent upon defining a simplified response which is equivalent to the actual response so that unnecessary complications may be eliminated from laboratory testing and so that the time duration of these tests may be shortened.

In keeping with the basic purpose of laboratory tests, each and every simplified response must duplicate the mode or modes of failure of the equipment. The above list of examples shows that several different types of failures can occur, with the possibility that different equivalent simplified responses are required for each different type of failure. Permanent types of failures associated with cumulative damage can be classified as fatigue failures. A discussion of the concepts of fatigue, cumulative damage, equivalent response for fatigue and appropriate methods for testing are presented in Sections III, IV, V. Cumulative damage is dependent upon the cyclical stressing of a component over a large number of cycles. For temporary equipment malfunctions, the essential parameter is deflection response. Displacements of equipment components and their elements alters the relative positions of these items with respect to neighboring components and elements producing electrical noise and arcing. For sufficiently large relative displacements, impacts may result causing either electrical shorts and the interruption of circuitry functions or shocks which in turn produce other malfunctions.

It should be noted that the fatigue of elements within electronic equipment components will have some what different characteristics than the fatigue of structural items because of the wide variety of materials used in equipment design, such as plastics, soft metal wires, brittle mica, carbon ceramics, etc.

On assessing the overall importance of equipment malfunctions relative to all equipment failures, it is difficult to assign a single number to the percentage of all failures due to malfunction. A review of the literature indicates that for different test programs involving various types of components, malfunctions

have accounted for from 5% to 50% of all equipment failures under shock and vibration environments. An exact figure need not be established here as this is of interest mainly to the estimation of statistical reliability of a space vehicle. The fact that certain programs have shown a 50% malfunction figure indicates that this problem area cannot be overlooked.

Unfortunately, only a limited amount of actual malfunction test data is available and therefore a detailed evaluation of this area is not presently possible. Specifically, it is difficult to evaluate present testing specifications and establish testing criteria which are both realistic and practical. Test programs discussed in the literature give no detailed information concerning the particular types of equipment tested, locations of accelerometers, and the actual environment that is to be duplicated in the laboratory. The present state of the art on equipment malfunction is in its infancy.

As with many engineering problems of this type in which the hardware involved is extremely complex and input excitations are complex random time functions, the approach consists of analyzing simplified, highly idealized dynamic models. These simple models, which generally consist of one or two degree of freedom linear oscillators, are used to provide a basic understanding of the phenomena involved, and the response solutions of these simple systems are used to provide engineering direction and order of magnitude results and establish better test procedures and indicate the significant parameters which should possibly be measured. Investigations in Reference 7, indicate that the responses of complex vehicle structures to random inputs may often be adequately approximated by the responses of single degree of freedom systems so that efforts to simplify the actual dynamic systems to ideal models may be very worthwhile. The dynamical complexities inherent in equipment, especially electronic components, probably stem from the fact that there exists a multitude of individual one and two degree of freedom systems each having different natural frequencies and damping characteristics, different directions of response (including rectilinear and rotation motions) and different transmission paths through which the excitational energy has been fed.

It is felt that cases do exist where coupled multimode response (say greater than two degrees of freedom) is significant, but these are very likely to be exceptional cases and not representative of the general type of response. Laboratory testing criteria are often rather arbitrary because of a lack of good data. The errors introduced by neglecting this type of multimode response may very well fall within the larger error introduced by present testing techniques.

Another approach to this problem is to determine what degree of reliability is required for an equipment package which will be compatible with the overall reliability of the vehicle and consistent with the cost of obtaining this reliability. It may be found that it is desirable in laboratory testing to reach for such multimode interactions.

The actual vibratory inputs to equipment components are generally complex random accelerations at the equipment mounting points and, where direct acoustic excitation is significant, the inputs consist of random pressure fluctuations over the surface of the components. The statistical characteristics of the excitation, such as spectrum level and shape, amplitude probability distribution, and degree of non-stationarity are usually unknown and must be estimated. Also the time duration and principal direction of input excitation are often not known. With a knowledge of a flight phase and the locations of the equipment within the vehicle, these estimations can be made by methods discussed in References 7 and 8.

The major sources of vibrational energy are the external acoustic field produced by the rocket exhaust, external hydrodynamic pressure fluctuations over the surface of the vehicle and direct mechanical excitation by thrust variations within the rocket engine. The vibration energy contained in these sources is broad band, i.e. contains a significant amount of energy at all frequencies.

For an equipment component located near the source, the excitation will be fairly broad band. Such is the case for equipment mounted to the external shell of the vehicle or in the aft section of the vehicle in the vicinity of the engine. When the vibratory energy is transmitted mechanically through various structural load paths, the filtering and transmission loss effects of the structure and equipment mounts narrows and reshapes the excitation spectrum. The amplitudes of the excitation are still distributed randomly after filtering, but if the frequency band has been sufficiently narrowed, the excitation will be nearly constant with a slowly varying amplitude envelope. Arguments for the use of sinusoidal laboratory testing of equipment are in part based on this filtering of the excitation by the structure. The actual effect of this filtering is not as pronounced as might be expected, however, when or where vibratory energy is transmitted to a point through multiple structural paths each having different filtering effects. The composite excitation at any point on the structure will then be wider band than that of its components.

Three simple dynamical models are discussed below which are considered to represent a wide variety of equipment elements that are likely to malfunction under shock and vibration environments. These systems are fully discussed in References 6 and 10 for random vibration excitation, and since they involve only single degree of freedom concepts (adequately discussed in References 7 and 9.) only the results of these analyses are presented here.

Figure 195a shows a single degree of freedom system B attached to a base A of infinite impedance and in close proximity to a third element C. The condition of an infinite impedance base means simply that the motion of the base is unaffected by the dynamic response of the oscillator. It is assumed that the surfaces A and C are structurally connected. Oscillations of the surfaces A and C are assumed to be identical with the same frequency content, same amplitudes at each

frequency and zero relative phasing in the frequency range from 0 to f_1 cps. This rigid body type oscillation of A and C may be due for example to the response of the space vehicle in its lower modes of vibration. The oscillations in the frequency range from f_1 to f_2 of both surfaces A and C are assumed to have the same frequency components with different, but known, amplitudes and phasing at each frequency in this range. Lastly it is assumed that in the frequency range above f_2 , the two surfaces have the same frequency content with different amplitudes at each frequency and arbitrary (unknown) phasing between the two at each frequency. This system, as defined, represents a very realistic condition insofar as the interdependencies of the oscillations of neighboring elements in the low, medium and high frequency range. The problem consists of first determining the response of the simple oscillator to its foundation excitation at the base and then determining the root mean square fluctuation of the spacing, S, between the oscillator and the adjacent surface.

For the latter problem it may be more desirable however to determine the probability that impact will occur at a given design and to determine the mean time between collisions. Further statistical analyses would be required for the system just discussed if this type of information is desired. Two simpler dynamic systems were analyzed by Himmelblau and Keer, Reference 10, which are special cases of the above system except that the emphasis was placed on solving the impact problem. The results of these analyses are presented below.

Figure 195b shows a simple one degree of freedom linear system having a mass m , spring constant k , viscous (linear) damper c , and attached to an infinite impedance base. Assume that the base experiences a random oscillation, characterized by a Gaussian white noise acceleration spectral density $F(f)$ [i.e. $F(f) = \text{constant}$ (g^2/cps^3), for all $0 < f < \infty$]. The rms relative displacement, $(x-y)_r$, between the mass m and the base is then given by the eq., Reference 10,

$$(x-y)_r = \frac{1}{\sqrt{32\pi^3}} \sqrt{\frac{QF}{f_0^3}} = 12.25 \sqrt{\frac{QF}{f_0^3}}$$

where

$$Q = \frac{1}{2} \frac{c_{cr}}{c} = \text{resonant amplification factor}$$

c = viscous damping constant (linear damping)

c_{cr} = critical damping constant

$f_0 = (K/M)^{\frac{1}{2}} = \text{system natural frequency, cps.}$

F = applied accelerations spectral density, g^2/cps^3 (= constant from $f = 0$ to $f = \infty$)

Although the above equation was derived on the basis of a constant acceleration spectral density from 0 to ∞ cps., the above rms. response equation is sufficiently accurate if all frequencies above $(4 f_0)$ are neglected. Integration of the Gaussian probability density function yields an equation for the probability that

the relative amplitude will exceed a given displacement in either the positive or negative direction. This probability distribution is given by the equation:

$$P\{|x - y| > a\} = 1 - \frac{1}{\sqrt{2\pi}} \int_{-a/(X-Y)_r}^{a/(X-Y)_r} e^{-\alpha^2/2} \cdot d\alpha$$

$(X-Y)_r$ = rms displacement response

Table XII lists this probability for various ratios $\frac{a}{(X-Y)_r}$.

This equation is useful in investigating such equipment vibration problems as:

- (a) Bottoming of equipment mounts during high acceleration peaks.
- (b) Impact of electron tubes against chasses and equipment covers when small clearances are available.
- (c) Shorting flexible tube elements with more rigid neighboring tube elements.
- (d) Relay chatter for relays having a flexible or moving contact point.
- (e) Change of electronic parameters due to an oscillating elements change of position with a chassis.

Many other examples could be given which may be adequately analyzed by this simple model. The complex geometry occurring in equipment items often disguises the actual simplicity with which the system may be analyzed. Such interpretations must be left to the ingenuity of the vibration engineer as a complete discussion of the many possible geometries that fall in this category cannot be presented here.

One very simple schematic is shown in Figure 195c, however, which should be representative of many types of geometries occurring in practice.

The specific problem of interest in Figure 195c is that of impact of the internal member against a relatively rigid casing. From Reference 10 the average number of impacts in time, t is

$$N = 2f_0 (\Delta t) \exp - \left[\frac{a^2}{2(X-Y)_r^2} \right]$$

Numerical values for the exponential appear in Table XII. The mean time between consecutive impacts is given by the equation for $N = 1$.

$$\Delta t = \frac{1}{2f_0} \exp \left[+ \frac{a^2}{2(X-Y)_r^2} \right]$$

The amplitude response of the mass is roughly that shown in Figure 196.

An assumption made in Reference 10 for the derivation of the above expression is that the Gaussian distribution of the response amplitudes remains unchanged by the impact or "clipping" of the response at $(X-Y)_r = a$. The above equations, which are approximate for this case, are considered by Himelblau, Reference 10, to be sufficiently accurate to give order of magnitude results.

This assumption, and the shape of the response time history shown in Figure 196 imply, however, that impacts, when they occur, are generally grouped into a set of successive impacts nearly $1/f_0$ in time apart with a relatively long time delay between groups. It is very likely that the response changes considerably after each impact, since energy is lost in the collision, so that the above grouping does not occur.

The mean time between collisions corresponds to a 50% probability of occurrence a collision during the time, Δt . H. Himelblau (Northrop Corporation) and J.S. Bendat (Ramo-Wooldridge) are presently investigating the problem of determining the time interval between successive collisions for various probabilities of occurrence of a collision during the corresponding time interval. With this information it is possible to estimate the probability that a given number of impacts (or say the closure of a relay) will occur during the service life of a space vehicle.

The idealized model shown in Figure 195d is also representative of vibratory systems internal to equipment components which may produce malfunctions under shock and vibration environments. This model consists of two single degree of freedom oscillators in close proximity to each other and attached to a common base of infinite impedance. When the base experiences random acceleration, each oscillator will respond in the fashion described in Example 1, so that the distance between the masses will have a random fluctuation. A derivation of the response of these two oscillators to a Gaussian white noise acceleration spectral density of the base is presented in Reference 10. Only the resulting response equations are presented and discussed here.

Of interest are the relative deflection and velocity of the separation distance between the two masses. These are given respectively by the equations:

$$(X-Z)_r = \left\{ (X-Y)_r^2 - 2 \langle (X-Y) (X-Z) \rangle \right\}^{1/2}$$

$$(\dot{Y}-\dot{Z})_r = \left\{ (\dot{X}-\dot{Y})_r^2 - 2 \langle (\dot{X}-\dot{Y}) (\dot{X}-\dot{Z}) \rangle \right\}^{1/2}$$

These responses are thus defined in terms of the relative mean square responses of each of the masses and the base and the cross-correlation of these responses.

The relative mean square responses are given by the equations:

$$\begin{aligned} (x-y)_r &= (12.25) \sqrt{\Phi_Y F / f_Y^3} & (\ddot{x} - \ddot{y})_r &= \frac{9}{\sqrt{8\pi}} \sqrt{\frac{\Phi_Y F}{f_Y}} = (17.1) \sqrt{\frac{\Phi_Y F}{f_Y}} \\ (x-z)_r &= (12.25) \sqrt{\Phi_Z F / f_Z^3} & (\ddot{x} - \ddot{z})_r &= 7.71 \sqrt{\frac{\Phi_Z F}{f_Z}} \end{aligned}$$

Q_z, Q_y = quality factors for the two systems = $\frac{1}{2} \frac{C_0 r}{C}$

f_z, f_y = natural frequencies of the two systems.

Noting that $(y-z)$ is the change in the separation distance between the two masses, (not the separation distance) the probability density that $(y-z)$ is equal to "a" is given by the expression:

$$\frac{1}{\sqrt{2\pi} (Y-Z)_r} \exp \left[-\frac{\alpha^2}{2} (Y-Z)_r^2 \right]$$

The probability of collision of the two masses separated by distance, a, can be determined by integrating this probability density function from (a) to ∞ , that is when the change in separation distance exceeds the static separation, and when the masses do not collide with the base. This probability distribution is given, by the equation

$$P\{(Y-Z) > a\} = \frac{1}{2} \left\{ 1 - \frac{1}{\sqrt{2\pi}} \int_{-a/(Y-Z)_r}^{a/(Y-Z)_r} \exp \left[-\frac{\alpha^2}{2} \right] d\alpha \right\}$$

Values of this probability are given in Table XIII for various ratios of $a/(y-z)_r$. The average number of collisions in time (t) is given by equation:

$$N = \frac{\Delta t}{2\pi} \frac{(\dot{Y} - \dot{Z})_r}{(Y-Z)_r} \exp \left[-\frac{\alpha^2}{2} (Y-Z)_r^2 \right]$$

and the mean time between two consecutive collisions is:

$$\Delta t = 2\pi \frac{(Y-Z)_r}{(\dot{Y} - \dot{Z})_r} \exp \left[\frac{\alpha^2}{2} (Y-Z)_r^2 \right]$$

Such collisions may occur in various types of equipment components and can result in serious malfunctions. Relay chatter, collisions between adjacent electron tubes, resistors and capacitors, circuit boards etc. are a few examples of this type of difficulty which may lead to malfunction.

The above three ideal systems have been analyzed and discussed very briefly. Further statistical analysis could be made which would provide other detailed information which could be of value in assessing the damage potential of these systems in any given environment. For example these systems should also be analyzed for shock excitation and for combined shock and vibration environments.

Response to shocks have not been discussed for these systems as the response of simple systems to shock pulses can be found throughout the literature.

Many other such ideal models could be constructed and analyzed which would aid in the overall understanding of equipment malfunctions. When more accurate results are desired in analytically predicting malfunction, the various statistical parameters could be obtained from more detailed models which account for such effects as:

- a) Impedances of the base and equipment mounts and their effects on shaping the acceleration spectral density of the applied excitation.
- b) Reshaping of the spectral accelerations at the mount points due to filtering and transmission loss effects of structural load paths which carry the vibratory energy from the source to the equipment.
- c) Influence of time temperature effects on tolerances, spacing and material properties.
- d) Influence of vibratory energy transfers along different axes of vibration.
- e) Influence of both rectilinear and rotational motions on the fluctuations in spacing and impact of neighboring components.
- f) Nonlinearities in spring constants such as the permanent set in soft wires and terminals and the slip of light weight components such as the movement of the pins of electron tubes within their sockets.

It is to be emphasized that the purpose of analyzing these ideal systems which represent potential malfunctions in equipment is to show that statistical parameters are significant and sensitive in various case of equipment malfunction. It is not expected that detailed analyses of any given piece of complex equipment will replace testing by theoretically predicting malfunction. The analyses may be used to obtain order of magnitude estimates of the serviceability and life of an individual element of a complex package during design and installation, but such analyses will never be sufficiently accurate to insure the necessary reliability of an equipment package for space vehicles. However, it is necessary at the present level of the state of the art of vibration testing that some indication be given as to what statistical parameters are significant in producing failure. Without these, the problem of developing equivalent simplified laboratory equipment tests which are both practical and realistic cannot proceed except by expensive trial and error. Further, the limits that must be imposed on the use of any equivalences in testing cannot be properly established without knowledge of these parameters and their associated modes of failure.

Theoretical analyses of the response of individual elements within equipment packages (such as tubes, wire connections, relays, etc.) can be circumvented, of course, by testing of each type of such element to determine the mode or modes of failure and the statistical parameters which must be dealt with.

As an example of the type of information desired here, some circuits containing electron tubes may be sensitive to the rms relative displacement of, say, the cathode and plate of a tube, while other circuits may be relatively insensitive to this rms response but may temporarily or permanently fail when 3σ (σ = rms value) relative displacements are experienced. Thus a sinusoidal test of this circuit which maintains an rms response which is equivalent to that produced by the random service environment would fail to disclose the latter type peak failure. Increasing the sinusoidal test level to the 3σ value of the random environment might fail other circuitry which would not fail in service.

Accurate proof testing for purposes of qualifying electronic and other equipment packages is clearly a difficult task in light of these complexities, and because the mechanisms of malfunction are dependent upon instantaneous responses and not the gradual accumulation of damage. The ideal test for malfunction consists in duplicating in the laboratory the actual equipment response experienced during flight. This generally would require a random excitation in three directions simultaneously, for the various excitation levels and spectrum shapes occurring during the various vehicle flight phases. The tests need not be conducted for time durations corresponding to real time flight phase durations since malfunctions themselves are generally not dependent upon cumulative deterioration of the equipment. It is important to note, however, that malfunction may depend upon cumulative damage as the gradual weakening and/or mean displacement of a component can lead to increased dynamic deflection and loss of spacing tolerances. Ultimately, combined fatigue and malfunction tests are desirable under the actual shock and vibration environments to insure that this interaction effect is properly assessed.

H. Himelblau (et.al.) presents a conceptual approach, in Reference 11, to defining an ideal laboratory test for evaluating the equipment failure problem. In this report, environmental and fragility surfaces and blankets are defined, and examples of these are presented in Figures 197 through 201. An environmental surface is a plot of the amplitudes of excitation versus frequency and time at a particular reference location on the structure, such as a point at the base of the equipment component. Figure 197 shows such a surface. A fragility surface is defined as a plot of the amplitudes of excitation at which a failure occurs versus the corresponding frequency of excitation used and the time at which failure occurs. Such a surface is shown in Figure 198.

Clearly such a surface can be defined only for a sinusoidal excitation of the equipment component at the same reference point used for defining the environment. If

multiple sinusoids were used, such as would be desirable to examine multi-mode failures, or if a random excitation were applied, then it would be necessary to use higher dimensional surfaces in order to show the coupling effect of two or more frequencies. (The number of frequency axes would have to correspond to the number of modes involved.)

If such sinusoidal tests were conducted, a scatter in the data would certainly be evident because of tolerances in materials and workmanship. Thus these surfaces would show a thickness due to the statistical spread in the sinusoidal amplitudes at which the same failures would occur. The fragility surface along with a plot of the amplitude probability density of failure occurrence constitutes a fragility blanket. Figure 199 shows such a fragility blanket. Similarly an environmental blanket could be defined since there exists a probability of occurrence of various amplitudes at each frequency and time, and such a blanket is shown in Figure 200. The environmental and fragility blankets for a given equipment component are shown combined into a single plot in Figure 201.

If no statistical scatter existed in the fragility and environmental surfaces, then at every point where the fragility surface falls below the actual environmental surface, failures would be expected to occur. These failures would include temporary malfunctions, the effects of deterioration of the components, and the cumulative damage fatigue type failures. Because of the overlapping statistical environmental and fragility blankets, however, failures would be expected to occur, at various probability levels, even when the fragility surface everywhere lies above the environmental surface.

The probability of occurrence of damage at any frequency f and time t can be determined from Table XIV in terms of the mean amplitude and standard deviation of the actual fragility and the actual environment (at the reference point described above). It is assumed for simplicity that the amplitude distributions of both the environment and the fragility are Gaussian. If other distributions were required, similar probability data could be tabulated.

Further discussions of these concepts are not presented here, however, Reference 11 gives a detailed discussion on how this method might be used, various problems associated with the actual laboratory testing (sine and sine sweep techniques) and discusses such topics as:

- a) Simulated Environment and Actual Fragility
- b) Actual Environment and Acceptable Fragility
- c) Simulated Environment and Acceptable Fragility

Because random vibration test equipment are not readily available in all testing

laboratories (especially for producing vibration in three directions simultaneously), and because random testing itself is a complex procedure, various simple excitation substitutes have been proposed and are being used in present testing specifications. These substitutes include:

- a) A set of constant amplitude constant frequency sinusoids to be applied individually in various directions and for predetermined times.
- b) A set of such sinusoids to be applied simultaneously in each of several directions (one direction at a time) for a predetermined time. (Such a set produces a composite wave which is complex and periodic).
- c) A continuous sinusoidal frequency sweep with either a constant or varying amplitude over the frequency band.
- d) Sinusoidal resonant dwell tests at frequencies corresponding to observed major resonances in the equipment. (special case of (a) above).
- e) A continuous sweep of a narrow band random excitation with constant or varying amplitudes over the frequency range.

The details associated with each of these techniques is discussed in Section VII and further discussion is not required here.

Methods for testing equipment to shocks were not included in this list of substitutes as the latter refer to steady vibration environments. Shock testing techniques are available in the form of drop tests which are able to very closely simulate the various pulse shapes, time durations, peak magnitudes and frequency spectrums of shocks experienced in service. The only problem associated with actual shock testing seems to be in measuring and analyzing a sufficient number of shocks to which the equipment will be subjected. Once these data are available, envelopes of the various shock characteristics can be made, and laboratory shocks can be designed to incorporate the desired features of many different types of shocks to be experienced. A major problem of "shock and vibration" testing does exist, however, as the intermixing of both shocks and random vibration can have a significant effect on the fatigue life of equipment components which experience cumulative damage in service.

Equipment failures in complex components may occur when the rms response of certain internal elements attain a given level, or when random response peaks exceed a given magnitude. The probability of occurrence of equipment failures is dependent upon the amplitude distribution of the response to the random vibration excitation and the shock excitation transmitted through the structure and those due to element impacts described earlier. This dependence upon distribution is especially important for cumulative damage fatigue failures. In addition, two mode type failures

may occur (and are common) when more than one natural frequency is excited simultaneously. In a few cases these failures are the result of responses in different directions.

The above listed excitation substitutes cannot simulate all of these statistical parameters each of which will be significant for the general equipment component, particularly electronic modules. Thus the use of these substitutes for qualification testing of all types of equipment components cannot insure that all potential failures will be discovered with a high degree of confidence. Usually this type of testing actually overtests certain equipment components by causing failures which would not normally occur in service, and undertests other components which may fail in the actual environment.

It is not to be construed here that the above simplified techniques are not without merit in each case. When the mode or modes of failure of a given type of equipment component are well understood, these substitutes may be judiciously used in very controlled tests to ascertain if failure will occur in one or more of these known modes of failure under a given vibration environment. The application of unidirectional sine and sine sweep excitations to search for all of the multitude of potential failures in all types of equipment components, however, does involve a risk - a risk which should be compatible with the overall preassigned reliability of the space vehicle and its mission.

Philosophically, it is important to redefine the problem of attaining laboratory equivalence by simulation. Frequently the subject of equivalence is discussed in terms of equivalent response, such as sine-random equivalence and sine sweep - random equivalence. More properly, equivalence should be referred to in terms of failure; that is, laboratory simulation of equivalent failure. Logically there is no difference between the two statements, but the connotation of the latter statement is sufficiently strong to rule out, in many cases, equivalences based purely upon equivalence between one or two of the statistical response parameters for only a portion of the total excitation.

As discussed in Reference 11, shock and vibration environmental testing involves two parameters: the environment and the fragility of the equipment. Laboratory simulation involves a risk in both of these parameters. If the actual environment for an equipment component is defined by a theoretical estimation or by a small number of samples of measured data, there exists a nonnegligible risk that the environment could be significantly more severe in terms of equipment failures. Similarly, laboratory tests of an equipment component will also have a nonnegligible risk that potential failures have not been discovered if the tests are performed with excitations that do not represent the actual environment with a high confidence that this environment will not be exceeded in severity. The risk naturally increases the further the simulated excitation departs from the actual environment.

The applicability of any given excitation substitute should be determined in terms of this risk for each essentially different type of equipment component tested. Very limited test data are presently available for evaluating the risk associated with any of the above substitutes for specific items of equipment. H. Spence, Reference 12, conducted sine and random shake tests on several missile electronic packages and found that the ratio of the rms random acceleration excitation to the equivalent rms sinusoidal acceleration excitation was 2.3, with a total variation of from 1.95 to 2.3. In these tests, emphasis was placed on cumulative fatigue damage. W.D. Trotter, Reference 13, tested complex electronic packages with both sinusoidal and random excitations to determine malfunctions thresholds for the two environments. Two methods were used to obtain sine-random equivalence. The first method provides for a sinusoidal input at each resonance such that the rms sine response in each resonant mode is made equal to the overall response to the entire random test envelope. The second method provides for a sinusoidal input which duplicates only the random rms response of each individual resonance. The conclusions arrived at were that both methods were unconservative, and if suitable corrections were made to make the two methods conservative, then many of the tested items would have experienced excessively severe excitation. It is of interest to note that this experiment showed that the greatest scatter in the results appeared for malfunction of electronic items as opposed to fatigue damage. Also, no instances of multi-mode malfunction were evidenced, which is encouraging.

TABLE XII

Gaussian Probability Distribution Function

Probability $a/(x - y)_r$	$P\{ x - y > a\}$	$\exp\left[a^2/2(x - y)_r^2\right]$
0	1.000	1.000
1	0.317	1.650
2	4.55×10^{-2}	7.390
3	2.70×10^{-3}	90.000
4	6.33×10^{-5}	$2.98 \times 10^{+3}$
5	5.73×10^{-7}	$2.68 \times 10^{+5}$
6	1.97×10^{-9}	$6.59 \times 10^{+7}$
7	2.56×10^{-12}	$4.37 \times 10^{+10}$
8	1.24×10^{-15}	$7.87 \times 10^{+13}$
9	2.28×10^{-19}	$3.86 \times 10^{+17}$
10	1.52×10^{-23}	$5.18 \times 10^{+21}$

TABLE XIII

Probability of Collision of Two Masses Separated by Distance

$a/(x - y)_r$	$P\{(y - z) > a\}$
0	0.500
1	0.159
2	2.28×10^{-2}
3	1.35×10^{-3}
4	3.17×10^{-5}
5	2.87×10^{-7}
6	9.86×10^{-10}
7	1.28×10^{-12}
8	6.22×10^{-16}
9	1.13×10^{-19}
10	7.62×10^{-24}

TABLE XIV

Probability of Occurrence of Damage at Any Frequency

N	Probability of Failure Occurrence
-3	99.87%
-2	97.73%
-1	84.13%
0	50.00%
1	15.87%
2	2.27%
3	0.13%
4	0.0032%
5	0.000029%

where

$$N = \frac{\mu_F - \mu_E}{\sqrt{\sigma_F^2 + \sigma_E^2}}$$

μ_F, μ_E = mean amplitude of the actual fragility and the actual environment at frequency f and time t respectively.

σ_F, σ_E = standard deviation of the fragility and environment at frequency f and time t respectively.

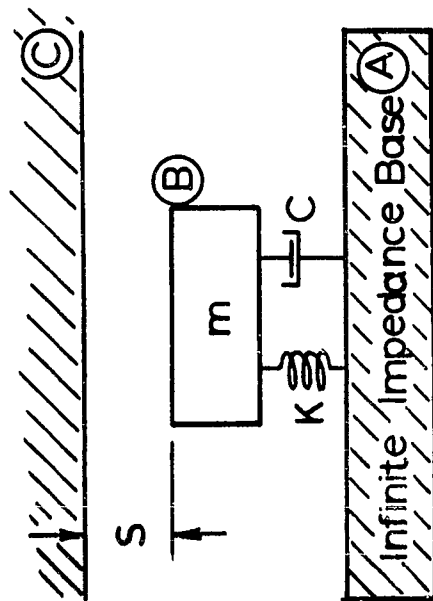


Figure 195a

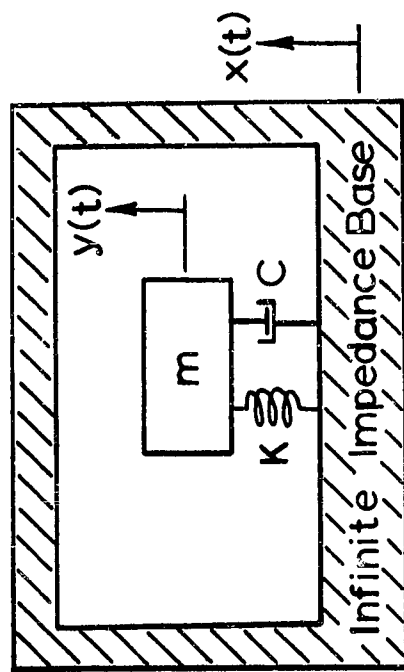


Figure 195b

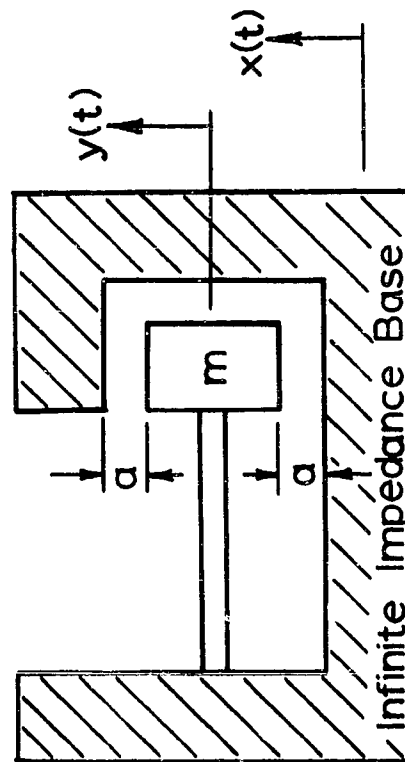


Figure 195c

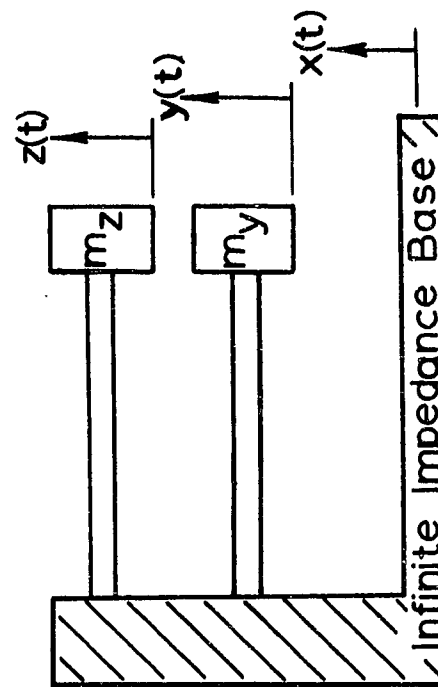


Figure 195d

Figure 195. Idealized Models of Equipment Packages for Which Spacing is Important

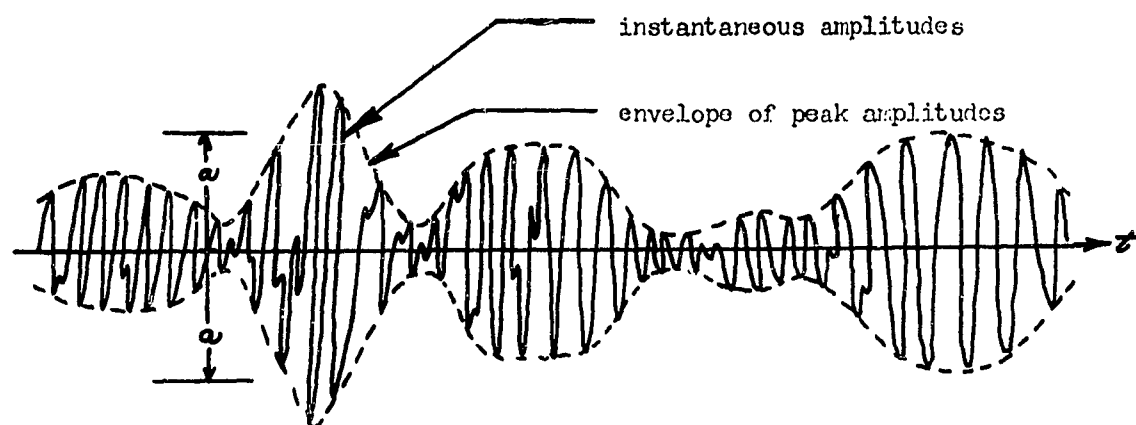


Figure 196. Response of the Single Degree of Freedom System
Shown in Figure 195c for the Case of Low Damping

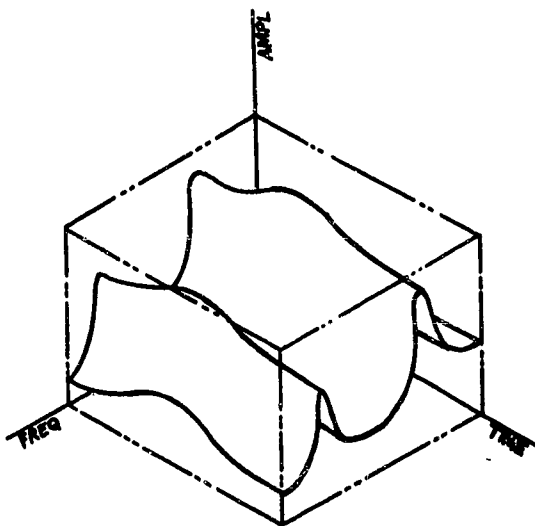


Figure 197 Actual Environmental Surface

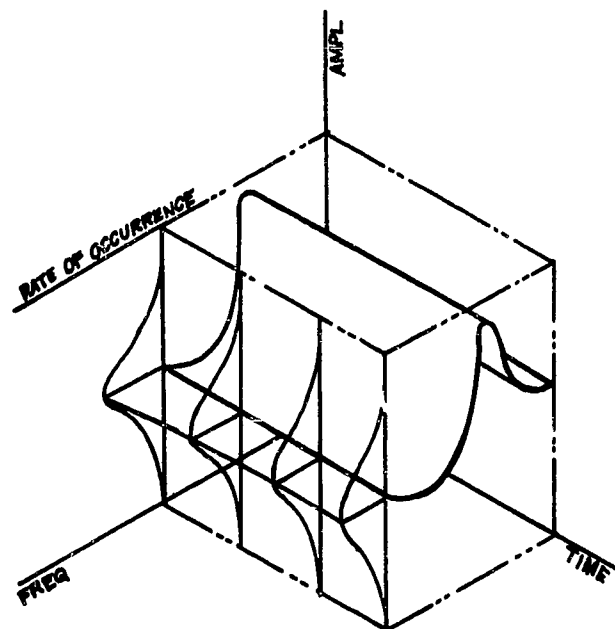


Figure 199 Actual Environmental Blanket

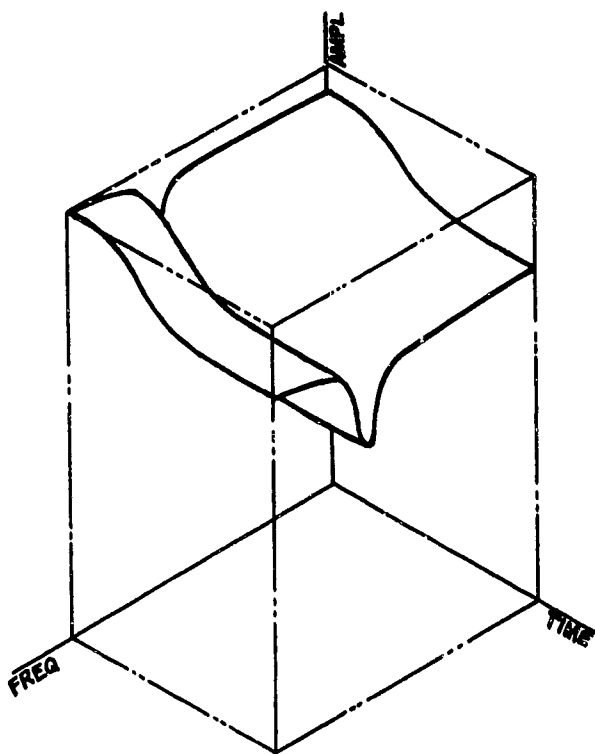


Figure 198 Actual Fragility Surface

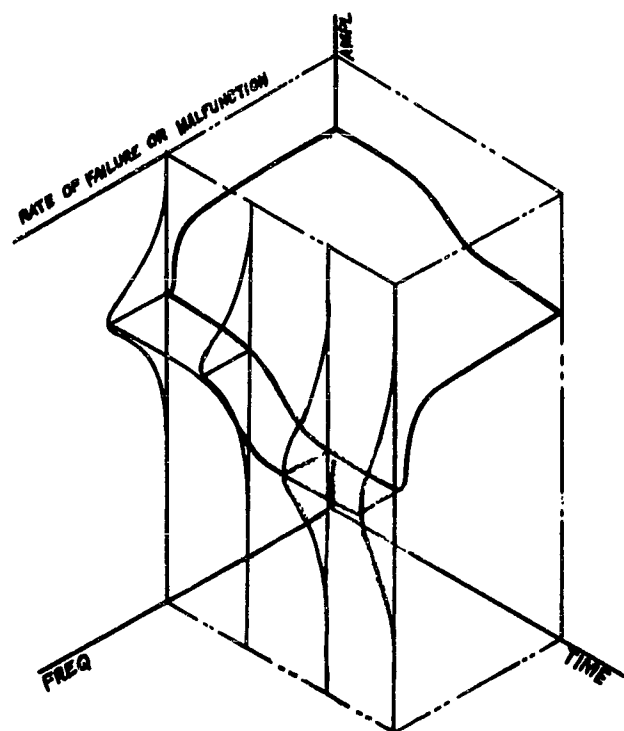


Figure 200 Actual Fragility Blanket

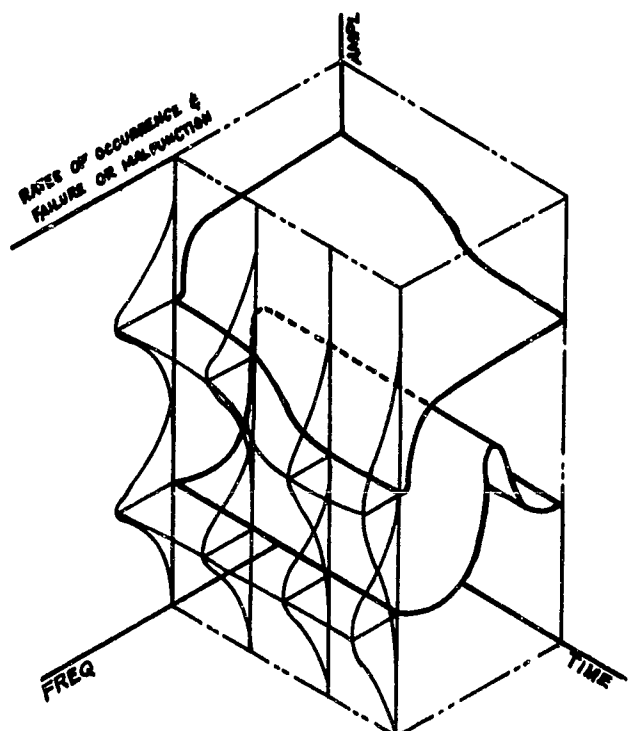


Figure 201 Comparison of Actual Environmental Blanket with actual fragility Blanket

VII. ANALYTICAL EQUIVALENCES FOR LABORATORY TESTING

The previous discussions on laboratory testing for structural fatigue and equipment malfunctions and damage have indicated that the modes of failure of structural and equipment items are often quite complex. This fact, coupled with the high reliability required for space vehicle components, generally necessitates careful laboratory duplication of the in-service environmental excitation forces and input accelerations applied to these components. Unfortunately, this has been, and still is, a difficult task because:

1. The in-service environment may consist of both acoustical and mechanical vibratory energy, and these are difficult to simulate simultaneously in the laboratory.
2. The input vibratory energy may be random and may include a broad band of frequencies.
3. High concentrations of energy may exist in one or several narrow frequency bands causing the input spectra to be shaped in a wide variety of patterns.
4. The source random processes are not actually stationary processes so that spectrum levels and shapes vary with time during flight.
5. Limited knowledge of the true environment of each component to be tested due to the time and cost associated with making in-flight environmental measurements and the associated data reduction to usable information.
6. Limited knowledge of the structural impedance between the source of excitation and the component to be tested, thus limiting the accuracy with which environmental predictions can be made.
7. The vibrational inputs associated with the environment are generally three dimensional.
8. Laboratory testing equipment with capabilities for producing either random excitation or excitation in two or three dimensions simultaneously are not readily available.

In order to circumvent some of these difficulties, and in order to simplify laboratory testing, thus saving time and money, it is desirable to use relatively simple substitutes, where possible, for complex environmental inputs to space vehicle components. These substitutes, which are often used whether the true environment has or has not been determined, include:

1. Sinusoidal acceleration of the component at a single frequency where high spectral energy concentrations are expected.

2. Sinusoidal acceleration of the component at each of the individual natural frequencies of the component and its internal elements.
3. Complex acceleration composed of several sinusoids each of a different frequency and amplitude.
4. Sinusoidal sweep in which the frequency of the applied sinusoidal acceleration is swept over the entire frequency range of interest.
5. Narrow band random sweep in which the applied acceleration contains all frequencies in a narrow frequency band which is slowly and continuously varied over the entire frequency range of interest. (The time history of a narrow band random acceleration appears very similar to an amplitude modulated sine wave except that the modulation has a more random character than a sinusoidal modulation.)

In using these substitutes for complex random excitation, the emphasis shifts from one of simulating the true excitation to one of simulating certain special characteristics of the structural and equipment response to the true excitation. For example, the response of a single degree of freedom system, having low damping, to a broad band random excitation is a nearly sinusoidal motion at the system natural frequency with a relatively low frequency amplitude modulation. Although this modulation is somewhat random in nature, it appears to be nearly sinusoidal, with the modulation frequency approximately equal to the bandwidth of the system. Such a response can be approximated by a resonant dwell test (i.e., a sinusoid applied at the system natural frequency) in which the rms response is duplicated by the proper choice of the sinusoidal input amplitude. Such a response could also be approximated by two sinusoidal inputs properly spaced about the natural frequency.

Since the basic purpose of qualification testing is to predict the in-service damage potential of the components, the use of simple substitutes automatically imposes the assumption that the damage potential for the simulated response is the same as that in the true environment. As discussed in the previous sections, these substitutes will not always produce a damage potential equivalent to that of the actual environment. Several factors may be significant to the damage potential of any component; and in using the above excitation substitutes, the influence of all factors during laboratory tests cannot be made equivalent to their influence in-service; e.g., rms response amplitude, amplitude distribution, peak amplitude distribution, multimode effect.

Hence, it is important in the choice of an equivalent substitute to consider the most important of these factors in order to minimize the error. In reference to the above example, it is true that the damage potential for a component is higher at the natural frequency than at any other frequency, but it must be noted even this damage potential may not be as high as for multiple frequency inputs such as random excitation of the system.

An equivalence relation is an equation relating the excitation parameters of a simple substitute to those of the true or estimated environment. Since the factors

which influence damage potential vary for different types of components, this relationship will depend upon the vibration characteristics of the component, major damage factors, type of environmental excitation, and the particular type of substitute to be used. The number of such equivalence relations that might be constructed is then quite large, especially when multimode systems are considered. A few of the more well-known and widely-used equivalence relations will be constructed and discussed below. Using these techniques, many other and more refined equivalences can be constructed for other systems and for inputs other than those considered below.

Ideal linear models of elastic systems are generally used to construct these relationships as these are mathematically tractable as opposed to systems occurring in practice which may contain nonlinearities, etc. Although this approach restricts the usefulness of the equivalence relations, these ideal relationships do indicate valuable functional forms, and provide a good base to which refinements can be added to account for other important effects.

Table IX lists the equations for the root-mean-square (rms) response, average power-developed, work dissipated, etc., for a single degree of freedom system excited by various sinusoidal and stationary random input forces and accelerations. This table is discussed in detail in material which follows. By equating the appropriate response quantities in this table for sinusoidal and random excitations, numerous sine-random equivalence relations can be constructed for the amplitude of the sinusoid necessary to produce the same response as for the random input.

The single degree of freedom system is emphasized here because the predominant contributor to the response of most elastic systems is the response in the fundamental mode. Such systems may then be analyzed as single-degree-of-freedom systems. These response expressions may also be applied to linear systems in which independent or uncoupled multimode response occurs. The total rms response of such systems is equal to the square root of the sum of the mean square response in each of the independent modes of vibration.

SINE-RANDOM EQUIVALENCES

Equating the rms displacement (velocity) for a sinusoidal force input, $F(t)$, at the natural frequency, ω_0 , to the rms displacement (velocity) for a Gaussian random force input with a constant power spectrum from $\omega = 0$ to $\omega = \infty$, gives the relation:

$$F_0 = \sqrt{\frac{\omega_0 \Phi_F}{2Q}}$$

In each case the base is held fixed, $Y(t)=0$. Similarly, equating the rms relative displacement (velocity) for a sinusoidal base acceleration, $Y(t)$, at the natural frequency and that for a constant spectral density Gaussian base acceleration gives the relation

$$\ddot{Y}_0 = \sqrt{\frac{\omega_0 \Phi_Y}{2Q}}$$

This is the familiar sine-random equivalence relation which appears extensively in the literature. It is interesting to note that in these two cases, the above equivalence relations also imply sine-random equivalence for both the average power developed by the damper and the total amount of work done in time (Δt) .

In all cases shown in this table, equivalence of the rms relative velocity implies the equivalence of the average power developed and the work done, because of the relations

$$\text{Avg. Power} = \frac{c}{g} \cdot \overline{\dot{X}}_{\text{Rel.}}^2$$

$$\text{Work} = \frac{c}{g} \cdot \overline{\dot{X}}_{\text{Rel.}}^2 \cdot (\Delta t)$$

$$\overline{\dot{X}}_{\text{Rel.}}^2 = \text{mean square relative velocity.}$$

The equations for the relative rms acceleration response to a Gaussian white noise input are

$$\overline{\ddot{X}} = \frac{1}{K} \sqrt{\frac{\omega_o^5}{2\pi} I_4 \Phi_F} \quad \begin{array}{ll} \Phi_F = \text{constant} & 0 \leq \omega \leq \omega_u \\ = 0 & \omega_u < \omega \end{array}$$

$$= \sqrt{\frac{\omega_o}{2\pi} I_4 \ddot{\Phi}_Y} \quad \begin{array}{ll} \ddot{\Phi}_Y = \text{constant} & 0 \leq \omega \leq \omega_u \\ = 0 & \omega_u < \omega \end{array}$$

$$I_4 = \frac{\pi Q}{2} \left[1 - \frac{1}{Q^2} \right] + \left(\frac{\omega_u}{\omega_o} \right) \quad \omega_u \gg 4 \omega_o$$

showing that the relative rms acceleration response is infinite if ω_u approach infinity. Thus, the above equivalence relations for displacement and velocity do not imply equivalence of the rms relative acceleration which depends upon the upper frequency limit of the excitation. The equivalence relations for accelerations are:

$$\begin{aligned} F_o &= \sqrt{\frac{\omega_o \Phi_F}{2Q}} \cdot \sqrt{1 + \frac{2}{\pi Q} \left(\frac{\omega_u}{\omega_o} \right)} \\ \ddot{Y}_o &= \sqrt{\frac{\omega_o \ddot{\Phi}_Y}{2Q}} \cdot \sqrt{1 + \frac{2}{\pi Q} \left(\frac{\omega_u}{\omega_o} \right)} \end{aligned}$$

Similarly, equating the absolute rms displacement, velocity, and acceleration for a sinusoidal and Gaussian white noise acceleration input gives the equivalence relations:

$$\ddot{Y}_0 = \sqrt{\frac{\omega_0 \Phi \ddot{Y}}{2Q(1-\frac{1}{Q^2})}} \cdot \sqrt{1 - \frac{2}{Q^2} + \frac{1}{Q^4} + \frac{1}{Q^3} \left(\frac{\omega_0}{\omega_L}\right) + \frac{1}{3Q} \left(\frac{\omega_0}{\omega_L}\right)^3} \quad \text{equiv. abs. displacement}$$

$$\dot{Y}_0 = \sqrt{\frac{\omega_0 \Phi \ddot{Y}}{2Q(1-\frac{1}{Q^2})}} \cdot \sqrt{1 + \frac{1}{Q^2} + \frac{2}{\pi Q} \left(\frac{\omega_0}{\omega_L}\right)} \quad \text{equiv. abs. velocity}$$

$$\ddot{Y}_0 = \sqrt{\frac{\omega_0 \Phi \ddot{Y}}{2Q(1-\frac{1}{Q^2})}} \cdot \sqrt{1 + \frac{1}{Q^2}}$$

where ω_L = lower cutoff frequency defined by

$$\begin{aligned} \Phi \ddot{Y} &= \text{constant} & 0 < \omega_L \leq \omega \leq \infty & \quad \omega_L \ll \omega_0 \\ &= 0 & 0 \leq \omega < \omega_L \end{aligned}$$

In this case, only the absolute rms acceleration remains finite for a constant excitation spectral density from $\omega = 0$ to $\omega = \infty$, while the absolute rms displacement and velocity become infinite when the lower cutoff frequency approaches zero.

If it can be assumed that for a high Q (say $Q \geq 10$) single degree of freedom systems, the excitation spectrum (either Φ_F or Φ_Y) has a lower and upper cutoff frequency within two to four bandwidths distance (bandwidth, $\Delta\omega = \omega_0/Q$) on either side of the natural frequency, ω_0 , of the system, then the major portion of the rms response (either relative or absolute) will be due to excitation frequencies very near the natural frequency, say within a single bandwidth about ω_0 . For this condition, the above sine-random equivalence relations reduce to the following very simple approximate forms for both relative and absolute displacement, velocity, and acceleration:

$$\begin{aligned}
 F_o &= \sqrt{\frac{\omega_o \Phi_F}{2Q}} & \left. \begin{aligned} \Phi_F &= \text{constant} \\ \Phi_Y &= \text{constant} \end{aligned} \right\} & \text{over the single degree} \\
 \ddot{Y}_o &= \sqrt{\frac{\omega_o \Phi_Y}{2Q}} & & \text{of freedom bandwidth.}
 \end{aligned}$$

Similar analyses can be applied to the case of constant velocity and constant displacement spectral density at the "base" or "foundation" of the single degree of freedom system shown in Table IX. The resulting approximate sine-random equivalence relations for both relative and absolute displacement, velocity, and acceleration response are:

$$\begin{aligned}
 \ddot{Y}_o &= \sqrt{\frac{\omega_o^3 \Phi_Y}{2Q}} & \left. \begin{aligned} \dot{\Phi}_Y &= \text{constant} \\ \Phi_Y &= \text{constant} \end{aligned} \right\} & \text{over the single degree} \\
 \ddot{Y}_o &= \sqrt{\frac{\omega_o^5 \Phi_Y}{2Q}} & & \text{of freedom bandwidth.}
 \end{aligned}$$

The accuracy of the latter equivalences is not expected to be as high as for Φ_F and Φ_Y inputs since, as the equations of Table IX show, the effect of the ratios of the lower and upper cutoff frequencies to the natural frequency, ω_o , is more pronounced. It was the elimination of the effect of these ratios which permitted the above elementary sine-random relationships. It is to be noted that these relationships imply an equivalence of power and work with the same accuracy as are the response equivalence if the test time duration is equal to the time duration of the random excitation.

Although the expressions are considerably more complex, these same techniques can be applied to the determination of sine-random equivalences for a combined random Gaussian white noise input force, $F(t)$, and foundation motion, $\ddot{Y}(t)$ or $\dot{Y}(t)$ or $Y(t)$.

Sine-random equivalences are not restricted to resonant dwell sinusoidal substitutes. High excitation energy concentrations at frequencies other than the natural frequency of the system is an example of a condition where sinusoids at other frequencies would be used. The simple and approximate form of the equivalence relations for a force input, $F(t)$, also for a base acceleration input at frequency ω are:

$$\begin{aligned}
F_o &= \sqrt{\frac{Q \omega_o \Phi F}{2H^2(\omega)}} \cdot \left(\frac{\omega_o}{\omega}\right) \\
\ddot{Y}_o &= \sqrt{\frac{Q \omega_o \Phi \ddot{Y}}{2H^2(\omega)}} \cdot \left(\frac{\omega_o}{\omega}\right) \quad \left. \begin{array}{l} \text{rms velocity equiv., ave. power} \\ \text{equiv., work equiv.} \end{array} \right\} \\
F_o &= \sqrt{\frac{Q \omega_o \Phi F}{2H^2(\omega)}} \cdot \left(\frac{\omega_o}{\omega}\right)^2 \\
\ddot{Y}_o &= \sqrt{\frac{Q \omega_o \Phi \ddot{Y}}{2H^2(\omega)}} \cdot \left(\frac{\omega_o}{\omega}\right)^2 \quad \left. \right\} \text{rms accel. equiv.}
\end{aligned}$$

where

$$H^2(\omega) = \frac{1}{\left[1 - \left(\frac{\omega}{\omega_o}\right)^2\right]^2 + \frac{1}{Q^2} \left(\frac{\omega}{\omega_o}\right)^2}$$

The approximation in these equivalence relations lies in the assumption that the effect of the ratios (ω_u/ω_o) and (ω_o/ω_L) can be neglected. These relations show that except for $\omega = \omega_o$, the rms displacement, velocity and acceleration response cannot be made equivalent simultaneously.

The number of response cycles occurring in a time duration Δt for high Q systems, say $Q \gg 5$, is given in Table IX as $\omega_o/2\pi \cdot (\Delta t)$. Hence a resonant dwell test produces the same number of response cycles in time Δt as does a random excitation of a single degree of freedom system acting for the same time duration. By application of a sinusoidal excitation at a frequency ω where $\omega > \omega_o$, the number of cycles in time Δt increases to $(\omega/2\pi) (\Delta t)$. Such inputs may be used in order to accelerate equipment testing in which cumulative damage depends upon the number of stress reversals such as fatigue. One disadvantage of this technique is that the peak amplitude (either F_o or Y_o) of the substitute sinusoid must be considerably greater (possibly by orders of magnitude) to produce the desired equivalent rms response than at the natural frequency ω_o .

The duration of the sinusoidal test must depend upon the type of damage occurring in the component. If the damage is of a malfunction type, this duration need be no longer than that required to determine if malfunction has or has not occurred.

For cumulative type damage, specification of this time duration is considerably more difficult if the simulated damage potential is to be equivalent to that occurring in-service. The influencing factors for this problem are discussed in detail in the previous chapters. Continuing with the ideal linear single degree of freedom model however, it might be assumed that cumulative damage is proportional to the total amount of work done in energy dissipation. Considering only the case in which a base acceleration $\ddot{Y}(t)$ is applied, the expressions for the work done are:

$$\begin{aligned}
W &= \frac{K \Phi \ddot{Y}}{4g \omega_0^2} (\Delta t) & \left\{ \begin{array}{l} \text{random Gaussian white noise} \\ \text{spectrum } \Phi \ddot{Y} \text{ from } \omega = 0 \text{ to } \omega = \infty \end{array} \right. \\
W &= \frac{K Q \ddot{Y}_0^2}{2g \omega_0^3} (\Delta t) & \left\{ \begin{array}{l} \text{resonant dwell sinusoid} \end{array} \right. \\
W &= \frac{K \omega^2 H^2 \ddot{Y}_0^2}{2g Q \omega_0^5} (\Delta t) & \left\{ \begin{array}{l} \text{sinusoid at frequency } \omega \end{array} \right.
\end{aligned}$$

This simpler condition was chosen here since the total work done for the random excitation remains finite for all random excitation frequencies. The approach used in the following discussion, however, applies equally well to other more complex sine-random equivalences for the single degree of freedom system.

Equating the work for the resonant sinusoid to the work for this random input gives

$$\ddot{Y}_0 = \sqrt{\frac{\omega_0 \Phi \ddot{Y}}{2Q}} \cdot \sqrt{\frac{T}{\Delta t}}$$

Δt = duration of the sinusoidal test

T = duration of the random excitation

If $\Delta t = T$, this reduces to the usual rms response equivalence.

From the standpoint of work done on a SDF system the test may be accelerated by choosing Δt smaller than T and increasing the input acceleration according to this equation. Thus it is possible to have a work equivalence without a response equivalence.

Similarly, equating the work done by the non-resonant sinusoid in time Δt to the work done by the random input in time T gives:

$$\ddot{Y}_0 = \sqrt{\frac{\omega_0 Q \Phi \ddot{Y}}{2H^2(\omega)}} \cdot \sqrt{\frac{T}{\Delta t}} \cdot \left(\frac{\omega_0}{\omega}\right)$$

If $\Delta t = T$, this reduces to the rms velocity equivalence at an arbitrary frequency ω . Once again, if the work done is the only factor leading to damage, the sinusoidal test may be accelerated by choosing $\Delta t < T$ and increasing \ddot{Y}_0 accordingly. It is to be noted that \ddot{Y}_0 increases with increasing ω since $H(\omega)$ decreases faster with increasing ω than does $1/\omega$.

As seen by Table IX, the probability density functions for both the instantaneous and peak response amplitudes of the single degree of freedom system are not at all equivalent for sinusoidal and random excitations. As discussed in Section IV the distribution of response peaks has a significant influence on the fatigue life

of structural elements in that the curve of stress vs. the number of life cycles is different for a sinusoidal than for a random excitation. In order to account for the influence on fatigue of the peak stresses at different levels, a set of sinusoids of different amplitude can be applied, which, with a random sequence of amplitude levels and with each level applied for a duration which is in proportion to the frequency of occurrence of that level in the probability density function, will produce a distribution of stress levels which approximates the random amplitude distribution.

SINUSOIDAL SWEEP - RANDOM EQUIVALENCES

Sinusoidal sweep tests have several applications. First, sweep tests may be used to determine the major natural frequencies of a complex component by sweeping the entire frequency range of interest. These natural frequencies can be detected visually or by the electrical output of strain gauges and accelerometers mounted at critical points throughout the component. Secondly, such sweep tests may be used to determine the transmissibilities between the point of force or motion application and critical response locations of the component. By integrating the areas under these transmissibility curves, the rms response to a random Gaussian white noise input force or motion can be predicted, as this area is theoretically proportional to the mean square response. Finally, sinusoidal sweep tests can be used to determine damage potential directly as a simple substitute for a white Gaussian random excitation. The latter case is of interest in this discussion.

The response of a single degree of freedom system to a sinusoidal excitation in which the input frequency changes with time at some given sweep rate is a complex problem and will not be considered here. It is sufficient to note that if the sweep rate through the system resonance is very fast, the response will not have sufficient time to build up to the desired maximum level. It is assumed in the following discussion that the sweep rate is sufficiently slow in order to assume that no transients exist and that the response is steady state at each frequency in the sweep band.

Present qualification testing specifications often require that the rms input acceleration level at each frequency in the frequency sweep band be equal to the total rms input acceleration of the predicted or known environment of the component. This is generally a conservative test sufficient to uncover the majority of equipment malfunctions. Some difficulty does occur at the various resonances of an equipment package, however, as the test may be overconservative, causing overstressing and damage which would not occur in service.

For the single degree of freedom system shown in Table IX, simple sine sweep-random equivalence relations can be derived by equating the total work done on the system in the sweep to the work done by the random excitation of deviation T.

Table IV gives the relationships for this work for three different sweep rates:

$$\dot{\omega} = \alpha \quad \text{constant sweep rate}$$

$$\dot{\omega} = \beta \omega \quad \text{log sweep rate}$$

$$\dot{\omega} = r \omega^2 \quad \text{log-log sweep rate}$$

Equating these expressions for work to those for the case of $\dot{\Phi}_F = \text{constant}$ and $\ddot{\Phi}_Y = \text{constant}$, Table IX, the following work equivalence relationships are obtained:

$\ddot{Y}_0 = \sqrt{\frac{\alpha}{\pi} \ddot{\Phi}_Y T}$	$F_0 = \sqrt{\frac{\alpha}{\pi} \dot{\Phi}_F T}$	$\dot{\omega} = \alpha$
$\ddot{Y}_0 = \sqrt{\frac{\beta \omega_0 \ddot{\Phi}_Y T}{\pi a}}$	$F_0 = \sqrt{\frac{\beta \omega_0 \dot{\Phi}_F T}{\pi a}}$	$\dot{\omega} = \beta \omega$
$\ddot{Y}_0 = \sqrt{\frac{r \omega_0^2 \ddot{\Phi}_Y T}{\pi}}$	$F_0 = \sqrt{\frac{r \omega_0^2 \dot{\Phi}_F T}{\pi}}$	$\dot{\omega} = r \omega^2$

It has been assumed in the derivation of these expressions that the spectra $\dot{\Phi}_F$ and $\ddot{\Phi}_Y$ are constant from $\omega = 0$ to $\omega = \alpha$. However, since almost all of the work is performed in the vicinity of the natural frequency of the single degree of freedom system, where the response magnification is highest, these spectra need be assumed constant only in the neighborhood of the natural frequency.

As with the sinusoidal substitute for the random excitation, the probability distributions of the instantaneous and peak amplitudes of the response are not approximated by the distribution produced by the sine sweep.

Complex equipment components generally contain many highly undamped and independent resonant frequencies. During a sinusoidal sweep test, all of these resonances having frequencies in the sweep band will be excited. Ideally, two conditions may exist:

1. The damping in all frequencies is the same; that is, the bandwidth, $\Delta \omega$, ($= \omega_0/Q$) increases in proportion with the natural frequency.
2. The bandwidth $\Delta \omega$ of each resonance is the same; that is, the damping is proportional to the magnitude of the natural frequency giving higher damping at the higher natural frequencies.

These are ideal conditions in that a complex component will probably show some evidence that neither of these conditions is valid, but that some intermediate condition exists with one merely predominating over the other. Table IV shows that:

1. A constant sweep rate gives the same sweep time deviation at each resonance for a constant bandwidth system.
2. A log sweep rate produces the same number of response cycles at each resonance for a constant bandwidth system, and allows for the same time deviation at each resonance for a constant Q system.

3. A log-log sweep rate produces the same number of response cycles at each resonance for a constant Q system (i.e. constant damping at all frequencies).

NARROW BAND RANDOM SWEEP EQUIVALENCES

When either the fixed frequency sinusoid or the sinusoidal sweep are used as laboratory substitutes for a wide band random excitation, the amplitude distributions of the response cannot be made equivalent to the distribution resulting from the response to the latter excitation. A testing technique is presented in Reference 3 by C. B. Booth in which a narrow band random excitation is applied and the center frequency of the band is swept at a log sweep rate over the frequency band of interest. With the proper choice of the β parameter, Table IV, it is possible to very closely duplicate the distribution of peak response amplitudes obtained for a wide band random excitation. This method is considered to be a valuable tool for laboratory testing, as the cost of producing a narrow band random excitation is well below equipment costs for producing a wide band random excitation.

The theoretical aspects of this method are described here very briefly. The bandwidth, $\Delta\omega$, of a single degree of freedom system is defined as

$$\Delta\omega = \omega_0/Q$$

Choosing a narrow frequency band $(\Delta\omega)'$ much smaller than $\Delta\omega$,

$$(\Delta\omega)' = K\omega_0/Q, \quad K \ll 1$$

and assigning to each such band in the neighborhood of the natural frequency a subscript, j , Figure 202, the rms response, σ_j , in this j -th band to an excitation σ_e in this frequency band is given by the equation

$$\sigma_j = T(\omega_j) \cdot \sigma_e = T_j \cdot \sigma_e$$

T_j is the appropriate transmissibility function, at ω_j , which relates the particular type of excitation and response parameters desired, and may be found by the use of Table IX. The probability P_j , that a peak response in this narrow band exceeds a certain level b is given by the equation

$$P_j = \exp \left[-\frac{1}{2} \frac{b^2}{\sigma_j^2} \right] = \exp \left[-\frac{1}{2} \frac{b^2}{T_j^2 \sigma_e^2} \right]$$

The functional form of P_j is obtained for integration of the Rayleigh probability density function for peak amplitudes, Table IX. Hence, the number of response peaks, N_j , exceeding b for this frequency band is

$$N_j = \frac{\omega_j}{2\pi} \cdot \Delta t_j \cdot P_j$$

where ω_j = center band frequency of the narrow band
 t_j = time duration for sweeping such a band

For a log sweep rate, Δt_j becomes

$$\frac{(\Delta\omega)_j}{\Delta t_j} = \frac{K\omega_0}{\Delta t_j \cdot Q} = \beta\omega_j \quad \therefore \Delta t_j = \frac{K\omega_0}{\beta Q \omega_j}$$

so that N_j is

$$N_j = \frac{K\omega_0}{2\pi\beta Q} P_j$$

Summing over-all $(\Delta\omega)_j$ in the entire frequency band of interest gives

$$N = \frac{\omega_0}{2\pi\beta Q} \left[K \sum P_j \right]$$

$$P_j = \exp \left[-\frac{1}{2} \frac{b^2}{T_j^2 \sigma_e^2} \right]$$

N = total number of response peaks above the level b in the entire frequency sweep band.

If T_m is used to denote the maximum value of the transmissibility function T , then P_j can be put into the more convenient mathematical form

$$P_j = \exp \left[-\frac{1}{2} \left(\frac{T_m}{T_j} \right)^2 \cdot \left(\frac{b}{T_m \sigma_e} \right)^2 \right]$$

where $\frac{b}{T_m \sigma_e}$ is a non-dimensional quantity. By numerical evaluation of the above summation, $\sum P_j$, a plot similar to that shown in Figure 203b can be constructed for various values of $(b/T_m \sigma_e)$.

A similar plot appears in Figure 203a. This curve is obtained from the equation

$$P = \exp \left[-\frac{1}{2} \frac{b^2}{\sigma_{WB}^2} \right]$$

σ_{WB} = rms response of the single degree of freedom system to random wide band excitation

which is the integral of the Rayleigh probability density function for the distribution of response peaks of a single degree of freedom system to a wide band random Gaussian excitation.

In Figure 203c the above curves are superimposed in such a manner as to obtain a "best fit" of one curve on the other. Let q and s denote the proportionality factors between the horizontal and vertical axes of Figure 203c according to the relations

$$\frac{b}{\sigma_{WB}} = q \cdot \frac{b}{T_m \sigma_e}$$

$$P = s \cdot \left[K \sum_j P_j \right]$$

The expression for σ_{WB} can be found from Table IX by choosing the rms response quantity for random excitation corresponding to the sinusoidal rms response quantity chosen above for σ_j , for which T_j is the transmissibility. With σ_{WB} prescribed,

$$\sigma_e = q \frac{\sigma_{WB}}{T_m}$$

For wide band excitation, the number of response peaks, N_{WB} , exceeding a given level b in the time duration, T , that the wide band excitation is applied, is

$$N_{WB} = \frac{\omega_0}{2\pi} TP$$

where P is defined above. Since it is desirable to have $N = N_{WB}$, the sweep rate can be determined as follows:

$$P = s \left[K \sum_j P_j \right]$$

$$\frac{2\pi N_{WB}}{\omega_0 T} = s \frac{2\pi N \beta Q}{\omega_0}, \quad N = N_{WB}$$

$$\therefore \beta = \frac{1}{sQT}$$

which is the desired relationship.

If the component being tested contains only one resonant frequency, the rms excitation level, σ_e , is to be held constant throughout the sweep test. However, most complex components will contain a multitude of high Q resonances with very narrow bandwidths. Since the expression for the rms wide band random response σ_{WB} is a function of the natural frequency ω_0 , and since many natural frequencies will be encountered during the sweep test, the magnitude of the excitation σ_e should be made to vary according to function frequency dependence of σ_{WB} . For example, Table IX shows that σ_{WB} for a constant spectral input force to the single degree of freedom system shown is

$$\sigma_{WB} = \frac{1}{2K} \sqrt{Q \omega_0} \Phi_F$$

Hence, for this case, where $T_m = Q$,

$$\sigma_e = \frac{q}{2KQ} \sqrt{Q \omega_o} \Phi_F = \frac{q}{2K} \sqrt{\frac{\omega_o}{Q}} \Phi_F$$

and the rms excitation level σ_e must increase as $\sqrt{\omega}$ since it is assumed that at each frequency during the sweep a different resonance could occur. For simulation of other response quantities, σ_e may have a different variation with frequency.

It is to be noted that the analysis presented above is for an ideal constant Q system. A similar analysis may be performed for constant bandwidth systems in which $\Delta\omega (= \frac{\omega_o}{Q})$ is held constant. Since this is but a minor variation of the above analysis, with the log sweep rate replaced by the constant sweep rate, only a brief description of the different expressions arrived at will be presented below.

$$\frac{(\Delta\omega)_j}{\Delta t_j} = \frac{K \omega_o}{\Delta t_j Q} = \alpha$$

$$\Delta t_j = \frac{K \omega_o}{\alpha Q}$$

Hence, N_j becomes

$$N_j = \frac{K \omega_o^2}{2\pi Q \alpha} \left[\frac{\omega_1}{\omega_o} P_j \right]$$

giving

$$N = \frac{\omega_o^2}{2\pi \alpha Q} \sum_j K \frac{\omega_1}{\omega_o} P_j$$

In this case, $\sum K \frac{\omega_1}{\omega_o} P_j$ is plotted for various values of $b/T\sigma_e$, as before, and compared with the curve for P. Then defining q and s as before, substitution into the equation

$$P = s \sum K \frac{\omega_1}{\omega_o} P_j$$

gives

$$\frac{2\pi N_{WB}}{\omega_o T} = \frac{2\pi \alpha N Q s}{\omega_o^2}, \quad N = N_{WB}$$

$$\therefore \alpha = \frac{\omega_o}{s T Q} = \frac{\Delta\omega}{s T}$$

which is the desired relationship for the constant sweep rate in terms of constant bandwidth $\Delta\omega$.

In the previous constant Q system, an example was given showing that,

$$\sigma_e = \frac{g}{2K} \sqrt{\frac{\omega_o \Phi_F}{Q}} = \frac{g}{2K} \sqrt{\Delta\omega \cdot \Phi_F}$$

and hence, the rms excitation level, σ_e , must remain constant during the narrow band random sweep test with a constant sweep rate for all frequencies.

The preceding discussions of sine-random, sine sweep-random, and narrow band random sweep-random equivalence relationships was not intended to be complete. Rather, its purpose was to indicate the analytical techniques whereby equivalence relations may be constructed from ideal dynamical models. Using these methods, other equivalence relations can be constructed for other types of excitation and for more complex models.

The single degree of freedom system has been used throughout the discussion as such a model is mathematically tractable, and since this system gives a first order approximation of the type of system which occurs frequently in practice.

It has been shown that even for this simplest of systems, the exact mathematical expressions for equivalence relations can be quite complex and can be simplified only when the proper assumptions have been imposed. Also, very ideal random excitations have been considered and these are not likely to occur in practice. Detailed mathematical analyses of the two degree of freedom system will be considerably more complex than that given above from the standpoint of equivalence relations. The use of IBM digital computers can be used to great advantage in numerically constructing more refined equivalences.

TABLE XV
SUMMARY OF SINUSOIDAL FREQUENCY SWEEP RELATIONS

INPUT	CONST. SINE SWEEP	LOG SINE SWEEP	LOG-LOG SINE SWEEP
SWEEP RATE	$\dot{\omega} = \alpha$	$\dot{\omega} = \beta \omega$	$\dot{\omega} = \tau \omega^2$
NUMBER OF CYCLES FROM ω_1 TO ω_2	$\frac{\omega_2^2 - \omega_1^2}{4\pi\alpha}$	$\frac{\omega_2 - \omega_1}{2\pi\beta}$	$\frac{1}{2\pi\tau} \ln \frac{\omega_2}{\omega_1}$
NUMBER OF CYCLES PER OCTAVE	$\frac{3\omega_1^2}{4\pi\alpha}$	$\frac{\omega_1}{2\pi\beta}$	$\frac{1}{2\pi\tau} \ln 2$
NO. OF CYCLES PER 1° FREEDOM BANDWIDTH	$\frac{\omega_2 \Delta \omega}{2\pi\alpha}$	$\frac{\Delta \omega}{2\pi\beta}$	$\frac{1}{2\pi\tau} \ln \frac{2Q+1}{2Q-1}$
TIME TO SWEEP FROM ω_1 TO ω_2	$\frac{\omega_2 - \omega_1}{\alpha}$	$\frac{1}{\beta} \ln \frac{\omega_2}{\omega_1}$	$\frac{\omega_2 - \omega_1}{\tau \omega_1 \omega_2}$
TIME TO SWEEP AN OCTAVE, $\omega_1 \rightarrow 2\omega_1$	$\frac{\omega_1}{\alpha}$	$\frac{1}{\beta} \ln 2$	$\frac{1}{2\tau \omega_1}$
TIME TO SWEEP A $\frac{1}{n}$ -th OCTAVE $\omega_1 \rightarrow 2^{1/n} \omega_1$	$\frac{2^{1/n} - 1}{\alpha} \omega_1$	$\frac{1}{n\beta} \ln 2$	$\frac{2^{1/n} - 1}{2^{1/n} \tau \omega_1}$
TIME TO SWEEP A 1° FREEDOM BANDWIDTH	$\frac{\Delta \omega}{\alpha}$	$\frac{1}{\beta} \ln \frac{2Q+1}{2Q-1}$	$\frac{4}{\tau \cdot (\Delta \omega)^2 (4Q^2 - 1)}$
WORK DONE IN SWEEP FROM 0 TO ∞; CONSTANT LEVEL INPUT, $\ddot{Y}(t)$	$\frac{\pi K \ddot{Y}_0^2}{4\alpha \omega_0^2 g}$	$\alpha \cdot \frac{\pi K \ddot{Y}_0^2}{4\beta \omega_0^3 g}$	$\frac{\pi K \ddot{Y}_0^2}{4\tau \omega_0^4 g}$
WORK DONE IN SWEEP FROM 0 TO ∞; CONSTANT LEVEL INPUT, $F(t)$	$\frac{\pi \omega_0^2 F_0^2}{4\alpha K g}$	$\alpha \cdot \frac{\pi \omega_0 F_0^2}{4\beta K g}$	$\frac{\pi F_0^2}{4\tau K g}$

$$N = \frac{1}{2\pi} \int_{\omega_1}^{\omega_2} \frac{\omega}{\dot{\omega}} d\omega$$

$$T = \int_{\omega_1}^{\omega_2} \frac{1}{\dot{\omega}} d\omega$$

$$W = \frac{K \ddot{Y}_0^2}{2Q\omega_0^3} \int_{\omega_1}^{\omega_2} \left(\frac{\omega}{\omega_0} \right)^2 H^2 \frac{d\omega}{\dot{\omega}}$$

$$\frac{9.94}{Q} \left| \frac{97}{5} \right| \frac{98}{10} \left| \frac{99}{15} \right| \frac{99}{20}$$

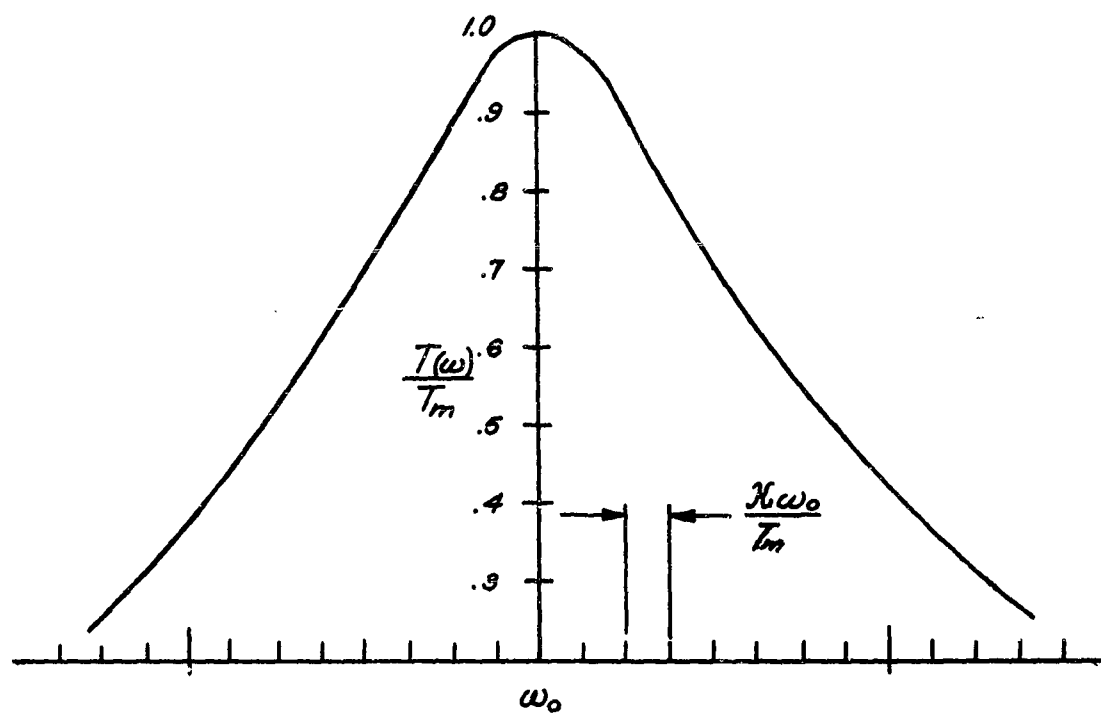


Figure 202. Non-dimensional Transmissibility Function For The Single Degree of Freedom System.

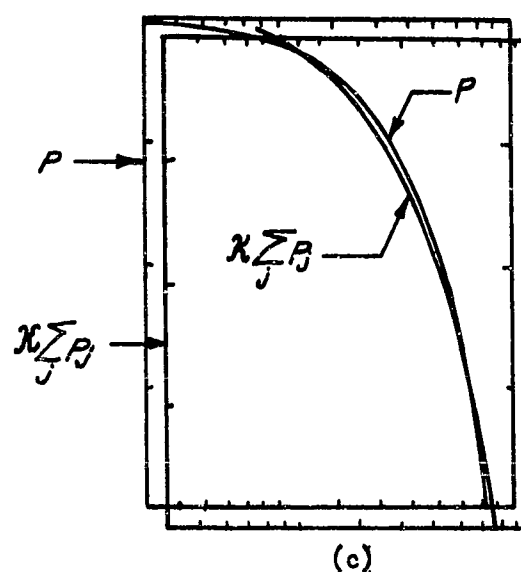
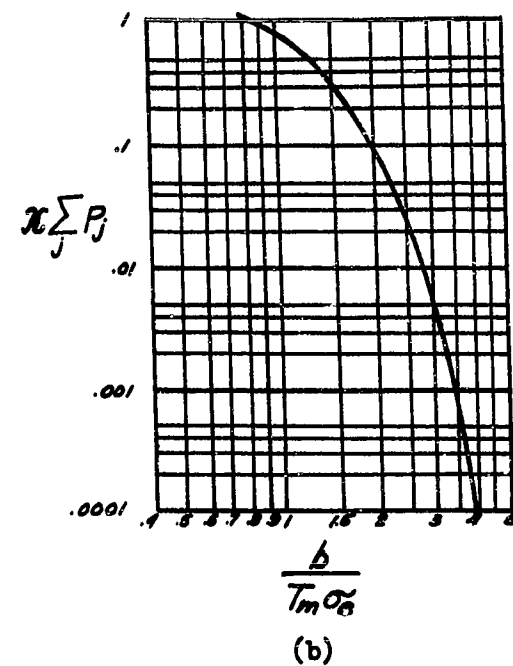
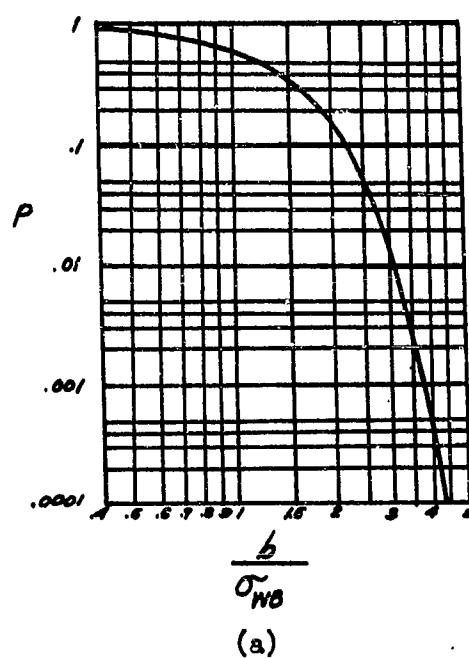


Figure 203. Probability Distributions For Peak Response of The Single Degree of Freedom System To Wide-Band Random Excitation and to Narrow-Band Random Sweep Excitation.

VIII. CONCLUSIONS

1. Judgments involving acceptable test procedures, confidence levels, safety margins, and environmental predictions should be made with cognizance of and reference to the vehicle over-all reliability requirements, and economic aspects of these judgments should be viewed in the context of the total vehicle or program reliability requirements. Thus, the cost of providing vehicle reliability by test must be weighed against the cost of providing insufficient vehicle reliability with its attendant risk of mission failure.
2. One of the fundamental attacks on the problem of reliability of structure and equipment must be through design innovation which avoids the problem of sensitive items. Miniaturizing, transistorizing, and potting of components are such fundamental approaches to the upgrading of equipment. The analogous advances in the field of structures may consist of sandwich structures, the use of bonding in place of riveting, and the addition of damping and the use of other techniques of vibration control.
3. The primary trend toward more severe environments and the need for continually improved vehicle performance should be recognized. The fact that an acoustic threshold has been crossed at which significant structural damage begins should be considered along with the trend of always more powerful propulsion systems which are available.
4. Certain questions to be answered in choosing sinusoidal or random testing are whether a damaging interaction between modes be present and whether fasteners exist which are sensitive to broad-band high-frequency excitation. However, the major reason for the need for random vibration testing is the additional damage done by stress interaction or intermixing of the loads.
5. The test design proceeds through the answers to these questions: (a) Can the test apply a duplication of the load history without acceleration in level or time? This type of test may be especially appropriate for missiles and space vehicles because of the limited service life. The margin of safety may be assigned to this case with more accuracy than usual. (b) If not the test above, is there a way to accelerate the test in time only? (c) If neither of the above tests apply, consideration can be given jointly to:
 - a. Is there an appropriate sinusoidal equivalent or should a random test be used?
 - b. Is the part sufficiently linear in response to allow acceleration in level?
6. The various equivalences are qualified equivalences in every case. The approximations and assumptions involved will provide something less than an exact equivalence.

7. The various equivalences presented have avoided the use of a cumulative damage theory. It is felt that no satisfactory cumulative damage theory is available which includes the influence of:
 - a. Intermixing
 - b. The variation in the endurance limit dependent on the degree of intermixing.
 - c. Stress concentrations

A satisfactory experimental correlation including these parameters is also not available.
8. An equivalence satisfactory for a certain problem may not be satisfactory for others. The many nonlinearities and significant parameters must be given adequate consideration; and before a method is accepted, it should be experimentally substantiated.
9. The statistical scatter in the data and the required confidence level should be considered in specifying the margin of safety. A fundamental reason for the margin of safety is the inability to do a sufficient number of tests with a significant number of parts to provide a statistically significant definition of the equipment fragility.

REFERENCES

1. McGlymonds, WADC TR-509 Sonic Fatigue Design.
2. Schelderup, "Structural Peak Distribution Under Random Vibration," WADC Minn. Acoustic Fatigue Conference, September 1959.
3. Galt Booth, "Sweep Random Vibration," IES Proceedings for 1960.
4. Shanley, "A Theory of Fatigue Based on Unbonding During Reversed Slip," Rand R-350, November 1952.
5. Stephenson, N., "Effect of Frequency on Fatigue Properties of Metals and Alloys," Mem. M320 National Gas Turbine, established June 1958.
6. Lassiter and Hess, "Calculated and Measured Stresses in Simple Panels Subject to Intense Field of Turbojet Engine," NASA TN-4076, September 1957.
7. Hess, Fralich, and Hubbard, "Studies of Structural Failure Due to Acoustic Loading," NASA TN-4050, July 1957.
8. Hess, Herr, and Mayers, "A Study of the Acoustic Fatigue Characteristics of Some Flat and Curved Aluminum Panels Exposed to Random and Discrete Noise," NASA TN D-1, August 1959.
9. Liu, Corten, "Fatigue Damage During Complex Stress Histories," NASA TN D-256, November 1959.
10. Hardrath, Utley, and Guthrie, "Rotating-Beam Fatigue Tests of Notched and Unnotched 7075-T6 Aluminum Alloy Specimens Under Stresses of Constant and Varying Amplitudes," NASA TN D-210, December 1960.
11. Hess, Lassiter, and Hubbard, "Response of Panels to Resonant Acoustic Excitation," NASA RM L55 E13C.
12. Fralich, R.W., "Experimental Investigation of Effects of Random Loading on the Fatigue Life of Notched Cantilever Beam Specimen of 7075-T6 Aluminum Alloy," NASA Memo, 12 April 1959.
13. Getline, G.L., "Correlation of Structural Fatigue Relative to Discrete Frequency, Constant Amplitude and Random Acoustic Excitation," Convair, San Diego, Newspaper.
14. Hall, B.M., "Correlation of Sinusoidal Random Vibration (BS)."
15. Lazan, "Structural Damping," December 1959.

16. Bingman, R. N., "Resonant Fatigue Failures Associated with Noise," SAE 164-B, April 1960.
17. Mustain, R. W., "Extended Environmental Test, SM-62 Components," Northrop Report NAI-57-954, December 1957.
18. Cook, Dr. Neal, "How Far to Go In Additional Random Vibration Equipment," 1960 IES Proceedings.
19. Spence, "Random Sinusoidal Vibration Tests on Missile Electronic Equipment."
20. Trotter, "Experience Evaluation of Sinusoidal Substitutes for Random Vibration."
21. Crandall, S. H., "Random Vibration," page 4.7.
22. Morrow, C. T., and Muchmore, R. B., "Shortcomings of Present Method of Measuring and Simulating Vibration Environments," JAM, September 1955.
23. Galef, A. E., "A Quasi-Sinusoidal Vibration Test as a Substitute for Random Testing," 28th Symposium on Shock and Vibration, February 1960.
24. Gertel, M., "Establishing Vibration and Shock Tests for Missile Electronic Equipment," Barry Report 230-C, February 1955.
25. Booth, "Sweep Random Vibration."
26. Blake, R. E., and Olson, M. W., "Substitute for Random Vibration Testing," 24th Shock and Vibration Bulletin, February 1957.
27. Riley, F. C., Schwartz, F. W., "Acceleration, Shock, and Vibration Criteria for Aircraft and Airborne Equipment," WADC TN 55-99, June 1955.
28. Barbieri, R. E., Hall, W., "Electronic Designs Shock and Vibration Guide for Airborne Applications," WADD TR 58-363, ASTIA No. AD-204095, December 1958.
29. Noisieux, D. U., "Response of Small Electronic Components to Intense Sound Fields and to Vibration," paper presented at SAE National Aeronautics Meeting, Los Angeles, October 1960.
30. "Specification for Environmental Requirements and Tests for XSM-68 and SM-68 Airborne Equipment," The Martin Company, 31 July 1956. Revised 22 February 1960.
31. "Basic Qualification Test Standards for Airborne Equipment," The Martin Co., Quality Control Specification No. Q.C. 103, September 1959.
32. Skoog, J. A., Setterbund, G. G., "Space Requirements for Equipment Items Subjected to Random Excitation Shock and Vibration," Bulletin No. 26, Part II, December 1958.

33. Eldred, K., Roberts, W., White, R. W., "Structural Vibrations in Space Vehicles," Phase II Report, "Determination of Structural Response to Vibratory Loading," NOR-60-268, 26 August 1960.
34. Eldred, K., Mustain, R., Roberts, W., White, R. W., "Structural Vibrations in Space Vehicles," Phase I Report, "Investigation of Structural Vibrations Sources and Characteristics," NOR-60-26, 29 January 1960.
35. "Random Vibration," Book edited by S. H. Crandall, The Technology Press of MIT, 1958.
36. Himmelblau, H., Keer, L. M., "Space Requirements for Simple Mechanical Systems Excited by Random Vibration," JASA, Vol. 32, No. 1, 76-80, January 1960.
37. Himmelblau, H., Kuoppamoki, K., Lahnala, E. H., Stafford, F. B., Mintz, F., "A Statistical Method for Determining Vibration Damage to Airborne Equipment," SAE Journal, Vol. 65, No. 12, November 1957.
38. Spence, H. R., "Random-Sine Equivalence Tests on Missile Electronic Equipment," Institute of Environment Sciences 1960 Proceedings.
39. Trotter, W. D., "An Experimental Evaluation of Sinusoidal Substitutes for Random Vibrations," paper presented at 29th Symposium on Shock, Vibration, and Associated Environments, November 1960.

APPENDIX A

RESONANCE ON RESONANCE

The equations of motion for the complete two-degree-of-freedom system shown in Figure 121 may be written as follows:

$$\ddot{x}_1 + \frac{\omega_0}{Q_1} \dot{x}_1 + \omega_0^2 x_1 + \mu \ddot{x}_2 = \omega_0^2 x_0 + \frac{\omega_0}{Q_1} \dot{x}_0 \quad (A1)$$

$$\ddot{x}_2 + \frac{\omega_0}{Q_2} \dot{x}_2 + \omega_0^2 x_2 = \omega_0^2 x_1 + \frac{\omega_0}{Q_2} \dot{x}_1 \quad (A2)$$

The straightforward analysis of the physical system described by the above equations would involve the direct calculation from Equations (A1) and (A2) of the square of the absolute value of the frequency response functions for \ddot{x}_1 and \ddot{x}_2 . An integration of these functions over all frequencies then yields the mean square values of x_1 and x_2 for a white noise input \ddot{x}_0 which has power spectral density of 1.0 g²/cps. If the functions are evaluated at any particular frequency, the values thus obtained are the mean square values for \ddot{x}_1 and \ddot{x}_2 corresponding to a sinusoidal input \ddot{x}_0 (having this frequency) with a 1.0 g rms amplitude.

Any of several methods involving various combinations of digital or analog computing equipment, rms voltmeters and/or power spectrum analysers may be used to obtain results along the above lines. Although the results were obtained by the above method, they were independently checked by another method involving the use of normal mode techniques. Although this technique is not applicable to cases where Q_1 and Q_2 differ appreciably, it gives rapid and economical results which are much more capable of physical interpretation than results obtained by the straightforward method.

The salient points of both of these methods are outlined below. Following this outline, results are presented in graphical form and interpretive conclusions are drawn.

The equations of motion (A1) and (A2) may be put in matrix form as follows:

$$A\ddot{x}(t) + \omega_0 B\dot{x}(t) + \omega_0^2 Cx(t) = D(t) \quad (A3)$$

where the following definitions hold:

$$A = \begin{bmatrix} 1 & 0 \\ 0 & \mu \end{bmatrix}, \quad B = \begin{bmatrix} Q_1^{-1} + \mu Q_2^{-1} & -\mu Q_2^{-1} \\ -\mu Q_2^{-1} & \mu Q_2^{-1} \end{bmatrix}, \quad C = \begin{bmatrix} 1 + \mu & -\mu \\ -\mu & \mu \end{bmatrix}$$

$$D(t) = \left[\omega_0^2 x_0(t) + \frac{\omega_0}{Q_1} \dot{x}_0(t) \right], \quad \mu = \frac{m}{M}, \quad x(t) = \begin{bmatrix} x_1(t) \\ x_2(t) \end{bmatrix}$$

Hence, the frequency response function matrix $\bar{\chi}_\delta(\omega)$ is

$$\bar{\chi}_\delta(\omega) = \left[-\omega^2 A + i \omega_0 \omega B + \omega_0^2 C \right]^{-1} \begin{bmatrix} \omega_0^2 + i \omega \omega_0 / Q_1 \end{bmatrix} \quad (A_4)$$

Calculation of $|\bar{\chi}_\delta(\omega)|^2$ is straightforward and yields the direct, but somewhat physically oblique results mentioned previously.

It may be readily verified that if the matrix Z is defined as follows

$$Z = \begin{bmatrix} 1 - (\frac{\omega_1}{\omega_0})^2 & 1 - (\frac{\omega_2}{\omega_0})^2 \\ 1.0 & 1.0 \end{bmatrix} \quad \text{where} \quad \begin{cases} (\frac{\omega_1}{\omega_0}) = \frac{1}{2} [2 + \mu - \sqrt{\mu^2 + 4\mu}] \\ (\frac{\omega_2}{\omega_0}) = \frac{1}{2} [2 + \mu + \sqrt{\mu^2 + 4\mu}] \end{cases}$$

then the matrices $Z^t A Z = A'$ and $Z^t A Z = C'$ have the following diagonal form (the superscript t indicates matrix transposition):

$$A' = \begin{bmatrix} a_1 & 0 \\ 0 & a_2 \end{bmatrix}, \quad C' = \begin{bmatrix} \omega_1^2 a_1 & 0 \\ 0 & \omega_2^2 a_2 \end{bmatrix} \omega_0^{-2}$$

where

$$a_n = \left[1 - (\frac{\omega_n}{\omega_0})^2 \right]^2 + \mu$$

and furthermore,

$$B' = Z^t B Z = \begin{bmatrix} P_1 Q_2^{-1} + P_2 Q_2^{-1} & \mu [Q_2^{-1} - Q_1^{-1}] \\ \mu [Q_2^{-1} - Q_1^{-1}] & P_3 Q_1^{-1} + P_4 Q_2^{-1} \end{bmatrix}$$

The constants p_n are easily determined for any particular value of ω by carrying out the indicated matrix multiplications. Further investigation shows that for $.7 \leq Q_1/Q_2 \leq 1.3$, a rapid approximate solution for \ddot{x}_1 and \ddot{x}_2 (as well as frequency response functions and rms values for random and sinusoidal inputs) can be obtained by the normal mode approach outlined below. (This method is exact for $Q_1 = Q_2$ and can be used to give rough estimates for Q_1/Q_2 outside the above range.)

Let the time dependent normal mode coordinates be denoted by the symbol $c_n(t)$ where the c_n satisfy the following equation:

$$\ddot{c}_n(t) + \frac{\omega_n}{Q(n)} \dot{c}_n(t) + \omega_n^2 c_n(t) = \omega_n^2 x_o^{(n)}(t) \quad (A5)$$

The above equations constitute a reformulation of Equation (A3) in terms of the $c_n(t)$ coordinates where the $x_n(t)$ coordinates and the $c_n(t)$ coordinates are related as follows:

$$\ddot{x}_1 = \left[1 - \left(\frac{\omega_1}{\omega_o} \right)^2 \right] \ddot{c}_1 + \left[1 - \left(\frac{\omega_2}{\omega_o} \right)^2 \right] \ddot{c}_2 \quad (A6)$$

$$\ddot{x}_2 = \ddot{c}_1 + \ddot{c}_2 \quad (A7)$$

(The term $(\omega_o/Q_1)\dot{x}_1$ in Equation (A1) has been ignored since it occurs in the absolute value of the transfer function as an additive term in Q_1^{-2} and is thus negligible for realistic values of Q_1).

The "quality factors" for the two equivalent single-degree-of-freedom systems described by Equation (A4) are determined from the matrix B' to be:

$$\frac{1}{Q(1)} = \frac{\omega_o}{\omega_1 a_1} (P_1 Q_1^{-1} + P_2 Q_2^{-1}) \quad (A8)$$

$$\frac{1}{Q(2)} = \frac{\omega_o}{\omega_2 a_2} (P_3 Q_1^{-1} + P_4 Q_2^{-1}) \quad (A9)$$

The equivalent acceleration input to the n^{th} equivalent single-degree-of-freedom system is given by the following relation:

$$\begin{aligned} \ddot{x}_o^{(n)}(t) &= \frac{1}{a_n} \left(\frac{\omega_o}{\omega_n} \right)^2 \left[1 - \left(\frac{\omega_n}{\omega_o} \right)^2 \right] \ddot{x}_o(t) = \left\{ (-1)^{n+1} \left(\frac{\omega_o}{\omega_n} \right)^2 \left[1 - \left(\frac{\omega_1}{\omega_o} \right)^2 \right] \frac{1}{a_1} \right\} \ddot{x}_o(t) \\ &= e_n \ddot{x}_o(t) \\ e_n &= (-1)^{n+1} \left(\frac{\omega_o}{\omega_n} \right)^2 \left[1 - \left(\frac{\omega_1}{\omega_o} \right)^2 \right] \frac{1}{a_1} \end{aligned} \quad (A10)$$

The power spectrum of any function $u(t)$ is denoted below by the symbol $\Phi_u(\omega)$. Thus, the power spectra of $\ddot{c}_n(t)$ and $\ddot{x}_n(t)$ are denoted by the symbols $\Phi_{\ddot{c}_n}(\omega)$ and $\Phi_{\ddot{x}_n}(\omega)$ respectively. Similarly, the cross spectral density for the two functions $\ddot{c}_1(t)$ and $\ddot{c}_2(t)$ is denoted by the symbol $\Phi_{\ddot{c}_1, \ddot{c}_2}(\omega)$.

It follows from Equations (A5) and (A7) that

$$\Phi_{\ddot{x}_1}(\omega) = \left[1 - \left(\frac{\omega_1}{\omega_0}\right)^2\right]^2 \Phi_{\ddot{c}_1}(\omega) + \left[1 - \left(\frac{\omega_2}{\omega_0}\right)^2\right]^2 \Phi_{\ddot{c}_2}(\omega) - \left[\Phi_{\ddot{c}_1 \ddot{c}_2}(\omega) + \Phi_{\ddot{c}_2 \ddot{c}_1}(\omega)\right] \quad (A11)$$

$$\Phi_{\ddot{x}_2}(\omega) = \Phi_{\ddot{c}_1}(\omega) + \Phi_{\ddot{c}_2}(\omega) + \Phi_{\ddot{c}_1 \ddot{c}_2}(\omega) + \Phi_{\ddot{c}_2 \ddot{c}_1}(\omega) \quad (A12)$$

where

$$\Phi_{\ddot{c}_n}(\omega) = \sigma_n^2 \Phi_{\ddot{x}_0}(\omega) \left\{ \left[1 - \left(\frac{\omega}{\omega_n}\right)^2\right]^2 + \left(\frac{\omega}{Q(n)\omega_n}\right)^2 \right\}^{-1}$$

$$\Phi_{\ddot{c}_1 \ddot{c}_2}(\omega) = \sigma_1 \sigma_2 \Phi_{\ddot{x}_0}(\omega) \left\{ \left[1 - \left(\frac{\omega}{\omega_1}\right)^2 - i \frac{\omega}{Q(1)\omega_1}\right] \left[1 - \left(\frac{\omega}{\omega_2}\right)^2 - i \frac{\omega}{Q(2)\omega_2}\right] \right\}^{-1}$$

$$\Phi_{\ddot{c}_2 \ddot{c}_1}(\omega) = \left[\Phi_{\ddot{c}_1 \ddot{c}_2}\right]^* \quad (\text{the asterisk denotes complex conjugation})$$

The maximum value of $\Phi_{\ddot{x}_2}(\omega)$ may be determined from a plot constructed with the aid of Equation (A12). This value occurs at the most critical frequency that can be applied to the primary structure insofar as the acceleration response of the secondary structure (or "black box") to a discrete input to the primary structure is concerned. If the secondary structure (or "black box") contains guidance or other equipment which is sensitive to some particular band of frequencies, the spectrum $\Phi_{\ddot{x}_2}(\omega)$ may be used to determine the rms response acceleration in that band.

For an input with a flat power spectral density (white noise), the rms accelerations of the primary and secondary structures may be determined by integrating the associated power spectral density function over all frequencies:

$$(\ddot{x}_{n_{rms}})^2 = \frac{1}{2\pi} \int_0^\infty \Phi_{\ddot{x}_n}(\omega) d\omega \quad (\Phi_{\ddot{x}_n}(\omega) \text{ is measured in } g^2/\text{cps units})$$

The results of these integrations (which are readily accomplished by application of the theory of residues) are presented on page 445.

$$\begin{aligned}
(\ddot{x}_{1\text{rms}})^2 = \omega_o \Phi \ddot{x}_o \left\{ \frac{\mu^2 Q^{(1)}}{4a_2^2 (\omega_1/\omega_o)^3} + \frac{\mu^2 Q^{(2)}}{4a_1^2 (\omega_2/\omega_o)^3} \right. \\
\left. + \frac{2\mu \left[1 - (\frac{\omega_1}{\omega_o})^2 \right]^2 (\gamma_2 + K\gamma_1)}{a_1^2 (\frac{\omega_2}{\omega_o})^3 \left[\beta_2^2 - K^2 \beta_1^2 - (\gamma_2 + K\gamma_1)^2 \right]^2 + 4\beta_2^2 (\gamma_2 + K\gamma_1)^2} \right\} \quad (A13)
\end{aligned}$$

$$\begin{aligned}
(\ddot{x}_{2\text{rms}})^2 = \omega_o \Phi \ddot{x}_o a_1^{-2} \left[1 - (\frac{\omega_1}{\omega_o})^2 \right] \left\{ \frac{Q^{(1)}}{4(\omega_1/\omega_o)^3} + \frac{Q^{(2)}}{4(\omega_2/\omega_o)^3} \right. \\
\left. + \frac{2(\gamma_2 + K\gamma_1)}{(\frac{\omega_2}{\omega_o})^3 \left[\beta_2^2 - K^2 \beta_1^2 - (\gamma_2 + K\gamma_1)^2 \right]^2 + 4\beta_2^2 (\gamma_2 + K\gamma_1)^2} \right\} \quad (A14)
\end{aligned}$$

where

$$\gamma_n = \frac{1}{2Q(n)}$$

$$\beta_n^2 = 1 - \gamma_n^2$$

$$K_2 = \omega_1/\omega_2$$

$$a_n = \left[1 - (\omega_n/\omega_o)^2 \right]^2 + \mu$$

It is worthwhile to note that Equations (A13) and (A14) can be used to develop check data for digital or analog computer programs where accurate results are desired for cases where $Q_1/Q_2 > 1.3$ or $Q_1/Q_2 < .7$. Such computing procedure is recommended for these cases since the analytical expressions for the power spectral densities and mean square values of x_1 and x_2 —which must be developed from Equation (A4)—are quite cumbersome.

It can be readily determined from Equation (A3) that the maximum values of the absolute values of the transfer functions of x_1 and x_2 , for the case $\frac{M}{m} = \infty$ are $\sqrt{Q_1^2 + 1}$ and $\sqrt{Q_2^2 + 1}$ respectively. (Where \ddot{x}_o is regarded as the input into the x_1 system and \ddot{x}_1 , in turn, is regarded as the input into the x_2 system.) Hence, for this case the net transfer function for \ddot{x}_2 (regarding \ddot{x}_o as the input) is the product $\sqrt{(Q_1^2 + 1)(Q_2^2 + 1)}$ which is the magnification factor $\ddot{x}_{2\text{rms}}/\ddot{x}_{o\text{rms}}$ for a

sinusoidal input \ddot{x}_0 at the resonant frequency ω_0 . The effect of mass ratio (M/m) on the magnifications $\ddot{x}_{1rms}/\ddot{x}_{0rms}$ and $\ddot{x}_{2rms}/\ddot{x}_{0rms}$ for a sinusoidal excitation at the lower of the coupled frequencies is shown by Figures 130a and 130b respectively. Only excitation at the lower normal mode frequency was used—as a brief inspection of Equation (A14) shows—the rms response to excitation at the higher frequencies is less than the response to excitation at the lower frequencies. This fact is clearly borne out by Figure 132. Input conditions should be noted.

The data for Figures 130 and 131 were obtained for the case $Q_1 = Q_2 = 15$ by means of the following equipment:

- (1) Electronic Associates Inc., EAI Analogue Computer Group 16-31R.
- (2) Hewlett Packard Low-Frequency Generator, Model 202-A.
- (3) Epsco Digital Voltmeter Model DV 803.

Figure 130a shows the expected initial decrease in $\ddot{x}_{1rms}/\ddot{x}_{0rms}$ as M becomes larger followed by a gradual trend toward the $(Q^2 + 1)^{1/2}$ asymptote as $M/m = \mu^{-1}$ approaches infinity. Figure 130b shows the expected increase of \ddot{x}_2/\ddot{x}_0 toward the asymptotic value $(Q^2 + 1)$ at $M/m = \infty$. Both asymptotes were checked on the EAI Computer by zeroing the potentiometer governing the $\mu \ddot{x}^2$ coupling term in Equation (A1). As $M/m \rightarrow \infty$, both systems approach resonance with \ddot{x}_1 acting as an input to the \ddot{x}_2 system in precisely the same way as \ddot{x}_0 is an input to the \ddot{x}_1 system. For this reason, the situation might be aptly termed as "resonance on resonance."

It is then reasonable to ask if a situation similar to "resonance on resonance" occurs for a random input. The well-known single-degree-of-freedom magnification for a white noise random input \ddot{x}_0 is

$$\frac{\ddot{x}_{1rms}}{\ddot{x}_{0rms}} = \sqrt{\frac{\omega_0 Q}{4 \Delta f}}$$

(This relation holds for $\frac{M}{m} = \infty$ —which is equivalent to $\mu = 0$ —where Δf = band width of $\ddot{x}_0(t)$.)

Since \ddot{x}_1 is essentially a randomly modulated sinusoid with a base frequency $\sqrt{k_1/M}$, it is reasonable to expect the magnification $\ddot{x}_{2rms}/\ddot{x}_{1rms}$ to approach a value somewhat less than $\sqrt{Q^2 + 1}$ as M/m approaches infinity. Hence, the over-all magnification $\ddot{x}_{2rms}/\ddot{x}_{0rms}$ is somewhat less than $\sqrt{Q^2 + 1} \sqrt{\frac{\omega_0 Q}{4 \Delta f}}$ or roughly of the order of $Q^{3/2} \sqrt{\omega_0 Q / 4 \Delta f}$. Data which resolve this question were determined with the above mentioned equipment as well as the following equipment:

(4) Hughes Electronic Noise Generator, Model 101, Serial 7.

(5) Technical Products Analyzer TP 627.

The power spectrum of the noise generator output obtained by use of the TP 627 analyzer is shown in Figure 132. The results of the random noise investigation are presented in Figures 131a and 131b. Figure 131a shows an initial decrease of $\ddot{x}_{1rms}/(\ddot{x}_{0rms}\sqrt{\frac{\omega_0}{4\Delta f}})$ (as in the sinusoidal case where $\ddot{x}_{1rms}/\ddot{x}_{2rms}$ initially decreased) followed by a gradual increase toward $Q^{\frac{1}{2}}$ asymptote at $M/m = \infty$.

Figure 131b shows a fairly rapid initial increase of $\ddot{x}_{2rms}/(\ddot{x}_{0rms}\sqrt{\frac{\omega_0}{4\Delta f}})$ followed by a leveling off toward an asymptotic value of approximately $.6 Q^{3/2}$ as M/m approaches infinity.

Hence, in both the random and sinusoidal cases, the effect of mass ratio (M/m) on the rms acceleration of the secondary structure is quite important when the frequencies of the primary and secondary structures are approximately equal. Consequently, it is clear that large and possibly destructive responses may result when small pieces of equipment or secondary structure are mounted on relatively large primary structures.

APPENDIX B

EXAMPLE OF THE ADDITION RULE FOR PROBABILITY DENSITIES: PROBABILITY DENSITY FUNCTION OF GAUSSIAN RANDOM NOISE AND A DISCRETE SINUSOID

A problem which is of interest in random noise analysis and which provides a useful example of the addition rules for probability density distributions is the problem of finding the resultant distributions for a noise consisting of normally distributed random components and a number of discrete frequency components. In such cases, the distribution of the envelope as well as the probability density of the noise is of interest. The case of a single sinusoid plus Gaussian random noise will be shown in some detail to illustrate the essentials of the addition process.

The main addition rule is stated as follows:

If $P_Z(b)$ is the probability density for a combined random process $Z(t)$ for which $N(t)$ and $S(t)$ are the constituent processes (i.e., $Z(t) = S(t) + N(t)$),

then

$$P_Z(b) = \int_{-\infty}^{\infty} P_S(a) P_N(b-a) da \quad (B1)$$

where $P_S(a)$ and $P_N(a)$ are the probability densities for the $S(t)$ and $N(t)$ processes respectively.

(Here, $P_f(b)db$ denotes the probability that, for any randomly chosen time t_1 , $f(t_1)$ lies between b and $b + db$.)

Another way of stating the same result is that if $\bar{P}_Z(u)$ is the Fourier transform of $P_Z(Z)$,

$$\bar{P}_Z(u) = \bar{P}_S(u) \bar{P}_N(u) \quad (B2)$$

where $\bar{P}_S(u)$ and $\bar{P}_N(u)$ are the Fourier transforms of $P_S(a)$ and $P_N(a)$ respectively.

This result follows directly from the application (to Equation (B2)) of the Fourier convolution theorem which states that the Fourier transform of a convolution is simply the product of Fourier transforms of the functions which are convoluted.

A statistical interpretation of the above Fourier transforms exists since, for instance,

$$\bar{P}_Z(u) = \text{F.T.} [P_Z(a)] = \int_{-\infty}^{\infty} P_Z(a) e^{iua} da = \text{Expectation of } e^{iua}. \quad (B3)$$

These Fourier transforms are usually termed characteristic functions in statistical literature. One of their main advantages is that, as shown above, the characteristic function for a combined random process is the product of the characteristic functions of the constituent processes. Then application of the Fourier inversion theorem yields

$$\text{F.T.}^{-1} \left\{ \text{F.T.} [P_Z(a)] \right\} = \text{F.T.}^{-1} \bar{P}_Z(u) = \frac{1}{2\pi} \int_{-\infty}^{\infty} \bar{P}_Z(u) e^{-iua} du = P_Z(a) \quad (B4)$$

The particular problem at hand consists of finding a probability density function $P_Z(Z)$ and an envelope distribution function $P_R(R)$ for the combined process $Z(t)$.

$$Z(t) = S(t) + N(t)$$

where $S(t) = A \cos(\omega t - \varphi)$

$N(t)$ = normally distributed random noise with standard deviation σ .

We shall first find $\bar{P}_S(u)$ (and incidentally $P_S(a)$). Then $\bar{P}_N(u)$ will be determined from $P_N(a) = e^{-a^2/2\sigma^2} / \sqrt{2\pi}$. Then the Fourier inversion theorem will be used to obtain the inverse transform of $\bar{P}_S(u) \bar{P}_N(u)$ which is $P_Z(a)$ according to Equation (B2). The distribution for the envelope of $Z(t)$ will then be developed and demonstrated to reduce the Rayleigh distribution for the case $A = 0$. Plots of the envelope probability density are presented for the cases $A = 0, \sigma, 2\sigma, 3\sigma, 4\sigma$, and 5σ in Figure 207.

Now choosing times t_i at random from the range $-\infty \leq t \leq +\infty$ is statistically the same as fixing t and choosing the equiprobable phases φ_i from the range $0 \leq \varphi \leq 2\pi$. Since the density in φ , $P_\varphi(\varphi)$ has the simple normalized form shown in Figure 204, it is much easier to calculate the characteristic function $\bar{P}_S(a)$ using the finite range phase distribution than it is to use the infinite range distribution for t .

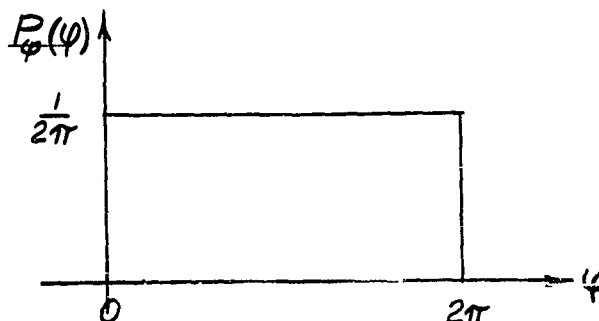


Figure 204. Probability Density of the Phase Angle

$$\bar{P}_S(u) = \text{Exp}(e^{iua}) = \int_{-\infty}^{\infty} P_{\varphi}(\varphi) e^{iu A \cos(\omega t - \varphi)} d\varphi = \frac{1}{2\pi} \int_0^{2\pi} e^{iu A \cos(\varphi - \omega t)} d(\varphi - \omega t) \quad (B5)$$

$$= J_0(Au)$$

where the last integral is the well-known integral expression for the zero order Bessel function.

The Fourier inversion theorem (B4) leads to the following expression for the probability density $P_S(a)$ for $S(t)$:

$$P_S(a) = \frac{1}{2\pi} \int_{-\infty}^{\infty} e^{-iua} J_0(Au) du = \begin{cases} \frac{1}{\pi \sqrt{A^2 - a^2}} & \text{for } |a| < A \\ 0 & \text{for } |a| > A \end{cases} \quad (B6)$$

where the integral representation (B5) for $J_0(Au)$ has been utilized to effect the last integration. This distribution is plotted in Figure 136. However, instead of convoluting $P_S(a)$ with the random noise probability density $P_N(a) = [e^{-a^2/2\sigma^2}]/\sigma\sqrt{2\pi}$ it is most convenient to obtain $P_Z(a)$ as the inverse Fourier transform of the product $\bar{P}_S(u) \bar{P}_N(u)$ where

$$\begin{aligned} \bar{P}_N(u) &= \text{F.T.} \left[\frac{e^{-\frac{a^2}{2\sigma^2}}}{\sigma\sqrt{2\pi}} \right] \text{Exp } e^{iua} = \int_{-\infty}^{\infty} e^{iua} \frac{e^{-a^2/2\sigma^2}}{\sigma\sqrt{2\pi}} da \\ \bar{P}_N(u) &= \frac{1}{\sqrt{2\pi}} \int_{-\infty}^{\infty} e^{-\frac{1}{2}(\frac{a}{\sigma} - i\sigma u)^2} e^{-(\sigma u)^2/2} d(a/\sigma) \\ \bar{P}_N(u) &= \frac{1}{\sqrt{2\pi}} e^{-(\sigma u)^2/2} \int_{-\infty}^{\infty} e^{-(1/2)v^2} dv = e^{-(\sigma u)^2/2} \end{aligned} \quad (B7)$$

$$\begin{aligned} \text{where } v &= \left(\frac{a}{\sigma} - i\sigma u\right) \\ dv &= d\left(\frac{a}{\sigma}\right) = \frac{da}{\sigma} \end{aligned}$$

Then since

$$\bar{P}_Z(u) = \bar{P}_S(u) \bar{P}_N(u) = e^{-\sigma^2 u^2/2} J_0(Au),$$

it follows from Equation (B4) that

$$P_Z(a) = \frac{1}{2\pi} \int_{-\infty}^{\infty} e^{-iua} \bar{P}_Z(u) du = \frac{1}{2\pi} \int_{-\infty}^{\infty} e^{-iua} e^{-\sigma^2 u^2/2} J_0(Au) du.$$

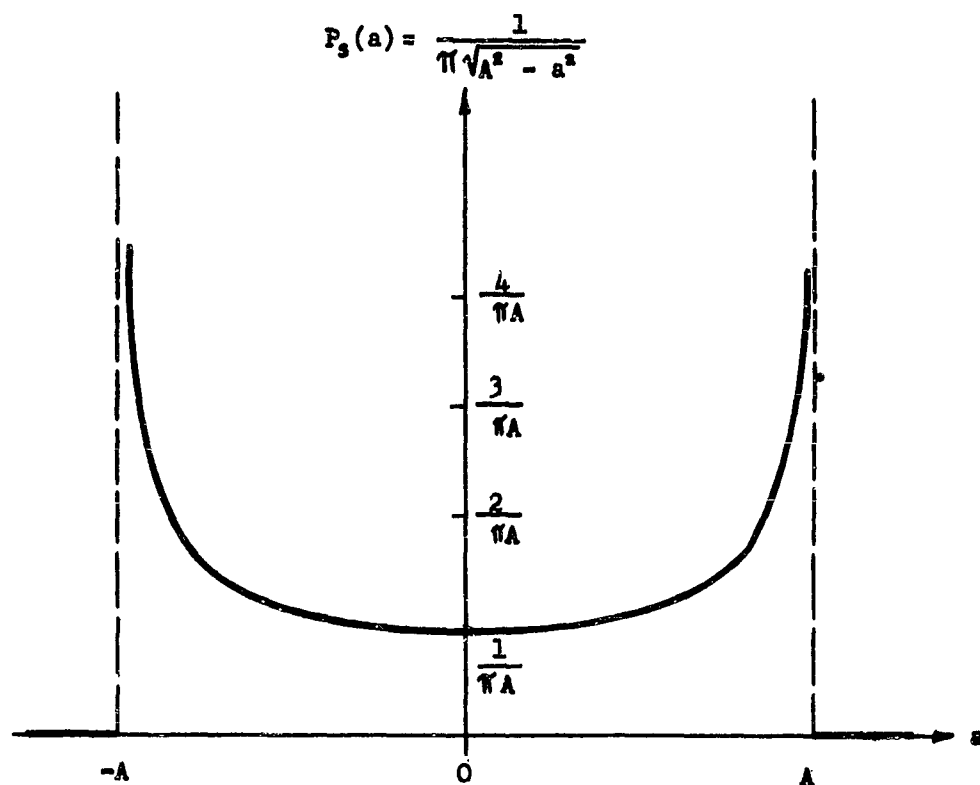


Figure 205. Probability Density of a Steady Sinusoidal Disturbance

This integral may be put in a more tractable form (relative to ease of numerical integration) by making use of the integral expression for $J_0(Au)$:

$$P_Z(a) = \frac{1}{2\pi} \int_{-\infty}^{\infty} \left\{ e^{iua - \sigma^2 u^2/2} \frac{1}{2\pi} \int_0^{2\pi} e^{iuA \cos \theta} d\theta \right\} du$$

$$= \frac{1}{2\pi} \int_0^{2\pi} \left\{ \frac{1}{2\pi} \int_{-\infty}^{\infty} e^{-iu(a-A \cos \theta)} e^{-\sigma^2 u^2/2} du \right\} d\theta$$

Now, according to Equation (B4), if $g = (a - A \cos \theta)$, then

$$\frac{1}{2\pi} \int_{-\infty}^{\infty} e^{-iug} e^{-\sigma^2 u^2/2} du = \text{F.T.}^{-1} \left[e^{-\sigma^2 g^2/2} \right],$$

where according to Equation (B7),

$$e^{-\sigma^2 g^2/2} = \text{F.T.} \left[\frac{e^{-g^2/2\sigma^2}}{\sigma\sqrt{2\pi}} \right],$$

and where "g" is the dummy variable of integration used in the Fourier integral which yields $e^{-\sigma^2 u^2/2}$ (just as "a" is the dummy variable in the two equations immediately preceding Equation (B7)).

$$\text{F.T.} \left[e^{-\sigma^2 u^2/2} \right] = \text{F.T.}^{-1} \left\{ \text{F.T.} \left[\frac{e^{-g^2/2\sigma^2}}{\sigma\sqrt{2\pi}} \right] \right\}$$

$$= \frac{e^{-g^2/2\sigma^2}}{\sigma\sqrt{2\pi}} = \frac{e^{-(a-A \cos \theta)^2/2\sigma^2}}{\sigma\sqrt{2\pi}}$$

Hence

$$P_Z(a) = \frac{1}{\pi\sigma\sqrt{2\pi}} \int_0^{\pi} e^{-(a-A \cos \theta)^2/2\sigma^2} d\theta \quad (\text{B8})$$

This reduces to a Gaussian distribution for $A = 0$. Now there is no loss in generality in any of the preceding results in not taking the sinusoidal portion of $Z(t)$ as $S'(t) = x_1 \cos(\omega t - \psi) + y_1 \sin(\omega t - \psi)$ since

$$S'(t) = \sqrt{x_1^2 + y_1^2} \cos(\omega t - \psi + \tan^{-1} x_1/y_1).$$

Hence $S'(t) = S(t)$ if $\varphi = \psi - \tan^{-1} \frac{x_1}{y_1}$, $A^2 = x_1^2 + y_1^2 = R_1^2$.

In the following development, the second representation for $Z(t)$ will be more convenient.

Now the envelope of $Z(t)$ is defined as $R(t)$, where

$$Z(t) = R(t) \cos (\omega t - \gamma(t)).$$

After expanding, there results

$$Z(t) = S(t) + N(t) = [R(t) \cos \gamma(t)] \cos \omega t + R(t) [\sin \gamma(t)] \sin \omega t.$$

Now $N(t)$ can be written as $N(t) = x_r(t) \cos \omega t + y_r(t) \sin \omega t$ where it can be shown that $x_r(t)$ and $y_r(t)$ are normally distributed with standard deviation σ .

Hence

$$R(t) \cos \gamma(t) = x_1 + x_r(t)$$

$$R(t) \sin \gamma(t) = y_1 + y_r(t)$$

and

$$R^2(t) = [x_1 + x_r(t)]^2 + [y_1 + y_r(t)]^2$$

A moment's reflection shows that the value of $R(t)$ then represents the magnitude of a vector $R(t) = \underline{x_1} + \underline{y_1} + \underline{x_r} + \underline{y_r}$, which is the sum of a fixed vector $R_1 = \underline{x_1} + \underline{y_1}$

and a random vector $R_r = \underline{x_r} + \underline{y_r}$.

Thus, the x density function $P_1(x)$ for $x = x_1 + x_r(t)$ is

$$P_1(x) = \frac{1}{\sigma\sqrt{2\pi}} e^{-(x-x_1)^2/2\sigma^2}$$

since x_1 is clearly the mean value of $P_1(x)$.

Similarly, the y density function $P_2(y)$ is

$$P_2(y) = \frac{1}{\sigma\sqrt{2\pi}} e^{-(y-y_1)^2/2\sigma^2}$$

Thus the joint probability density function $P(x, y)$ is

$$P(x,y) = \frac{1}{2\pi\sigma^2} \cdot e^{-\frac{1}{2\sigma^2} \left\{ (x-x_1)^2 + (y-y_1)^2 \right\}}$$

This may be conveniently converted to polar coordinates with the aid of Figure 206.

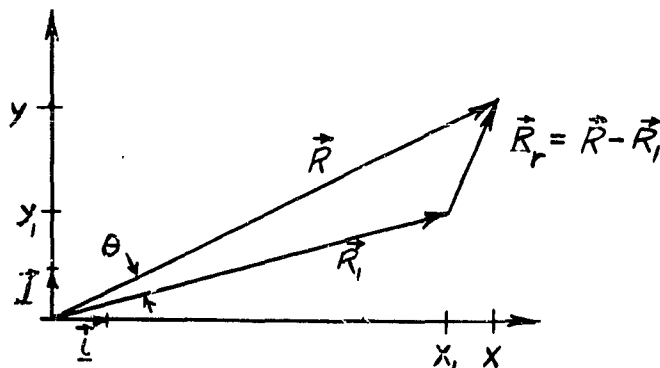


Figure 206. Relations between the Coordinates

so that

$$P(x,y) dx dy \rightarrow P(R,\theta) R dR d\theta$$

Hence, the probability $P_R(R) dR$ that the envelope $R(t)$ will lie between R and $(R + dR)$ for all θ is obtained by integrating over the entire range of θ .

$$\begin{aligned} P_R(R) dR &= \frac{1}{2\pi\sigma^2} \int_0^{2\pi} R dR \cdot e^{-\frac{1}{2\sigma^2} (R^2 + R_1^2 - 2RR_1 \cos \theta)} d\theta \\ &= \frac{R dR}{\sigma^2} \cdot e^{-(R^2 + R_1^2)/2\sigma^2} \left\{ \frac{1}{2\pi} \int_0^{2\pi} e^{(-iRR_1/\sigma^2) \cos \theta} d\theta \right\} \end{aligned} \quad (B9)$$

Thus

$$P_R(R) = \frac{R}{\sigma^2} \cdot e^{-(R^2 + R_1^2)/2\sigma^2} J_0\left(-i\frac{RR_1}{\sigma^2}\right) = \frac{R}{\sigma^2} \cdot e^{-(R^2 + R_1^2)/2\sigma^2} I_0\left(\frac{RR_1}{\sigma^2}\right)$$

where $I_0(\bar{x}) = J_0(-i\bar{x})$ is the zero order, modified Bessel function of the first kind. Since $I_0(0) = J_0(0) = 1$, $P_R(R)$ reduces to the familiar Rayleigh distribution. As mentioned before, $P_R(R)$ is plotted (Figure 207) for the cases $R_1 = 0, \sigma, 2\sigma, 3\sigma, 4\sigma$, and 5σ .

In fact, $P_R(R)$ and $P_Z(a)$ might be called non-central Rayleigh and non-central normal distributions.

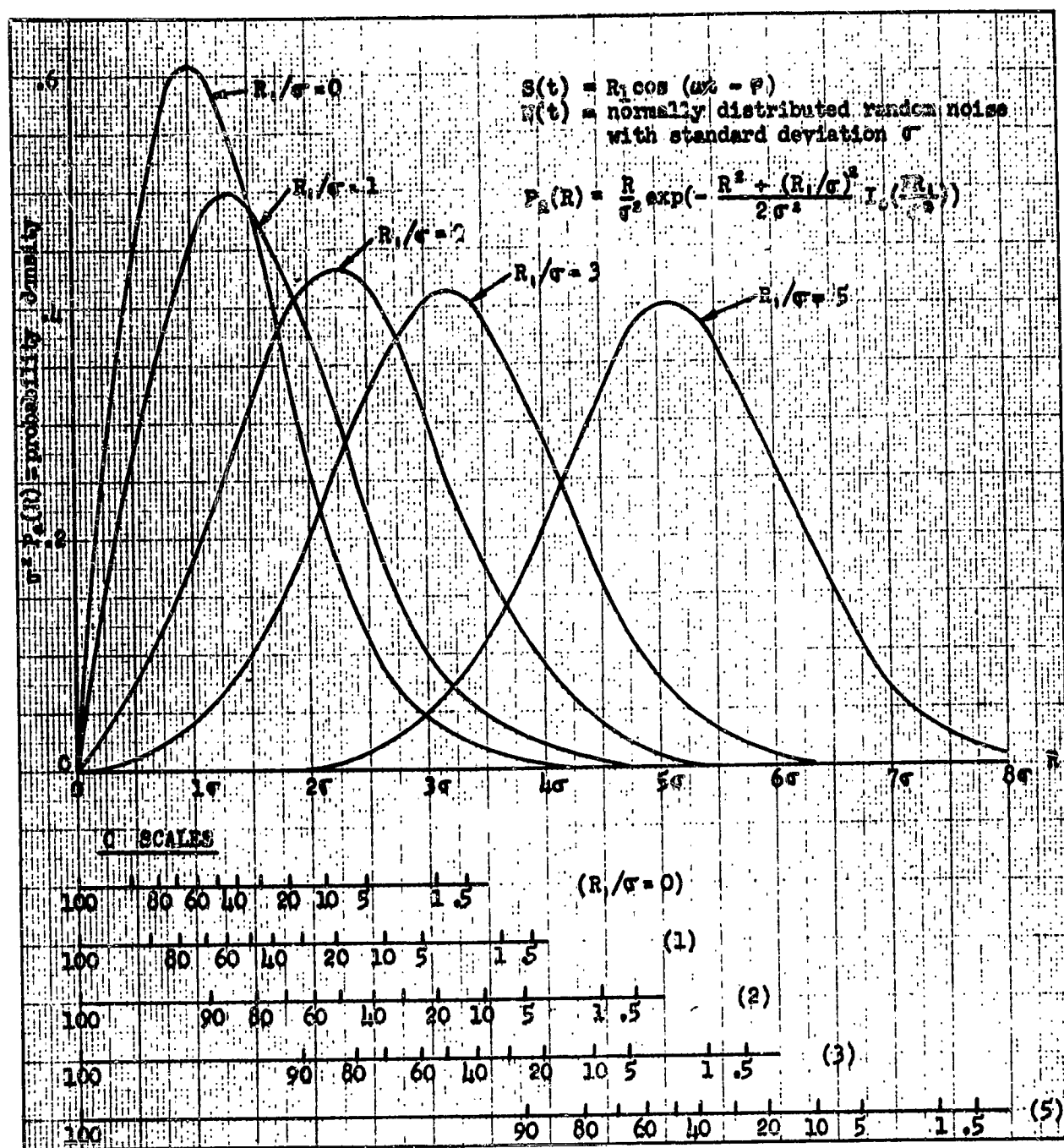
If the combined process $Z(t)$ consists of n discrete sinusoidal components plus normally distributed random noise

(that is, $Z(t) = \sum_{i=1}^n A_i \cos \omega_i t + N(t)$ where $\frac{\omega_i}{\omega_j}$ is irrational for $i \neq j$),

application of the foregoing methods results in the following expression for the probability density of the resulting envelope:

$$P_{n,R}(R) = R \int_0^\infty r J_0(Rr) \prod_{i=1}^n J_0(A_i r) e^{-r^2/2} dr$$

For the cases $n = 0$ and $n = 1$, the above expression specializes (after integration) to the Rayleigh distribution and the distribution given by Equation (B9) respectively.



c = probability in percent that R exceeds the value of the R axis.

Figure 207. Probability Density of Envelope R of $Z(t) = S(t) + N(t)$